GEOCHEMISTRY OF STREAM SEDIMENTS AND SURFICIAL DEPOSITS AT PASCUA-LAMA HIGH SULFIDATION EPITHERMAL GOLD DEPOSIT, CHILE-ARGENTINA

By

Emily Ann Chastain

B.Sc. – Colorado School of Mines, 1998.

A THESIS SUBMITTED IN PARTIAL FULFILLMENT OF
THE REQUIREMENTS FOR THE DEGREE OF
MASTER OF SCIENCE

in

THE FACULTY OF GRADUATE STUDIES

Department of Earth and Ocean Sciences

We accept this thesis as conforming

to the required standard

THE UNIVERSITY OF BRITISH COLUMBIA
March, 2001

In presenting this thesis in partial fulfilment of the requirements for an advanced degree at the University of British Columbia, I agree that the Library shall make it freely available for reference and study. I further agree that permission for extensive copying of this thesis for scholarly purposes may be granted by the head of my department or by his or her representatives. It is understood that copying or publication of this thesis for financial gain shall not be allowed without my written permission.

Department of Earth & Ocean Sciences

The University of British Columbia
Vancouver, Canada

Date 20 March 2001

DE-6 (2/88)

Abstract

Pascua-Lama is a 17.1 moz Au and 560 moz Ag high sulfidation epithermal gold deposit on the crestline of the High Andes of Argentina and Chile. In this arid, mountainous terrain, talus cones and alluvial fans flank deeply incised valleys and debris flows infill valley floors decoupling streams from valley walls. Glacial till is preserved locally.

Surficial deposits, stream sediments and waters were sampled along valleys draining the deposit. Samples were wet sieved and fractions finer than –150μm analyzed for gold by FA-AAS. The -53μm fraction of medium energy sediments was also analyzed by ICP-MS after total, aqua regia, and a weak hydroxylamine leach. Heavy mineral concentrates (HMCs) were analyzed by NAA and SEM-EDS. Water samples were analyzed by ICP-MS.

Geochemical patterns at Lama-Pascua developed as a result of both mechanical and chemical processes. The occurrence of gold and associated elements (e.g., Ag, As, Pb, Hg, Sb, Bi) in HMCs allows their progressive enrichment as light minerals are selectively removed during erosion and transport of surficial materials. Thus, till, with the greatest abundance of fines, has the lowest geochemical contrast. Conversely, sediments have the highest concentration of HMC associated elements. More mobile elements such as Cu have similar concentrations in surficial deposits and stream sediments, but under extremely acidic conditions are depleted close to the deposit.

In stream sediments, gold provides the best anomaly contrast with the longest and most consistent anomalies in the fine fractions (-75μm or finer). Based on sediment texture, ~2 kg –2 mm field samples should provide 50 g of -75μm material for analysis. Stream water pH should be measured and analysis of stream waters could be a valuable adjunct to sediment data, particularly in areas where debris flows decouple streams from their valley sides or headwalls. Follow-up to drainage anomalies would involve base-of-slope sampling of talus and alluvial fans and should consider the possible depletion of more mobile metals close to a deposit.

TABLE OF CONTENTS

List of Tables

List of Figures

List of plates

ACKNOWLEDGEMENTS

Funding for this project was provided by Barrick Gold Corporation in the form of a grant to K. Fletcher. This grant provided for analyses, travel to Argentina-Chile, and room and board. Thanks to Dave Heberlein for his information, feedback and willingness to support this project. Sandra Schiattino was indispensable in getting reports, data and myself to and from San Juan.

I'm very grateful to K. Fletcher for his patience the last 2 ½ years and especially the last couple of months. Thanks to his ability to read the same chapters many times there are a lot few fewer mistakes and inconsistencies. Also thanks to committee members Dr. Sinclair, Lee Groat, Dick Tosdal and Dick Chase for reviewing and commenting on the thesis in a short time period.

Many thanks to the geologists at both Lama and Pascua for making a gringa feel welcome, including Annick Chouinard. The help of numerous field assistants was invaluable. Melissa Montgomery deserves praise for her perseverance in sample preparation at UBC.

A special thanks to Cari Deyell for helping me from the moment I stepped into Chile to providing ore and alteration descriptions today. Thanks for listening to my rants, always being supportive and knowing what to say. Thanks for sushi and beer at the Eatery!

Thanks to Jen Hobday, Katye McConaghy, Vanessa Gale, Kate Bone, Tina Roth and everyone else for making me be social and putting up with my drastic mood swings. Special thanks to Keith Patterson for taking me skiing (and letting me use his printer right now at 3 am without having to ask!). I did NOT push you off the cliff at Whistler. I'll always have coffee cravings Thursday at 10:30 am. Steven, I will miss your yoga class. Thanks to the Wednesday night crew for letting me teach yoga.

Final acknowledgements to my family whose tolerance exceeds expectations and to my friends in Colorado. Without Scott, MC, Larry and Wendy Harrison I would never have survived the move to Canada, let alone finishing.

CHAPTER 1

INTRODUCTION

1.1 Objectives

The Chilean/Argentinean Andean cordillera host a number of epithermal precious metal deposits which include El Indio, Tambo and the focus of this research, Pascua/Lama, a 17.1 moz Au and 560 moz Ag high sulfidation deposit (Figure 1.1) (Barrick, 1999). Despite a suitable environment, very little previous work has been reported on Andean epithermal stream sediment geochemistry and in particular on the effectiveness of sediment sampling in relation to the complex supply of sediment by glacial till, alluvial fan, talus cone and debris flow material. This research is focused on improving regional stream sediment geochemistry through a better understanding of processes that link mineral deposits, via surficial deposits, to geochemical anomalies in stream sediments and waters. Recommendations are made with respect to optimizing reconnaissance and property scale geochemical exploration.

1.2 Literature review

There is a paucity of previous work in the public domain on regional exploration geochemistry in the Andes. Moranzana (1972) examined the applications of talus sampling to exploration in the desert Andes, and gold dispersion by ephemeral streams in the Atacama region, Chile was reported by Herail, et. al. (1999). More generally relevant literature includes the traditional stream sediment anomaly dilution model proposed by Hawkes (1976). This model has been modified to explain enrichment of heavy minerals (including gold) by fluvial processes and includes work done by Day and Fletcher (1991), Hou and Fletcher (1996), Fletcher and Loh

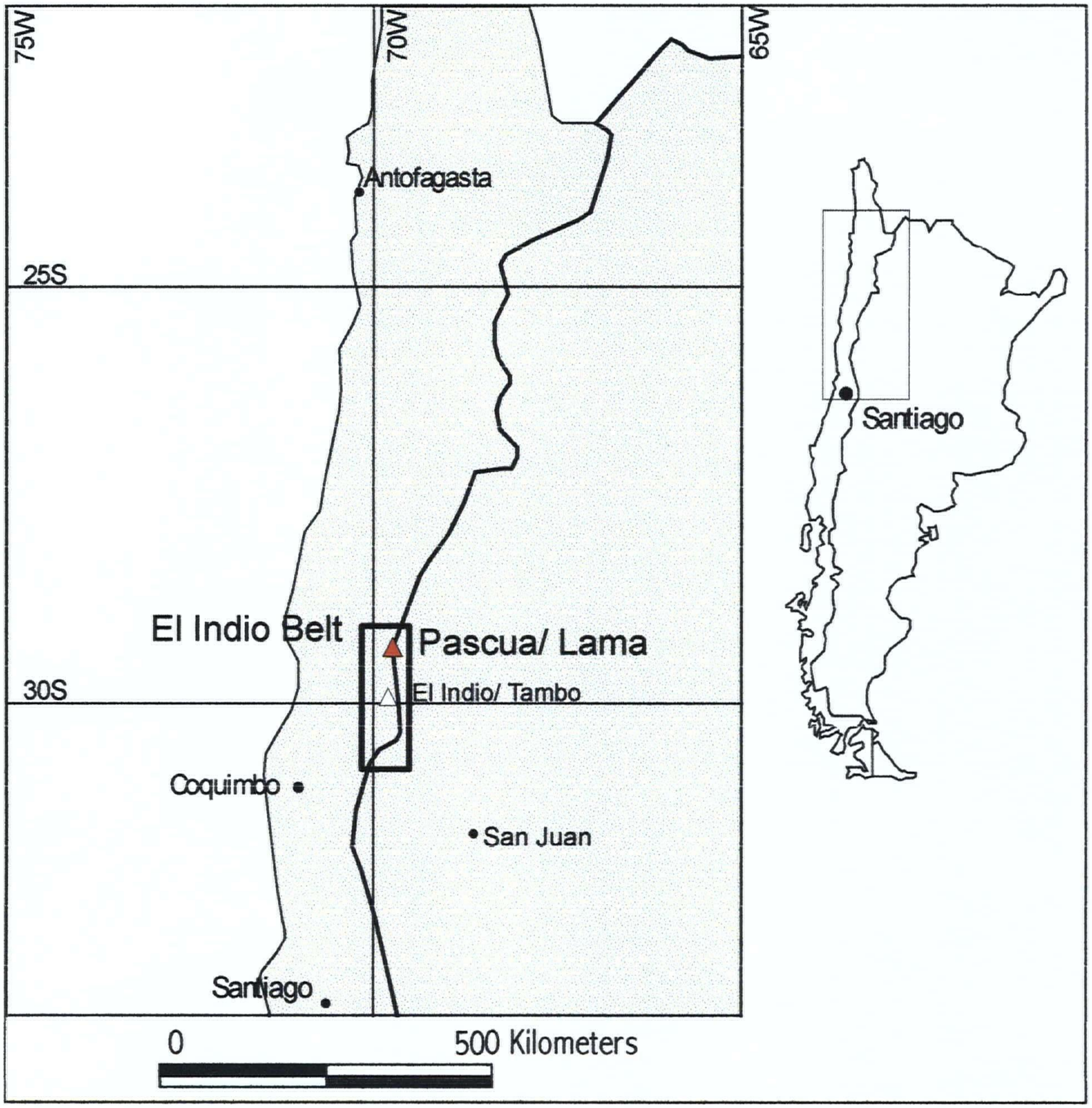

Figure 1.1 Location map of El Indio belt in Chile/Argentina with El Indio/Tambo and Pascua/Lama deposits indicated.

(1996) and Fletcher et. al., (1987). The use of selective chemical extractions to capture previously mobile elements has been reported by Chao (1972 and 1984), Chao and Theobald (1976), Hall (1998), and Hall et. al., (1996). Fletcher (1997) and Stanley and Smee (1989) examined the statistical problems of sampling gold (and other rare grains) as applied to exploration programs.

1.3 High sulfidation epithermal geochemical suite

High sulfidation (acid-sulfate) epithermal deposits are formed at shallow depths and are associated with subaerial volcanic rocks (Evans, 1993). The alteration mineralogy contains many acid-stable minerals such as alunite, kaolinite, dickite and pyrophyllite (Hedenquist et. al., 1996). The ore is hosted by leached silicic rock associated with acidic fluids (less than pH 2) generated in the volcanic hydrothermal environment (Hedenquist et. al., 1996). The ore mineralogy includes many sulfides (e.g. chalcopyrite, tennanite, sphalerite, galena, arsenopyrite, cinnabar and stibnite) and sulfosalts (e.g. enargite), tellurides and selenides which produces the multi-element 'epithermal' suite reported in Cox and Singer (1986) and White and Hedenquist (1995) of Au, Ag, As, Cu, Sb, Bi, Hg, Te, Sn, Pb and Mo. High sulfidation deposits tend to have areally extensive and visually prominent alteration zones related to acid alteration (Hitzman, 1997).

1.4 Stream sediment geochemical model

Stream sediment geochemistry is used to identify anomalous dispersion trains and follow them upstream to their source. The traditional model of downstream dilution of sediment anomalies was proposed by Hawkes (1976) and has the form:

$$Me_m A_m = A_a(Me_a - Me_b) + A_m Me_b \qquad (1)$$

where:

A_m and A_a are the areal extent of the mineralized area and the area above the sampling site, respectively, and Me_m, Me_a and Me_b are the concentrations of an element in the deposit, anomalous sample site and background, respectively (Figure 1.2). If the drainage basin is large relative to the size of mineralization, it can be considered a point source and the model reduces to:

$$Me_m A_m = A_a (Me_a - Me_b) \qquad (2)$$

This model is valid under specific assumptions of equal rates of erosion, constant geochemical background concentrations, no interaction between waters and sediment, no sampling or analytical errors and only one source of mineralization. The decay pattern is expected to be the same regardless of whether the anomaly occurs as residual detrital grains or as precipitates of hydromorphic origin (Rose et. al., 1979).

This model was shown to predict Cu concentrations in stream sediments draining porphyry copper deposits (Hawkes, 1976). However, there is a substantial amount of work that repudiates the assumptions of the traditional model as a result of fluvial and chemical processes that modify downstream dilution patterns. There are also sampling and analytical problems inherent in sampling for rare grains such as gold.

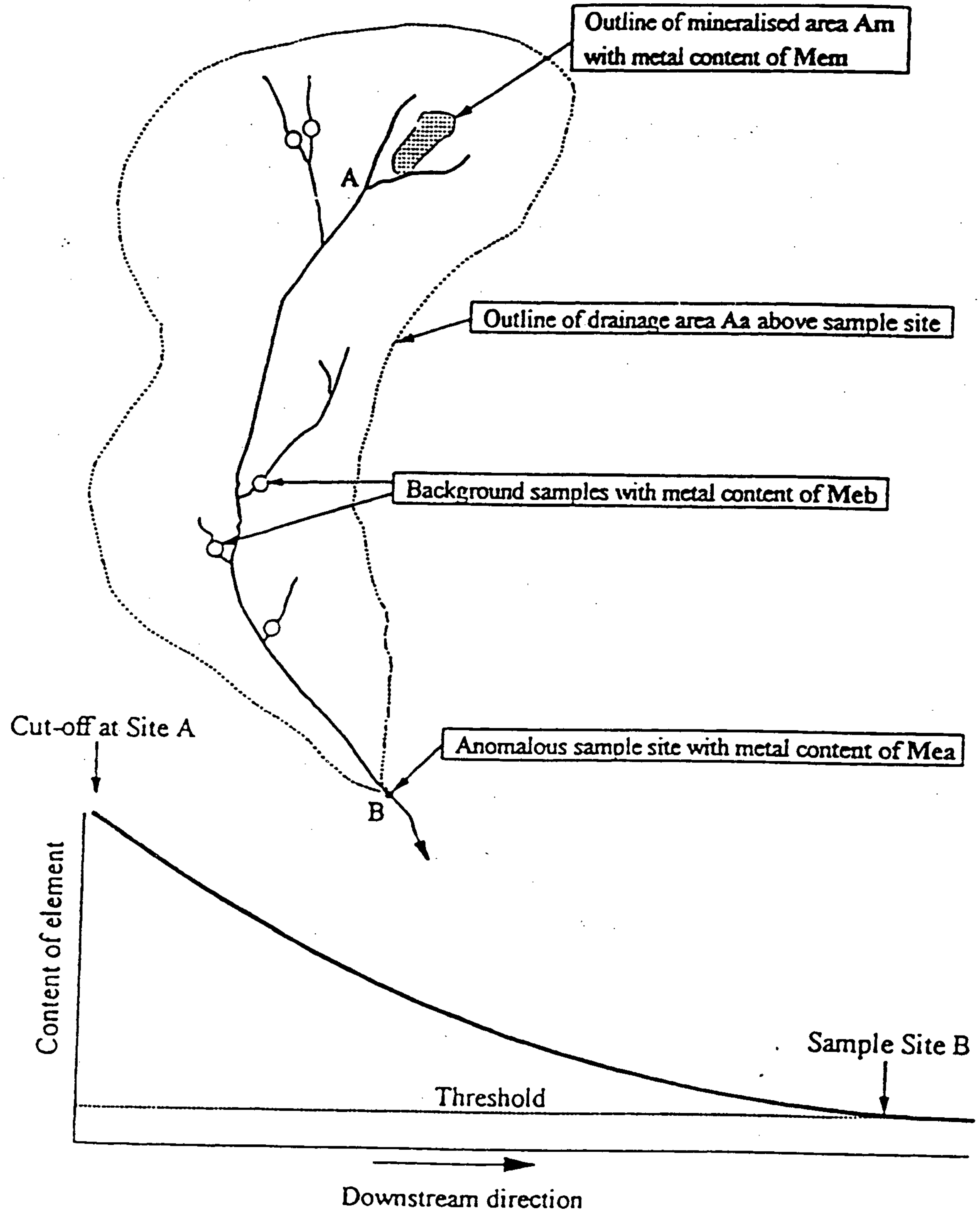

Figure 1.2. Definition of parameters used in Hawkes' dilution model, equation 1. (from Hou, 1997 after Hawkes, 1976).

1.4.1 Fluvial effects

Water-deposited sediment is sorted according to the size, shape and specific gravity of the particles. Both geomorphic (e.g. stream gradient and morphology, proximity to sources) and hydraulic factors (e.g. stream velocity, depth to width ratio) can lead to enriched concentrations of heavy minerals in streams (Slingerland, 1984). It is known that there are a number of locations in streams that tend to concentrate heavy minerals (Table 1.1). A more extensive discussion of local fluvial processes that concentrate heavy minerals is found in Day (1985).

Five major sorting mechanisms have been proposed to explain placer formation: (1) entrainment equivalence (Slingerland, 1977); (2) hydraulic equivalence (Rubey, 1933); (3) dispersive equivalence (Sallenger, 1979); (4) interstice trapping (Reid and Frostick, 1985); and (5) turbulent flow around obstacles and at stream junctions where there is flow separation (Best and Brayshaw, 1985). Entrainment sorting removes particles from the stream bed by overcoming the inertial forces keeping them in place. The Shields diagram relating critical shear Reynolds number to a dimensionless critical shear stress for entrainment is often used to define the stability of stream beds under different hydraulic conditions (Boggs, 1995). Hydraulic equivalence is based on theoretically derived terminal settling velocities (e.g. Stokes Law) that predict small high-density particles will settle at the same rate as large less dense particles. Sallenger (1979) proposed dispersive sorting as a mechanism for producing concentrations of high density minerals at different horizons within a concentrated granular dispersion by grain collisions producing dispersive pressures. Interstices trapping attempts to explain heavy mineral concentrations by assuming those fine particles will move into the interstices between coarse particles following a flood event, hence the fine matrix is not in hydraulic equivalence with the

Table 1.1 Examples of locations of extreme high-density mineral concentrations (after Day, 1985).

1) In riffled bedrock depressions.
2) Downstream of large boulders and islands.
3) Any zone of flow separations (Best and Brayshaw, 1985).
4) Downstream of counfluences in suction eddies.
5) Bar to bank flow convergence zones.
6) Heads of point bars and channel bars.
7) Decrease in channel gradient.
8) Emergence of streams from canyons (abrupt channel widening).
9) At the contact between alluvial sediments and bedrock.
10) At "false bottoms" above clay layers and pans.

coarse framework (Best and Brayshaw, 1985). All these processes can lead to the development of highly variable, localized increases of heavy minerals on the stream bed.

Although it is accepted that heavy minerals are preferentially enriched by fluvial processes in stream sediments, the traditional geochemical dilution model of Hawkes (1976) does not allow for this and downstream profiles of elements found in heavy minerals (such as Au, Sn, W and Ba) are erratic, typically with concentrations that increase downstream away from the source (e.g. Day and Fletcher, 1991 and Hou and Fletcher, 1996 for Au; Saxby and Fletcher, 1986a for W; Fletcher and Loh, 1996 for Sn; and Sleath and Fletcher, 1982 for Ba).

In geochemical exploration, the erratic nature of heavy minerals resulting from fluvial processes causes difficulties in interpretation. Rittenhouse (1943) used coefficients of variation to determine hydraulically equivalent low and high density fractions. Fletcher et. al., (1987) used analysis of variance to assess reduction of within-site-variance versus between-site-variance using ratios of concentrations of low-density minerals in one fraction with concentrations of cassiterite in another fraction. Saxby and Fletcher (1986b) used geometric mean concentration ratios (GMCR) to estimate the variability introduced into stream sediment data by local hydraulic effects. Concentration ratios (XR) are defined as:

$$XR_s = X_{s,\,he} / X_{s,le} \qquad (3)$$

where XR_s is the concentration ratio for size fraction s; $X_{s,\,he}$ is the concentration of mineral (or element) in size fraction s for high energy sample; and $X_{s,\,le}$ is the equivalent paired data for the low energy sample. The GMCR is then calculated as the:

$$GMCR = \text{antilog}\,\{(\sum_{n}^{1} \log_{10} XR)/n\} \qquad (4)$$

where n is the number of paired data. GMCRs of Au, Sn (as cassiterite) and W (as sheelite) were shown to decrease with decreasing size fractions. This suggests that differences in heavy mineral concentrations between fluvial environments are minimized in the finer size fractions.

Fletcher et. al. (1987) showed that ratioing of heavy mineral of interest to a ubiquitous heavy mineral, such as magnetite, had a two fold effect on downstream dispersion patterns of Sn as cassiterite. The ratios lowered the overall geochemical contrast, but more importantly, reduced high Sn concentrations resulting from fluvial processes. This simplified downstream profiles, and the remaining downstream peaks were related to mineralization and not local fluvial effects. Ratioing gold concentration to magnetite was also used at Slesse Creek, British Columbia to reduce noise downstream Au patterns (Hobday and Fletcher, 2001). Preparation of magnetite (and other heavy mineral) separates is impractical for most exploration surveys where time and money are limited. Fletcher and Muda (1999) showed that the use of Ti and V concentrations, as surrogates for heavy mineral separates, from multi-element digestions also reduces the effect of fluvial concentration.

A final counter to the traditional dilution model was presented by Hou and Fletcher (1996), where peak gold concentrations were found to occur downstream from active landslides. While unable to determine if the breaks in stream gradient at the landslides were coincidental, they were able to trace the dilution of gold concentrations by erosion of fine grained sediment supplied by mass wasting events. Geochemical patterns downstream of the landslide depended on whether elemental concentrations of the eroded material were higher or lower than in stream sediments. Christie and Fletcher (1999) showed that road building produced new sediment sources which elevated the concentrations of elements associated with fine grained material (such as Co, Mg and Ni) above previously established levels.

1.4.2 Chemical effects

While fluvial modification tends to explain the downstream dispersion of heavy resistate minerals, many economic and pathfinder elements are also dispersed hydromorphically. The relative mobility of elements in the surficial environment is dependent on factors which include pH, Eh, and mode of occurrence. Rose et. al. (1979) outline four modes of occurrence of trace metals in solids: (1) as a major element in a trace material, such as Cu in enargite (Cu_3AsS_4) or Au as a native metal; (2) as a trace constituent in the crystal structure of a well crystallized mineral, such as Cu in biotite; (3) as a trace metal in a poorly crystallized material or adsorbed on a material and trapped by further precipitation, such as Cd or Zn in Fe-Mn oxides, and (4) as trace element adsorbed on the surface of a colloidal particle of Fe-Mn oxide, clay or organic material or in the exchange layer of a clay mineral. Under acidic and oxidizing conditions, such as those associated with natural acid rock drainage and surface oxidation of sulfides and sulfosalts, many minerals are leached or have appreciable aqueous solubility (Figure 1.3). This results in the primary mobilization of metals into solution, after which they must be readsorbed or precipitated (modes of occurrence 3 and 4) on stream sediments to form a hydromorphic anomaly. Adsorption-desorption processes between sediments and stream waters are ignored by Hawkes dilution model which assumes no interchange of material between stream waters and sediments.

a) Cu-S-O-H_2O at 25°C and 1 atm. Solubility is defined as a Cu activity of 10^{-6}. Total activity of sulfur species = 10^{-2}.

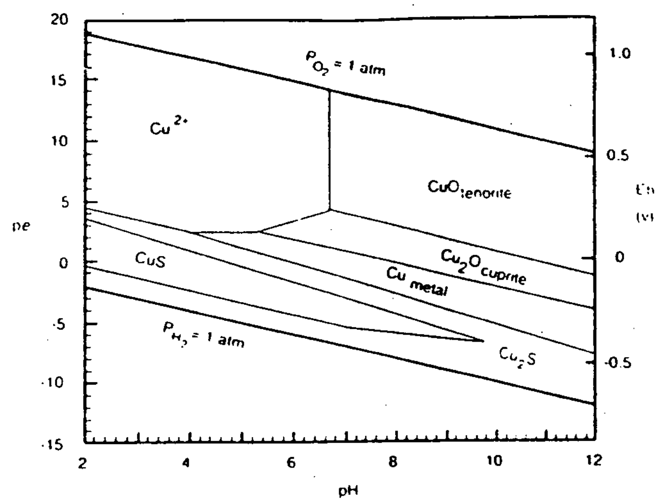

b) b) Zn-CO_2-S-O-H_2O at 25°C and 1 atm. Solubility is defined as a Zn activity of 10^{-6}. Total activity of sulfur species = 10^{-2}, $P_{CO_2} = 10^{-2}$.

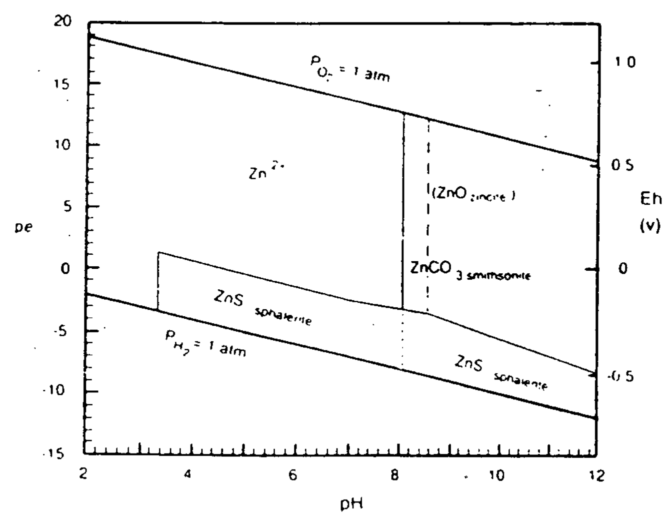

Figure 1.3. Simplified pe-pH diagrams for Cu and Zn heavy mineral systems (Drever, 1997). Copper and Zn are mobile in acidic and oxidizing conditions.

1.4.2.1 Chemical dispersion in surface waters

Elements in waters can occur simply as cations (e.g. Zn^{2+}, Cu^{2+}) and anions (e.g. SO_4^{2-}, MoO_4^{2-}), uncharged species (e.g. O_2, undissociated $H_4SiO_4^0$), organic complexes, suspended colloidal particles (Fe, Al and Mn oxides and hydroxides) and as ions adsorbed on suspended matter (Rose et. al., 1979). Element abundances in waters vary according to the solubility of minerals which, in turn, is controlled by acidity, redox conditions and salinity (total dissolved solids) (Giblin, 1994). In areas with acid rock drainage, such as Iron Mountain, California, extremely low pH values of –3.6 and high total dissolved metal concentrations of 200g/l have been reported (Nordstrom et. al., 2000).

Dissolved major and trace elements (including hydrogen as pH) can be used as hydrogeochemical guides to mineral deposits. The major element composition of natural waters can indicate presence of a group of rocks which has been identified from previous discoveries to be favorable for mineralization. For example, waters in contact with the crystalline basement at the Olympic Dam deposit in South Australia have lower [Ca^{2+}]/[total cation] than ground waters from overlying Late Proterozoic formations and Cambrian limestones (Giblin, 1994). Thus determination of Ca^{2+} normalized to total cation concentration can be used to locate aquifers with similar basement rocks as those hosting Olympic Dam. Deering et. al. (1983) found that Ca^{2+}, Mg^{2+}, SO_4^{2-} and total dissolved solid concentrations can be used to explore for Mississippi Valley Type base metal deposits. Trace metals can also be used as vectors to mineralization. Groundwaters from the Abitibi region, Quebec, showed two trace metal associations. Arsenic, Mo and Fe were indicative of base metal mineralization and As, Ni, F and Mn were related to Au mineralization (Lalonde, 1983). While many sulfide ore minerals are relatively insoluble in pure water, they are vulnerable to attack in oxidizing environment especially when pyrite or marcasite is present and generate sulfuric acid upon oxidation.

When taken with other sampling media, hydrogeochemical anomalies can be effectively used as guides to mineralization (Leybourne et. al., 1999 and Tianxiang et. al., 1998), and use of hydrogeochemical anomalies has grown since the development of ICP-mass spectrometry to measure concentrations in ppb (μg/l) range. Water samples have the advantage of being small (15ml) and are relatively easy to collect and suitable for multi-element ICP-MS analysis. However, since metal mobility in the surface environment is extremely pH dependent, pH must be measured to interpret the results.

1.4.2.2 Hydromorphic anomalies

Precipitation of metals from surface water is used to account for the rapid decay of water anomalies (Rose et. al. 1979). Precipitation barriers occur where changes in environmental conditions (typically pH) cause metals to drop out of solution and be precipitated or adsorbed onto sediment. Major types of precipitation barriers include (Perel'man, 1967): (1) oxidation type, Fe and Mn oxides precipitated out usually caused by water emergence to the surface; (2) alkaline type where Ca, Mg, Sr, Mn, Fe, Cu, Zn, Pb, Cd and other elements are precipitated by increased pH, usually caused by mixing of acid and alkaline waters; and, (3) adsorptive type where ions accumulate by adsorption or coprecipitation on accumulating Fe-Mn oxides, clays and organic matter. Generally, transition and higher valence cations tend to be more strongly adsorbed than anions and low valence cations. Precipitation barriers are generally a combination of the above types, combining Fe-Mn oxide precipitation with adsorption/coprecipitation of trace metals in response to increasing pH.

The ability of secondary oxides to scavenge trace metals results from their fine grained nature and cation exchange capacity in excess of some clay minerals (Carpenter and Hayes, 1980). In natural systems, composition of Fe-Mn oxides is often a complex mixture of both phases. However, experiments conducted by Robinson (1983) indicate that Fe-Mn coating in stream sediments display similar trace metal adsorption characteristics despite mineralogical and geochemical diversity. Surface complexation is regarded as the most accurate model to describe adsorption onto Fe-Mn oxides (Drever, 1997). At low pH values, cation adsorption is minimal, but rapidly goes to completion over a narrow change in pH (Figure 1.4a). Adsorption of anions is complementary to cations (Figure 1.4b). The precise pH range of adsorption is unique to each metal.

The use of selective extractions to capture the previously mobile (in solution) elements that have been subsequently immobilized in the surficial environment has been of great interest to geochemists and extensively studied (Chao, 1972 and 1984; Chao and Theobald, 1976; Hall, 1998; Hall et. al., 1996). It is impossible to extract *only* the phases sought during a selective extraction, and as a result selective leaches have been operationally defined (Caughlin, 1999). A number of chemical digestions have been created to liberate the trace metals associated with secondary oxides (e.g. hydroxylamine hydrochloride, hydroquinone, hydrogen peroxide, ammonium oxalate, sodium dithionite). The partitioning of an element into a hydromorphic phase can be seen by comparing ratios concentrations in selective leach (e.g. cold hydroxylamine) to a total or *aqua regia* digestion. The strong influence of pH on controlling the concentrations of hydromorphic metals is seen in data from a disseminated copper deposit in the Philippines (Figure 1.5) (Coope and Webb, 1963). Where pH is less than 4.0, cold extractable Cu:total Cu is low; as the pH increases, so does the amount of Cu in the cold extractable phase.

a)

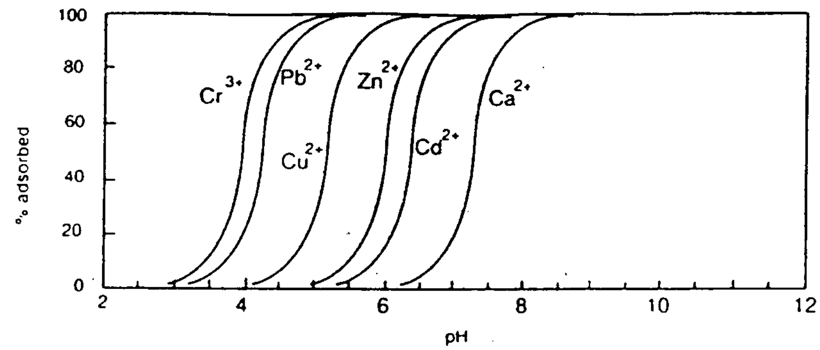

b)

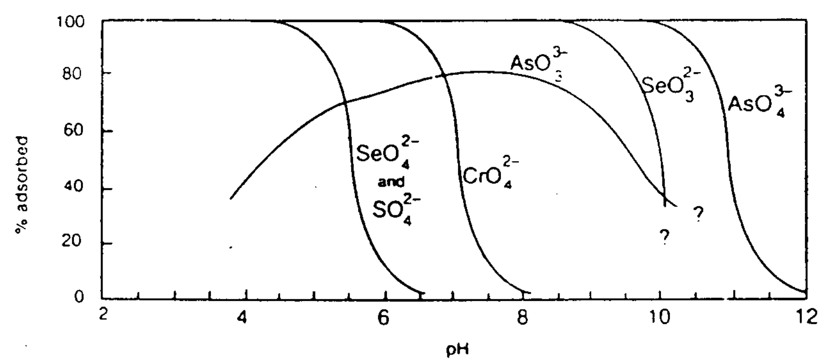

Figure 1.4. Adsorption of metal cations (a) and anions (b) on hydrous ferric oxide as a function of pH (Drever, 1997).

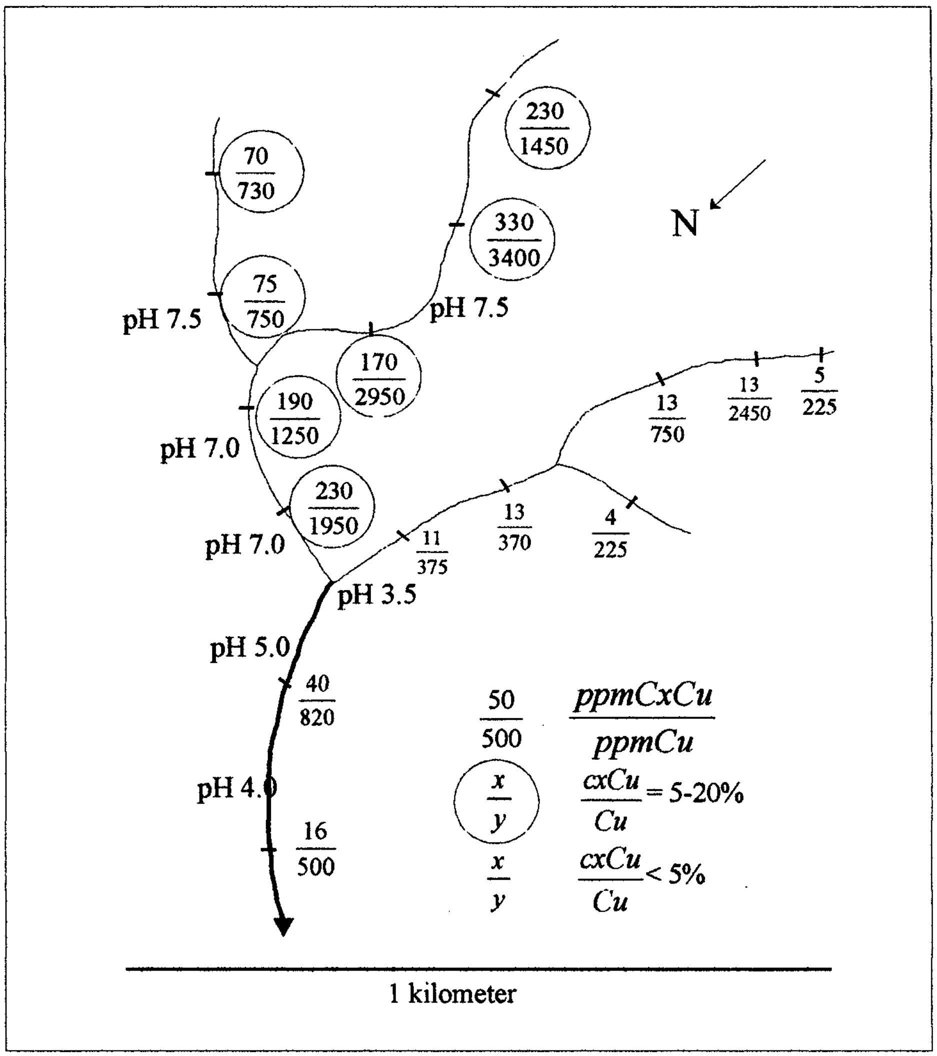

Figure 1.5. Influence of pH on selective extraction of Cu in stream sediments, Cebu Project, Republic of Phillipies (after Rose *et al.*, 1979). Where pH is low, the ratios of cold extractable Cu (cxCu) to total Cu is low. As pH of the streams increases, a greater fraction of the total copper is held in the cxCu phase.

1.5 Problems with sampling for gold

Gold has three characteristics which contribute to the difficulties in obtaining a proper sample for gold determination (Nichol et. al., 1994): it occurs in low concentrations, it generally occurs as a native metal rather than as a trace component of a major constituent; and it has a very high specific gravity (19.3 for pure gold). Rather than using the binomial distribution, the sampling distribution of very rare particles (e.g. gold, diamonds, cassiterite) can be described by the Poisson distribution (Ingamells, 1981):

$$P(n) = \mu^n e^{-\mu}/n! \qquad (5)$$

where μ is the expected (mean) number of particles in a sample and P(n) is the probability of obtaining n particles in the sample. The Poisson distribution has the unique characteristics that the mean (μ) is equal to variance. Therefore, the relative error (RE) can be approximated as RE $= 1/\sqrt{\mu}$.

Clifton et. al. (1969) used the binomial distribution to illustrated how sampling precision and the average number of gold particles present in a sample are related assuming that:

(1) gold particle size is uniform,

(2) gold particles represent less than 0.1% of all particles,

(3) the sample contains at least 1000 grains

(4) analytical errors are absent, and

(5) the gold particles are randomly distributed through the material being sampled.

Based on these conditions Clifton et. al. (1969) determined a minimum of 20 gold particles are required in a sample to achieve a precision of ± 50% at the 95% confidence level. However, Clifton et. al., were attempting to estimate grades of placer deposits. Stanley and Smee (1989) argue that for exploration samples, precision of ± 50% is adequate if the anomaly is to be defined by a single sample. If more samples are collected over the anomalous zone (i.e. an increase in sample density) the level of precision necessary for each sample becomes even lower. Similarly, Fletcher (1997) argued that for stream sediment surveys a probability of missing an anomaly of approximately 5% might be acceptable. This corresponds to an average of three particles of gold in a subsample of given size (Fletcher, 1997).

The effects of a rare grain of gold on initial sampling or subsampling can be illustrated by example. An original 500 g sample, having bulk composition of 150 ppb gold, was taken from stream sediment downstream of prospective high sulfidation epithermal gold mineralization. The sediment was homogeneously composed of grains 100μm in diameters and contained trace amounts of gold. If the gold is present as spheres 100μm diameter and is pure gold ($\rho = 19.3$ g/cm^3), each gold grain will weigh 10.1 μg. The weight of gold within the original sample is 75μg representing, on average, 7.43 particles of gold. A 30 g subsample will therefore, contain on average 0.446 particles of gold. Using the Poisson distribution (3), the probability that a 30 g subsample will contain zero particles of gold is $p(0) = 0.640$ (Figure 1.6), Thus, 64.0% of these subsamples will not contain any gold resulting in the true gold concentration being undetected. A 28.8% probability exists that one particle of gold will exist in the subsample resulting in a gold concentration of 337 ppb, approximately 2.2 times greater than the true concentration. The

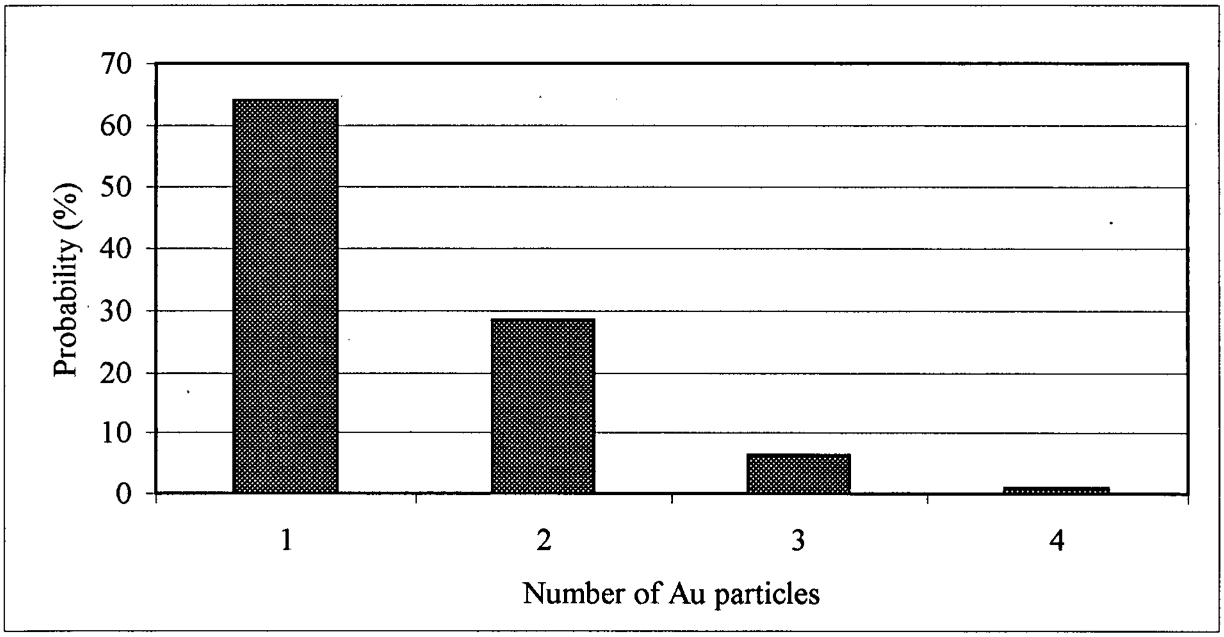

Figure 1.6. Probability of detecting a given number of gold particles in a 30 gram subsample using the Poisson distribution. Based on an original 500 g sample with true concentration of 150 ppb.

effect of elevated gold analysis produced by the random inclusion of a single gold particle within a subsample is termed the "nugget effect" (Ingamells, 1981).

Gold results are influenced by variations in both size fractions and the sample size being analyzed since representativity of the subsamples is highly dependent upon the number of Au particles present in the original sample and the size in which they occur. Nichol et. al. (1987) suggest that when gold is present as coarse particles, the size of the samples must be increased in order for them to be representative. For example, an original 1200 g sample is wet sieved into four size fractions (200 μm, 150 μm, 75 μm and 50 μm) each weighing 300g and having a gold concentration of 500 ppb gold. The mass of gold in each size fraction is thus 150μg. Assuming the gold particles are present as spheres of pure gold with a diameter equal to the grain size of each fraction, the weight of one gold particle is 80.84 μg, 34.11 μg, 4.26 and 1.263 μg for each fraction, respectively. This represents, on average, 6.18, 14.66, 117.3 and 395.9 particles of gold in the respective size fractions. The effect of grain size and subsample size on sample representativity is illustrated in Figure 1.7. If ten 30 g or six 50 g subsamples were to be taken from each size fraction, using the Poisson equations, the probability of detecting zero grains of gold in the subsamples decreases with decreasing grain size and increasing subsample size. For example, the 200μm size fraction contains 0.62 particles of gold. Therefore, there is only a 33% chance than a 30 g subsample will contain one particle of gold, giving a concentration 5.4 times the true sample concentration. In contrast, since the number of gold particles increases in the finer fractions, the probability of containing zero gold particles in a 30 g subsample from the 200 μm fraction is 53.9%, which decreases to 23.1% for the 150 μm fraction and is negligible for the 75 μm and 50 μm fractions. For each subsample size, the 75 μm and 50 μm fractions have a 0%

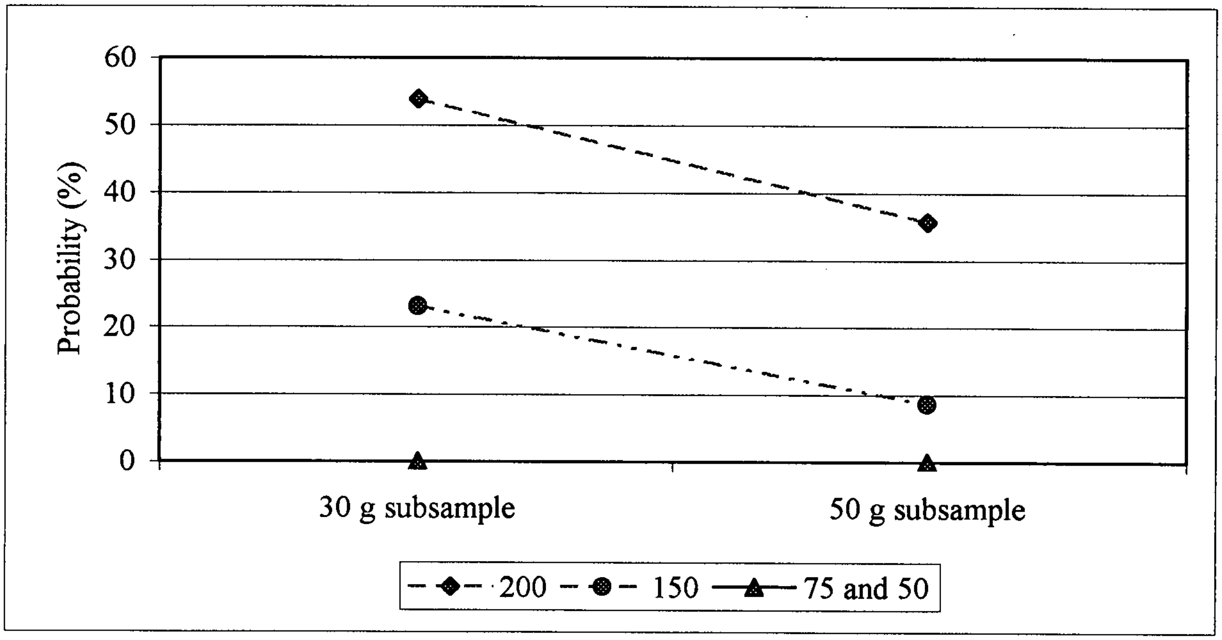

Figure 1.7. Effect of subsample size and size fraction on detecting zero particles of gold. The probability of missing the anomaly (detecting no Au particles) decreases with decreasing size fraction and increasing subsample size. Size fractions are in μm.

probability of detecting no gold particles and would yield the most representative subsample gold results.

1.6 Research approach

Based on the above the objective of this thesis is to improve regional stream sediment geochemistry for high sulfidation epithermal Au deposits in the High Andes by examining and interpreting the:

1) distribution of gold between fluvial environments and size fractions in stream sediments and associated surficial deposits;
2) physical and chemical distribution and behavior of elements of the epithermal suite (eg. Au, Ag, As, Sb, Hg, Bi, Te) in stream sediments and related surficial deposits such as glacial till, talus cones, alluvial fans and debris flows using strong and weak chemical digestions to provide insight to the mode of the elements occurrence in stream sediments;
3) effects of pH on metals mobility in the surficial environment and the exchange of metals between stream sediments and waters with changes in acidity;

Results are used to make recommendations for optimum sampling media, size fraction and chemical digestion to maximize anomaly contrast and dispersion distance for regional and property scale geochemical surveys in arid mountainous terrain.

CHAPTER 2

STUDY AREA DESCRIPTION

2.1 Location and access

The Lama/Pascua property, at the northern end of the El Indio belt, is approximately 200 km NW of San Juan, Argentina and 180 km NE of Coquimbo, Chile at 4500-4800 meters elevation on the crest of the Andean Cordillera, (Figure 1.1). Lama camp is reached by an eight hour, 4 wheel drive through the Argentine pre-Cordillera and Cordillera, reaching a maximum elevation of 5100 meters. Road access to sampling sites on the property was good along the R. Turbio and R. Canito drainages. Access to the Pascua property from Lama was accommodated by a property border crossing. Travel to Pascua from Chile is by aircraft or truck originating in the coastal resort town of La Serena. Road access to the R. Estrecho and tributary sampling sites was good.

2.2 Regional geology and tectonic setting

The Andean Cordillera is interpreted to be an eastward-migrating Mesozoic and Cenozoic magmatic arc built over Paleozoic and Precambrian basement (Coira et. al., 1982). The pre-Jurassic basement is comprised of discrete fragments of Precambrian through late Paleozoic terranes of the Gondwana continent (Davidson and Mpodozis, 1991). An early Carboniferous magmatic arc formed along the length of the Andes, bounded toward the ocean by an accretionary prism and by foreland sedimentary basins toward the Gondwana continental interior (Davidson and Mpodozis, 1991). During the Mesozoic, large volumes of calc-alkaline volcanics and related plutons were emplaced along a belt parallel to present coastline in northern and central Chile (Davidson and Mpodozis, 1991). During the middle Cretaceous collapse of backarc basins occurred related to an increase in westwards velocity of South American Plate with the beginning of South Atlantic spreading (Davidson and Mpodozis, 1991). After a Late Cretaceous magmatic lull, intense calc-alkaline magmatism resumed periodically through the late Miocene. Volcanism recommenced in the Paleocene and is associated with porphyry copper and epithermal precious metal ore deposits including El Indio, Tambo and Sancarron (Davidson and Mpodozis, 1991). Magamatism ceased during the late Miocene when the subduction angle of the Nazca Plate shallowed between 27° S and 33° S latitude; this area constitutes the modern nonvolcanic, "flat-slab" region of the Andes (Kay et. al., 1997, Davidson and Mpodozis, 1991).

The El Indio belt, which hosts the Pascua/Lama property, is a 150 km long, 10 km wide north-south region defined by an almost continuous line of hydrothermal alteration zones that extends across the Chile-Argentina border and lies above the flat slab segment of the present Andean subduction zone (Kay et. al., 1991). The mountain ranges of the Andes Cordillera in this region result from basement uplifts and thrusts that formed between 16-11 m.y. (Jannus, 1995). The El Indio belt, between latitude 29° and 31° S, has seen only insignificant volcanism for approximately the last 9 million years (Kay et. al., 1999). Hydrothermal alteration is comprised of argillic, advanced argillic and silicification of Paleozoic intrusions and volcanic rocks and Oligocene-middle Miocene volcanics. These alteration zones are preserved due to their location in north-south trending graben systems bounded by regionally extensive high-angle reverse faults (Mpodozis and Cornejo, 1988; Nasi et. al., 1990 from Davidson and Mpodozis, 1991).

2.3 Local and deposit geology

Geological and age constraints are not well known in Pascua area, but general information is taken from Martin et. al.. (1995) and Maksaev et. al.. (1984) as summarized by Deyell (2000). Geologic and alteration maps are from Heberlein (2000).

The oldest exposed basement rocks belong to the Pastos Blancos Group (Martin et. al.., 1995) of Permian to Early Jurassic age (Figure 2.1). This group includes:

1. Guanaco Sonso sequence of rhyolitic ash flow tuff;
2. Chollay Unit of intermediate to felsic granitoids;
3. Los Tilos sequence of volcanic and sedimentary rocks; and
4. the Colorado Unit of diorites, monzongranites and dacitic porphyries.

The Pastos Blancos group is overlain by a series of Mesozoic to early Cenozoic marine sediments, volcaniclastics and andesitic lava flows. Rocks in the Pascua/Lama area are intruded by plutons and dioritic intrusions of the Bocatoma Unit (Eocene-Oligocene) (Figure 2.2). Younger volcanic and intrusive rocks from Late Oligocene to Middle Miocene are present, including tuffs of the Vacas Heladas Formation. Mapped lithologies on the property scale include tuffaceous units belonging to the Pastos Blancos Group, and two intrusive units (a quartz monzonite and quartz porhyry) contemporaneous with the Chollay Unit. Younger diorite, granodiorite, and dacite units provisionally are included in the Bocatoma Group. A thick sequence of ignimbritic pyroclastic rocks have been correlated with the Vacas Heladas Formation. Numerous generations of felsic dikes cut the basement rocks. Hydrothermal

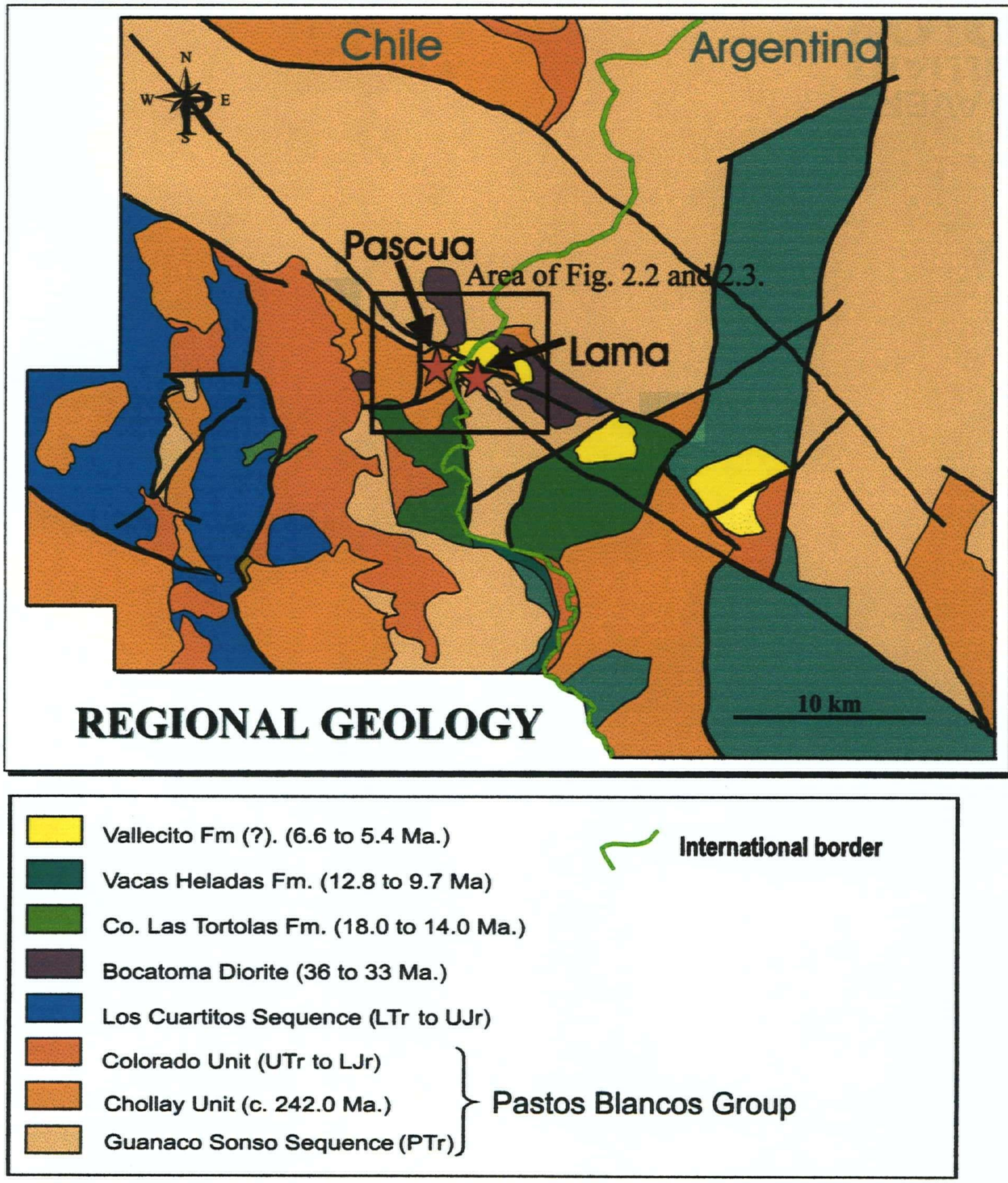

Figure 2.1 Regional geology of Pascua/Lama.

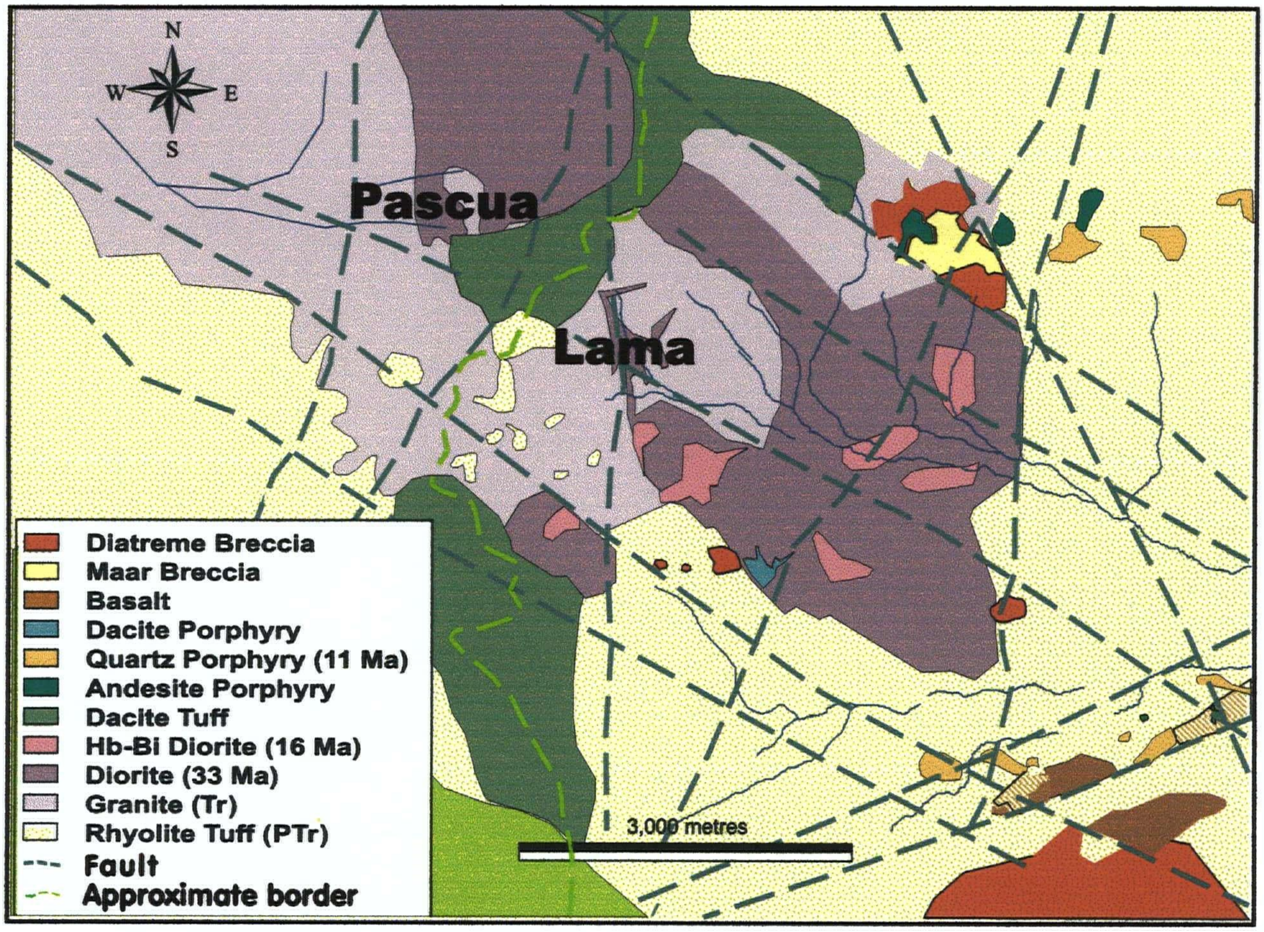

Figure 2.2 Deposit scale geology of Pascua, Chile and Lama, Argentina (Heberlein, 2000).

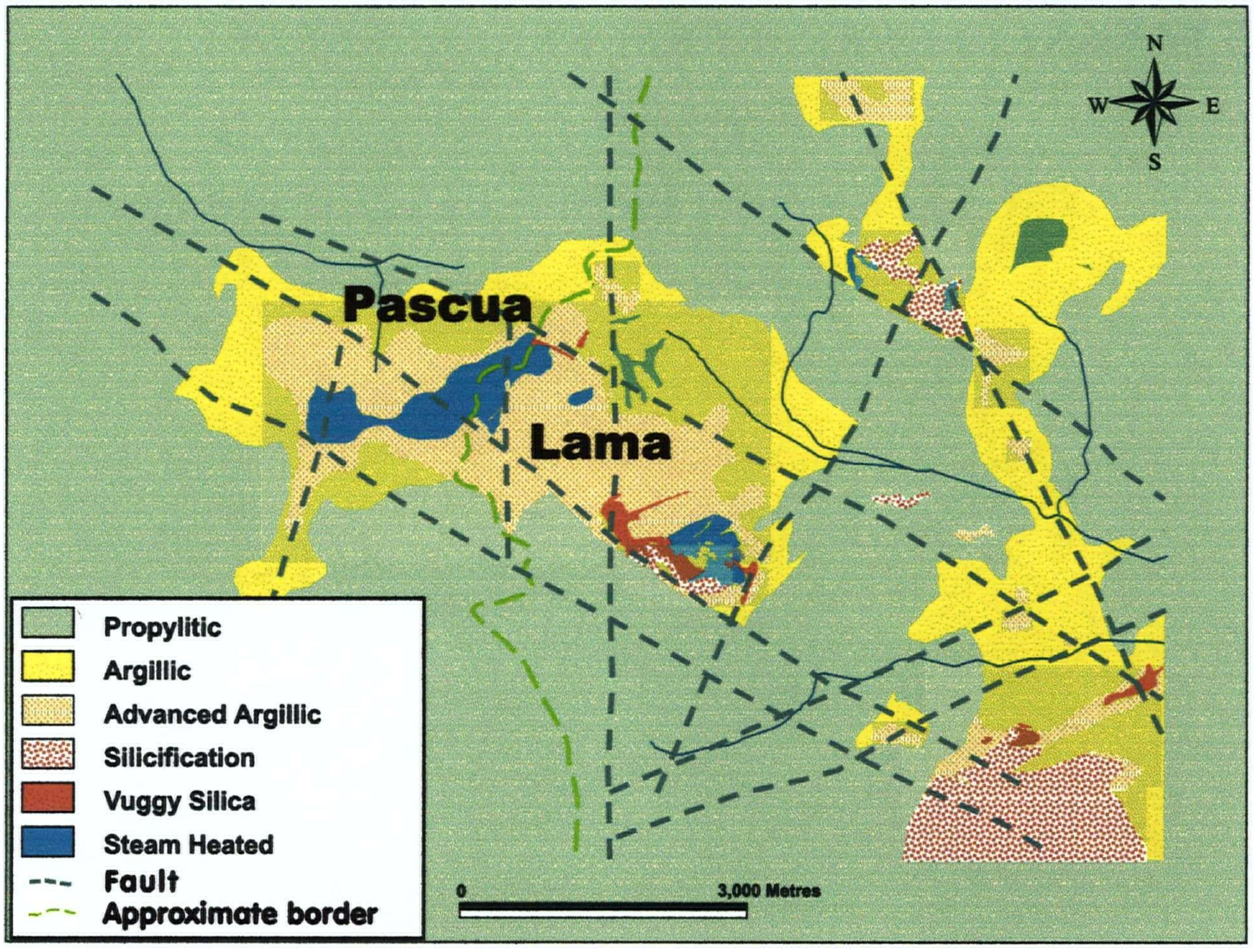

Figure 2.3. Hydrothermal alteration of Pascua, Chile and Lama, Argentina (Heberlein, 2000).

alteration includes advanced argillic, silicification, vuggy silica and a steam heated zone (Figure 2.3)

The Andean subduction zone is part of the earthquake prone Circum-Pacific. The Pascua/Lama study area is encompassed in an area expected to experience earthquakes of magnitude 5, 6, 7, 8 and 8.5 with a periodicity of 0.8, 12.5, 180, 2600, and 10,000 years, respectively (Inform Geostudies, 1994).

2.3.1 Styles of mineralization

Pascua/Lama is a 17.1 moz Au and 560 moz Ag deposit (Barrick, 1999). Mineralization occurred over a short interval at 7.8 Ma (Deyell, 2001) and is spatially associated with Vacas Heladas volcanics. Discussion of ore and alteration assemblages is given for Pascua, Chile, by Chouinard and Williams-Jones (1999).

Gold occurs in two major mineralized facies: alunite-pyrite-enargite (APE), pyrite-szomolnokite ($FeSO_4 \cdot H_2O$) (PZ). PZ type mineralization is subordinate to APE. APE mineralization occurs as disseminations, open-space fillings and as banded alunite-sulfide veins. Barite is common and occurs as individual grains and massive aggregates. Native sulfur co-precipitates with alunite and enargite-pyrite in disseminated and open-space filling zones, but is rarely observed in the banded veins (Deyell, 2001). Accessory minerals include diaspore, anglesite, pyrophyllite, stibnite, cassiterite, goldfieldite, covellite and trace chalcopyrite. Native gold and calaverite ($AuTe_2$) are the most abundant gold minerals of APE mineralization and occur mainly as inclusions in enargite (Chouinard and Williams-Jones, 1999). Enargite, which is very unstable under surface conditions at Pascua (Deyell, pers comm, 2000) occurs as irregular grains to massive aggregates and contains a variety of solid inclusions. This is the largest mineralizing event with average gold grades of about 1.2-2 g/t Au.

The PZ facies is characterized by pyrite-szomolnokite deposition in strongly silicified, partially leached alteration zones. Minor enargite is associated with this event and is commonly partly replaced by arsenolite and/or szomolnokite. Other accessory minerals includes anglesite, barite, rare covellite. gypsum, voltatie and paracoquimbite. Gold and silver in pyrite-szomolnokite mineralization are thought to occur as sub-microscopic inclusions in pyrite and enargite. Mean Au grades in the PZ facies are slightly higher than the APE event (2.1 g/t) and Cu contents average 0.2% (Deyell, 2001). Pyrite-szomolnokite and APE mineralization do not show cross cutting relations and are thought to be mutually exclusive (Chouinard and Williams-Jones, 1999). Overall, the deposit is highly acidic.

Penelope is a relatively small high grade breccia and vein system with little-to-no copper. Mineralization occurs as free Au associated with jarosite, ± quartz, alunite, barite, scorodite in oxidized and/or silicified tuffs and breccias (Deyell, 2001).

No information was available on the grain size of gold in the deposit. However, gold grains in heavy mineral separates of stream sediments have an average size of 1.46μm (n = 15) ranging from less than one micron to approximately 2.5μm.

Sulfides are not common at Veladero, the adjacent property south of Lama (Diego Charchaflie, pers. comm.). Pyrite has be found, but in concentrations much less than at Pascua-Lama.

2.4 Quaternary geology

2.4.1 Andean glaciation

Pascua/Lama is part of a larger area extending from lat 17°30'S to 31°S categorized as the desert dry Andes, where most of the current glaciation is found as small ice-and-snow areas along the Argentine-Chilean border (Lliboutry, 1997). Presence of U-shaped valleys, cirques and other glacial features such as developed morainic systems are evidence of a historically more developed glacial system (Caviedes and Paskoff, 1975). Field observations to the south of the Pascua/Lama area in the Argentine Rio Mendoza and Chilean Rio Juncal-Aconcagua have recognized four morainic systems terminating at the elevations indicated in parenthesis (Caviedes and Paskoff, 1975, and Lliboutry, 1997):

Chilean	Argentine
Portillo (2650 m)	Horcones (2750 m)
Ojos de Aqua (2100 m)	Penitentes (2500 m)
Guardia Vieja (1600 m)	Puntas de Vacas (2350 m)
Salto del Soldado (1300 m)	Uspallata (1870 m)

Determination of the extent of glaciation is compounded by the following: 1) in very high, semiarid regions of the Central Andes, glaciers did not leave clear terminal moraines, 2) glaciers flowed in the middle of valleys without modifying V-shaped profiles, and 3) glaciers transported older deposits (Lliboutry, 1997).

2.4.2 Drainages and surficial deposits

The Rio Turbio and Rio Estrecho are second order streams draining the Lama/Pascua deposit on the Argentine and Chilean sides, respectively (Figure 2.4 and 2.5). The R. Turbio stream gradient decreases from a maximum of 14% at the headwaters to 3% near the confluence with the R. Tagus as it flows on and through debris flows (Figure 2.4). Topography is generally steep except along the debris flow- filled valley floor. The R. Estrecho has a steeper gradient then the R. Turbio with a maximum of 11% at the headwaters decreasing to 7% at the R. Toro confluence (Figure 2.5). The topography is steep, with flat U-shaped valley floors at the headwaters of the R. Estrecho and Q. Barriales. Both drainages are decoupled from valley walls by large mass wasting events that fill valley floors. Flow volumes vary seasonally (Table 2.1) and are greatest in the summer months (December- February).

Field classification of surficial deposits was based on morphology and texture (Figure 2.6 and 2.7). Glacial till, talus cone, alluvial fans and debris flow deposits have distinct origins and unique processes controlling material transport and deposition.

Glacial deposits are the oldest surficial material, contain multiple clast types and abundant fines with subrounded clasts ranging in size from gravel to boulder (Plate 2.1) (Table 2.2). Although vegetation is very sparse on the property, glacial till tends to have more vegetation than other surficial materials. Glacial deposits are found in both the main R. Turbio and R. Tagus basins and in the R. Canito and R. Barriales tributaries where valleys have a U-shaped profile. Till forms a series of E-W trending ridges coalescing between the R. Turbio and R. Canito drainages east of Penelope Ridge (perhaps lateral moraines?) at Lama. It is also found as hummocky topography along the edges of valleys and ultimately terminates at the R. Tagus/ R. Turbio

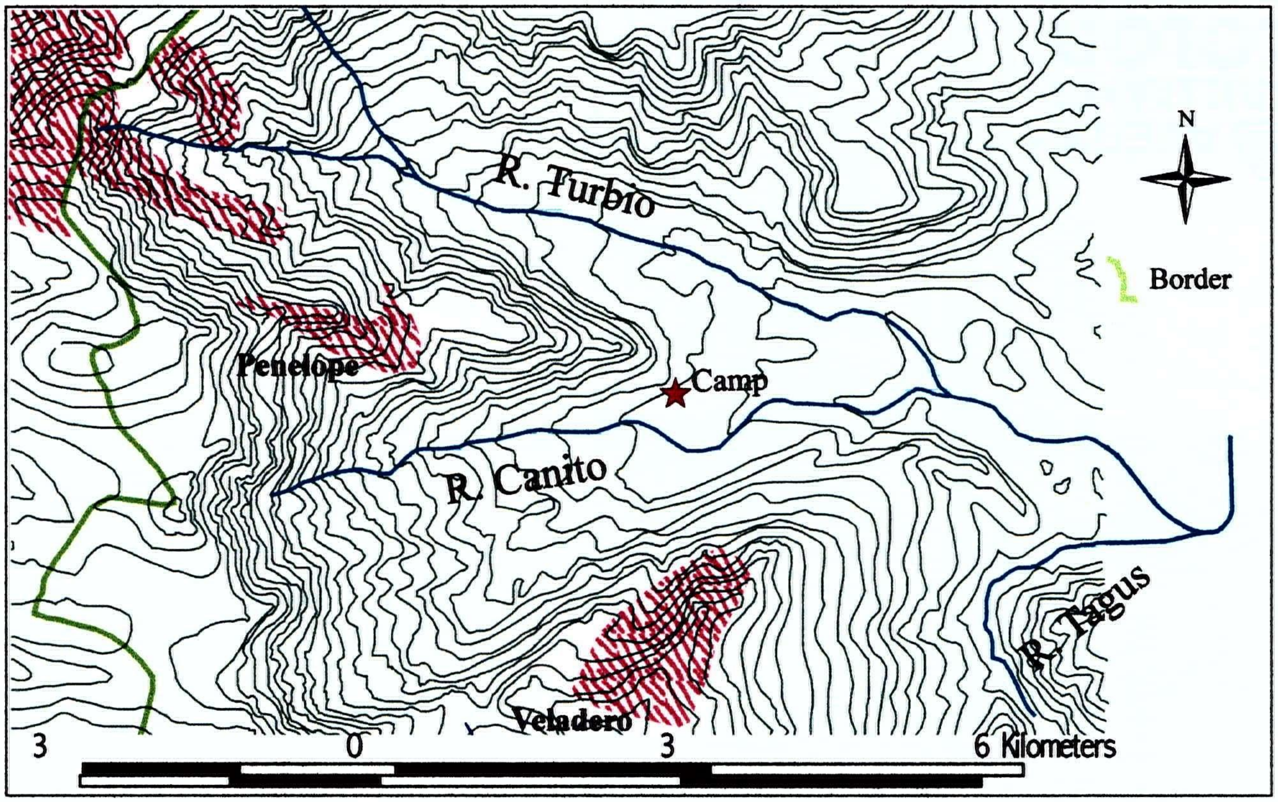

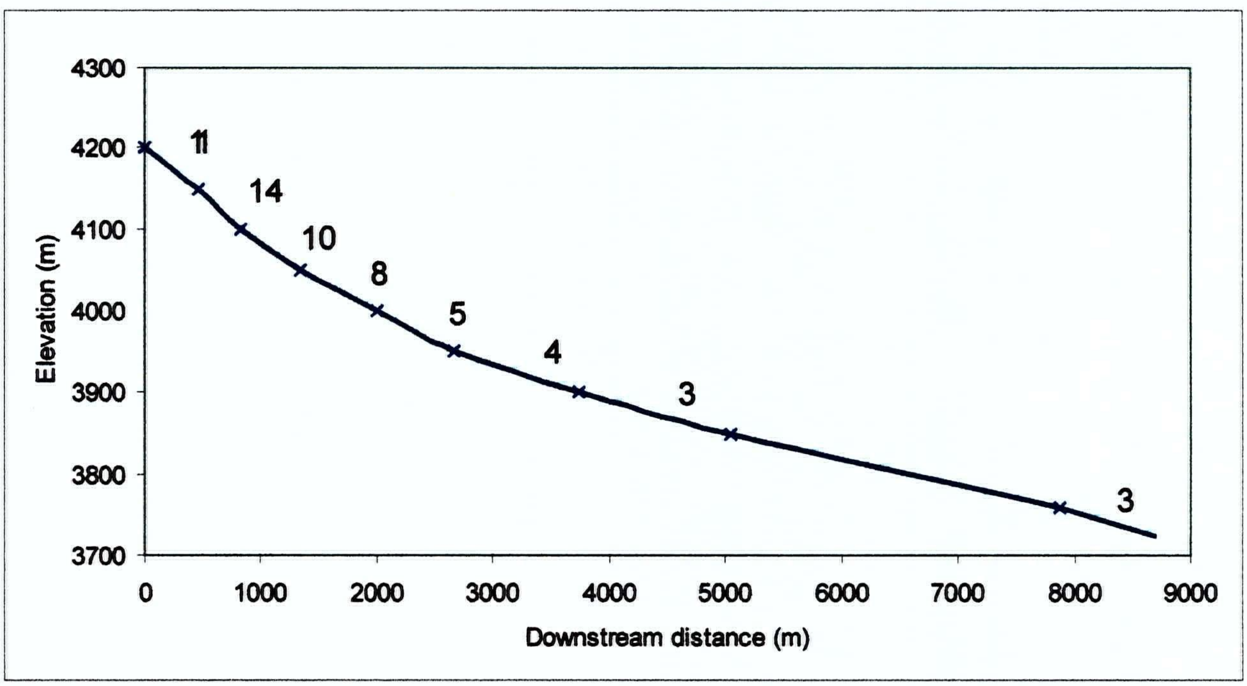

Figure 2.4. Topography (50 meter contours) and stream gradient (%) of R. Turbio drainage, Argentina. Approximate zones of mineralization are shown in red.

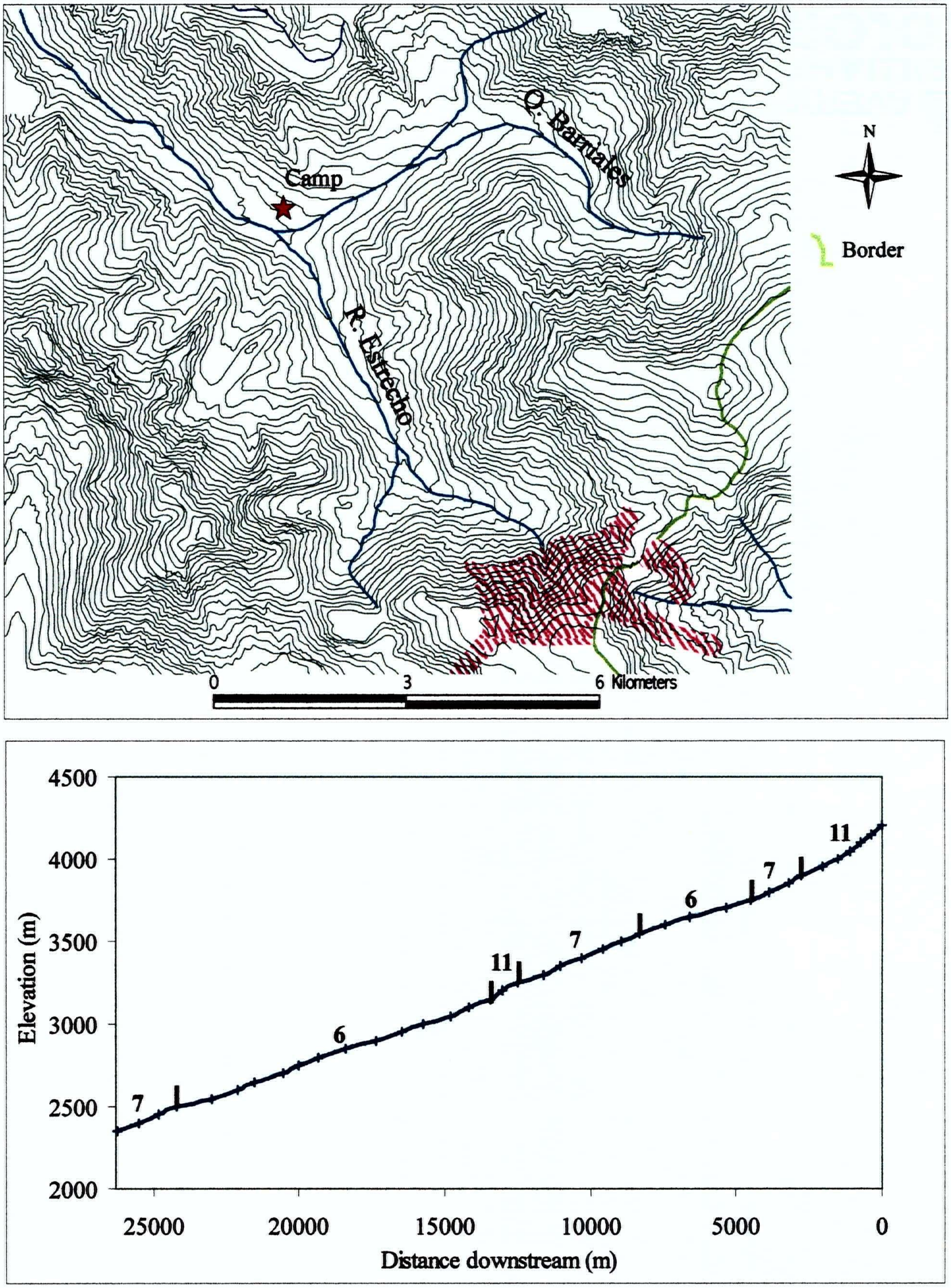

Figure 2.5. Topography (50 meter contours) and stream gradient (%) of upper R. Estrecho drainage, Chile.

Location	Dec-98	Feb-99	Apr-99	Jun-99
R. Turbio above R. Canito	0.10	0.18	0.25	0.09
R. Canito	0.08	0.54	0.11	0.06
R. Tagus below R. Turbio			1.68	1.48
R. Estrecho above Q. Barriales		0.47	0.13	0.09
R. Estrecho above Q. Falda	0.59	0.85	0.31	0.19
R. Estrecho below Q. Falda	0.76	0.89	0.43	0.34

Table 2.1. Volume capacity of R. Turbio and R. Estrecho (m^3/s) (CONIC -BF, 1999).

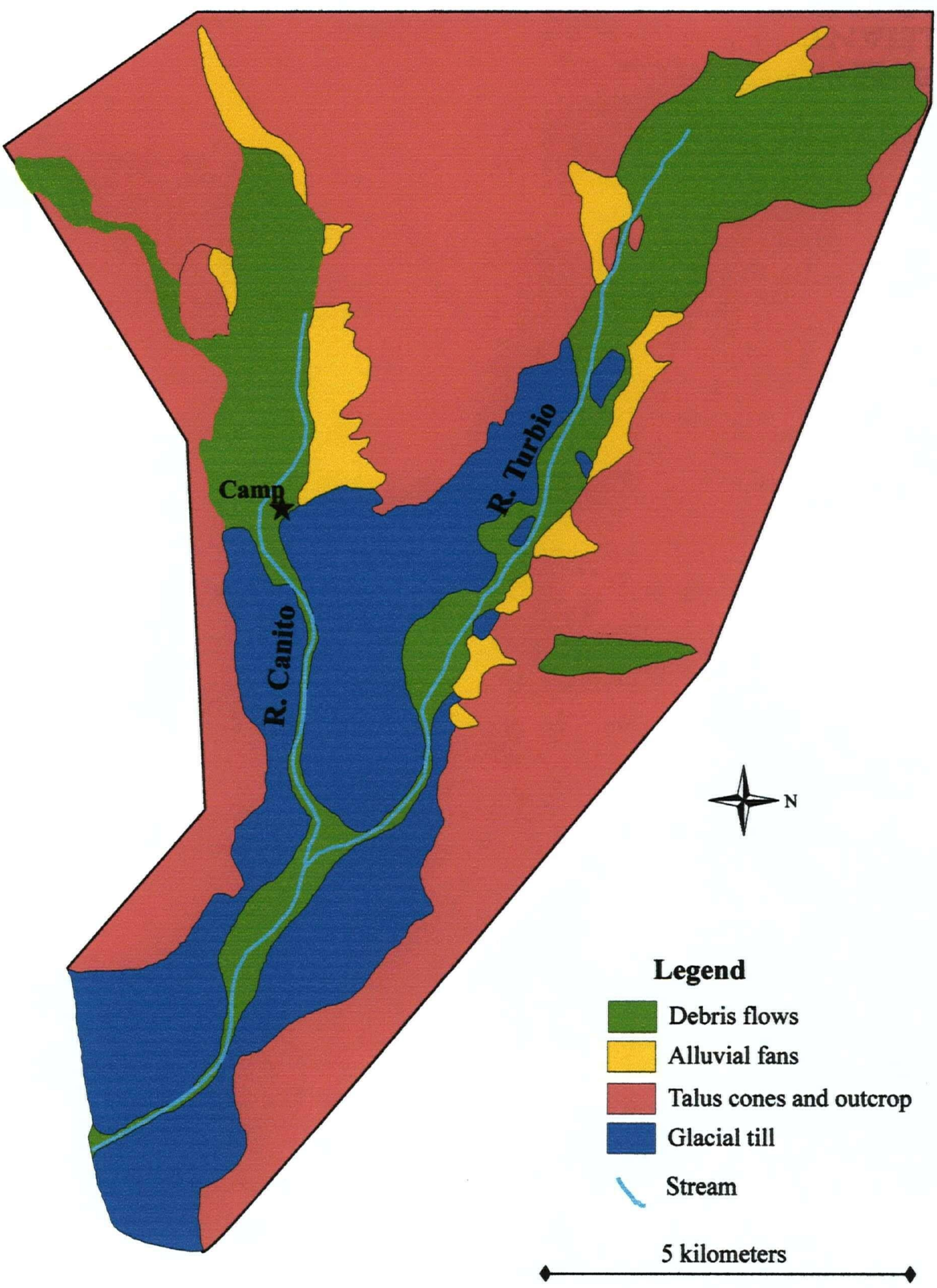

Figure 2.6. Sketch of surficial deposits distribution at Lama, Argentina. Based on 1: 40 000 air photo.

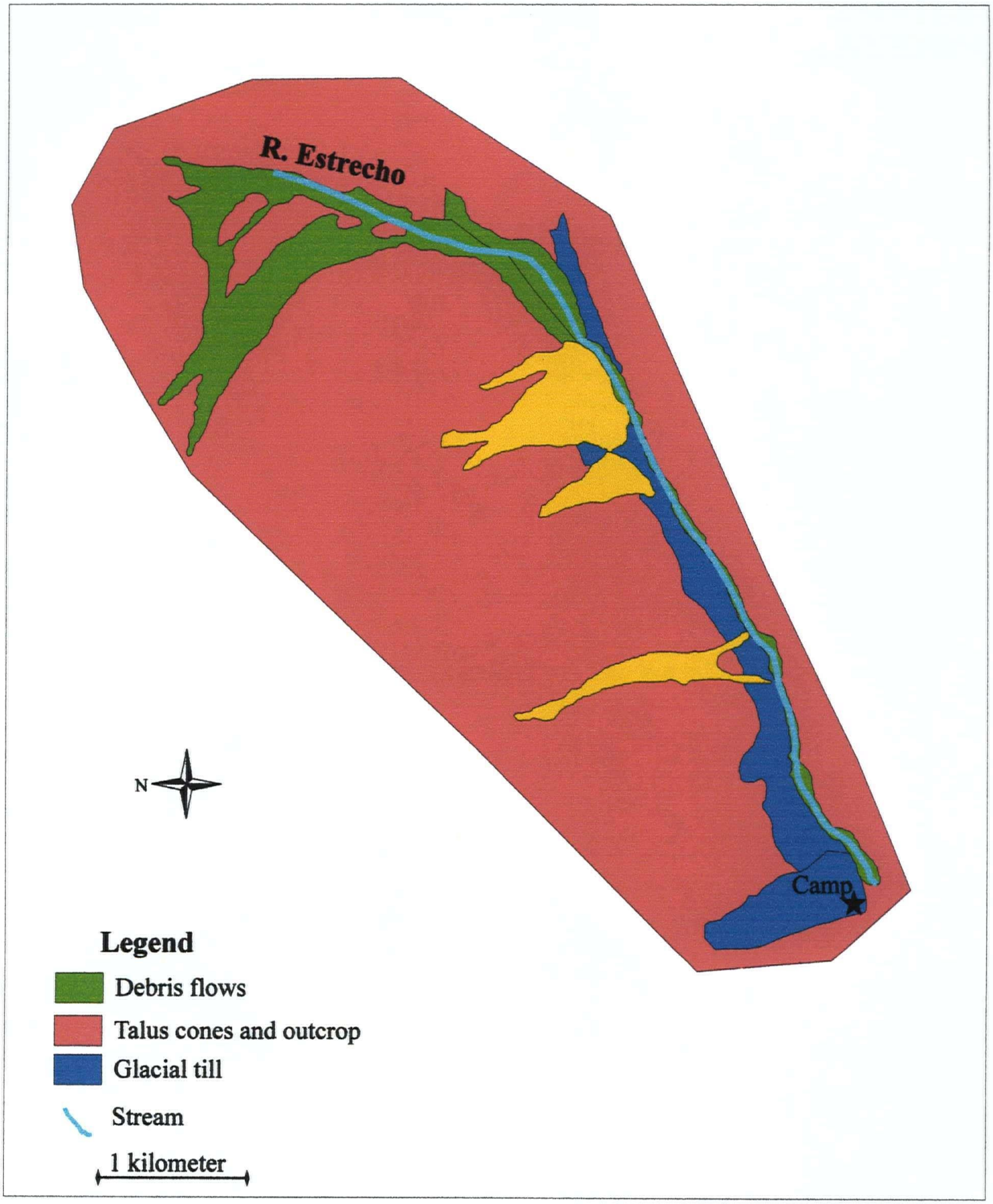

Figure 2.7. Sketch of surficial deposits distribution at Pascua, Chile. Based on 1: 30 000 air photo.

Lama

Size Fraction	Debris flows (n=28)	Glacial till (n=18)	Talus fines (n=32)	Alluvial fans (n=25)
-4+2mm	25.5	21.4	23.6	32.1
-2mm+850μm	18.8	16.5	18.3	20.3
-850+425μm	188	13.7	15.2	12.6
-425+212μm	17.4	17.9	16.5	11.3
-212+106μm	8.9	11.2	10.8	7.9
-106+53μm	4.2	5.9	4.9	4.8
-53μm	6.3	13.5	10.8	11.0

Pascua

Size Fraction	Debris flows (n=10)	Glacial till (n=12)	Talus fines (n=18)
-4+2mm	25.9	25.5	44.4
-2mm+850μm	18.8	20.1	19.4
-850+425μm	20.2	16.1	10.1
-425+212μm	17.6	12.3	8.6
-212+106μm	8.0	8.0	5.2
-106+53μm	3.8	6.1	3.2
-53μm	5.8	11.9	9.2

Table 2.2 Average weight percentages of sieved size fractions of surficial media at Pascua/Lama.

Plate 2.1.A. Glacial till at Lama being eroded into R. Turbio. Stream is approximately 2.5 meters wide.

Plate 2.1.B. Glacil till erosion into R. Estrecho at Pascua. Stake is appoximately 45 cm tall.

confluence. Till at Pascua is found in the upper reaches of the R. Estrecho drainage basin and extends to approximately one kilometer below the camp. Glacial material from the Q. Barriales drainage intersects and appears to overlie R. Estrecho till. Glacial till is currently being eroded into both the R. Turbio and R. Estrecho (Plate 2.1). Glaciers flowed from the topographically higher headwaters down-valley to lower elevations.

Talus cones and alluvial fans share a number of field characteristics. They have limited lateral extent onto the valley floor, often terminating within 300 meters from the slope front. Also, winnowing of fines by strong winds has led to the development of a surface lag deposit, with finer material beneath the pavement. Both deposits types have similar texture and are coarser than till deposits (Table 2.2). Talus cones are ubiquitous in the mountainous terrain of the study area (Plate 2.2). Below the Q. Barriales confluence at Pascua, talus cones are the major sediment source of the R. Estrecho. Alluvial fans differ from talus cones by being water transported deposits, as opposed to gravity transport of talus material. The surface of the fans is generally dissected by numerous flow channels. Alluvial fans have a rounded terminus, concave towards the slope (Plate 2.2).

Debris flow deposits at Pascua/Lama fill valley floors and have transported material up to 10 kilometers from stream headwaters. Deposits contain multiple lithologies of sub-rounded clasts and are poorly sorted. At Lama, there are several debris flows (Plate 2.3); an upper western flow, a lower eastern flow and a flow in the R. Canito basin. The R. Turbio flows have several terraces, often marked by color gradations. The flows are often indurated and cemented by a red (iron?) ferricrete at stream level. At several locations, the R. Turbio is incised up to 5 meters below the surface of the flows (Plate 2.4). There is evidence that much of this downcutting took place over the course of one year (1997-1998) due to large amounts of snowfall in the winter

Plate 2.2.A. View east from Lama down the R. Turbio showing the upper western debris flow, alluvial fans and talus cones.

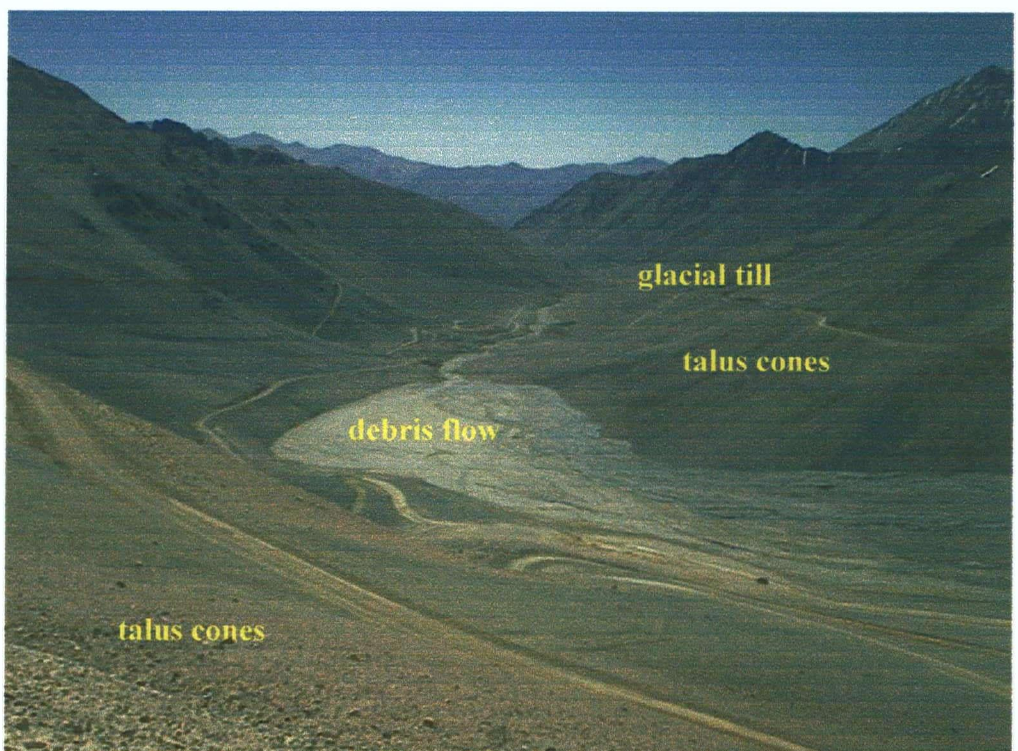

Plate 2.2.B. View west along the R. Estrecho valley showing talus cones, debris flows and glacial till.

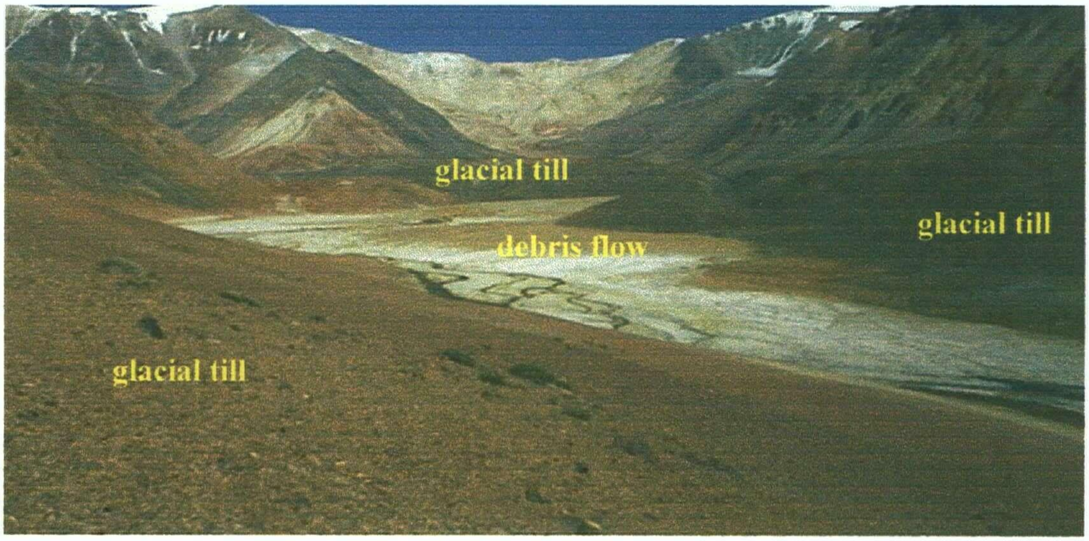

Plate 2.3. View west towards Lama of lower eastern debris flow. The R. Turbio channel is braided with meanders across the level debris flow. The white material is efflourescent chemical precipitates.

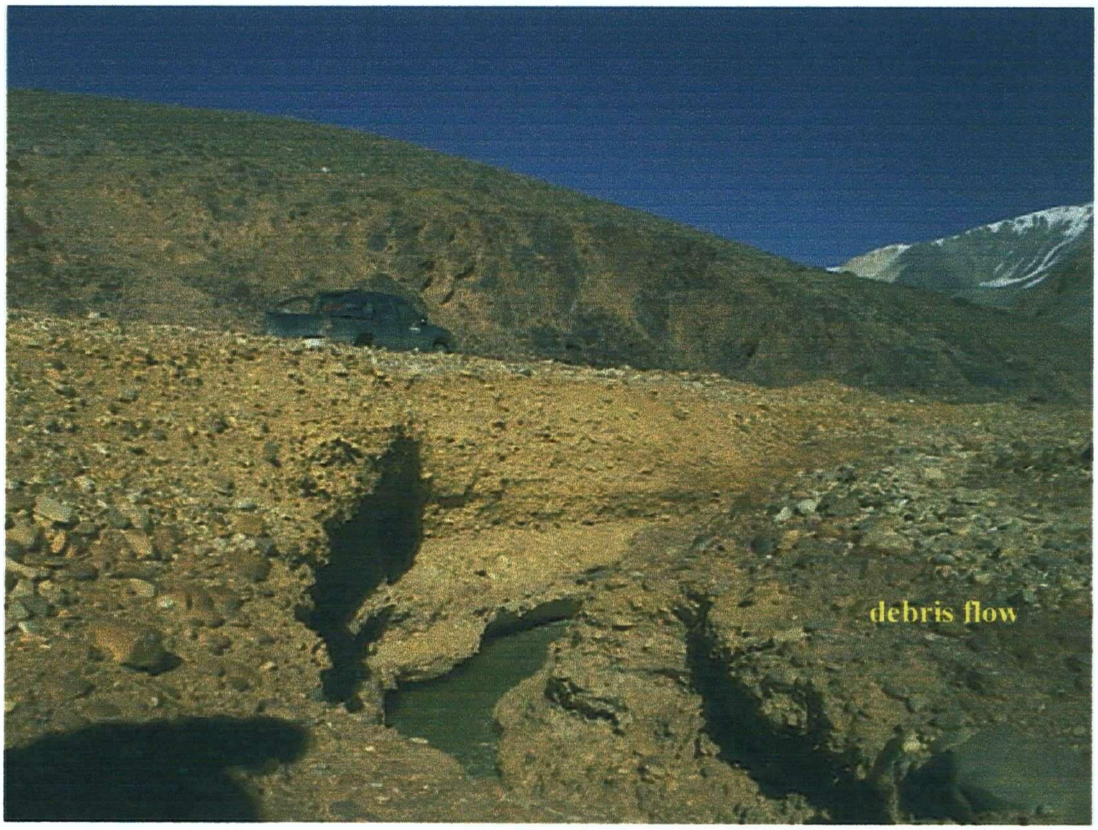

Plate 2.4. Incision of R. Turbio into lower eastern debris flow. The R. Turbio is approximately three meters below the surface of the debris flow.

months; a road used for sampling during the 1997 field season was dissected by the R. Turbio to a depth of approximately three meters in 1998 (Plate 2.5).

Chemical precipitates are found in two environments; as efflorescent coatings adjacent to the streambed and as base-of-slope seeps along the southern bank of the R. Canito (Plate 2.5). There are five large (over 3 meters width) precipitate seeps which are zoned symmetrically about their effluent seep from brown and yellow precipitates to white precipitates. The effluent generally runs down a red, indurated hard pan layer.

2.5 Climate

The climate at Pascua is dominated by the Pacific anticyclone which results in a warm, dry climate. Winter snowfall is associated with west to east travelling cyclonic fronts. Average annual temperatures at the Pascua camp are on the order of 1° to 3° C (elevation approximately 3700 m), and -8° to -10° C at 5000 m, near the Chilean-Argentine border (Informe Geoestudios, 1994). Most precipitation occurs as snowfall during the winter months of June to August, with accumulations of 300-400 mm/year near the Pascua camp increasing with elevation towards the border (Informe Geoestudios, 1994). Evaporation rates are estimated at 3-6 mm/day at the Pascua Camp (Informe Geoestudios, 1994).

Climate at Lama is similar to Pascua: dry and warm in the summer and cold in the winter with precipitation occurring predominately as snow in the winter (Geotecnica, 1999).

Plate 2.5. Base of slope chemical precipitate seep along the R. Canito. Stream is approximately 1.5 meters across.

CHAPTER 3

SAMPLING AND ANALYTICAL METHODS

Fieldwork was during January and February 1999. Samples were collected from the main stream and tributaries draining each property. The author was accompanied by sundry workers during sediment and surficial material sampling. Sample preparation was done from March through December 1999 at the University of British Columbia by two laboratory assistants.

3.1 Sample collection

Seven sample types were collected: stream sediments are the most numerous sample medium, followed by surficial deposits, surface waters and chemical precipitates (Table 3.1). Figures 3.1 and 3.2 show detailed sample location for all media.

3.1.1 *Stream Sediments*

Sediments sites were chosen, where possible, from the active stream channel to ensure that samples were representative of recently transported material. If suitable material could not be found in the active channel, samples were taken within the area defined by bank full flow. At each site, three different samples were collected: one each from a high, medium and low energy environment of the stream. Plate 3.1 shows a photograph of typical locations for each environment in the stream. Field discrimination of the three energy environments was based on streambed texture. The high energy environment (ideally) was taken from areas with a gravel-cobble surface, medium energy from gravel-sand, and low energy from fine sand to silt. Plate

Table 3.1. Number of samples collected for each media at Pascua/Lama.

Sample type		**Pascua**	**Lama**	**Total**
Stream sediments		42	47	89
Glacial till		12	18	30
Alluvial fans		0	25	25
Talus fines		18	32	50
Debris flow		10	28	38
Chemical precipitates		5	22	27
Surface waters	Stream	26	23	49
	Seepage	5	4	9

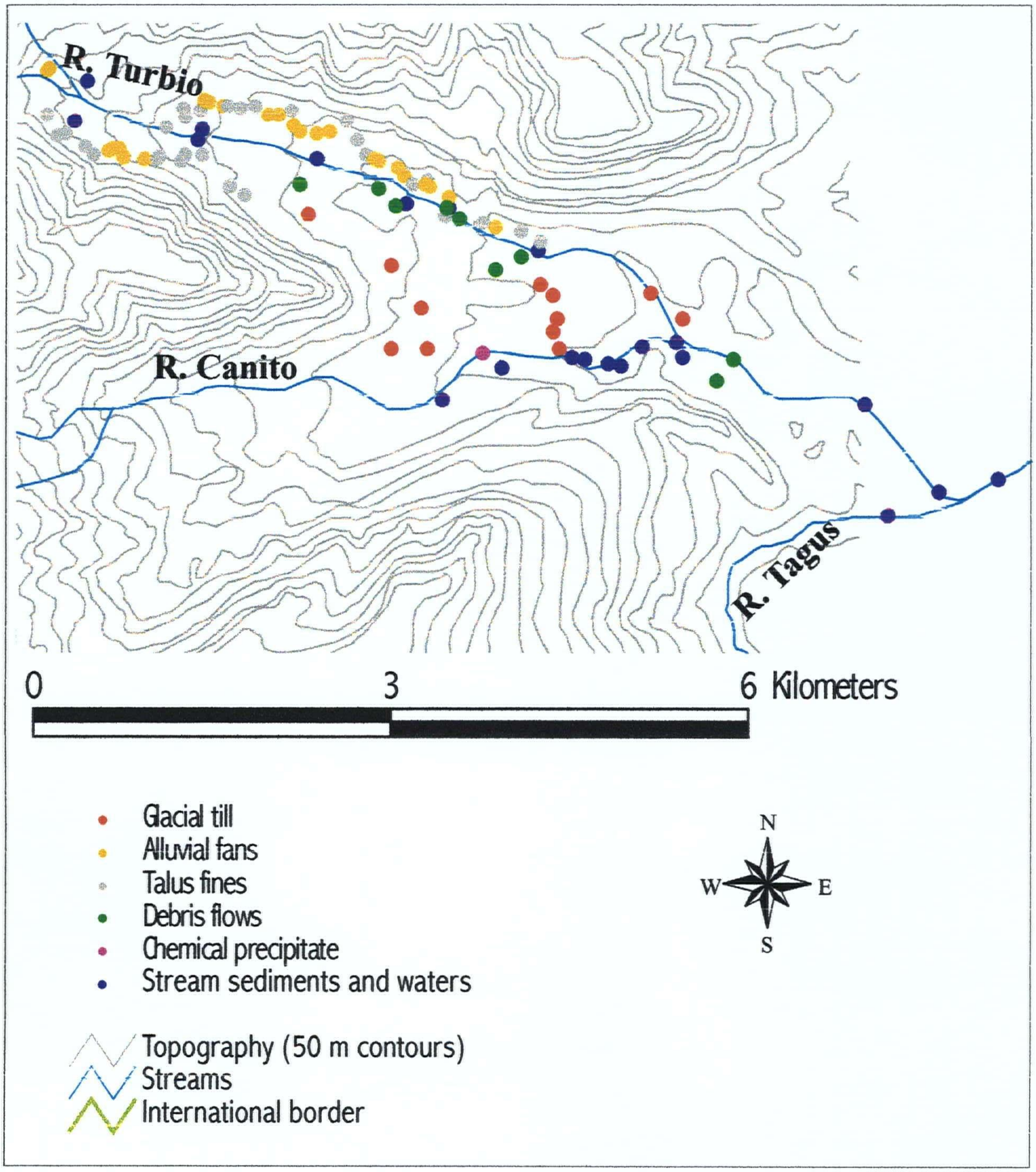

Figure 3.1. Sample location map for Lama, Argentina.

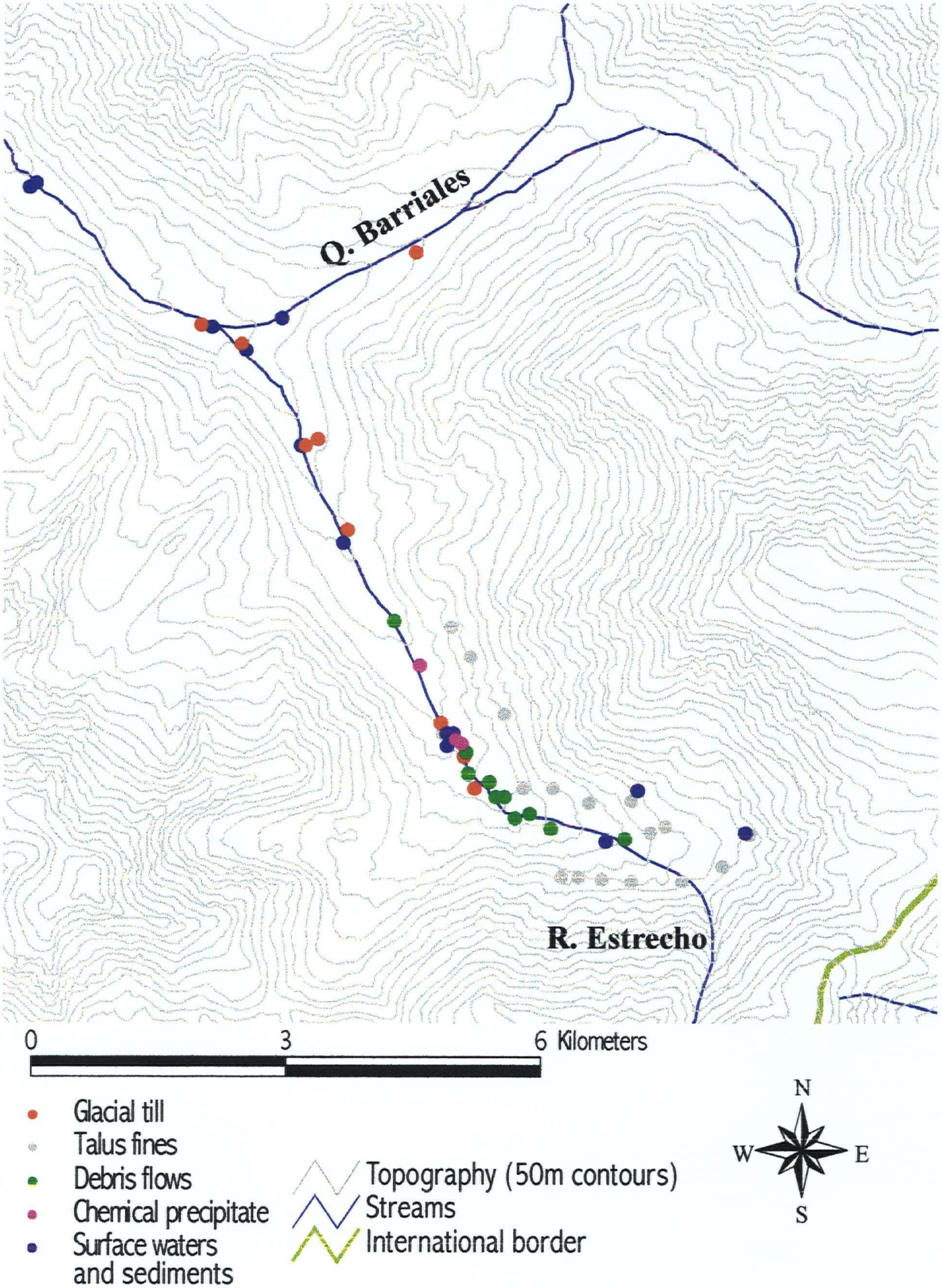

Figure 3.2. Sample location map at headwaters of R. Estrecho, Pascua, Chile.

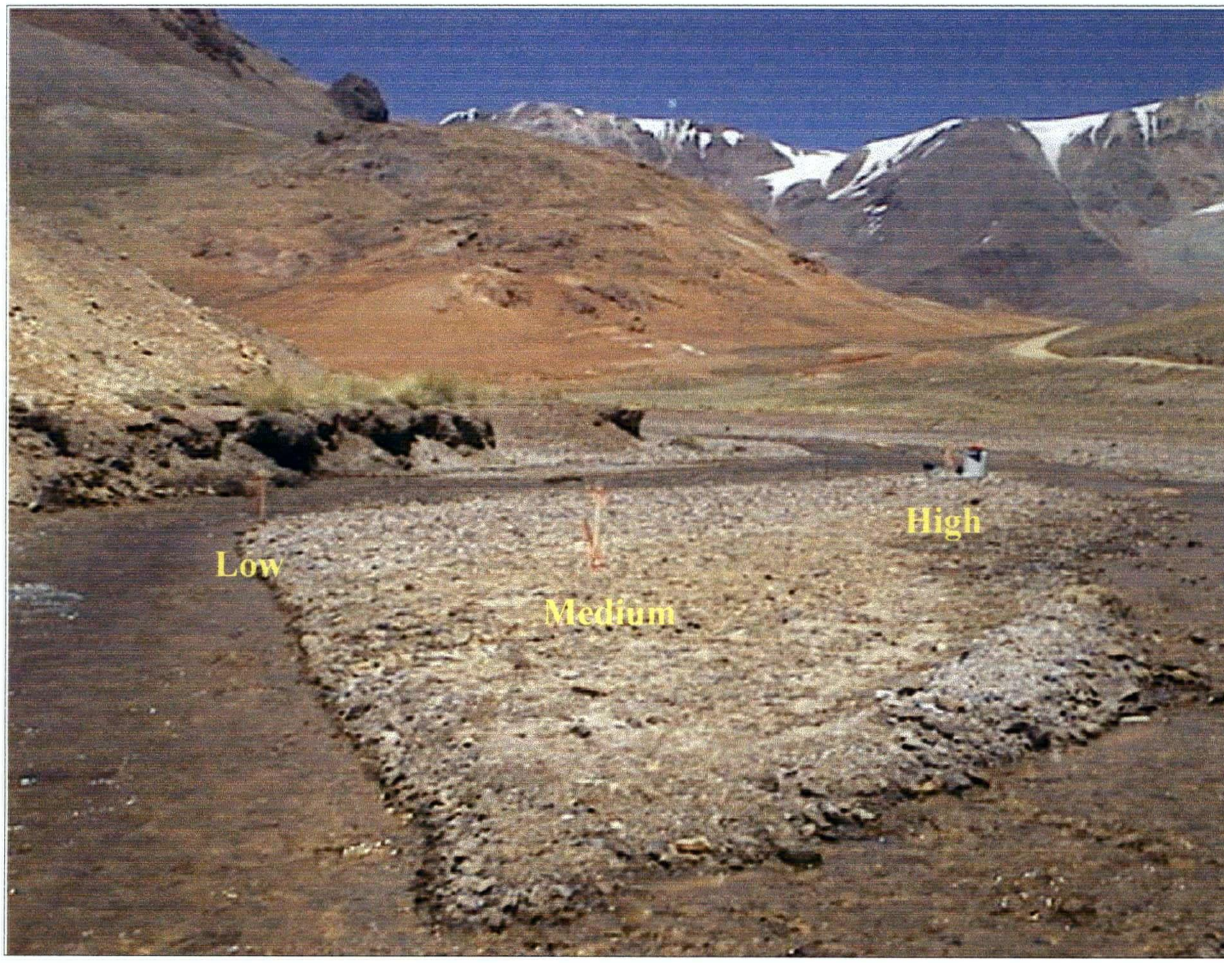

Plate 3.1. Photograph of typical locations for high medium and low energy stream sediments. Flow is toward bottom of page.

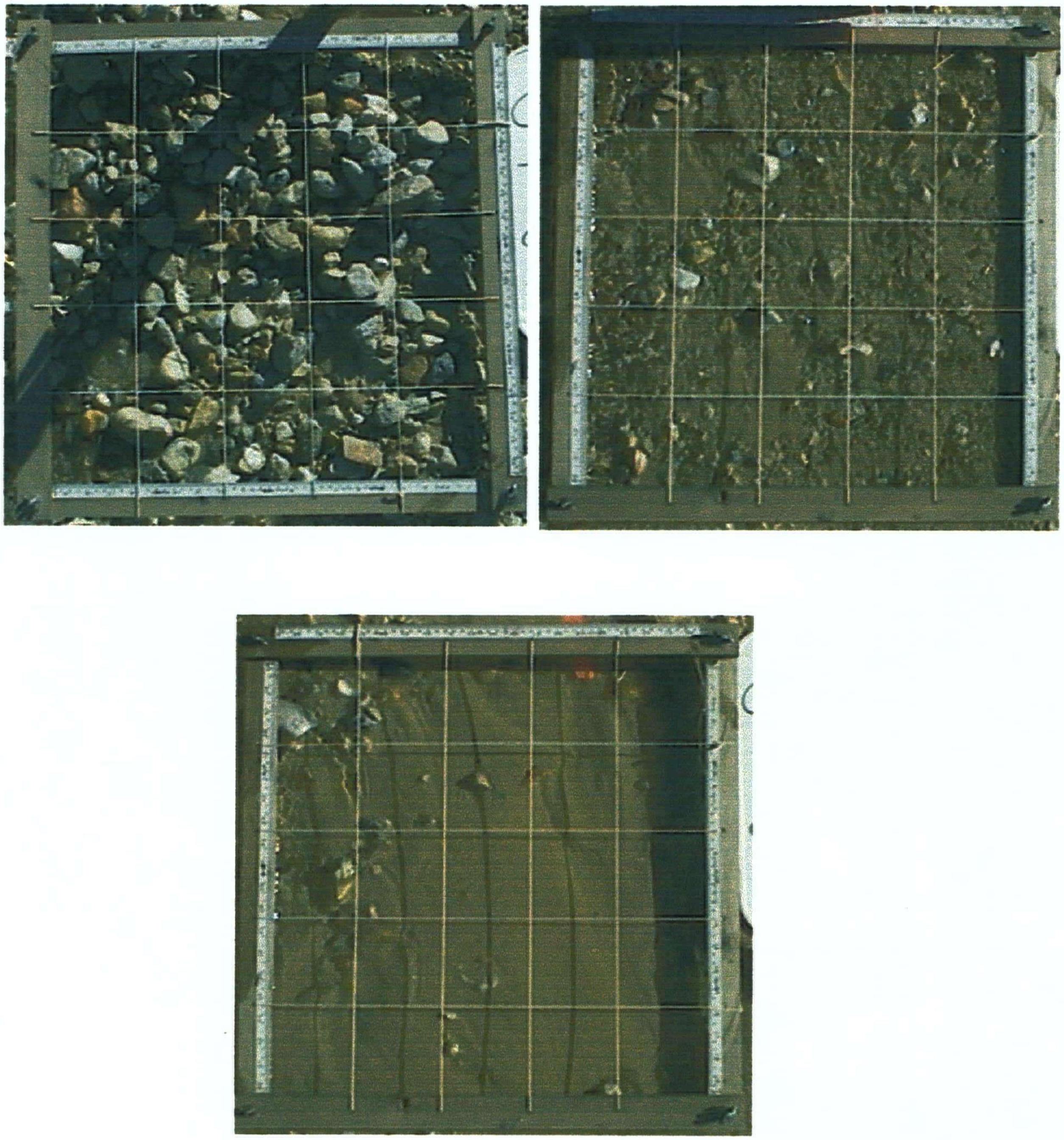

Plate 3.2. Typical textures for high, medium and low energy (clockwise from top left) stream sediment samples.

3.2 shows ideal sample textures for each energy environment. At all sites, samples were collected from downstream to upstream to avoid between-environment contamination.

Sampling procedure for high- and medium- energy environments involved wet field screening to obtain 15- 20 kg of <2mm sediment. The >2mm fraction was weighed in the field and discarded. Three to 5 kg of the low energy environment sample were taken from sandy sections of the stream, frequently with visible heavy mineral accumulations, and did not require field screening. Sediment texture was estimated with a 2500 cm^2 form containing a 10cm by 10cm grid. Additionally, the stream channel and bedforms were characterized and measured, bank material was classified to identify potential sediment inputs, and pH was measured. In total, 30 high energy, 35 medium energy and 24 low energy samples were collected.

3.1.2 Surficial materials

Glacial tills, alluvial fans, talus fines, and debris flows were sampled to geochemically characterize material supplying sediment to the streams. Determination of material sampled was based on air-photo interpretation, landform, and textural analysis and field recognition of geomorphological features unique to each sample type. Figures 2.7 and 2.8 show the distribution of the surficial materials.

Sampling was conducted in two phases. Initially, the stream bank material, outside of the active channel, was sampled at every sediment site. A second round of sampling, for both Lama and Pascua, involved sampling from the road and walking transects to sample other surficial features. Figure 3.1 and 3.2 show sampling location as a function of sample type. Samples were collected about 20 cm from the surface to minimize contamination from wind (and truck) transported material. Approximately 3-5 kg of <4mm material was field screened for each sample. A total of 30 glacial till, 25 alluvial fan, 50 talus fines, and 38 debris flow samples were collected (Table 3.1).

3.1.3 Surface waters

Surface water samples were taken at every sediment site and also at locations such as groundwater seeps. Waters from sediments sites were collected in three mornings to avoid times of high runoff and turbidity from afternoon snowmelt. Sulfate concentration, as SO_4^{-2}, was estimated using a Hach sulfate kit (SF-1), and pH was measured with a waterproof pHTestr 2 digital meter at every site. Samples were collected in a 20 ml sterile, latex free plastic syringe (Luer Lox Recorder No. 309661) and filtered in the field through a 0.45 μm filter (Nalgene surfactant-free cellulose acetate membrane filter in an acrylic housing, into a 15 ml metal free, polypropylene centrifuge tube (Elkay Lot No 11955). For preservation, 100 μl of ultrapure (Seastar Lot No. 128100) nitric acid was pipetted into each sample. Table 3.2 lists the concentration of selected elements in the nitric acid. Previous tests of this equipment with blank water samples showed no significant contamination (Table 3.3) (W. K. Fletcher, pers. comm.). In total, fifty-eight surface water samples were collected.

3.1.4 Chemical precipitates

Chemical precipitates are found predominately on the Lama property where they are associated with surface outlets of ground water seeps. They are visually distinct from other surficial materials with an efflorescent texture and are white to yellow to brown (Plate 2.5). Two types of chemical precipitates were collected, the first being a bulk sample of 0.5 -1 kg to be analyzed for

Table 3.2. ICP-MS analysis of Seastar baseline quality nitric acid used in preservation of water samples (Seastar Chemicals Inc, certificate of analysis, lot no.128100).

Element	oncentration (ppt)
Al	<10
Sb	<10
As	<10
Ba	<1
Be	<5
Bi	<1
Cd	<1
Ca	<20
Cr	<10
Co	<1
Cu	<3
Fe	<20
Pb	<1
Mg	3
Mn	<1
Hg	<100
Mo	<1
Ni	<10
P	NA
K	<10
Se	<10
Ag	<1
Na	4
Sr	<1
Sn	<10
Ti	<20
Tl	<1
U	<0.1
V	<1
Zn	<3

Table 3.3. Results of contamination test for water sampling equipment and nitric acid (W.K. Fletcher, pers.comm.). All samples are deionized water filtered through a 0.45 μm syringe filter. 100 μl ultra-pure nitric acid added were added to samples 5-9. All concentrations are in mg/l.

Sample No.	Units	1	2	3	4	5 (+HNO_3)	6 (+HNO_3)	7 (+HNO_3)	8 (+HNO_3)	9 (+HNO_3)
Ag	μg/l	<10.00	<10.00	<10.00	<10.00	<10.00	<10.00	<10.00	<10.00	<10.00
Al	mg/l	<.002	<.002	0.002	<.002	<.002	0.002	0.002	0.004	0.004
As	μg/l	<2	<2	<2	<2	<2	<2	<2	<2	<2
Ba	μg/l	<.10	<.10	<.10	<.10	<.10	<.10	0.2	0.3	0.2
Be	μg/l	<1.0	<1.0	<1.0	<1.0	<1.0	<1.0	<1.0	<1.0	<1.0
Bi	μg/l	<.10	<.10	<.10	<.10	<.10	<.10	<.10	<.10	<.10
Ca	mg/l	<.10	<.10	<.10	<.10	<.10	<.10	<.10	<.10	<.10
Cd	μg/l	<.2	<.2	<.2	<.2	<.2	<.2	<.2	<.2	<.2
Co	μg/l	<.04	<.04	<.04	<.04	<.04	<.04	<.04	<.04	<.04
Cr	μg/l	<1.0	<1.0	<1.0	<1.0	<1.0	<1.0	<1.0	<1.0	<1.0
Cu	μg/l	0.2	<.2	0.2	<.2	1	1.4	0.6	1.4	0.8
Fe	mg/l	<.02	<.02	<.02	<.02	<.02	<.02	<.02	<.02	<.02
Hg	μg/l	<2	<2	<2	<2	<2	<2	<2	<2	<2
K	mg/l	<.10	<.10	<.10	<.10	<.10	<.10	<.10	<.10	<.10
Mg	mg/l	<.002	<.002	<.002	<.002	<.002	<.002	0.004	<.002	<.002
Mn	μg/l	<.10	<.10	<.10	<.10	<.10	<.10	<.10	<.10	<.10
Mo	μg/l	<.2	<.2	<.2	<.2	<.2	<.2	<.2	<.2	<.2
Na	mg/l	<.10	<.10	<.10	<.10	<.10	<.10	<.10	<.10	<.10
Ni	mg/l	<.4	<.4	<.4	<.4	<.4	<.4	<.4	0.4	0.4
P	mg/l	<.2	<.2	<.2	<.2	<.2	<.2	<.2	<.2	<.2
Pb	μg/l	<4	<4	<4	<4	<4	<4	<4	<4	<4
Sb	μg/l	<.10	<.10	<.10	<.10	<.10	<.10	<.10	<.10	<.10
Se	μg/l	<2	<2	<2	<2	<2	<2	<2	<2	<2
Sn	μg/l	<1.0	<1.0	<1.0	<1.0	<1.0	<1.0	<1.0	<1.0	<1.0
Sr	μg/l	0.1	0.2	0.1	0.1	0.5	0.2	0.7	0.2	0.7
Ti	μg/l	<2	<2	<2	<2	<2	<2	<2	<2	<2
Tl	μg/l	<.10	<.10	<.10	<.10	<.10	<.10	<.10	<.10	<.10
U	μg/l	<.10	<.10	<.10	<.10	<.10	<.10	<.10	<.10	<.10
V	μg/l	<2	<2	<2	<2	<2	<2	<2	<2	<2
Zn	μg/l	2	1	1	1	4	6	3	5	4

general chemical composition. The second was a small (15ml) vial filled with crystalline precipitate to be analyzed by XRD and SEM for mineralogical constituents. Sample selection was guided by color and crystallinity differences between the precipitates.

3.2 Sample preparation

Samples were sent to the University of British Columbia for preparation prior to analysis: summary flow charts for sample preparation are shown in Figures 3.3-3.5.

3.2.1 Sediments

Preparation for samples from the three energy environments differed only in the initial step, with a 5 kg sub-sample of the high and medium energy sites being saved by coning and quartering. The remainder of the high and medium energy samples, and all low energy samples were then processed as described below.

Samples were wet sieved in the laboratory through a series of seven stainless steel ASTM sieves to obtain the following eight size fractions: -2mm+850μm, -850+425μm, -425+212μm, -212+150μm, -150+106μm, -106+ 75μm, -75+53μm, -53μm. Between sample contamination was minimized by sieving in order of lowest anticipated geochemical values to highest anticipated geochemical values based on proximity to source, presence of visible secondary oxides, and principle versus tributary streams. During sieving, the water from the pail was recirculated with a pump to minimize loss of fines. The final wash of each sieve was completed with clean water. The -53 μm material and wash water were retained in plastic pails to allow the

Figure 3.3. Sample preparation flowchart for high and medium energy stream sediments.

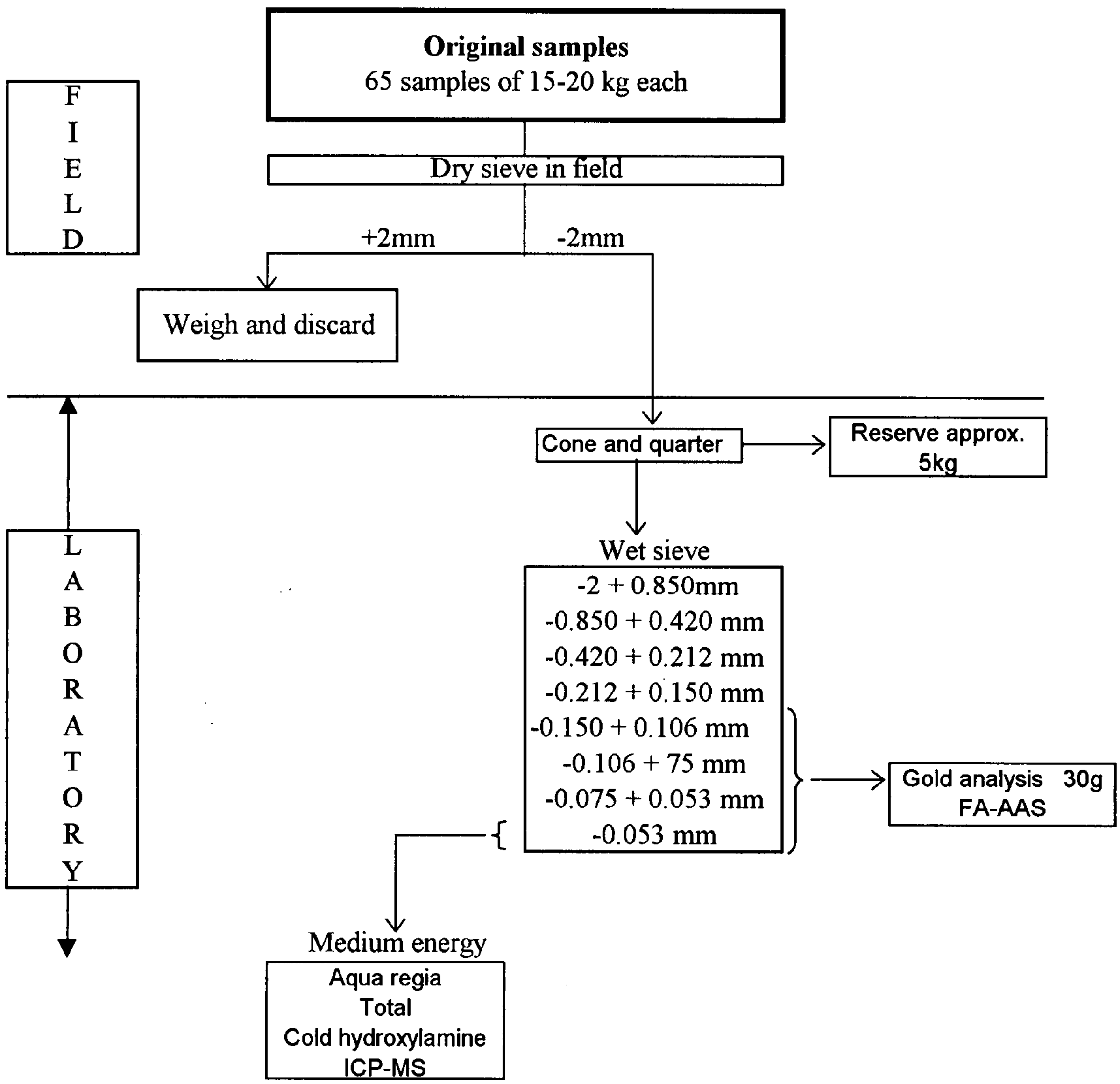

Figure 3.4. Sample preparation flowchart for low energy stream sediments.

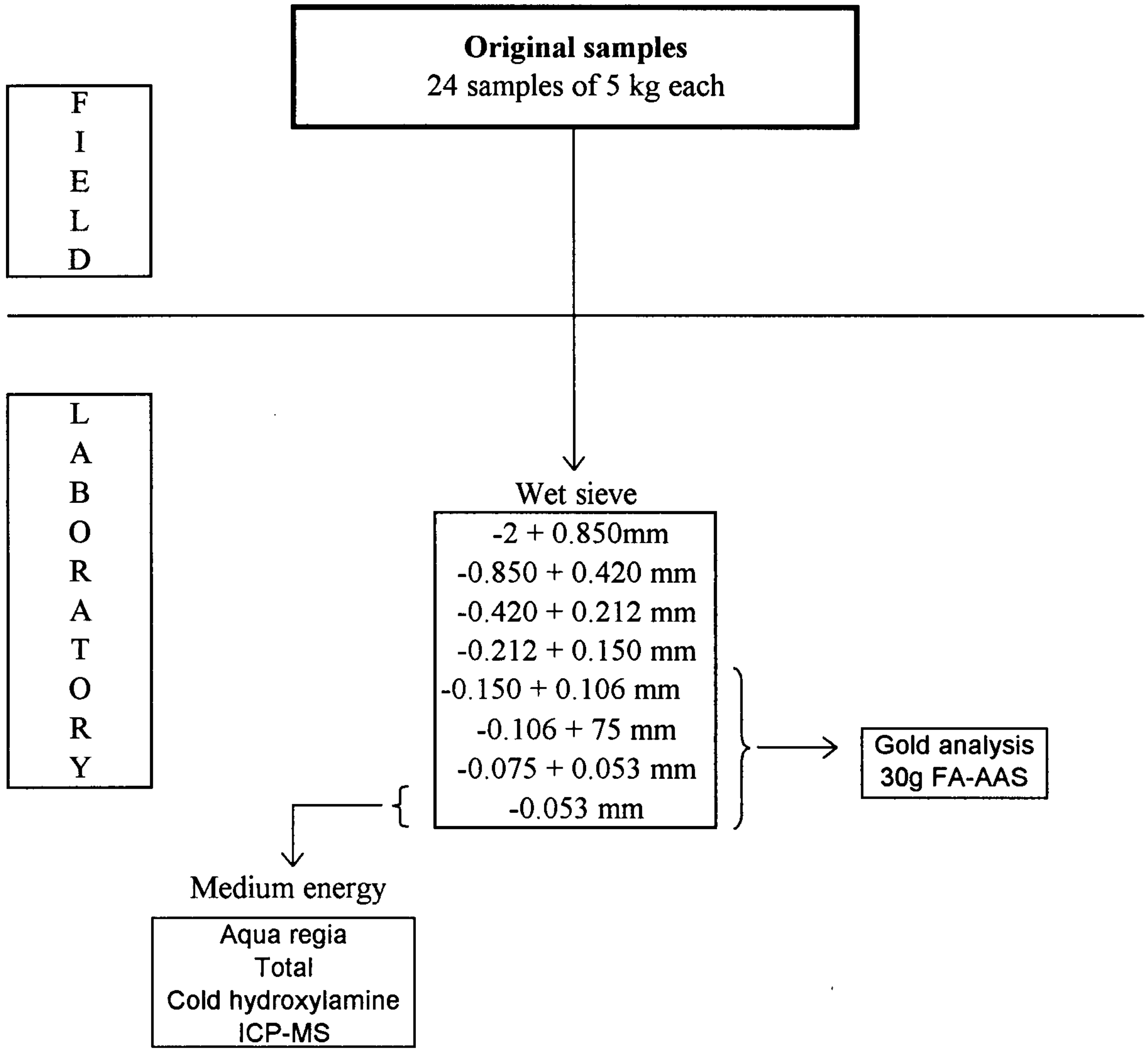

Figure 3.5. Sample preparation flowchart for surficial materials.

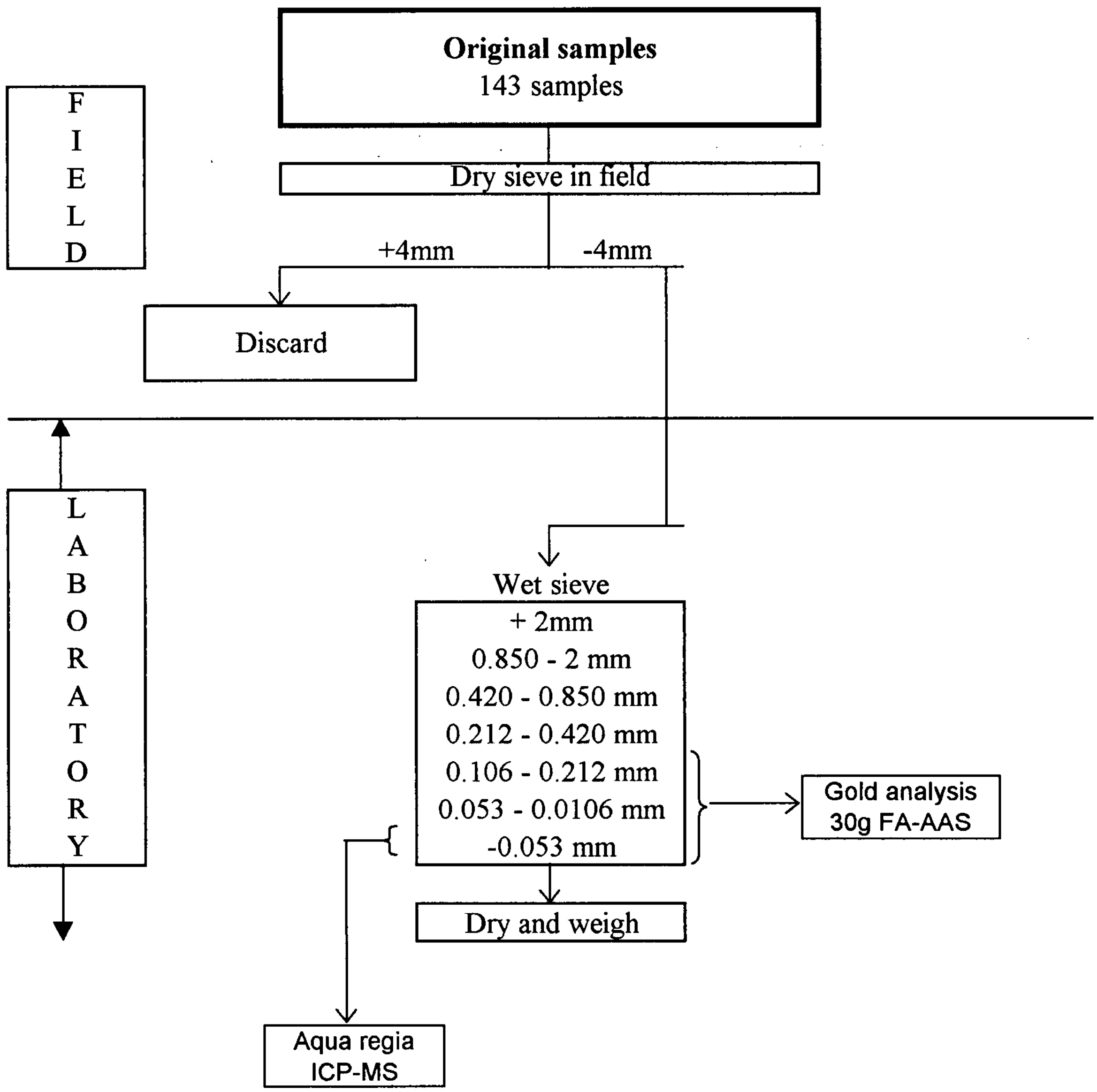

fine suspended material to settle. The pH of the water column above the settled -53µm sediments was measured. Excess water was then pumped out of the pail and the sediment scraped and rinsed into glass drying trays. Each of the size fractions was then oven-dried overnight at approximately 80°C, cooled to room temperature and placed in plastic sample bags. The four coarsest size fractions, -2mm+850µm, -850+425µm, -425+212µm and -212+150µm were weighed and stored. The four finest size fractions, -150+106µm, -106+ 75µm, -75+53µm and -53µm were weighed and sub-sampled for chemical analysis. A representative 40-70 g sub-sample for determination of gold was obtained using a Jones riffle splitter. The -53µm size fraction was disaggregated with a stainless steel rolling pin prior to splitting. The remaining material was stored in plastic bags.

Sub-samples were submitted for analysis grouped by size fraction from coarsest (-150+106 µm) to finest (-53 µm), preserving preparation order. In each size fraction, four random laboratory duplicates and one gold standard (Canmet GTS-2) were added.

3.2.2 Surficial materials

Preparation of the surficial materials duplicated the sediment procedure except that 100g of material was held aside for storage and future work, and only seven size fractions were sieved: +2mm, -2mm+850µm, -850+425µm, -425+212µm, -212+106µm, -106+53µm, -53µm.

3.3 Sample analysis

After preparation at UBC, stream sediment, surficial materials and water samples were submitted to a commercial laboratory, Chemex Labs of North Vancouver, BC, for multi-element analysis using a variety of analytical methods. Raw geochemical data are found in Appendix A.

Gold determinations on the stream sediments and surficial materials were made by a 30 g sub-sample fire assay fusion followed by an atomic absorption finish (Chemex Code 983, detection limit 5 ppb). Two *aqua regia* digestions (Chemex Codes G132 and G32m) were used. The standard *aqua regia* leach (G32m) was used for surficial materials, whereas the ultra-trace, low detection limit *aqua regia* leach (G 132) was employed for stream sediments. The total digestion (Chemex Code T27) uses a mixture of nitric (HNO_3), perchloric ($HClO_4$) and hydrofluoric (HF) acids to destroy silicate matrices and liberate trace elements. The third chemical attack employed was a cold hydroxylamine leach. The cold hydroxylamine leach (0.1 M hydroxylamine in 0.01 M nitric acid) is intended to selectively dissolve manganese oxides (Chemex, 1999). A description of these chemical attacks can be found in Appendix C.

In summary, the -150+106μm, -106+ 75μm, -75+53μm and -53μm fractions of every sediment sample was analyzed for gold. The -53μm fraction from the medium energy environment was also analyzed with the *aqua regia*, total digestion and the cold hydroxylamine leach. For the surficial materials, the -212+106μm, -106+53μm and -53μm size fractions were analyzed for gold, and the -53μm was also analyzed after digestion by *aqua regia*. Surface waters were submitted without additional sample preparation for multi-element ICP-MS analysis at Chemex Labs.

3.4 Quality control

All sample media, excluding chemical precipitates, were subjected to a quality control program. Analytical and sub-sampling precision and accuracy were determined for stream sediments and surficial materials with laboratory duplicates and the geochemical standard GTS-2 (Leaver, 2000). Only total variability (i.e. field and laboratory variation) was quantified for surface waters. Precision was estimated using X-Y scatter and Thompson-Howarth plots (Thompson and Howarth, 1978; and Fletcher, 1981).

3.4.1 Gold precision and accuracy

Table 3.4 shows estimates of laboratory sub-sampling and analytical precision at the 95% confidence level for all size fractions and sample types analyzed for gold. Analytical and sub-sampling precision for stream sediments improves significantly with a corresponding decrease in grain size; ± 10% for -53μm and approximately ± 100% for -150+106μm samples. Figures 3.6 and 3.7 compare the X-Y scatter and Thompson-Howarth plots for Au in the -150+106μm and -53μm fractions of sediments. Duplicate data for all size fractions can be found in Appendices 3.2 and 3.3. Estimates of precision for surficial samples also shows a trend toward better precision with a decrease in size fraction; i.e. ±35% for –212+106 μm versus ±15% for -53μm fraction (Table 3.4).

The accuracy of gold determinations for stream sediment and surficial materials is ±10 % based on seven replicate analysis of the gold standard, GTS-2, for which an average value of 266 ppb was obtained versus the recommended value of 263 ± 5ppb (Leaver, 2000).

Table 3.4. Estimate of gold sub-sampling and analytical precision for stream sediments and surficial material. Precision at the 95% confidence level estimated using Thomson-Howarth short method.

Size fraction (μm)	Sample type	Thompson-Howarth (%	n
-150+106	sediment	100	5
-106+75	sediment	100	5
-75+53	sediment	75	5
-53	sediment	10	9
-212+106	surficial	35	13
-106+53	surficial	20	13
-53	surficial	15	14

Table 3.5. Thompson-Howarth estimates of total precision at 95% confidence using high and medium energy stream sediments as field duplicates.

Size fraction (μm)	Lama (n=13)	Pascua (n=16)
-150+106	100	155
-106+75	100	150
-75+53	75	95
-53	55	75

An estimate of field precision (i.e. field plus analytical) can be obtained by assuming high and medium energy stream sediment samples are field duplicates. This is not strictly correct, but seems reasonable insofar as t-tests show no significant difference between sediment texture of high and medium energy samples. (see Chapter 4.3.1 and 5.3.1). Table 3.5 reports the Thompson-Howarth estimates of field precision. Field precision is worse than ± 100% at 95% confidence for the –150+106μm and –106+75μm size fractions at both Pascua and Lama, but improves to ±55% in the –53μm fraction at Lama and ±75% in the -53μm fraction at Pascua.

3.4.2 Chemical digestions and selective leaches

Duplicate data for all sample types, size fractions and chemical digestions can be found in Appendix A. The majority of elements have sub-sampling and analytical precision better than ±10% at the 95% confidence level. Exceptions to this are mainly found with the cold hydroxylamine leach (Au, As, Cr, I, Li, U and Pb have precision worse than ±25%). For surficial samples with the *aqua regia* digestion precision was worse than ±20% at the 95% confidence level for Be, Ni and gold (as determined by fire assay) in the –212+106 and –106+53μm fractions. Mercury precision, for all analyses, was worse than ±40% at the 95% confidence level. Figure 3.8 shows Thompson-Howarth plots for Cu, Sb, and Ag.

3.4.3 Water samples

By collecting duplicate water samples at every fourth sample site, total variability (field and analytical) was determined using the methods outlined above. Appendix A contains duplicate

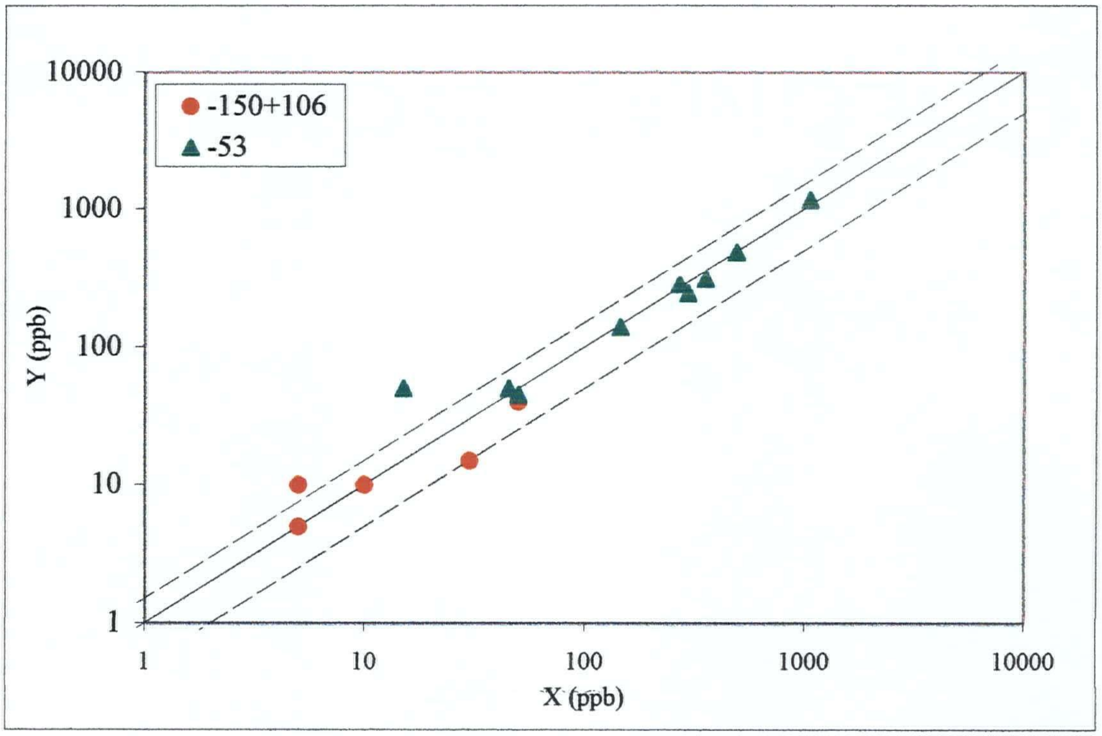

Figure 3.6. X-Y scatter plot of sub-sampling and analytical precision for gold in the 150+106μm and -53mm fractions. Control lines are at +/- 50% precision.

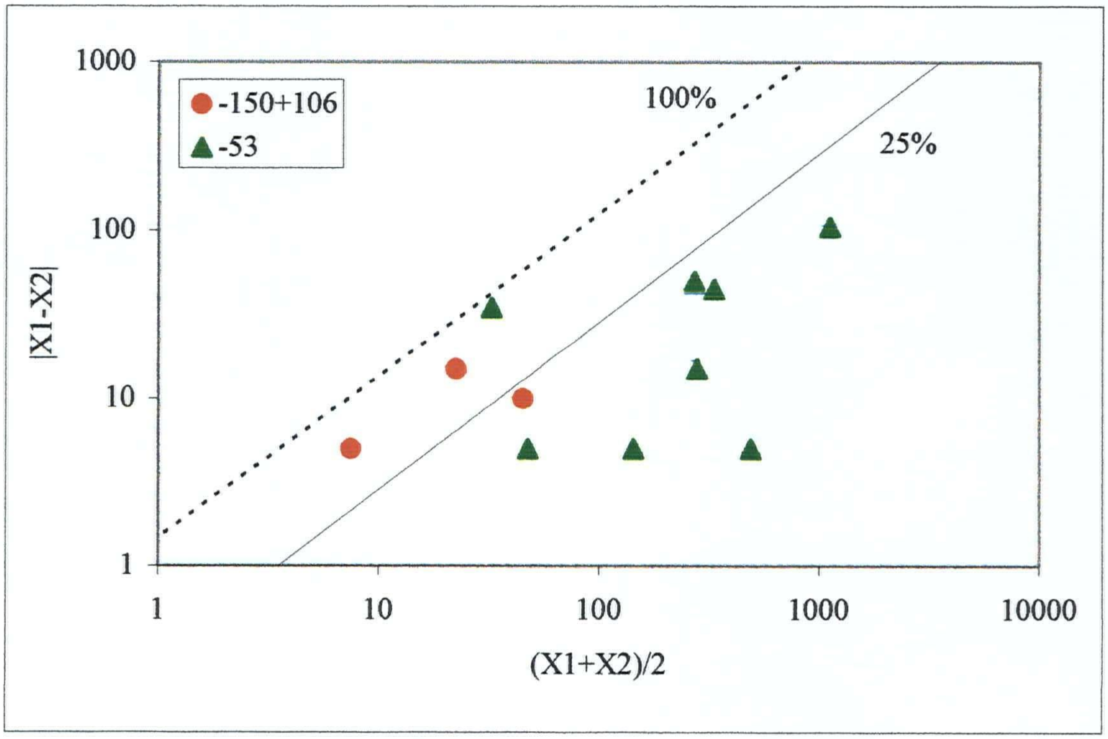

Figure 3.7. Thompson and Howarth plot of laboratory duplicates for the -150+106μm and -53 mm fractions. Control lines at the 95% confidence level are shown for 100% and 25% precision.

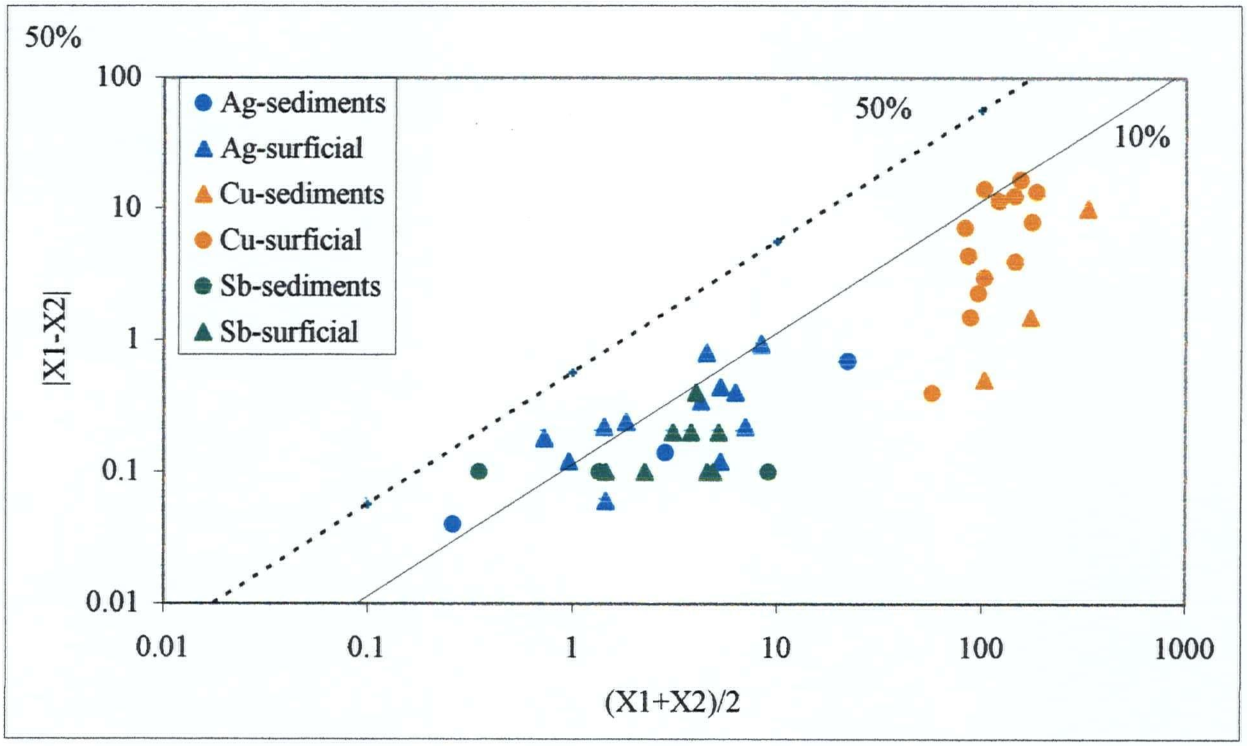

Figure 3.8. Thompson-Howarth plots of 10% precision at 95% confidence levels for laboratory duplicates of Ag, Cu and Sb after aqua regia digestion for stream sediments and surficial samples.

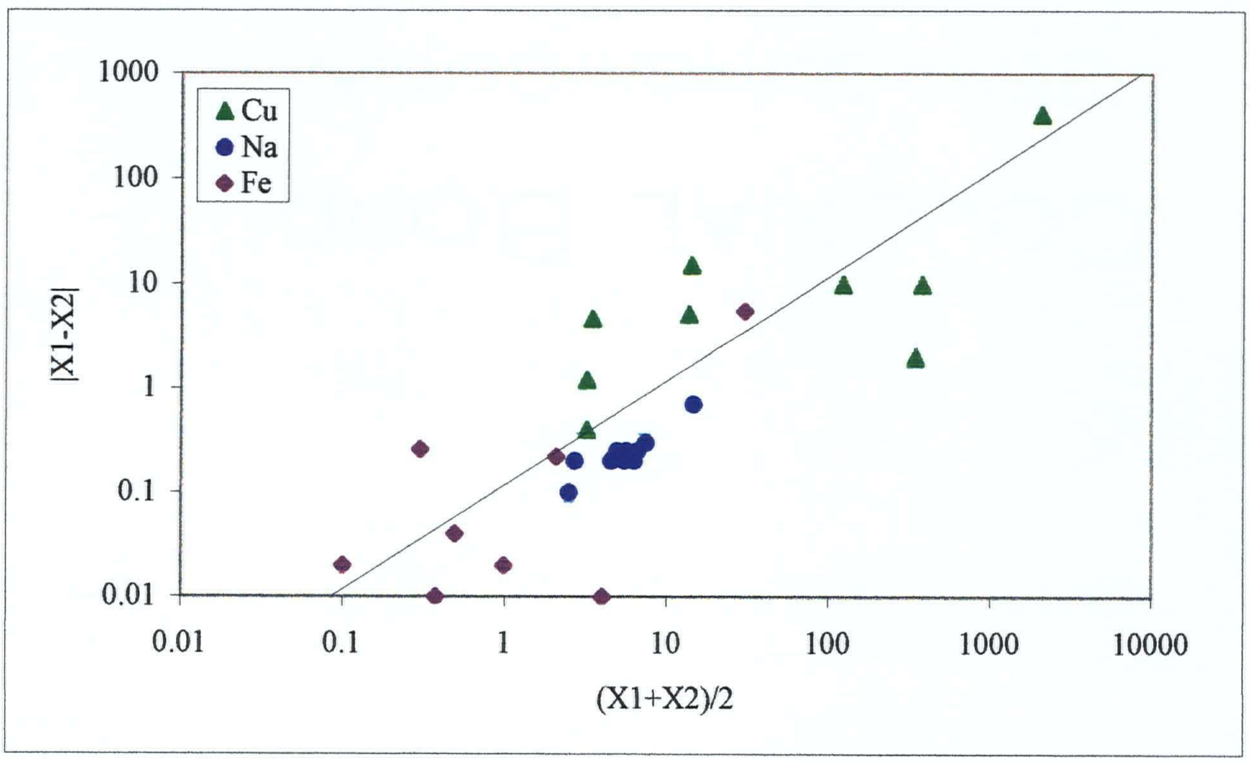

Figure 3.9. Thompson-Howarth plots of 10% precision at 95% confidence levels for field duplicates of Cu, Na and Fe in water samples.

data for water samples. Figure 3.9 shows Thompson-Howarth plot for Cu, Na and Fe. Only Cu, with a precision of ±35%,was worse than ±15% at 95% confidence (Figure 3.9).

3.5 Other analytical methods

Heavy mineral separates were taken from two stream sediment sites, one each from Pascua and Lama. The −106+75μm and +53μm size fractions were separated into heavy (S.G. > 3.3) and light mineral fractions using methylene iodide (CH_2I_2). Both heavy and light fractions were retained and weighed. Approximately 10 grams of the light mineral fraction was analyzed with total (triple acid) digestion. The heavy mineral fraction was further divided into magnetic and non-magnetic fractions using a hand-held piston magnet. After taking a representative sub-sample of the magnetic and non-magnetic heavy minerals, the samples were mounted in cylindrical holders (diameter = 18 mm) and set with epoxy resin for examination and analysis with the scanning electron microscope and energy dispersive spectrometer. Polished grain mounts were carbon coated and examined with a Phillips XL-30 scanning electron microscope and a Princeton-Gamma-Tech ED spectrometer at spot 6 and 20 kV. Samples were examined to identify minerals of high average atomic weight such as Au, Ag, Hg, Bi, As, Sb, Cu, Pb and Zn species. Results of these supplemental methods are in Appendix C.

CHAPTER 4

RESULTS LAMA, ARGENTINA

4.1 Surficial media

To complement stream sediment sampling, one hundred thirty two surficial samples of glacial till, talus fines, debris flow and alluvial fan material were collected. Classification of the media was determined in the field based on morphology, texture and air-photo interpretation. Field discrimination and spatial distribution of the materials is detailed in Chapter 2.

4.1.1 Glacial till

Eighteen glacial till samples were collected north and east of the Lama camp. The till forms a series of sub-parallel ridges aligned approximately east-west that appear to have originated from the heads of both the R. Turbio and R. Canito basins, converging to the east of Penelope Ridge.

4.1.1.1 Texture and geochemistry

The weight percent distributions of the seven size fractions show the -212μm material (fine sand and finer) accounts for 30.6% of the average sample mass, with 44.1% of fines in the -53μm fraction (Table 4.1).

Gold concentrations are greatest in the -53μm fraction (Table 4.1), which also has the lowest maximum to minimum contrast due to a minimum value of 50 ppb. Geochemically, there are no obvious down-ice dispersion patterns or differences between the R. Turbio and R. Canito basins (

Table 4.1. Descriptive statistics of glacial till after aqua regia digestion (n=18). Maximum/minimum ratios greater than ten are in bold. Elements of the high sulfidation geochemical suite (Hedenquist et.al.,1996) are grouped together. Median values reported for gold.

Element	Units	Mean	Minimum	Maximum	Max/Min
Au (-212+106μm)	ppb	17.5	10.0	825.0	**82.5**
Au (-106+53μm)	ppb	17.5	5.0	70.0	**14.0**
Au (-53μm)	ppb	85.0	50.0	280.0	5.6
pH		8.2	5.3	10.4	2.0
Cu	ppm	138.2	62.9	186.5	3.0
Ag	ppm	1.8	0.6	3.4	5.3
As	ppm	220.6	115.0	428.0	3.7
Pb	ppm	206.7	104.0	620.0	6.0
Hg	ppm	0.2	0.0	0.6	**21.0**
Sb	ppm	3.2	1.9	6.4	3.4
Te	ppm	1.0	0.6	1.8	3.3
Mo	ppm	5.8	3.4	19.6	5.8
Bi	ppm	3.5	1.8	5.6	3.2
Al	%	1.5	1.0	2.0	2.0
Ba	ppm	337.2	230.0	440.0	1.9
Ca	%	0.4	0.2	1.3	6.7
Cd	ppm	0.6	0.3	1.3	4.5
Co	ppm	7.6	3.6	11.2	3.1
Cr	ppm	13.8	8.0	23.0	2.9
Fe	%	4.4	3.7	5.3	1.4
K	%	0.4	0.3	0.5	1.8
Mg	%	0.5	0.3	0.6	1.8
Mn	ppm	814.7	320.0	1435.0	4.5
Na	%	0.1	0.1	0.1	2.0
Ni	ppm	8.4	5.0	11.0	2.2
P	ppm	816.7	530.0	1120.0	2.1
S	%	0.7	0.4	1.2	3.3
Se	ppm	2.6	1.5	4.0	2.7
Sr	ppm	94.2	61.0	135.0	2.2
V	ppm	44.6	32.0	61.0	1.9
W	ppm	0.2	0.1	0.4	3.5
Zn	ppm	170.2	106.0	334.0	3.2
-4+2mm	%	21.4	8.0	45.8	
-2mm+850μm	%	16.5	8.8	22.7	
-850+425μm	%	13.7	7.3	19.1	
-425+212μm	%	17.9	7.9	32.6	
-212+106μm	%	11.2	1.1	21.7	
-106+53μm	%	5.9	0.6	9.3	
-53μm	%	13.5	3.1	31.1	

Table 4.2. Correlation coefficients with -53μm gold for selected elements of Lama glacial till samples (df = 16, r significant at >0.468 at P= 0.05). Significant values in **bold**.

	r
Cu	0.36
Ag	**0.76**
As	**0.63**
Pb	0.17
Hg	0.22
Sb	**0.71**
Te	**0.69**
Mo	0.03
Bi	**0.74**
Al	0.46
Ba	0.45
Cd	**0.77**
Ca	0.17
Cr	0.10
Co	-0.08
Fe	**0.49**
Mg	0.34
Mn	-0.17
Ni	-0.02
P	0.31
K	**0.49**
Sc	0.16
Se	0.42
Na	0.37
Sr	0.42
S	0.37
U	0.20
W	0.40
V	0.13
Zn	**0.76**

Figure 4.1. Gold in -53μm fraction of glacial tills at Lama.

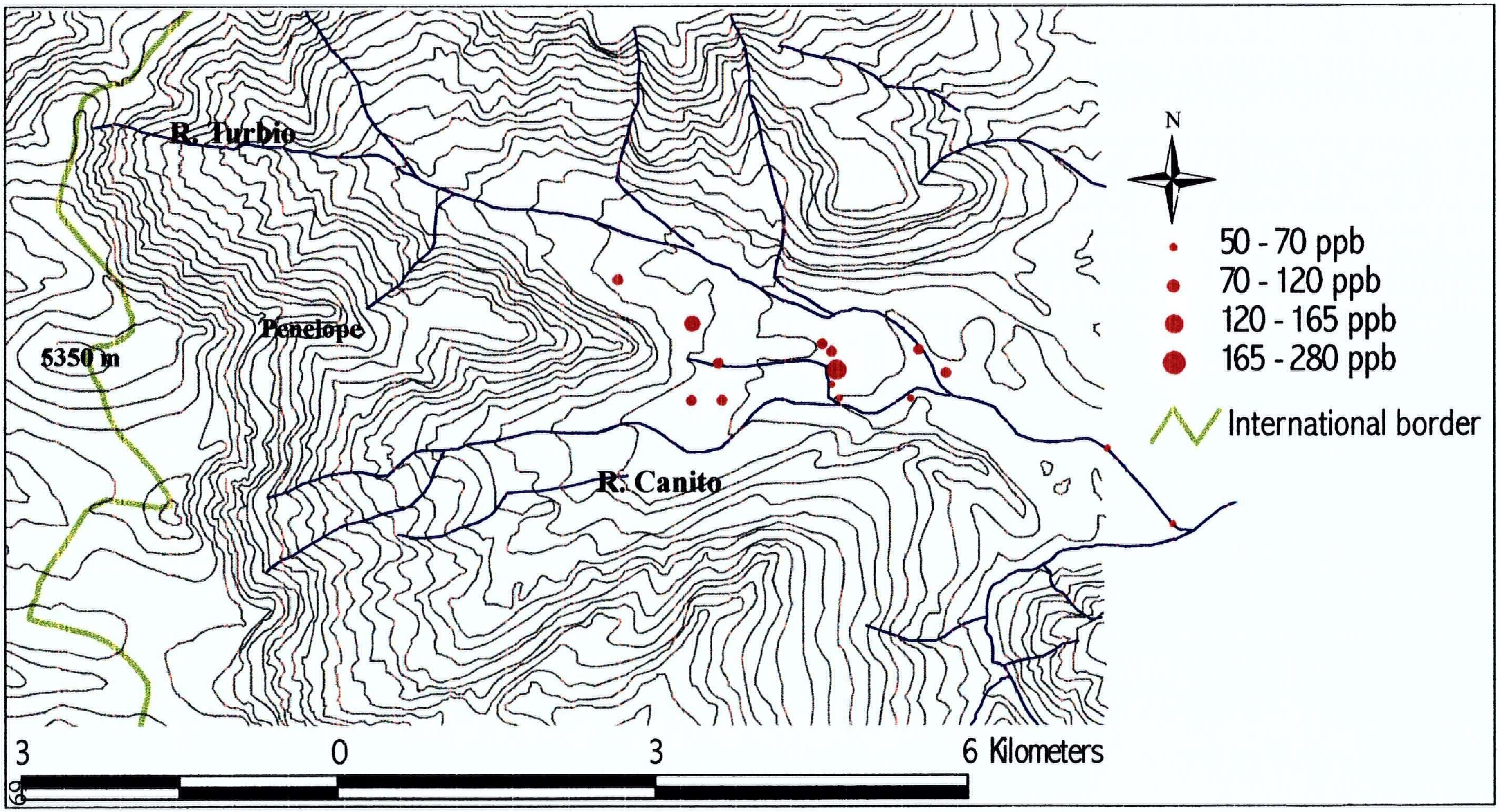

Figure 4.2. Copper concentrations in glacial till at Lama.

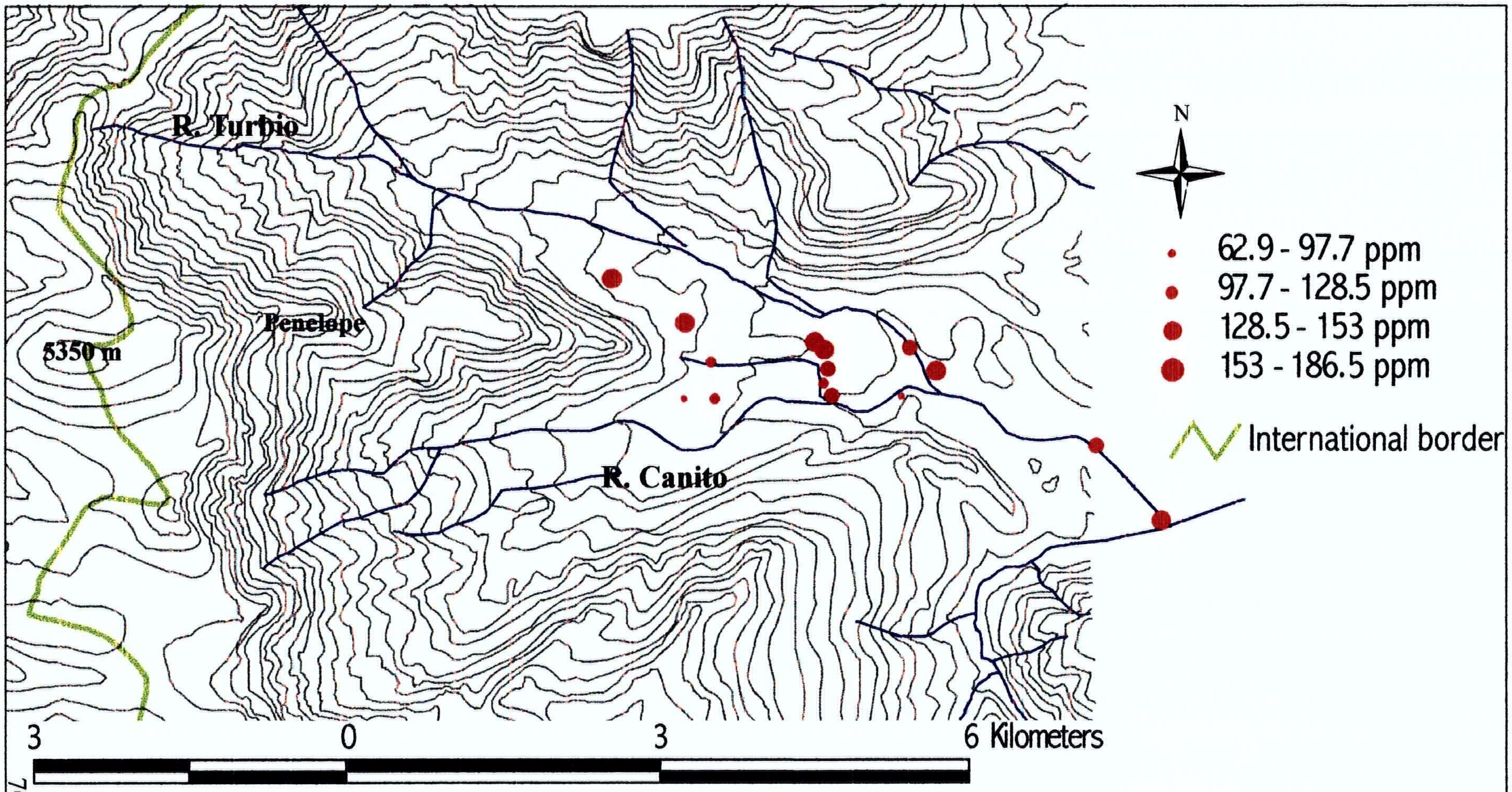

e.g. Au and Cu in Figures 4.1 - 4.2). Twenty-one elements have maximum/minimum ratios of less than or equal to three. Examination of correlation coefficients shows Al, Sb, As, Bi, Cd, Fe, K, Te and Zn have significant positive correlations with Au. Copper, Pb, Hg and Mo also have positive but not significant positive relation to Au (Table 4.2). The pH of till samples range from 5.3-10.4 with an average of 8.2.

4.1.2 Debris flows

Debris flow is used to describe poorly sorted landforms with minor rounding of clasts and imbrication (with other flow features) that appear to flow around topographic highs and occupy valley bottoms. Twenty-eight debris flow samples were collected at Lama. The majority of the sampling was adjacent to stream sediment sites on the valley floor.

4.1.2.1 Texture and geochemistry

Debris flows are coarser than other surficial materials, with only approximately 20% of the sample mass in the –212μm fraction (Table 4.3). The eastern, lower debris flow (near the R. Canito confluence) is coarser than the western, upper flow (Figure 4.3). Maximum median gold concentrations of 252.5 ppb are found in the –53 μm fraction compared to only 30 ppb in the –212+106μm fraction. Gold in the -53μm fraction is approximately evenly distributed throughout the debris flows (Figure 4.4), with slightly higher concentrations at the upper end of the western flow. Boron, Ge, Fe, La, Mg, P, K, Na, S and Tl all have maximum to minimum ratios of less than three and hence tend not to have strongly developed distribution patterns. Antimony, As, Bi, Te, W, Na, Ag, Se and Mo have both a significant correlation (Table 4.4) with ($r \geq 0.42$) and a similar spatial distribution to gold (e.g. Ag in Figure 4.5). Conversely,

Table 4.3. Descriptive statistics of debris flows after aqua regia digestion (n=28). Maximum/minimum ratios greater than ten are in bold. Elements of the high sulfidation geochemical suite (Hedenquist et.al., 1996) are grouped together. Median values reported for gold.

Element	Units	Mean	Minimum	Maximum	Max/Min
Au (-212+106μm)	ppb	30.0	5.0	85.0	**17.0**
Au (-106+53μm)	ppb	72.5	10.0	555.0	**55.5**
Au (-53μm)	ppb	252.5	65.0	490.0	7.5
pH		4.1	3.3	5.1	1.6
Cu	ppm	150.3	82.6	399.0	4.8
Ag	ppm	5.6	1.2	10.1	8.5
As	ppm	386.4	190.5	602.0	3.2
Pb	ppm	289.2	138.0	1515.0	**11.0**
Hg	ppm	1.0	0.2	3.3	**13.7**
Sb	ppm	3.9	2.0	12.3	6.2
Te	ppm	1.8	0.5	3.2	6.4
Mo	ppm	5.7	1.4	13.8	9.9
Bi	ppm	6.5	3.0	12.9	4.2
Al	%	1.6	0.8	2.4	3.0
Ba	ppm	337.6	150.0	590.0	3.9
Ca	%	0.2	0.0	0.5	**15.3**
Cd	ppm	0.4	0.1	1.0	**10.4**
Co	ppm	6.5	2.2	18.0	8.2
Cr	ppm	11.6	6.0	18.0	3.0
Fe	%	6.1	3.8	11.0	2.9
K	%	0.5	0.3	0.8	2.4
Mg	%	0.5	0.3	0.8	2.6
Mn	ppm	698.9	260.0	3360.0	**12.9**
Na	%	0.1	0.1	0.2	2.5
Ni	ppm	6.4	2.0	10.0	5.0
P	ppm	718.2	480.0	970.0	2.0
S	%	1.0	0.6	1.8	2.9
Se	ppm	3.7	1.5	7.0	4.7
Sr	ppm	86.8	45.0	141.0	3.1
V	ppm	49.3	31.0	63.0	2.0
W	ppm	0.3	0.1	1.2	**12.0**
Zn	ppm	144.4	60.0	324.0	5.4
-4+2mm	%	25.5	9.7	45.3	
-2mm+850μm	%	18.8	10.3	30.1	
-850+425μm	%	18.8	9.6	27.3	
-425+212μm	%	17.4	7.1	25.6	
-212+106μm	%	8.9	2.1	19.0	
-106+53μm	%	4.2	0.8	9.1	
-53μm	%	6.3	0.7	14.4	

Table 4.4. Correlation coefficients with -53µm gold for selected elements of Lama debris flow samples (df = 26, r significant at >0.374 at P= 0.05). Significant values in **bold**.

	r
Cu	-0.25
Ag	**0.82**
As	**0.60**
Pb	-0.30
Hg	0.18
Sb	**0.54**
Te	**0.74**
Mo	**0.52**
Bi	**0.77**
Al	-0.06
Ba	-0.09
Cd	-0.16
Ca	**-0.40**
Cr	-0.31
Co	**-0.42**
Fe	-0.22
K	**0.49**
Mg	0.17
Mn	**-0.38**
Ni	-0.34
P	0.31
Sc	-0.32
Se	**0.42**
Na	**0.59**
Sr	0.31
S	0.14
W	**0.72**
U	**-0.43**
V	-0.28
Zn	**-0.53**

Figure 4.3. Distribution of coarse and fine material at Lama in debris flows.

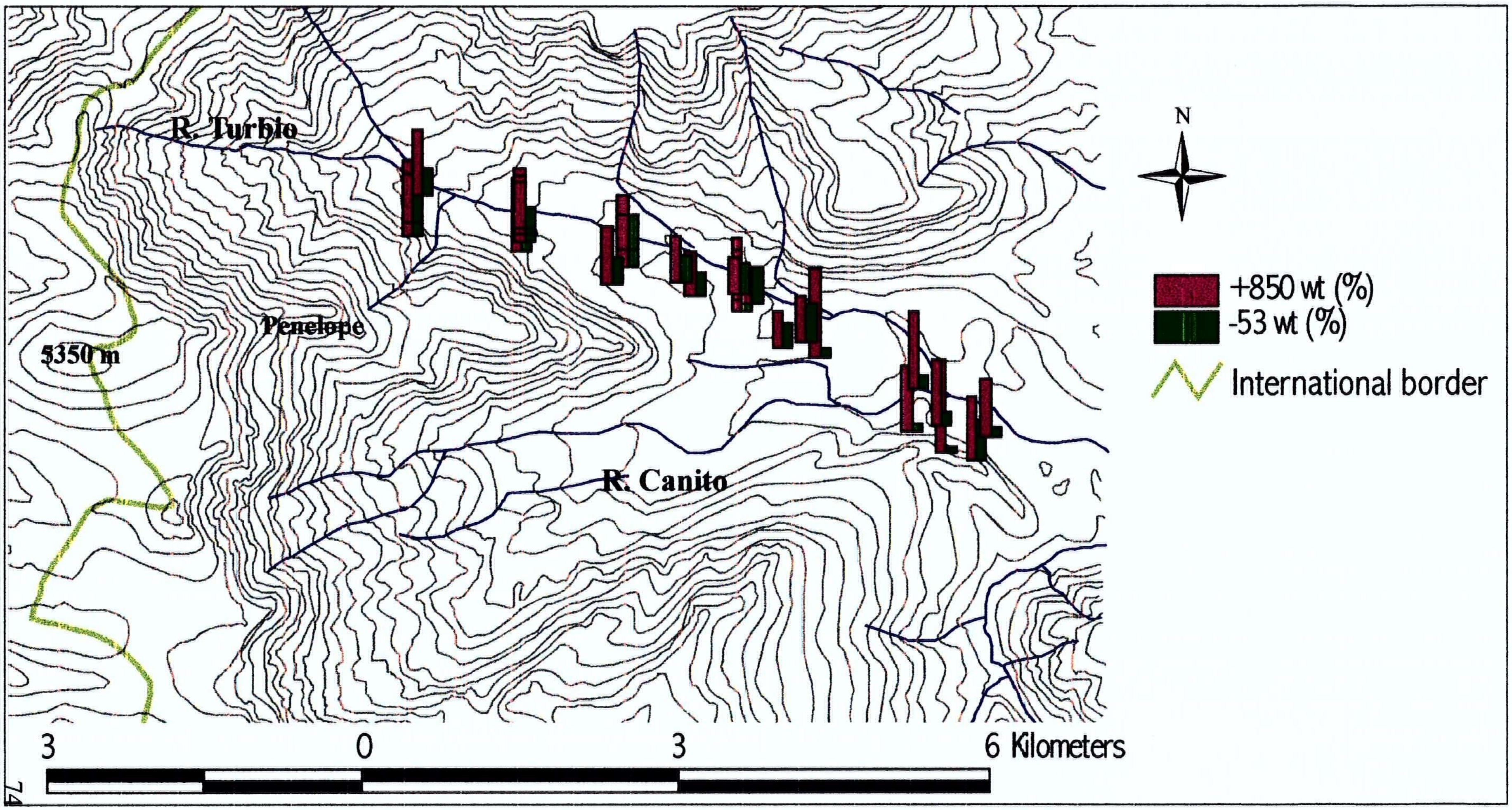

Figure 4.4. Gold in -53μm fraction of debris flows at Lama.

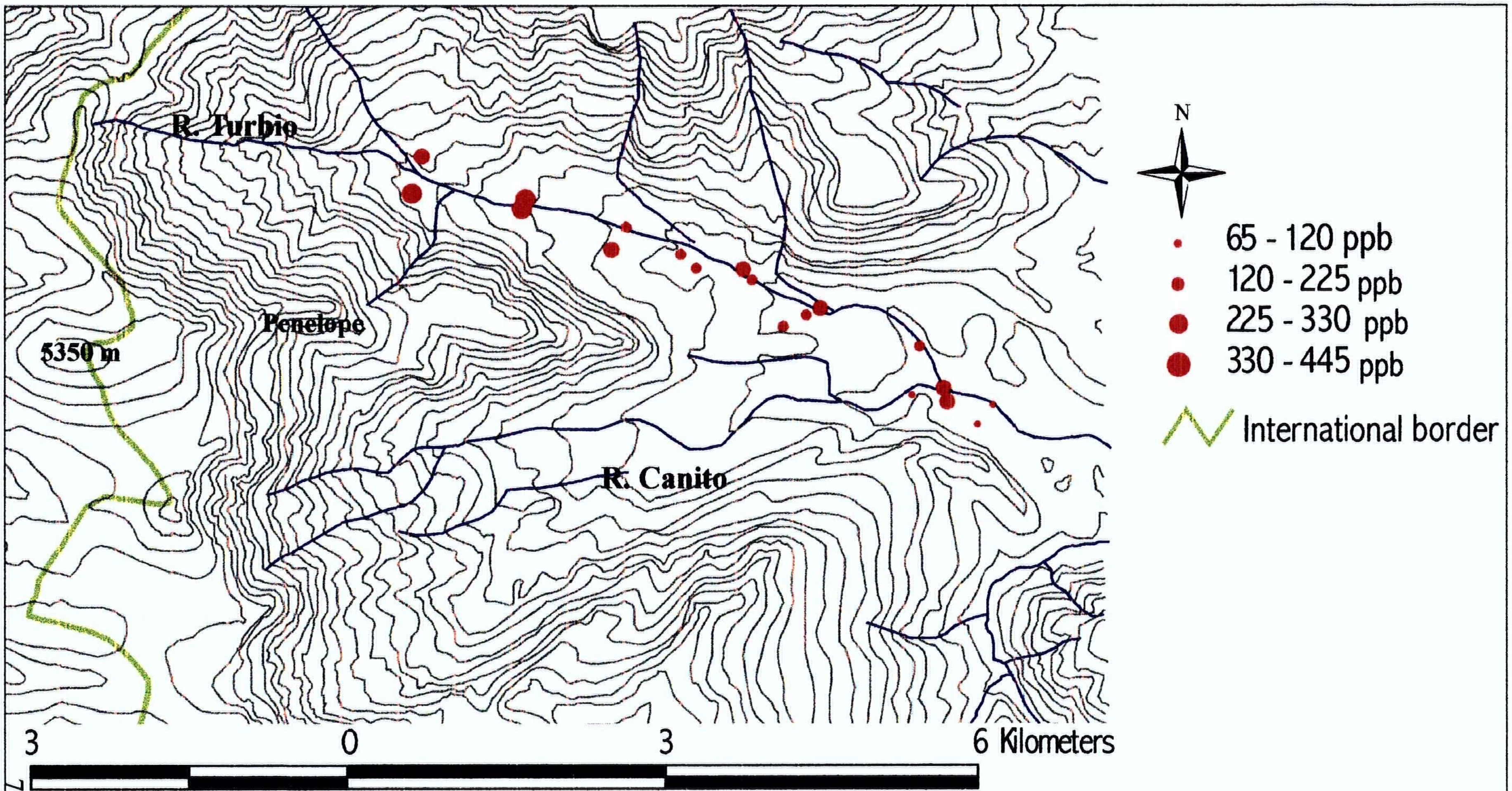

Figure 4.5. Silver concentrations in debris flows at Lama.

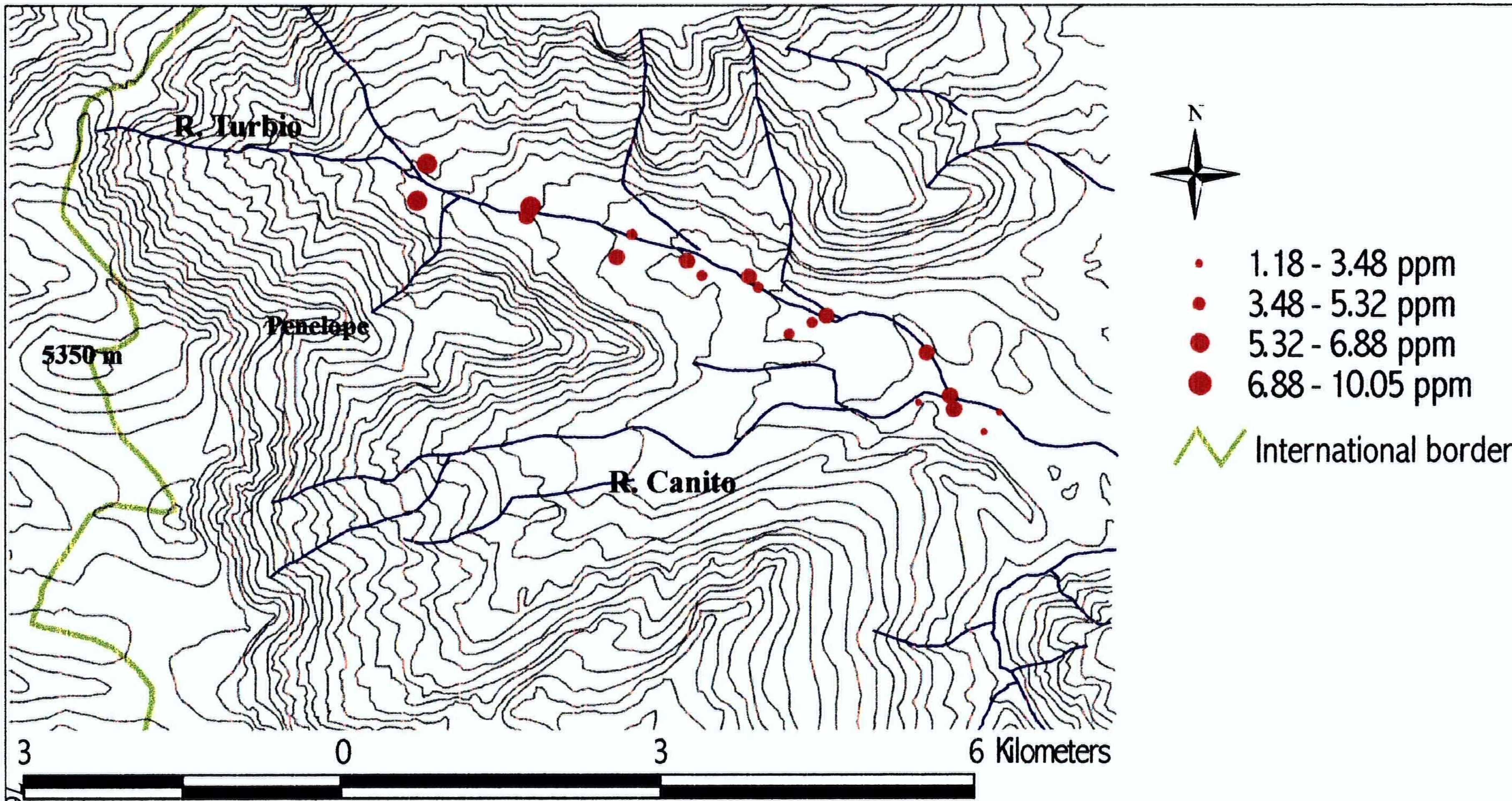

Figure 4.6. Zinc concentrations in debris flows at Lama.

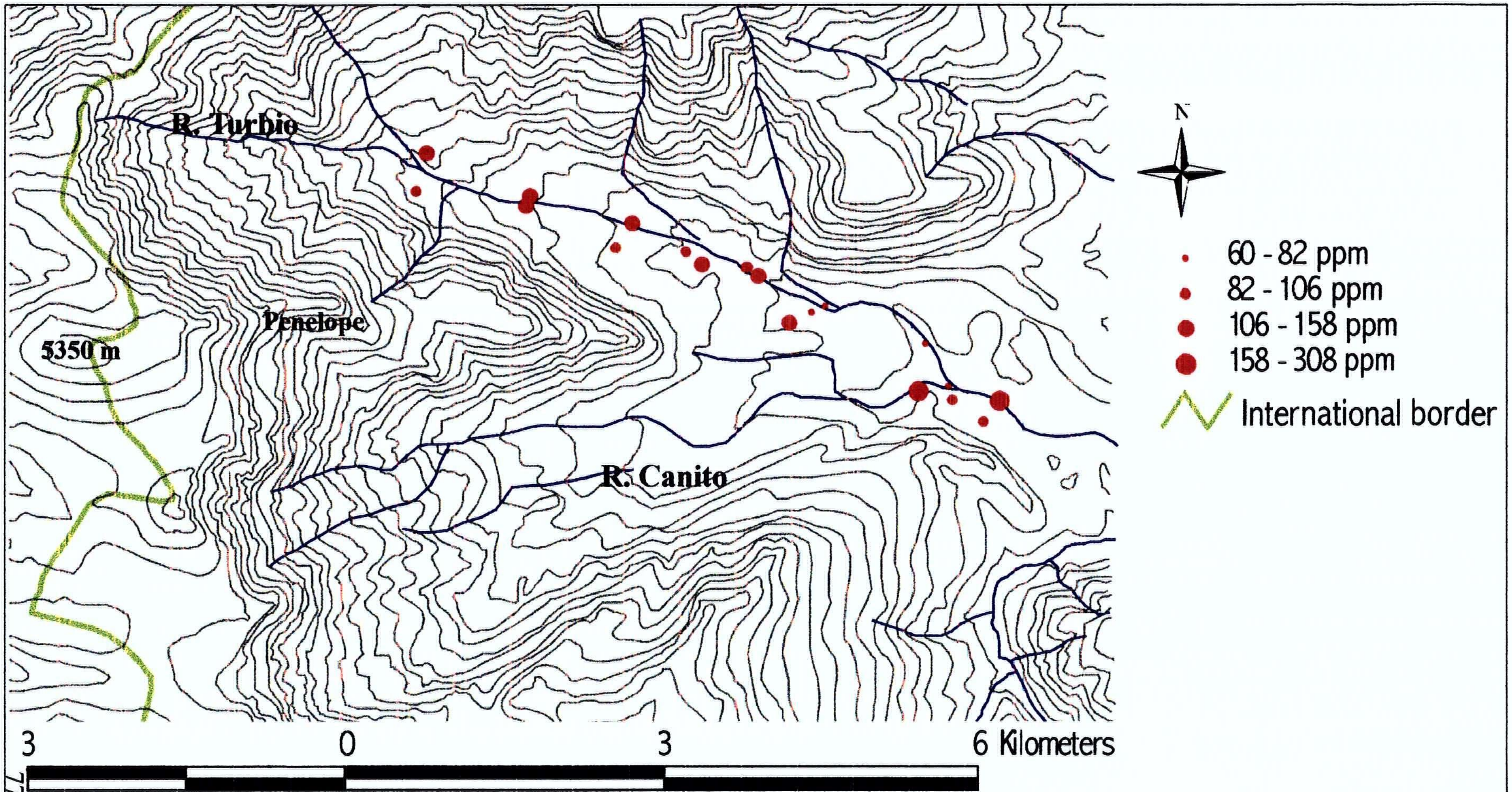

Figure 4.7 Copper concentrations in debris flows at Lama.

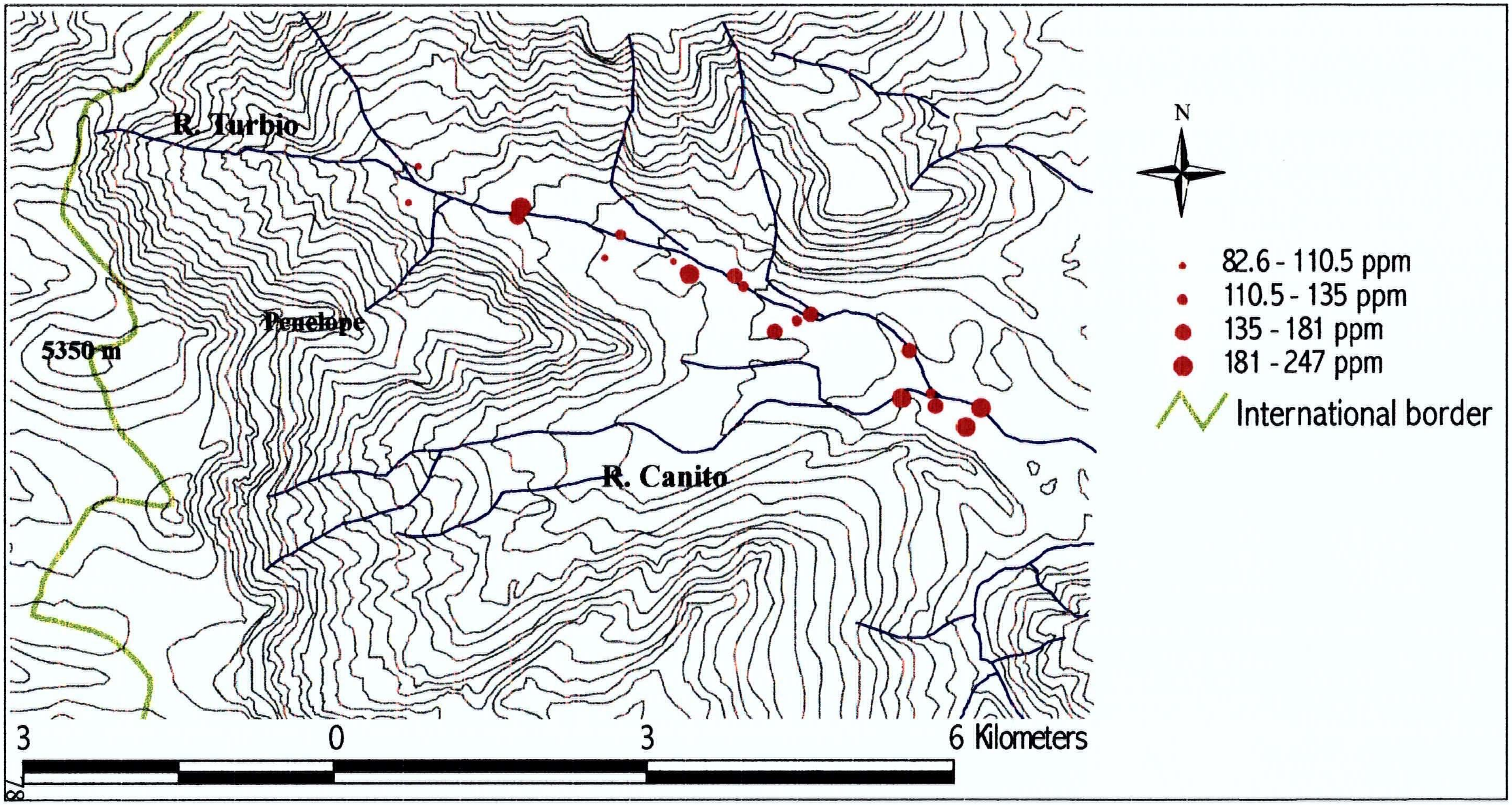

chromium, Ca, Co, Mn, Ni, U and Zn exhibit both high values corresponding to gold lows and negative correlation to gold (e.g. Zn in Figure 4.6). The upper, western flow has high Te values, while Cu is elevated in the lower, eastern debris flow (Figure 4.7 for Cu). Debris flows are very acidic with an average pH of 4.1 and a range of 3.3 to 5.1. Elements with a negative correlations with Au (such as Zn) tend to have higher concentrations where pH values are high.

4.1.3 Talus fines

A total of fifty talus samples were collected on the Pascua/Lama properties. At Lama, thirty-two samples were taken along Penelope ridge and the southern edges of the R. Turbio valley. No distinction was made between talus material and other gravity transported colluvium.

4.1.3.1 Texture and geochemistry

The weight percent distributions of the seven size fractions suggests that while there is no dominant size fraction, relative abundances decrease with decreasing grain size and talus cones appear to be deficient in –106+53μm material (Table 4.5). In general, talus cones on the upper reaches of the R. Turbio drainage contain more coarse material relative to the easterly, downstream cones (Figure 4.8). The -212μm material accounts for 26% of the average sample mass, with 40% of these fines comprised of the -53μm (silt and clay) fraction.

Maximum gold concentrations are in the –53 μm fraction (median 95 ppb) (Table 4.5) and show a strong dependence on which talus cone was sampled with talus cones developed at the base of Penelope ridge on the southern edge of the basin most anomalous in gold, regardless of size

Table 4.5. Descriptive statistics of talus cones after aqua regia digestion (n=32). Maximum/minimum ratios greater than ten are in bold. Elements of the high sulfidation geochemical suite (Hedenquist et.al., 1996) are grouped together. Median values reported for gold.

Element	Units	Mean	Minimum	Maximum	Max/Min
Au (-212+106μm)	ppb	20.0	5.0	95.0	**19.0**
Au (-106+53μm)	ppb	45.0	5.0	345.0	**69.0**
Au (-53μm)	ppb	95.0	20.0	1045.0	**52.3**
pH		4.9	3.5	7.2	2.1
Cu	ppm	152.1	87.6	290.0	3.3
Ag	ppm	3.9	0.8	13.1	**15.5**
As	ppm	375.8	123.5	896.0	7.3
Pb	ppm	348.8	98.0	984.0	**10.0**
Hg	ppm	0.3	0.1	0.6	6.6
Sb	ppm	4.1	1.4	12.6	9.0
Te	ppm	2.0	0.7	9.3	**13.2**
Mo	ppm	5.9	2.4	11.0	4.6
Bi	ppm	5.4	1.9	12.7	6.8
Al	%	2.0	1.4	3.1	2.2
Ba	ppm	347.5	50.0	560.0	**11.2**
Ca	%	0.3	0.1	0.7	**14.2**
Cd	ppm	0.7	0.1	2.2	**27.0**
Co	ppm	8.2	1.6	15.2	9.5
Cr	ppm	14.3	4.0	28.0	7.0
Fe	%	5.8	4.4	8.9	2.0
K	%	0.5	0.3	0.9	3.0
Mg	%	0.6	0.3	1.1	3.5
Mn	ppm	1038.4	220.0	2860.0	**13.0**
Na	%	0.1	0.1	0.3	5.0
Ni	ppm	8.9	1.0	19.0	**19.0**
P	ppm	907.2	620.0	1210.0	2.0
S	%	1.0	0.5	2.5	4.9
Se	ppm	3.9	2.0	10.0	5.0
Sr	ppm	122.7	67.0	241.0	3.6
U	ppm	907.2	620.0	1210.0	2.0
V	ppm	47.5	32.0	64.0	2.0
W	ppm	0.3	0.1	1.1	**22.0**
Zn	ppm	193.9	48.0	468.0	9.8
-4+2mm	%	23.6	2.4	59.0	
-2mm+850μm	%	18.3	8.5	29.0	
-850+425μm	%	15.2	6.9	26.3	
-425+212μm	%	16.5	7.8	30.3	
-212+106μm	%	10.8	3.9	24.1	
-106+53μm	%	4.9	1.1	12.6	
-53μm	%	10.8	2.7	27.9	

Table 4.6. Correlation coefficients with -53μm gold for selected elements of Lama talus fines samples (df = 30, r significant at >0.349 at P= 0.05). Significant values in **bold**.

	r
Cu	-0.24
Ag	**0.92**
As	**0.84**
Pb	**0.67**
Hg	-0.04
Sb	**0.64**
Te	**0.76**
Mo	-0.10
Bi	**0.84**
Al	**-0.70**
Ba	**-0.37**
Cd	-0.22
Ca	**-0.62**
Cr	**-0.56**
Co	**-0.73**
Fe	**0.61**
Mg	**-0.46**
Mn	**-0.50**
Ni	**-0.65**
Na	**0.67**
P	**-0.45**
K	**0.56**
Sc	**-0.51**
Se	**0.72**
Sr	**0.44**
S	**0.73**
U	**-0.59**
V	**-0.39**
W	**0.70**
Zn	**-0.42**

Figure 4.8. Distribution of coarse and fine material at Lama in talus fines.

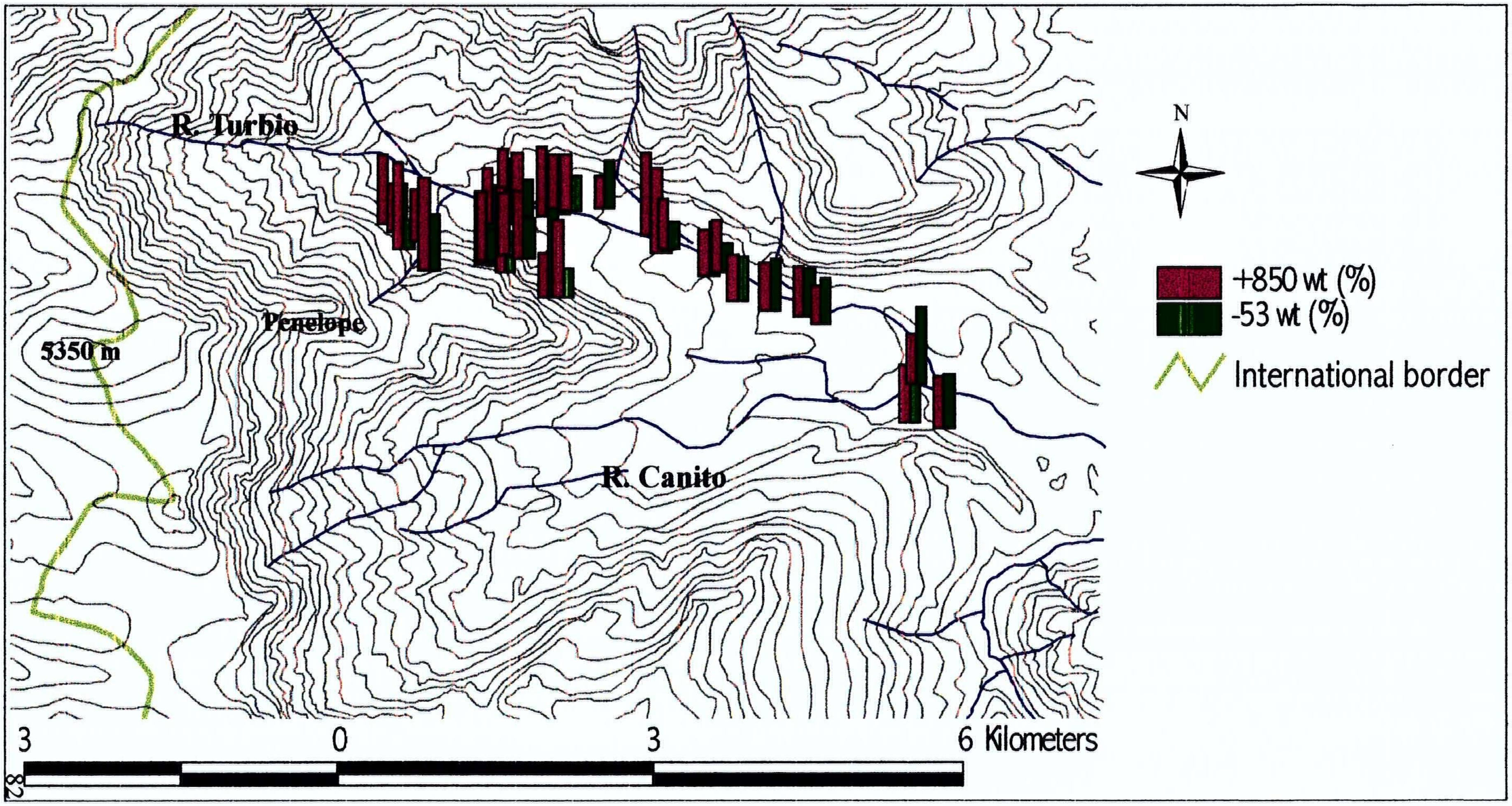

Figure 4.9. Gold in -53μm fraction of talus fines at Lama.

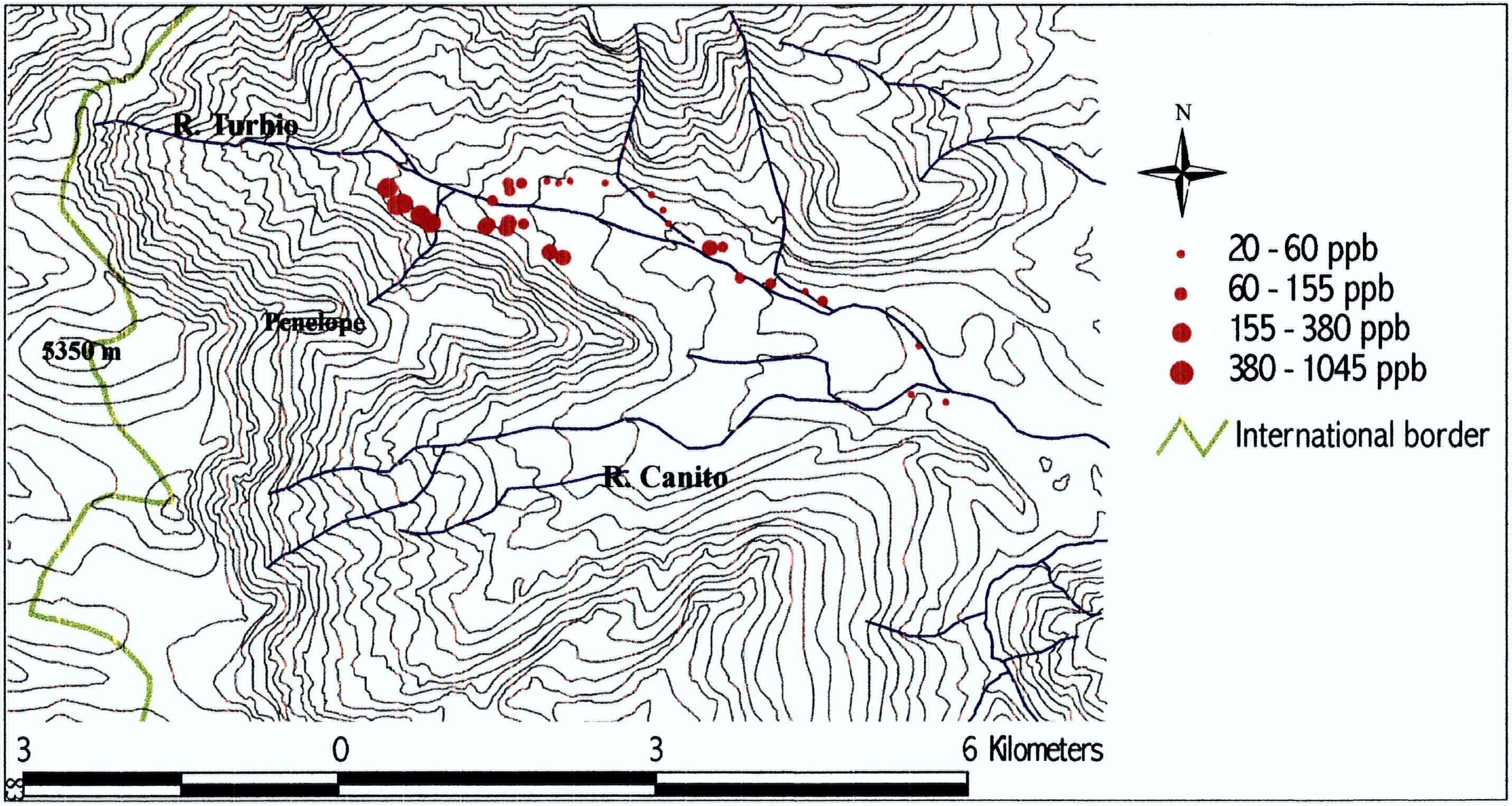

Figure 4.10. Silver concentrations in talus fines at Lama.

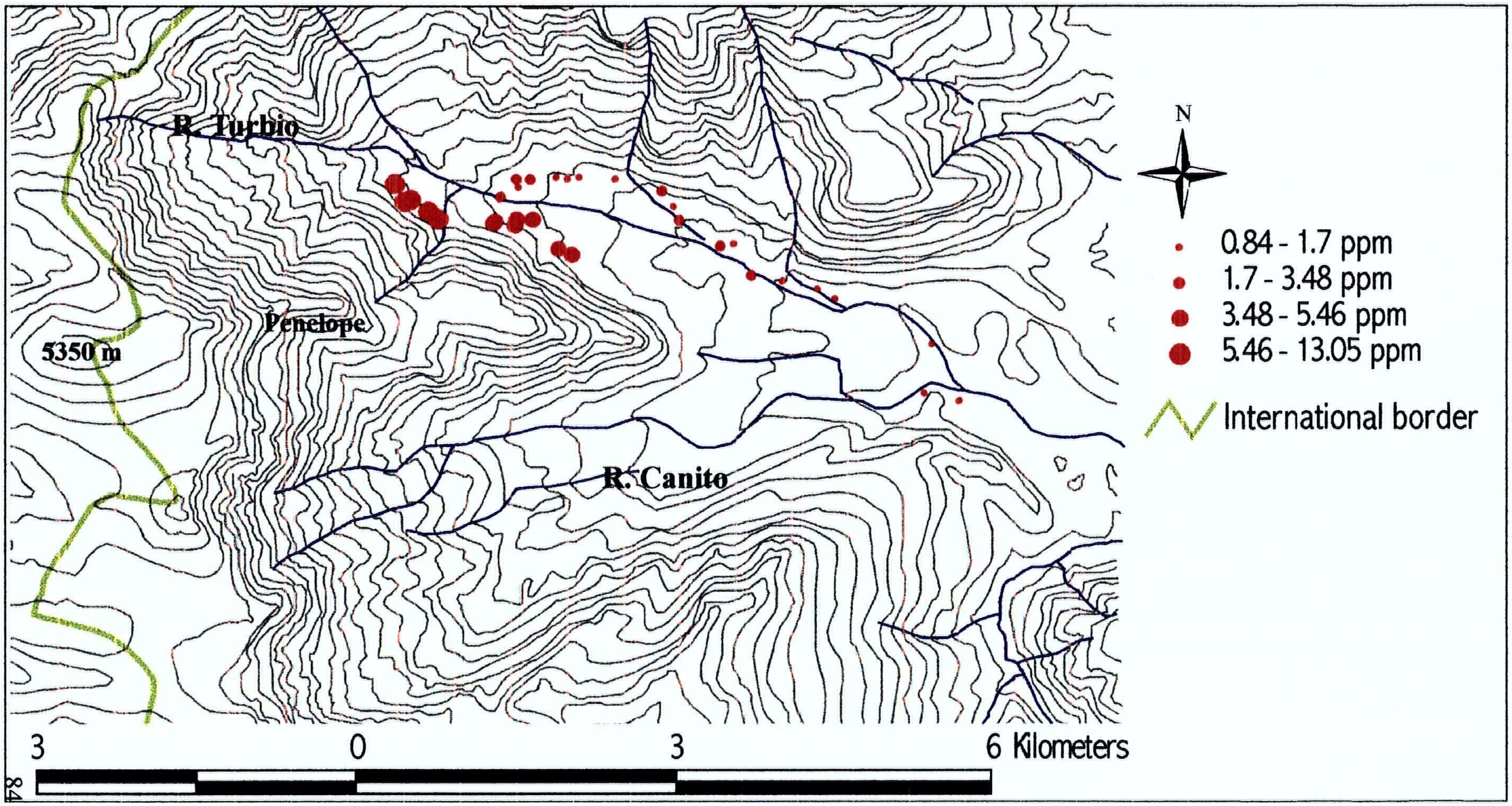

Figure 4.11. Zinc concentrations in talus fines at Lama.

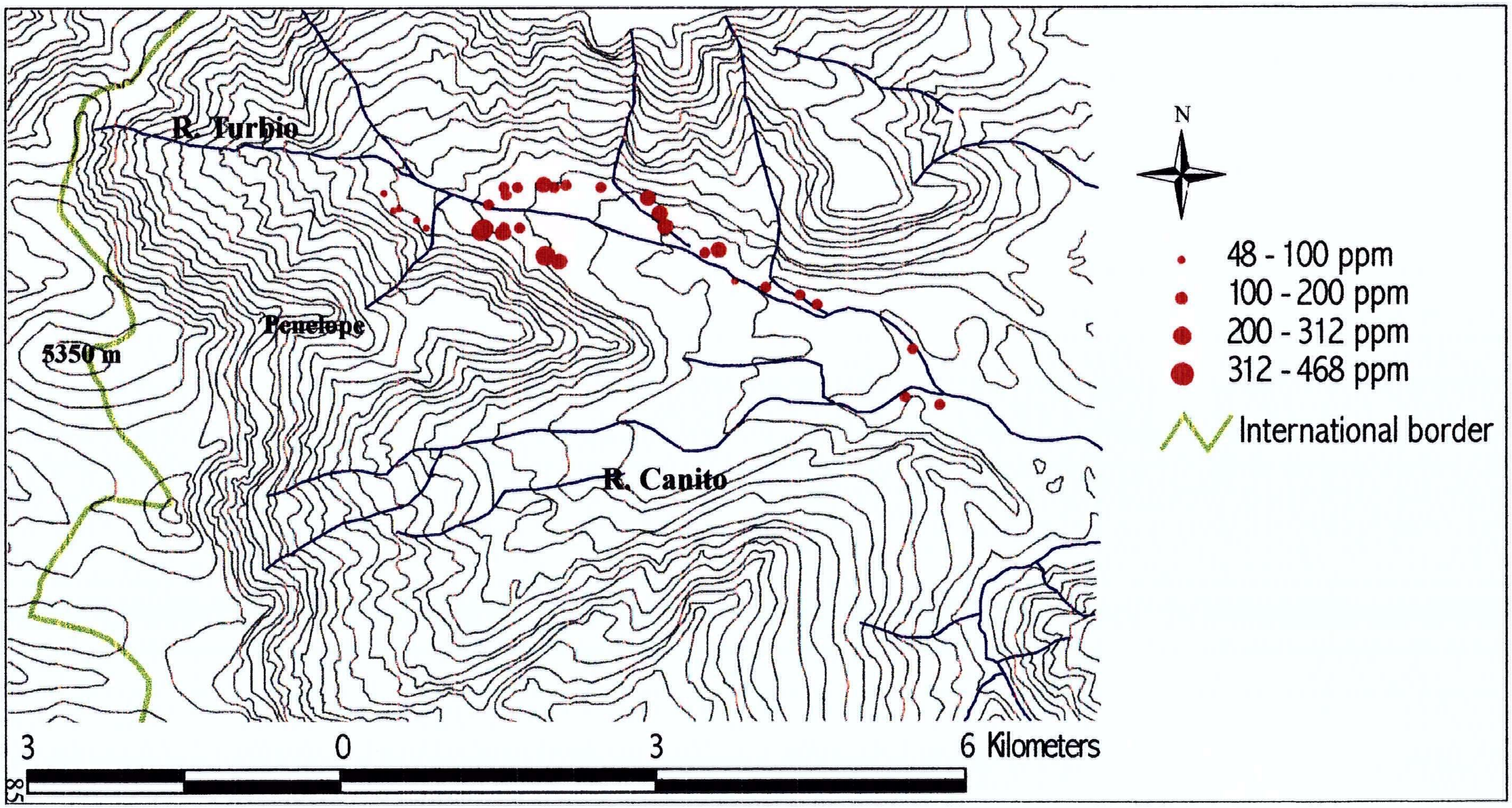

Figure 4.12. Selenium concentrations in talus fines at Lama.

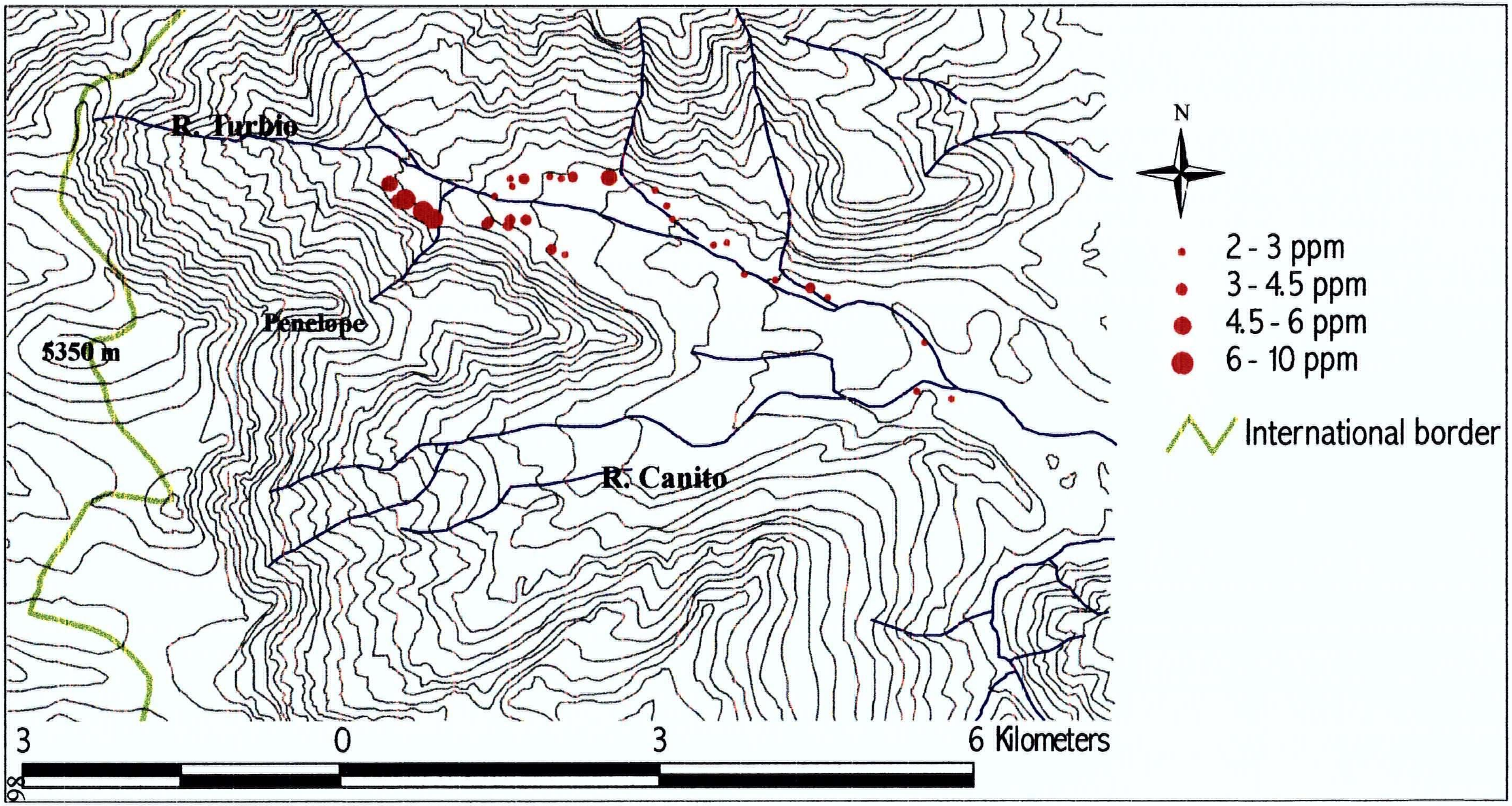

fraction. (Figure 4.9). Antimony, As, Bi, Pb, Ag, Te, Se, Na, Sr, S, Fe and W are significantly correlated with gold (Table 4.6).

Multi- element geochemistry shows maximum Sb, As, Bi, Pb, Ag, Te and W concentrations corresponding to areas of high gold (e.g. Ag in Figure 4.10) and correlation coefficients of at least 0.64. Cadmium, Cr, Co, Cu, Mg, Mn, Ni, P, U, V, Zn and Ca show both very low values corresponding to high gold concentrations (e.g. Zn in Figure 4.11) and negative correlations to Au. Se and Tl also have high concentrations in the west decreasing downstream (e.g. Se in Figure 4.12). Ba, Hg, Sr and Be do not have any coherent patterns with relation to Au. Boron, Ga, Ge and Sc are at or below their detection limits and Al, Fe, K, P, U and V have maximum to minimum ratios of less than three. Talus cones close to mineralization at Penelope ridge are acidic, while cones on the northern valley sides are of neutral pH. The average pH is 4.9, ranging from 3.5-7.2. The most acidic talus cones are found at the R. Turbio headwaters. Talus cones along the northern edge of the valley tend to be more neutral and have greater concentrations of elements with negative correlations with gold.

4.1.4 Alluvial fans

Alluvial fans were sampled only at Lama. Twenty-five samples were taken along the northern and southern edges of the R. Turbio valley. Alluvial fans are distinguished from talus cones by being composed of water deposited material and are generally more developed with further lateral extent onto the valley floor relative to talus cones (Chapter 2).

4.1.4.1 Texture and geochemistry

While no single size fraction dominates alluvial fans, there is more –4mm+2mm and –2mm+850μm material than is found in the sum of the remaining fractions (Table 4.7). As with talus fines, alluvial fans become finer with increasing distance eastward (Figure 4.13). On average, the -212μm material accounts for 24% of the samples, with 46% of the –212 μm comprised of the -53μm fraction.

The same geochemical patterns are developed in alluvial fans as in talus fines. Highest gold concentrations (maximum 1050 ppb) are found in the -53μm (Table 4.7), where it has significant positive correlation ($r > 0.60$) with Sb, As, Bi, Pb, Ag, Te, Mo, S, Se and W and strong negative correlations with Al, Ca, Cr, Co, Cu, Fe, Mg, Mn, Ni, P, Sc, U, V and Zn (Table 4.8). There is a spatial dependence of gold concentration, with fans from the southwest margin of the R. Turbio basin showing the highest concentrations of gold below Penelope ridge (840-1050 ppb) (Figure 4.14). Alluvial fans to the northeast, furthest from mineralization, range from 10-15 ppb gold.

As with gold, the concentration of other elements is a function of location (e.g. Sb in Figure 4.15). Ten elements either are at detection limits (B and Ge), or have maximum to minimum ratios less than three (Ga, Fe, K, S and La) and tend not to have strongly developed distribution patterns (Ba, Sr and Ti). The remaining elements are classed into three categories: (1) elements with high values associated with high gold concentrations; (2) elements with high values associated with low gold concentrations; and, (3) elements with high values in the west decreasing to the east. The first group of elements (As, Sb, Bi, Pb, Mo, S, Ag, Te and W) show maximum values in alluvial fans below Penelope Ridge and the western extreme of the R. Turbio

Table 4.7. Descriptive statistics of alluvial fans after aqua regia digestion (n=25). Maximum/minimum ratios greater than ten are in bold. Elements of the high sulfidation geochemical suite (Hedenquist et.al., 1996) are grouped together. Median values reported for gold.

Element	Units	Mean	Minimum	Maximum	Max/Min
Au (-212+106μm)	ppb	10.0	5.0	150.0	**30.0**
Au (-106+53μm)	ppb	10.0	5.0	190.0	**38.0**
Au (-53μm)	ppb	45.0	10.0	1050.0	**105.0**
pH		6.5	4.5	8.0	1.8
Cu	ppm	150.9	67.3	309.0	4.6
Ag	ppm	2.1	0.3	7.1	**22.1**
As	ppm	297.4	22.6	746.0	**33.0**
Pb	ppm	308.8	18.0	1115.0	**61.9**
Hg	ppm	0.3	0.0	0.9	**89.0**
Sb	ppm	4.1	0.4	16.4	**41.0**
Te	ppm	1.5	0.2	3.8	**18.8**
Mo	ppm	16.7	2.0	54.7	**27.4**
Bi	ppm	4.7	0.5	12.5	**23.5**
Al	%	1.5	0.5	2.1	4.0
Ba	ppm	307.2	140.0	550.0	3.9
Ca	%	0.2	0.0	0.5	**11.5**
Cd	ppm	0.5	0.1	2.0	**14.0**
Co	ppm	7.0	0.8	13.0	**16.3**
Cr	ppm	12.7	4.0	23.0	5.8
Fe	%	4.8	2.6	5.8	2.2
K	%	0.5	0.3	0.8	2.2
Mg	%	0.5	0.1	0.9	6.8
Mn	ppm	867.2	95.0	3110.0	**32.7**
Na	%	0.1	0.0	0.2	4.0
Ni	ppm	8.0	1.0	14.0	14.0
P	ppm	741.2	260.0	1020.0	3.9
S	%	0.9	0.6	1.7	2.9
Se	ppm	4.3	0.5	9.0	**18.0**
Sr	ppm	82.5	38.0	162.0	4.3
U	ppm	1.5	0.3	3.7	**14.8**
V	ppm	37.6	14.0	63.0	4.5
W	ppm	0.3	0.1	1.8	**35.0**
Zn	ppm	166.7	26.0	486.0	**18.7**
-4+2mm	%	32.1	8.2	54.7	
-2mm+850μm	%	20.3	6.0	28.6	
-850+425μm	%	12.6	4.1	16.7	
-425+212μm	%	11.3	3.3	19.4	
-212+106μm	%	7.9	1.1	16.8	
-106+53μm	%	4.8	0.5	20.5	
-53μm	%	11.0	1.0	39.5	

Table 4.8. Correlation coefficients with -53μm gold for selected elements of Lama alluvial fan samples (df = 23, r significant at >0.396 at P= 0.05). Significant values in **bold.**

	r
Cu	**-0.41**
Ag	**0.81**
As	**0.91**
Pb	**0.97**
Hg	0.18
Sb	**0.96**
Te	**0.82**
Mo	**0.80**
Bi	**0.89**
Al	**-0.69**
Ba	-0.20
Cd	-0.39
Ca	**-0.76**
Cr	**-0.60**
Co	**-0.81**
Fe	**-0.54**
Mg	**-0.64**
Mn	**-0.45**
Ni	**-0.79**
P	**-0.79**
K	-0.13
Sc	**-0.86**
Se	**0.68**
Na	0.29
Sr	0.15
S	**0.46**
Tl	0.03
Ti	0.07
W	**0.97**
U	**-0.57**
V	**-0.61**
Zn	**-0.48**

Figure 4.13. Distribution of coarse and fine material at Lama in alluvial fan.

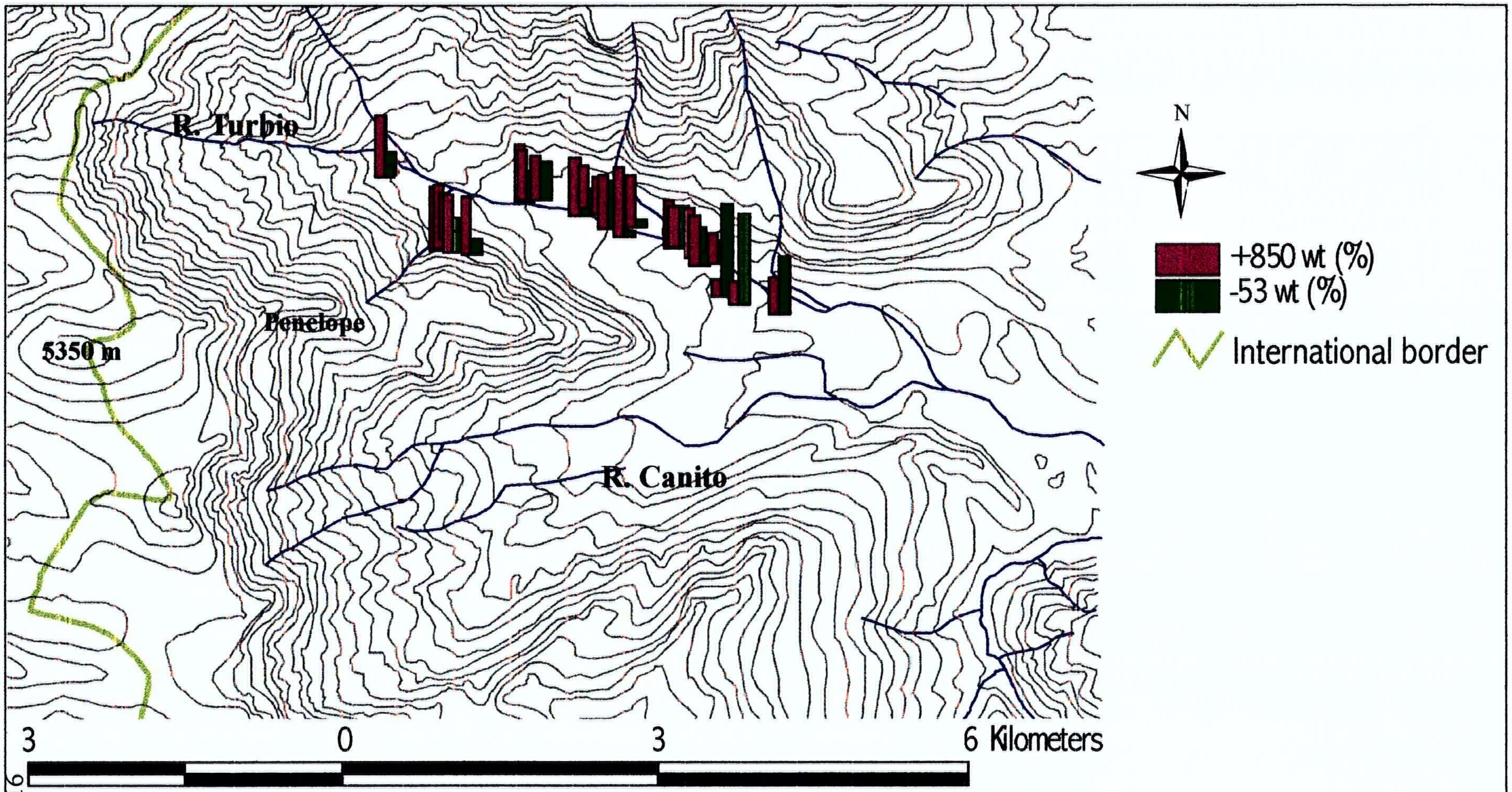

Figure 4.14. Gold in -53μm fraction of alluvial fans at Lama.

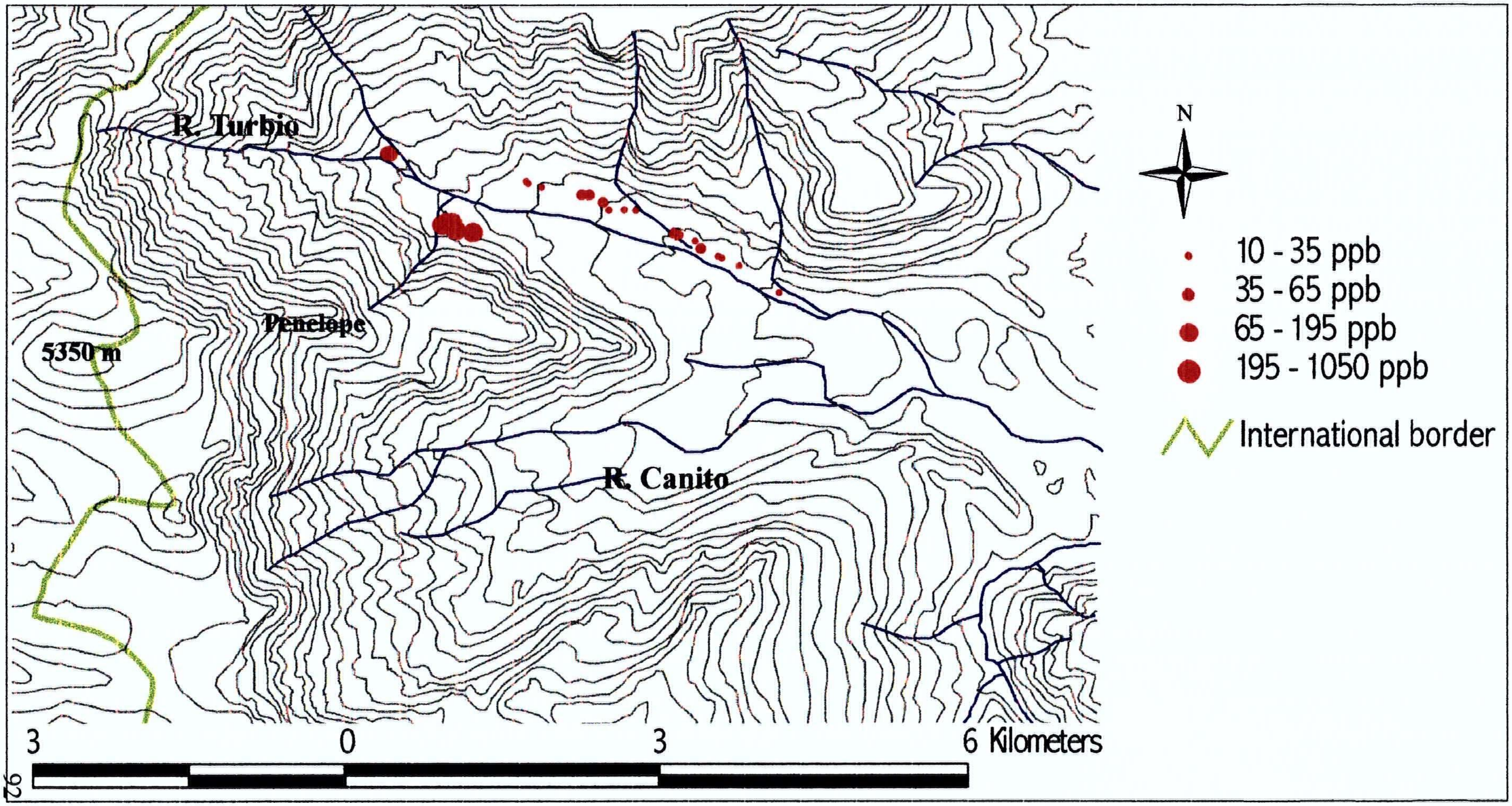

Figure 4.15. Antimony concentrations in alluvial fans at Lama.

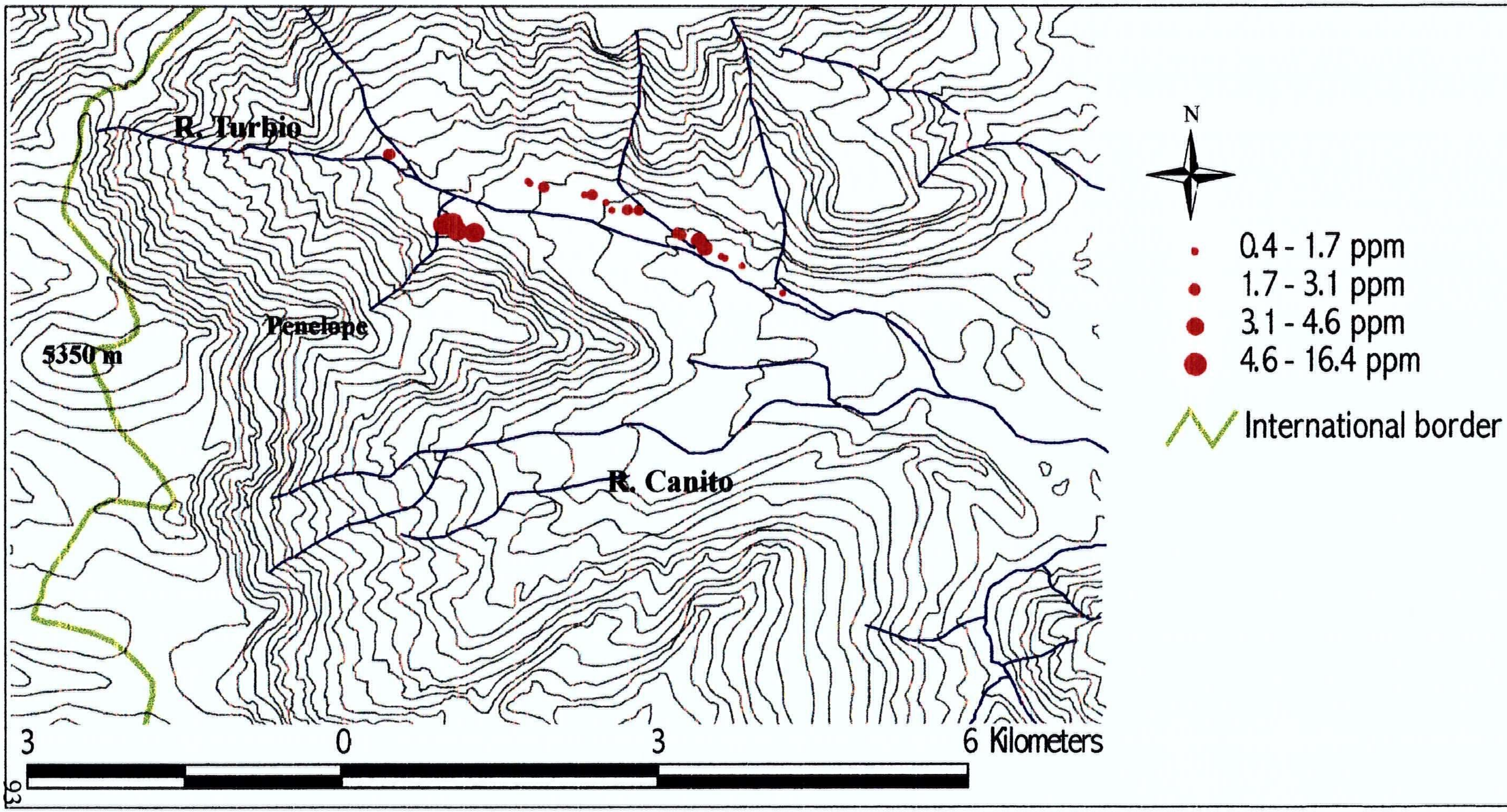

Figure 4.16. Silver concentrations in alluvial fans at Lama.

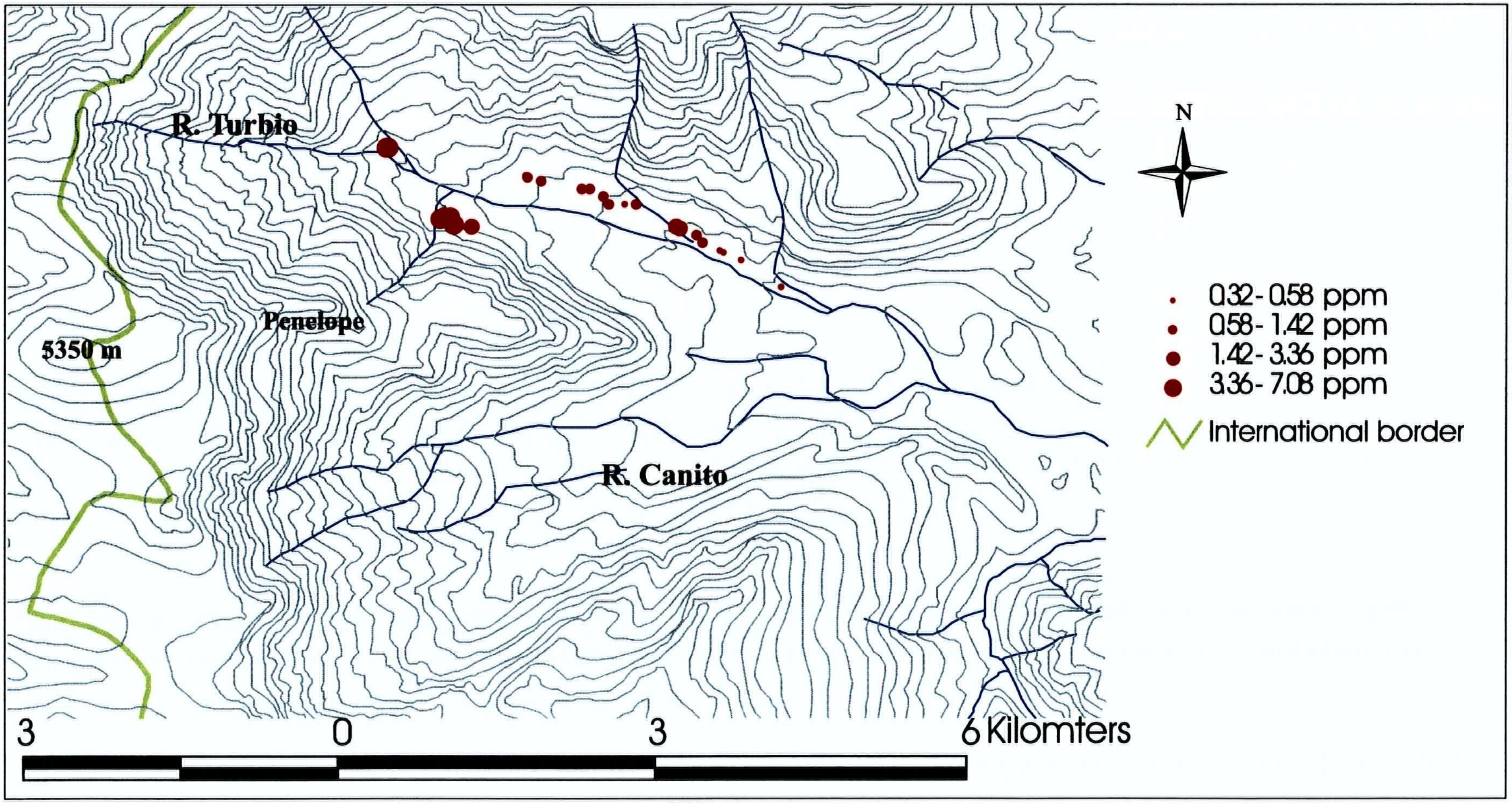

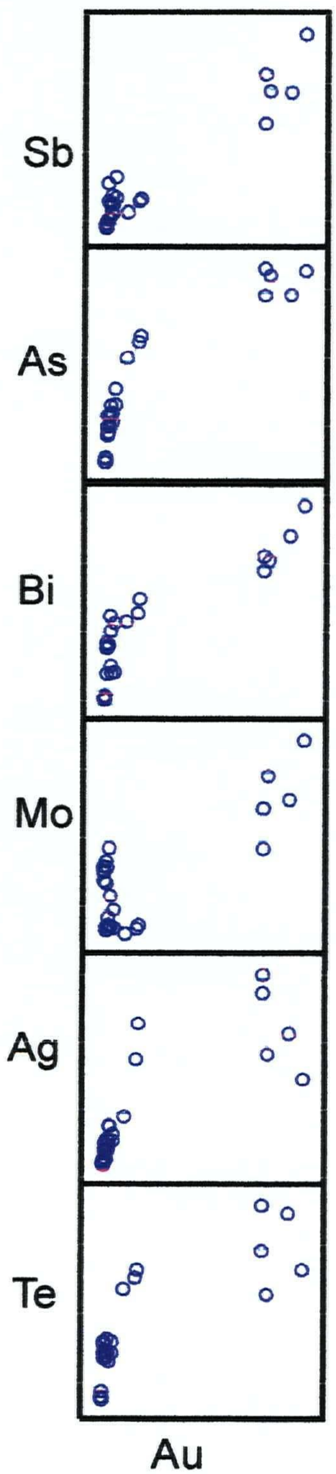

Figure 4.17. X-Y scatter plots of selected elements with -53mm Au in alluvial fans at Lama.

Figure 4.18. Selenium concentrations in alluvial fans at Lama.

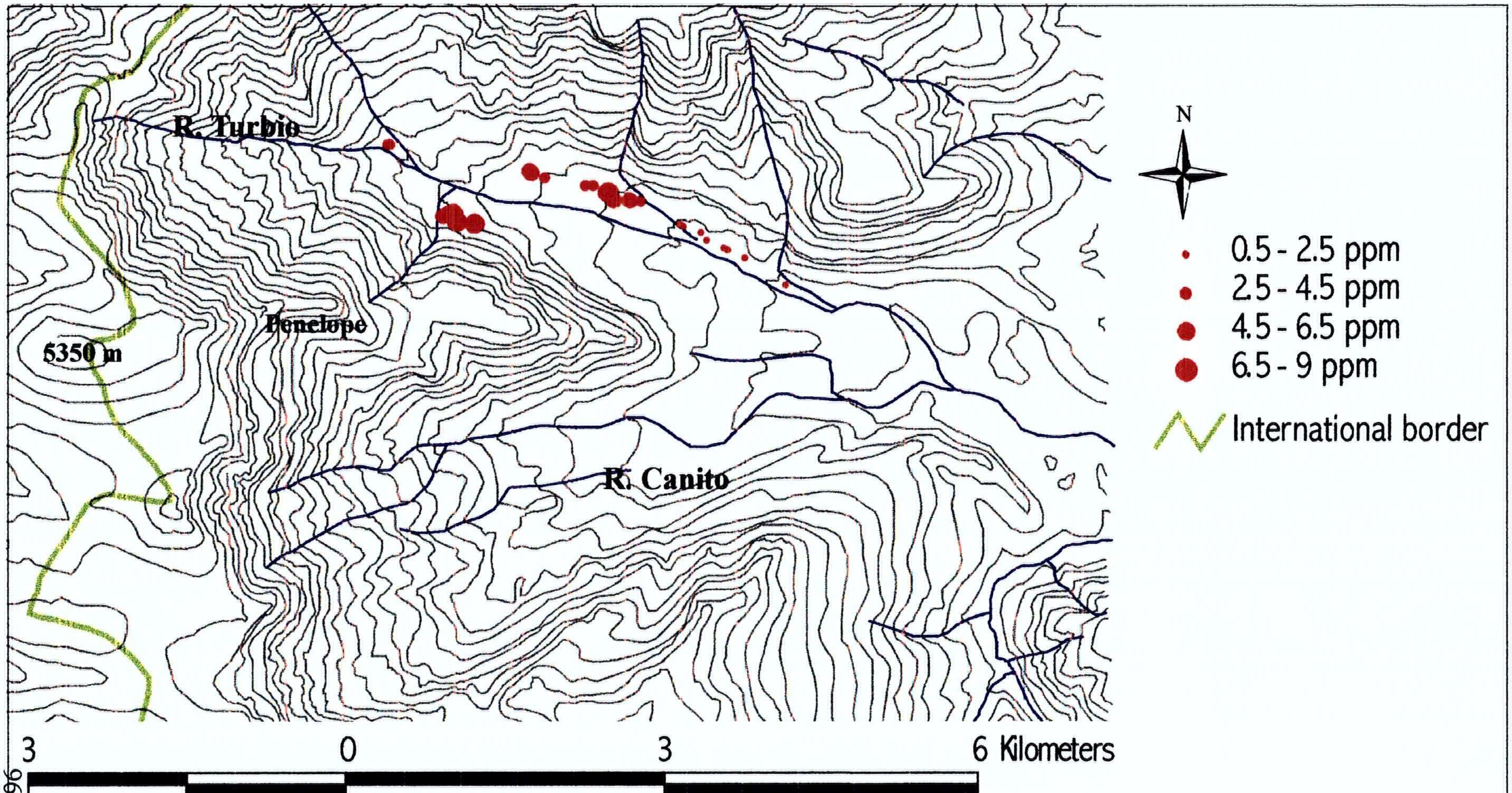

basin and lower concentrations at the northern margin (e.g. Sb in Figure 4.15 and Ag in Figure 4.16). This group of elements are strongly inter-correlated and have high positive correlation with Au (Table 4.8, Figure 4.17). Group 2 contains elements with concentrations that are inversely related to gold (Al, Cr, Co, Cu, Ca, Fe, Mg, Mn, Ni, P, Sc, U, V and Zn, Table 4.8). Se and Tl comprise the final group with high concentrations near the headwaters of the R. Turbio that decrease downstream (e.g. Se in Figure 4.18). Although Hg has considerable contrast (max/min = 89.0), it is only weakly correlated with Au (r = 0.18) and gold-associated elements. In general, Hg concentrations are higher in alluvial fans originating from Penelope Ridge and in the upper stretches of the R. Turbio valley. Alluvial fans have an almost neutral pH of 6.5, ranging from 4.5-8.0, with fans near Penelope Ridge and R. Turbio headwaters generally being more acidic than distal fans.

4.1.5 Comparison of surficial materials

Glacial till has the greatest quantity of -212μm material (average 30.6%) and debris flows the least (average 19.4%). Comparison of mean values for each surficial media shows glacial till has lower values than talus fines, alluvial fans or debris flows for 13 elements (Cu, Ag, As, Pb, Hg, Sb, Te, Bi, Tl, Fe, K, Se and S) (Table 4.9). Of these, elements that are generally associated with Au (As, Bi, Fe, Ag, S, Te, Hg and Mo) are significantly less abundant in glacial till than in one or more of the other three surficial deposits (Table 4.9) as determined by the Bonferroni adjustment. Concentrations of Au, As, Bi, Hg, Ag and V are the greatest in debris flows, but these have the lowest average concentrations for Cd, Cr, Co, Mn, Ni, P, Zn and Mo. Glacial till is the least acidic of surficial materials at Lama having an average pH of 8.2 versus debris flows which are the most acidic, with an average pH of 4.1 (Figure 4.19).

Table 4.9. Comparison of mean (median for Au) concentrations for surficial samples at Lama. Elements of the high sulfidation geochemical suite (Hedenquist et.al., 1996) are grouped together. Significant differences in mean values between deposits are shown in bold (e.g. for Hg: D Δ all means debris flows are significantly different than all other deposits). G = glacial till, D = debris flows, T= talus cones, A= alluvial fans.

Element	**Units**	**Glacial till** (n=18)	**Debris flows** (n=28)	**Talus fines** (n=32)	**Alluvial fans** (n=25)	**Significant difference (Bonferroni adjustment)**
Au (-212+106μm)	ppb	17.5	30.0	20.0	10.0	
Au (-106+53μm)	ppb	17.5	72.9	45.0	10.0	
Au (-53μm)	ppb	**85.0**	252.5	95.0	45.0	G Δ all
pH		8.2	4.1	4.9	6.5	
Cu	ppm	138.2	150.3	152.1	150.9	
Ag	ppm	1.8	**5.6**	**3.9**	2.1	D Δ all, T Δ all
As	ppm	**220.6**	386.4	375.8	**297.4**	G, A, Δ D, T
Pb	ppm	206.7	289.2	348.8	308.8	
Hg	ppm	0.2	**1.0**	0.3	0.3	D Δ all
Sb	ppm	3.2	3.9	4.1	4.1	
Te	ppm	**1.0**	1.8	2.0	1.5	G Δ T
Mo	ppm	5.8	5.7	5.9	**16.7**	A Δ all
Bi	ppm	**3.5**	6.5	5.4	4.7	G Δ D, T
Al	%	1.5	1.6	2.0	1.5	
Ba	ppm	337.2	337.6	347.5	307.2	
Cd	%	0.6	**0.4**	0.7	0.5	D Δ all
Ca	ppm	0.4	**0.2**	0.3	0.2	D Δ all
Cr	ppm	13.8	11.6	14.3	12.7	
Co	ppm	7.6	6.5	8.2	7.0	
Fe	%	4.4	**6.1**	**5.8**	4.8	D Δ all. T Δ all
Mg	%	0.5	0.5	0.6	0.5	
Mn	%	814.7	698.9	1038.4	867.2	
Ni	ppm	8.4	**6.4**	8.9	8.0	D Δ T
P	%	816.7	718.2	907.2	741.2	
K	%	0.4	0.5	0.5	0.5	
Se	ppm	2.6	3.7	3.9	4.3	
Na	%	0.1	0.1	0.1	0.1	
Sr	ppm	94.2	86.8	122.7	82.5	
S	ppm	**0.7**	1.0	1.0	0.9	G Δ D. T
Tl	ppm	1.2	2.3	2.3	2.2	
W	ppm	0.2	0.3	0.3	0.3	
V	ppm	44.6	49.3	47.5	37.6	
Zn	ppm	170.2	**144.4**	193.9	166.7	D Δ T
-4+2mm	%	21.4	25.5	23.6	**32.1**	A Δ T,G
-2mm+850μm	%	16.5	18.8	18.3	20.3	
-850+425μm	%	13.7	18.8	15.2	12.6	
-425+212μm	%	17.9	17.4	16.5	11.3	
-212+106μm	%	11.2	8.9	10.8	7.9	
-106+53μm	%	5.9	4.2	4.9	4.8	
-53μm	%	**13.5**	6.3	10.8	11.0	G Δ D

Table 4.10. Correlation coefficents for gold in surficial materials at Lama. Significant positive values in red, significant negative values in blue. Glacial till n = 18, r_{sign} >0.468; debris flows n = 28, r_{sign} >0.374; talus fines n = 32, r_{sign} >0.349; alluvial fans n = 25, r_{sign}>0.396 at P = 0.05.

	Glacial till	Debris flows	Talus cones	Alluvial fans
Cu	0.36	-0.25	-0.24	**-0.41**
Ag	**0.76**	**0.82**	**0.92**	**0.81**
As	**0.63**	**0.60**	**0.84**	**0.91**
Pb	0.17	-0.30	**0.67**	**0.97**
Hg	0.22	0.18	-0.04	0.18
Sb	**0.71**	**0.54**	**0.64**	**0.96**
Te	**0.69**	**0.74**	**0.76**	**0.82**
Mo	0.03	**0.52**	-0.10	**0.80**
Bi	**0.74**	**0.77**	**0.84**	**0.89**
Al	**0.46**	-0.06	**-0.70**	**-0.69**
Ba	0.45	-0.09	**-0.37**	-0.20
Cd	**0.77**	-0.16	-0.22	-0.39
Ca	0.17	**-0.40**	**-0.62**	**-0.76**
Cr	0.10	-0.31	**-0.56**	**-0.60**
Co	-0.08	**-0.42**	**-0.73**	**-0.81**
Fe	**0.49**	-0.22	**0.61**	**-0.54**
K	**0.49**	**0.49**	**0.56**	-0.13
Mg	0.34	0.17	**-0.46**	**-0.64**
Mn	-0.17	**-0.38**	**-0.50**	**-0.45**
Ni	-0.02	-0.34	**-0.65**	**-0.79**
P	0.31	0.31	**-0.45**	**-0.79**
Sc	0.16	-0.32	**-0.51**	**-0.86**
Se	0.42	**0.42**	**0.72**	**0.68**
Na	0.37	**0.59**	**0.67**	0.29
Sr	0.42	0.31	**0.44**	0.15
S	0.37	0.14	**0.73**	**0.46**
U	0.20	**-0.43**	**-0.59**	**-0.57**
W	0.40	**0.72**	**0.70**	**0.97**
V	0.43	-0.28	**-0.39**	**-0.61**
Zn	**0.76**	**-0.53**	**-0.42**	**-0.48**
No. positive	10	10	13	10
No. negative	0	5	13	14

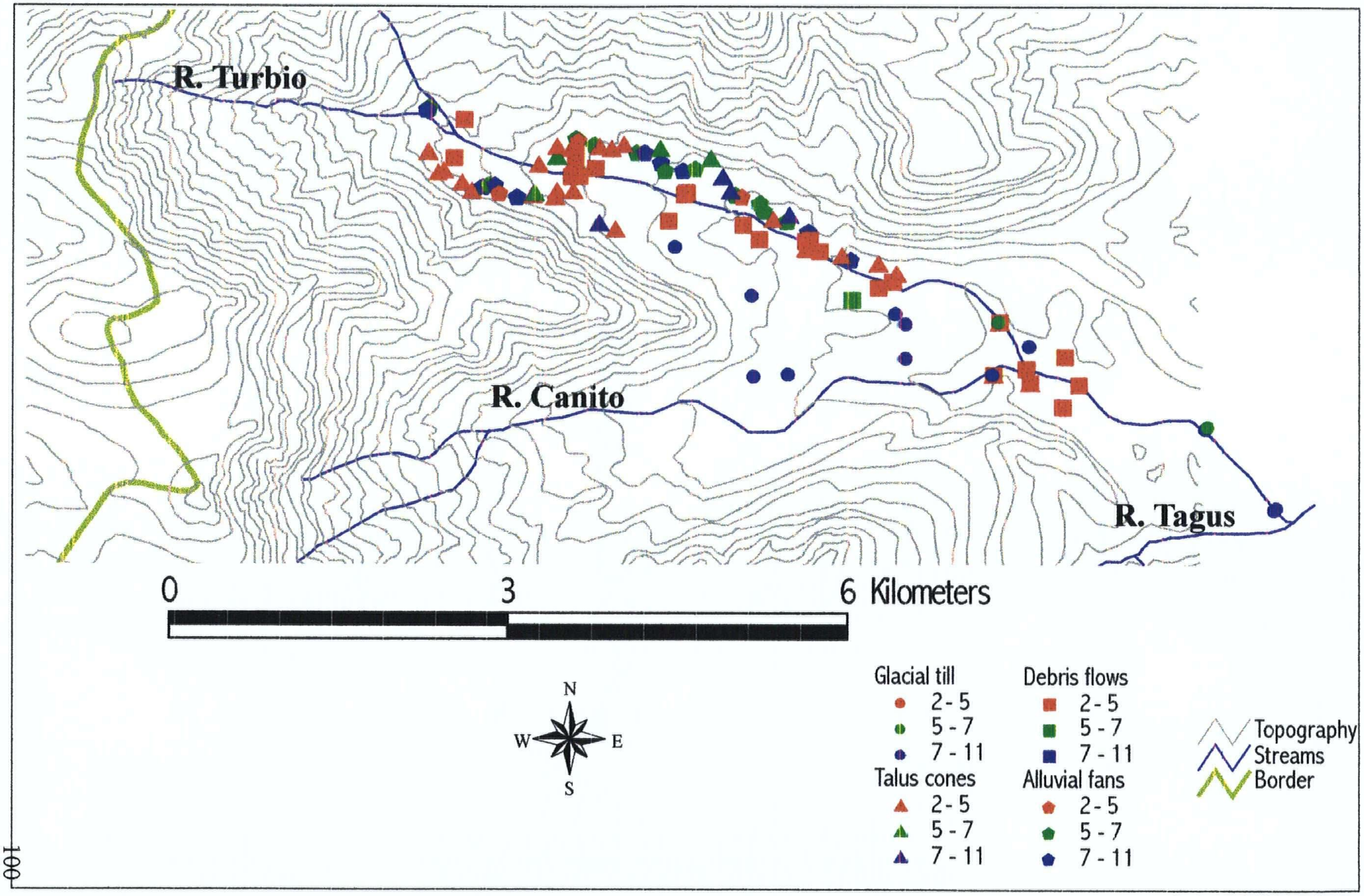

4.19. pH of surficial media at Lama.

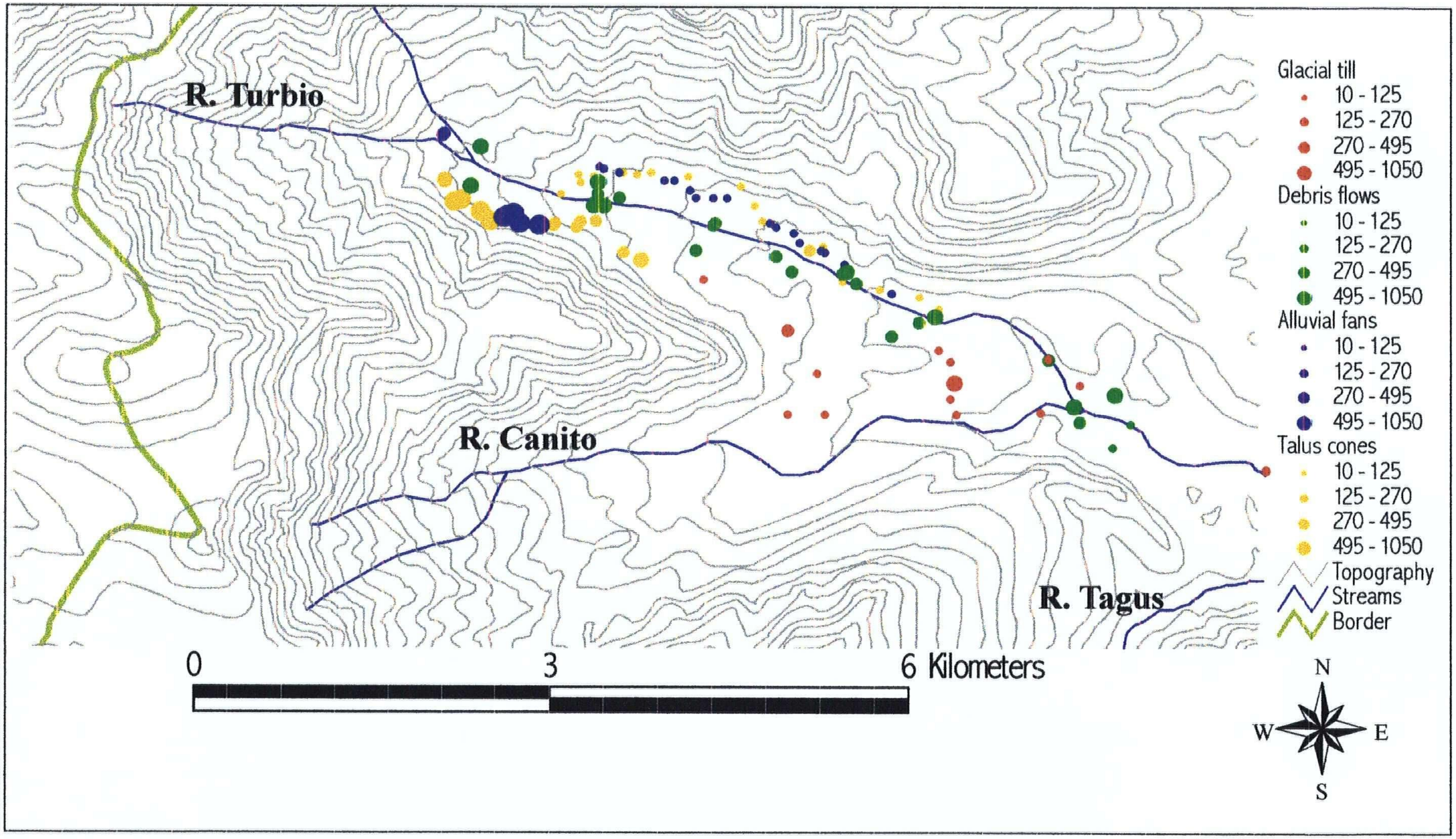

4.20. Gold concentrations (ppb) in the -53µm fraction of surficial deposits at Lama.

Silver, As, Sb, Te and Bi have positive correlation with Au in all surficial deposits (Table 4.10). Lead, Se, Na, S and W also have strong positive correlation with Au in debris flows, talus cones and glacial till. Conversely, Al, Ca, Cr, Co, Mg, Mn, Ni and Zn, in talus cones and alluvial fans have significant negative correlations with gold. The most obvious difference between element associations in the surficial media is the absence of significant negative correlations with Au in glacial till versus the presence of strong positive and negative correlations in the other media.

All surficial materials have maximum median gold concentrations in the -53μm size fraction. Overall, greatest concentrations of gold are at the headwaters of the R. Turbio and decrease downstream (Figure 4.20). Elements that tend to have a positive correlation with Au (As, Sb, Bi, Hg, Te, S, Fe, Cu, Pb and Ag) also have greater concentrations close to the deposit, decreasing downstream. Conversely, elements that generally correlate negatively with Au are found in lower concentrations at the headwaters with concentrations increasing down-valley.

4.2 Stream waters

Water samples were taken in conjunction with stream sediments at every sampling site and at precipitate seeps. Results presented here will be only for samples collected at sediments sites. Water samples taken at chemical precipitate sites are presented in Section 4.5 with precipitate mineralogy and geochemistry.

4.2.1 Elemental concentrations and pH

R. Turbio stream waters are very acidic, with pH values ranging from a minimum of 2.5 to a maximum of 5.9 below the R. Turbio-R. Tagus confluence. The concentrations of many elements in the waters have minimum/maximum ratios in excess of 10 (Table 4.11), although seven elements were at or below their detection limits of the ICP-MS (Ag, Bi, Hg, Mo, P, Se and Sn). Field sulfate measurements were all greater than 200 mg/l.

Analysis of variance (ANOVA) shows that between site variances are significant compared to within site variances on field duplicates except for Se (Table 4.12). Examination of $F/F_{critical}$ ratios shows that most elements are in excess of ten times $F_{critical}$, excepting As, Be, Mo and Se.

Rio Canito waters are neutral with an average pH of 7.5. The R. Canito has lower average concentrations of all elements except Ba. Silver, Be, Bi, Cd, Hg, P, Pb, Se, Sn, Ti, Pb and V are all at or below detection limit in this stream.

For all elements except Ba and Sb, correlations with pH are strongly negative suggesting that most elements are responsive to changes in acidity (Table 4.13). Examination of X-Y scatter plots of selected elements shows that the very high correlations seen in Table 4.13 result from pH effects in the R. Turbio and are not the results of outliers (Figure 4.21). Element concentrations are generally higher at sites with correspondingly lower pH values (e.g. Cu in Figure 4.22). Most elements above detection limits have concentrations that decrease an average of 30% below the confluence with the R. Canito and are at a minimum at Site 21 below the confluence with the R. Tagus (Figures 4.23 - 4.24 for Zn and Ni). However, concentrations of Mg, As, Sr, and Ca increase at Site 21, probably relating to high concentrations upstream in the R. Tagus relative to the R. Turbio (e.g. As in Figure 4.25).

The upper reaches of the R. Turbio have an almost constant pH resulting in essentially stable water chemistries (e.g. Cu and Zn in Figures 4.22 and 4.23). Below the confluences with the R.

Table 4.11. Descriptive statistics of stream waters (n=13). Maximum/minimum ratios greater than ten are in bold.

	R.Turbio (n=10)				
	Units	**Mean**	**Minimum**	**Maximum**	**Max/Min**
pH		2.9	2.5	3.3	1.3
Cu	µg/l	8142.0	1830.0	24000.0	**13.1**
As	µg/l	133.6	7.0	343.0	**49.0**
Pb	µg/l	3.0	<2.0	8.0	4.0
Sb	µg/l	0.1	0.1	0.5	**10.0**
Al	mg/l	132.5	34.1	330.0	**9.7**
Ba	µg/l	7.0	1.7	19.3	**11.4**
Ca	mg/l	199.9	103.0	302.0	2.9
Cd	µg/l	26.1	7.7	71.9	9.3
Co	µg/l	98.0	32.2	246.0	7.6
Cr	µg/l	11.1	2.5	30.5	**12.2**
Fe	mg/l	172.1	26.3	505.0	**19.2**
K	mg/l	5.2	3.1	10.8	3.5
Mg	mg/l	33.2	15.7	68.7	4.4
Mn	µg/l	9297.0	2980.0	22600.0	7.6
Na	mg/l	7.2	6.6	7.9	1.2
Ni	µg/l	71.6	22.4	180.5	8.1
Sr	µg/l	717.7	360.0	1545.0	4.3
V	µg/l	37.8	<1.0	120.0	**120.0**
Zn	µg/l	5641.5	1430.0	15400.0	**10.8**

	R. Canito (n=3)				
	Units	**Mean**	**Minimum**	**Maximum**	**Max/Min**
pH		7.5	7.1	8.2	1.2
Cu	µg/l	6.9	0.6	16.2	**27.0**
As	µg/l	10.7	4.0	22.0	5.5
Pb	µg/l	2.0	<2.0	<2.0	1.0
Sb	µg/l	0.3	0.2	0.4	2.0
Al	mg/l	0.2	0.02	0.3	**16.9**
Ba	µg/l	32.7	31.4	34.3	1.1
Ca	mg/l	87.9	69.0	103.0	1.5
Cd	µg/l	0.1	<0.1	<0.1	1.0
Co	µg/l	1.1	0.2	1.8	**10.2**
Cr	µg/l	0.5	<0.5	<0.5	1.0
Fe	mg/l	1.1	0.2	2.2	**10.4**
K	mg/l	1.8	1.3	2.2	1.7
Mg	mg/l	11.0	8.8	12.4	1.4
Mn	µg/l	716.7	244.0	1095.0	4.5
Na	mg/l	4.9	4.0	5.5	1.4
Ni	µg/l	1.1	<0.2	2.0	**10.0**
Sr	µg/l	148.8	114.5	180.5	1.6
V	µg/l	1.0	<1.0	<1.0	1.0
Zn	µg/l	43.7	5.0	81.0	**16.2**

Table 4.12. Summary of analysis of variance (ANOVA) performed on field duplicate for water samples. $F_{critical} = 3.02$ (n= 15).

Element	F	F/Fcrit
Cu	98.7	32.7
As	17.0	5.6
Sb	133.4	44.2
Al	99.8	33.0
Ba	1009.2	334.2
Be	20.0	6.6
Ca	17106.9	5664.5
Cd	2139.3	708.4
Co	2543.8	842.3
Fe	111.1	36.8
K	2722.8	901.6
Mg	149.0	49.3
Mn	441.0	146.0
Mo	6.1	2.0
Na	489.6	162.1
Ni	242.2	80.2
Se	0.9	0.3
Sr	55646.1	18425.9
Tl	22596.6	7482.3
U	1404.0	464.9
Zn	2488872.2	824129.9

Table 4.13. Correlation coefficients for selected elements of Lama stream water samples. df = 13, r significant at greater than 0.514 at P= 0.05. Significant values in bold.

	pH
Cu	**-0.66**
As	**-0.66**
Sb	0.39
Al	**-0.73**
Ba	**0.71**
Ca	**-0.80**
Co	**-0.74**
Cr	**-0.67**
Fe	**-0.66**
K	**-0.73**
Pb	-0.21
Mg	**-0.73**
Mn	**-0.74**
Na	**-0.84**
Ni	**-0.73**
Sr	**-0.76**
Tl	**-0.83**
U	**-0.71**
Zn	**-0.70**

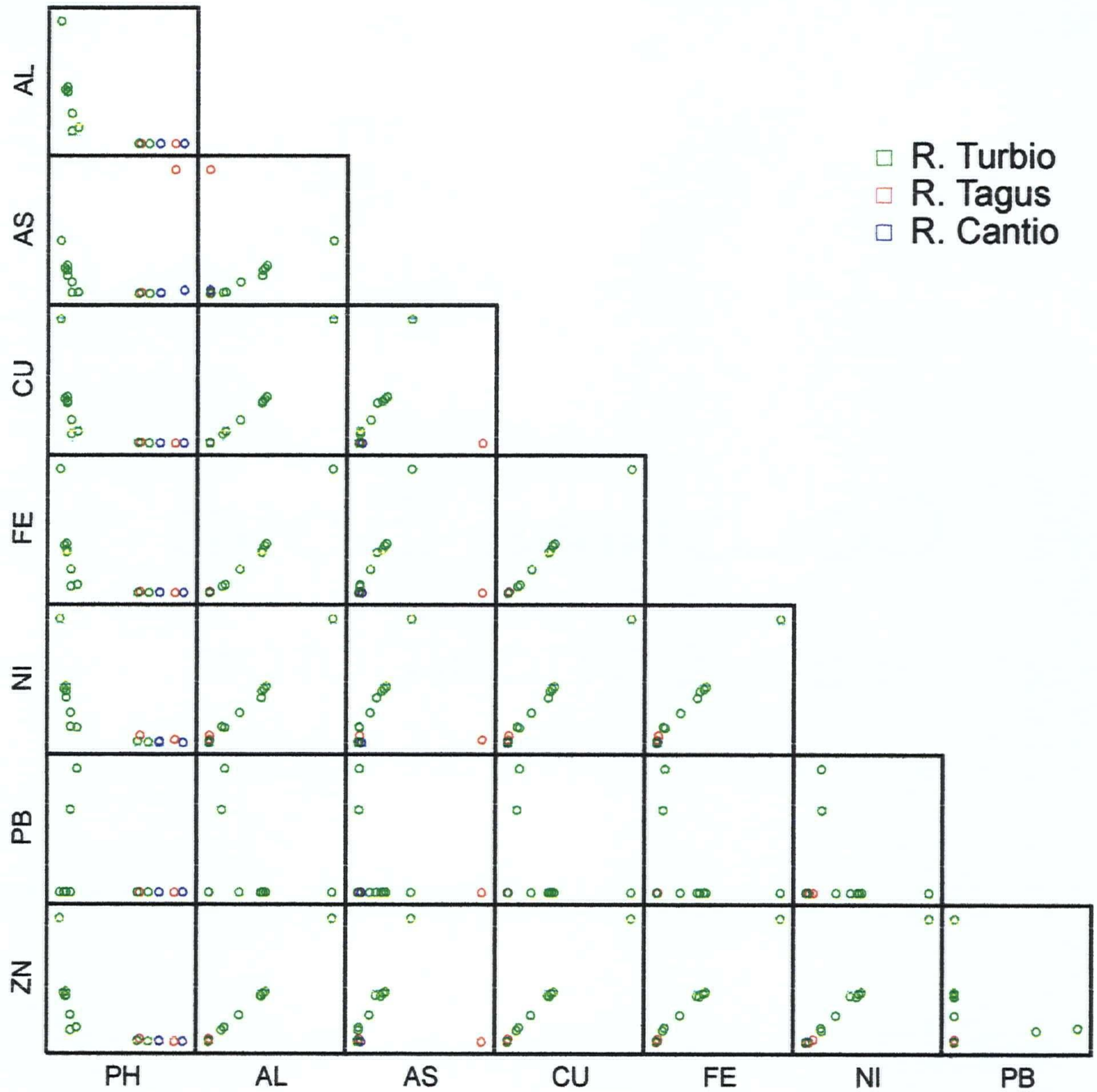

4.21. X-Y scatter plots of selected elements in stream waters at Lama.

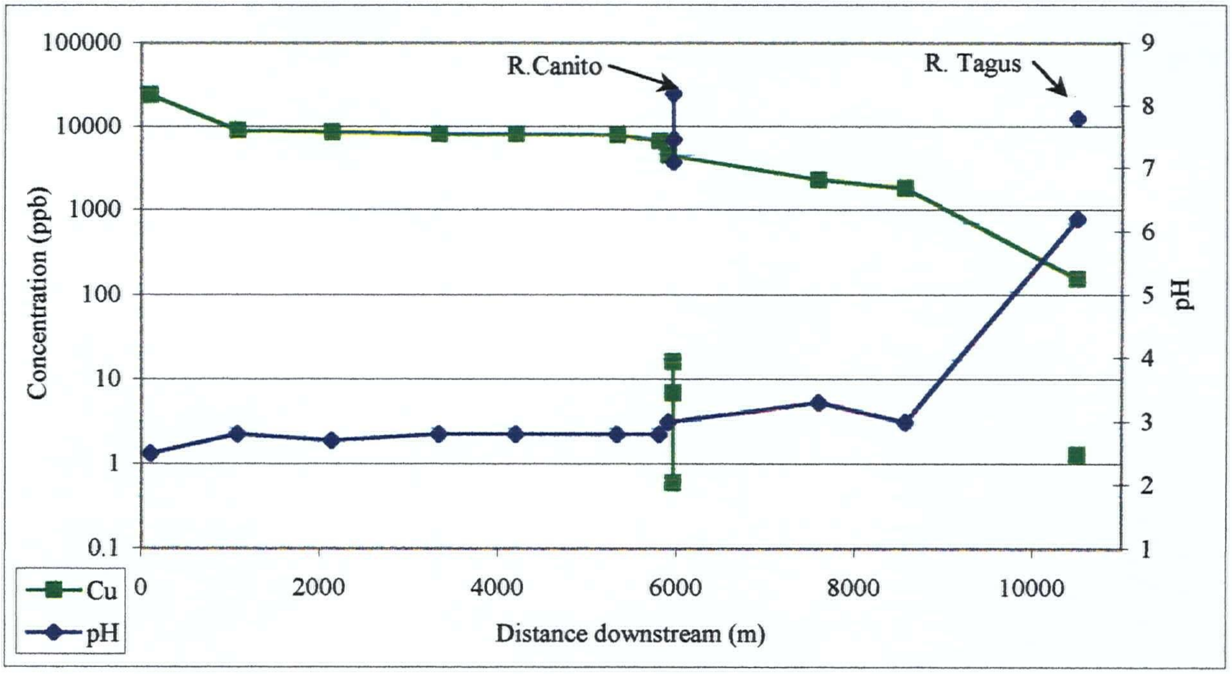

Figure 4.22. Downstream profile of Cu in stream waters. Rio Cantio data is shown as average and range at 5.9 km, Site 22 on the R. Tagus is shown as a point at 10.5 km downstream.

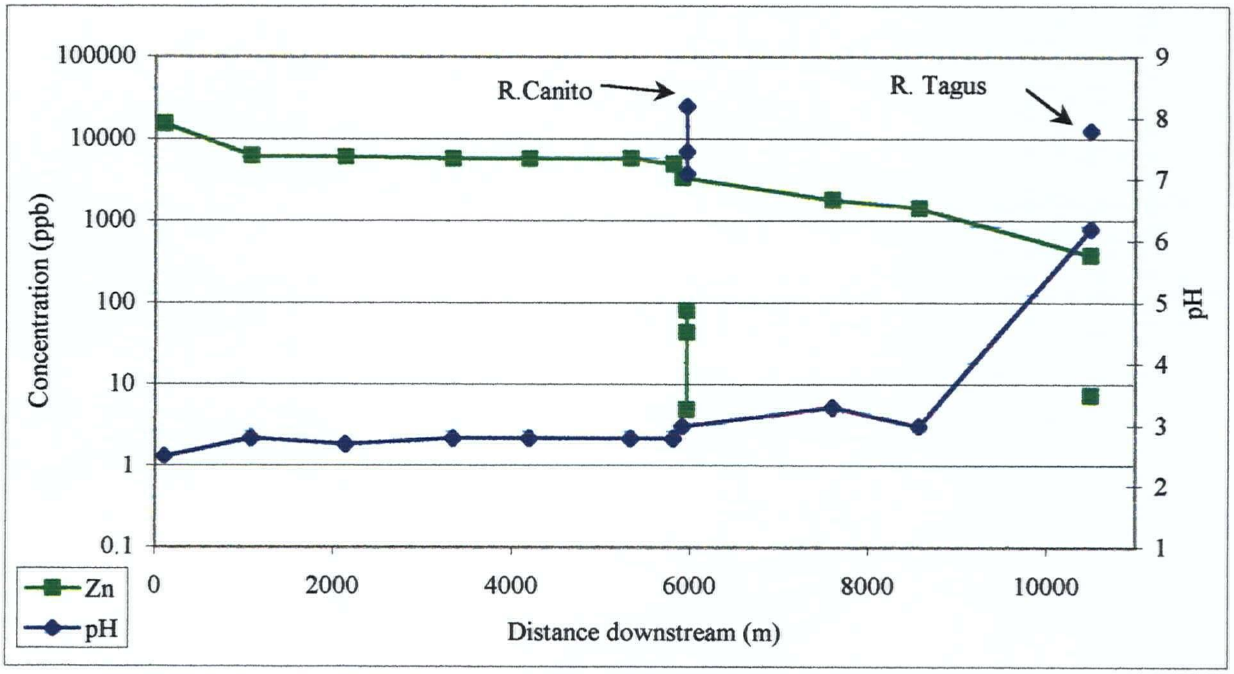

Figure 4.23. Downstream profile of Zn in stream waters. Rio Canito data is shown as average and range at 5.9 km, Site 22 on the R. Tagus is shown as a point at 10.5 km downstream.

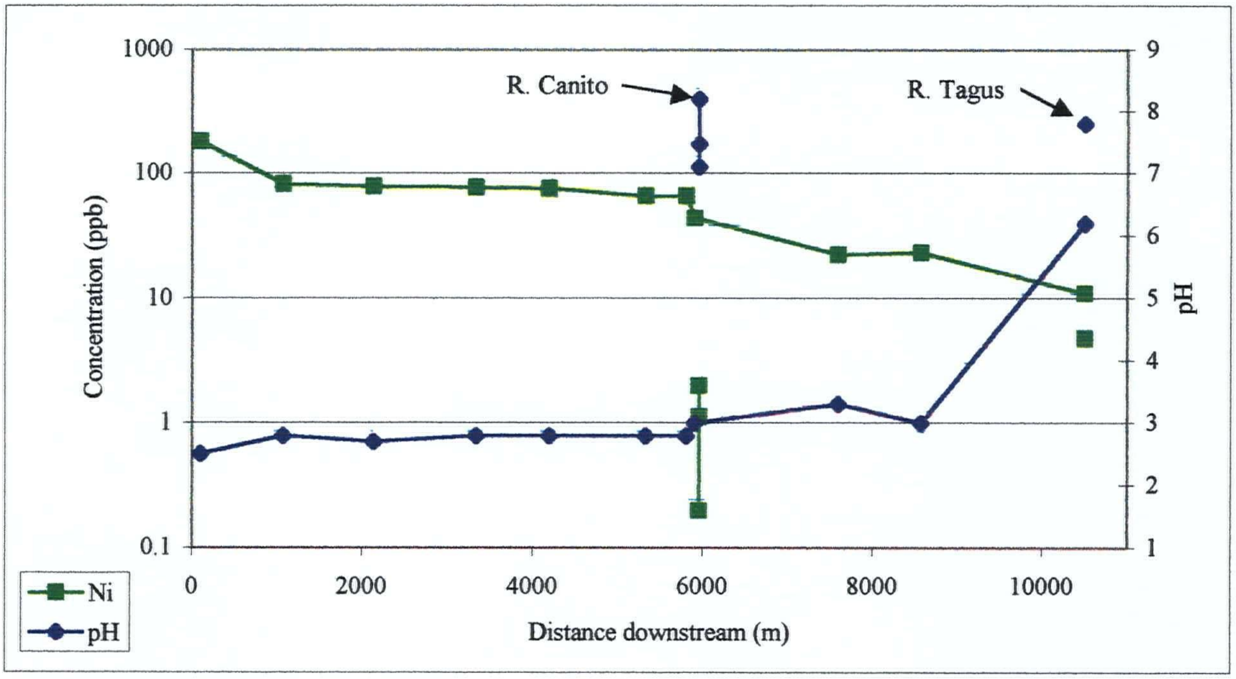

Figure 4.24. Downstream profile of Ni in stream waters. Rio Cantio data is shown as average and range at 5.9 km, Site 22 on the R. Tagus is shown as a point at 10.5 km downstream.

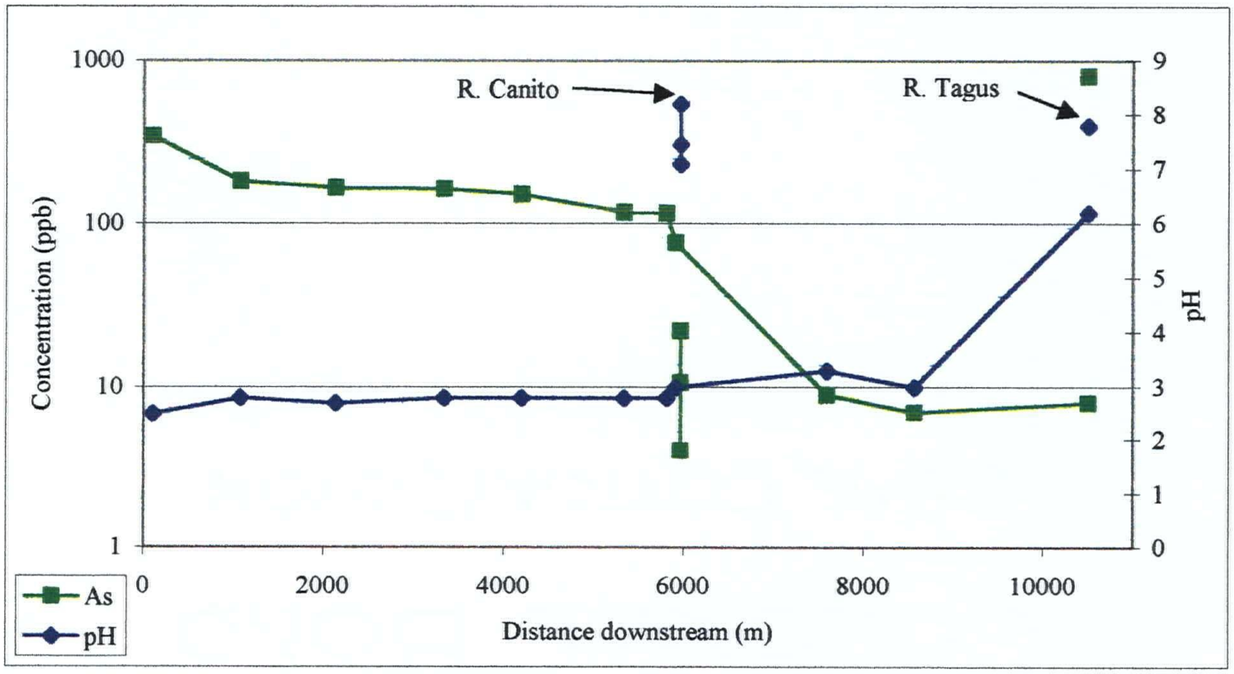

Figure 4.25. Downstream profile of As in stream waters. Rio Cantio data is shown as average and range at 5.9 km, Site 22 on the R. Tagus is shown as a point at 10.5 km downstream.

Canito and R. Tagus, however, pH of the R. Turbio rises and the streambed is coated with visible red staining. By assuming that changes in concentration are due solely to differences in relative flow volumes of the streams, it is possible to calculate an apparent dilution factor for confluences. The apparent dilution factor is determined by:

$$DF = 1 + ((A-C)/(C-B))$$

where, A, B, and C are the concentrations of an element on the principle stream above the confluence, on the tributary stream (diluting the main stream), and on the principle stream below the confluence, respectively.

A dilution factor greater than that calculated for a conservative element (e.g. Na^{2+}) would presumably indicate a mechanism other than dilution is lowering elemental concentrations in solution (e.g. precipitation onto secondary oxides). All of the dissolved metals analyzed in the water samples have an apparent dilution greater than 1.29, the dilution factor for Na at the R. Turbio- R. Canito confluence (Table 4.14), but there is remarkable similarity in the calculated dilution factors for all elements (avg. 1.49 with Sb removed), excepting Na and Sb. Mixing curves of pH vs. metal concentration show a linear trend between samples at sites 5, 6 and 3 (Figure 4.26). Additional samples taken from the R. Turbio at sites 1 and 2 before its confluence with the R. Tagus deviate from the linear trend with metal concentrations below the mixing curve (Figure 4.26).

The R. Tagus- R. Turbio confluence has a dilution factor of 1.28 for Na. Unlike the R. Tagus-R. Canito confluence, the dilution factors of the elements are much more variable, relations are more complex than the first confluence, and range from 793 for As to less than one for Ca and U

Table 4.14. Calculated dilution ratios for stream confluences at Lama.

Element	Site 5	Site 6	Site 3	Dilution of R. Turbio by R. Canito	Site 23	Site 1	Site 21	Dilution of R. Tagus by R. Turbio
pH*	2.8	7.1	3.0	1.58	7.8	3.0	6.2	1.00
Al	118.0	0.3	81.1	1.46	0.1	34.1	0.3	1.01
As	117.0	4.0	77.0	1.55	800.0	7.0	8.0	793
Ba	2.8	31.4	12.2	1.49	14.5	19.1	15.6	1.30
Ca	195.0	103.0	158.0	1.67	106.0	103.0	115.5	0.24
Cd	22.6	0.1	15.0	1.51	0.1	7.8	1.9	1.31
Co	89.4	1.8	61.9	1.46	3.6	32.2	11.3	1.37
Cr	10.0	0.5	6.5	1.58	0.5	2.5	0.5	1.00
Cu	6760.0	16.2	4570.0	1.48	1.3	1830.0	155.5	1.09
Fe	143.5	2.2	96.3	1.50	0.3	26.3	5.0	1.22
K	4.9	2.2	4.1	1.46	25.2	3.1	18.9	1.40
Mg	30.8	12.4	24.7	1.50	17.7	15.7	17.7	1.00
Mn	8550.0	1095.0	6010.0	1.52	555.0	2980.0	1525.0	1.67
Na	7.7	5.5	7.2	1.29	195.0	7.3	154.5	1.28
Ni	65.8	2.0	44.2	1.51	4.8	23.4	11.0	1.50
Sb	0.1	0.2	0.2	3.00	6.9	0.1	4.2	1.66
Sr	670.0	180.5	502.0	1.52	645.0	365.0	563.0	1.41
Tl	1.9	0.3	1.3	1.55	0.5	0.8	0.5	1.17
U	5.6	0.3	4.0	1.41	2.0	2.2	0.2	0.08
Zn	4890.0	81.0	3350.0	1.47	7.5	1430.0	383.0	1.36

* pH estimate based on H^+ concentrations

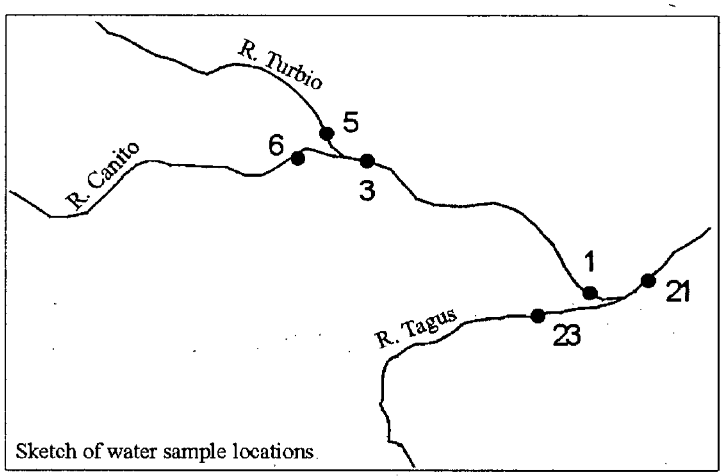

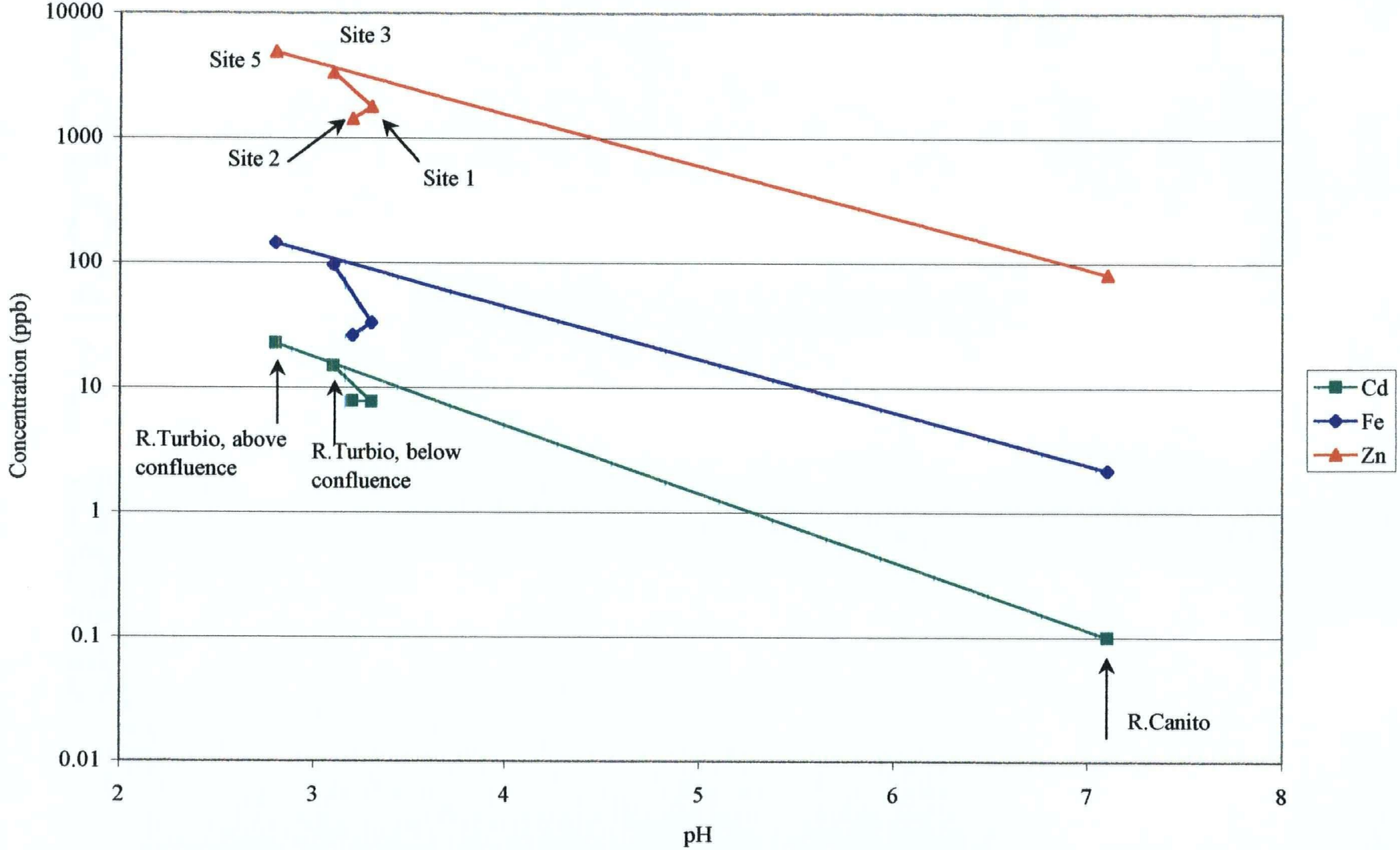

Figure 4.26. Mixing trends for Cd, Fe, and Zn at and below the R. Turbio- R. Canito confluence. Sites downstream from the confluence deviate from the linear trend.

(Table 4.14). Arsenic, Cd, Co, K, Mn, Ni, Sb, Sr and Zn all have factors exceeding 1.28. For elements where concentrations at site 1 (R. Turbio) are greater than site 23 (R. Tagus, upstream from confluence) dilution factors greater than 1.28 indicate that dissolved concentrations increase below the confluence more than can be explained by simple mixing (e.g. Ba, Cd, Co, Mn, Ni and Zn). Conversely, for elements with greater concentrations as site 23 than site 1, a dilution factor greater than 1.28 indicates that dissolved concentrations decrease more than can be explained by mixing below the confluence (e.g. Sb, K, As and Sr). This is especially notable for As with concentrations that decrease from 800 ppb in the R. Tagus to 8 ppb below the confluence. These situations are reversed for elements with dilution factors less than 1.28 so that concentrations of Cu, Fe, Al, Cr, U and Tl are less than would be expected and dissolved Ca and Mg concentrations increase.

4.3 Drainage sediments

Stream sediments were collected at seventeen locations along the R. Turbio, R. Canito and R. Tagus in Argentina. Thirteen high energy samples were taken from stream sections with a cobble-gravel surface, seventeen medium energy samples from gravel coarse-sand surfaces and seventeen low energy samples from areas with fine sand and silt surfaces (Figure 4.27).

4.3.1 Texture

Effort was made to sample material consistently from the same environment based on streambed texture, however the average weight percents of the high and medium energy samples are very similar (Table 4.15). Plate 4.1 shows the similarity of high vs. medium energy environments at one location. t-tests confirm there is no statistical difference between average abundances of

Figure 4.27. Sample locations for stream sediments at Lama.

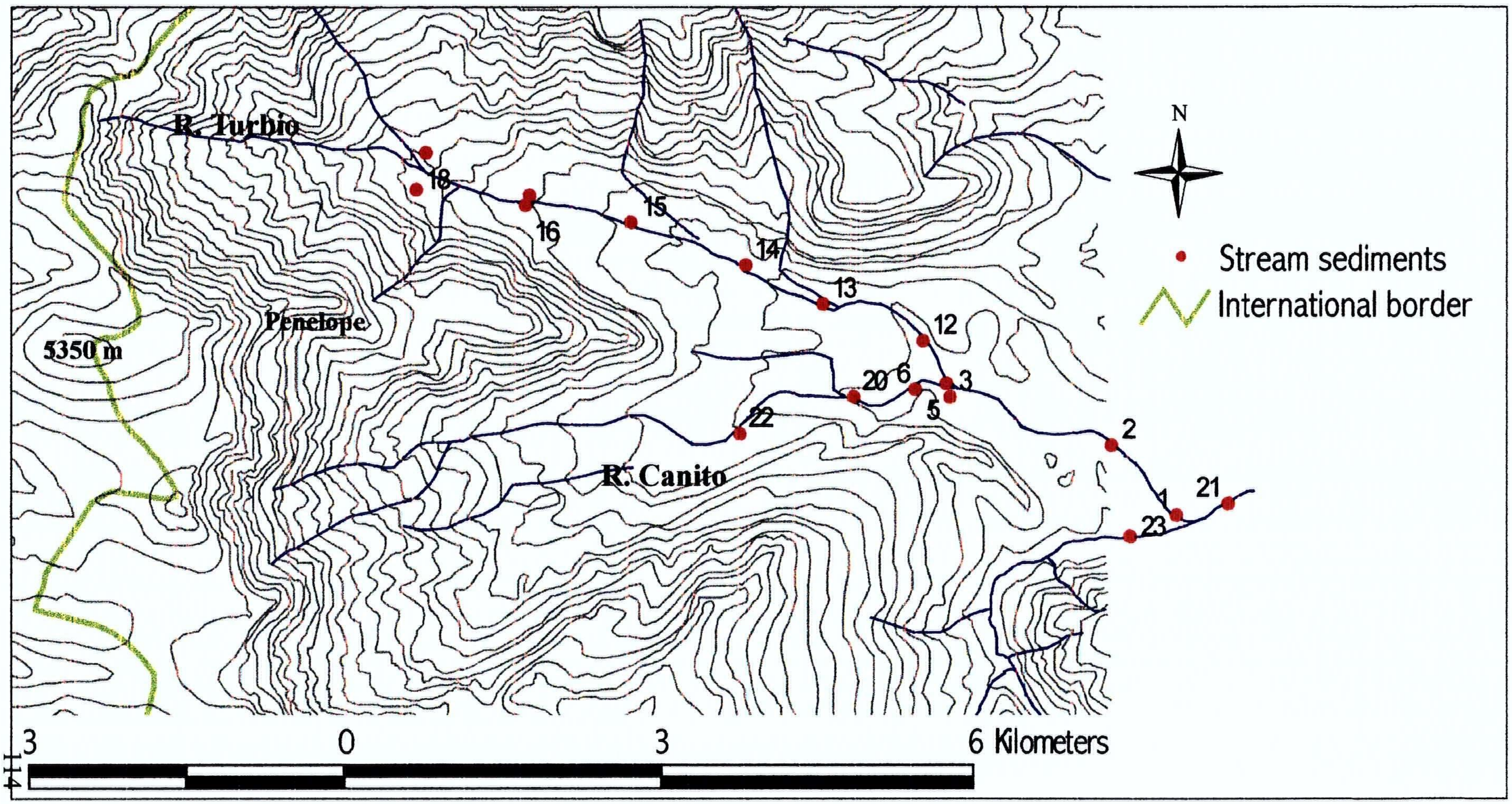

Table 4.15. Average weight percents for high, medium and low energy stream sediments at Lama.

Size fraction (μm)	High (n=13)	Medium (n=17)	Low (n=17)
-2mm+850	37.6	37.5	16.3
-850+425	27.4	29.4	25.1
-425+212	20.7	20.8	31.0
-212+150	4.7	4.2	10.7
-150+106	2.9	2.4	7.1
-106+75	2.0	1.6	3.8
-75+53	1.4	1.1	2.0
-53	3.4	3.1	4.1

Table 4.16. Results of two tailed t-test on weight percentages of stream sediments between high and medium energy samples ($t_{critical}$ = 2.09).

Size fraction (μm)	t_{stat}	Accept or Reject
-2mm+850	0.02	Accept
-850+425	-1.43	Accept
-425+212	-0.04	Accept
-212+150	0.66	Accept
-150+106	0.86	Accept
-106+75	1.03	Accept
-75+53	1.09	Accept
-53	0.53	Accept

material in the eight size fractions of the high and medium energy environments (Table 4.16). Stream sediments are the most coarse grained of all sampled media, with approximately 24% of the total –212μm material comprised of the -53μm faction.

Although, textural data is extremely noisy without coherent patterns, several trends relating to the effects of confluences can be recognized. High energy samples show an increase in abundance of –212μm and finer material immediately below the R. Canito, decreasing in abundance through the last sample site (Figure 4.28 where -53μm is representative of –212μm fractions). Medium energy samples show a smooth decline in abundance of -53μm below both the R. Turbio-R. Canito and R. Turbio-R. Canito confluences (Figure 4.29) with a concurrent increase in –425+212μm material and a slight increase in the –2mm+850μm and –850+425μm fractions. Low energy samples are exceedingly noisy and with no discernible downstream patterns (Figure 4.30). In general for all energies, as the percentage of coarse material (+425μm and coarser) increases there is a corresponding loss of –53μm sediment.

4.3.2 Geochemistry

4.3.2.1 Gold

Examination of gold concentration in the three energy environments shows that: (1) Au in Lama has greater absolute values in the fine fractions regardless of fluvial energy (median 515 ppb vs. 70 ppb for high energy -53μm and –150+106μm fractions, respectively); (2) the medium energy fluvial environments contain on average the most gold in all fractions except the –150+106

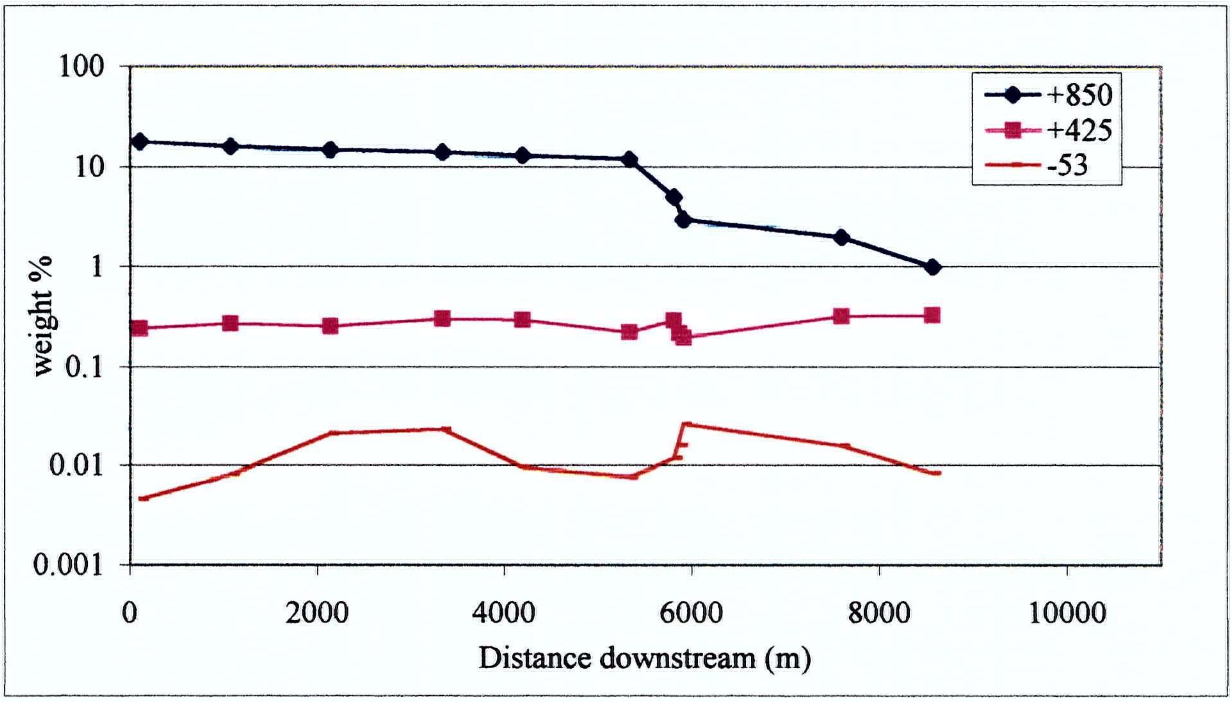

Figure 4.28. Downstream profile of weight percent of selected size fractions in high energy stream sediments. R. Canito shown as mean and range at 5.9 km. Grain size in μm.

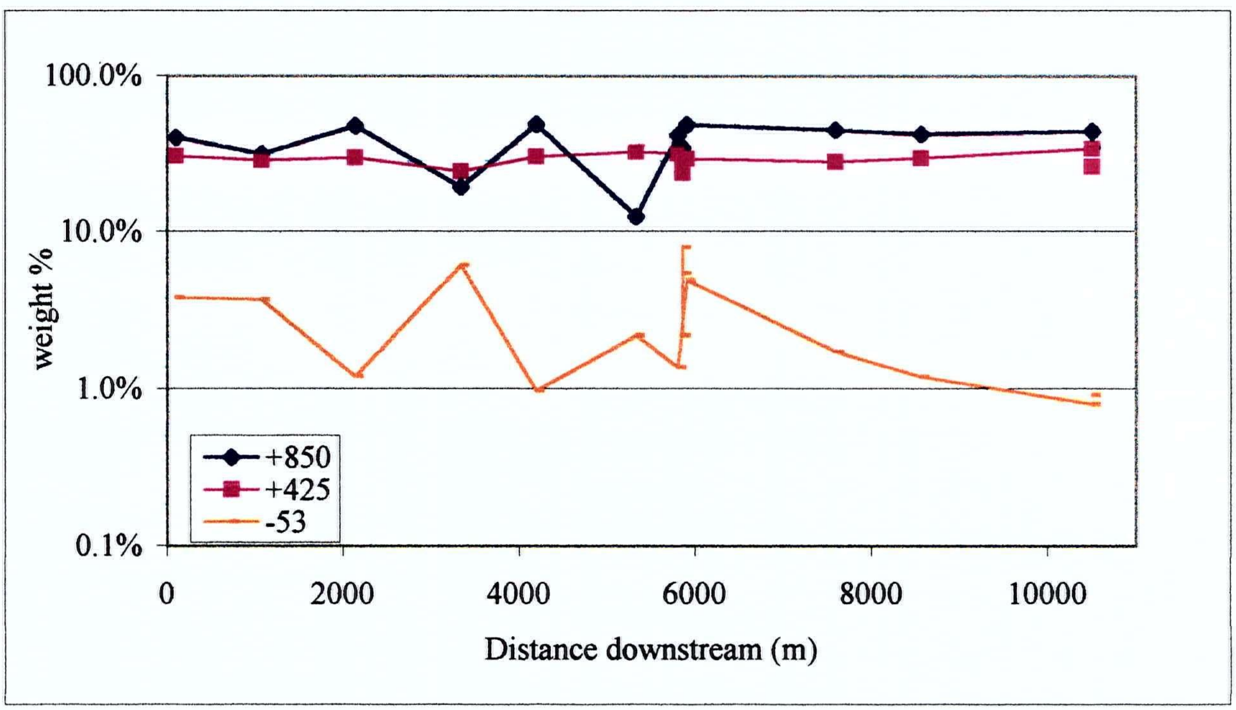

Figure 4.29. Downstream profile of weight percent of selected size fractions in medium energy stream sediments. R. Canito shown as mean and range at 5.9 km, Site 22 on the R. Tagus is shown as a point at 10.5 km downstream. Grain size in mm.

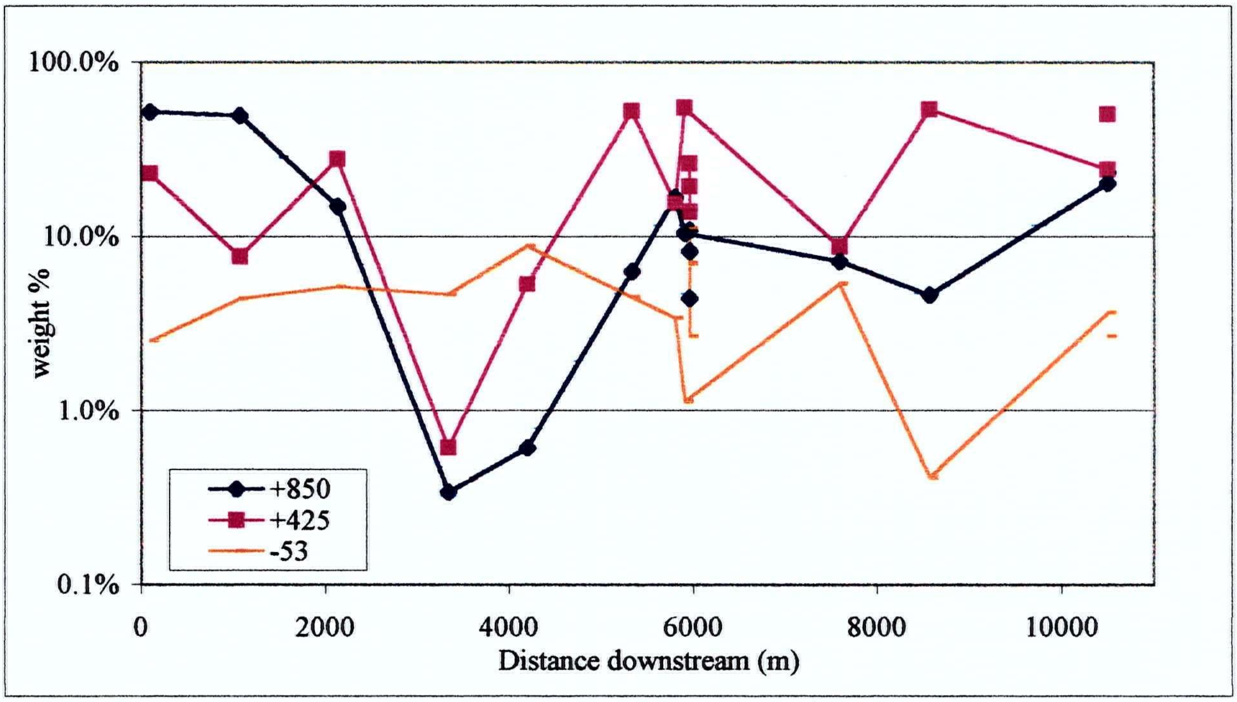

Figure 4.30. Downstream profile of weight percent of selected size fractions in low energy stream sediments. R. Canito shown as mean and range at 5.9 km, Site 22 on the R. Tagus is shown as a point at 10.5 km downstream.

(Table 4.17); and, (3) the R. Turbio contains appreciably more gold than the R. Canito for all size fractions and all energies (Table 4.17).

In light of poor quality control results for coarse gold (Table 3.4) most attention will be given to the –75+53 and -53μm fractions, although data will be presented for all size fractions. Results of analysis of variance (ANOVA) conducted for gold suggest that the between site variability is not significantly greater then within site variability (Table 4.18). However, $F/F_{critical}$ ratio increases with decreasing grain size and between site variability is greater than within site variability when medium and low energy are considered.

Downstream profiles of gold in the R. Turbio are shown in Figures 4.30, 4.31 and 4.32 for medium, high and low energy, respectively. In the medium energy, all size fractions, except for the –150+106 μm fraction, have maximum gold values at site 14, and then erratic downstream (Figure 4.31). The peak at site 14 is also apparent at high energy sites (Figure 4.32). Gold concentrations generally decrease downstream from the peak in all size fractions. However, in high energy sediments gold values generally increase downstream to a maximum, distal anomaly immediately above the R. Turbio- R. Tagus confluence at site 1. The low energy environment has three noticeable, but low magnitude peaks at 1.1, 5.3 and 8.6 km downstream, but overall profiles are relatively 'flat' (Figure 4.33). In low energy sites gold concentration decreases below the R. Turbio- R. Tagus confluence, with peak concentrations at Site 1 in the R. Turbio drainage, just upstream from the confluence with the R. Tagus.

The R. Turbio stream gradient exhibits a smooth decrease with no perturbations which might cause local increases in gold concentration relating to fluvial energy (Figure 4.31 to 4.33). In the high energy samples, a relation can be seen between the increase in the weight percent of

Table 4.17. Median gold values for Lama stream sediments. No high energy sites were sampled along the R. Canito. R. Turbio medians include site 21, below the R. Tagus confluence.

Size fraction (μm)	High energy	Medium energy		Low energy	
	R. Turbio (n=15)	R. Turbio (n=11)	R. Canito (n=3)	R. Turbio (n=11)	R. Canito (n=3)
-150+106	70	60	10	45	10
-106+75	120	150	15	70	10
-75+53	205	300	10	175	15
-53	515	560	60	430	70

Table 4.18. Summary of ANOVA results for gold between fluvial energies. n = 13 for high energy, n= 17 medium and low energy.

	-150+106μm		-106+75μm		-75+53μm		-53μm	
	F	$F/F_{critical}$	F	$F/F_{critical}$	F	$F/F_{critical}$	F	$F/F_{critical}$
High-medium ($F_{crit} = 2.52$)	0.965	0.38	0.753	0.3	1.266	0.5	2.083	0.83
High-low ($F_{crit} = 2.52$)	1.278	0.51	1.138	0.45	1.386	0.55	2.136	0.85
Medium-low (F_{crit}=2.29)	1.57	0.68	1.267	0.55	3.108	1.36	3.193	1.36

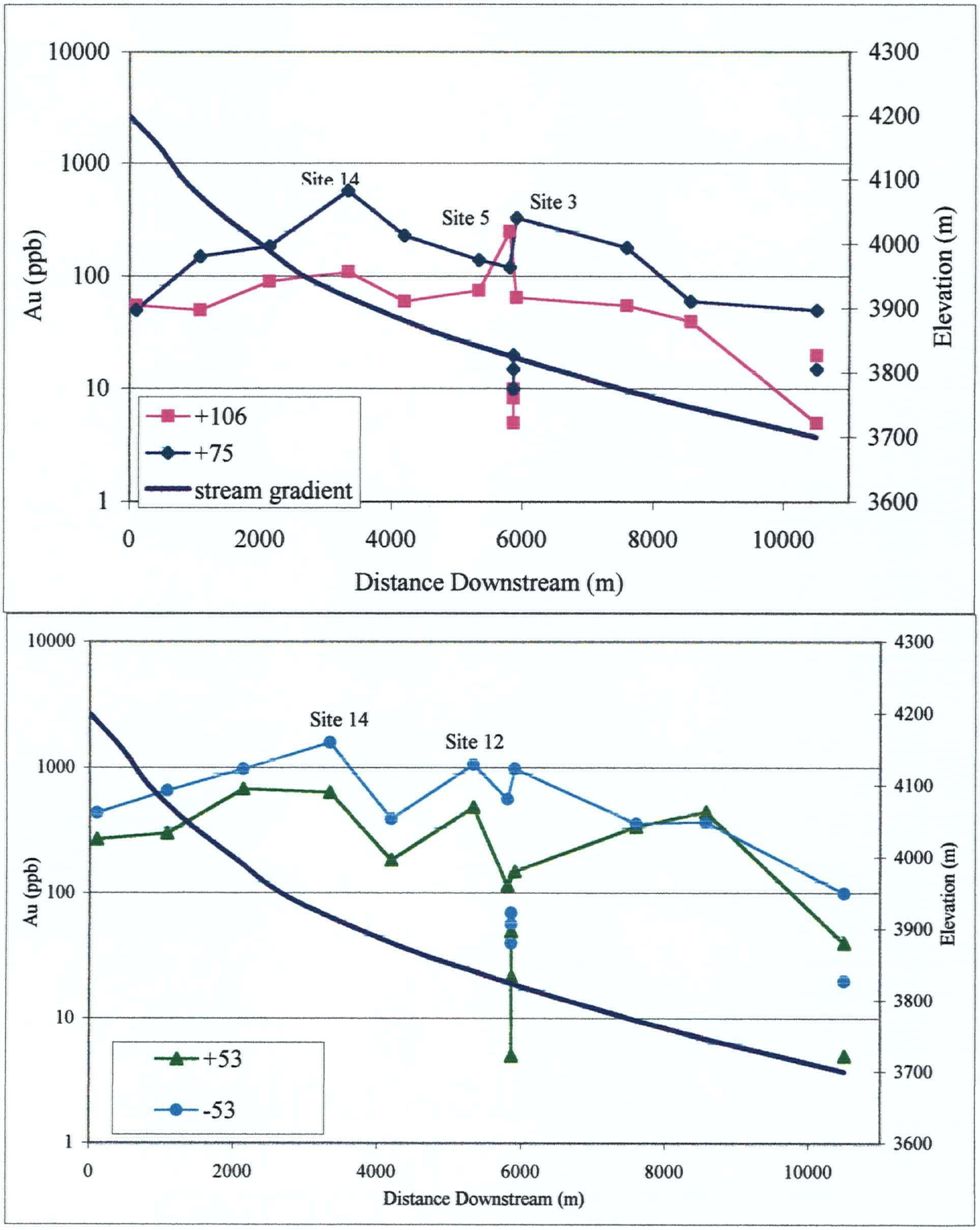

Figure 4.31. Gold in medium energy stream sediments of Lama. R. Canito is represented by mean and range at 5.9 km downstream. R Tagus is shown as a point at 10.5 km downstream.

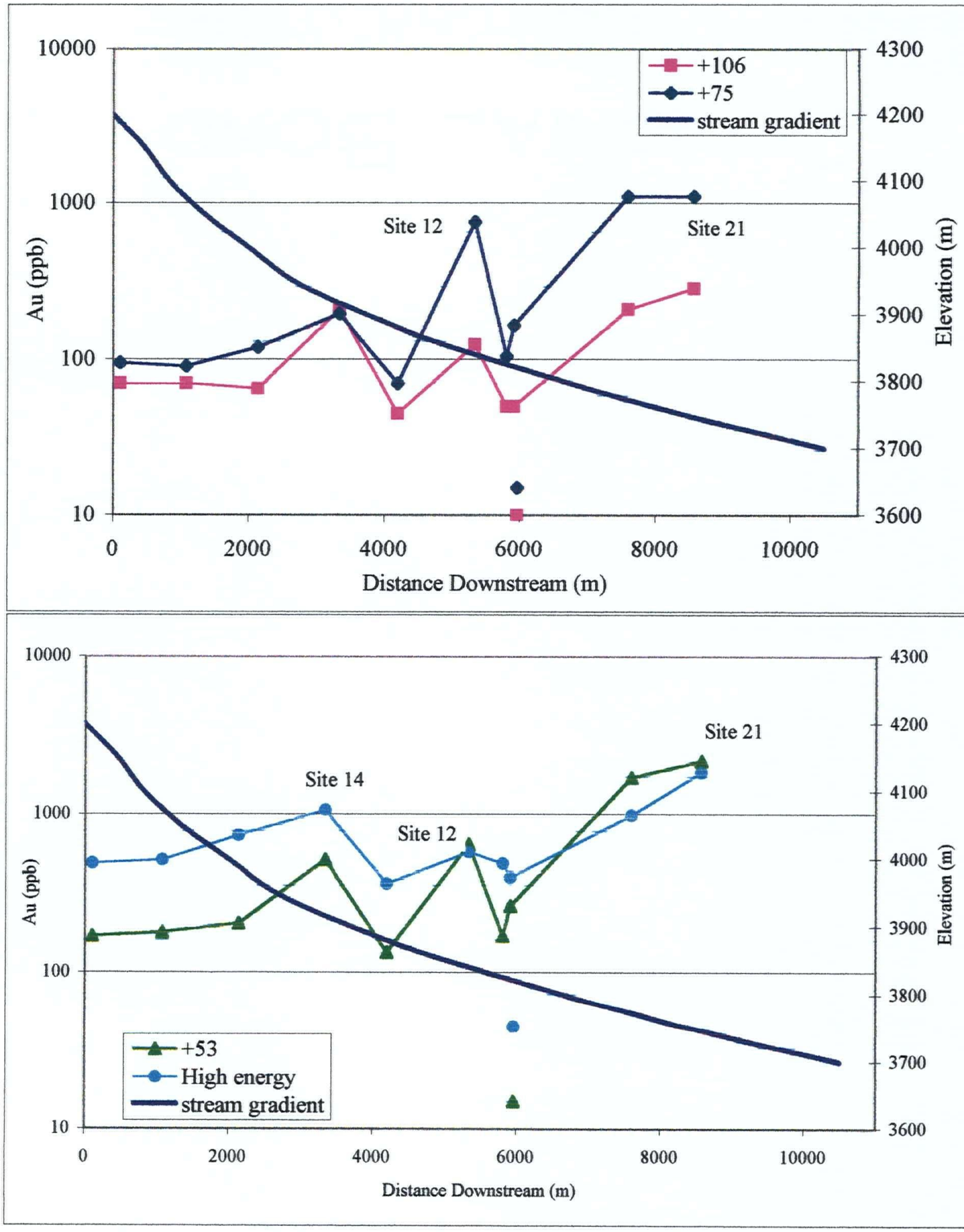

Figure 4.32. Gold in high energy stream sediments of Lama. R. Canito is by a point 6 km downstream. There is no high energy sample on the R. Tagus.

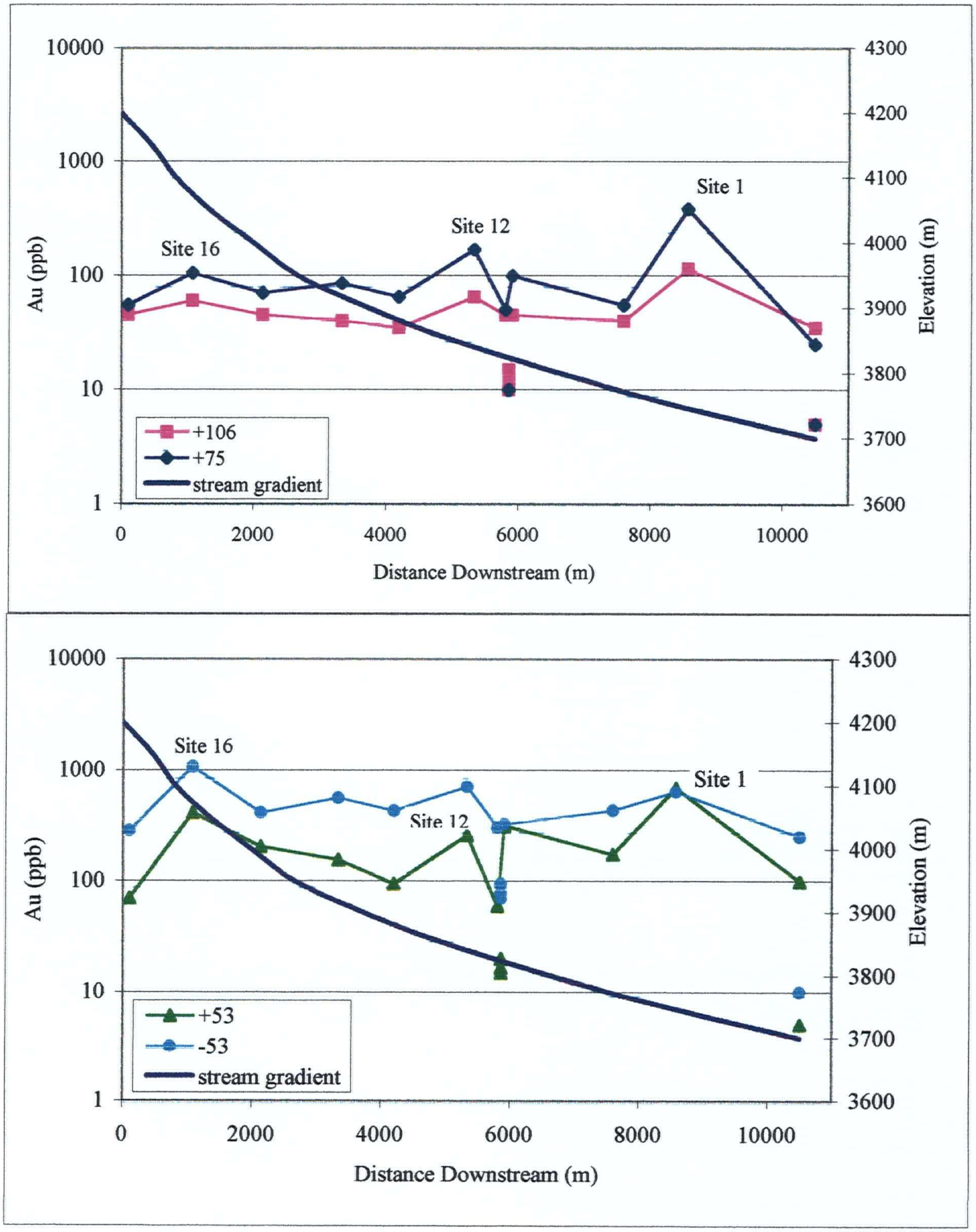

Figure 4.33. Gold in low energy stream sediments of Lama. R. Canito is represented by mean and range at 5.9 km downstream. R Tagus is shown as a point at 10.5 km downstream.

coarse material (-2mm+850μm,-425+212μm), the substantial decrease in mass of the -53μm fraction and the increase of gold concentration in all size fractions except the -53μm, immediately below the confluence of the R. Turbio and R. Canito (Figure 4.34). All size fractions of gold from high energy samples show strong, positive correlation with the –850+425μm (r values from 0.41-0.64) (Table 4.19).

At site 6, immediately below the R. Turbio- R. Canito confluence, medium energy sediments show a decrease in the weight percent abundances of all size fractions (except for –2mm+850μm and -53μm fractions) and an increase in gold for all fractions except the –150+106μm despite lower gold values in the R. Canito. Gold concentration continues to decrease below the R. Tagus confluence and there is a slight increase in coarse material (-2mm+850μm and –850+425μm), and a decrease in the weight percentages of all other size fractions (Figure 4.35). Except for –150+106μm fraction, gold in medium energy sediments has significant negative correlations with –850+425μm sediment (Table 4.19) and is generally positively correlated with sediment in the finer size fractions.

Low energy samples have considerable 'noise' in the downstream texture profiles and lower concentrations of gold. Regardless, the influence of the R. Tagus on the R. Turbio is evident as a decrease of the weight percentages of the fine material (all size fractions below –212+150μm except for the -53μm fraction) with a corresponding decrease in gold concentration (Figure 4.36) relative to the R. Turbio. Gold in the –106+75μm and –75+53μm fraction has significant positive correlations with sediment from the –850+425μm fraction.

Table 4.19. Summary of correlation coefficients for gold in stream sediments and texture at Lama.

High energy (df=9, r_{signf}> 0.602)	**-2mm+850µm**	**-850+425µm**	**-425+212µm**	**-212+150µm**	**-150+106µm**	**-106+75µm**	**-75+53µm**	**-53µm**
Au -212+106µm	-0.39	**0.62**	0.24	0.12	-0.02	0.05	0.00	0.24
Au -106+75µm	-0.13	0.41	0.06	0.09	-0.21	-0.13	-0.17	-0.1
Au -75+53µm	-0.3	0.59	0.19	0.13	-0.12	-0.05	-0.11	-0.01
Au -53µm	-0.42	**0.64**	0.28	0.1	0.05	0.05	0.00	0.22

Medium energy (df=13, r_{signf}> 0.514)	**-2mm+850µm**	**-850+425µm**	**-425+212µm**	**-212+150µm**	**-150+106µm**	**-106+75µm**	**-75+53µm**	**-53µm**
Au -212+106µm	-0.10	-0.06	0.03	0.23	0.20	0.18	0.17	0.03
Au -106+75µm	-0.31	**-0.77**	0.25	0.43	**0.56**	**0.59**	**0.65**	**0.71**
Au -75+53µm	-0.46	**-0.56**	0.49	**0.57**	**0.58**	**0.58**	**0.58**	0.23
Au -53µm	**-0.61**	**-0.59**	**0.56**	**0.65**	**0.70**	**0.70**	**0.71**	**0.70**

Low energy (df=13, r_{signf}> 0.514)	**-2mm+850µm**	**-850+425µm**	**-425+212µm**	**-212+150µm**	**-150+106µm**	**-106+75µm**	**-75+53µm**	**-53µm**
Au -212+106µm	-0.07	0.58	-0.21	-0.38	-0.50	-0.50	-0.49	**-0.56**
Au -106+75µm	-0.25	**0.61**	-0.14	-0.24	-0.40	-0.41	-0.41	-0.50
Au -75+53µm	-0.08	**0.55**	-0.16	-0.38	-0.50	-0.48	-0.47	**-0.53**
Au -53µm	0.19	-0.05	-0.18	-0.01	-0.02	-0.01	0.08	0.07

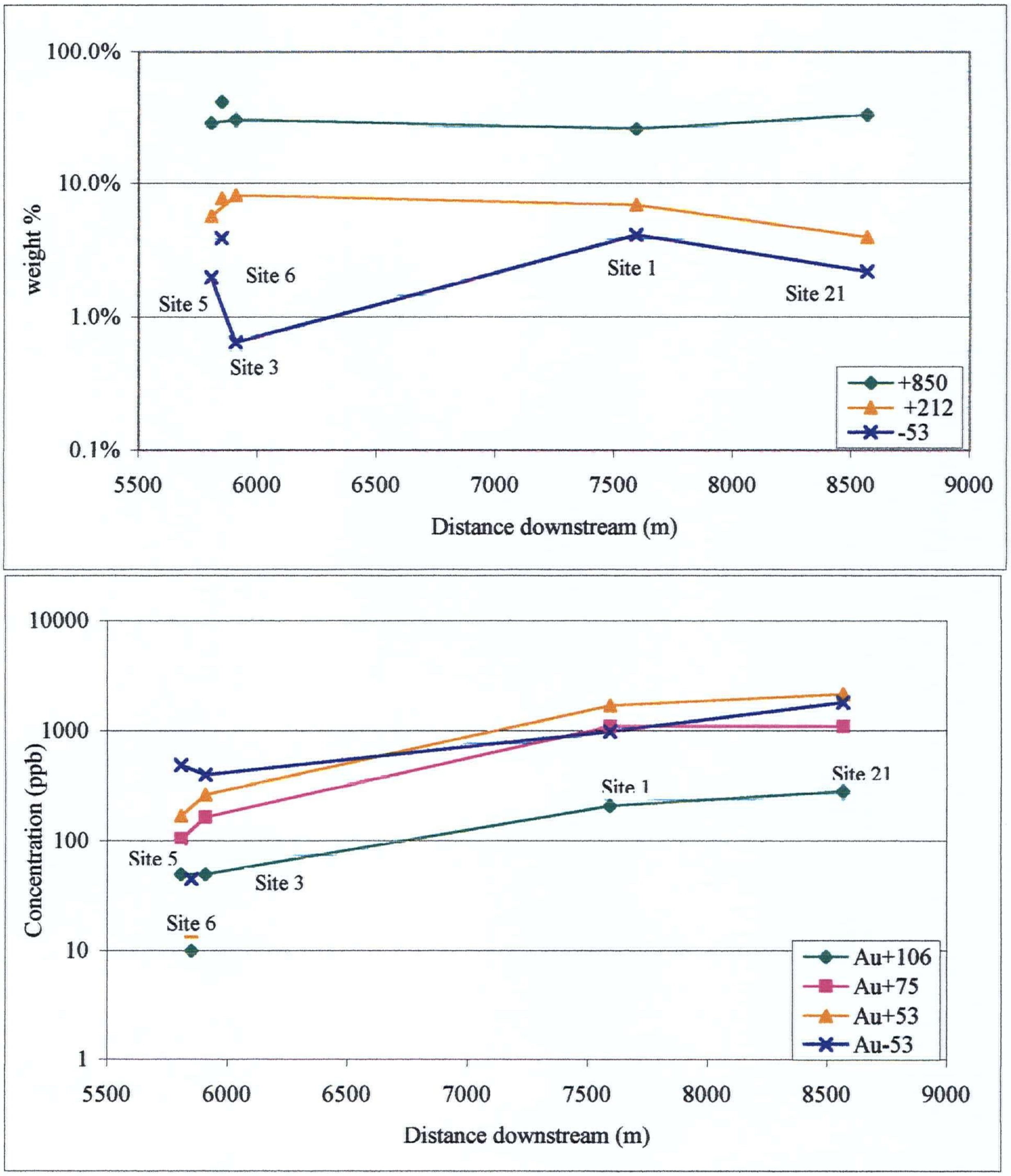

Figure 4.34. Effects of confluences on stream texture and gold concentration for Lama high energy stream sediments. Site 6 is along the R. Canito. All grain sizes in μm.

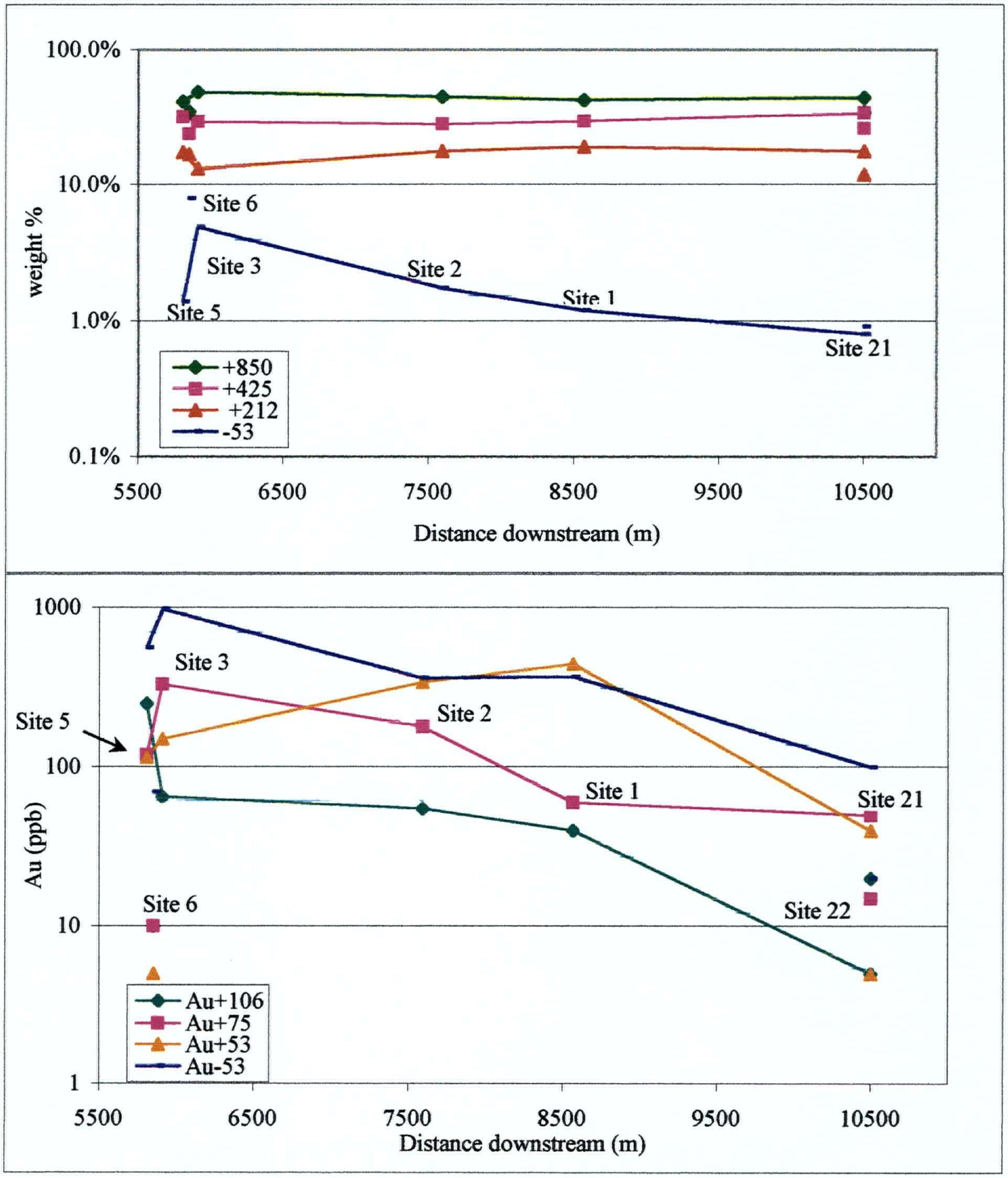

Figure 4.35. Effects of confluences on stream texture and gold concentration for Lama medium energy stream sediments. Site 6 is along the R. Canito, site 22 is in the R. Tagus upstream from confluence with the R.Turbio. All grains size in µm.

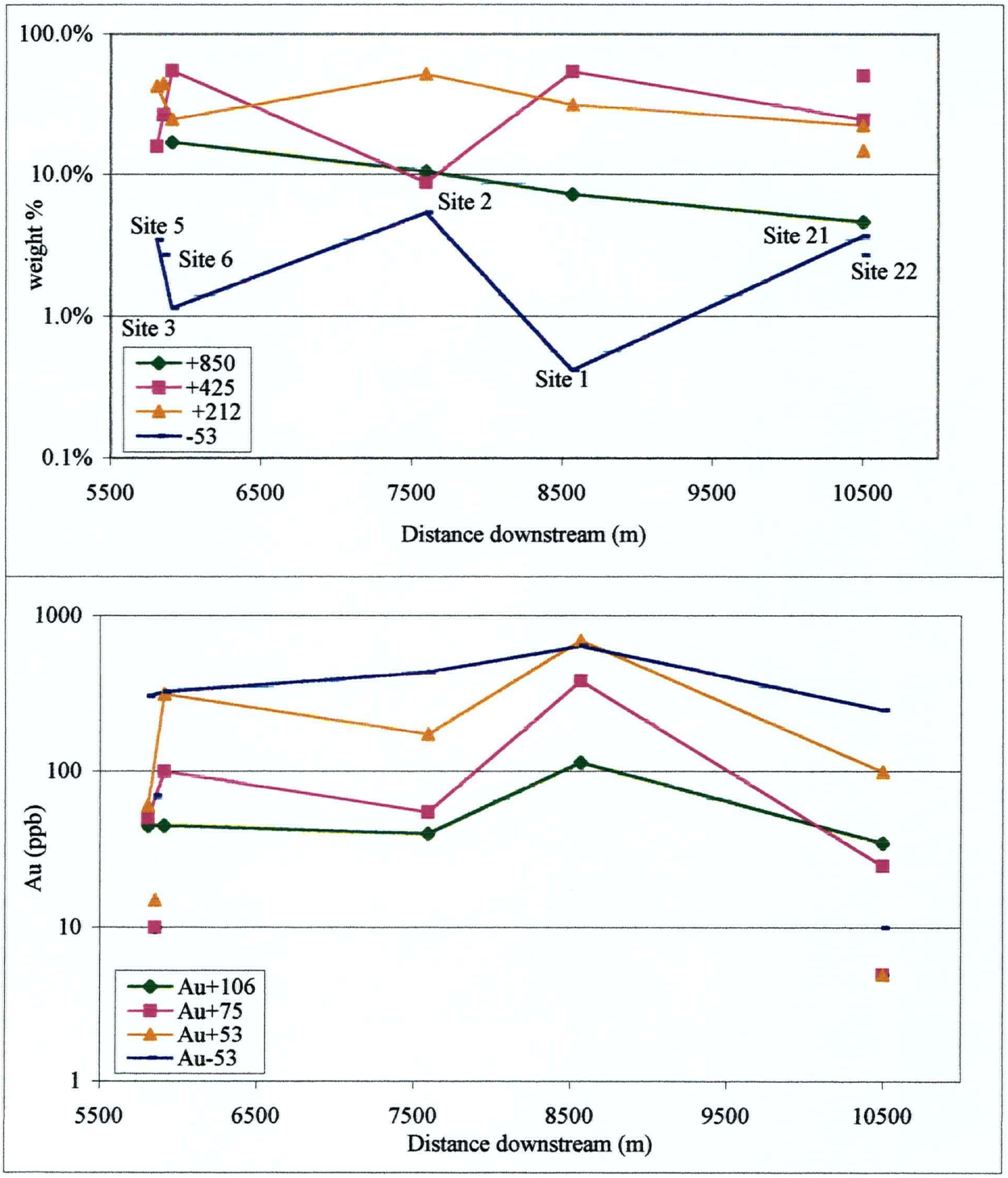

Figure 4.36. Effects of confluences on stream texture and gold concentration for Lama low energy stream sediments. Site 6 is along the R. Canito, site 22 is in the R. Tagus upstream from confluence with the R.Turbio. All grain sizes in µm.

4.3.2.2 Other elements and digestions

Aqua regia, total and cold hydroxylamine digestions were performed on the -53µm fraction, medium energy stream sediments. Presentation of results will focus on the *aqua regia* digestion, followed by presentation and comparison of the total digestion and cold hydroxylamine selective leach results.

Aqua regia digestion

Following ICP-MS analysis after *aqua regia* digestion of the medium energy –53 µm fraction sediments, only La, B, Ga, Ge, Cr, and Ni have maximum to minimum ratio of less than three (Table 4.20), where ratios less than three are deemed insufficient to develop strong geochemical trends. Of the remaining elements, there are two primary classes describing the downstream distribution: (1) elements acting similar to gold in the R. Turbio (Ag, Hg, Sb, As, Bi, Te, Pb, S and V) (e.g. Ag and Sb in Figure 4.37); and, (2) elements with dispersion patterns that are apparently controlled by pH and water chemistry (Cu, Zn, Mn, Cd, Ca, Al, Fe, Mg, Mo and Sr). Elements in the first group are generally positively correlated with Au in the R. Turbio (Table 4.21). Unlike gold, As has higher values in the R. Canito than the R. Turbio and increases in concentration downstream of the R. Turbio/R. Tagus confluence (Figure 4.38). Comparatively, gold has lower values in the R. Canito and concentrations in the -53µm fraction decrease below this confluence. This disparity in behavior manifests as non-significant correlation coefficients for these elements in the R. Turbio (Table 4.21).

Elements of the second class generally show a positive correlation to pH, a negative correlation to Au, and a negative relation to metal concentrations in water samples for R. Turbio samples,

Table 4.20. Descriptive statistics of aqua regia digestion of stream sediments (n=15). Maximum/minimum ratios greater than ten are in bold. Elements of the high sulfidation geochemical suites (Hedenquist et.al.,1996) are grouped together. Median values reported for gold.

Element	Units	Mean	Minimum	Maximum	Max/Min
Au (-53μm)	ppb	325.0	10.0	1080.0	**108.0**
pH		4.0	1.5	8.8	5.9
Cu	ppm	132.8	48.6	412.0	8.5
Ag	ppm	12.8	0.2	23.8	**99.2**
As	ppm	525.0	316.0	1265.0	4.0
Pb	ppm	483.9	22.0	2140.0	**97.3**
Hg	ppb	6.0	0.1	16.5	**165.0**
Mo	ppm	5.4	1.0	12.2	**12.2**
Sb	ppm	6.9	1.9	9.8	5.2
Te	ppm	2.3	0.3	4.3	**14.3**
Bi	ppm	12.1	1.2	21.7	**17.6**
Al	%	1.1	0.5	2.6	4.9
Ba	ppm	254.7	110.0	680.0	6.2
Ca	%	0.5	0.1	3.1	**61.8**
Cd	ppm	0.6	0.2	1.9	**10.4**
Co	ppm	9.4	2.0	41.2	**20.6**
Cr	ppm	12.2	8.0	19.0	2.4
Fe	%	6.7	4.7	15.0	3.2
K	%	0.4	0.2	0.6	3.2
Mg	%	0.3	0.2	0.8	4.4
Mn	ppm	1208.0	190.0	6210.0	**32.7**
Na	%	0.1	0.0	0.1	3.5
Ni	ppm	9.7	6.0	15.0	2.5
P	ppm	532.7	280.0	1060.0	3.8
S	%	1.3	0.3	2.1	6.8
Sr	ppm	69.0	40.0	151.0	3.8
U	ppm	0.6	0.3	1.5	5.0
V	ppm	45.9	24.0	98.0	4.1
W	ppm	0.4	0.2	0.9	4.3
Zn	ppm	180.7	64.0	612.0	9.6

Table 4.21. Correlation coefficients with Au and pH for stream sediments. The first columns are for all stream sediments (df=13, r significant at >0.514 at 95%) and the remaining are for R. Turbio samples including site 21 on the R. Tagus (df=9, r significant at >0.602).

	Lama (n=15)		**R. Turbio (n=11)**	
	Au	**pH**	**Au**	**pH**
Au	1.00	**-0.71**	1.00	-0.34
Cu	0.12	-0.06	-0.39	**0.86**
Ag	**0.75**	**-0.91**	**0.78**	**-0.76**
As	-0.18	0.49	-0.50	**0.81**
Pb	-0.44	**0.71**	0.49	**-0.81**
Hg	**0.66**	**-0.74**	**0.88**	-0.44
Sb	**0.66**	**-0.55**	**0.76**	-0.46
Te	**0.77**	**-0.95**	0.52	**-0.94**
Mo	0.02	0.11	0.29	**-0.86**
Bi	**0.76**	**-0.87**	**0.82**	**-0.70**
Al	**-0.59**	**0.66**	-0.49	**0.75**
Ba	**-0.58**	**0.85**	-0.53	**0.74**
Ca	-0.42	**0.54**	-0.46	**0.85**
Cd	**-0.55**	**0.83**	-0.49	**0.73**
Co	**-0.51**	**0.61**	-0.42	**0.83**
Cr	0.01	-0.05	0.00	0.08
Fe	0.25	-0.02	-0.23	0.13
K	**0.73**	**-0.90**	0.55	**-0.90**
Mg	**-0.54**	**0.51**	-0.52	**0.67**
Mn	**-0.60**	**0.90**	-0.48	**0.81**
Na	0.15	-0.46	0.03	-0.44
Ni	**-0.52**	**0.70**	-0.35	**0.65**
P	**-0.69**	**0.93**	**-0.60**	**0.72**
S	**0.76**	**-0.93**	**0.66**	**-0.77**
Sr	-0.40	0.41	-0.43	0.50
Ti	-0.35	0.41	-0.45	**0.85**
Tl	**0.75**	**-0.91**	**0.66**	**-0.87**
U	**-0.67**	**0.87**	-0.47	**0.84**
V	-0.09	0.28	-0.53	**0.69**
W	0.00	0.01	-0.13	**0.67**
Zn	**-0.65**	**0.86**	-0.50	**0.76**
pH	**-0.71**	1.00	**-0.60**	1.00

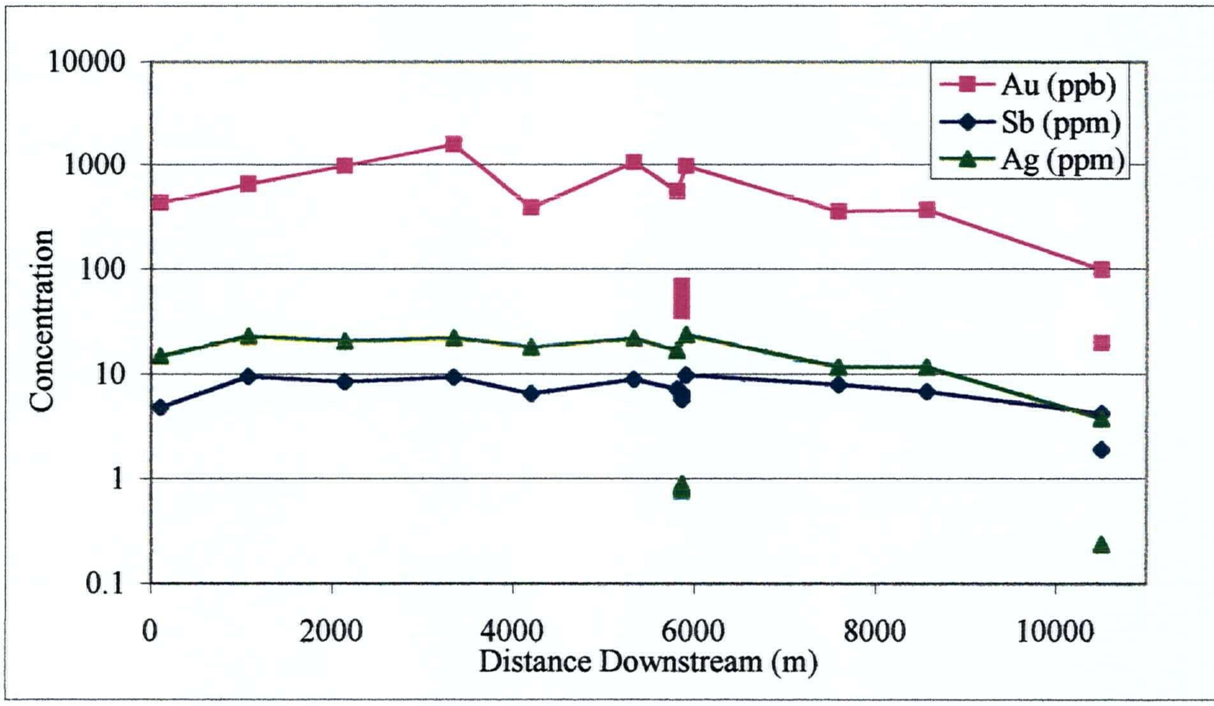

Figure 4.37. Downstream profile for aqua regia digestible Ag and Sb in -53µm medium energy sediments. R. Canito shown by mean and range 5.9 km downstream, R. Tagus is a point at 10.5 km.

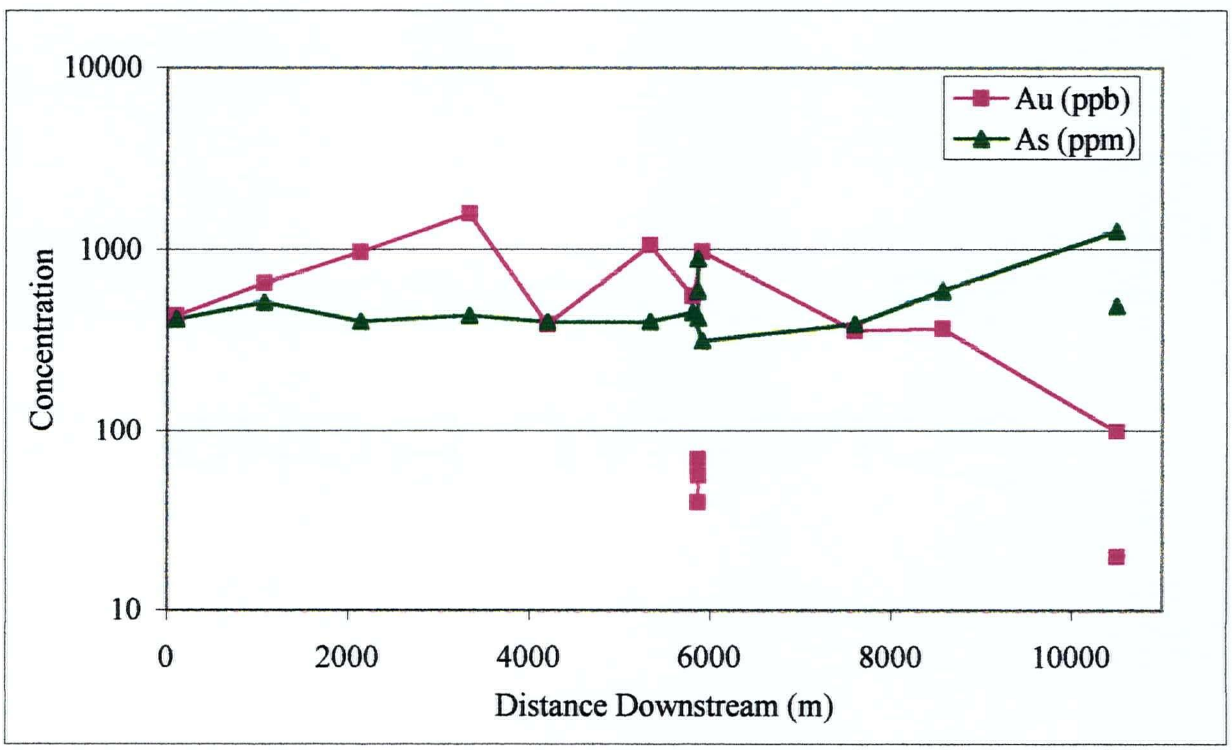

Figure 4.38. Downstream profile for aqua regia digestible As in -53µm medium energy sediments. R. Canito shown by mean and range 5.9 km downstream, R. Tagus is a point at 10.5 km.

the exception being Mo (Table 4.21). In general, as the pH rises above 4, element concentration increases in sediments (e.g. Zn in Figure 4.30). The low pH of the upper reaches of the R. Turbio results in all of the second group of elements, except Mo, having approximately constant values in the Rio Turbio (average pH of 2.5 not including site 21 below the R. Turbio- R. Tagus confluence) that increase to maximum concentrations below the R. Tagus confluence. The remaining elements (Na, K, P, Be, Co, Sr, U and Ba) do not have downstream profiles that relate to either of the aforementioned patterns.

Total digestion

The total (triple acid) digestion returns average elemental concentrations in excess of the *aqua regia* for all but eight elements (Ag, As, Bi, Cd, Fe, Hg, Mn and Ni) (Table 4.22). The percent extraction of the *aqua regia* digestion relative to the total (triple acid) is dependant on the element (Table 4.23): (1) Ag, As, Bi, Cd, Co, Cu, Fe, Hg, Mn, Mo, Ni, Te and Zn are readily extractable with *aqua regia*/total values of >100-76%, (2) partially extracted elements of Ba, Be, Ca, Cr, La, Mg, P, Pb, Sb, Tl, U and V at 40-75% and (3) elements that are weakly extracted at less than 40% (Al, K, Na, Sr, W and Ti). High *aqua regia*/total correlation coefficients (0.53-0.99) generally coincide with groups 1 and 2 above (Table 4.23). Downstream profiles of elements generally associated with heavy minerals show a strong relation between *aqua regia* and total digestions (e.g. Cr and V in Figure 4.40).

Cold hydroxylamine leach

The cold hydroxylamine leach, which is designed to dissolve amorphous manganese oxides and associated trace elements, removed an average of 20.6% of the *aqua regia* digestible manganese

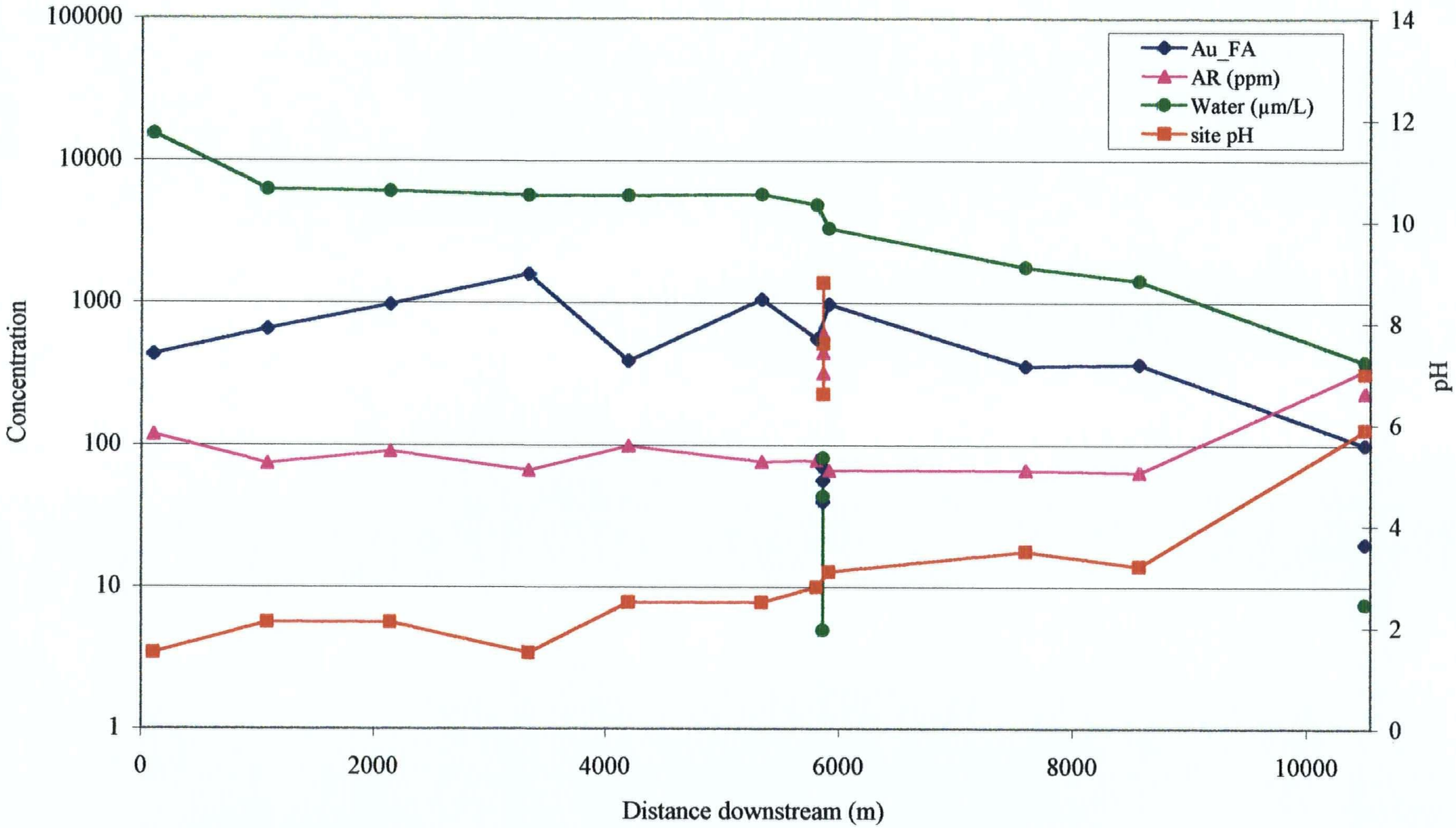

Figure 4.39. Downstream dispersion for aqua regia digestible Zn in medium energy -53µm sediment. R. Canito is shown by mean and range at 6 km downstream. R. Tagus is shown by a point 10.5 km downstream.

Table 4.22. Descriptive statistics of total digestion of stream sediments (n=15). Maximum/minimum ratios greater than ten are in bold. Elements of the high sulfidation geochemical suites (Hedenquist et.al., 1996) are grouped together. Median values reported for gold.

Element	Units	Mean	Minimum	Maximum	Max/Min
Au (-53mm)*	ppb	325.0	10.00	1080.0	**108**
pH	ppm	4.0	1.5	8.8	5.9
Cu	ppm	137.3	52.00	432.0	**8**
Ag	ppm	10.55	1.40	21.40	**15**
As	ppm	509.1	302.0	1290	4
Pb	ppm	610.7	32.00	1955	**61**
Hg	ppb	4265	90.00	15930	**177**
Sb	ppm	14.47	4.80	20.70	4
Te	ppm	2.64	0.35	4.80	**14**
Mo	ppm	6.52	2.00	14.20	7
Bi	ppm	7.19	1.04	13.25	**13**
Al	%	7.87	5.59	10.10	2
Ba	ppm	814.7	140.0	2230	**16**
Ca	%	0.76	0.24	3.56	**15**
Cd	ppm	0.51	0.06	1.60	**27**
Co	ppm	9.72	1.00	43.20	**43**
Cr	ppm	24.47	19.00	31.00	2
Fe	%	6.21	4.25	14.10	3
K	%	2.28	1.56	2.85	2
Mg	%	0.53	0.29	1.23	4
Mn	ppm	1173	255.0	5450	**21**
Na	%	1.07	0.81	1.44	2
Ni	ppm	9.97	2.40	21.60	9
P	ppm	812.7	640.0	1320	2
Sr	%	264.6	163.0	362.0	2
Ti	%	0.4	0.2	0.6	3
V	ppm	106.8	70.00	180.0	3
W	ppm	2.87	1.00	4.30	4
Zn	ppm	185.6	74.00	576.0	8

* Au by FA-AAS

Table 4.23. Percent extraction of aqua regia to total and cold hydroxylamine to aqua regia. Correlation coefficient (df = 13, r significant at >0.514 at 95% confidence) values reported are for aqua regia to total.

Element	Ratio (%)	Average	Min	Max	r
Silver	AR/Total	112.9	17.1	312.0	0.97
	CH/AR	3.8	0.8	10.8	
Aluminum	AR/Total	13.4	6.7	34.2	0.21
	CH/AR	6.1	0.1	8.9	
Arsenic	AR/Total	103.8	98.1	109.4	0.94
	CH/AR	0.8	0.0	7.4	
Barium	AR/Total	43.4	8.9	120.0	0.73
	CH/AR	6.3	0.7	25.7	
Beryllium	AR/Total	44.9	13.6	100.0	0.92
	CH/AR	20.0	2.0	40.0	
Bismuth	AR/Total	182.3	112.4	500.0	0.93
	CH/AR	0.1	0.0	0.4	
Mercury	AR/Total	166.0	104.0	454.0	0.97
Calcium	AR/Total	41.9	20.0	89.2	0.99
	CH/AR	55.9	1.5	71.1	
Cadmium	AR/Total	114.4	78.6	300.0	0.99
	CH/AR	26.2	10.0	59.0	
Cobalt	AR/Total	101.2	84.2	220.0	0.99
	CH/AR	19.9	8.0	50.0	
Chromium	AR/Total	49.3	40.0	65.4	0.85
Copper	AR/Total	96.6	79.2	107.5	0.99
	CH/AR	12.1	1.5	31.1	
Iron	AR/Total	108.0	85.8	118.8	0.97
	CH/AR	2.2	0.2	3.7	
Potassium	AR/Total	16.1	9.4	22.3	0.65
	CH/AR	3.5	0.1	18.1	
Lanthanum	AR/Total	73.2	37.7	250.0	0.63
	CH/AR	1.4	0.7	4.0	

Element	Ratio (%)	Average	Min	Max	r
Magnesium	AR/Total	63.8	58.0	73.3	0.90
	CH/AR	4.7	2.6	10.6	
Manganese	AR/Total	88.6	73.1	114.3	0.99
	CH/AR	20.6	4.7	60.9	
Molybdenum	AR/Total	87.7	35.7	230.0	0.90
Sodium	AR/Total	7.9	3.1	12.6	0.20
	CH/AR	8.4	0.7	43.8	
Nickel	AR/Total	112.2	64.8	250.0	0.92
	CH/AR	24.0	2.1	142.3	
Phosphorus	AR/Total	62.9	43.8	89.7	0.95
	CH/AR	2.1	0.5	10.6	
Lead	AR/Total	63.8	42.1	109.7	0.97
	CH/AR	4.0	0.0	40.9	
Antimony	AR/Total	51.9	32.9	142.9	0.82
	CH/AR	2.5	0.1	27.9	
Strontium	AR/Total	26.2	14.5	44.3	0.53
	CH/AR	8.1	1.2	33.3	
Tellurium	AR/Total	94.3	60.0	231.8	0.85
Titanium	AR/Total	4.2	2.4	11.3	0.89
Thallium	AR/Total	59.9	35.4	145.5	0.53
	CH/AR	6.6	2.4	19.3	
Uranium	AR/Total	41.0	21.4	100.0	0.62
	CH/AR	7.0	0.4	17.5	
Vanadium	AR/Total	41.7	20.9	69.0	0.85
	CH/AR	5.1	1.7	10.4	
Tungsten	AR/Total	14.4	8.1	30.0	0.47
Zinc	AR/Total	93.2	80.5	106.3	0.93
	CH/AR	12.6	8.1	28.6	

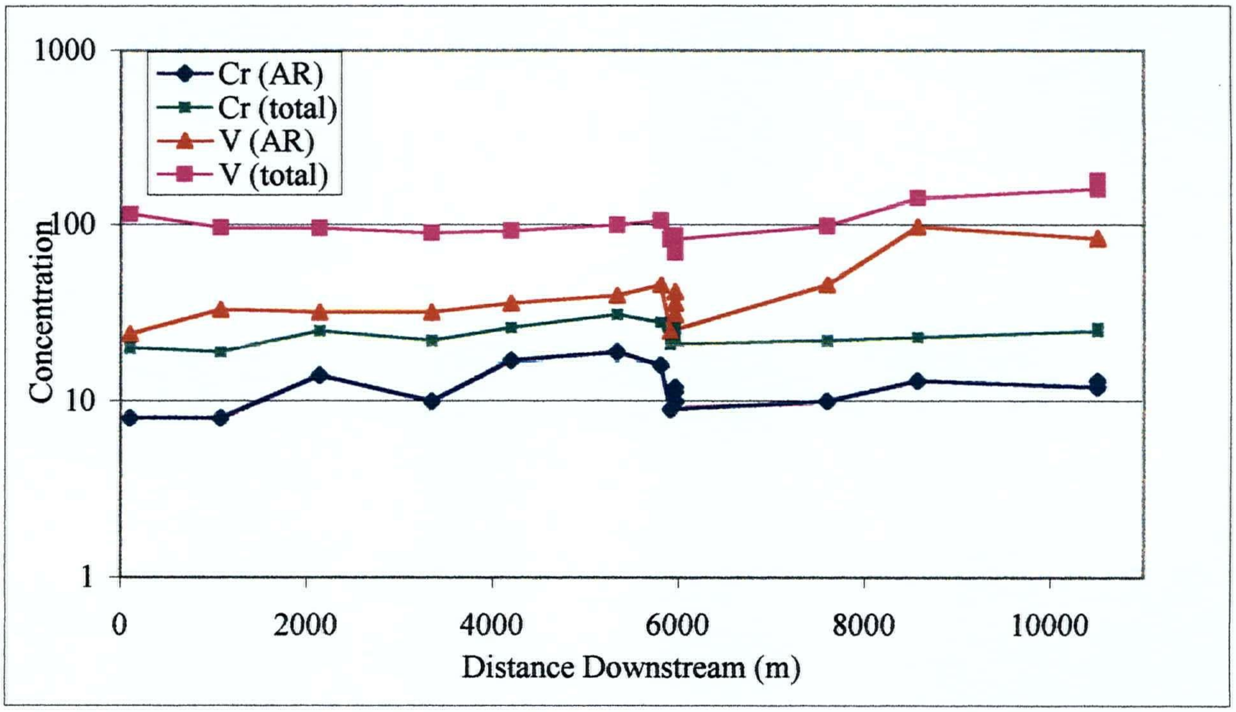

Figure 4.40. Comparison of Cr and V after aqua regia and total digestions.
R. Canito shown by mean and range 5.9 km downstream, R. Tagus is a point at 10.5 km.

Table 4.24. Descriptive statistics of cold hydroxylamine leach of stream sediments (n=15). Maximum/minimum ratios greater than ten are in bold. Elements of the high sulfidation geochemical suites (Hedenquist et.al., 1996) are grouped together. Median values reported for gold.

Element	**Units**	**R. Turbio (n=10)**	**R. Canito (n=3)**	**Minimum**	**Maximum**	**Max/Min**
Au (-53μm)*	ppb	325.00	325.00	10.00	1080.00	108.0
Au**	ppm	0.08	0.08	0.05	0.20	4.0
pH		2.9	7.5	1.50	8.80	5.9
Cu	ppm	21.04	2.25	1.15	36.10	31.4
Ag	ppm	0.47	0.05	0.01	1.02	170.0
As	ppm	5.48	0.47	0.10	30.70	307.0
Pb	ppm	1.55	195.50	0.10	409.00	4090.0
Sb	ppm	0.03	0.02	0.01	0.53	106.0
Bi	ppm	0.02	0.01	0.01	0.05	9.0
Al	ppm	565.25	350.67	19.00	1370.00	72.1
Ba	ppm	1.96	98.32	1.15	169.80	147.7
Ca	ppm	527.50	2506.67	310.00	8620.00	27.8
Cd	ppm	0.04	0.67	0.02	1.11	55.5
Co	ppm	0.34	3.82	0.20	20.60	103.0
Fe	ppm	1527.50	1151.67	110.00	5380.00	48.9
I	ppm	6.88	1.10	0.70	62.40	89.1
K	ppm	17.50	118.33	5.00	380.00	76.0
Mg	ppm	96.75	256.67	62.00	456.00	7.4
Mn	ppm	21.80	2020.00	13.80	3780.00	273.9
Na	ppm	10.00	36.67	10.00	570.00	57.0
Ni	ppm	1.98	5.58	0.15	15.65	104.3
Sr	ppm	1.01	8.68	0.80	47.00	58.8
Tl	ppm	0.08	0.17	0.06	0.24	4.3
U	ppm	0.04	0.03	0.01	0.07	14.0
V	ppm	2.28	0.98	0.80	4.70	5.9
Zn	ppm	10.50	76.33	5.80	118.00	20.34

* Au by FA-AAS

** Au from cold hydroxylamine leach

Table 4.25. Summary of correlations for pH and cold hydroxylamine leach and water for selected elements (df= 13, r significant at > 0.514 at 95% confidence).

	pH	Water
Al	-0.29	0.24
As	-0.27	0.43
Ba	**0.83**	**0.72**
Ca	**0.65**	-0.42
Cd	**0.88**	**-0.51**
Co	**0.61**	-0.48
Cu	**-0.76**	**0.70**
Fe	-0.31	-0.07
K	**0.70**	**0.82**
Mg	**0.77**	-0.36
Mn	**0.83**	-0.50
Na	0.47	**0.99**
Ni	0.42	-0.28
Sb	0.37	**0.97**
Sr	**0.58**	-0.10
V	**-0.51**	0.04
Zn	**0.83**	-0.43

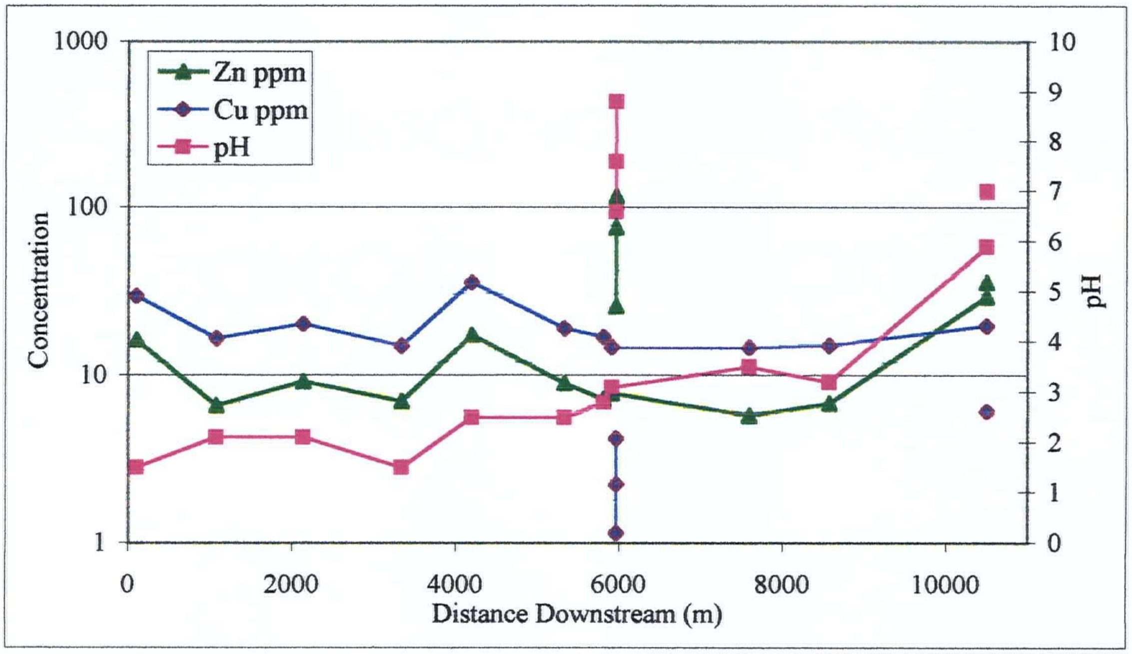

4.41. Cold hydroxylamine concentrations of Zn and Cu on -53µm stream sediments at Lama. R. Canito shown by mean and range 5.9 km downstream, R. Tagus is a point at 10.5 km.

in the –53 μm fraction of medium energy sediments. Elemental concentrations are much lower than those returned after *aqua regia*, i.e. mean Sb value of 0.07 ppm vs. 6.95 ppm and mean Zn values of 25.83 ppm and 180.7 ppm for cold hydroxylamine and *aqua regia*, respectively (Table 4.24). Barium, Mn, Mg, Ca, Co, Cd, Ni, Zn, K Pb, Na, Tl and Sr have average cold hydroxylamine values greater in the R. Canito compared to the R. Turbio (Table 4.24). Barium, Sb, Mn, Mg, Co, Cd, Zn, K, Na, Cs, Li, Tl and Sr all have peak concentrations at Site 21. downstream from the R. Tagus- R. Tagus confluence (e.g. Zn in Figure 4.41). Correlations between cold hydroxylamine and water data show that As, Ba, Sb, Cu, K and Na have a positive relation with water chemistry (Table 4.25). Correlation coefficients between pH and cold hydroxylamine are positive for Ba, Mn, Mg, Ca, Co, Cd, Zn, K, Tl and Sr, but negative for Cu and V. In general, as stream pH increases the concentration of all elements, except Fe, increases.

4.4 Heavy minerals in drainage sediments

The –106+75μm and –75+53μm fractions of one stream sediment sample (site 1, high energy) were separated into heavy (S.G. >3.3) and light (S.G. < 3.3) mineral fractions. The light mineral fraction was analyzed with a total (triple acid) digestion. A representative sub-sample of the heavy mineral fraction was submitted for neutron activation analysis (NAA). Concentrations of elements common to both analytical techniques and *aqua regia* digestion of the -53μm medium energy are presented in Table 4.26. In an attempt to further concentrate rare, presumably non-magnetic grains, the remaining sample was further segregated into magnetic and non-magnetic heavy mineral fractions. A representative sub-sample of magnetic and non-magnetic separates for both size fractions was mounted in epoxy resin, polished and carbon coated for identification of heavy mineral phases using the scanning electron microscope and concurrent energy dispersive spectra.

Table 4.26. Comparison of concentrations between original sample and light and heavy mineral fractions. Original analysis is aqua regia digestion on -53µm medium energy sample. Light mineral fraction is total digestion of high energy sample for respective size fractions. Heavy mineral concentrations are from neutron activation analysis of high energy sample for each size fraction. All concentrations in ppm except Au (ppb).

	Site 1 -106+75µm high energy		
	Lights	**Heavies**	**HM (% total)**
Au	30.00	7800.00	96.9
Ag	1.40	10*	---
As	311.00	624.00	19.2
Ba	500.00	37700.00	89.9
Co	3.20	53.00	66.3
Cr	9.00	220.00	74.4
Hg	0.07	10*	---
Mo	3.20	34.00	55.8
Sb	7.10	25.00	29.4
U	1.20	31.00	75.4
W	1.80	27.00	64.0
Zn	158.00	550.00	29.2

	Site 1 -75+53µm high energy		
	Lights	**Heavies**	**HM (% total)**
Au	40.00	37200.00	98.1
Ag	1.55	17.00	49.5
As	322.00	700.00	16.3
Ba	200.00	53400.00	96.0
Co	3.60	47.00	4.8
Cr	11.00	230.00	65.1
Hg	0.16	10*	---
Mo	3.00	5.80	38.5
Sb	7.50	30.00	26.3
U	1.40	56.00	78.1
W	1.60	45.00	71.5
Zn	176.00	610.00	23.6

* indicates value at or below detection limit

Light minerals account for approximately 90% of the sample mass in both size fractions (Table 4.27). Elements are found in greater concentration in the heavy mineral fraction than in the light mineral fractions (Table 4.26), e.g. Au is 260 and 930 times greater in HM separate for the –106+75 and –75+106μm fractions, respectively. The heavy mineral fraction accounts for between a minimum of 19.2% (As) and a maximum of 96.9% (Au) of total concentration (HM plus LM) in the –106+75μm fraction and between 16.3% (As) and 98.1% (Au) in the –75+53μm fraction. Results of fire assay gold can be directly compared with the Au concentration calculated from a weighted average of heavy and light mineral fractions (Table 4.28).

Scanning electron microscopy confirmed the presence of Ba, S, Fe, Ti, Pb, Hg, Au, Ag, Cu, Sb, As, Zn and Te in the heavy mineral fraction of –106+75 and –75+53μm stream sediments. Relative abundances of minerals found in the magnetic and non-magnetic heavy mineral fractions are qualitatively classified as rare, subordinate, common and dominate (Table 4.29). Mineralogy of the magnetic fraction was dominated by magnetite, titaniferous magnetite and pyrite grains. Mineralogy of the non-magnetic fraction was dominated by barite, pyrite, zircon and monazite grains.

4.5 Chemical precipitates

Semi-qualitative mineralogy was determined with step-scan X-ray powder diffraction (XRD) for 15 samples (Table 4.30). Scanning electron microscopy and energy dispersive spectra were also collected to confirm XRD results. Ten precipitate samples from Lama were assigned qualitative relative abundances from XRD results with gypsum and epsomite being the dominant phases.

Table 4.27. Breakdown of weight percentage of sample mass between light mineral, magnetic and non-magnetic heavy mineral fractions.

	weight LM (%)	Weight HM (%)	
		magnetic	non-magnetic
-106+75μm	89.40	6.40	4.20
-75+53μm	91.80	4.40	3.70

Table 4.28. Calculated concentrations of gold (ppb) from HM and LM results.

	Calculated		**Fire assay**	
	-106+75μm	**-75+53μm**	**-106+75μm**	**-75+53μm**
Au	853.60	3087.12	1110.00	2180.00

Mineral	-106+75μm non-magnetic	-106+75μm magnetic	-75+53μm non-magnetic	-75+53μm magnetic
Barite	d	c/s	d	s
Zircon	s	s	c	
Magnetite (Fe3O4)	c/s	d	r	d
Ti-magnetite	s/c	c	s	c/d
Pyrite	c	s	c	s
Galena (PbS)	c	r	c	
Pb,As,S	c	r	c	
Pb,As,Fe,S	c	r	c	
Monazite	c	s	c	r
Cinnabar (HgS)		r	r	
Illmenite	c	s	r	
Au (with Ag)	2 grains	0 grains	6 grains	0 grains
Enargite (?CuAsS)	c	s	r	
Bismuthinite (?)	s			
AgS (Acanthite)	1 (pure Ag)		1 grains	
Cu,Sb,As,S (stibnite with sub?	r		r	
Sphalerite (ZnS)	c			
AgI	r (3 grains)			
Hg,As,S,Sb			r	
Au,Ag, Te			1 grain	

r = rare
s = subordinate
c = common
d = dominate

Table 4.29. Relative abundances of heavy mineral and unidentified phases at site 1 stream sediment sample.

Sample 20, taken from sediment site 5 along the R. Turbio, is unique with alunogen ($Al_2(SO_4)_3 \cdot 17\ H_2O$), roemerite ($Fe_3(SO_4)_4 \cdot 14\ H_2O$) and coquimbite ($Fe_3(SO_4)_3 \cdot 9\ H_2O$) as the main phases.

Waters emerging from the precipitate seeps appear to be intermediate to both the R. Turbio and R. Canito water chemistries (Table 4.31) but have pH values similar to the R. Turbio. Concentrations of Al, As, Ca, Cd, Co, Fe, K, Mg, Mn, Na, Ni, Sr and Zn are two to ten times higher in the seepage water than in the R. Canito. Rio Turbio waters have higher average concentrations of all elements except Ca (2.4 times greater in seepage waters). Twelve bulk samples of chemical precipitates were analyzed after a total decomposition. All but seven elements (Hg, Cd, Cr, Co, Ag, Ar, and U) have maximum/minimum ratios greater than ten (Table 4.32). The iron concentration of four samples exceeds 25%. Calcium and Fe are the only elements found in greater concentrations in chemical precipitates than in stream sediments (total digestion).

Table 4.30. Relative abundances of mineral phases in chemical precipitates as determined by XRD (H= high, M= medium, L= low).

Mineral	Chemical formula	20	29	30	31	32	41	42	44	48	70
Color*		lt. yellow	white	yellow	dk. tan	white	white	brown	lt. brown	yellow	white
Gypsum	$CaSO_4 \cdot 2H_2O$		H	H	H	H	H	H	H	H	H
Epsomite	$MgSO_4 \cdot 7H_2O$		M	M	M			M		M	L
Tamarugite	$NaAl(SO_4)_2 \cdot 6H_2O$			L	L	L					
Jarosite	$KFe_3(SO_4)_2(OH)_6$						L		M		
Quartz	SiO_2			L		M			L		
Muscovite	$KAl_2(AlSi_3O_{10})(OH)_2$							L		L	
Biotite	$K(Mg,Fe)_3(AlSi_3O_{10})(OH)_2$				M						
Ferricopiapite	$Fe_{4.67}(SO_4)_6(OH)_2 \cdot 20H_2O$					L		L			
Magnesite	$MgCO_3$	M									
Barrerite	$(Na,K,Ca)_2(Si,Al)_9O_{18} \cdot 7H_2O$				L						
Marcasite	FeS_2				L						
Magnetite	MnOOH				L						
Metavoltine	$Na_6K_2Fe_7$			L							
Bassanite					L						
Alunogen	$Al_2(SO_4)_3 \cdot 17H_2O$	H									
Coquimbite	$Fe_3(SO_4)_3 \cdot 9H_2O$	L									
Roemerite	$Fe_3(SO_4)_4 \cdot 14H_2O$	M									

* Color of precipitate when collected.

Table 4.31. Descriptive statistics of waters associated with chemical precipitates (n=4).

	Units	Mean	Minimum	Maximu	Max/Min
pH		2.9	2.8	3	1.1
Ag	µg/l	0.05	<0.05	<0.05	1.0
As	µg/l	24.50	<1.0	95.0	95.0
Bi	µg/l	0.05	<0.05	<0.05	1.0
Hg	µg/l	1.00	<1.0	<1.0	1.0
Pb	µg/l	2.50	2.0	4.0	2.0
Al	mg/l	8.46	7.54	9.15	1.2
Ba	µg/l	6.39	2.45	9.4	3.8
Ca	mg/l	486.75	350	808	2.3
Cd	µg/l	0.35	<0.1	0.6	6.0
Co	µg/l	10.46	6.28	13.7	2.2
Cr	µg/l	0.63	<0.5	1.0	2.0
Cu	µg/l	5.13	3.4	10.1	3.0
Fe	mg/l	8.43	1.06	22.2	20.9
K	mg/l	11.01	9.55	12.0	1.3
Mg	mg/l	34.03	28.3	46.0	1.6
Mn	µg/l	6212.50	3780	12480	3.3
Mo	µg/l	0.10	<0.1	<0.1	1.0
Na	mg/l	16.55	14.25	21.8	1.5
Ni	µg/l	12.00	8.6	14.6	1.7
P	mg/l	0.10	<0.1	<0.1	1.0
Sb	µg/l	0.05	0.05	0.05	1.0
Se	µg/l	1.25	<1.0	2.0	2.0
Sn	µg/l	0.50	<0.5	<0.5	1.0
Sr	µg/l	801.00	588	1340	2.3
Ti	µg/l	1.00	<1.0	<1.0	1.0
U	µg/l	0.36	0.25	0.4	1.6
V	µg/l	2.25	<1.0	6	6.0
Zn	µg/l	417.25	347	545	1.6

Table 4.32. Descriptive statistics of bulk chemical precipitates after total digestion (n = 12).

Element	Units	Mean	Median	Minimum	Maximum	Max/Min
As	ppm	171.0	95.5	2	641	320.5
Hg	ppb	11.67	10	10	20	2.00
Sb	ppm	1.34	0.75	0.3	5	16.67
Bi	ppm	0.38	0.215	0.04	1.44	36.00
Pb	ppm	40.71	27	10.5	160	15.24
Ag	ppm	0.20	0.175	0.05	0.5	10.00
Al	%	1.06	0.63	0.08	4.84	60.50
Ba	ppm	123.3	75	10	550	55.00
Be	ppm	0.35	0.25	0.05	1	20.00
Cd	ppm	0.05	0.03	0.02	0.14	7.00
Ca	%	10.52	14.6	0.06	21.2	353.3
Cr	ppm	3.17	2	1	9	9.00
Co	ppm	2.15	2.4	0.6	4.2	7.00
Cu	ppm	9.42	8	1	34	34.00
Fe	%	11.54	11.55	0.11	25 (+)	227.27
Li	ppm	5.10	4.8	0.2	12.4	62.00
Mg	%	0.21	0.14	0.01	0.66	66.00
Mn	ppm	324.6	210	30	795	26.50
Mo	ppm	1.20	0.4	0.2	4.8	24.00
Ni	ppm	3.67	4.5	0.2	6.8	34.00
Na	%	0.28	0.24	0.02	0.67	33.50
Ti	%	0.03	0.015	0.01	0.14	14.00
W	ppm	3.69	2.7	0.6	15.3	25.50
U	ppm	0.28	0.2	0.2	1	5.00
V	ppm	42.25	38	1	102	102.00
Zn	ppm	67.50	70	6	112	18.67

CHAPTER 5

PASCUA, CHILE RESULTS

5.1 Surficial media

To complement stream sediment sampling, one hundred thirty two surficial samples of glacial till, talus fines, debris flow and alluvial material were collected. Classification of the media was determined in the field based on morphology, texture and air-photo interpretation. Field discrimination and spatial distribution of the materials is detailed in Chapter 2. No alluvial fans were sampled on the Pascua property.

5.1.1 Glacial till

Twelve glacial till samples were collected along the R. Estrecho valley adjacent to and east of the Pascua camp. Tills are aligned laterally to the R. Estrecho and form discontinuous ridges terminating west of the confluence of the R. Estrecho and Quebrada Los Barriales (Figure 2.7).

5.1.1.1 Texture and geochemistry

Weight percent abundances of the seven size fractions is dominated by fine gravel and coarse sand (-2mm+850μm) with a decrease in relative abundance with size to a minimum of 6.1 % in the –106+53μm fraction (Table 5.1). Abundance of the -53μm fraction, which comprises 45.8% of the fine sand and finer material, does not have a discernable pattern in glacial till (Figure 5.1).

Table 5.1. Descriptive statistics of glacial till samples after aqua regia digestion (n=12). Maximum/minimum ratios greater than ten are in bold. Elements included in the high sulfidation epithermal geochemical suite (as defined by Hedenquist et.al., 1996) are grouped together. Median values reported for gold.

Element	Units	Mean	Minimum	Maximum	Max/Min
Au	-212+106μm	7.5	5	600	**120.0**
Au	-106+53μm	7.5	5	165	**33.0**
Au	-53μm	35	5	190	**38.0**
pH		7.70	4.7	9.5	2.0
Cu	ppm	130.85	21	467	**22.2**
Ag	ppm	0.66	0.08	2.46	**30.8**
As	ppm	40.58	3.4	131	**38.5**
Pb	ppm	59.83	8	150	**18.8**
Hg	ppm	0.14	0.01	0.58	**58.0**
Sb	ppm	0.67	0.1	2	**20.0**
Te	ppm	0.26	0.05	0.8	**16.0**
Mo	ppm	2.37	0.8	5.4	6.8
Bi	ppm	1.72	0.52	3.52	6.8
Al	%	1.71	0.81	2.84	3.5
Ba	ppm	154.17	80	230	2.9
Be	ppm	1.12	0.5	1.9	3.8
B	ppm	10.00	10	10	1.0
Cd	ppm	0.45	0.08	0.8	**10.0**
Ca	%	0.38	0.04	0.73	**18.3**
Cr	ppm	22.17	11	35	3.2
Co	ppm	9.58	5.4	17.4	3.2
Ga	ppm	5.93	3.7	9.9	2.7
Ge	ppm	0.10	0.1	0.1	1.0
Fe	%	4.28	1.94	13.75	7.1
La	ppm	21.67	10	40	4.0
Mg	%	0.67	0.33	1.37	4.2
Mn	ppm	958.33	360	1430	4.0
Ni	ppm	14.50	5	26	5.2
P	ppm	790.83	530	1470	2.8
K	%	0.18	0.06	0.25	4.2
Sc	ppm	4.92	3	9	3.0
Se	ppm	0.54	0.5	1	2.0
Na	%	0.03	0.01	0.04	4.0
Sr	ppm	39.00	21	64	3.0
S	%	0.14	0.02	0.39	**19.5**
Tl	ppm	0.59	0.02	2.9	**145.0**
Ti	%	0.08	0.02	0.12	6.0
W	ppm	0.19	0.1	0.25	2.5
U	ppm	1.95	0.8	4.45	5.6
V	ppm	52.25	32	81	2.5
Zn	ppm	121.83	52	152	2.9
-4mm+2mm	%	25.5	12.8	46.5	
-2mm +850μm	%	20.1	14.0	34.1	
-850+425μm	%	16.1	8.8	28.3	
-425+212μm	%	12.3	6.5	17.7	
-212+106μm	%	8.0	3.1	13.5	
-106+53μm	%	6.1	2.1	13.6	
-53μm	%	11.9	2.3	23.6	

Table 5.2. Correlation coefficients for selected elements of Pascua glacial till (df = 10), r significant at greater than 0.576 at P=0.05 with 95% confidence. Significant values in **bold**.

	Au
Cu	**0.81**
Ag	**0.95**
As	**0.89**
Pb	0.49
Hg	0.31
Sb	**0.84**
Te	**0.88**
Mo	**0.69**
Bi	**0.70**
Al	-0.09
Ba	0.31
Be	-0.47
Cd	-0.26
Ca	**-0.58**
Cr	-0.32
Co	-0.45
Fe	**0.85**
Mg	-0.42
Mn	-0.55
Ni	**-0.58**
P	0.05
K	0.21
Se	**0.90**
Na	0.17
Sr	-0.43
S	**0.88**
Sc	-0.32
Tl	**0.94**
Ti	-0.08
W	0.15
U	-0.26
V	-0.01
Zn	-0.01

Figure 5.1. Distribution of coarse and fine material in glacial till at Pascua.

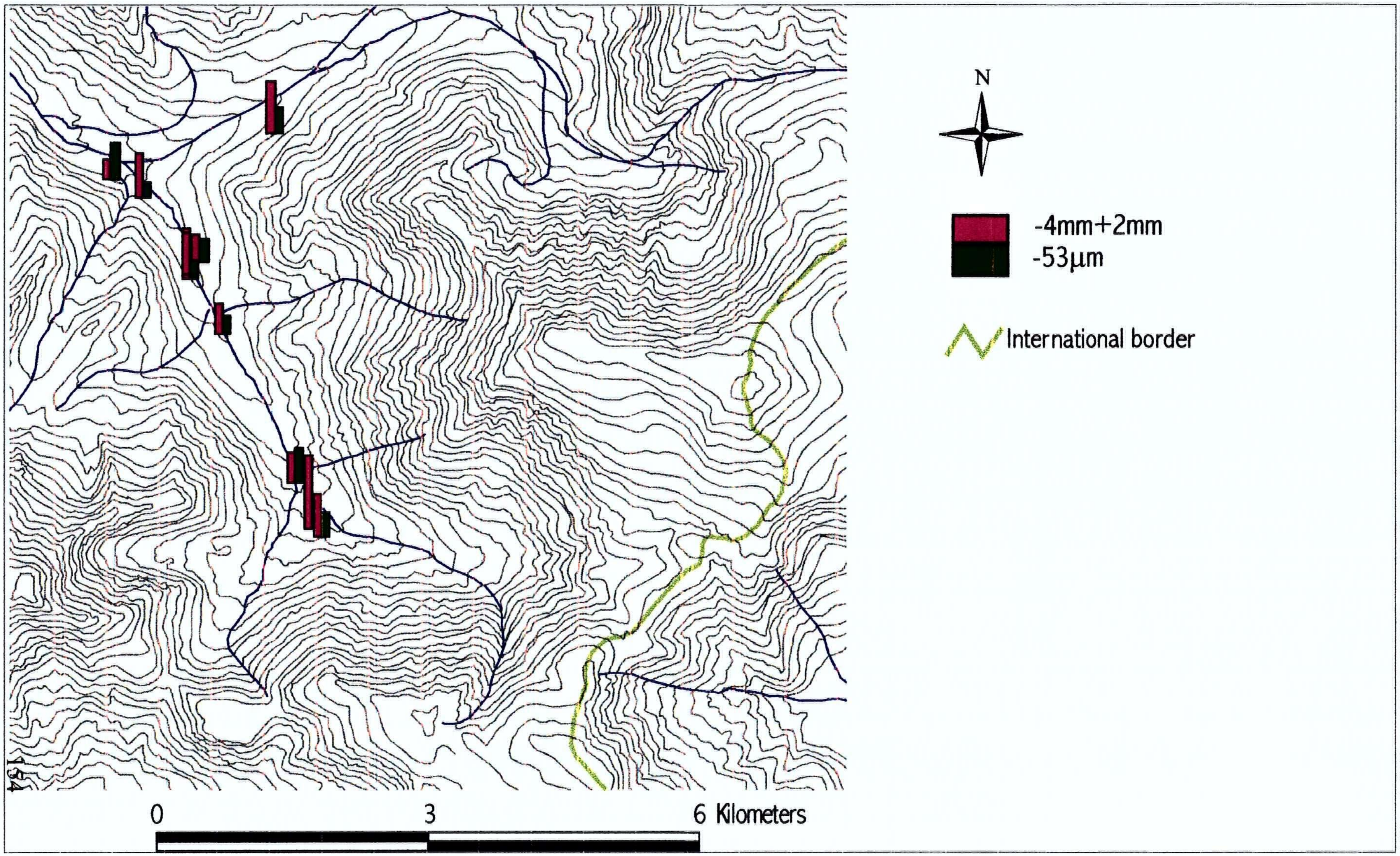

Figure 5.2. Gold in -53 µm fraction of glacial till at Pascua.

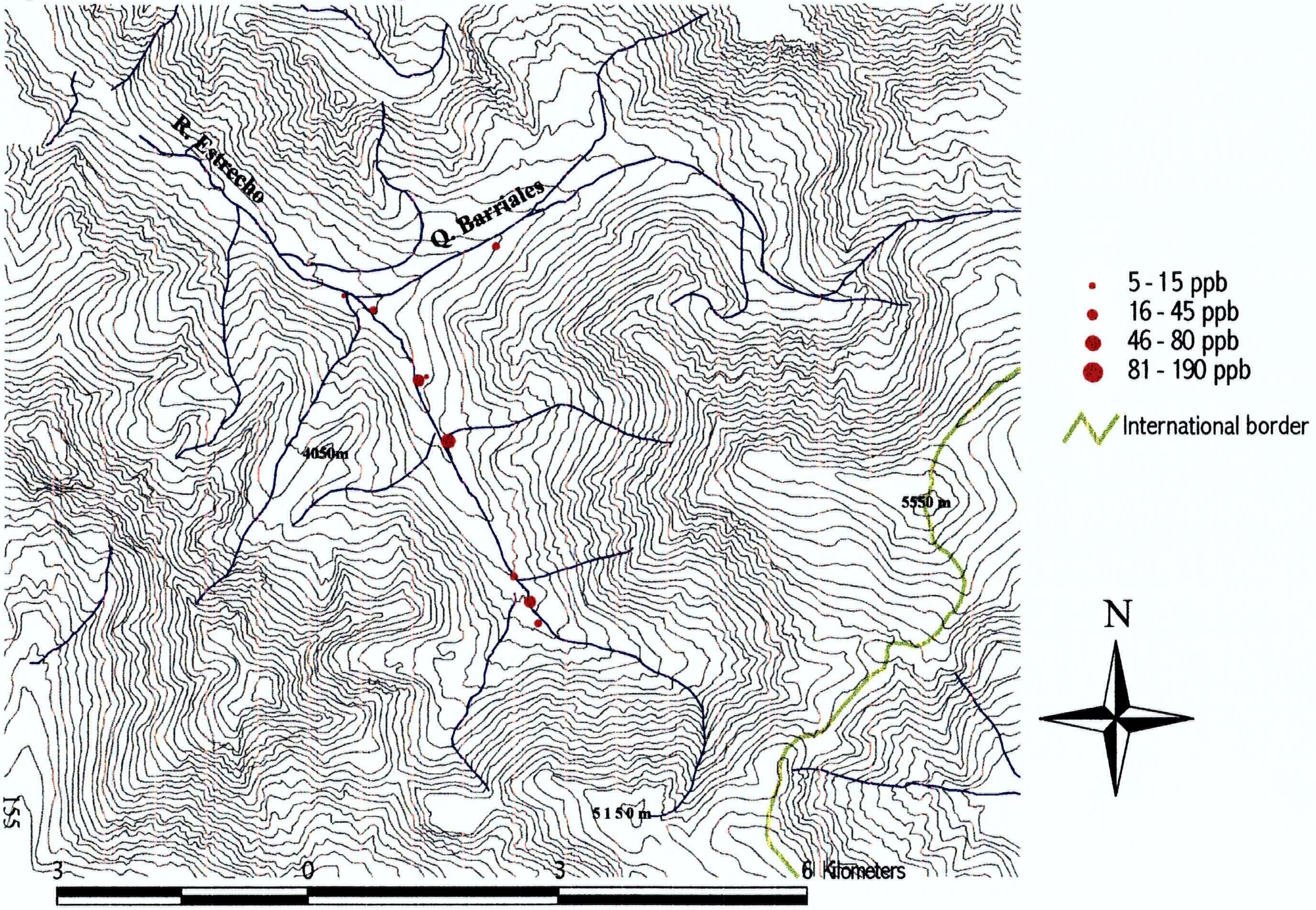

Figure 5.3. Cu in glacial till.

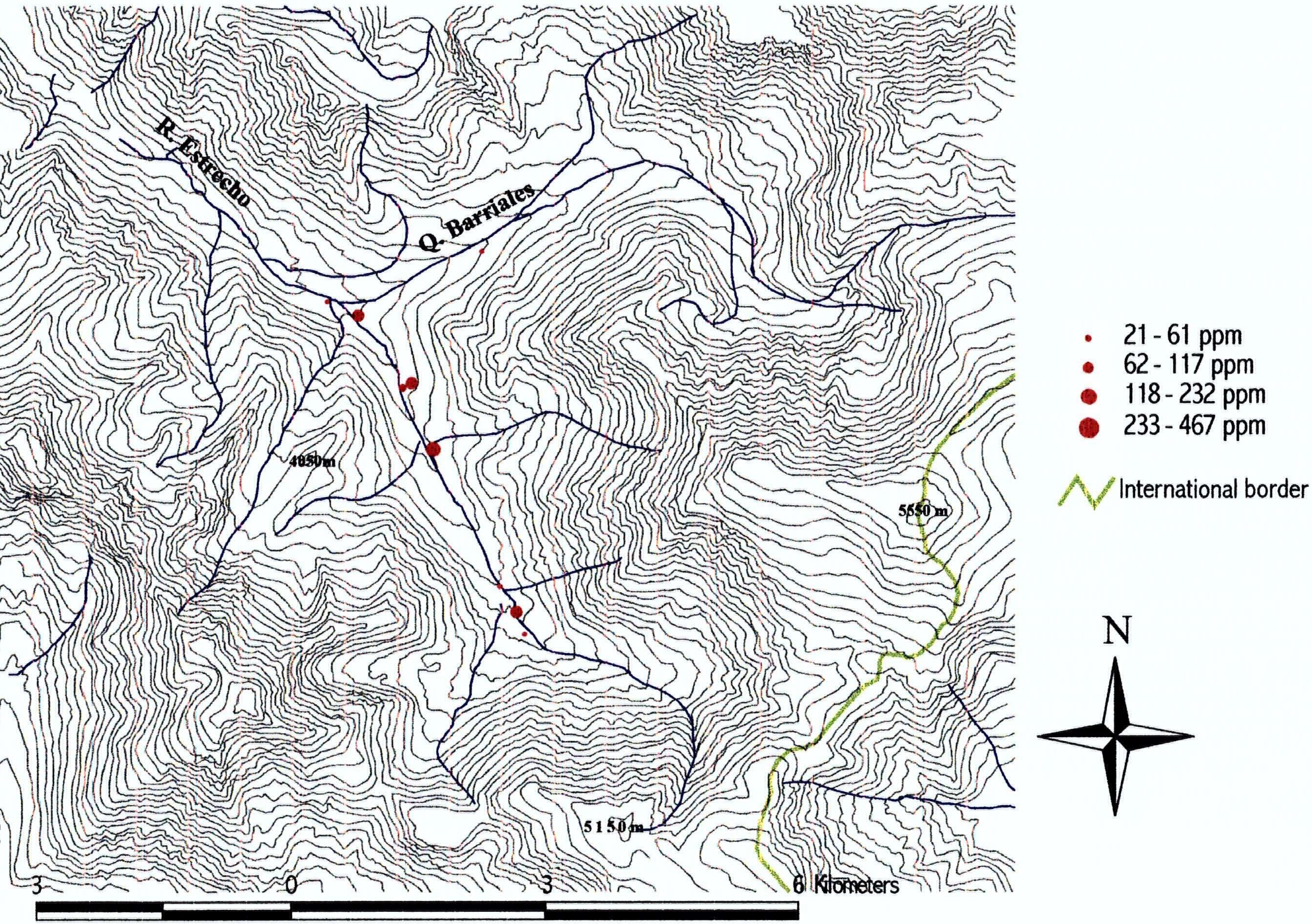

Figure 5.4. Ni in glacial till.

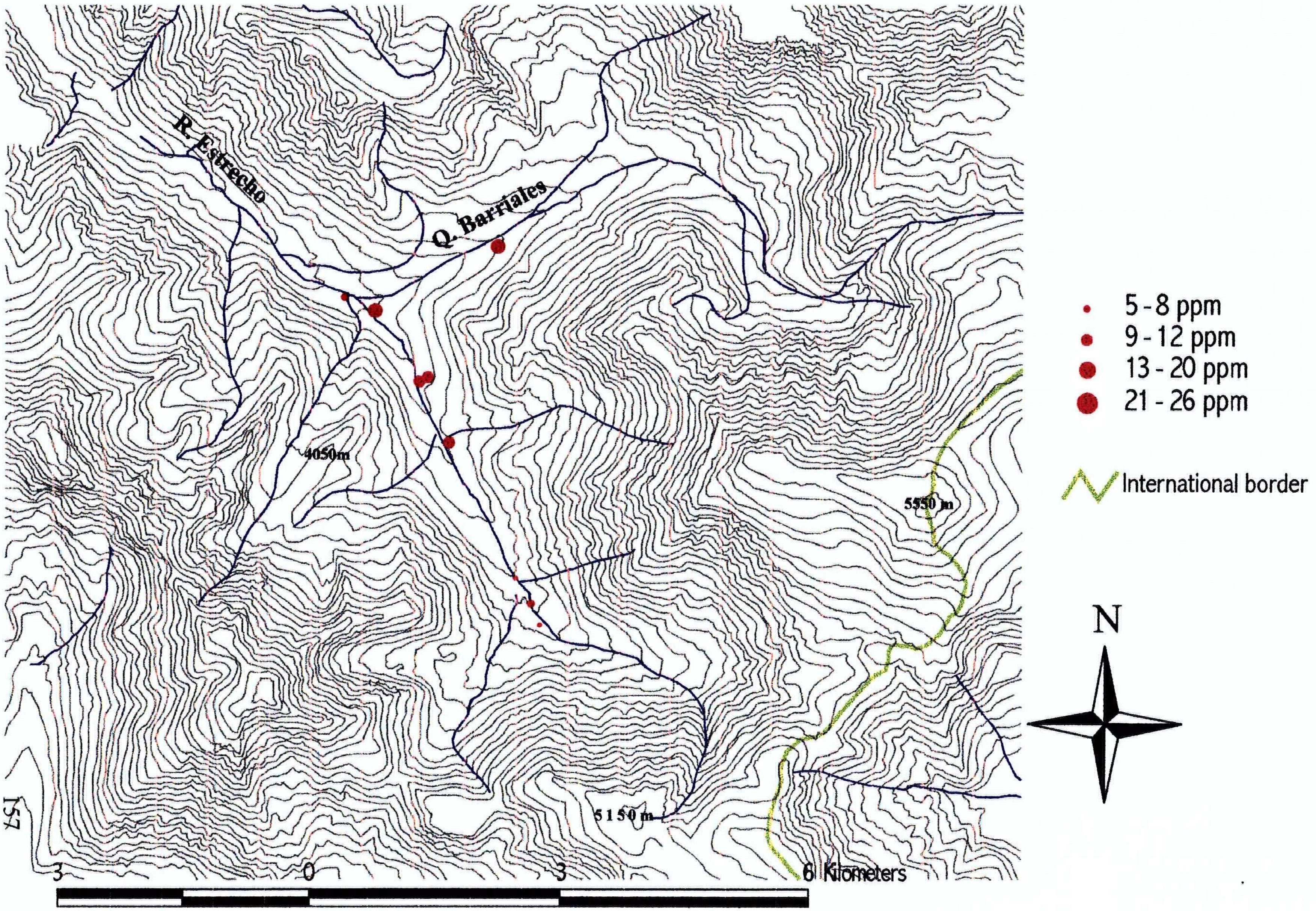

Figure 5.5. Pb in glacial till.

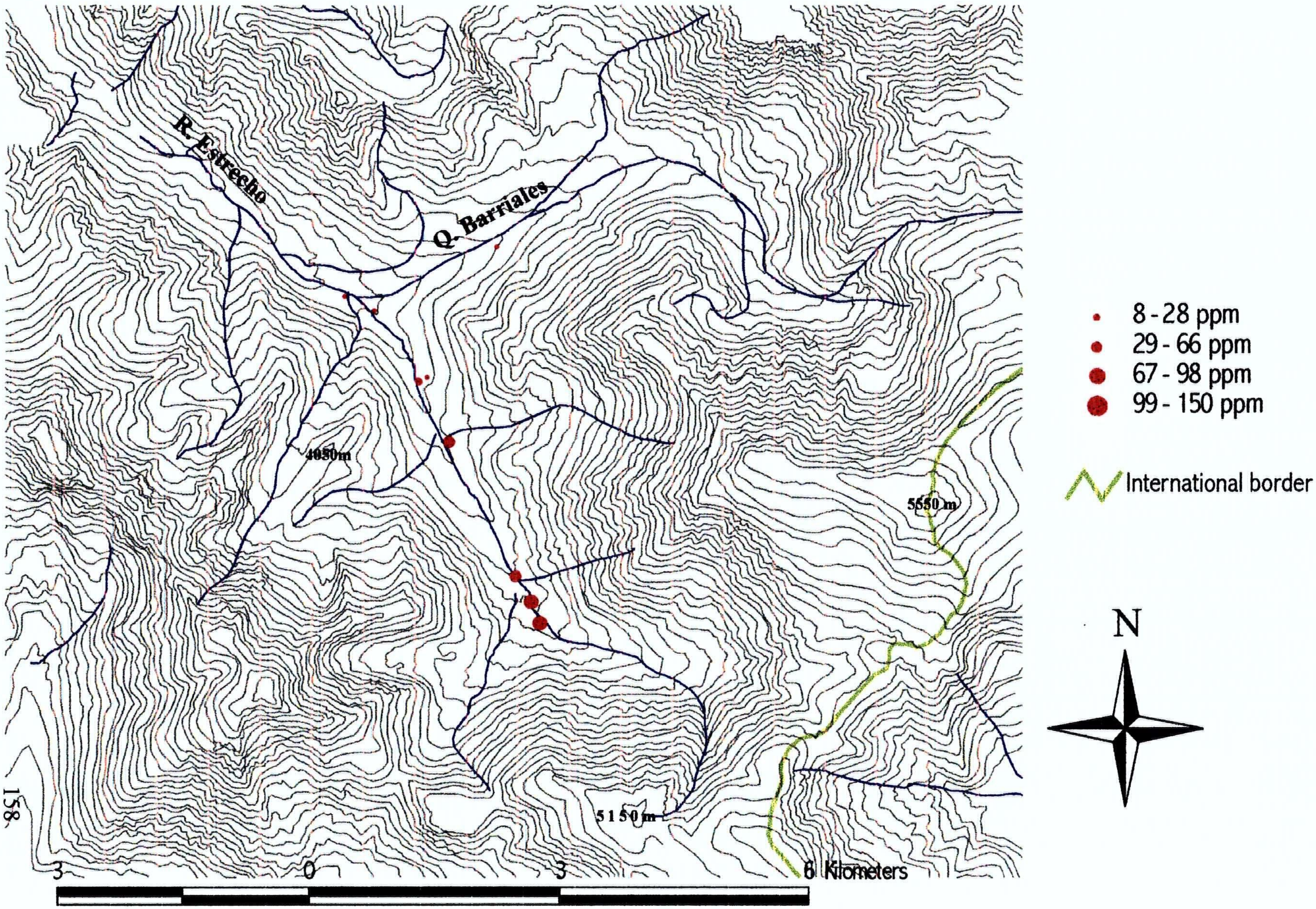

Figure 5.6. Ca in glacial till.

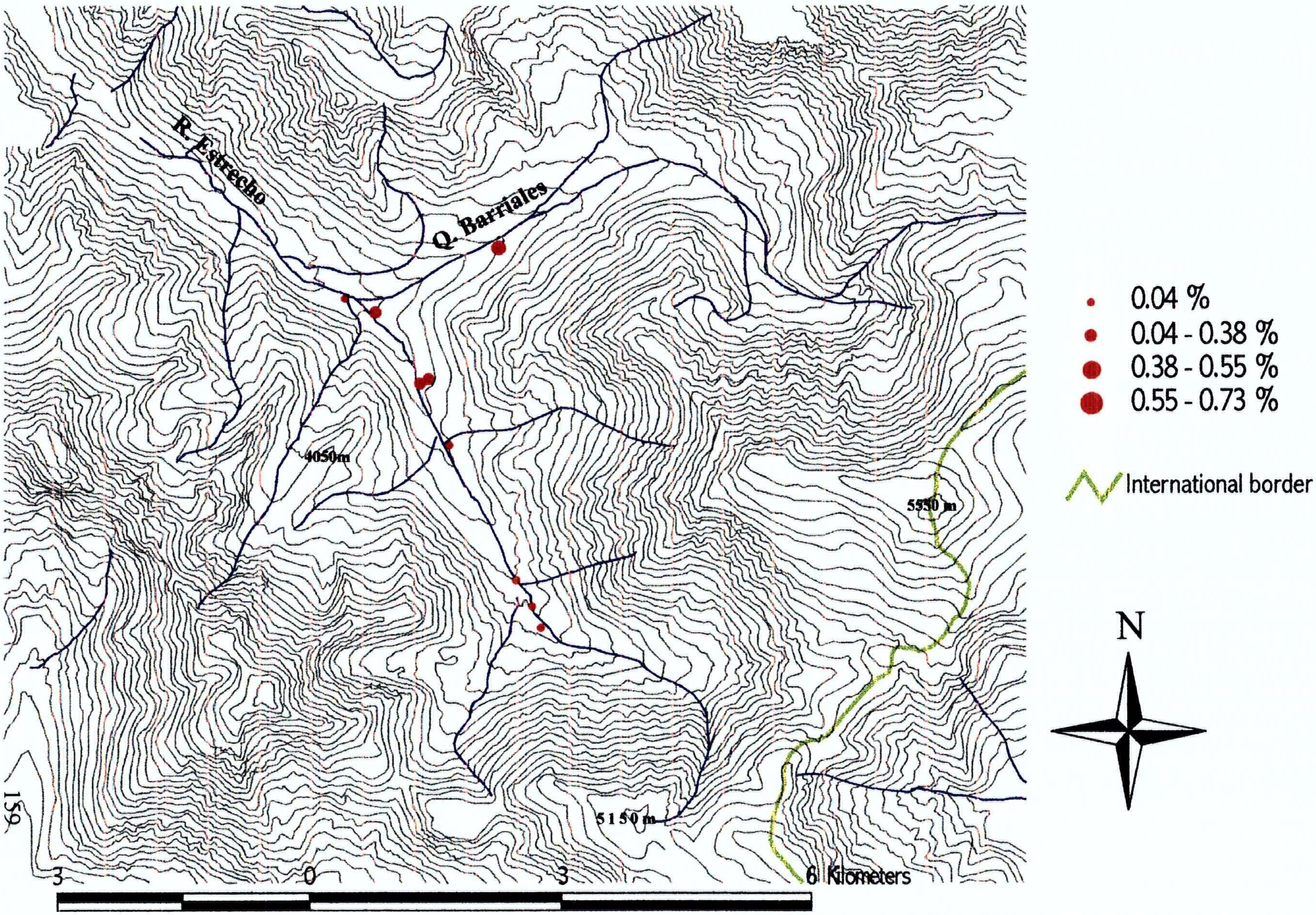

Geochemically, there are no obvious down ice glacial dispersion patterns (Figure 5.2-5.6). Eleven elements are either at their detection limits (B and Ge) or have maximum to minimum ratios of less than three (Ba, Ga, P, Sc, Se, Sr, W, V and Zn) (Table 5.1). Examination of element dispersion maps and correlation coefficients shows two element groups: (1) antimony, As, Bi, Cu, Fe, Mo, Se, Ag, S, Te and Tl are positively correlated with gold ($r > 0.576$) (Table 5.2). Aluminum, Be, Ca, Cr, Co, Fe, Mg, Mo, Sr, Ni, K, Ti and U show maximum values associated with gold lows (e.g. Ni in Figure 5.4). Beryllium, Ca, Cd, Cr, Co, Mn, Mg, Ni, Sc, U and Sr have negative, but except for Ca and Ni, non-significant correlations with gold (Table 5.2).

While there does not appear to be consistent down-ice dispersion, each valley has a unique and identifiable geochemical signature (e.g. Pb in Figure 5.5). Tills from Q. Los Barriales are lower in -53µm gold (average 17.5 ppb) and higher in Ca (average 1.97%), than the R. Estrecho tills (Au average of 76 ppb and average Ca of 1.3%) (Figures 5.2 and 5.6). The same patterns are seen with As, Sb, Bi, Cu, Pb, Ag, S, Ca, Na and Tl. Only one glacial till sample has an acidic pH (4.7), all others are neutral to alkaline, averaging 7.7.

5.1.2 Debris flows

Debris flow is used to describe poorly sorted landforms with minor rounding and imbrication of clasts (with other flow features) that were deposited around topographic highs and occupy valley bottoms. Ten debris flow samples were collected at Pascua, two to five kilometers southeast of the camp along the R. Estrecho headwaters.

5.1.2.1 Texture and geochemistry

Debris flow samples tend to be coarse, with only 17.6% of the sample mass in the -212μm (fine sand and smaller) fraction. On average, the -53μm fraction comprises 32.9% of the -212μm mass. The size fraction distribution of material in each sample remains relatively constant and does not vary consistently between upstream and downstream samples (Figure 5.7). Maximum median gold concentration of 267.5 ppb occurs in the -53μm fraction (Table 5.3), and is (almost) uniformly distributed through the debris flow, except the eastern most sample which contains only 50 ppb (Figure 5.8). Elements with strong (significant) positive correlations to gold include Sb, As, Bi, Pb, Hg, Ag, S, Te, Tl, W (Table 5.4). However, only Hg and W have maximum to minimum ratios greater than three. The spatial distribution of these elements is similar to gold (e.g. Ag and Sb in Figures 5.9 and 5.10). Aluminum, Ca, Co, Mg and Ti have both high values associated with gold lows (e.g. Mg in Figure 5.11), and are negatively correlated with gold. Although a trend in pH values is not well defined, it does tend to increase down valley, from 3.9 at the headwaters to 7.3 at the most distal sample (mean 6.7).

5.1.3 Talus cones

Eighteen samples were taken in Pascua along the northern and southern edges of the R. Estrecho valley. No distinction was made between talus material and other gravity transported colluvium. Talus fans were the most frequently sampled surficial media at Pascua other than stream sediments.

Table 5.3. Descriptive statistics of debris flow samples after aqua regia digestion (n=10). Maximum/minimum ratios greater than ten are in bold. Elements included in the high sulfidation epithermal geochemical suite (as defined by Hedenquist et.al., 1996) are grouped together. Median values reported for gold.

Element	Units	Mean	Minimum	Maximum	Max/Min
Au	-212+106μm	37.5	20	60	3.0
Au	-106+53μm	97.5	40	295	7.4
Au	-53μm	267.5	80	490	6.1
pH		6.72	3.9	9.9	2.5
Cu	ppm	158.90	90.5	399	4.4
Ag	ppm	5.83	3.28	7.88	2.4
As	ppm	286.65	190.5	380	2.0
Pb	ppm	266.60	154	390	2.5
Hg	ppm	1.43	0.53	3.28	6.2
Sb	ppm	3.40	2	4.8	2.4
Te	ppm	1.70	1.1	2.6	2.4
Mo	ppm	1.84	1.4	3	2.1
Bi	ppm	7.23	4.33	10.75	2.5
Al	%	1.65	1.32	2	1.5
Ba	ppm	467.00	350	590	1.7
Be	ppm	0.84	0.6	1.4	2.3
B	ppm	10.00	10	10	1.0
Cd	ppm	0.71	0.4	1.04	2.6
Ca	%	0.38	0.22	0.46	2.1
Cr	ppm	10.10	6	15	2.5
Co	ppm	9.26	6.2	10.8	1.7
Ga	ppm	5.60	4.8	6.1	1.3
Ge	ppm	0.10	0.1	0.1	1.0
Fe	%	4.22	3.8	4.67	1.2
La	ppm	20.00	10	30	3.0
Mg	%	0.57	0.37	0.77	2.1
Mn	ppm	1051.00	820	1390	1.7
Ni	ppm	6.70	5	8	1.6
P	ppm	741.00	580	810	1.4
K	%	0.42	0.37	0.48	1.3
Sc	ppm	3.90	3	5	1.7
Se	ppm	2.45	1.5	3.5	2.3
Na	%	0.13	0.11	0.14	1.3
Sr	ppm	73.40	54	89	1.6
S	%	0.80	0.65	0.96	1.5
Tl	ppm	1.92	1.28	2.54	2.0
Ti	%	0.04	0.02	0.05	2.5
W	ppm	0.58	0.2	1.2	6.0
U	ppm	1.56	1.2	2.3	1.9
V	ppm	42.60	31	50	1.6
Zn	ppm	226.40	178	324	1.8
-4mm+2mm	%	25.9	17.1	34.9	
-2mm +850μm	%	18.8	15.2	22.6	
-850+425μm	%	20.2	15.3	26.6	
-425+212μm	%	17.6	10.8	23.3	
-212+106μm	%	8.0	5.0	13.4	
-106+53μm	%	3.8	2.4	5.6	
-53μm	%	5.8	3.0	11.7	

Table 5.4. Correlation coefficients for selected elements of Pascua debris flows (df = 8), r significant at greater than 0.632 at P=0.05 with 95% confidence. Significant values in **bold**.

	Au
Cu	0.56
Ag	**0.77**
As	**0.77**
Pb	**0.83**
Hg	**0.80**
Sb	**0.87**
Te	**0.85**
Mo	0.17
Bi	**0.81**
Al	-0.50
Ba	0.26
Cd	0.16
Ca	-0.55
Cr	0.39
Co	**-0.73**
Fe	0.25
Mg	**-0.81**
Mn	-0.11
Ni	0.28
P	-0.36
K	0.32
Se	0.53
Na	-0.42
Sr	-0.45
S	**0.67**
Tl	**0.74**
Ti	**-0.79**
W	**0.64**
U	0.16
V	-0.38
Zn	0.46

Figure 5.7 .Comparison of coarse and fine material at Pascua in debris flows.

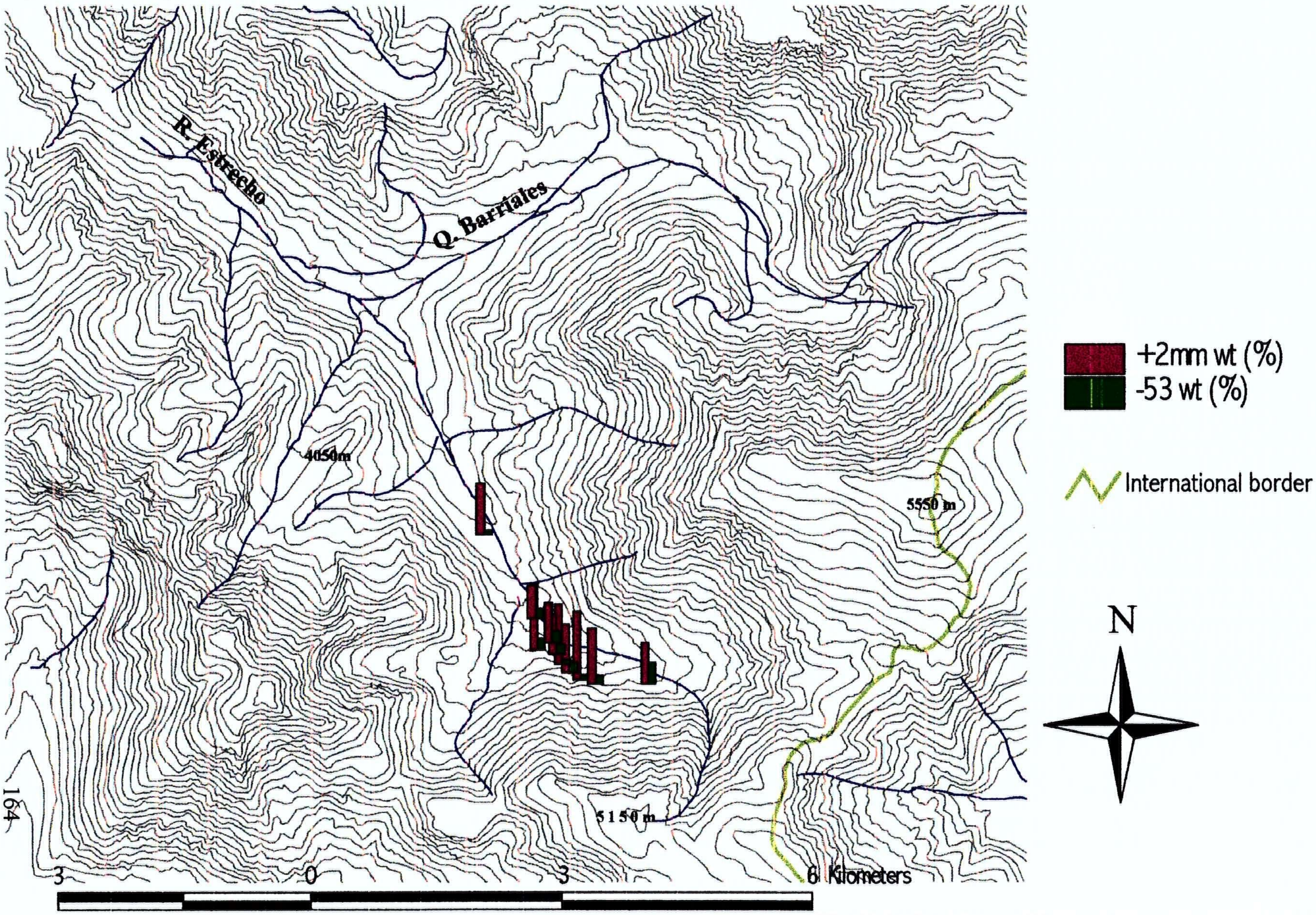

Figure 5.8. Gold in the -53μm fraction of debris flows.

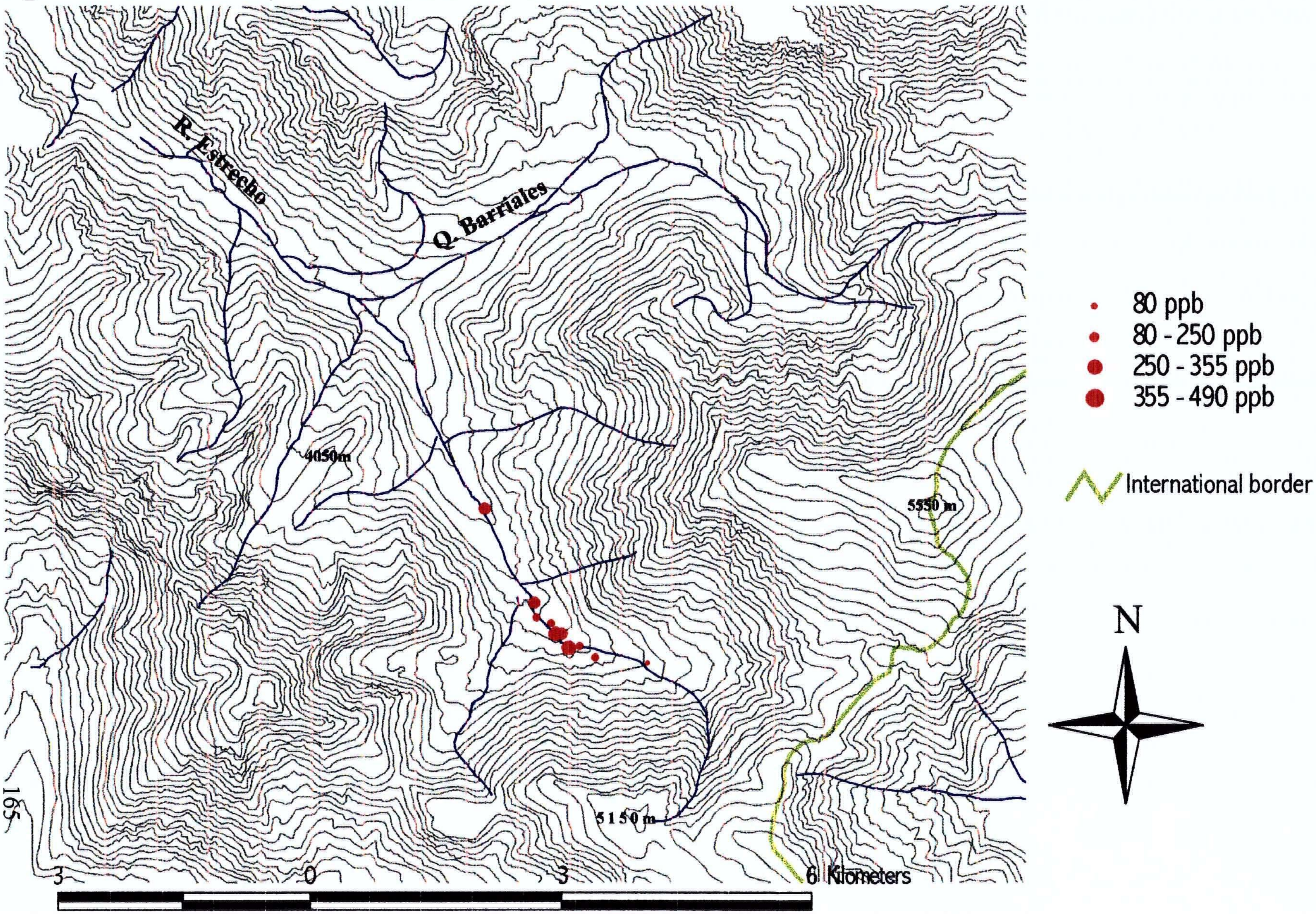

Figure 5.9. Ag in debris flows

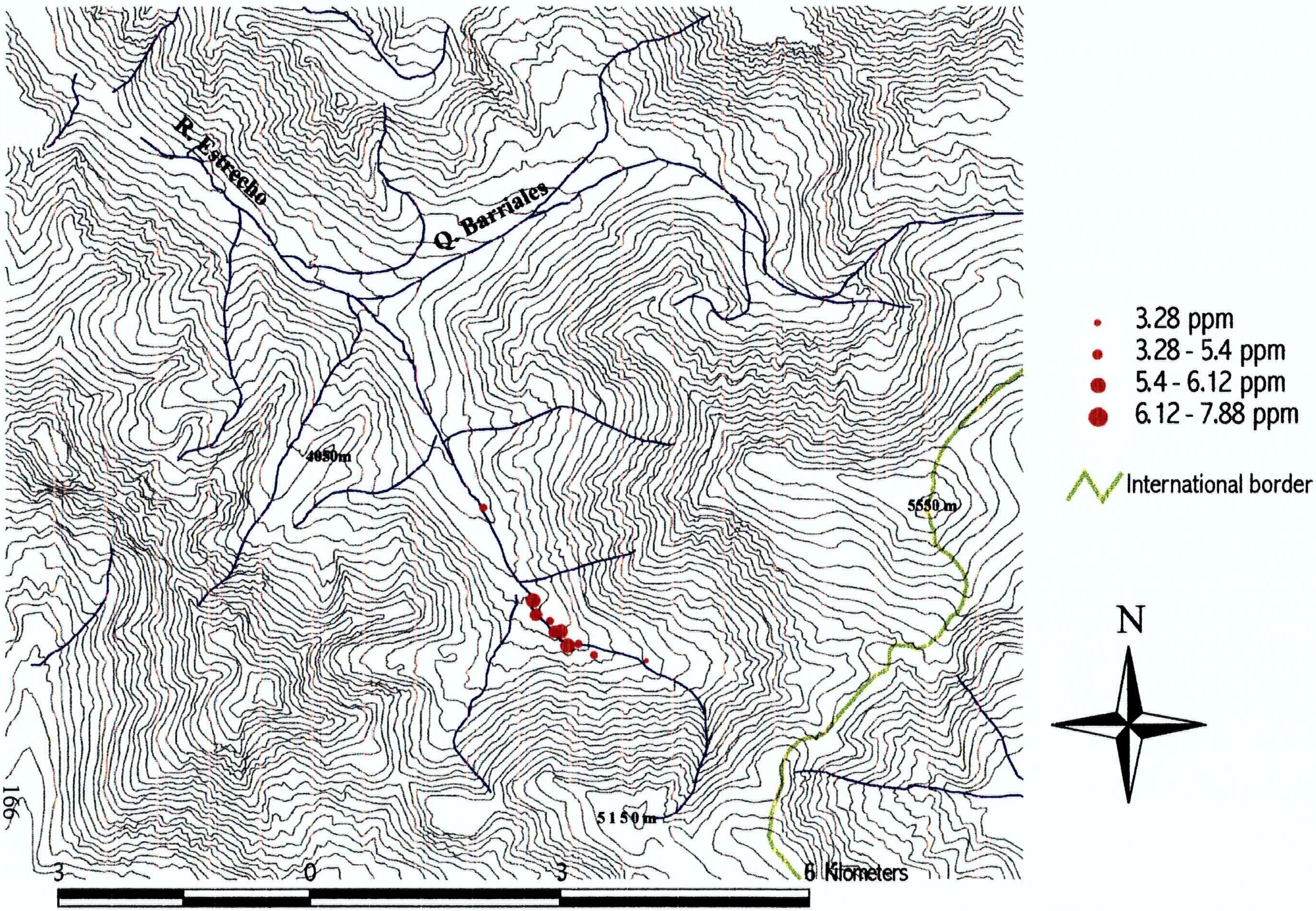

Figure 5.10. Sb in debris flows

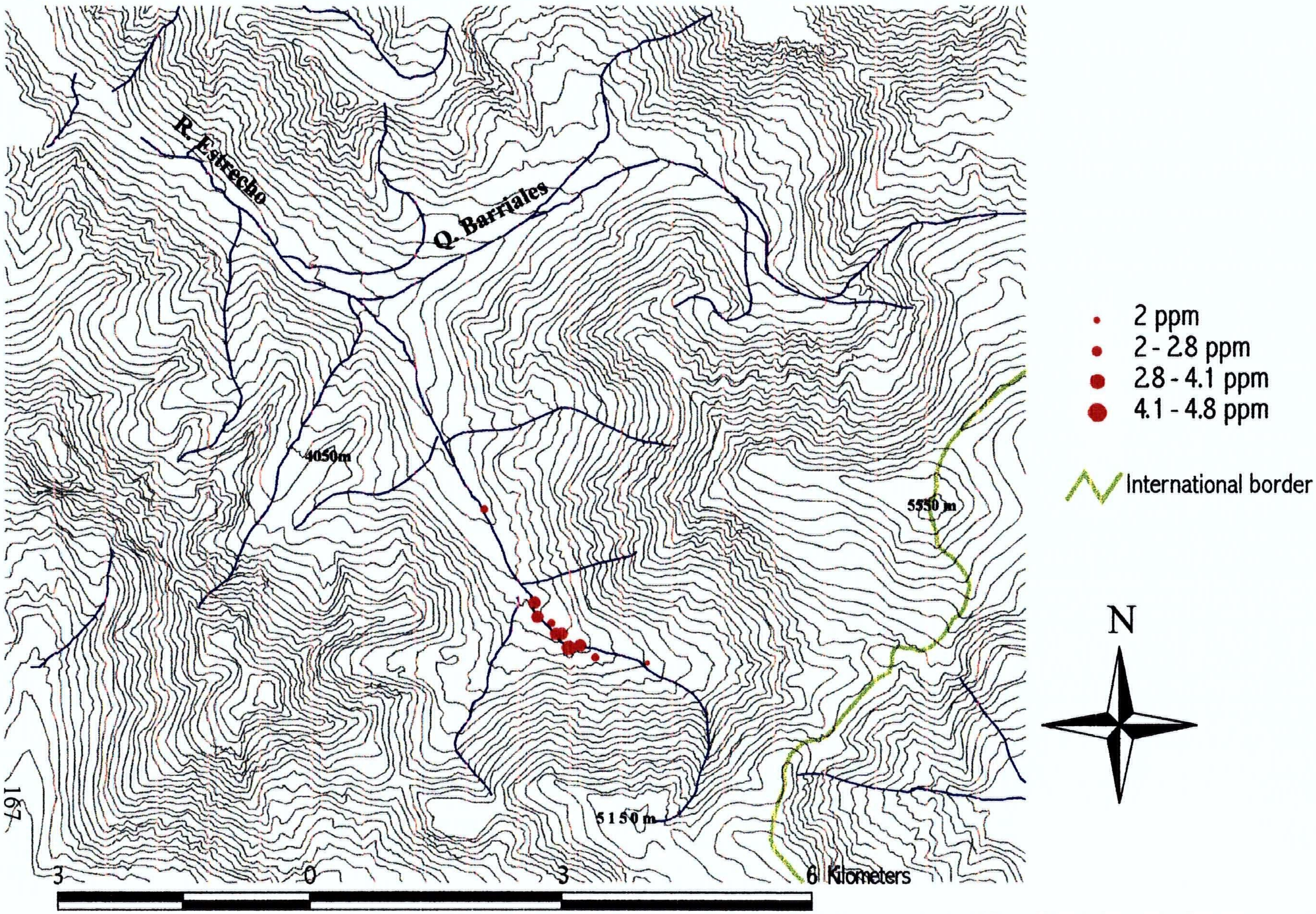

Figure 5.11. Mg in debris flows.

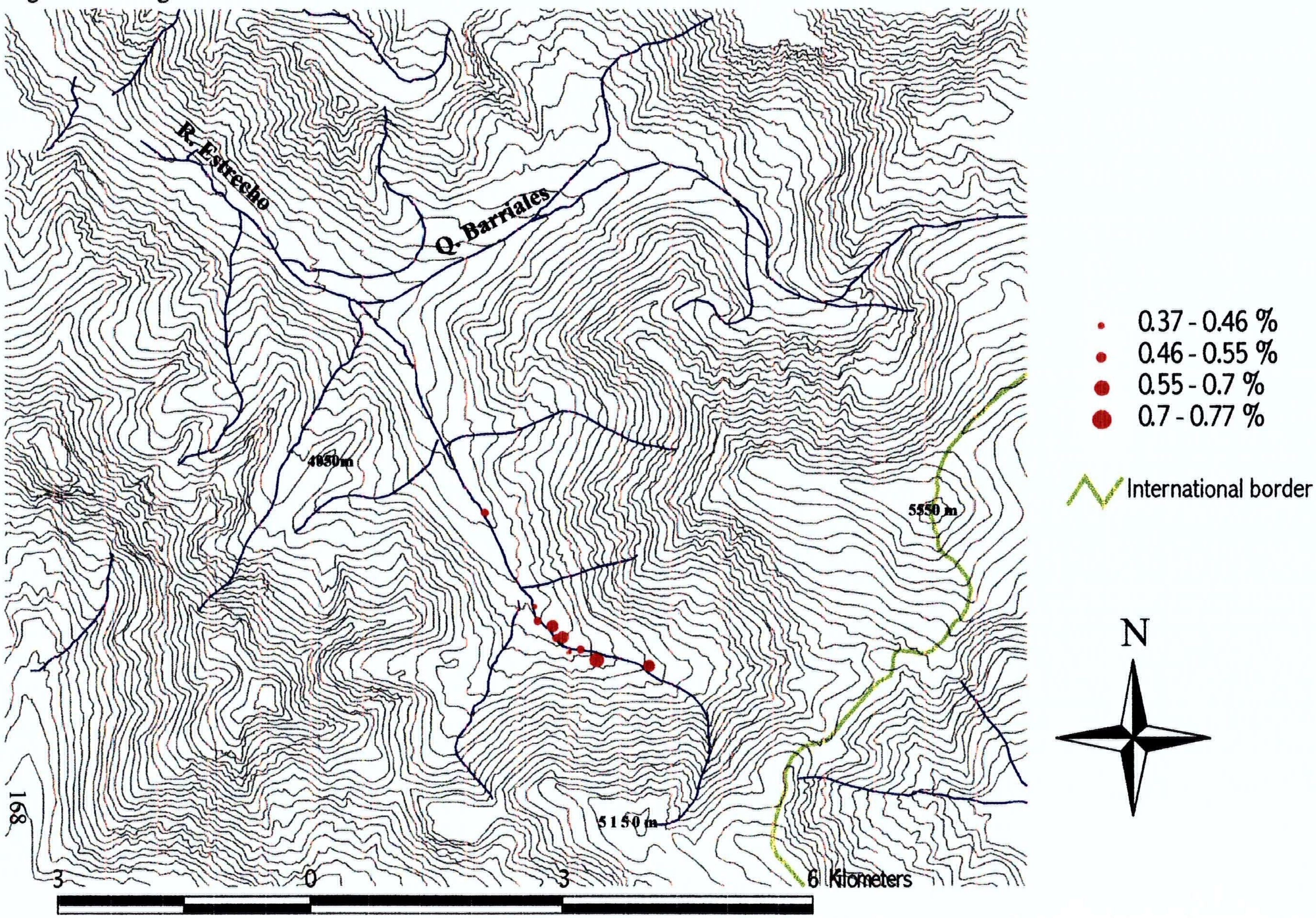

5.1.3.1 Texture and geochemistry

Weight percent distribution of the seven size fractions shows talus cones are dominated by coarse material of the -4mm+2mm fraction (Table 5.5) and fractions decrease in abundances as size decreases. The relative amount of coarse and fine material vary between individual talus cones, with the southwestern most cone containing up to 64.2% in the –4mm+2mm fraction, while a sample from the northwest cone consists of only 33.9% in the coarsest fraction (Figure 5.12). The -212μm material (fine sand and smaller) accounts for an average of 17.6% of the sample, with 52.3% of the fines comprised of the -53μm (silt and clay) fraction.

Greatest median gold concentrations (70 ppb) are found in the -53μm fraction. Gold in the -53μm fractions has significant positive correlation ($r > 0.47$) with Sb, As, Bi, Pb, Hg, K, Se, Ag, S and Te (Table 5.6), and significant negative correlations with Al, Be, Ca, Cr, Co, Mg, Ni, P, Sc, Sr, Ti, U and V. Gold concentration is dependant on which cone was sampled (Figure 5.13); cones along the southern and eastern margin of the R. Estrecho basin contain higher concentrations of gold with values ranging from 120 to 1195 ppb.

The distribution of other elements is also dependent on talus cone location (e.g. Ag in Figure 5.14). Eight elements are either at their detection limit (B and Ge), show no meaningful pattern (Ba, Be, W and U) or have maximum to minimum ratios less than three (Ga and Fe). The remaining elements are classed into two patterns: (1) those associated with elevated gold concentrations; and, (2) elements that are negatively associated with gold. The first group of elements (Sb, As, Bi, Pb, Hg, Mo, K, Se, Ag, S, Te and Tl) have a positive relationship with Au (Table 5.6). They show maximum values in talus cones along the southern and eastern most edge of the R. Estrecho drainage, with values decreasing to the north and west (e.g. Ag in Figure

Table 5.5. Descriptive statistics of talus cone samples after aqua regia digestion (n=18). Maximum/minimum ratios greater than ten are in bold. Elements included in the high sulfidation epithermal geochemical suite (as defined by Hedenquist et.al., 1996) are grouped together. Median values reported for gold.

Element	Units	Mean	Minimum	Maximu	Max/Min
Au	-212+106μm	7.5	5	325	**65**
Au	-106+53μm	12.5	5	1810	**362.0**
Au	-53μm	70	5	1195	**239.0**
pH		5.8	4.5	8.4	1.9
Cu	ppm	111.8	35.4	298	8.4
Ag	ppm	2.2	0.12	12.95	**107.9**
As	ppm	320.4	18.6	1230	**66.1**
Pb	ppm	438.9	36	1490	**41.4**
Hg	ppm	0.2	0.01	1.38	**138.0**
Sb	ppm	3.7	0.4	28.5	**71.3**
Te	ppm	2.3	0.05	10.05	**201.0**
Mo	ppm	4.3	0.6	21	**35.0**
Bi	ppm	8.8	0.73	52.3	**71.6**
Al	%	2.0	0.41	3.4	8.3
Ba	ppm	182.8	60	470	7.8
Be	ppm	1.4	0.05	3.8	**76.0**
B	ppm	10.0	10	10	1.0
Cd	ppm	1.2	0.08	5.56	**69.5**
Ca	%	0.5	0.01	1.01	**101.0**
Cr	ppm	22.3	7	41	5.9
Co	ppm	9.5	0.2	20.2	**101.0**
Ga	ppm	7.9	4.4	11.5	2.6
Ge	ppm	0.1	0.1	0.1	1.0
Fe	%	4.9	2.99	8.79	2.9
La	ppm	30.6	10	70	7.0
Mg	%	0.8	0.04	1.59	**39.8**
Mn	ppm	1380.0	50	5010	**100.2**
Ni	ppm	14.4	1	33	**33.0**
P	ppm	705.0	250	1070	4.3
K	%	0.5	0.17	0.99	5.8
Sc	ppm	5.3	1	10	10.0
Se	ppm	2.8	0.5	13	**26.0**
Na	%	0.1	0.03	0.16	5.3
Sr	ppm	55.6	18	124	6.9
S	%	0.7	0.01	2	**200.0**
Tl	ppm	2.9	0.34	7.78	**22.9**
Ti	%	0.1	0.01	0.17	**17.0**
W	ppm	0.3	0.15	1.1	7.3
U	ppm	1.8	0.25	3.55	**14.2**
V	ppm	47.3	12	69	5.8
Zn	ppm	249.9	20	1090	**54.5**
-4mm+2mm	%	44.4	22.0	81.0	
-2mm +850μm	%	19.4	9.9	33.1	
-850+425μm	%	10.1	1.0	19.1	
-425+212μm	%	8.6	0.4	24.2	
-212+106μm	%	5.2	0.4	15.5	
-106+53μm	%	3.2	0.5	6.5	
-53μm	%	9.2	1.5	20.0	

Table 5.6. Correlation coefficients for selected elements of Pascua talus fines (n = 16), r significant at greater than 0.468 at P=0.05 with 95% confidence. Significant values in **bold**.

	Au
Cu	-0.13
Ag	**0.93**
As	**0.86**
Pb	**0.50**
Hg	**0.89**
Sb	**0.96**
Te	**0.94**
Mo	0.12
Bi	**0.89**
Al	**-0.73**
Ba	-0.29
Be	**-0.59**
Cd	-0.32
Ca	**-0.65**
Cr	**-0.61**
Co	**-0.71**
Fe	0.06
Mg	**-0.66**
Mn	-0.45
Ni	**-0.62**
P	**-0.71**
K	**0.47**
Sc	**-0.73**
Se	**0.94**
Na	0.06
Sr	**-0.56**
S	**0.53**
Tl	0.32
Ti	**-0.47**
W	0.32
U	**-0.69**
V	**-0.79**
Zn	-0.36

Figure 5.12. Distribution of coarse and fine material in talus fines.

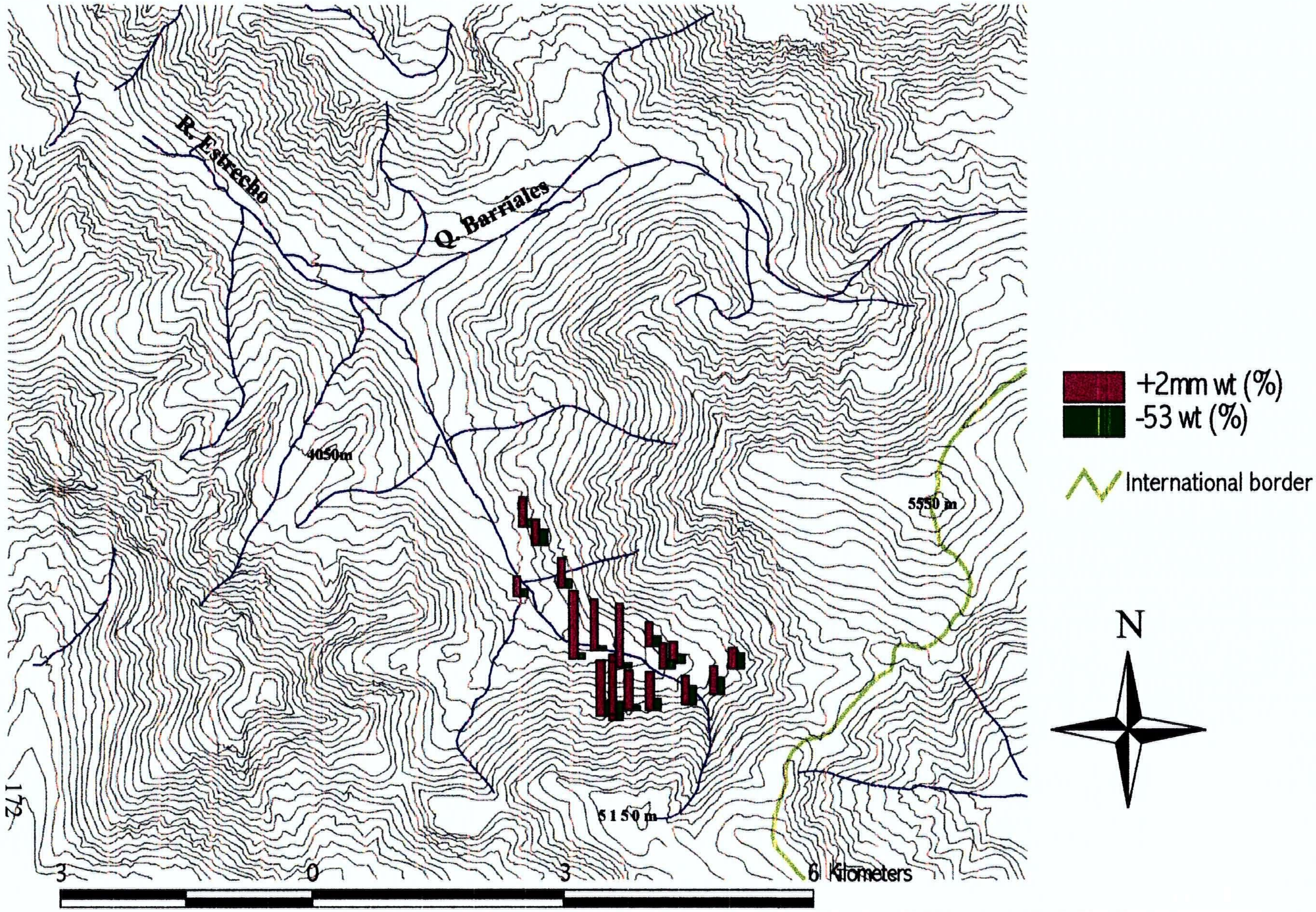

Figure 5.13. Gold in -53μm fraction of talus fines.

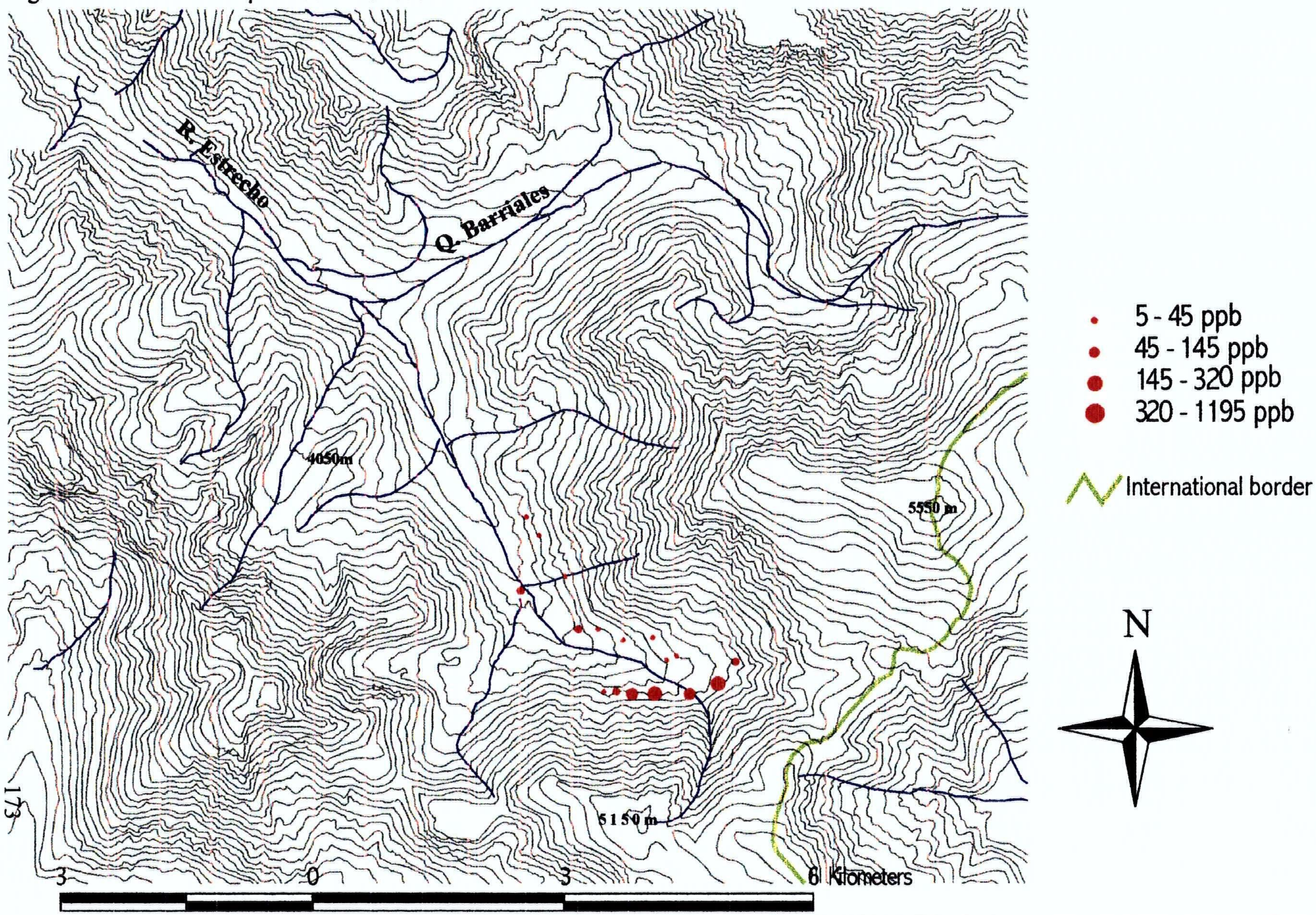

Figure 5.14. Ag in talus fines.

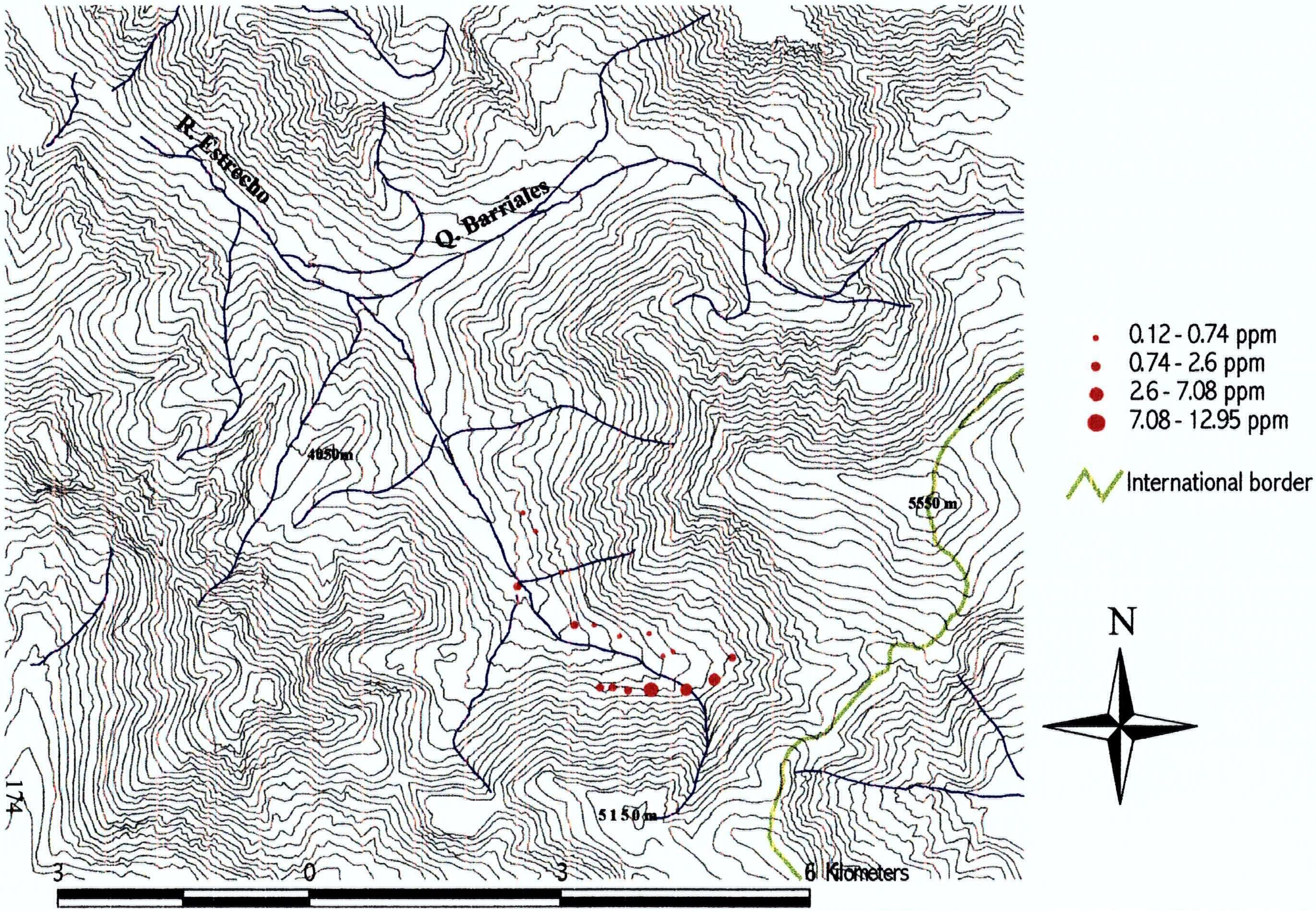

Figure 5.15. Zn in talus fines.

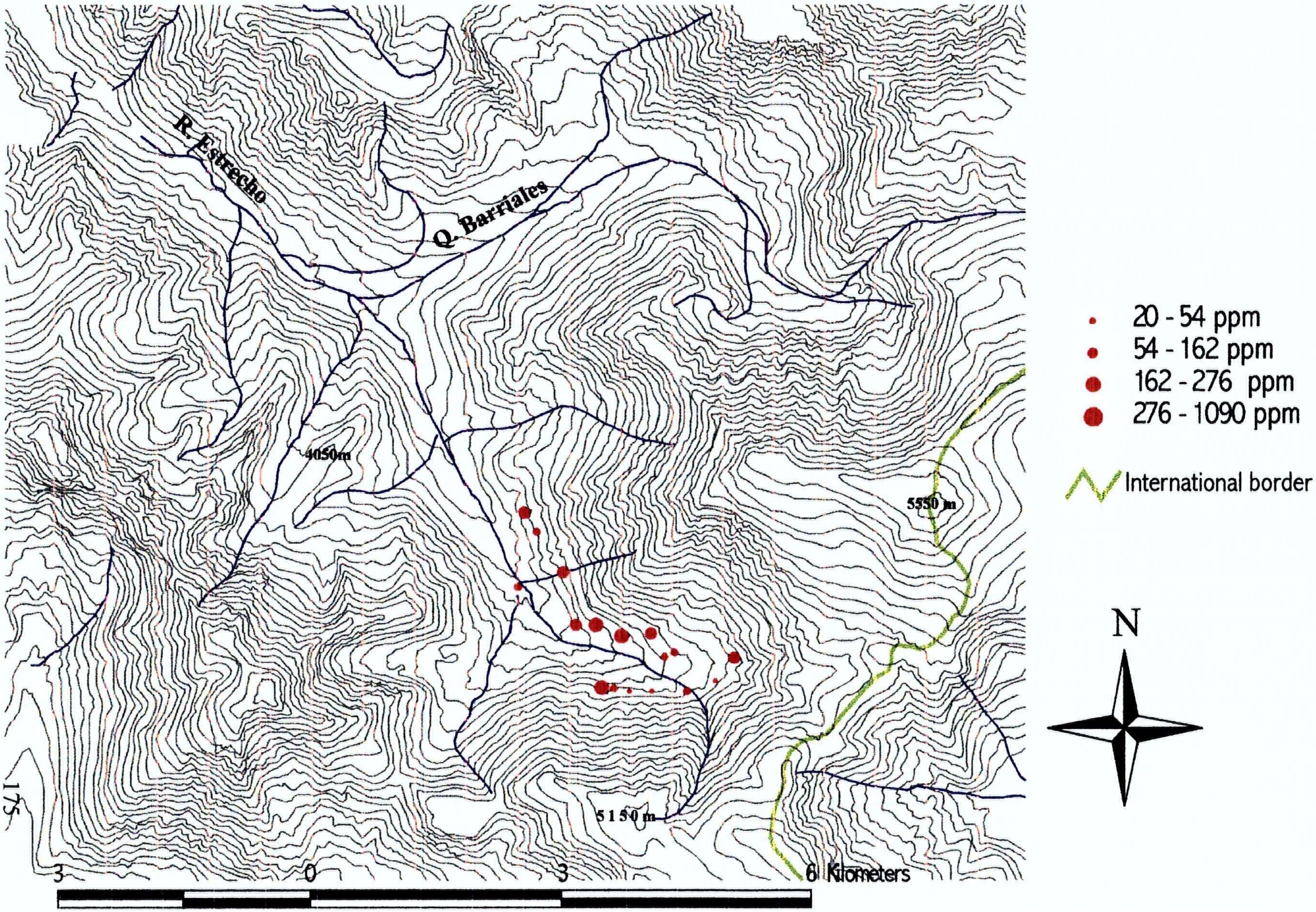

5.14). The second group of elements (Al, Ca, Cd, Cr, Co, Cu, Mg, Mn, Ni, P, Sc, Sr, Ti, V, Zn are inversely related to high Au concentrations and have negative correlations (Table 5.6, Figure 5.15). Talus cones are acidic (as measured by pH of -53μm settling water) with an average pH of 5.8. The lowest pH cones occur at the headwaters along the north edge of the R. Estrecho valley.

5.1.3. Comparison of surficial materials

Comparison of textures between the three sample media shows decreasing average weight percentages with a decrease in size for all sieved fractions (Table 5.7). Talus fans are the coarsest grained (average 44.4% in –4+2mm fraction compared to 25.9% and 25.5% for debris flows and glacial till, respectively) and glacial till has the greatest relative abundance of fines (average 18.0% in -106μm fraction compared to 12.4% and 9.6% for talus fines and debris flows) (Table 5.7).

Peak median gold values are found in the -53μm fraction of debris flows (median, 267.5 ppb), while the lowest concentrations are in glacial till (median 35 ppb) (Figure 5.16). Differences in mean values between surficial media are significant for the following cases (as determined by the Bonferroni adjustment): (1) debris flows have a higher average concentration than both talus fines and glacial till for Au, Ba, Hg, Sr, W and –425+212μm fraction; (2) debris flows and talus fines have higher average concentrations than glacial till for As, K, Ag and S; (3) debris flows have significantly less Cr than talus cones and glacial till. Overall, glacial till has lowest average concentrations for nineteen elements (Au, As, Sb, Ba, Bi, Cd, Pb, Mn, Hg, K, Se, Ag, Na, Sr, S, Te, Tl, W, and Zn). Twelve elements have their lowest average values in debris flows (Al, Cr,

Table 5.7. Comparison of mean (median for Au) concentrations for surficial samples at Pascua. Elements of the high sulfidation geochemical suite (Hedenquist et.al., 1996) are grouped together. Significant differences in mean values between deposits are shown in bold (e.g. for Hg: D D all means debris flows are significantly different than all other deposits). G = glacial till, D = debris flows, T= talus cones.

Element	Units	Talus fines (n=18)	Debris flow (n=10)	Glacial till (n=12)	Significant difference (Bonferroni adjustment)
Au (-212+106µ	ppb	7.5	37.5	7.5	
Au (-106+53µm	ppb	12.5	97.5	7.5	
Au (-53µm)	ppb	70	**267.5**	35	D Δ all
pH		5.8	6.7	7.7	
Cu	ppm	111.8	158.9	130.9	
Ag	ppm	2.2	5.83	**0.66**	G Δ all
As	ppm	320.4	286.7	**40.58**	G Δ all
Pb	ppm	438.9	266.6	59.83	
Hg	ppm	0.2	**1.43**	0.14	D Δ all
Sb	ppm	3.7	3.40	0.67	
Te	ppm	2.3	1.70	0.26	
Mo	ppm	4.3	1.84	2.37	
Bi	ppm	8.8	7.23	1.72	
Al	%	2.0	1.65	1.71	
Ba	ppm	182.8	**467.0**	154.2	D Δ all
Cd	ppm	1.2	0.71	0.45	
Ca	%	0.5	0.38	0.38	
Cr	ppm	22.3	**10.10**	22.17	D Δ all
Co	ppm	9.5	9.26	9.58	
Fe	%	4.9	4.22	4.28	
Mg	%	0.8	0.57	0.67	
Mn	ppm	1380	1051	958.3	
Ni	ppm	14.4	6.70	14.50	
P	ppm	705.0	741.0	790.8	
K	%	0.5	0.42	**0.18**	G Δ all
Sc	ppm	5.3	3.90	4.92	
Se	ppm	2.8	2.45	0.54	
Na	%	0.1	0.13	0.03	
Sr	ppm	55.6	**73.40**	39.00	D Δ all
S	%	0.7	0.80	**0.14**	G Δ all
Tl	ppm	2.9	1.92	0.59	
Ti	%	0.1	0.04	0.08	
W	ppm	0.3	**0.58**	0.19	D Δ all
U	ppm	1.8	1.56	1.95	
V	ppm	47.3	42.60	52.25	
Zn	ppm	249.9	226.4	121.8	
-4mm+2mm	%	44.4	25.9	25.5	
-2mm +850µm	%	19.4	18.8	20.1	
-850+425µm	%	10.1	20.2	16.1	
-425+212µm	%	8.6	**17.6**	12.3	D Δ all
-212+106µm	%	5.2	8.0	8.0	
-106+53µm	%	3.2	3.8	6.1	
-53µm	%	9.2	5.8	11.9	

Table 5.8. Correlation coefficents for gold in surficial materials at Pascua. Significant positive values in red, significant negative values in blue. Glacial till n = 12, r_{sign} >0.576; debris flows n = 10, r_{sign} >0.632; talus fines n = 18, r_{sign} >0.468 at P = 0.05.

	Glacil till	Debris flows	Talus cones
Cu	**0.81**	0.56	-0.13
Ag	**0.95**	**0.77**	**0.93**
As	**0.89**	**0.77**	**0.86**
Pb	0.49	**0.83**	**0.50**
Hg	0.31	**0.80**	**0.89**
Sb	**0.84**	**0.87**	**0.96**
Te	**0.88**	**0.85**	**0.94**
Mo	**0.69**	0.17	0.12
Bi	**0.70**	**0.81**	**0.89**
Al	-0.09	-0.50	**-0.73**
Ba	0.31	0.26	-0.29
Cd	-0.26	0.16	-0.32
Ca	**-0.58**	-0.55	**-0.65**
Cr	-0.32	0.39	**-0.61**
Co	-0.45	**-0.73**	**-0.71**
Fe	**0.85**	0.25	0.06
Mg	-0.42	**-0.81**	**-0.66**
Mn	-0.55	-0.11	-0.45
Ni	**-0.58**	0.28	**-0.62**
P	0.05	-0.36	**-0.71**
K	0.21	0.32	**0.47**
Se	**0.90**	0.53	**0.94**
Na	0.17	-0.42	0.06
Sr	-0.43	-0.45	**-0.56**
S	**0.88**	**0.67**	**0.53**
Tl	**0.94**	**0.74**	0.32
Ti	-0.08	**-0.79**	**-0.47**
W	0.15	**0.64**	0.32
U	-0.26	0.16	**-0.69**
V	-0.01	-0.38	**-0.79**
Zn	-0.01	0.46	-0.36
No. positive	11	10	10
No. negative	2	3	11

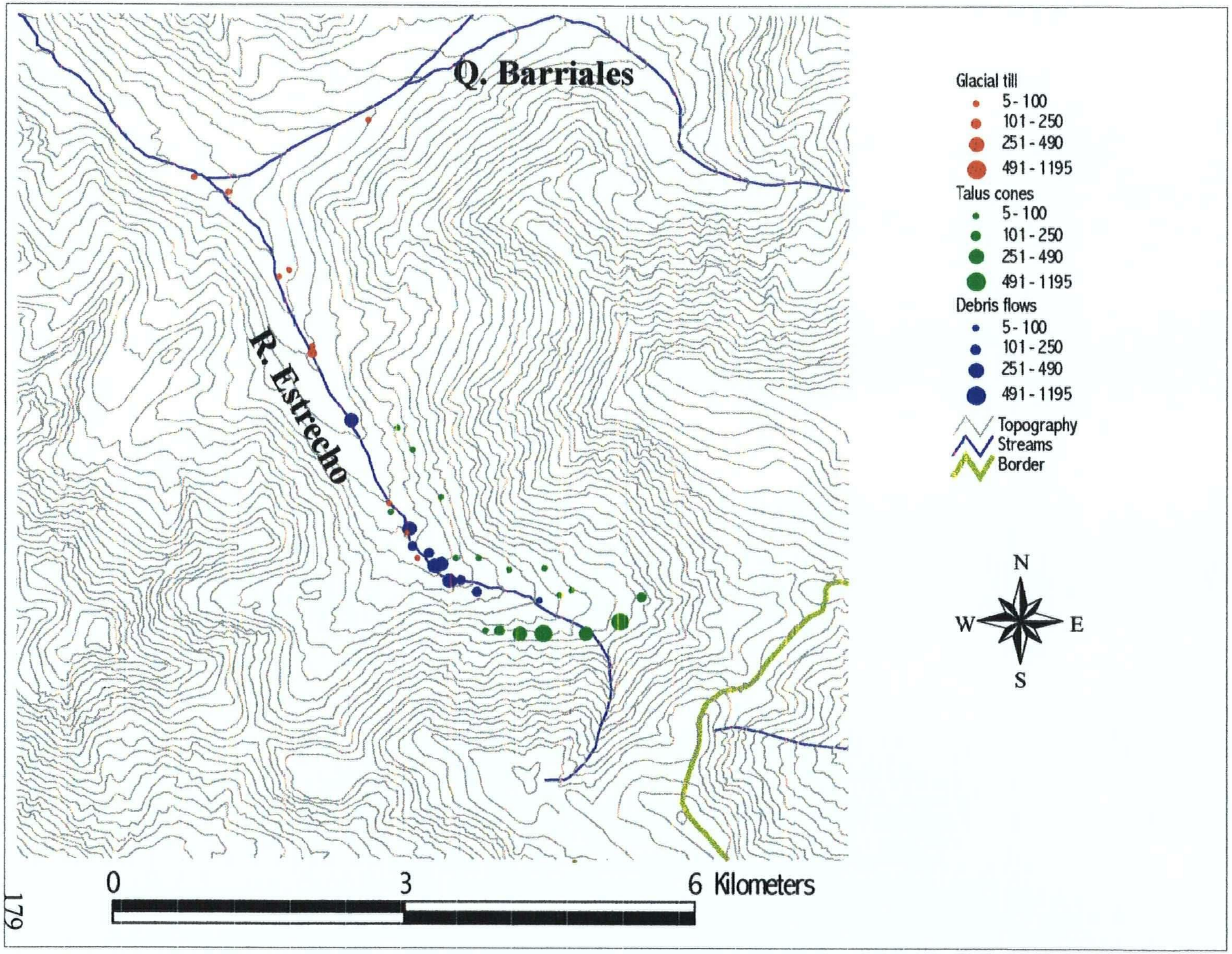

Figure 5.16. Gold concentrations in -53μm fraction of surficial deposits at Pascua, Chile.

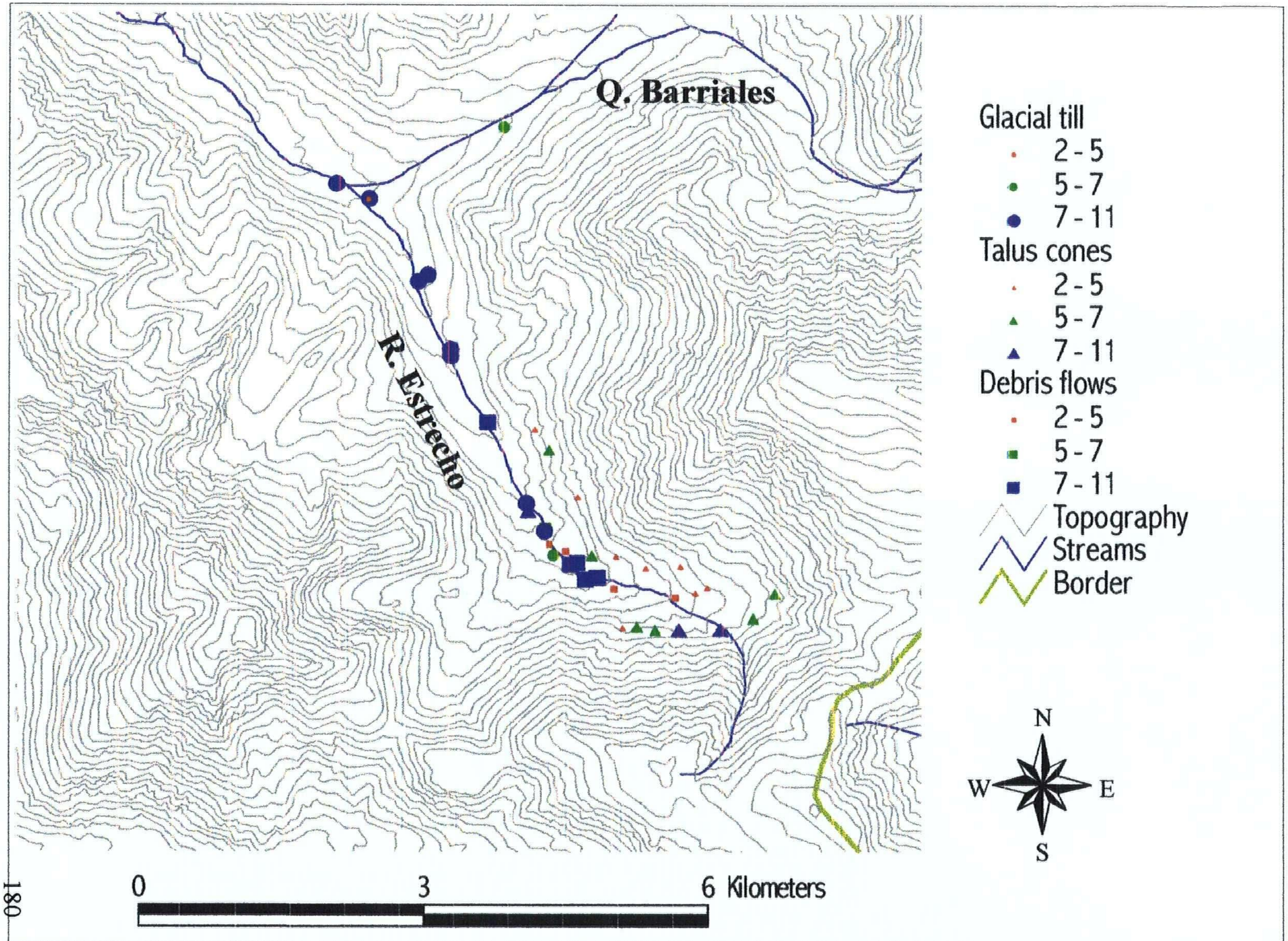

Figure 5.17. pH of surficial deposits at Pascua, Chile.

Co, Cu, Fe, Mg, Mo, Ni, Sc, Ti, U and V), however average values are approximately equal between media except where otherwise indicated by the Bonferroni adjustment (Table 5.7).

Debris flows have higher minimum values and hence lower contrast relative to other surficial materials; thirty-four elements have maximum to minimum ratios of less than three for debris flows. All surficial deposits have significant positive correlations of gold with As, Sb, Bi, Ag, S and Te. Talus cones, the most acidic media (average 5.8), have negative correlations with gold for eleven elements. In pH neutral glacial till (average 7.7), gold only has negative correlations with Ca and Ni (Table 5.8). Surficial deposits tend to be more acidic near the deposit (Figure 5.17).

5.2 Stream waters

Water samples were taken in conjunction with stream sediment at every sampling site and at precipitate seeps (Figure 5.18). Only results for samples collected at sediment sites will be presented here. Water samples collected at chemical precipitate sites are described in Section 5.5 with precipitate mineralogy and geochemistry.

5.2.1 Elemental concentrations and pH

Stream waters of the R. Estrecho range from a minimum, acidic value of 3.5 to a maximum, neutral pH of 7.8. Low pH values are found at the headwaters and values of less than 5 persist until below the Q. Barriales confluence, where they increase to pH 7 and higher, until the most distal sample site 26 km downstream, where pH drops to 6.6 (Figure 5.20). Ten elements were at or below their detection limit of the ICP-MS (Ag, As, Bi, Cr, Hg, P, Sb, Sn, Ti and V) (Table

Figure 5.18. Stream water sampling sites at Pascua, Chile.

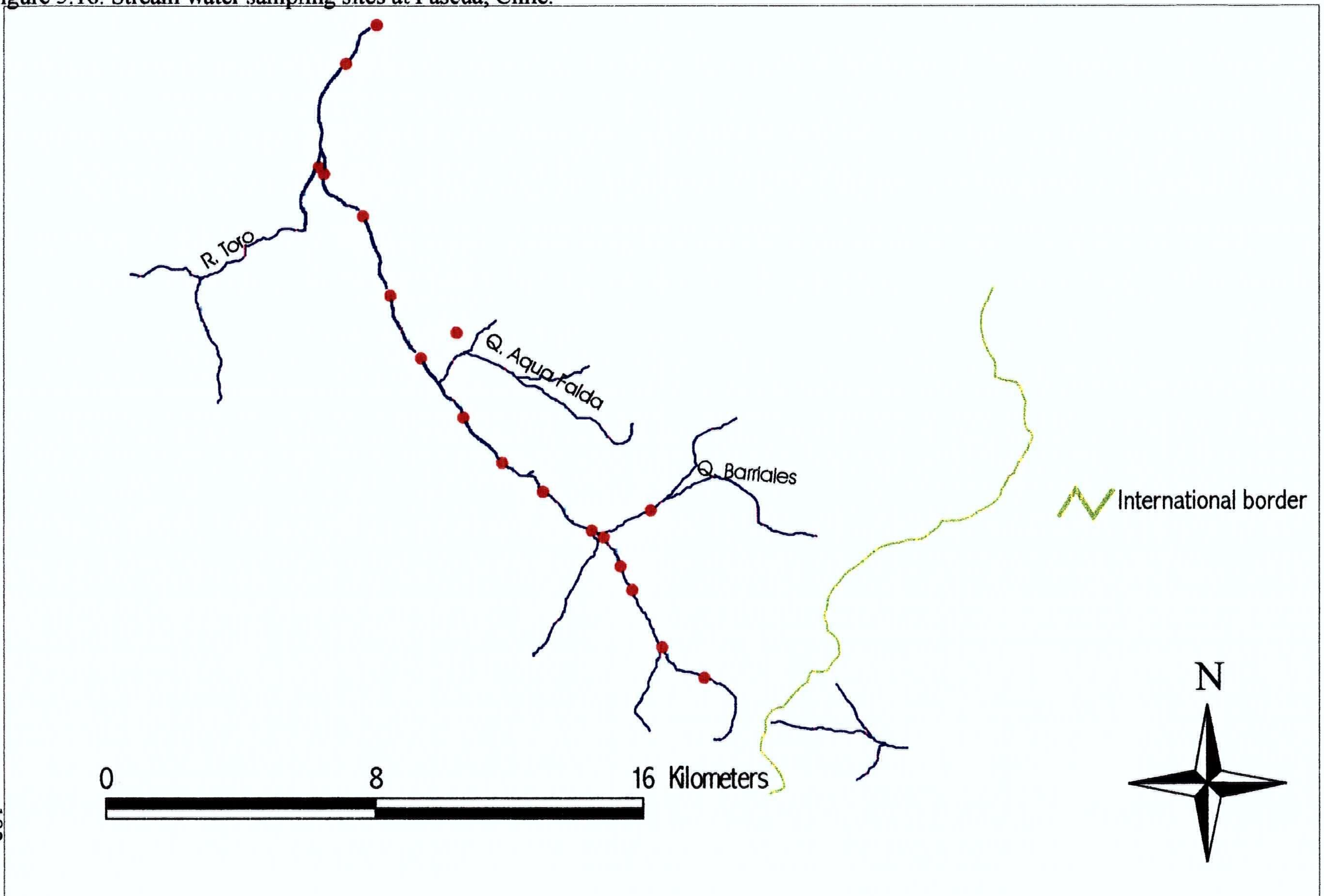

5.9). Analysis of variance (ANOVA) shows that between site variances are significant compared to within site variances based on field duplicate data (Table 4.11).

Tributaries of the R. Estrecho have pH values between 6 and 7.8. All metals, except U, have lower average concentrations in the three tributaries relative to the R. Estrecho. However, although the tributaries do not have the maximum average values, Mo, U, Ba and Sr concentrations are greater in the tributaries than in the immediately adjacent sites along the R. Estrecho. Field sulfate values were greater than 200 mg/l at all sample sites along the R. Estrecho. Tributaries have much lower sulfate concentrations, approximately 50 mg/l.

In the R. Estrecho, water chemistry has a negative relation with pH (generally $r > -0.59$), suggesting that most metal cations (with the exception of Pb), are responsive to changes in acidity (Table 5.10). Molybdenum, the lone metal anion, has a strong positive correlation with pH ($r = 0.79$). Examination of X-Y scatter plots of selected elements show that the high correlation coefficients seen are not caused by outliers, but relate to changes in pH values (Figure 5.19). Elemental concentrations are generally higher at sites with correspondingly lower pH values (e.g. Cu in Figure 5.20). In general, elements (except for Mo) have higher dissolved concentrations in the acidic, upper reaches of the R. Estrecho, decreasing downstream to the final sample site (Site 24) over 20 kilometers downstream where concentrations increase again (e.g. Ni, Cd and Zn in Figure 5.21). Below the confluence with Q. Los Barriales, metal concentrations decrease between 28-78% (Table 5.11) while the pH increases to above 5.2. Molybdenum, which has higher concentrations in the Q. Los Barriales (2.7 ppb) than the R. Estrecho, increases below the confluence by 1200%, to 1.3 ppb. At subsequent confluences there are no steps in downstream metal profiles, pH changes are negligible, and water chemistry does not show consistent changes (Table 5.11).

Table 5.9. Descriptive statistics of water samples associated with sediments (n=17). Max/min ratios greater than 10 are in bold.

	Units	Mean	Minimum	Maximum	Max/Min
pH		5.8	4.0	7.1	1.8
Cu	µg/l	109.5	<0.1	507	**5070.0**
As	µg/l	1.0	<1.0	<1.0	1.00
Pb	µg/l	3.6	<2.0	24	**12.00**
Hg	µg/l	1.0	<1.0	<1.0	1.00
Sb	µg/l	0.05	<0.05	<0.05	1.00
Mo	µg/l	2.6	<0.1	11.2	**112.0**
Bi	µg/l	0.05	<0.05	<0.05	1.00
Al	mg/l	2.5	0.003	14.2	**4733**
Ba	µg/l	22.2	9.8	34.7	3.54
Be	µg/l	0.6	<0.5	1.5	3.00
Ca	mg/l	53.1	26.7	107.5	4.03
Cd	µg/l	4.4	<0.1	15.9	**159.0**
Co	µg/l	8.7	0.06	26.3	**438.3**
Cr	µg/l	0.5	<0.5	<0.5	1.00
Fe	mg/l	0.5	0.07	2.16	**30.86**
K	mg/l	1.7	0.45	3.8	8.44
Mg	mg/l	9.7	2.69	17.5	6.51
Mn	µg/l	2604.5	1.6	8640	**5400.0**
Na	mg/l	5.0	2.55	7.05	2.76
Ni	µg/l	10.3	<0.2	33.4	**167.0**
P	mg/l	0.1	<0.1	<0.1	1.00
Se	µg/l	1.2	<1.0	3.0	3.00
Sn	µg/l	0.5	<0.5	<0.5	1.00
Sr	µg/l	90.5	52.8	137	2.59
Ti	µg/l	1.0	<1.0	<1.0	1.00
Tl	µg/l	0.2	<0.05	0.55	**11.00**
U	µg/l	2.0	0.15	10.1	**67.33**
V	µg/l	1.0	<1.0	<1.0	1.00
Zn	µg/l	821.7	<0.5	3550	**7100.0**

Table 5.10. Correlation coefficients for selected elements of R. Estrecho stream water samples. df=12, r signficant at greater than 0.532 at P= 0.05 and 95% confidence.

	pH	*Al*	*Ba*	*Be*	*Ca*	*Cd*	*Co*	*Cu*	*Fe*	*K*	*Mg*	*Mn*	*Mo*	*Na*	*Ni*	*Pb*	*Se*	*Sr*	*Tl*	*U*	*Zn*
Al	-0.79	1.00																			
Ba	-0.24	0.27	1.00																		
Be	-0.51	0.82	-0.12	1.00																	
Ca	-0.86	0.98	0.36	0.75	1.00																
Cd	-0.85	0.98	0.21	0.77	0.98	1.00															
Co	-0.83	0.94	0.45	0.73	0.98	0.94	1.00														
Cu	-0.88	0.98	0.26	0.76	0.99	0.99	0.94	1.00													
Fe	-0.85	0.99	0.20	0.81	0.98	0.99	0.94	0.99	1.00												
K	-0.86	0.98	0.27	0.75	0.99	0.99	0.95	1.00	0.99	1.00											
Mg	-0.85	0.93	0.45	0.69	0.98	0.95	0.99	0.95	0.94	0.95	1.00										
Mn	-0.85	0.98	0.25	0.75	0.98	1.00	0.94	0.99	0.99	1.00	0.95	1.00									
Mo	0.79	-0.70	0.06	-0.44	-0.72	-0.81	-0.65	-0.78	-0.76	-0.79	-0.72	-0.80	1.00								
Na	-0.81	0.92	0.57	0.59	0.96	0.90	0.95	0.93	0.90	0.94	0.95	0.92	-0.62	1.00							
Ni	-0.84	0.97	0.35	0.78	0.99	0.98	0.99	0.97	0.98	0.97	0.98	0.97	-0.71	0.93	1.00						
Pb	0.33	-0.22	-0.18	-0.13	-0.27	-0.21	-0.25	-0.26	-0.25	-0.25	-0.25	-0.22	0.14	-0.31	-0.23	1.00					
Se	-0.59	0.74	-0.14	0.90	0.69	0.70	0.66	0.71	0.75	0.69	0.64	0.68	-0.45	0.52	0.70	-0.17	1.00				
Sr	-0.39	0.49	0.89	0.25	0.58	0.43	0.68	0.47	0.44	0.47	0.65	0.45	-0.01	0.72	0.59	-0.21	0.15	1.00			
Tl	-0.86	0.98	0.24	0.78	0.98	0.99	0.94	0.99	0.99	0.99	0.94	0.99	-0.77	0.92	0.97	-0.26	0.72	0.46	1.00		
U	-0.85	0.92	0.32	0.65	0.92	0.89	0.84	0.94	0.91	0.92	0.85	0.91	-0.65	0.91	0.86	-0.34	0.66	0.46	0.93	1.00	
Zn	-0.85	0.98	0.14	0.81	0.96	0.99	0.93	0.98	0.99	0.98	0.93	0.98	-0.80	0.87	0.97	-0.21	0.75	0.38	0.98	0.88	1.00

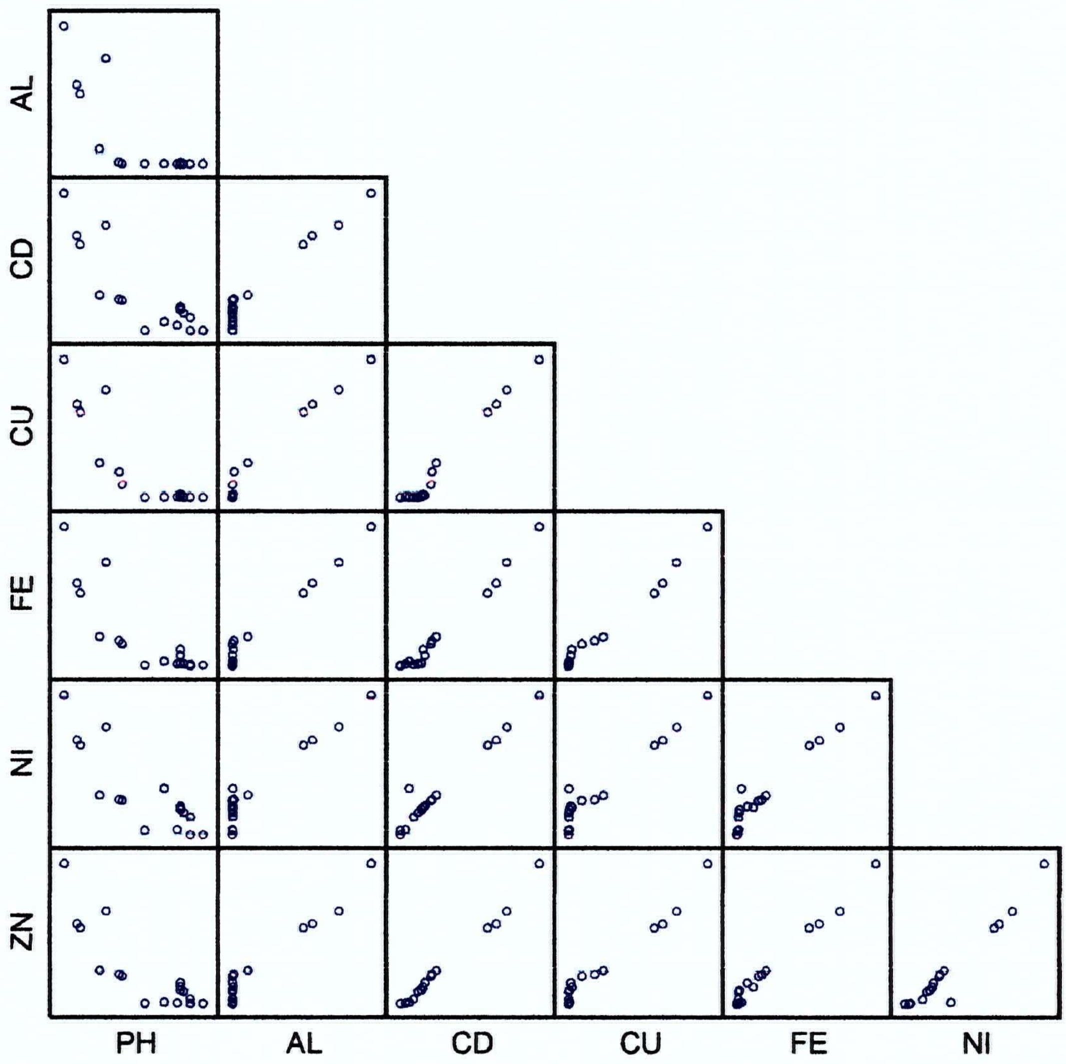

Figure 5.19. X-Y Scatter plors of pH and selected elements from stream waters at Pascua, Chile.

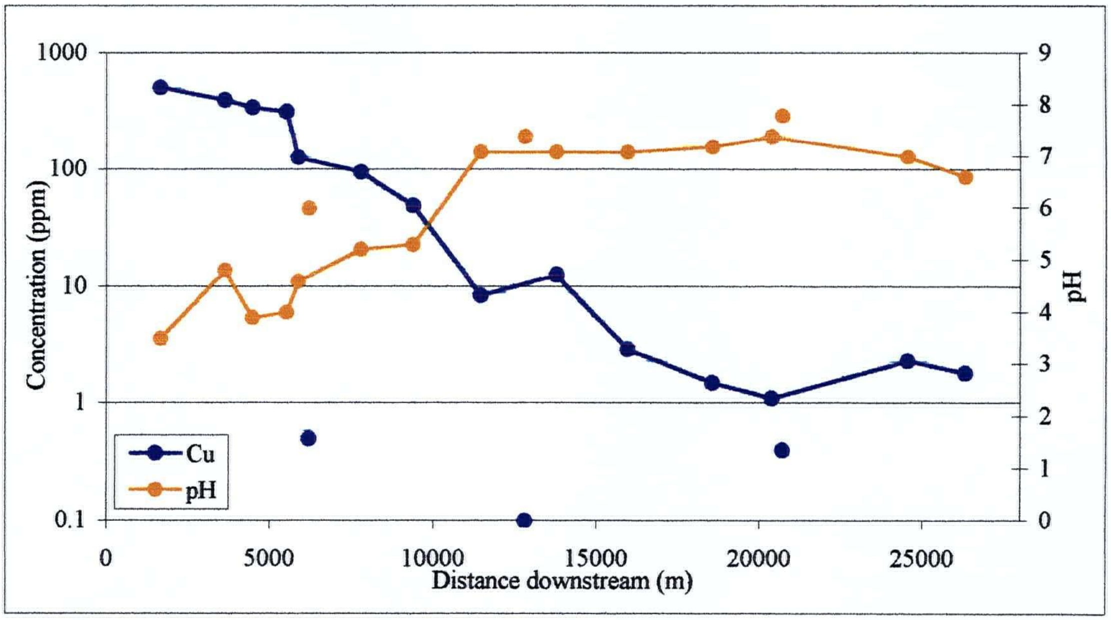

Figure 5.20. Downstream profile of Cu in stream waters. Q. Barriales, Q. Agua Falda and R. Toro are shown as points 6.2, 12.8, and 20.7 km downstream, respectively.

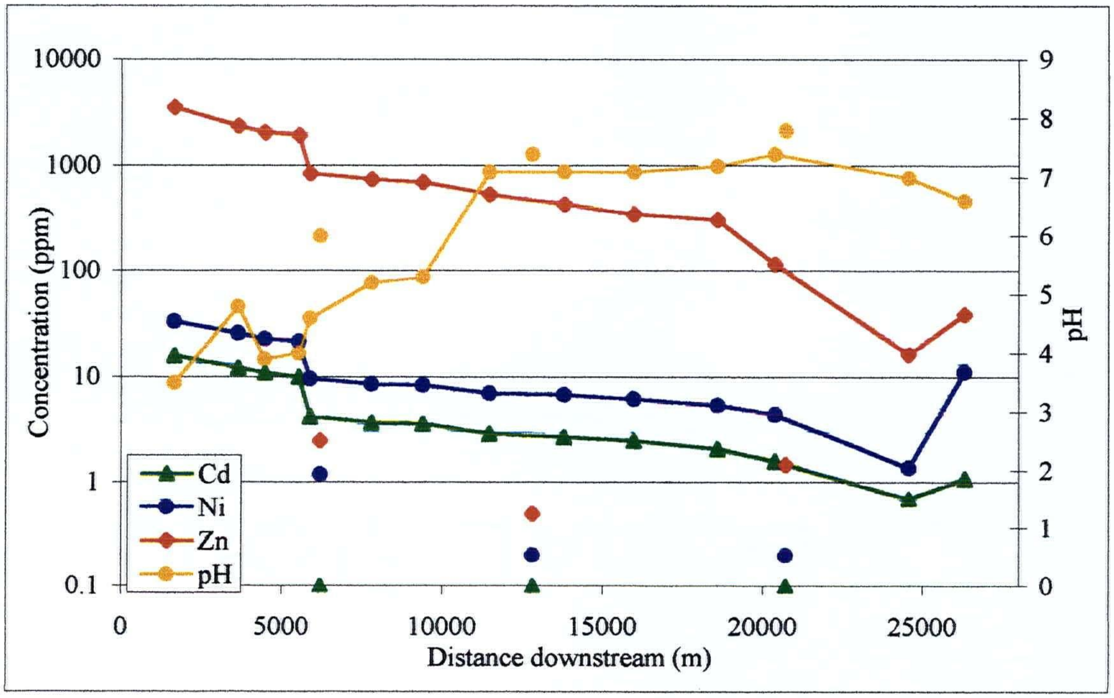

Figure 5.21. Downstream profile of Cd, Ni and Zn in stream waters. Q. Barriales, Q. Agua Falda and R. Toro are shown as points 6.2, 12.8, and 20.7 km downstream, respectively.

As with water data from the R. Turbio at Lama, by assuming that changes in dissolved metal concentration are due solely to differences in relative flow volumes of the streams, it is possible to calculate an apparent dilution factor for confluences. The apparent dilution factor is determined by:

$$DF = 1 + ((A-C)/(C-B))$$

where, A, B, and C are the concentrations of an element on the principle stream above the confluence, on the tributary stream (diluting the main stream), and on the principle stream below the confluence, respectively.

A dilution factor greater than the calculated ratio for a conservative element (e.g. Na^{2+}) indicates a mechanism other than dilution is changing elemental concentrations in the stream below the confluence. At the R. Estrecho- Q. Barriales confluence, all elements except U and Mo, have apparent dilution factors between 1.9 (Mg) and 4.7 (Al) with most elements slightly greater than the Na value of 2.0. There is thus a greater than expected loss of most elements, relative to Na, below the confluence. The dilution factor for Mo, which has higher concentrations in the Q. Barriales v. the R. Estrecho, decreases suggesting a loss of Mo from solution below the confluence.

5.3 Drainage sediments

Stream sediments were collected at eighteen locations along the R. Estrecho and three of its tributaries; the Q. Los Barriales, Q. Aqua de la Falda and the R. del Toro (Figure 5.22). Sixteen

Table 5.11. Apparent dilution ratio for the R.Estrecho- Q. Barriales confluence and percentage decrease in metal concentration below all confluences.

	R. Estrecho (Site 36)	Q. Barriales (Site 40)	Downstream (Site 35)	Dilution ratio	Q. Barriales	Q. Aqua Falda	R. Toro
pH	4	6	4.6	4.1	-15%	0%	5%
Al	7.26	0.037	1.59	4.7	78%	-485%	-61%
Ba	29.9	9.8	21.5		28%	-14%	6%
Ca	84.7	27.4	54	2.2	36%	10%	-2%
Cd	10	0.1	4.2	2.4	58%	7%	56%
Co	18	1.36	8.42	2.4	53%	15%	68%
Cu	313	0.5	127.5	2.5	59%	-50%	-109%
Fe	1.16	0.08	0.51	2.5	56%	-39%	-11%
K	2.85	0.95	1.8	2.2	37%	14%	4%
Mg	14.8	5.66	10.6	1.9	28%	5%	27%
Mn	6110	30.3	2480	2.5	59%	19%	31%
Mo	0.1	2.7	1.3	1.9	-1200%	-37%	-73%
Na	6.55	3.55	5.05	2.0	23%	2%	-7%
Ni	21.6	1.2	9.6	2.4	56%	3%	68%
Sr	110	52.8	79.3	2.2	28%	-8%	-10%
Tl	0.3	0.05	0.15	2.5	50%	0%	0%
U	2.25	1.5	1.45	-15.0	36%	-67%	-150%
Zn	1935	2.5	845	2.3	56%	20%	86%

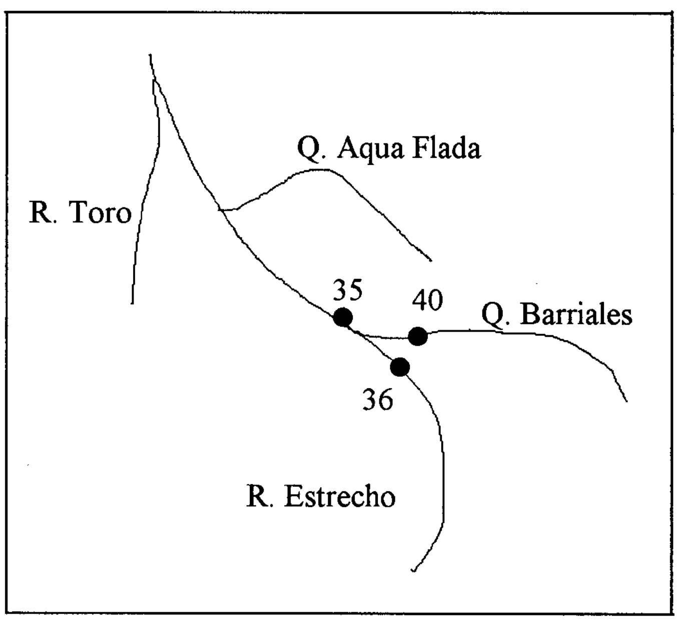

Figure 5.22. Sketch of stream sediment sample locations.

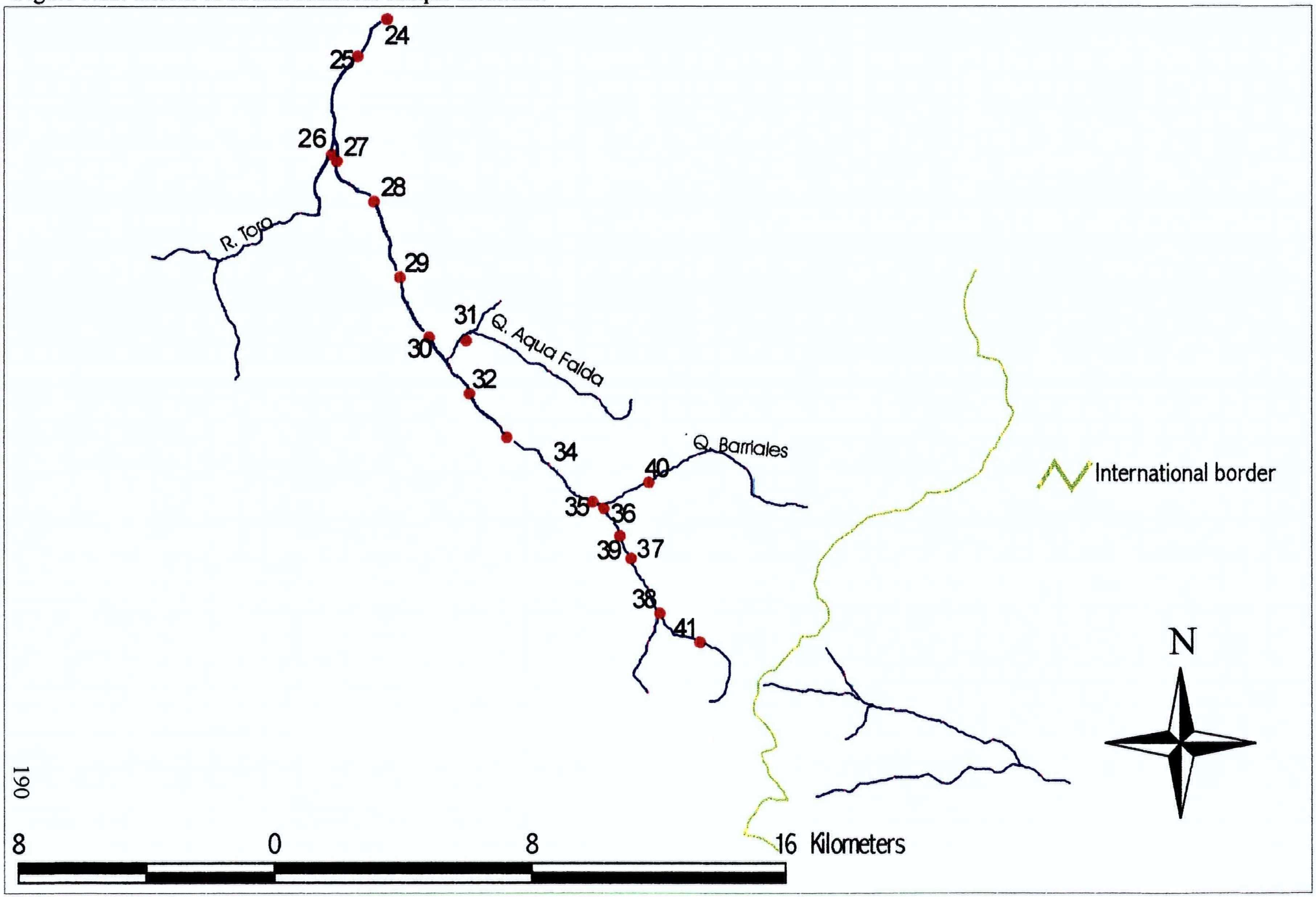

high energy samples were taken from stream sections with a cobble-gravel surface, eighteen medium energy samples were taken from gravel and coarse sand surfaces and seven low energy samples from areas with fine sand and silt surfaces.

5.3.1 Texture

An effort was made to sample material consistently from the same environment based on streambed texture, however, the average weight percents of the high and medium energy samples are similar (Table 5.12) with t-test results confirming there are no statistical differences between average abundances of material in these environments (Table 5.13). High and medium energy stream sediments are relatively coarse grained material compared to surficial media, with less than 10% of the sample mass in the -212μm (fine sand and finer) material.

Textural data is noisy at the R. Estrecho headwaters and does not relate to changes in stream gradient (Figure 5.23- 5.25). In the high energy environment, –2mm+850μm material increases as other size fractions decrease in relative abundance (Figure 5.23.). The coarse fractions of medium energy samples are noisy at the headwaters with less variation in texture below the Q. Aqua Falda confluence. The relative abundance of the –53μm fraction decreases below the Q. Barriales confluence, until the final sample site where relative abundance increases (Figure 5.24). The seven low energy samples, collected from the upper reaches of the R. Estrecho, all show the most variation in relative abundance material of all of the environments but do not have any definable trends in texture (Figure 5.25).

Table 5.12. Average weight percentages for high, medium and low energy stream sediments at Pascua.

Size fraction (μm)	High (n=16)	Medium (n=18)	Low (n=7)
-2mm+850	53.6	51.9	4.6
-850+425	24.5	26.3	10.5
-425+212	13.2	13.8	26.4
-212+150	2.5	2.4	17
-150+106	1.8	1.7	15
-106+75	1.1	1.1	10.3
-75+53	0.9	0.8	6
-53	2.4	2	10.2

Table 5.13. Results of two tailed t-test on weight percentages of stream sediments between high and medium energy samples ($t_{critical} = 2.04$).

Size fraction (μm)	t_{stat}	Accept/Reject
-2mm+850	-0.44	Accept
-850+425	0.92	Accept
-425+212	0.47	Accept
-212+150	-0.13	Accept
-150+106	-0.67	Accept
-106+75	0.89	Accept
-75+53	0.73	Accept
-53	0.21	Accept

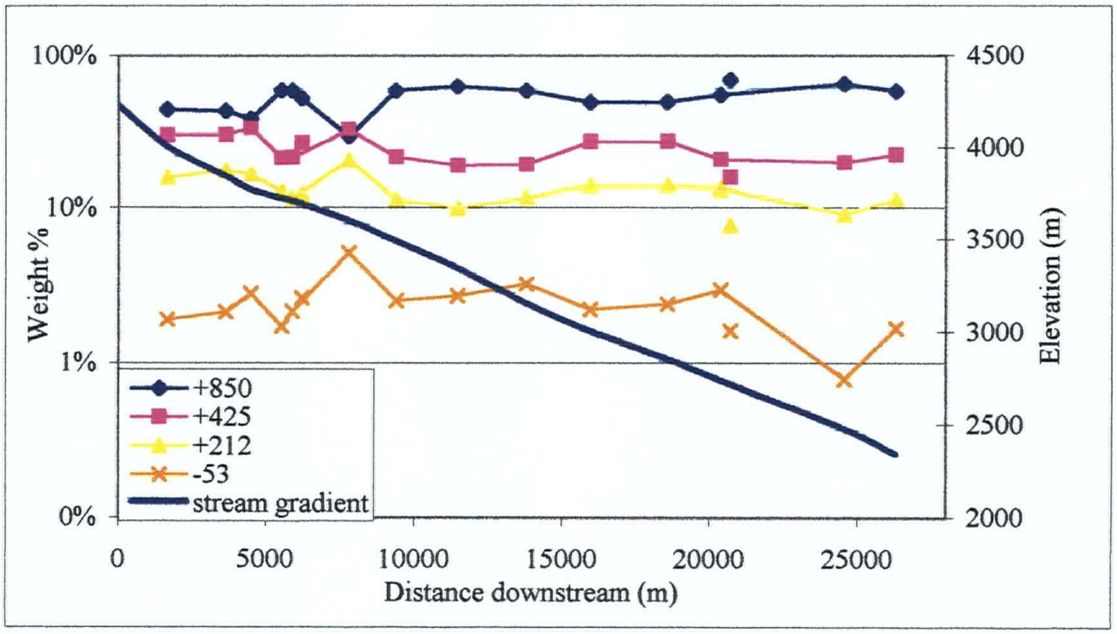

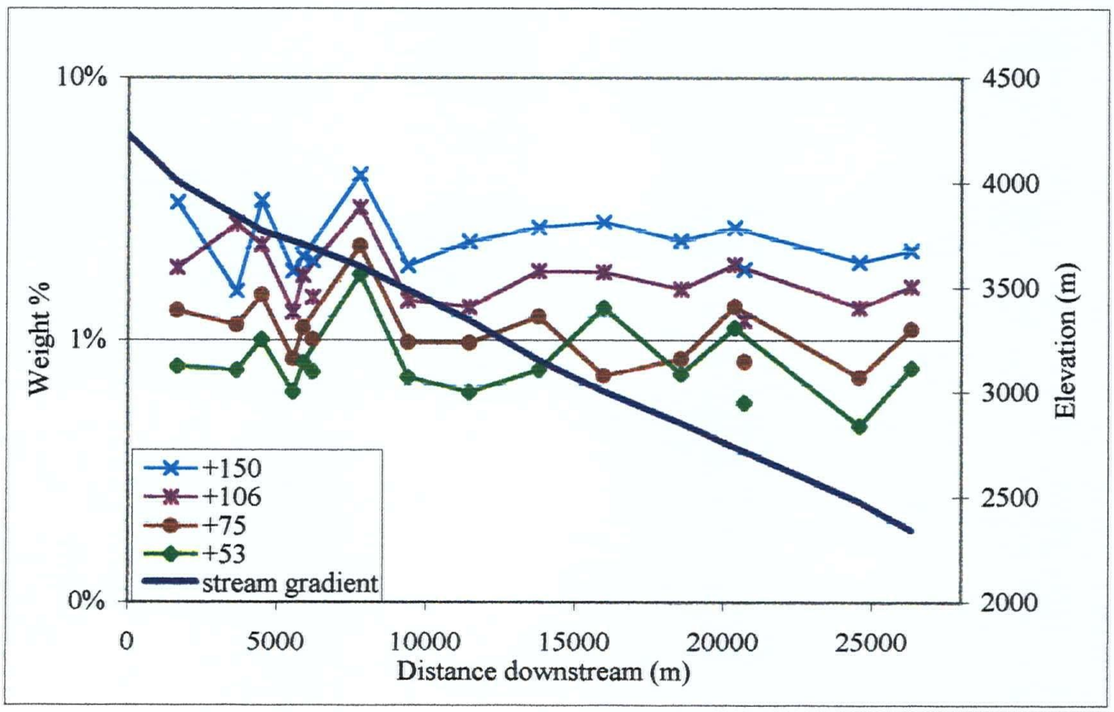

Figure 5.23. Downstream profiles of weight percentages of size fractions in high energy stream sediments. Q. Barriales, Q. Agua Falda and R. Toro are shown as points 6.2, 12.8, and 20.7 km downstream, respectively. All grain sizes in μm.

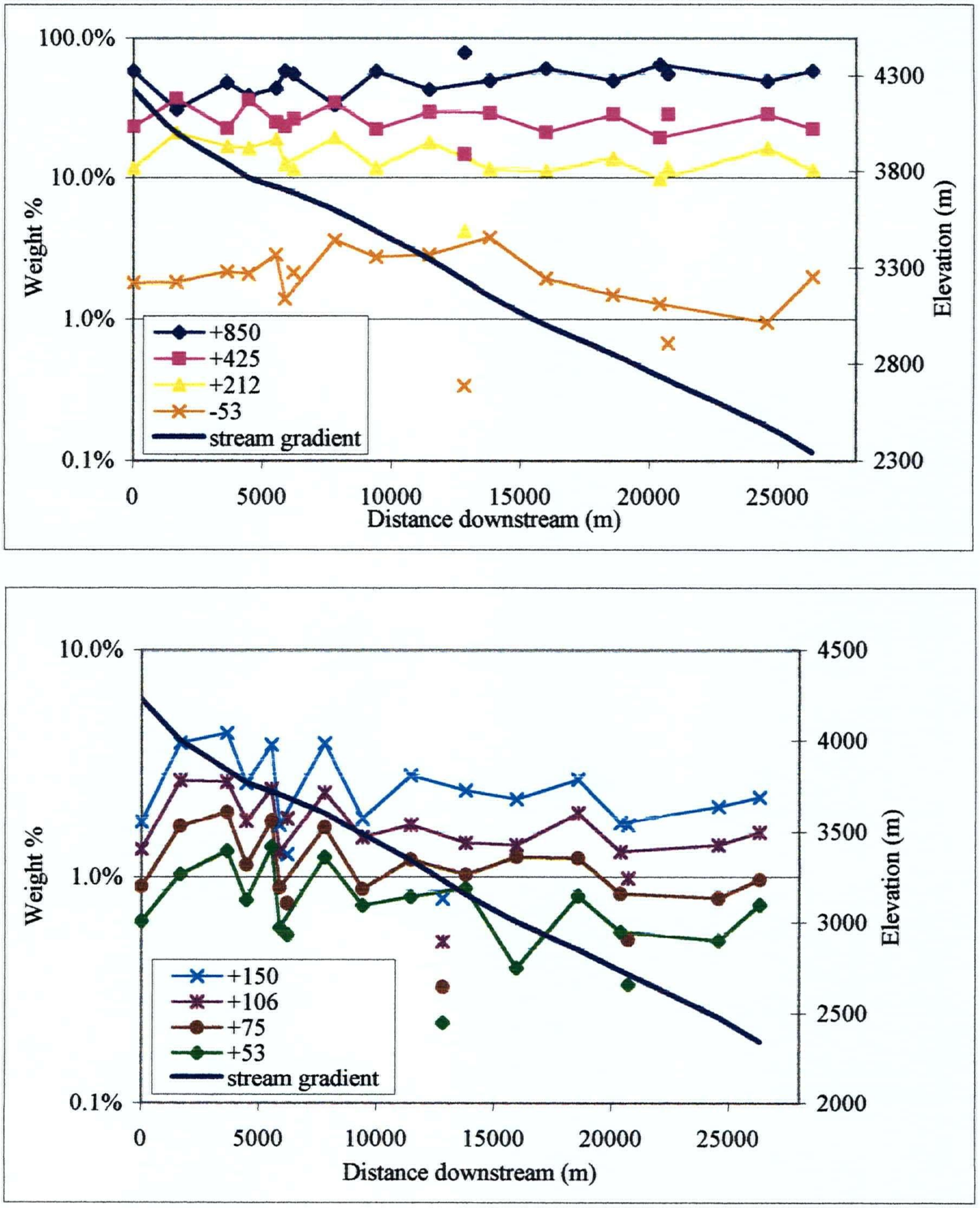

Figure 5.24. Downstream profiles of weight percentages of size fractions in medium energy stream sediments. Q. Barriales, Q. Agua Falda and R. Toro are shown as points 6.2, 12.8, and 20.7 km downstream, respectively. All size fractions in μm.

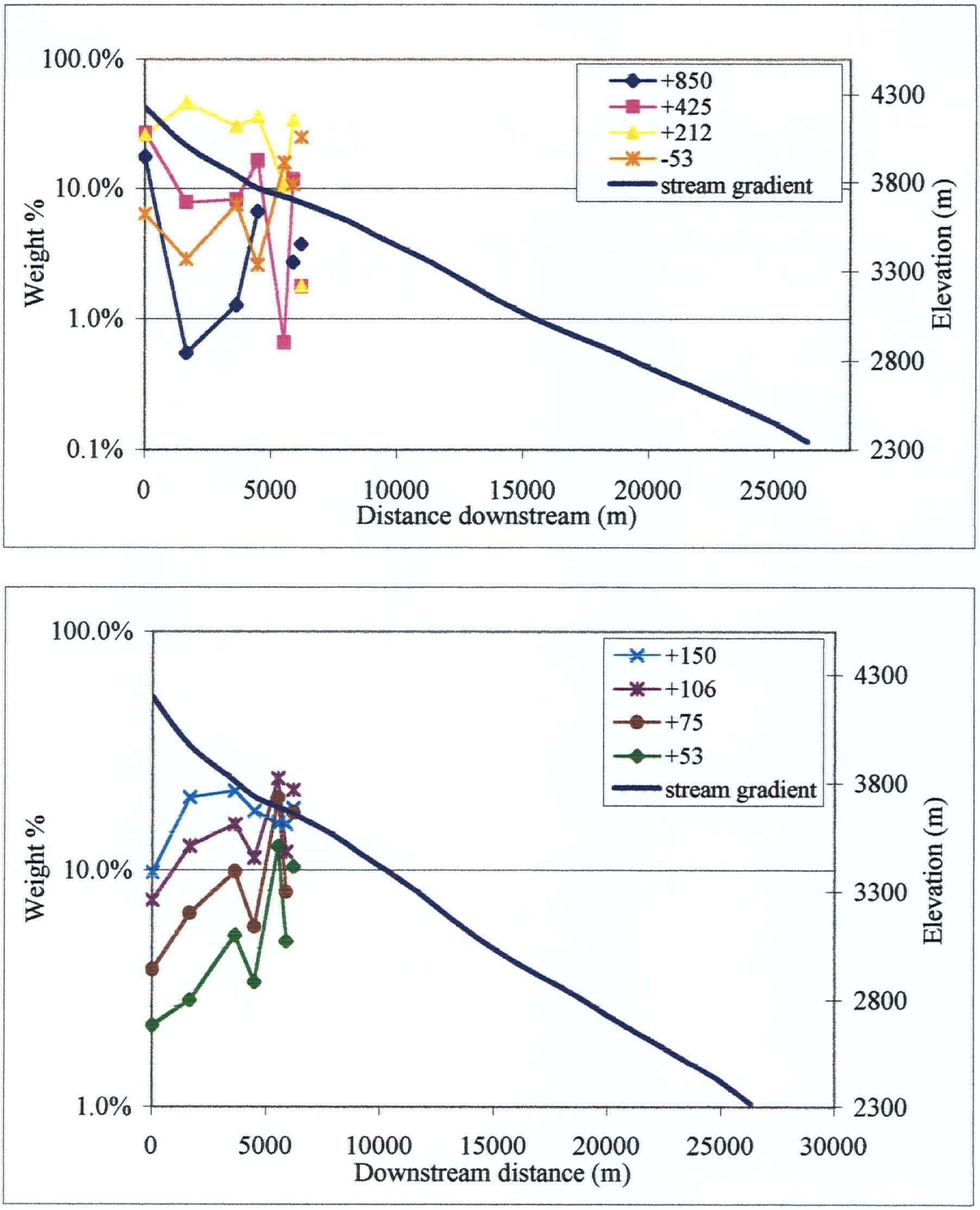

Figure 5.25. Downstream profiles of weight percentages of size fractions in low energy stream sediments. Q. Barriales, Q. Agua Falda and R. Toro are shown as points 6.2, 12.8, and 20.7 km downstream, respectively. All size fractions in μm.

5.3.2 Geochemistry

5.3.2.1 Gold

Comparison of average and median gold concentrations shows: (1) Au in the R. Estrecho has the greatest absolute values in the –75+53μm fraction in high and medium energy (median 340 ppb in –75+53μm vs. 270 and 150 ppb in the -53μm and –106+75μm fractions, respectively); (2) the high energy environment has the greatest median gold concentrations (Table 5.14); and, (3) the R. Estrecho has greater gold concentrations than the three tributaries for all size fractions and all energies (Table 5.14).

The poor quality control results discussed in Chapters 3 and 4 for coarse gold are applicable to gold at Pascua. Data are presented for all size fractions, but most attention will be given to the –75+53μm and -53μm fractions. Analysis of variance of gold values suggests that the between site variability is not significant compared to within site variances (Table 5.15). Only the –150+106μm fraction has between site variances at least as great as between site variances for high and medium energy. The remaining three fractions show a trend to increasing $f/f_{critial}$ ratio with decreasing grain size between high and medium energy samples (Table 5.15).

In the high energy environment, all size fractions have maximum gold concentrations at site 37, except for the –150+106μm fraction which peaks at site 36 (Figure 5.26). Although, site 37 is approximately 800 meters upstream from a decrease in stream gradient, the change in stream slope does not appear to be linked to changes in gold concentrations. Gold in the –150+106 and –106+75μm fractions is erratic, (e.g. 980 ppb to 25 ppb to 545 ppb in –106+75μm fraction

Table 5.14. Median gold values found in Pascua steam sediments.

Size fraction (μm)	High		Medium		Low	
	R. Estrecho (n=14)	Pascua (n=16)	R. Estrecho (n=15)	Pascua (n=18)	R. Estrecho (n=6)	Pascua (n=7)
-150+106	27.5	25	30	25	12.5	10
-106+75	150	30	135	125	12.5	10
-75+53	341	310	275	215	20	20
-53	270	250	250	243	113	110

Table 5.15. F values and $F/F_{critical}$ ratios from ANOVA tests for gold between fluvial energies (Fcritcal = 2.23).

	-150+106μm		-106+75μm		-75+53μm		-53μm	
	F	$F/F_{critical}$	F	$F/F_{critical}$	F	$F/F_{critical}$	F	$F/F_{critical}$
High-medium	2.93	1.31	0.75	0.34	1.08	0.48	1.419	0.64

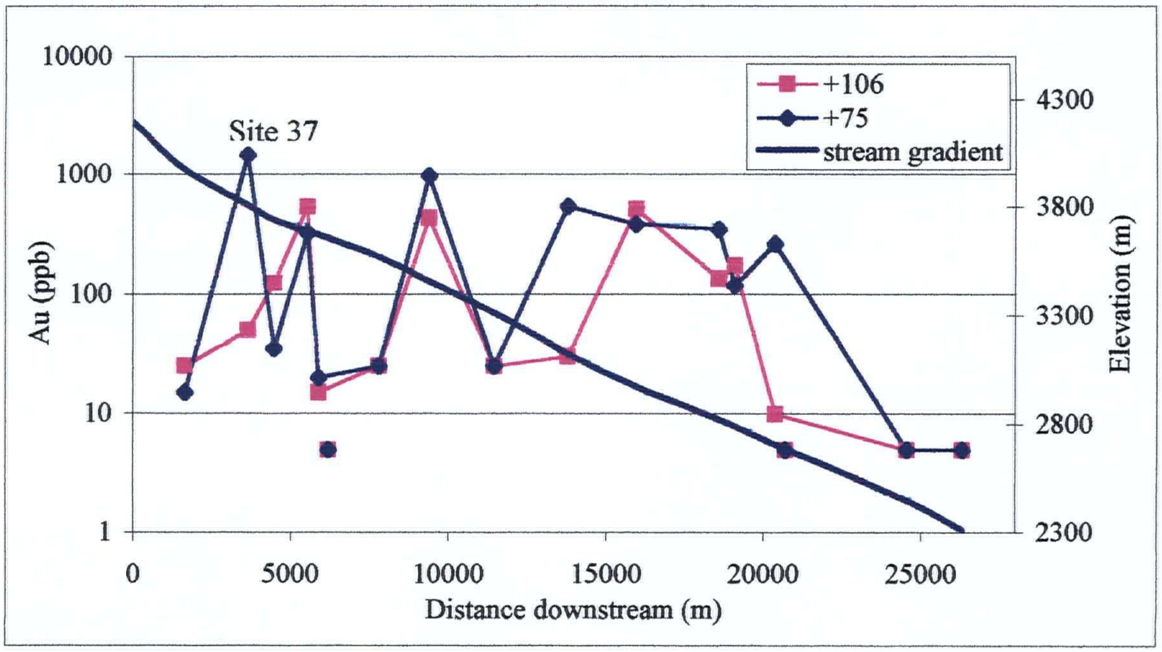

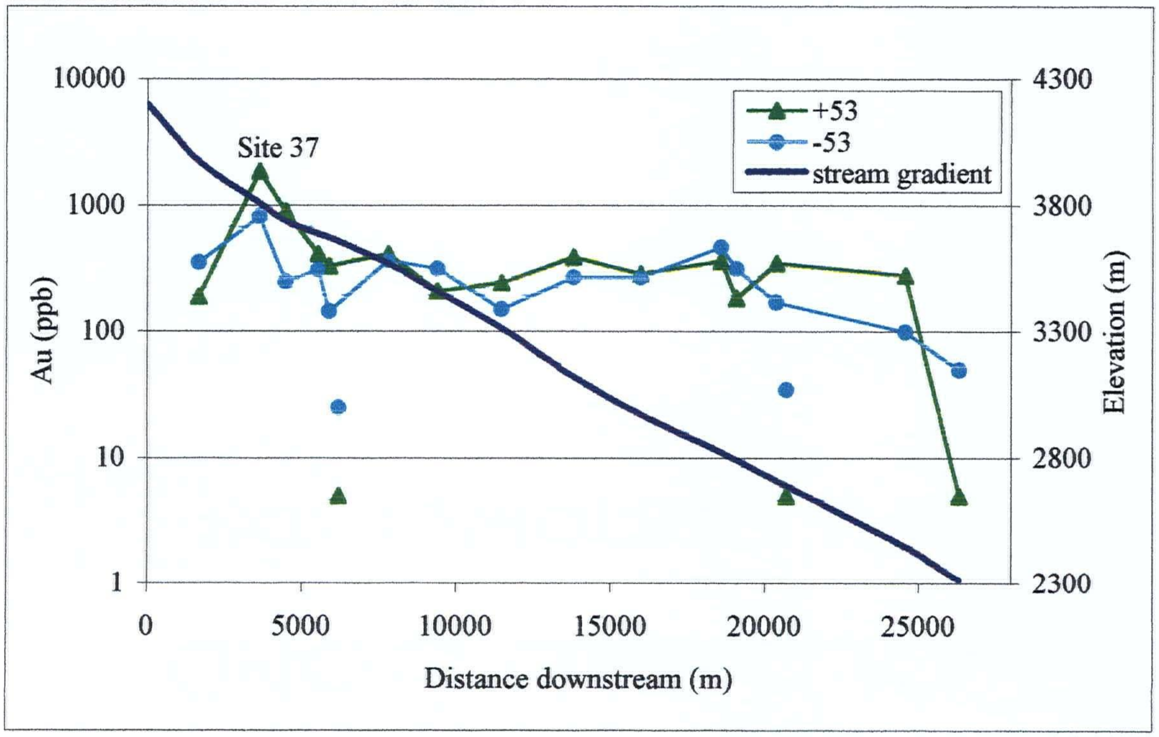

Figure 5.26. Gold in high energy stream sediments at Pascua. Q. Barriales, Q. Agua Falda and R. Toro are shown as points 6.2, 12.8, and 20.7 km downstream, respectively. Size fractions in μm.

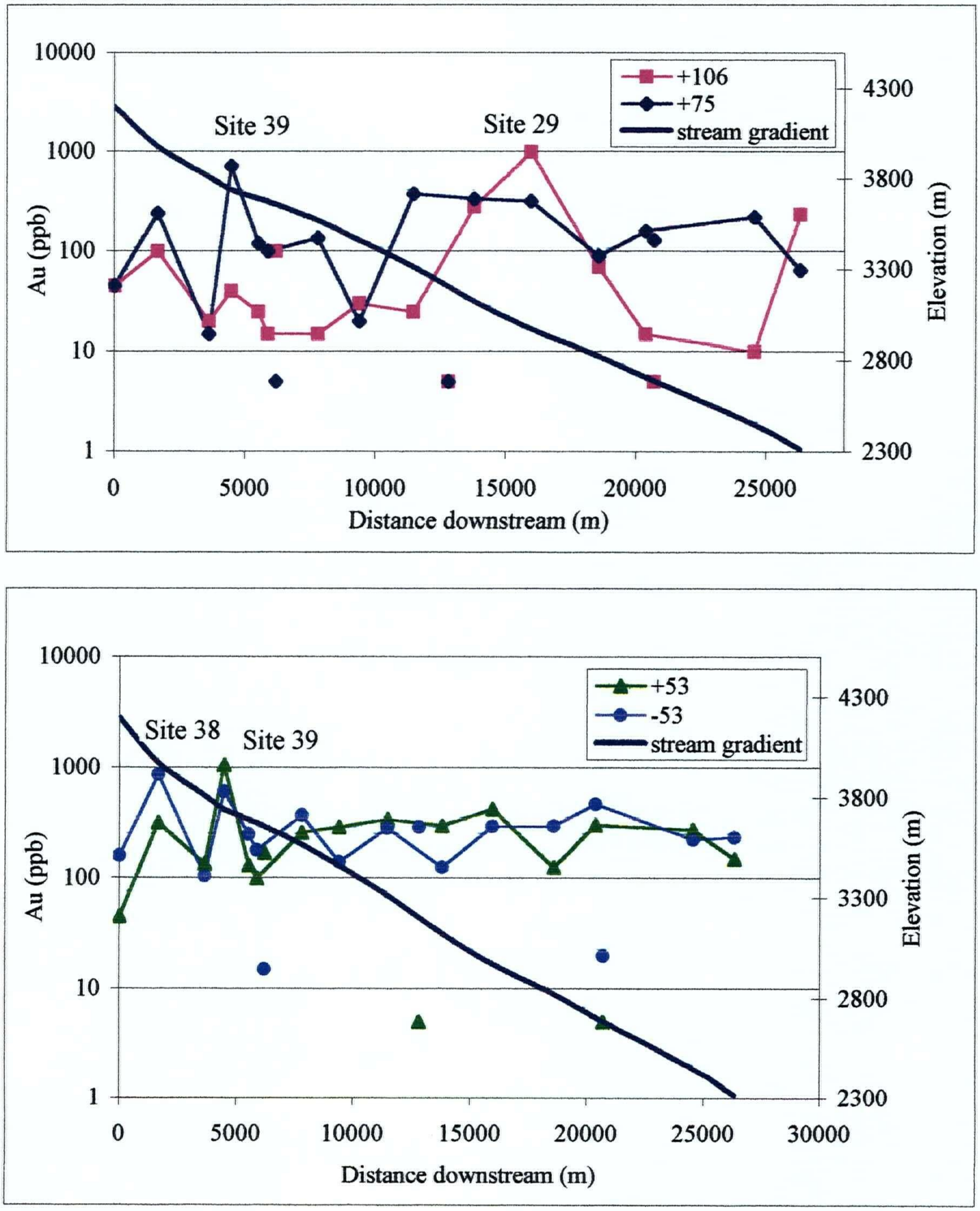

Figure 5.27. Gold in medium energy stream sediments at Pascua. Q. Barriales, Q. Agua Falda and R. Toro are shown as points 6.2, 12.8, and 20.7 km downstream, respectively. All grains sizes in μm.

between three adjacent samples sites over a 4.4 kilometers stretch) (Figure 5.26). The downstream profiles for the –75+53 and -53μm fractions are less irregular, decreasing from peak values at site 37. Concentrations are greater than 185ppb (-75+53μm) and 100 ppb (-53μm) for the remaining samples sites. Gold concentrations for all size fraction are the lowest at the most distal site, 26.3 kilometers downstream, below the confluence with the R. Blanco which drains an area approximately the same as the R. Estrecho. Below this major confluence, gold values for all size fraction are at or below the detection limit of 5 ppb, except for the –53 μm fraction with a concentration of 50 ppb. Tributaries are at or below the detection limit of 5 ppb, except for –53 fraction which has values of 25 and 35 ppb.

Medium energy samples have similar patterns as the high energy (Figure 5.27). Gold values are erratic in the coarser fractions, peaking at site 29 (990 ppb) in the –150+106μm fraction and at site 39 (715 ppb) for the –106+75μm fraction. Gold values in the –75+53μm and -53μm fractions have two pronounced peaks at site 38 (320 and 865 ppb, respectively) and site 39 (1060 and 605 ppb). The Q. Barriales has a gold value of 100 ppb in the –150+106μm fraction and the R. del Toro returns a value of 130 ppb in the –106+75μm fraction. All three tributaries have elevated gold concentrations in the –53 μm fraction (Figure 5.27).

The R. Estrecho and its tributaries do not have many low energy sample sites. However, the limited data from the headwaters of the R. Estrecho shows similar behavior to high and medium energy sample sites with greater gold concentrations in the finer fractions for both the main stream and the Q. Barriales.

values at sites 38 and 39 (Figure 5.30). Profiles for Cr, Na, Sr and V do not relate to either of the aforementioned trends.

Correlation coefficients with Au produce similar groupings as the dilution profiles (although only Ag, Bi, Fe, and V have significant correlations). Elements with higher concentrations in the R. Estrecho headwaters tend to be positively correlated to Au in the -53μm fraction medium energy sediments (Table 5.17) except for S (r = -0.01). Elements with high concentrations in the middle reaches of the R. Estrecho are generally negatively correlated with gold (although not significantly so). However X-Y scatter plots of element concentration versus Au shows that even elements with non-significant r values still have recognizable relations to gold , e.g. Zn in Figure 5.32. The majority of elements have a negative relation to their water chemistry (Table 5.18).

Total digestion

Mean concentrations from the total digestion are in excess of the *aqua regia* for all but eight elements (As, Bi, Cd, Cu, Fe, Mn, U and Zn) (Table 5.18). The percent extraction of the *aqua regia* digestion relative to the total is a function of the element (Table 5.19): (1) Ag, As, Bi, Cd, Co, Cu, Fe, Mg, Mn, Hg, Mo, Ni, P, Te and Zn are all readily extractable by *aqua regia* with *aqua regia*/total values of >100-76%; (2) partially extractable elements of Ba, Be, Ca, Cr, Pb and V at 40-75%; and, (3) elements that are weakly extracted at less than 40% (Al, Ga, K, Na, Sb, Sr and Ti). High *aqua regia*/total correlation coefficients (greater 0.79) coincide with readily and partially extractable elements, except for Ba (r = 0.55). Downstream profiles have the same trend between total and *aqua regia* for each element (i.e. Cu and Bi Figure 5.33).

Table 5.16. Descriptive statistics of aqua regia digestion of Pascua medium energy stream sediments (n=18). Max/min ratios greater than 10 in bold. Elements of the high sulfidation epithermal geochemical suite (Hedenquist et.al., 1996) are grouped together. Median value for Au.

Elements	Units	Mean	Minimum	Maximum	Max/Min
Au (-53μm)	ppb	243.0	15.00	865.00	**57.7**
pH		5.76	4.00	7.10	1.8
Cu	ppm	328.94	68.90	943.00	**13.7**
Ag	ppm	2.84	0.24	6.72	**28.0**
As	ppm	119.64	14.00	354.00	**25.3**
Pb	ppm	99.33	16.00	302.00	**18.9**
Hg	ppm	1.01	0.13	2.46	**18.9**
Te	ppm	0.93	0.05	1.85	**37.0**
Sb	ppm	1.54	0.30	3.60	**12.0**
Mo	ppm	11.64	1.80	30.00	**16.7**
Bi	ppm	3.96	0.96	7.96	8.3
Al	%	2.82	1.72	5.65	3.3
Ba	ppm	320.56	160.00	440.00	2.8
Be	ppm	1.52	0.95	3.05	3.2
Ca	ppm	0.52	0.21	1.51	7.2
Cd	ppm	3.85	0.26	14.70	**56.5**
Co	ppm	19.62	7.60	38.60	5.1
Cr	ppm	27.00	17.00	73.00	4.3
Fe	ppm	5.35	3.87	8.31	2.1
Ga	ppm	6.56	4.80	12.40	2.6
Ge	ppm	0.10	0.10	0.10	1.0
K	%	0.29	0.11	0.57	5.2
La	ppm	16.11	10.00	30.00	3.0
Mg	%	0.70	0.39	1.35	3.5
Mn	ppm	2977.78	655.00	9720.00	**14.8**
Na	%	0.09	0.04	0.17	4.3
Ni	ppm	21.11	13.00	33.00	2.5
P	ppm	837.22	640.00	1690.00	2.6
S	%	0.53	0.06	1.15	**19.2**
Sc	ppm	4.72	4.00	7.00	1.8
Sr	ppm	84.50	38.00	173.00	4.6
Ti	%	0.07	0.04	0.20	5.0
Tl	ppm	1.58	0.08	2.68	**33.5**
U	ppm	24.73	1.60	229.00	**143.1**
V	ppm	57.11	39.00	82.00	2.1
W	ppm	0.73	0.15	2.65	**17.7**
Zn	ppm	870.39	82.00	3330.00	**40.6**

* Au by FA-AAS

Table 5.17. Correlation coefficients of R. Estrecho stream sediments after aqua regia digestion. df= 1f, r significant at 0.514 for P= 0.05 at 95% confidence. Significant values in **bold.**

	Au	*pH*
Au	1.00	-0.38
pH	-0.38	1.00
Cu	-0.39	0.49
As	0.21	**-0.51**
Pb	0.18	-0.42
Hg	0.49	-0.16
Te	0.35	**-0.56**
Mo	-0.46	0.41
Bi	**0.75**	**-0.60**
Ag	**0.71**	**-0.73**
Al	-0.46	-0.02
Ba	0.07	0.49
Be	-0.51	0.28
Ca	-0.26	**0.75**
Cd	-0.35	**0.59**
Co	-0.36	**0.62**
Cr	0.19	-0.38
Fe	**0.55**	**-0.83**
K	0.02	-0.33
Mg	-0.07	0.44
Mn	-0.39	**0.59**
Na	-0.07	-0.02
Ni	-0.32	**0.67**
P	0.02	-0.43
S	-0.01	**-0.71**
Sb	0.34	**-0.64**
Sc	-0.11	-0.44
Sr	-0.19	0.23
Ti	-0.07	**0.58**
Tl	0.09	-0.37
U	-0.38	**0.65**
V	**0.63**	-0.19
W	-0.18	0.22
Zn	-0.37	**0.56**

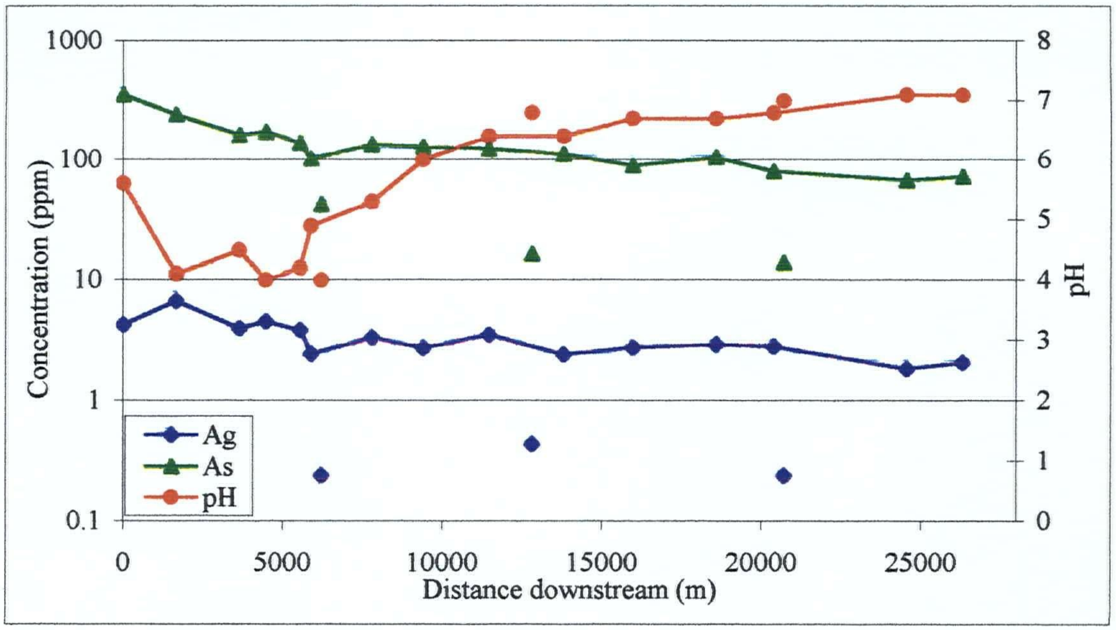

Figure 5.28. Downstream profile of aqua regia digestible Ag and As in -53µm medium energy sediments. Q. Barriales, Q. Agua Falda and R.Toro are shown as points 6.2, 12.8, and 20.7 km downstream, respectively.

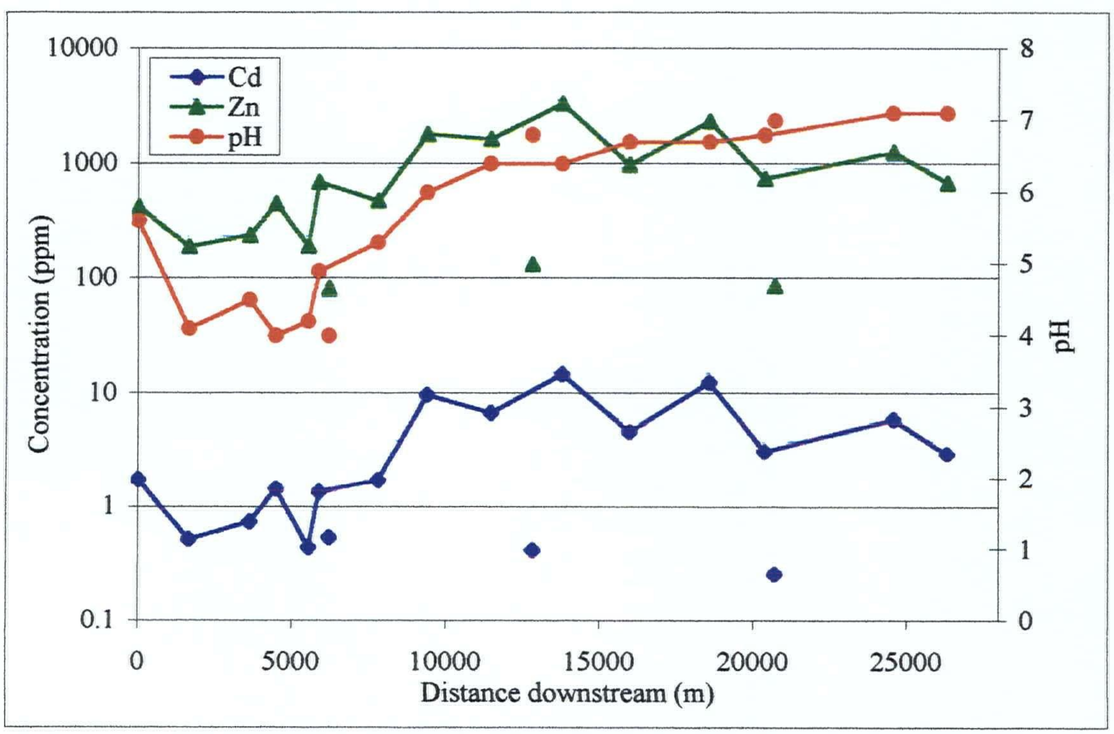

Figure 5.29. Downstream profile of aqua regia digestible Cd and Zn in - 53µm medium energy sediments. Q. Barriales, Q. Agua Falda and R.Toro are shown as points 6.2, 12.8, and 20.7 km downstream, respectively.

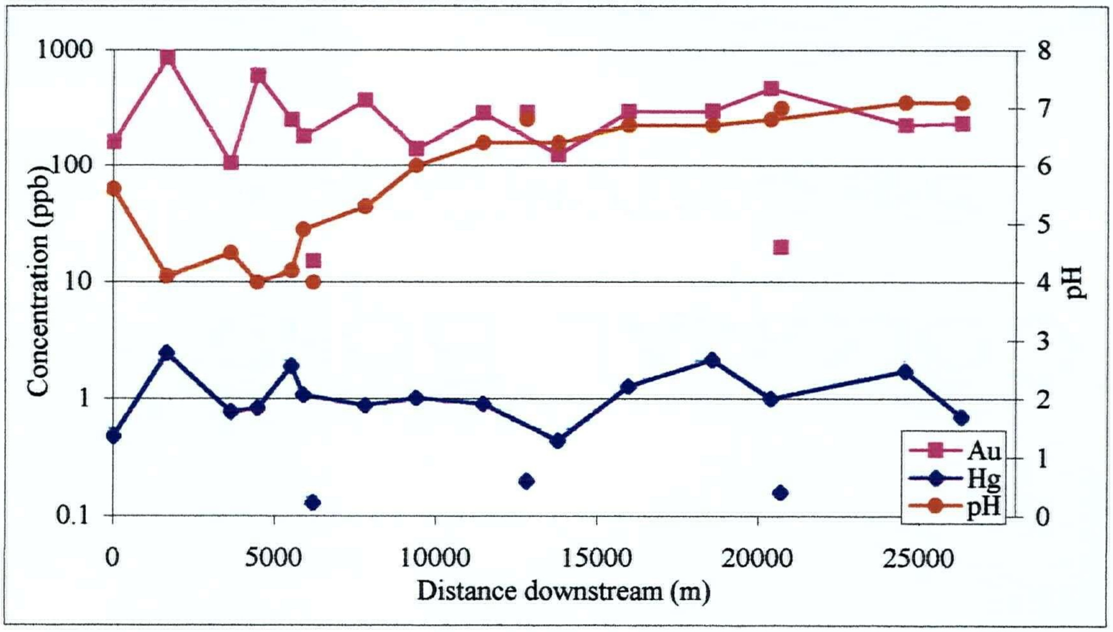

Figure 5.30. Downstream profile of aqua regia digestible Hg in -53μm medium energy sediments. Q. Barriales, Q. Agua Falda and R. Toro are shown as points 6.2, 12.8, and 20.7 km downstream, respectively.

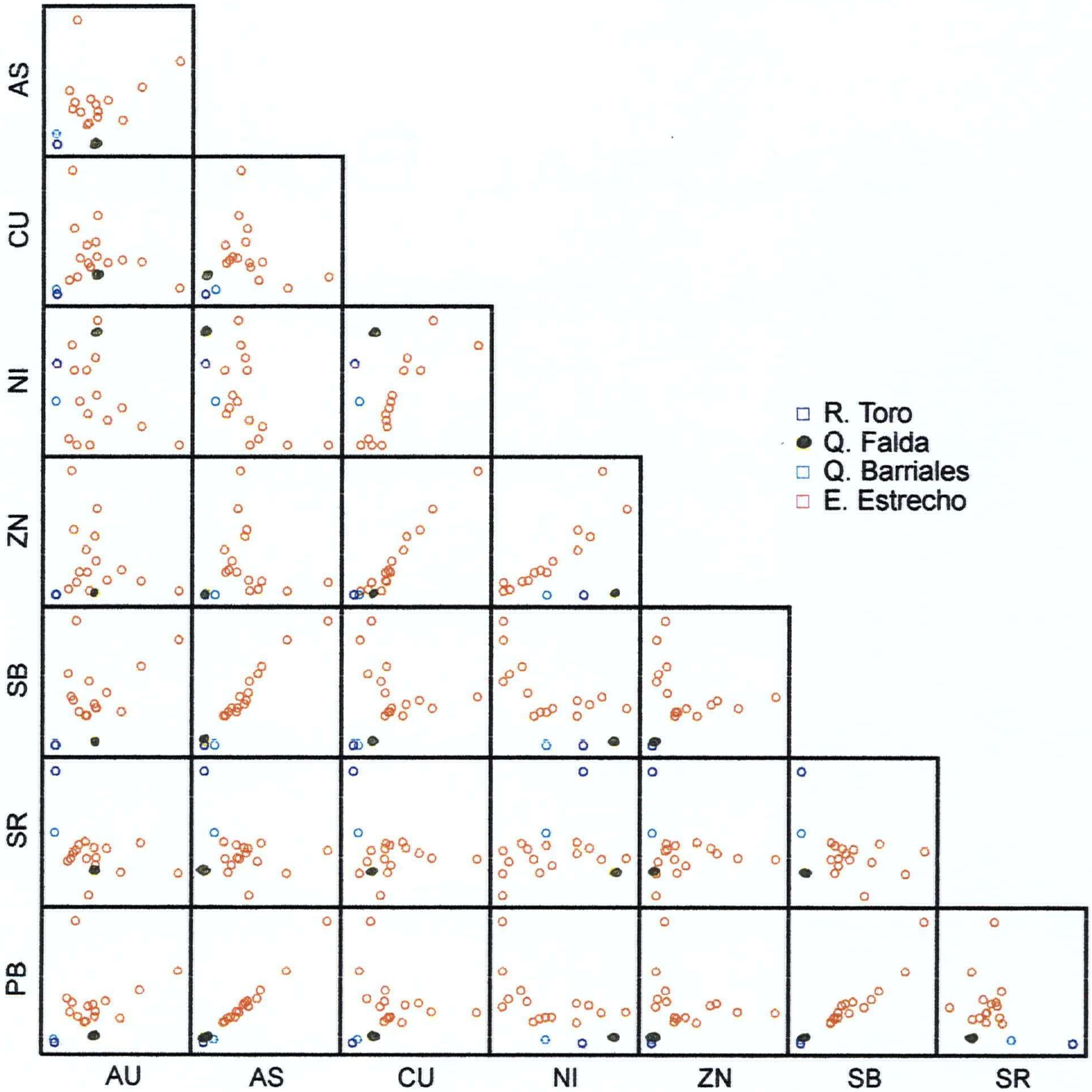

Figure 5.32. X-Y scatter plots of selected elements for stram sediments after aqua regia digestions at Pascua.

values at sites 38 and 39 (Figure 5.30). Profiles for Cr, Na, Sr and V do not relate to either of the aforementioned trends.

Correlation coefficients with Au produce similar groupings as the dilution profiles (although only Ag, Bi, Fe, and V have significant correlations). Elements with higher concentrations in the R. Estrecho headwaters tend to be positively correlated to Au in the -53μm fraction medium energy sediments (Table 5.17) except for S (r = -0.01). Elements with high concentrations in the middle reaches of the R. Estrecho are generally negatively correlated with gold (although not significantly so). However X-Y scatter plots of element concentration versus Au shows that even elements with non-significant r values still have recognizable relations to gold , e.g. Zn in Figure 5.32. The majority of elements have a negative relation to their water chemistry (Table 5.18).

Total digestion

Mean concentrations from the total digestion are in excess of the *aqua regia* for all but eight elements (As, Bi, Cd, Cu, Fe, Mn, U and Zn) (Table 5.18). The percent extraction of the *aqua regia* digestion relative to the total is a function of the element (Table 5.19): (1) Ag, As, Bi, Cd, Co, Cu, Fe, Mg, Mn, Hg, Mo, Ni, P, Te and Zn are all readily extractable by *aqua regia* with *aqua regia*/total values of >100-76%; (2) partially extractable elements of Ba, Be, Ca, Cr, Pb and V at 40-75%; and, (3) elements that are weakly extracted at less than 40% (Al, Ga, K, Na, Sb, Sr and Ti). High *aqua regia*/total correlation coefficients (greater 0.79) coincide with readily and partially extractable elements, except for Ba (r = 0.55). Downstream profiles have the same trend between total and *aqua regia* for each element (i.e. Cu and Bi Figure 5.33).

Table 5.18. Descriptive statistics of total digestion of Pascua medium energy stream sediments (n=18). Max/min ratios greater than 10 in bold. Elements of the high sulfidation epithermal geochemical suite (Hedenquist et.al., 1996) are grouped together. Median reported for Au.

Element	Units	Mean	Minimum	Maximu	Max/Min
Au*	ppb	242.5	15	865	**57.7**
pH		5.76	4.00	7.10	1.8
Cu	ppm	328.56	76	869	**11.4**
Ag	ppm	2.90	0.6	6.6	**11.0**
As	ppm	111.83	17	352	**20.7**
Pb	ppm	142.33	26	342	**13.2**
Hg	ppb	704.44	10	2430	**243.0**
Sb	ppm	4.14	0.7	8.9	**12.7**
Te	ppm	1.16	0.05	2.15	**43.0**
Mo	ppm	12.43	2.2	31.6	**14.4**
Bi	ppm	2.59	0.69	5.22	7.6
Al	%	8.32	6.14	9.41	1.5
Ba	ppm	787.78	380	1310	3.4
Be	ppm	2.75	2.1	3.75	1.8
Ca	%	1.22	0.79	2.26	2.9
Cd	ppm	3.50	0.26	13.55	**52.1**
Co	ppm	20.49	8.6	39.8	4.6
Cr	ppm	44.33	30	86	2.9
Cs	ppm	12.61	7.65	25.8	3.4
Fe	%	5.06	3.73	7.94	2.1
Ga	ppm	21.46	17.9	26.2	1.5
K	%	1.98	1.36	2.45	1.8
Mg	%	0.91	0.63	1.71	2.7
Mn	ppm	2879.17	775	8600	**11.1**
Na	%	1.92	1.66	2.18	1.3
Ni	ppm	24.29	14.6	38	2.6
P	ppm	983.33	740	1980	2.7
Sr	ppm	235.28	170	391	2.3
Ti	%	0.37	0.27	0.56	2.1
Tl	ppm	2.54	0.56	4.84	8.6
U	ppm	24.51	2	264	**132.0**
V	ppm	95.78	66	136	2.1
W	ppm	3.06	1.4	7.1	5.1
Zn	ppm	802.61	92	2840	**30.9**

* Au by FA-AAS

Table 5.19. Percent extraction of aqua regia to total and cold hydroxylamine to aqua regia. Correlation coefficients (r) values reported are for aqua regia to total.

Element	Ratio (%)	Min	Max	Average	r
Silver	AR/tot	16.0%	129.1%	90.4%	0.94
	CH/AR	0.0%	35.2%	18.9%	
Aluminum	AR/tot	20.9%	60.0%	33.7%	0.49
	CH/AR	0.0%	57.7%	20.8%	
Arsenic	AR/tot	82.4%	126.8%	105.1%	0.99
	CH/AR	0.0%	6.4%	0.5%	
Barium	AR/tot	20.6%	49.3%	41.3%	0.55
	CH/AR	0.0%	49.0%	22.9%	
Beryllium	AR/tot	41.7%	81.3%	54.3%	0.90
	CH/AR	0.0%	21.1%	13.2%	
Bismuth	AR/tot	129.5%	190.5%	153.5%	0.98
	CH/AR	0.0%	0.5%	0.1%	
Calcium	AR/tot	23.2%	70.6%	40.3%	0.89
	CH/AR	0.0%	0.5%	0.3%	
Cadmium	AR/tot	95.7%	119.4%	107.2%	1.00
	CH/AR	0.0%	87.8%	59.4%	
Cobalt	AR/tot	82.6%	103.7%	94.6%	0.99
	CH/AR	0.0%	80.6%	45.2%	
Chromium	AR/tot	37.8%	84.9%	60.1%	0.90
Copper	AR/tot	88.3%	108.5%	98.2%	1.00
	CH/AR	0.0%	23.5%	14.3%	
Iron	AR/tot	87.2%	113.2%	105.9%	0.98
	CH/AR	0.0%	1.0%	0.6%	
Ga	AR/tot	24.8%	58.8%	30.6%	0.21
	CH/AR	0.8%	2.1%	1.6%	
Mercury	AR/tot	5.4%	1600.0%	267.0%	0.79
Potassium	AR/tot	5.9%	23.3%	14.4%	0.62
	CH/AR	0.0%	10.5%	4.5%	
Magnesium	AR/tot	59.3%	97.8%	75.1%	0.94
	CH/AR	0.0%	56.6%	23.3%	
Manganese	AR/tot	68.9%	113.0%	96.7%	1.00
	CH/AR	0.0%	70.3%	48.4%	
Molybdenum	AR/tot	80.0%	109.5%	92.4%	1.00
Sodium	AR/tot	2.4%	9.8%	4.7%	-0.41
	CH/AR	0.0%	8.6%	3.8%	
Nickel	AR/tot	74.3%	98.0%	86.5%	0.97
	CH/AR	0.0%	118.1%	22.9%	
Phosphorus	AR/tot	75.3%	90.6%	85.3%	0.99
	CH/AR	0.0%	4.5%	1.1%	
Lead	AR/tot	60.7%	88.3%	67.6%	0.98
	CH/AR	0.0%	1.9%	0.7%	
Antimony	AR/tot	23.1%	45.7%	36.9%	0.97
	CH/AR	0.0%	1.7%	0.7%	
Strontium	AR/tot	22.4%	44.2%	35.5%	0.87
Tellurium	AR/tot	72.0%	300.0%	92.7%	0.98
Titanium	AR/tot	9.3%	39.1%	19.4%	0.74
Uranium	CH/AR	0.0%	5.6%	1.9%	
Vanadium	AR/tot	45%	70%	60%	0.85
	CH/AR	0.0%	4.1%	1.8%	
Zinc	AR/tot	89.1%	117.3%	102.9%	1.00
	CH/AR	0.0%	44.0%	19.7%	

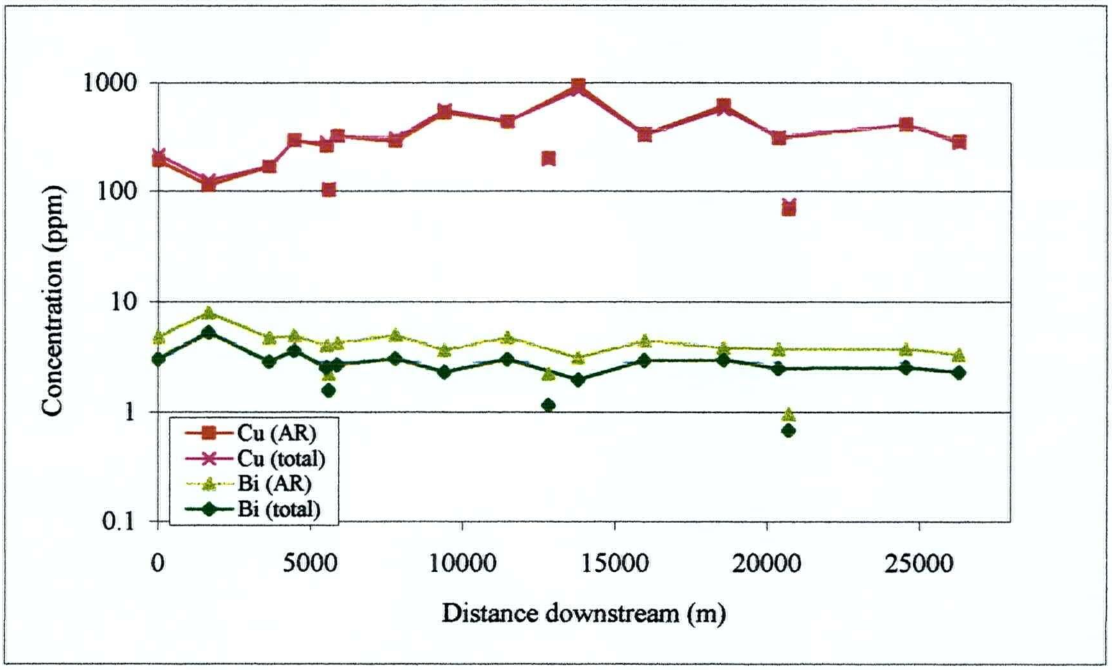

Figure 5.33. Downstream profiles for Cu and Bi in stream sediments after aqua regia and total digestions. Q. Barriales, Q. Agua Falda and R. Toro are shown as points 6.2, 12.8, and 20.7 km downstream, respectively.

size fractions was mounted in epoxy resin, polished and carbon coated for identification of heavy mineral phases using the scanning electron microscope and concurrent energy dispersive spectra.

Light minerals account for between 84% and 90% of the sample mass in both size fractions (Table 5.23). Elements are found in greater concentrations in the heavy mineral fraction than in the light mineral fractions (Table 5.22), e.g. Au is 127 and 84 times greater in HM separates for the –106+75 and –75+106μm fractions, respectively. The heavy mineral fraction accounts for between a minimum of 17.6% (As) and a maximum of 95.9% (Au) of total concentration (HM plus LM) in the –106+75μm fraction and between 12.1% (Zn) and 91.0% (Au) in the –75+53μm fraction.

Scanning electron microscopy confirmed the presence of Ba, S, Fe, Ti, Pb, As, Cu, Hg, Au, Ag, Cu, Sb, As, Zn and Te in the heavy mineral fraction of –106+75 and –75+53μm stream sediments. Relative abundances of minerals found in the magnetic and non-magnetic heavy mineral fractions are qualitatively classified as rare, subordinate, common and dominate (Table 5.23). Mineralogy of the magnetic fraction was dominated by magnetite, titaniferous magnetite and monazite grains. Barite and zircon dominated the non-magnetic fraction mineralogy.

5.5 Chemical precipitates

Semi-qualitative mineralogy was determined with step-scan X-ray powder diffraction for fifteen samples (Table 5.24). Scanning electron microscopy and energy dispersive spectra were collected to confirm results. Five precipitate samples from Pascua were assigned relative abundances from XRD results with halotrichite ($FeAl_2(SO_4)_4 \cdot 22H_2O$), epsomite ($MgSO_4 \cdot 7H_2O$) and apjohnite ($MnAl(SO_4)_4 \cdot 22H_2O$) being the dominate phases. Sample 313, taken above

Table 5.20. Descriptive statistics of cold hydroxylamine leach of Pascua medium energy stream sediments (n=14). Max/min ratios greater than 10 in bold. Elements of the high sulfidation epithermal geochemical suite (Hedenquist et.al. 1996) are grouped together. Median values for Au.

Elements	Units	Mean	Minimum	Maximu	Max/Min
Au*	ppb	242.5	15	865	**57.7**
pH		5.76	4.00	7.10	1.8
Cu	ppm	70.88	9	222	**24.67**
Ag	ppm	0.68	0.344	0.908	2.64
As	ppm	0.38	0.1	4	**40.00**
Pb	ppm	0.94	0.3	3.5	**11.67**
Sb	ppm	0.01	0.005	0.045	9.00
Ni	ppm	5.71	0.5	24.8	**49.60**
Al	ppm	658.14	257	1685	6.56
Au	ppm	0.09	0.05	0.15	3.00
Ba	ppm	89.42	23.8	206	8.66
Be	ppm	0.22	0.15	0.3	2.00
Bi	ppm	0.01	0.005	0.005	1.00
Ca	ppm	1450.71	530	2380	4.49
Cd	ppm	3.75	0.27	12.9	**47.78**
Co	ppm	12.46	1.8	31.1	**17.28**
Cs	ppm	0.10	0.07	0.175	2.50
Fe	ppm	326.79	200	535	2.68
K	ppm	137.50	80	210	2.63
Mg	ppm	161.00	17	379	**22.29**
Mn	ppm	2135.29	281	5000	**17.79**
Na	ppm	35.71	20	60	3.00
P	ppm	7.14	5	30	6.00
Sr	ppm	9.43	5.05	15.1	2.99
Tl	ppm	0.19	0.135	0.26	1.93
U	ppm	0.24	0.035	0.93	**26.57**
V	ppm	1.05	0.35	1.95	5.57
Zn	ppm	323.79	20	1035	**51.75**

*Au by FA-AAS

Table 5.21. Correlation coefficients for stream sediments after cold hydroxylamine leach with pH and water chemistry. df = 12, r significant at 0.532 for P = 0.05 and 95% confidence. Significant values in **bold**.

Elemen	Water	pH
Cu	**-0.59**	**0.61**
Al	**0.59**	**-0.56**
Ba	0.27	**0.61**
Ca	-0.42	0.29
Cd	-0.49	**0.59**
Co	**-0.68**	**0.61**
Fe	0.33	-0.16
K	-0.07	0.13
Mg	-0.51	0.28
Mn	**-0.58**	**0.66**
Na	-0.12	0.13
Ni	-0.21	0.38
Sr	-0.08	0.45
Tl	-0.22	0.22
U	-0.50	0.35
Zn	-0.52	**0.66**

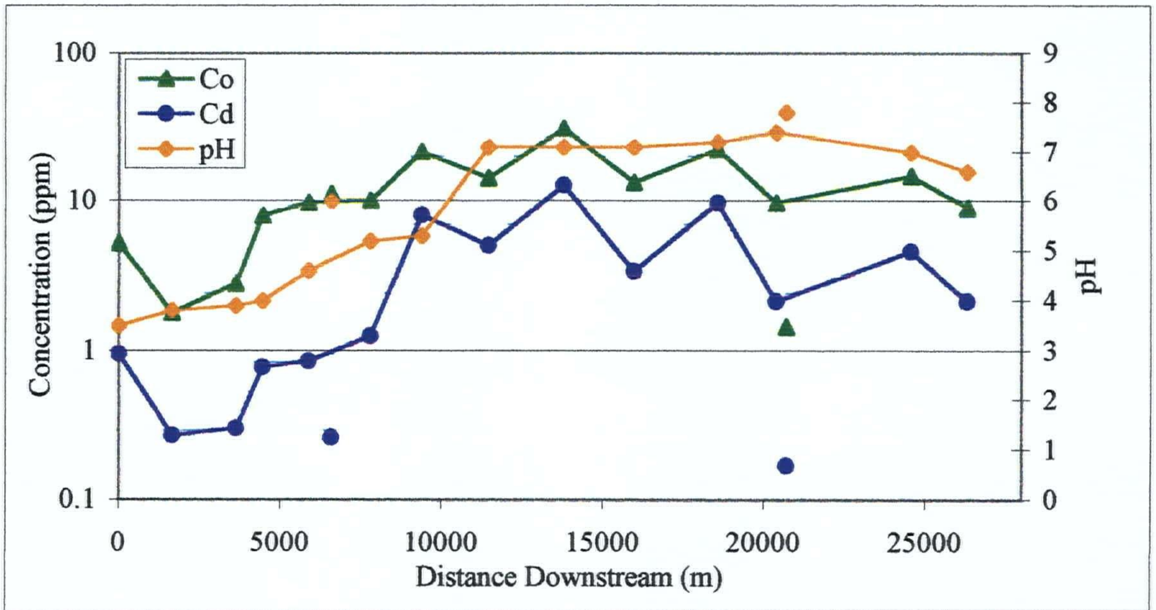

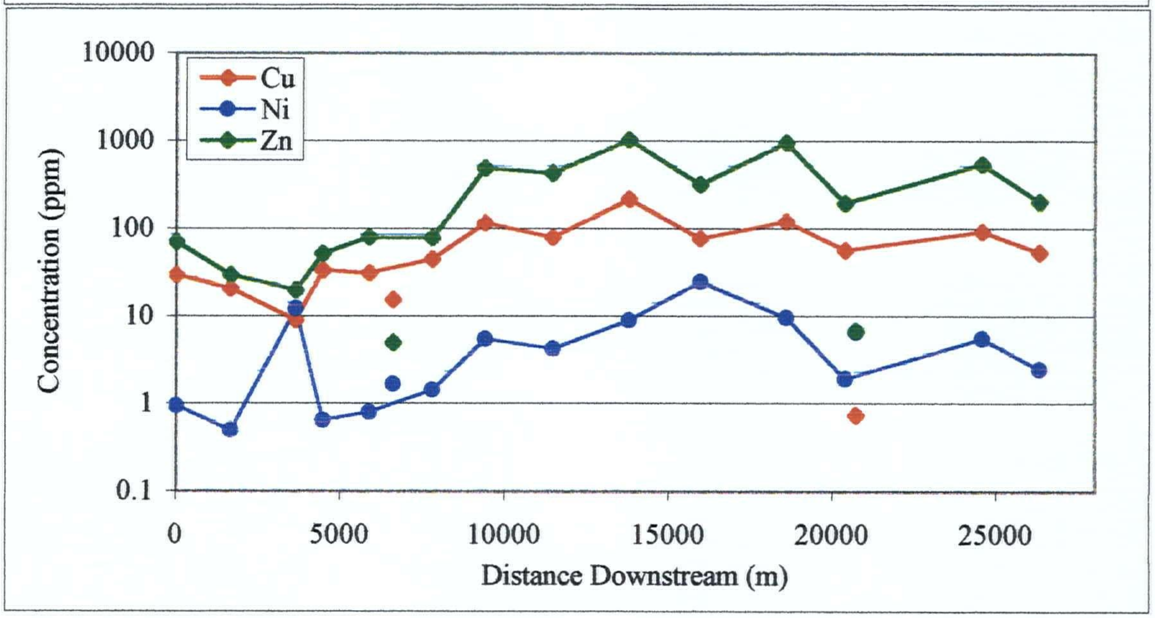

Figure 5.34. Downstream profiles for Cu, Ni, Zn, Co and Cd after cold hydroxylamine selective leach. Q. Barriales, Q. Agua Falda and R. Toro are shown as points 6.2, 12.8, and 20.7 km downstream, respectively.

Table 5.22. Comparison of concentrations between original sample and light and heavy mineral fractions. Original analysis is aqua regia digestion on -53μm medium energy sample. Light mineral fraction is total digestion of high energy sample for respective size fractions. Heavy mineral concentrations are from neutron activation analysis of high energy sample for each size fraction. All vonventrations in ppm, except Au (ppb).

	Site 37 -106+75μm high energy		
	Lights	**Heavies**	**HM (% total)**
Au	30.00	3800.00	95.90
Ag	1.45	10*	---
As	96.00	110.00	17.6
Ba	520.00	10900.00	79.6
Co	9.20	58.00	54.0
Cr	12.00	160.00	71.3
Hg	0.05	10*	---
Mo	4.00	9.00	29.5
Sb	3.70	10.00	33.5
U	2.20	14.00	54.2
W	1.60	9.00	51.2
Zn	432.00	600.00	20.6

* indicates value at or below detection limit

	Site 37 -75+53μm high energy		
	Lights	**Heavies**	**HM (% total)**
Au	155.00	13000.00	91.00
Ag	1.45	10*	---
As	105.00	160.00	15.6
Ba	550.00	19400.00	81.0
Co	10.40	55.00	39.0
Cr	13.00	280.00	72.3
Hg	0.07	10*	---
Mo	4.80	11.00	21.7
Sb	4.20	17.00	32.9
U	2.40	29.00	59.4
W	1.80	20.00	57.4
Zn	528.00	600.00	12.1

size fractions was mounted in epoxy resin, polished and carbon coated for identification of heavy mineral phases using the scanning electron microscope and concurrent energy dispersive spectra.

Light minerals account for between 84% and 90% of the sample mass in both size fractions (Table 5.23). Elements are found in greater concentrations in the heavy mineral fraction than in the light mineral fractions (Table 5.22), e.g. Au is 127 and 84 times greater in HM separates for the –106+75 and –75+106μm fractions, respectively. The heavy mineral fraction accounts for between a minimum of 17.6% (As) and a maximum of 95.9% (Au) of total concentration (HM plus LM) in the –106+75μm fraction and between 12.1% (Zn) and 91.0% (Au) in the –75+53μm fraction.

Scanning electron microscopy confirmed the presence of Ba, S, Fe, Ti, Pb, As, Cu, Hg, Au, Ag, Cu, Sb, As, Zn and Te in the heavy mineral fraction of –106+75 and –75+53μm stream sediments. Relative abundances of minerals found in the magnetic and non-magnetic heavy mineral fractions are qualitatively classified as rare, subordinate, common and dominate (Table 5.23). Mineralogy of the magnetic fraction was dominated by magnetite, titaniferous magnetite and monazite grains. Barite and zircon dominated the non-magnetic fraction mineralogy.

5.5 Chemical precipitates

Semi-qualitative mineralogy was determined with step-scan X-ray powder diffraction for fifteen samples (Table 5.24). Scanning electron microscopy and energy dispersive spectra were collected to confirm results. Five precipitate samples from Pascua were assigned relative abundances from XRD results with halotrichite ($FeAl_2(SO_4)_4 \cdot 22H_2O$), epsomite ($MgSO_4 \cdot 7H_2O$) and apjohnite ($MnAl(SO_4)_4 \cdot 22H_2O$) being the dominate phases. Sample 313, taken above

Table 5.23. Breakdown of weight percentage of sample mass between light mineral, magnetic and non-magnetic heavy mineral fractions.

	weight LM (%)	Weight HM (%)	
		magnetic	non-magnetic
-106+75μm	84.30	12.00	3.60
-75+53μm	89.20	7.50	3.50

Mineral	-106+75µm magnetic	-106+75µm non-magnetic		-75+53µm non-magnetic	-75+53µm magnetic
Barite	c	d		NS	c
Zircon	s	c		NS	s
Magnetite (Fe3O4)	d	s		NS	d
Ti-magnetite	d	s		NS	d
pyrite				NS	
galena (PbS)		r		NS	s
Pb,As,S		s		NS	
Pb,As,Fe,S	r	r		NS	
monazite	s	s		NS	c
Cinnabar (HgS)		r		NS	
illmenite	d	s		NS	d
Au (Ag)	6 grains	9 grains		NS	10 grains
Spahlerite (w/ Fe)	s			NS	s
Cu,Sb,Pb,S (stibnite with sub?)	r			NS	
S,As,Pb		r		NS	
Bi,S		r		NS	
Pb,Sb,S		r		NS	
Sb,Bi,S		r		NS	

r = rare
s = subordinate
c = common
d = dominate

Table 5.24. Relative abundances of heavy mineral and unidentifed phases at site 1 stream sediment sample.
NS = no sample

Table 5.25. Relative abundances of mineral phases in chemical precipitates as determined by XRD (H= high, M= medium, L= low).

Mineral	**Chemical formula**	**313**	**314**	**315**	**316**	**317**
Color*		white	white	ylw/bwn	white	yellow
Gypsum	$CaSO_4 \cdot 2H_2O$			M		L
Epsomite	$MgSO_4 \cdot 7H_2O$			M	M	M
Quartz	SiO_2	M				
Albite	$NaAlSi_3O_8$	H				
Alunogen	$Al_2(SO_4)_3 \cdot 17H_2O$	L				
Apjohnite	$MnAl(SO_4)_4 \cdot 22H_2O$		H			H
Halotrichite	$FeAl_2(SO_4)_4 \cdot 22H_2O$		M	H	M	M
Wattevilleite	$Na_2Ca(SO_4)_2 \cdot 4H_2O$		M			
Pickeringite	$MgAl_2(SO_4)_4 \cdot 22H_2O$				M	
Jurbanite	$AlSO_4(OH) \cdot 5H_2O$					L
Montmorillonite	$(Al,Mg)_8(Si_4O_{10})_4(OH)_8 \cdot 12H_2O$	L				
Pargasite	$NaCa_2Mg_4Al_3Si_6O_{22}$	L				

* Color of precipitate when collected.

Table 5.26. Descriptive statistics for waters associated with chemical precipitates (n=5) Maximum/ minimum ratios greater than ten in **bold**.

(n=5)	Units	Mean	Minimum	Maximum	Max/Min
pH		5.0	3.4	6.5	1.9
Ag	µg/l	0.1	<0.05	0.1	1.0
Al	mg/l	3.2	0.01	12.1	**1728.6**
As	µg/l	1.6	<1.0	3.0	3.0
Ba	µg/l	20.5	1.0	70.9	**70.9**
Ca	mg/l	53.1	16.9	100.0	5.9
Cd	µg/l	4.4	<0.1	18.1	**181.0**
Co	µg/l	7.5	0.1	26.8	**446.7**
Cu	µg/l	108.8	0.4	381.0	**952.5**
Fe	mg/l	0.2	0.1	0.4	7.6
K	mg/l	1.8	1.0	2.9	2.9
Mg	mg/l	10.1	2.8	19.3	6.8
Mn	µg/l	2454.6	4.9	9960.0	**2032.7**
Mo	µg/l	0.4	<0.1	1.1	11.0
Na	mg/l	4.9	4.1	6.4	1.6
Ni	µg/l	8.4	<0.2	29.8	**149.0**
Se	µg/l	1.2	1.0	2.0	2.0
Sr	µg/l	81.1	12.3	154.0	**12.6**
Tl	µg/l	0.2	<0.05	0.6	**11.0**
U	µg/l	1.1	0.2	2.9	**19.3**
Zn	µg/l	878.4	2.5	3620.0	**1448**

sediment site 38 along the R. Estrecho, is unique with quartz and albite and minor amounts of alunogen)$Al_2(SO_4)_3 \cdot 17H_2O$), montmorillonite ($(Al,Mg)_8(Si_4O_{10})_4(OH)_8 \cdot 12H_2O$) and pargasite ($NaCa_2Mg_4Al_3Si_6O_{22}$). Water samples associated with chemical precipitates have maximum/minimum ratios greater than 70 for Al, Ba, Cd, Co, Cu, Mn, Ni and Zn (Table 5.25). Only Al, Mg, Mn, As and Zn concentrations are greater in chemical precipitate waters (albeit by small amounts) than average values from the R. Estrecho.

CHAPTER 6

DISCUSSION

To understand the patterns developed in stream sediment geochemistry, it is necessary to examine the source of metals and the processes responsible for creating and modifying sediment inputs. Comparison of mechanical and chemical processes that redistribute elements from the deposit into surficial media and the supply of sediment to the stream system enables the identification of surface anomalies and modifications of deposit geochemistry occurring prior to fluvial dispersion. Knowledge of the effects of mechanical and chemical segregation of elements by the fluvial system is the final step in comprehending stream sediment geochemistry and its exploration implications.

6.1 Deposit chemistry and mineralogy

In depth presentation of Pascua ore and alteration mineralogy and petrology is given in Section 2.3.1. Salient features relevant to surficial chemistry are summarized here (from Chouinard and Williams-Jones, 1999).

At Pascua, gold occurs in two main styles of mineralization: alunite-pyrite-enargite (APE) and pyrite-szomolnokite (PZ). Enargite in the APE facies can contain a variety of solid inclusions which are the likely source for many metals in stream sediments. Enargite inclusions contain pyrite, stibnite (Sb_2S_3), cassiterite (SnO_2), muthmannite ([Ag,Au]Te), goldfieldite ($Cu_{12}[Te,Sb]_4S_{13}$) and unidentified Cu-Sn-Zn-S and Cu-Bi-Sb-S phases. The Py-Sz facies contains Au and Ag, which are thought to be present as submicroscopic inclusions in pyrite and enargite. These styles of mineralization are responsible for the presence of enriched concentrations of Au, Ag, Te, Cu, As, Sb, Bi, S and Zn in the surficial system.

6.2 Mechanical and chemical dispersion in surficial media

6.2.1 Surficial deposits

A brief review of the significant geochemical results (Chapters 4.1 and 5.1) of surficial deposits prefaces the discussion. The distribution of the various media is presented in Chapter 2.4.2.

Glacial till

Greatest median gold concentrations are found in the -53μm fraction. Glacial till has the lowest geochemical contrast of all surficial media for most elements associated with epithermal mineralization (Au, Ag, Sb, As, Bi, Pb, Hg, Se, S, Te, Tl, and also for Cu at Lama), where contrast is defined as the ratio of the maximum to the minimum concentration for each element (Figure 6.1 and 6.2). Elements that have a significant correlation with gold at both Pascua and Lama include Ag, As, Sb, Bi and Fe. There are no significant negative correlations with Au at Lama, but Ca and Ni have significant negative correlations at Pascua. Although not statistically significant, glacial till has the greatest relative abundance of fine sand and finer material and, conversely, the least fine gravel to medium sand material of all surficial deposits. The abundance of fine material suggests that washing of till is minimal or absent at Pascua/Lama. At Lama, till extends at least as far as the confluence with the R. Tagus (Figure 2.6), where till with gold values of 60 and 70 ppb is being currently eroded into the stream near site 1. Till at Pascua, is present from the headwaters of R. Estrecho, downstream to the west of the camp, below the confluence with the Q. Barriales (Figure 2.7).

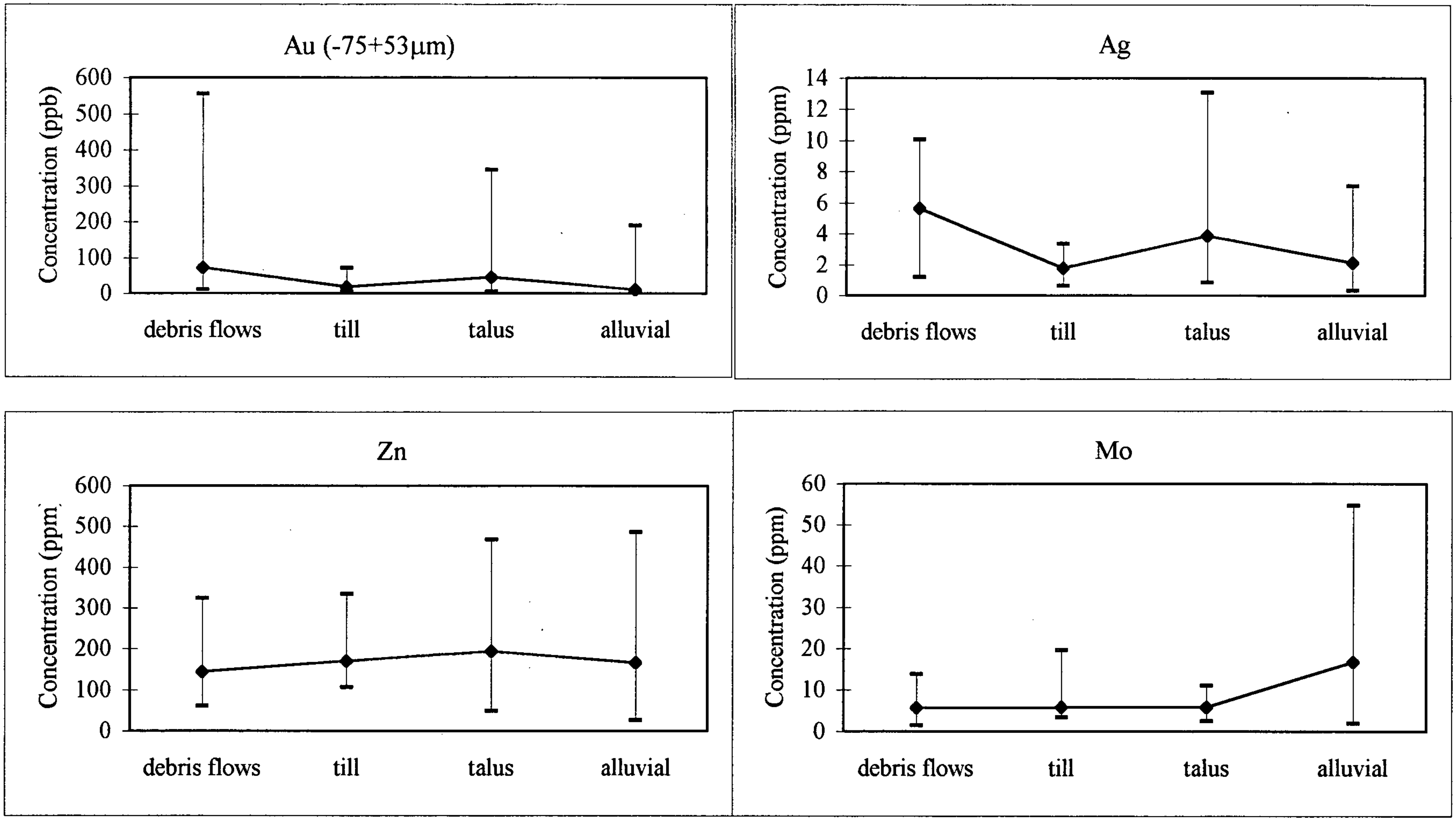

Figure 6.1. Range and mean plots (Au median) for surficial deposits at Lama, Argentina.

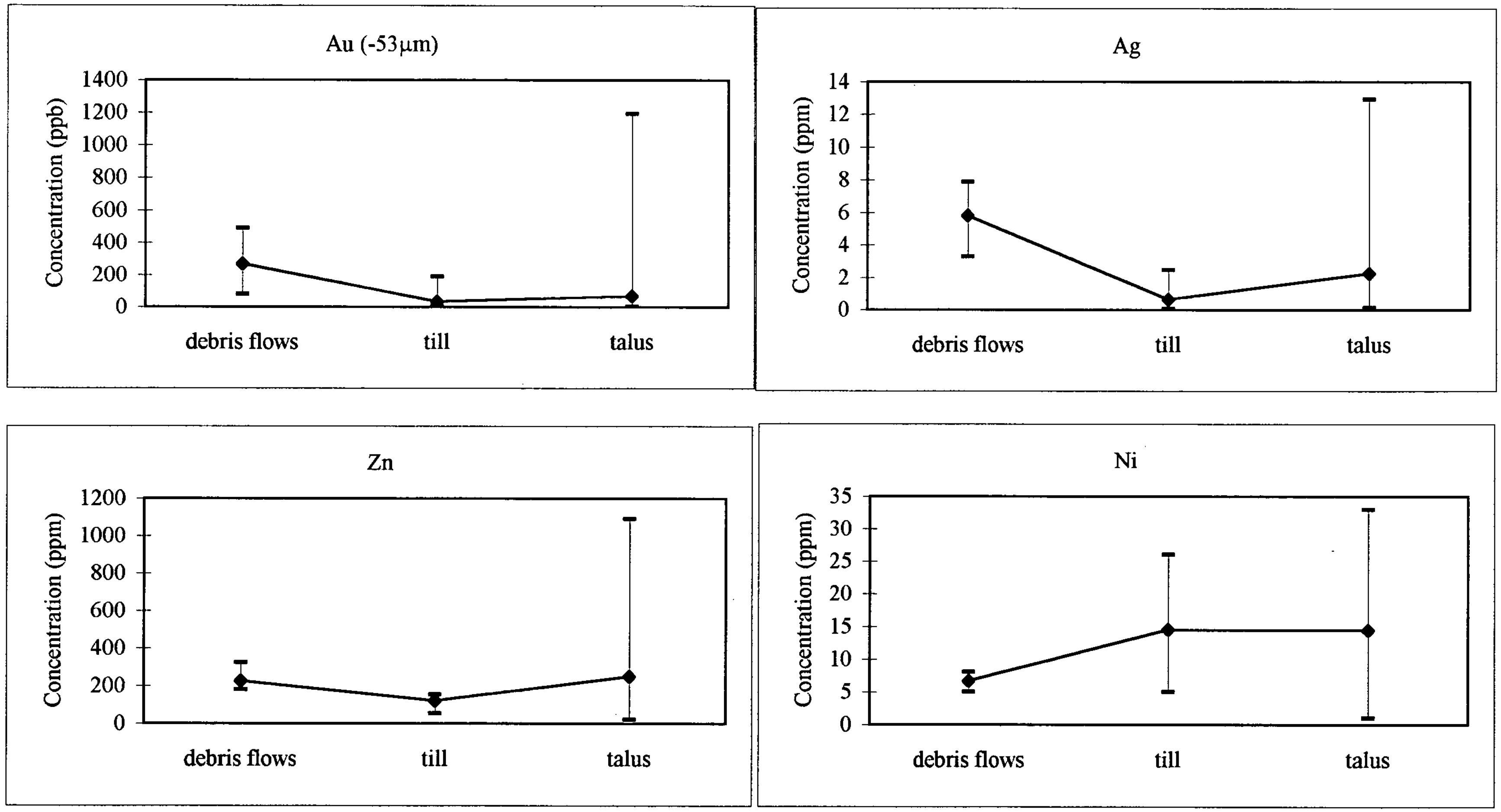

Figure 6.2. Range and mean plots (Au median) for surficial deposits at Pascua, Chile.

Talus cones

Talus cones at Lama are generally coarse, having similar relative abundances of sieved material to debris flows and alluvial fans (Table 4.9). Concentrations of elements associated with mineralization do not differ significantly from other surficial materials except for Ag (mean of 3.85 ppm) and Fe at Lama. However, the range is greater and mean values are generally less than debris flows for heavy mineral associated elements (Figure 6.1 and 6.2). Silver, Sb, As, Bi, Pb, K, Se and S have significant positive correlations with gold at both Pascua and Lama, but Al, Ca, Cr, Co, Mg, Ni, P, U and V have significant negative correlations at both locations.

Anomalous talus cones at the western limit of sampling at Lama extend to the R. Turbio. All other talus cones near Pascua/Lama terminate on either glacial till or debris flows and can not be considered direct sediment inputs (Figure 2.6 and 2.7). Downstream from Pascua where the R. Estrecho valley becomes v-shaped, talus cones are the dominant sediment source supplying (assumed) background concentrations of sediment.

Debris flows

Mass wasting events are common in steep mountainous terrain, especially where valley walls may have been over steepened by glacial erosion. The debris flows deposited by mass wasting are the most common sediment source at Pascua/Lama, and have undergone the greatest amount of transport. Debris flows would have entrained glacial till and older talus cones and alluvial fans that had formed prior to mass wasting. Extensive transport away from the deposit and reworking of older surficial media would allow for more washing away of fines and enrichment of heavy mineral elements. Debris flows are the coarsest surficial material (although not statistically significant) and have the greatest mean concentrations for Au, Ag and Hg at both Pascua and Lama, whereas elements (including Al, Co, Cd, Mn, Ni and Zn) that are more mobile have lower means in debris flows (Figure 6.1 and 6.2). Significant positive correlations with gold include Ag, As, Sb, Te, Mo, Bi, K and W at Lama and Ag, As, Sb, Bi, Pb, Hg, S, Te, and W a Pascua. However, Ca, Co, Mn, U and Zn at Lama and Co, Mg and Ti at Pascua have significant negative correlations with gold. Most of the R. Turbio flows though debris flows and is actively eroding debris flow material so that it has locally downcut 3-5 meters below the surface (Plate 2.4). Debris flows have moved anomalous material at Lama at least as far as the R. Tagus confluence (Figure 2.6). The R. Estrecho at Pascua flows through debris flows from its headwaters to approximately four kilometers below camp (Figure 2.7).

Alluvial fans

Fans were only sampled at Lama. They have significantly more –4+2mm material, and on average more -212μm material than debris flows. They are the youngest surficial media, topographically overlaying all other deposits to terminate on debris flows along the R. Turbio (Figure 2.6). Alluvial fans reach the R. Turbio along the western reaches of Penelope Ridge and directly contribute anomalous material to the stream. Geochemically, alluvial fans are similar to other surficial deposits except for Mo which has a mean value over two times greater (Table 4.9 and Figure 6.1). Molybdenum and copper (as well as other metal cations) show reciprocal behavior in alluvial fans with Mo generally higher in concentration where Cu values are low. The same reciprocal behavior between Cu and Mo was reported by Hansuld (1966) and attributed to the different response of Cu as a cation to Mo as an anion under changing pH conditions. This effect is only seen in alluvial fans since they are the only surficial medium with appreciable amounts of Mo. The range and value of other elements in alluvial fans is generally intermediate between glacial till and talus cones (Figures 6.1 and 6.2).

Dispersion in surficial deposits

There are subtle geochemical differences between the surficial media as summarized above and in Table 6.1. The differences among surficial media must be partly related to different geochemistry and proportions of background and anomalous sample in the data sets. However, they can also be viewed as a continuum from deposits with the least amount of mechanical and chemical modification to deposits with more extensive mechanical and chemical modification (Table 6.2).

With respect to mechanical modification, washing of material can preferentially entrain light minerals and concentrations of elements associated with heavy minerals (Hou and Fletcher, 1998), including Au, Ag, Sb, Hg, Te, S, As, Pb and Bi, tend to increase as the relative abundance of -212μm material decreases from a maximum of 30.6% in glacial till to a minimum of 19.4% in debris flows. In this context, mechanical enrichment of heavy minerals is greatest in debris flows, because they have been transported furthest of all surficial deposits and because they incorporate older till, talus cone and alluvial fan material and have had the greatest opportunity for reworking, loss of fines and concentration of heavy minerals. By incorporating older surficial deposits, mechanical sorting within debris flows creates a younger anomaly that amplifies the mechanical and chemical modification of the original media.

The acidic nature of Pascua/Lama has resulted in variable amounts of acid leaching and removal of mobile elements in the surficial deposits proximal to mineralization. Taking the pH of water in the -53μm settling buckets to reflect the acid producing capacity of surficial media, the difference in concentrations of the more mobile elements (such as Cu, Ni, Zn and Cd) can be explained by varying amounts of acid leaching both within media and (to a lesser extent)

Table 6.1. Significant differences between means of surficial materials of selected elements and size fractions determined by Bonferroni adjustment. Statistically significant differences between media are indicated by Δ and **bold** mean values. Gold concentrations are median values. All values are in ppm except where noted.

Lama					
Element	Debris flows	Glacial till	Talus fines	Alluvial fans	Significant differences by Bonferroni adjustment
Au (ppb)	252	**85**	95	45	G Δ all
Ag	**5.6**	1.8	**3.8**	2.1	D Δ all, T Δ all
As	386.4	**220.6**	375.8	**297.4**	G, A Δ D, T
Bi	6.5	**3.5**	5.4	4.7	G Δ D, T
Hg	**1.0**	0.22	0.28	0.3	D Δ all
Mo	5.7	5.8	5.9	**16.7**	A Δ all
Te	1.8	**1.0**	2.02	1.5	G Δ T
S	1.0	**0.7**	1.0	0.9	G Δ D, T
Cd	**0.4**	0.6	0.7	0.5	D Δ all
Ca (%)	**0.2**	0.4	0.3	0.27	D Δ all
Fe (%)	**6.1**	4.4	**5.8**	4.8	D Δ all, T Δ all
Ni	**6.4**	8.4	8.9	8.0	D Δ T
Zn	**144.4**	170.2	193.9	166.7	D Δ T
-4+2mm	25.5	21.4	23.6	**32.1**	A Δ T, G
-53μm (%)	6.3	**13.5**	10.8	11.0	G Δ D

Pascua				
Element	Debris flows	Glacial till	Talus fines	Significant differences by Bonferroni adjustment
Au (ppb)	**268**	35	70	D Δ all
Ag	5.8	**0.7**	2.2	G Δ D, T
As	286.7	**40.58**	329.4	G Δ D, T
Ba	**467.0**	154.2	182.8	D Δ G, T
Hg	**1.4**	0.1	0.2	D Δ G, T
S	**0.8**	0.1	0.7	D Δ G, T
Cr	**10.1**	22.2	22.3	D Δ G, T
-425+212μm (%)	**17.6**	12.3	8.6	D Δ G, T

G = glacial till
A = alluvial fans
T = talus cones
D = debris flows

Table 6.2. Continuum of mechanical processes modifying surficial media geochemistry. Removal of fine material leads to enrichment of HME by fluvial processes. Values are means for all elements.

Lama

	Mechanical			
	Texture	=	HME enrichment	
Increasing mechanical modification	Σ wt% -212μm		Au (ppb)	Bi (ppm)
Glacial till	30.6		95	3.5
Talus cones	26.5		202	5.4
Alluvial fans	23.7		226	4.7
Debris flows	19.4		257	6.5

Pascua

	Mechanical			
	Texture	=	HME enrichment	
Increasing mechanical modification	Σ wt% -212μm		Au (ppb)	As (ppm)
Glacial till	26.0		35	40.6
Talus cones	17.6		70	320.4
Debris flows	17.6		268	386.7

between media. Figure 6.3 shows concentrations of Ni in debris flows and talus cones, Zn in alluvial fans and Cd in glacial till at Lama at high pH values relative to concentrations with acidic values. In general, concentrations of trace metals increases with increasing pH in all media. Debris flows at Pascua range from acidic (minimum 3.9) to slightly alkaline (maximum 9.9) and have lower trace metal concentrations in acidic samples than in alkaline samples (e.g. Cu in Figure 6.4). Although, the trend is not as strongly developed, the same relationship between Zn concentrations and pH is preserved in glacial till samples. Talus cones at Pascua appear to be controlled more by sampling anomalous and background cones than by acid leaching, where nickel concentrations are high near the deposit (with corresponding low pHs) with lower value relating to 'background', neutral talus cones (Figure 6.4). Debris flows are the most acidic surficial deposit (average pH 4.0 at Lama) and, on average, are generally depleted in mobile elements relative to other media, although this maybe related to the different chemistry of anomalous and background samples.

Although all surficial media transport anomalous material away from the deposit, not all of the media can be considered a direct source of stream sediment. At Lama, debris flows restrict the input of glacial till, alluvial fan and talus cones to the R. Turbio and R. Canito which flow through, and actively erode, valley filling debris flows that decouple the streams from valley walls. At Pascua, debris flows commonly detach other surficial materials from the R. Estrecho proximal to the deposit. From approximately four kilometers below the headwaters to just west of the camp, the R. Estrecho continues to be decoupled from valley sides as it flows through a small flood plain and glacial till deposits. Glacial till and talus cones contribute minor amounts of anomalous material to the stream system, but the majority of the sediment is contributed by debris flows. Sediment supply to the middle and lower reaches of the R. Estrecho is dominated by talus cones of presumed 'background' geochemical values.

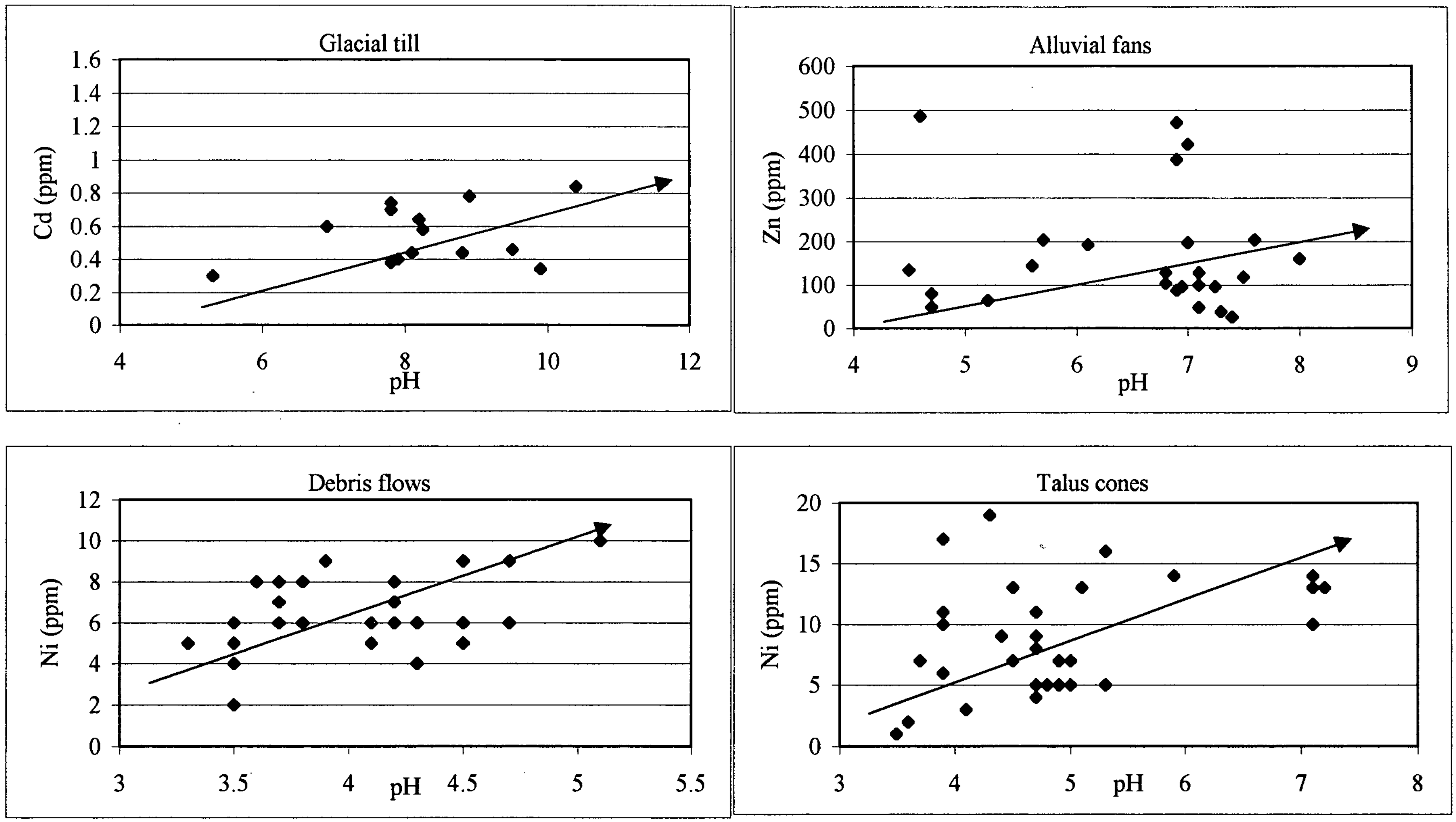

Figure 6.3. Variations of metals concentration as a function of pH in surficial deposits at Lama.

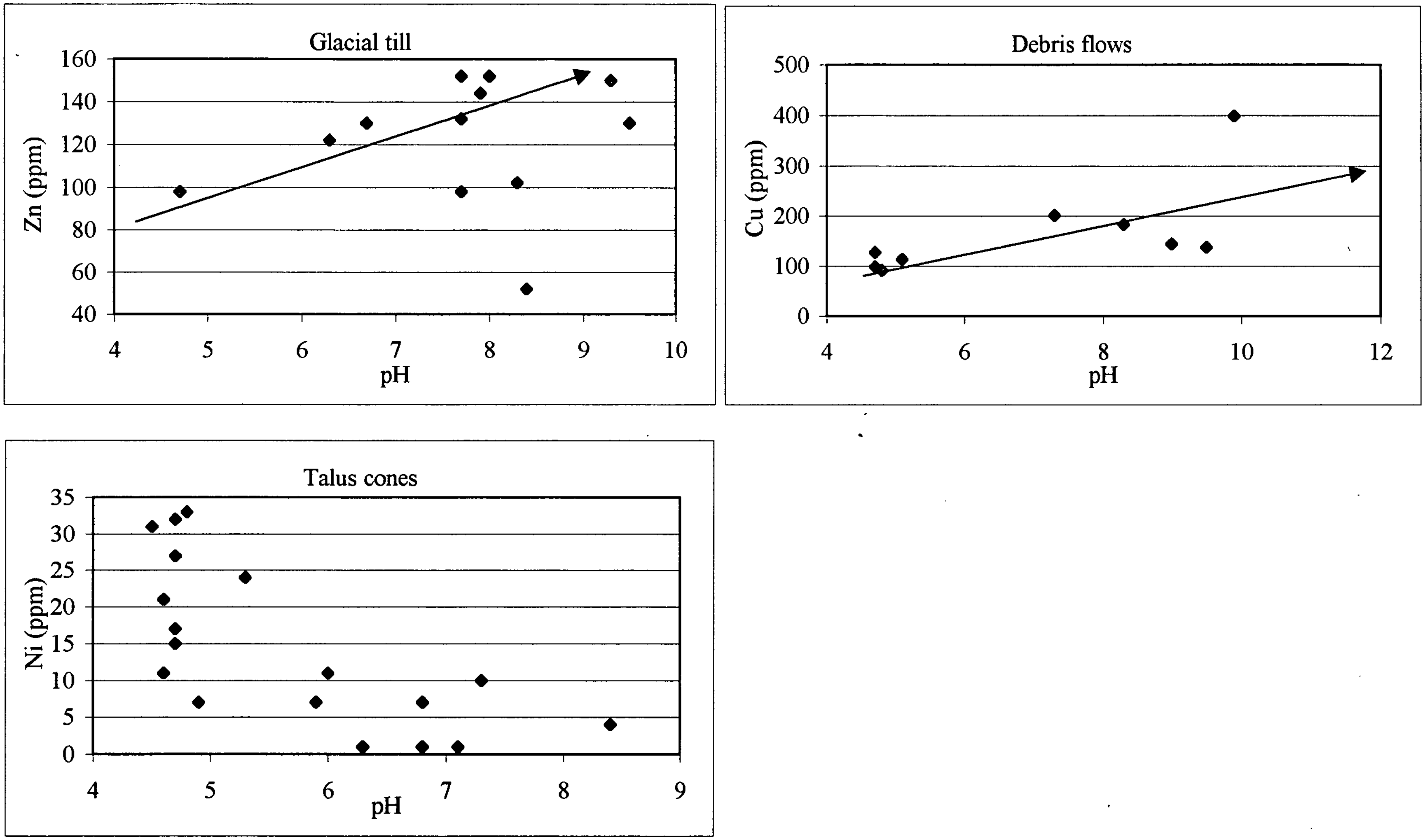

Figure 6.4. Variations of metals concentration as a function of pH in surficial deposits at Pascua. Talus cones do not show the relation with pH, but reflect sampling of both background and anomalous cones.

Geochemical dispersion by debris flows, and to a lesser extent glacial till, extends the metal dispersion train at Pascua/Lama 4-10 km downstream from the deposits. This effects stream sediment geochemistry in two ways: 1) it creates a linear anomaly through which the stream flows (i.e. not a point source); and, 2) the chemical heterogeneity of the surficial materials may mask the effects of any fluvial modifications of stream sediments. In addition, in the case of debris flows, the anomalous material has relatively enhanced values of Au and other heavy mineral associated elements, but is depleted in elements such as Cu that are easily leached under acidic conditions.

6.2.2 Chemical precipitates, surface waters and acid rock drainage

Ferricrete

Ferricrete cementation of older surficial deposits and recent debris flows is the most visible chemical modification of surficial materials and was noted by B. Smee (1998). Debris flows have significantly more iron (mean 6.1%) than glacial till and alluvial fans (Table 4.9). These high iron concentrations and extensive iron oxide precipitates and cements suggest that a large volume of rock has been acid leached and the iron redeposited in debris flows. The presence of iron (maximum 505 mg/l) in the acidic stream waters substantiates that acid leaching is an ongoing process.

Chemical precipitates and associated low pH waters

Base of slope seeps with precipitates are located along the southern edge of the R. Canito drainage near the Veladero property. Less extensive, more efflorescent precipitates are found on the surface of debris flows at both Pascua and Lama. Assuming that precipitate seeps are groundwater outlets (as opposed to surface waters), water chemistry and bulk precipitate chemistry can be explained by the oxidation of sulfide and acid sulfate minerals. The low pHs created by oxidation liberates iron, sulfate (sulfate concentration of all samples was much greater then 200 mg/l) and associated trace elements (e.g. As, Cd, Ni and Zn). Acid rock drainage generation can be explained by the oxidation of pyrite:

$$FeS_2 + 7Fe_2(SO_4)_3 + 8H_2O = 15FeSO_4 + 8H_2SO_4 \quad (1)$$

$$FeS_2 + Fe_2(SO_4)_3 = 3FeSO_4 + 2S \quad (2)$$

$$4FeSO_4 + O_2 + 2H_2SO_4{}^{\text{bacteria}} = 2Fe_2(SO_4)_3 + 2H_2O \quad (3)$$

$$2S + 3O_2 + 2H_2O^{\text{bacteria}} = 2H_2SO_4 \quad (4)$$

$$4FeS_2 + 15O_2 + 2H_2O = 2Fe_2(SO_4)_3 + 2H_2SO_4 \quad (5)$$

$$S + 3Fe_2(SO_4)_3 + 4H_2O = 6FeSO_4 + 4H_2SO_4 \quad (6)$$

The bacteria in equations (3) and (4) are *Thiobacillus ferroxidans* (Mills and Robertson, 1999). As oxidation proceeds, ferric iron acts as an oxidant and can dissolve heavy metal sulfides (including As, Pb and Cu) according to the following schematic reaction:

$$MS + nFe^{3+} = M^{n+} + S + Fe^{2+} \quad (7)$$

where MS is a heavy metal sulfide, and M^{n+} is an aqueous heavy metal ion. Although there is no direct evidence for pyrite and metal sulfide (sulfosalt) oxidation, the low pH values and high trace metal contents are consistent with the expected products of acid rock drainage.

Leaching of non-sulfide minerals by oxidized, acid waters may be the source of high concentrations of Ca, Mg, Mn, Al and K in seepage waters. The center of several seeps were iron indurated and iron nodules were found in precipitates at depths of 15-20 cm. Hydrated sulfates including gypsum, epsomite ($MgSO_4 \cdot 7H_2O$), tamarugite ($NaAl(SO_4)_2 \cdot 6H_2O$) at Lama and halotrichite ($FeAl_2(SO_4)_4 \cdot 22H_2O$) at Pascua are deposited where seepage waters emerge to surface temperature, pressure and pH conditions. Bulk precipitate samples which were classified in the field as dominantly gypsum, tend to have lower concentrations of trace metals compared to iron-rich (greater than 25% Fe) samples (Table 6.3). The high trace metal content of iron rich samples is probably caused by adsorption or coprecipitation onto amorphous or poorly crystalline oxides, and is consistent with the enrichment of As (641 ppm v. 75 ppm). The strong enrichment of As on precipitates is consistent with its preferential adsorption to secondary oxides in low pH conditions.

Trace metal inputs from seepage waters do not appear to appreciably affect the metal concentration of R. Canito waters. Where the acidic seeps (pH 2.5) intersect the neutral pH R. Canito there is a sequential occurrence of yellow (pH 3.0) and white (pH 5.5) oxides; presumably these are hydrous iron and aluminum oxides which adsorb or coprecipitate trace metals from the water (Figure 1.4).

6.3 Stream sediments and waters

The traditional downstream dilution model for metals in stream sediments, as proposed by Hawkes (1976), relates the surface area and metal content of the mineralized area to the surface area and metal content of tributary drainages and the part of the drainage basin above the sample site (Section 1.3). The principle assumptions of this models are: (1) equal rates of erosion throughout the entire drainage basin; (2) constant geochemical background; (3) no interaction between stream waters and sediments; (4) no sampling or analytical errors; and, (5) there is only

Table 6.3. Concentrations of selected elements on two types of chemical precipitates from a seep at Lama after total digestion.

Sample color	Dominate mineralogy	Fe (%)	Ca (%)	As (ppm)	Pb (ppm)	Bi (ppm)	Cu (ppm)
white	gypsum	1.0	15.9	75.0	29.0	0.3	9.0
red	Fe-oxides	>25.0	0.1	641.0	44.0	0.6	10.0

one source of mineralization (Rose et. al. 1979). In addition, this model does not distinguish between mechanical and hydromorphically transported anomalies.

6.3.1 Gold distribution

There are two mechanisms that may result in downstream variations of gold and other HME concentrations in addition to the dilution by barren tributaries described by Hawkes model: 1) erosion or entrainment of bank material of different geochemistry and texture (e.g. not a point source); or, 2) increases in gold (HME) concentrations by preferential winnowing of light mineral elements from stream sediments (e.g. Fletcher and Loh, 1996).

Neither Pascua or Lama can be considered a point source of mineralization as debris flows and glacial till have transported anomalous material up to 4-10 kilometers downvalley where it is currently being eroded into the R. Turbio and R. Estrecho. Where geochemistry of local bank material prevails, downstream patterns between the different energy environments in the stream would be more similar and there would be less relation between gold concentrations and texture because the stream would not have had sufficient time to fluvially rework the sediment based on size and density differences of mineral grains. Where fluvial processes dominate, an inverse relation between the abundance of high-density heavy mineral elements and fine grained sediment texture should be prominent (as described by Fletcher and Loh, 1996). This can lead to the development of displaced anomalies, where peak concentrations may occur kilometers below source, and greater differences in HME concentrations between different fluvial energies (e.g. Saxby and Fletcher, 1986; Sleath and Fletcher, 1982; Fletcher and Loh, 1996).

Both difference in bank material geochemistry and winnowing of fine grained sediments can explain downstream gold (and other HME) variations at Lama. Near R. Turbio headwaters, gold patterns are similar between all energy environments for approximately four kilometers downstream to site 13 (two sites above R. Canito confluence) suggesting that gold concentration is controlled by local sediment input from surficial materials (Figures 4.30-4.32). Evidence for the upgrading of gold and associated elements by winnowing of fines, relative to sediment sources, is provided by the appreciably higher concentrations of gold and lower fines content of stream sediments compared to debris flows, glacial till, talus cones and alluvial fans at both Lama and Pascua (Table 6.4). Similar increases in heavy mineral content versus sediment sources has been described by Hou and Fletcher (1996) and Fletcher and Muda (1999). There is also evidence for continued upgrading of gold values within the sediments. In particular, in the R. Turbio below the R. Canito confluence there is a tenuous relation between sediment texture and gold concentrations (Figures 4.30 and 4.31). All size fractions of the high-energy environment have an increase in gold concentration between the confluence of the R. Canito and site 1, with an associated decrease in relative abundance of –212+53μm material. This results in a displaced gold anomaly. The same relation is not, however, observed for gold in the medium energy sediments in the lower reaches of the R. Turbio. Gold concentrations of the most distal medium energy sample collected below the confluence with the R. Tagus, probably reflects dilution from the much larger R. Tagus drainage basin and does not preserve the relation with texture.

The same processes affect gold (and HME) concentration at Pascua (Table 6.4) where an interesting feature is the almost constant texture and constant gold concentrations for the –75+53μm and -53μm fractions below site 33, where the majority of new sediment is from 'background' talus cones (Figures 5.23 and 5.25). This suggests that elimination of fines by

Table 6.4. Enrichment of Au and Bi by removal of fine grained material at Pascua/Lama. Samples form a continuum between higher HME concentrations and lower abundances of fine grained material. na = not analyzed. All values reported are mean concentrations except for Au (median).

LAMA

		Relative abundance (%) Σ -212μm	Relative abundance (%) -53μm	Au* (ppb) -53μm	Bi (ppm)
Surficial deposits	Glacial till	30.6	13.5	95.3	3.5
	Debris flows	19.4	6.3	256.6	6.5
Stream sediments	Low energy	27.7	4.1	430.0	na
	Medium energy	12.4	3.1	560.0	13.0
	High energy	14.4	3.4	515.0	na

* R. Turbio only

Enrichment of HME by removal of fine material

PASCUA

		Relative abundance (%) Σ -212μm	Relative abundance (%) -53μm	Au* (ppb) -53μm	Bi (ppm)
Surficial deposits	Glacial till	26.0	11.9	35.0	1.7
	Debris flows	17.6	5.8	70.0	7.2
Stream sediments	Low energy	58.8	10.2	113.0	na
	Medium energy	8.0	2.0	250.0	4.0
	High energy	8.7	2.4	270.0	na

* R. Estrecho only

Enrichment of HME by removal of fine material winnowing approximately balances inputs from tributaries and erosions of talus cones so that gold values remain roughly constant. A similar effect has been reported by Hobday and Fletcher (2001) for gold in a mountain stream in British Columbia, Canada. The dramatic drop in gold values at site 24 (the most distal sampling site), below the confluence with the R. Blanco can be related to anomaly dilution by barren sediments from the R. Blanco ($A_{drainage}$= 160.3 km^2) which drains an area slightly larger than the R. Estrecho basin ($A_{drainage}$= 128.1 km^2).

6.3.2 Other elements

As in surficial media, dispersion of elements in stream sediments is controlled by mechanical and chemical processes and can be divided into two groups of elements. The first group is generally positively correlated with Au and present in heavy minerals (e.g. Ag, As, Pb, Hg, Sb, Te, S, Bi, Cu and Zn) but exhibits both mechanical and chemical mobility. The second group of elements has a strong relation to pH and water chemistry (e.g. Mn, Mg, Cd, Al, Fe, and Ni) so that their dispersion is dominated by sediment-water geochemistry.

Downstream dispersion of elements in stream sediments is a balance between mechanical (clastic) and aqueous transport. Evidence of mechanical transport would be: 1) enrichment of elements in heavy mineral concentrates over stream sediments; 2) a positive correlation with gold (and thus, controlled by the phenomena outlined in 6.3.1); and, 3) a lack of response to changes in acidity. Conversely, a chemical (aqueous) component is suggested by: 1) current mobility as measured by detectable concentrations in stream waters; 2) a negative relation between pH and water chemistry for cations; and 3) relatively high proportions of elements extracted by the cold hydroxylamine leach which is designed to measure trace elements associated with amorphous Mn oxides.

Dispersion is evident as distinct, non-linear trends in X-Y scatter plots of Au versus *aqua regia* digestible metal concentrations. An extreme case of chemical dispersion is at Lama. In the R. Turbio extremely low pH values result in almost constant metal concentrations (e.g. As in Figure 6.5a and 4.38 and Zn in Figure 4.39), however, metal concentrations are typically greater in the higher pH tributaries (Figure 6.5a). The balance between mechanical and chemical dispersion is well developed at Pascua which has less acidic pHs than Lama (Figure 6.5b). The positive diagonal trend from low Au /low HME to high Au/high HME is interpreted to represent the mechanical component of the anomaly. The negative sloping low Au/high HME to high Au/low HME trend is probably caused by transport away from high gold concentration, low pH headwaters to the distal sites with lower Au and neutral pH waters. Generally, low concentrations of trace metals (such as Zn, Cd, Cu, and Ni) and high gold values tend to correspond to lower pH waters, suggesting there is a strong component of aqueous dispersion. This also implies that at Lama, with low pHs throughout the drainage, the hydromorphic component of the anomaly has not been strongly developed (Table 4.14).

The interpretation suggested here of non-linear trends of metal versus gold concentration is one possibility. However, the interpretation may not be universally applicable and should not be applied to similar X-Y trends without supporting data (e.g. heavy mineral concentrates, stream waters, cold hydroxylamine leach). For example, an alternative interpretation is that the high Cu/low Au to low Cu/high Au trend could result from proximal versus distal sampling where the Cu anomaly extends a few hundred meters, but the Au anomaly is displaced from source and extends for approximately twenty kilometers downstream.

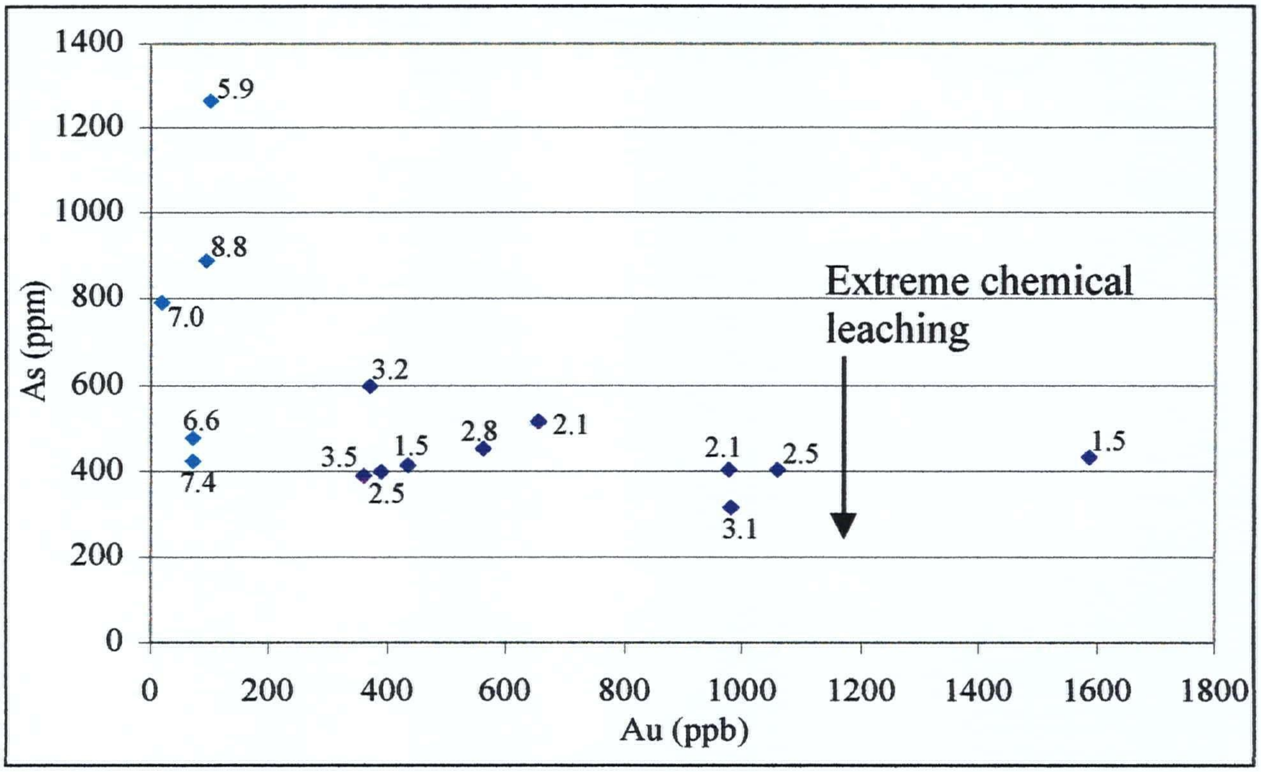

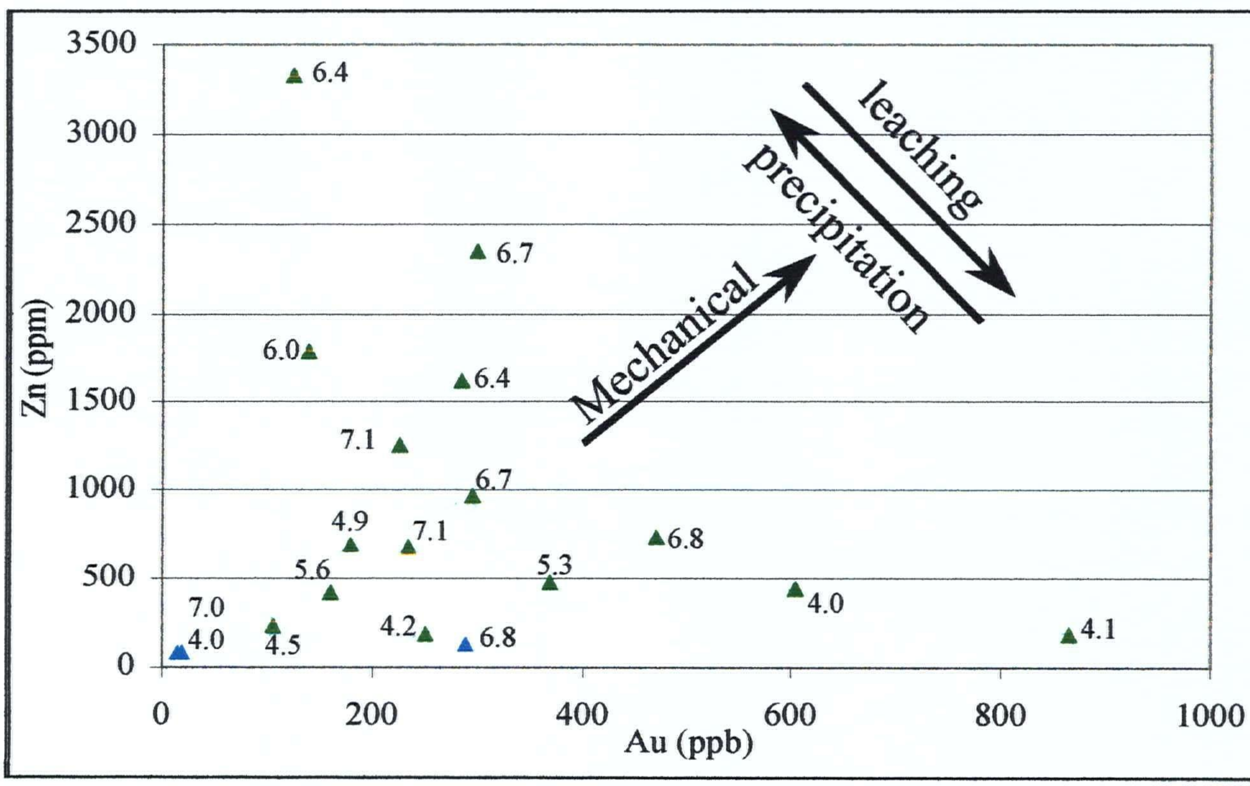

Figure 6.5. X-Y scatter plots for Au-As (Lama) and Au-Zn (Pascua). The sympathetic, positve trend results from mechanical transport. The antipathetic, negative sloping trend results from hydromorphic transport. Tributaries are light blue symbols. pH of samples is adjacent to each symbol.

Differences in pH between Lama and Pascua result in very different response for the relatively mobile elements as shown in Figure 6.6, where the ratios of cold hydroxylamine/total digestion of stream sediments from the less acidic R. Estrecho at Pascua are greater than at the highly acidic R. Turbio at Lama. It is worthwhile to note that at Lama (with few exceptions) only deposit-associated elements have greater mean concentrations in stream sediments than in surficial deposits. However, at Pascua there are a number of elements with higher concentrations (Ba, Cd, Cr, Co, Fe, Mn, Ni, Sr, and Zn) in stream sediments than in surficial deposits. This probably results from the less acidic nature of the R. Estrecho stream waters.

As with gold, elements identified in the heavy mineral fractions (Ag, Hg, Sb, As, Bi, Te, Pb, Fe and S) by SEM and NAA have higher mean concentrations in stream sediments than in surficial media (Table 4.26 and 5.22). The relative importance of clastic (heavy mineral) dispersion is shown in Figure 6.7. Elements with low chemical mobility, such as Ba, are concentrated in the heavy mineral fraction relative to the light mineral fraction (average of 86.6% of Ba is in HMC). Arsenic and Zn, which have already been shown to have chemical and mechanical transport, have lower concentrations in HMC versus LM separates (averages of 17.2% and 21.4% for As and Zn, respectively).

For elements with a significant amount of chemical mobility, which is not exclusive of elements that are also present as constituents in heavy minerals, (including Zn, Cu, Mn, Mg, Cd, Al, Fe, Sr and Mo) evidence of hydromorphic transport is found in: 1) the interrelations between *aqua regia* and cold hydroxylamine digestions; 2) water chemistry and pH; and, 3) the presence of secondary oxides and precipitation (dissolution?) barriers.

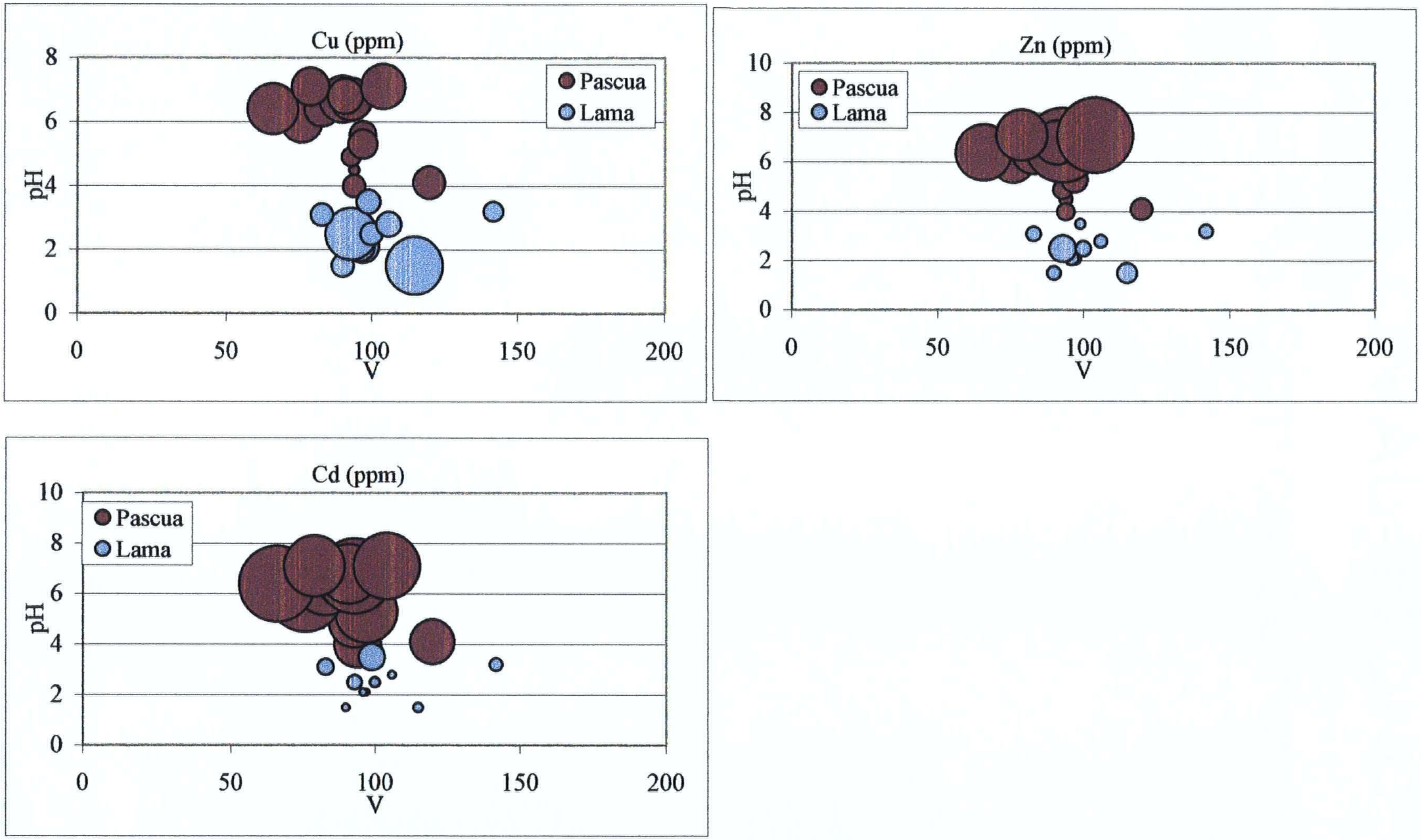

Figure 6.6. Effect of pH on stream sediments. Bubbles are proportiona to the cold hydroxylamine/total ratio in stream sediments

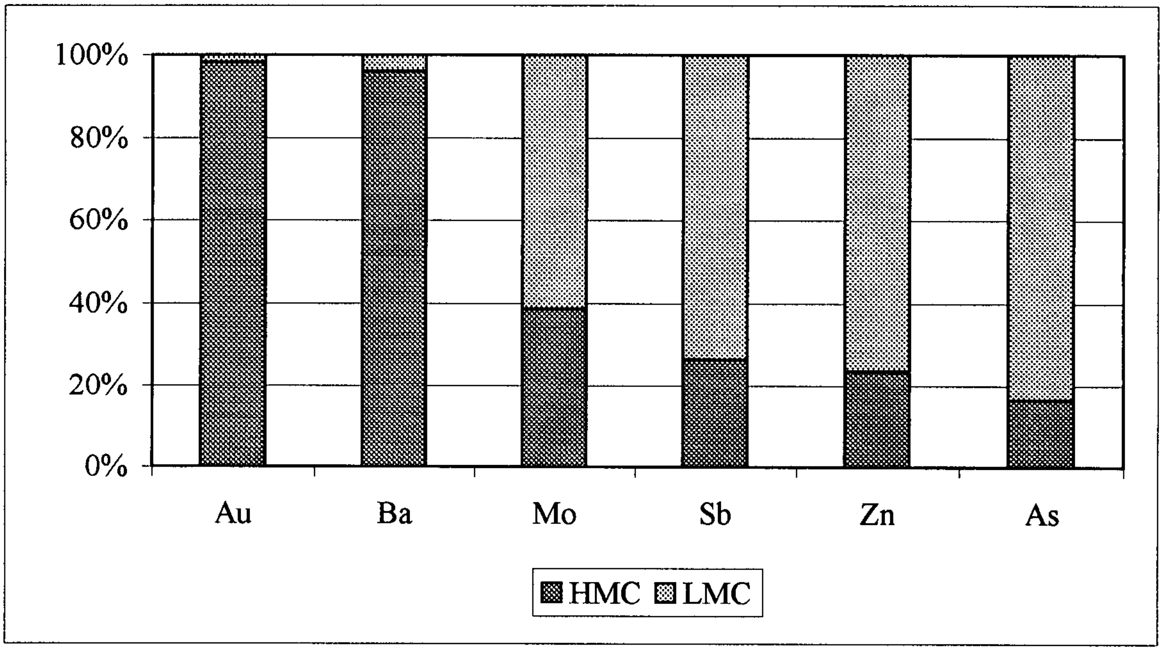

a) Lama -75+53μm, site 1

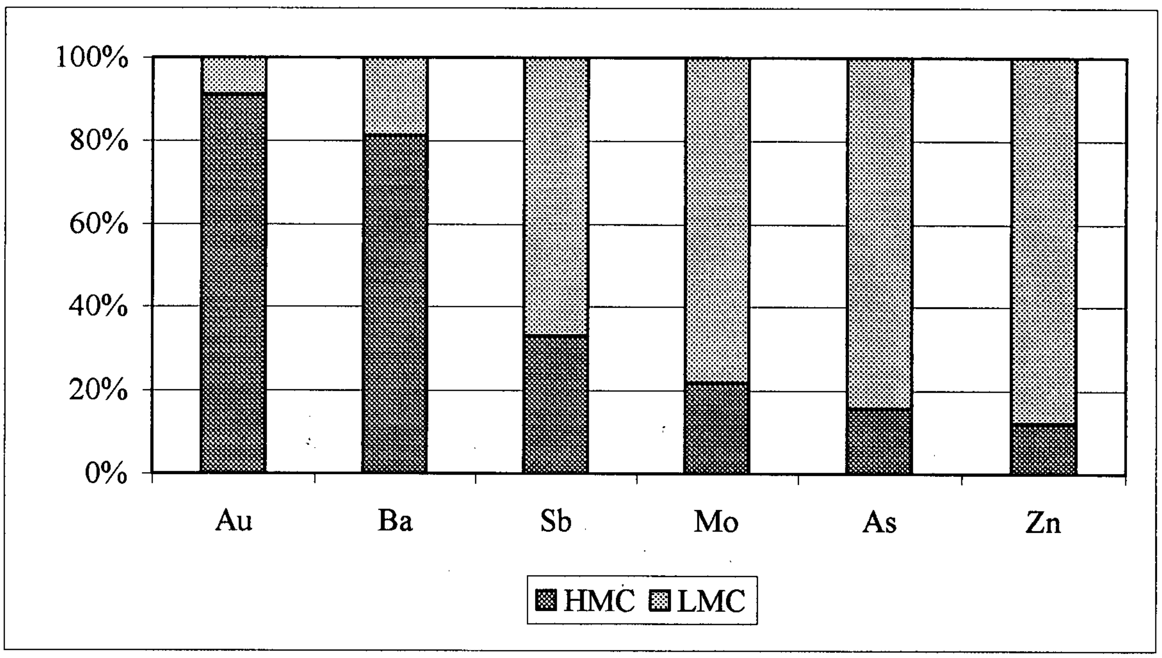

b) Pascua -75+53μm, site 37

Figure 6.7. Relative concentrations of metals in heavy mineral concentrates (HMC) and light mineral concentrates (LMC).

Secondary iron and manganese oxides coat the stream beds of both R. Turbio and R. Estrecho. The efficiency of these oxides to control the fate and transport of aqueously mobile elements has been well documented (Rose et. al.., 1979; Chao and Theobald, 1976). Recalling the dilution coefficients presented in Chapters 4 and 5, Na was taken as a conservative element (i.e. dilution was assumed to be the only mechanism controlling changes in concentration of Na at confluences). Where dissolved metal concentrations decrease more than expected from simple dilution, it is probable that precipitates of secondary oxides are responsible (Table 4.14 and 5.11). Another reason for suggesting that precipitation onto secondary oxides is occurring is the deviation from the linear mixing trends (Figure 4.26). The water sample immediately below the R. Turbio-R. Canito confluence is generally along the mixing trend, but samples further downstream have lower metal concentrations than would be expected if mixing was the only controlling parameter. This suggests that at the confluence dilution is controlling aqueous metal concentrations, however, downstream from the mixing zone, precipitation is decreasing concentrations of dissolved metals.

Additional evidence that hydrous oxides contribute to the decrease in dissolved metals is the concurrent increase in the concentrations on metals stream sediments (Figure 6.8). Thus at, and downstream from, the R. Canito/R. Turbio confluence, adsorption and/or coprecipitation onto secondary oxides is affecting both water and stream sediment concentrations of the mobile suite of elements (Cu, Zn Mn, Mg, Cd, Al, Fe and Sr).

The R. Turbio/R. Tagus confluence is more complex. Dilution factor data suggest that concentrations of dissolved Ba, Cd, Co, Mn, Mg, Ca, Ni and Zn increase below the confluence whereas concentrations of dissolved Tl, U, Cr, Al, Fe, Cu, Sb, K, As and Sr decrease (Table 6.5). Also, twelve elements (As, Sr, Mn, Sb, Ba, Ca, Co, Fe, K, Mg, Na, Ni and Zn) have higher cold

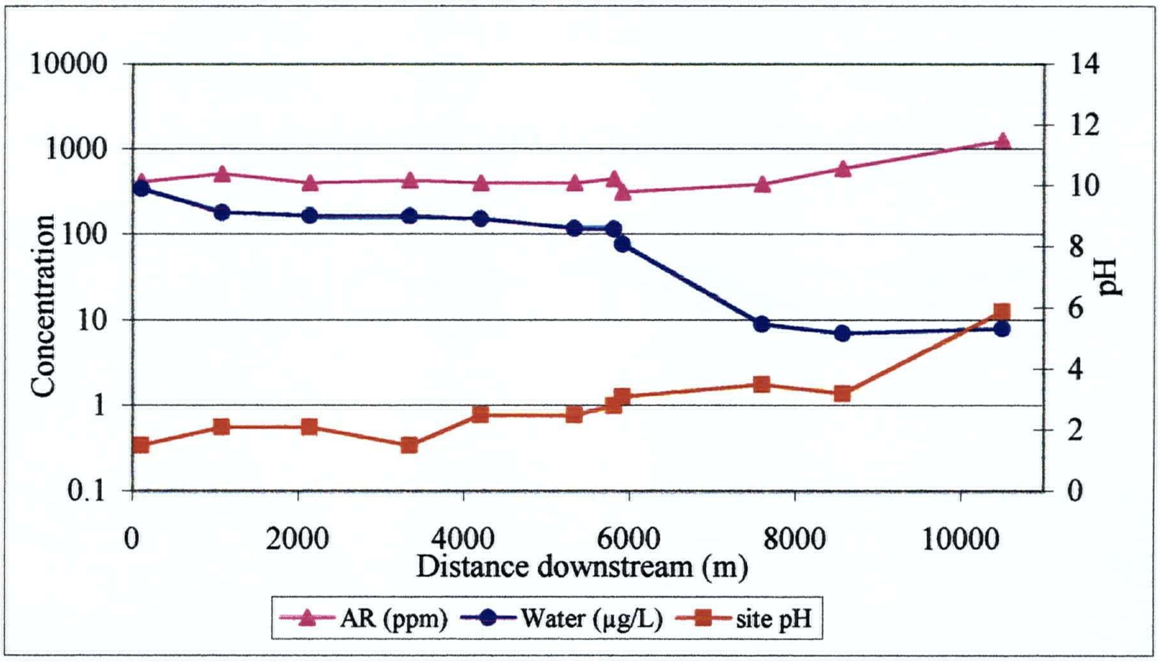

a) Lama -53mm medium energy, As

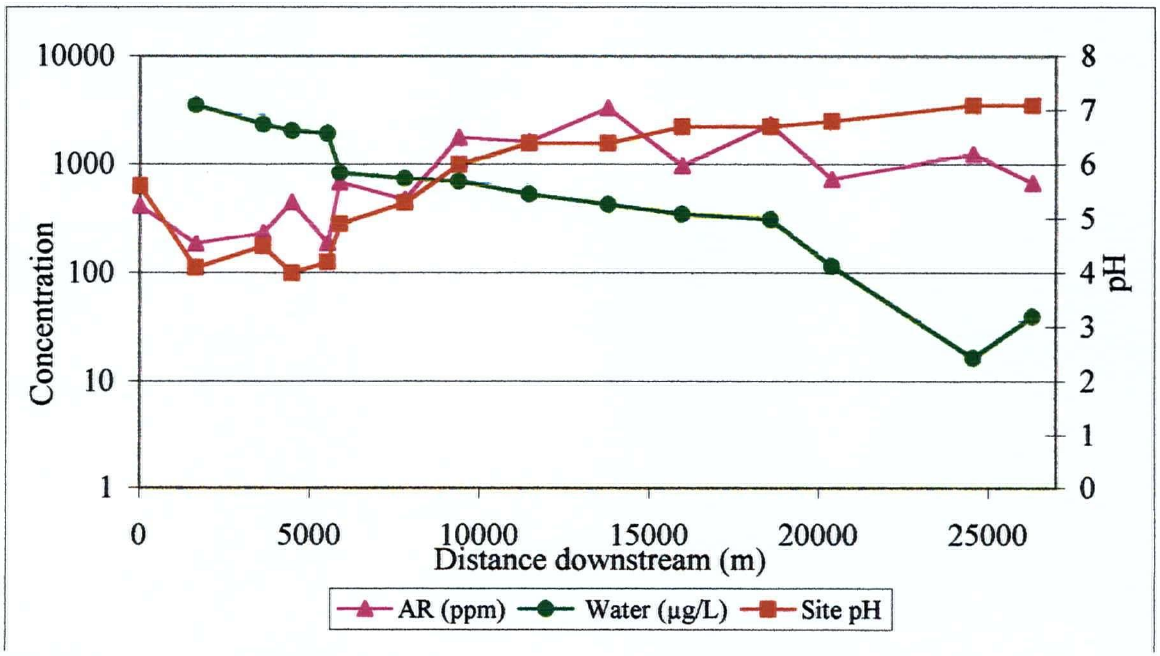

a) Pascua -53mm medium energy, Zn

Figure 6.8. Arsenic (Lama) and Zn (Pascua) concentrations after aqua regia digestion. As aqua regia (AR) concentrations increase as pH increases, and dissolved metals in stream waters decrease.

Table 6.5. Relative increase or decrease of dissoled metals at the R. Turbio-R. Canito confluence (from dilution ratios).

Decrease		Increase
Cu, Fe, Al, Cr, U,	site 1 > site 23	Zn, Ni, Ba, Cd, Co, Mn,
Sb, As, Sr, K	site 23 > site 1	Ca, Mg

Table 6.6. Cold hydroxylamine concentrations of stream sediments on the R. Tagus above and below the confluence with the R. Canito. Concentrations as Site 21 are lower suggesting the presence of a 'dissolution barrier'.

Element	Units	Site 21	Site 23
pH		5.9	7.0
Ba	ppm	31.2	46.2
Sb	ppm	0.2	0.5
Fe	ppm	110.0	175.0
Mn	ppm	1370.0	1320.0
As	ppm	2.8	6.5
Mg	ppm	452.0	456.0
Ca	ppm	452.0	8620.0
Co	ppm	14.2	20.6
Ni	ppm	1.8	3.7
Zn	ppm	29.4	36.0
K	ppm	285.0	380.0
Sr	ppm	1.1	1.0
Cd	ppm	1.2	1.0
Na	ppm	350.0	570.0

hydroxylamine leach concentrations on the R. Tagus upstream of the R. Turbio- R. Tagus confluence than downstream (Table 6.6), suggesting that there has been dissolution of metals from stream sediments into solution after the mixing of the two streams. This suggests that the R. Turbio- R. Canito confluence is actually a dissolution barrier for Ba, Cd, Co, Mn, Mg, Ca, Ni and Zn, whereby the acidic R. Turbio waters leach metals from the neutral R. Tagus sediments. Conversely, it is a precipitation barrier for Tl, U, Cr, Al, Fe, Cu, Sb, K, As and Sr. Samples taken further downstream on the R. Tagus should have higher metal concentrations in the stream sediments as the pH continues to rise and metals can no longer be transported in solution.

At Pascua, higher concentrations of chemically mobile elements in middle reaches of the R. Estrecho corresponds to areas of Fe/Mn staining on the stream bed and more neutral pH values (Figure 5.29). The gradual increase of pH with distance downstream from the headwaters, results in a gradual decrease in dissolved metal load and increase in *aqua regia* and cold hydroxylamine in stream sediments. Manganese behaves similar to mobile elements suggesting Mn-oxides may be controlling the concentrations of Al, Mo, Cd, Cu, Ni, Zn, Co and U. For all elements, except K and Na, there is a decrease in concentrations at the final sample site, below the confluence with the R. Blanco.

The strong hydromorphic component of anomalies at Pascua is clearly shown in the relation between (for example) cold hydroxylamine Cu and Zn values and pH (Figure 6.9). In these plots, increasing pH values are used to represent increasing hydromorphic component of anomalies, whereas, increasing V (as a surrogate for magnetite, a ubiquitous heavy mineral (Fletcher, 1999)) is used to represent mechanical enrichment. The size of the bubble is proportional to the cold hydroxylamine concentrations. In the R. Estrecho, the cold hydroxylamine anomaly is greater than in the acidic R. Turbio for Cu and Zn.

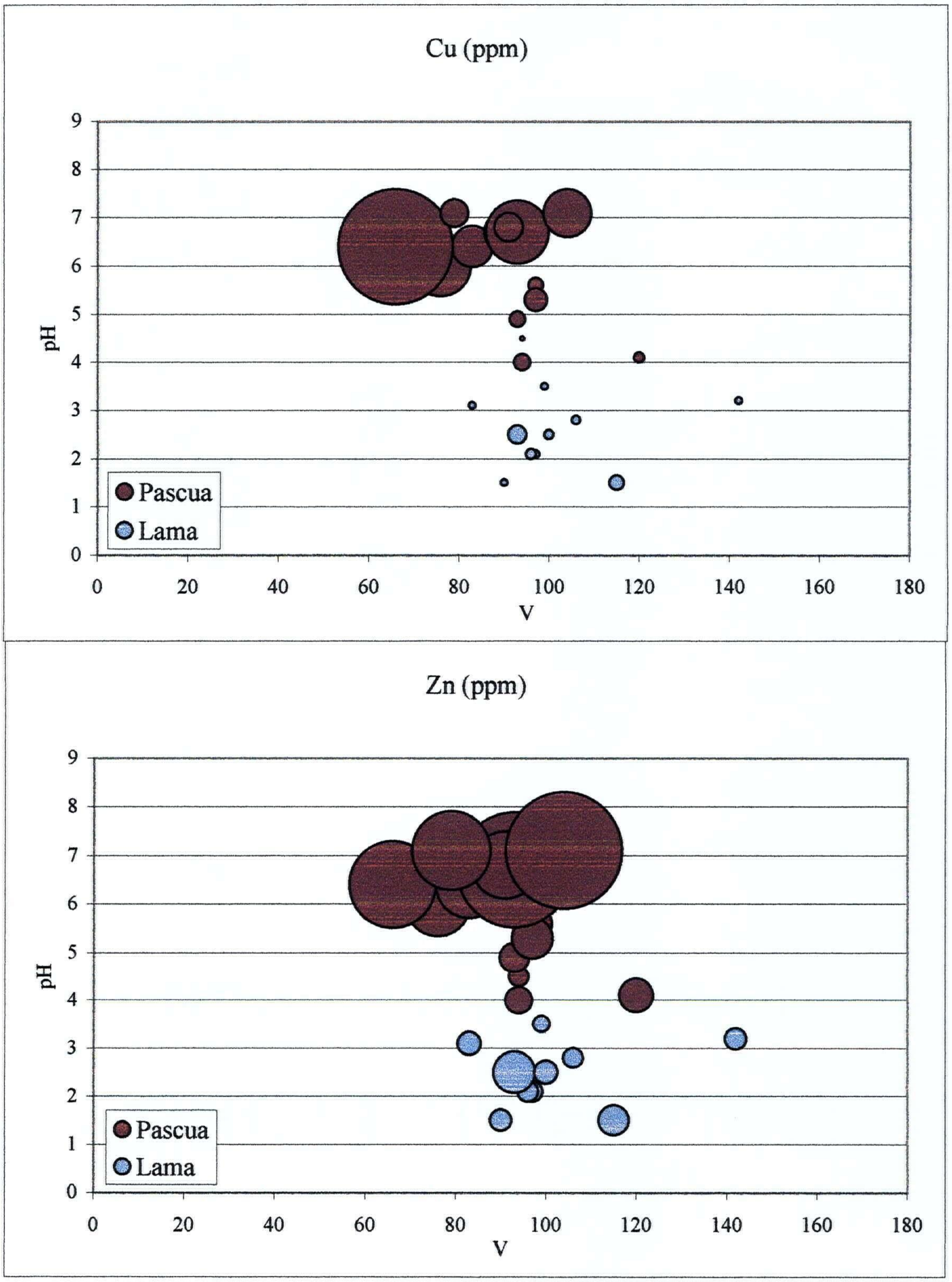

Figure 6.9. Plots of cold hydroxylamine Cu and Zn as a function of V and pH. Size of the buble is proportional to the cold hydroxylamine concentration.

6.3.3 Summary

Based on these results, several conclusions can be made about the occurrence and distribution of elements in the surficial environment around Pascua/Lama.

- Washing of material preferentially entrains light minerals and enriches elements associated with heavy minerals including Au, Ag, Sb, Hg, Te, S, As, Pb and Bi.

- Acid leaching has removed mobile elements (i.e. Cu, Ni, Zn, Cd, Al, Mn and Mg) close to the deposit, redepositing them in stream sediments at distal locations where pH values are more neutral.

- Most elements of the high sulfidation epithermal suite(Ag, As, Pb, Hg, Sb, Te, S and Bi) are present in heavy minerals, but have variable and limited chemical mobility.

- Surficial deposits of glacial till, talus fines, alluvial fans and debris flows have different genesis and this is reflected as subtle differences in geochemistry and texture. Glacial till has the most fines (mean 30.6 % and 26.0% of -212μm material at Lama and Pascua, respectively), and lowest median Au concentration (95.8 ppb Lama and 35 ppb Pascua in -53μm fraction). Debris flows have the least amount of fine material (mean 19.4% and 17.6% of -212μm material at Lama and Pascua, respectively) and higher median Au concentrations (256.6 ppb Lama and 267.5 ppb Pascua in -53μm fraction).

- Debris flows have restricted the input of other surficial materials into R. Turbio and R. Estrecho by decoupling the streams from the valley sides. Debris flows have also created a linear anomaly (i.e. not a point source), transporting anomalous material 4-10 km down valley.

- Stream sediments have the least amount of fines of all sampled media (mean 14.4% and 8.7% of –212μm material at Lama and Pascua) and greater concentrations of Au (median 515 ppb Lama and 250 ppb Pascua in -53μm fraction) and HME (i.e. Ag, Hg, Sb, Bi, Te, Pb, Fe, and S). Streams are acidic proximal to the deposit where dissolved metal concentrations are high. As pH increases, metal concentrations decrease in stream waters and concurrently increase in stream sediments.

- Gold and other HME concentrations in stream sediments are controlled by dilution with barren tributaries, erosion of chemically and texturally heterogeneous bank material, and enrichment of Au and HMEs by preferential entrainment of light mineral.

- Cu, Zn, Ni, Mn, Mg, Cd, Al, Fe and Sr concentrations in stream sediments are strongly affected by downstream variations in pH, especially at precipitation/dissolution barriers below confluences.

- The presence of base of slope chemical precipitates suggests oxidation of sulfides and sulfosalts at depth. Precipitates can have high trace metal content.

6.4 Implications for stream sediment surveys

Four questions need to be answered for stream sediment explorations surveys: 1) what to sample; 2) where to sample; 3) what to analyze; and, 4) how to interpret and follow-up the data. Results at Pascua-Lama show that Au has the longest dispersion trains and the greatest anomaly contrast. However, surveys should also be designed to capture and take advantage of the multi-element pathfinder signature (e.g., Ag, As, Sb, Bi, Hg, Cu, Pb, Zn and Te) including those elements that are transported hydromorphically.

6.4.1 Gold

A major problem with stream sediment exploration for gold is the erratic nature of its dispersion caused by: 1) spatial variation on the stream bed in response to varying fluvial conditions (e.g., Day and Fletcher, 1991); and, 2) the difficulty of collection of representative samples (e.g. Nichol et. al.., 1994). It is therefore necessary to determine the optimum environment to sample, and the size fraction and amount of material that gives the most consistent response and least probability of missing an anomaly.

6.4.1.1 *Where to sample*

Stream sediments were collected from three different depositional environments (high, medium and low energy). The ideal sample location should minimize within site variability for gold, maximize geochemical contrast, and be ubiquitous in the survey area so that it can be samples consistently. Fine grained, low energy samples do not meet these requirements insofar as this environment is not present at every site (at Pascua it is only found near the deposit) and also tends to have lower gold concentrations than associated high and medium energy samples (Tables 4.17 and 5.14). Low energy sediments are therefore not considered further.

Statistically, there are no significant textural differences between high (cobble-gravel) and medium (gravel-coarse sand) energy sediments (Tables 4.16 and 5.13). Furthermore, although average gold values are greater in high energy (median 515 ppb and 390 ppb in –53 μm at Lama and Pascua, respectively) than in medium energy (median 250 ppb and 243 ppb in –53 μm at Lama and Pascua, respectively), values are not consistently greater for high energy (i.e., at any given site medium energy samples may have a greater gold concentration (Sections 4.3.2.1 and 5.3.2.1).

Site selection can also be considered with respect to anomaly contrast (i.e., the ratio between anomalous sites and a background value). At the most distal site on the R. Turbio at Lama, gold in the –53 μm fraction is 368 and 20 times greater than background in high and medium energy samples, respectively (Table 6.7). However, high energy sediments have the greatest contrast in all size fractions. Conversely, medium energy sediments produce the longest dispersion train at Pascua with contrast 30 and 47 times background at site 24 (most distal) for the –75+53 μm and –53 μm fractions, respectively. Medium energy may be giving a stronger anomaly at Pascua since it is, on average, slightly more coarse (Table 5.13).

Thus, both high and medium energy environments can be sampled for gold. The low energy environment should not be sampled as it has low gold concentrations and is not ubiquitous.

Lama

	-150+106μm		-106+75μm		-75+53μm		-53μm	
	High	**Medium**	**High**	**Medium**	**High**	**Medium**	**High**	**Medium**
Average	21	15	69	34	110	62	129	127
Peak (site #)	57 (1)	50 (5)	22 (1)	115 (14)	436 (1)	135 (15)	368 (1)	317 (14)
Most distal	57	1	22	10	436	8	368	20

Pascua

	-150+106μm		-106+75μm		-75+53μm		-53μm	
	High	**Medium**	**High**	**Medium**	**High**	**Medium**	**High**	**Medium**
Average	28	26	64	39	89	55	58	61
Peak (site #)	108 (36)	198 (29)	298 (37)	143 (39)	371 (37)	212 (39)	164 (37)	173 (38)
Most distal	1	47	1	13	1	30	10	47

Table 6.7. Contrast ratios for Au (background = 5 ppb). Averages calculated with tributaries and background sites removed.

6.4.1.2 Size fraction and sample representativity

Choice of optimum size fraction must consider optimizing anomaly contrast, and sampling and subsampling reliability. The reliability of Au results is closely related to the nugget problem and subsampling statistics that depend on the number of gold particles in a sample or subsample (Nichol et. al., 1994; Fletcher, 1997). The number of gold particles in a 30 g FA-AAS subsample was calculated using the maximum gold concentrations (ppb) for each size fraction, where gold was assumed to occur either as spheres or flakes (thickness = 1/10 diameter) of pure gold (ρ = 19.3 g/cm^3) (Table 6.8). Results of SEM work suggest that Au is actually much smaller than the diameters used here and contain silver, increasing the estimated number of gold grains.

Since each size fraction has an upper and lower sieve size except for –53 µm fraction, the minimum number of grains is determined by the maximum sieve size and the maximum number of grains for the size fraction by the minimum sieve size. There are many more gold grains and lower relative error in the finer fractions where gold concentrations are the greatest. Estimates of sampling and subsampling precision (Table 3.4) also decrease with decreasing size fraction and are of the same order of magnitude as the relative errors determined from the number of gold grains (Table 6.8). If an anomaly threshold concentration of 100 ppb was chosen, then the samples do not meet the criteria for anomaly detection outlined by Fletcher (1997), of at least 3 particles of gold in the analytical sub-sample, until the grain size decreases to –53µm for gold as spheres and –106+75µm for gold as flakes (Table 6.9).

Further evidence of the reliability of the finer fractions is provided by analysis of variance of between versus within site variability. For differences in gold concentrations between site to be

Spheres*

Sieve size	Au (ppb)	No. grains (min)	No. grains (max)	Relative error[1]	Pecision estimate[2]
-150+106μm	990	1	2	127-245	100
-106+75μm	1490	4	10	62-104	100
-75+53μm	2180	15	43	35-51	75
-53μm	1840	37	293	33-11	10

* gold grains occur as spheres, 100% Au ($\rho = 19.3\ g/cm^3$), 30 g sample

Flakes**

Sieve size	Au (ppb)	No. grains (min)[1]	No. grains (max)[2]	Relative error[3]
-150+106μm	990	5	13	55-95
-106+75μm	1490	20	57	26-44
-75+53μm	2180	840	237	13-22
-53μm	1840	200	1601	14-5

** gold grains occur as flakes (thickness = 1/10 diameter), 100% Au (ρ = 19.3 g/cm^3), 30 g sample

[1]Relative error from NUGGET output

[2] Sampling and subsampling precision from Chapter 3

Table 6.8. Maximum number of gold grains per size fraction in stream sediments. Calculations performed with NUGGET (Stanley), relative error is at two standard deviations. A radius of 26.5μm was choosen for the lower size limit of Au grains.

Spheres*

Sieve size	Au (ppb)	No. grains (min)	No. grains (max)	Relative error[1]
-150+106μm	100	0.1	0.3	674-400
-106+75μm	100	0.3	0.7	400-238
-75+53μm	100	0.7	2.0	238-142
-53μm	100	2.0	16.0	142-50

* gold grains occur as spheres, 100% Au (ρ = 19.3 g/cm^3), 30 g sample

Flakes**

Sieve size	Au (ppb)	No. grains (min)[1]	No. grains (max)[2]	Relative error[3]
-150+106μm	100	0.5	1.4	289-171
-106+75μm	100	1.4	3.8	171-102
-75+53μm	100	3.8	5.4	102-61
-53μm	100	5.4	87.0	61-21

** gold grains occur as flakes (thickness = 1/10 diameter), 100% Au (ρ = 19.3

[1]Relative error from NUGGET output

Table 6.9. Number of gold grains present in each size fraction with a concentration of 100 ppb. Calculations performed with NUGGET (Stanley), relative error is at two standard deviations. A radius of 26.5μm was choosen for the lower size limit of Au grains.

meaningful (i.e., related to geochemical dispersion), between site variance must be significantly greater than within site variance. A two-factor ANOVA (without) replication for combined Lama-Pascua data suggests that between site variability is significantly greater than within site variability for both the –150+106μm and –53 μm fractions (Table 6.10). However, the results for the –150+106μm fractions are almost certainly an artifact of the very poor precision (+100% at 95% confidence, Table 3.4) in these fractions. Between versus within site variability is not significant for the two fractions between 53 and 106μm. True between site differences in gold concentrations can therefore only be reliably detected in the -53μm fraction.

With respect to anomaly contrast, gold concentrations and contrast are both generally higher in the –75+53μm and -53μm fractions than in either of the two coarser fractions (Table 6.7). Furthermore, with the exception of poor contrast at site 23 in the –75+53μm high energy fraction, contrast generally remains high in these fractions at the most distal sites.

The finer the size fraction to be analyzed, the larger the field sediment samples needed to provide sufficient material for analysis. To obtain a 50g sub-sample of -53μm material (sufficient for 30g FA for Au and multi-element ICP analysis) at least 1.5 kg at Lama and 2.0 kg at Pascua of –2mm material needs to be collected (Table 6.11). Conversely, if -212μm samples are used for analysis, the field sample can be much smaller (often 50-75% reduction in sample mass). However, as discussed above, use of size fractions coarser than 75μm will result in much poorer precision (Table 3.4), lower gold values, and reduced anomaly contrast.

Based on the preceding discussion, -53μm material is the optimum size fraction for analysis for gold, although results of -75μm fractions can also be used.

Table 6.10. Results of two factor analysis of variance for gold in Pascua/Lama stream sediments (combined) reported as either significant (S) or not significant (NS). Not significant means that the between site variation of gold concentration in not significantly great than the within site variation.

	-150+106µm	**-106+75µm**	**-75+53µm**	**-53µm**
Between site	S	NS	NS	S
Within sites	NS	NS	NS	NS

Table 6.11. Average sample size (g) needed to obtain 50 g of -53μm and -212μm material, respectively. Smaller samples are needed for 0.212μm sample, however, precision of elements associated with rare minerals (e.g. Au, Ag, Hg) is much worse in the coarser fractions).

Media		-53μm		-212μm	
		Pascua	**Lama**	**Pascua**	**Lama**
Surficial	Glacial till	420	370	190	160
	Debris flows	860	790	285	260
Sediments	High energy	2100	1500	575	350
	Medium energy	2500	1600	625	400

6.4.1.3 *Summary for gold*

Sampling medium and/or high energy environments and using the –75 or -53μm size fractions will result in the best precision, the longest dispersion trains and the greatest anomaly contrast. Using these procedures, sediments at the mouths of second order streams (1:100 000 scale and an approximate drainage basin area of 50 km^2) contain anomalous concentrations of gold. For example, 370 ppb and 1840 ppb in the –53μm fraction from medium and high energy sites, respectively, on the R. Turbio upstream from the R. Tagus confluence. Similarly, at the R. Estrecho upstream from the Q. Barriales confluence, medium and high energy -53μm samples have strongly anomalous gold values that continue down the R. Estrecho for approximately another 15 km despite input of non-anomalous material from tributary drainages and erosion of talus cones.

6.4.2 *Other elements in stream sediments*

Only the -53μm fraction was submitted for ICP-MS multi element determinations after digestion by *aqua regia*, triple-acid (total) or cold hydroxylamine. This discussion, therefore, focuses on the differences between the digestions without considerations of size fraction effects.

At Lama, CRs are reported for the R. Turbio at site 1 and the R. Tagus at site 21 relative to the R. Tagus at background site 23 (Table 6.12). Both the total and *aqua regia* digestions give strong CRs for heavy mineral associated elements (e.g., Ag and Pb) immediately above the confluence of the R. Turbio and R. Tagus. Contrast decreases below the confluence, presumably because of simple mechanical dilution by sediment from the R. Tagus: in this respect the mechanically

	Site 1:23			Site 21:23		
Element	TOT	AR	CH	TOT	AR	CH
Au (FA)	64.0			25.0		
Ag	48.8	91.7	6.1	2.2	15.8	68.3
Pb	10.1	41	11.4	3.1	2.6	0.05
Cu	1.6	2.45	1.4	3.9	4.6	3.23
Zn	0.3	0.2	0.3	1.3	1.5	0.8

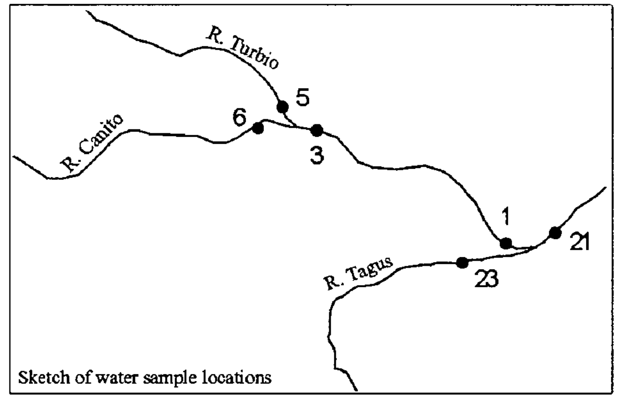

	Site 27:26			Site 24:26		
Element	TOT	AR	CH	TOT	AR	CH
Au (FA)	23.5			11.3		
Ag	11.8	3.2	1.7	1.6	8.7	3.0
Pb	4.6	10.0	4.7	4.2	4.1	7.0
Cu	4.5	75.7	4.2	3.7	4.2	72.4
Zn	8.6	28.8	7.2	6.5	7.9	30.3

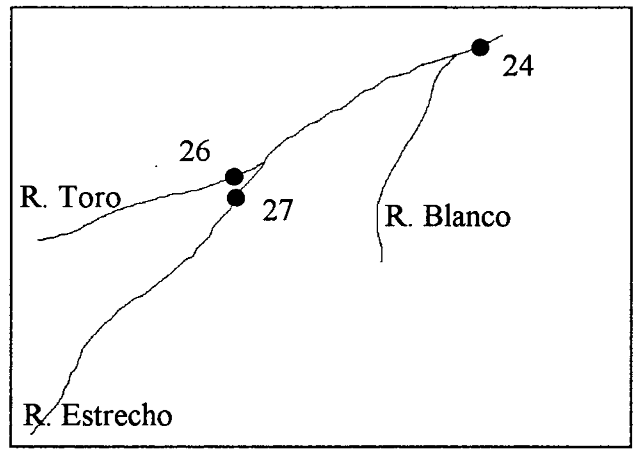

Table 6.12. Contrast ratios of gold and selected elements for aqua regia (AR), cold hydroxylamine (CH) and triple acid (TOT) digestions. FA-AAS Au on medium energy 53μm sediments.

dispersed anomalous elements behave like gold. Conversely, CRs of the more chemically mobile elements (e.g., Cu and Zn) are less than 1 in the strongly acidic environment upstream of the confluence (i.e. concentrations are depleted relative to background values) and increase downstream because of the increase in pH and input of unleached sediment by the R. Tagus. However, even below the confluence anomaly contrast for the mobile pathfinder elements is generally much lower than for Au and Ag.

At Pascua, CRs are reported for site 24 and 27 on the R. Estrecho relative to the background site 26 on the R. Toro: site 24 is below the confluence with the large drainage basin of the R. Blanco. The input from this large drainage basin probably explains why CRs for most elements (e.g., Au, Pb, Cu and Zn) decrease below the confluence. However, despite the dilution, contrast remains reasonable at site 24 with CRs of 8.7, 4.1, 4.2, and 7.9 for Ag, Pb, Cu and Zn, respectively, by the *aqua regia* digestion. The neutral pH of the R. Estrecho (unlike the very acidic R. Turbio) probably accounts for the very high CRs for Cu and Zn in the R. Estrecho at site 27 above the confluence with the R. Toro. The cold hydroxylamine leach gives very high CRs for mobile pathfinder elements Cu and Zn at site 24 relative to background at site 26. This probably results from development of a hydromorphic anomaly under near-neutral pH conditions and suggests that the weak leach may be useful in detecting distal anomalies in non-acidic conditions.

Based on comparison of detection limits to anomalous concentrations in the R. Turbio and R. Estrecho, the *aqua regia* digestion followed by ICP-MS produces the most complete suite of elements (Table 6.12). At both Lama and Pascua, Ag and Sb concentrations in tributaries are less than five times the detection limit (an acceptable lower concentration limit to achieve adequate analytical precision), and Te is not reported for ICP-ES technology. In addition, at Lama, Mo and Bi are below ICP-ES detection limits in tributary streams. Thus, the less expensive ICP-ES package ($8.50 with increased Hg sensitivity) could be used instead of ICP-MS ($14.00) but at the loss of Sb, Ag, Bi, Mo and Te.

Contrast ratios suggests that the *aqua regia* digestion combined with ICP-MS provide the best overall contrast for both heavy mineral associated elements (mechanical anomaly) and hydromorphic anomalies of the more mobile elements. The cold hydroxylamine anomaly at Pascua is very strong at distal sites, and as pH increases further downstream the anomaly might increase down the R. Tagus at Lama. Thus, in areas of neutral-pH waters (i.e., distal from the deposit), weak leaches may also provide good anomaly contrast for the more mobile elements. Whatever method of analysis is used, pH of stream waters should be measured to facilitate interpretation of results for the more mobile pathfinder elements.

6.4.3 Use of other media for reconnaissance and follow-up surveys

Talus cones, alluvial fans, debris flows and glacial till all detect mineralization at Pascua-Lama. While these surficial deposits have generally similar compositions, some textural and geochemical differences do exist. It is therefore imperative that surficial samples be properly classified and separately interpreted. For example, glacial till and debris flow samples taken within a few hundred meters of each other have very different Au concentrations (e.g., a till (60 ppb) and debris flow (200 ppb) sample taken from adjacent locations at Lama, and at Pascua 40 meters separated glacial till of 60 ppb from debris flow of 355 ppb).

Both glacial till and debris flow deposits have anomalies that extend over ten kilometers down valley from the mineralization. Both these media could therefore be used as substitutes for stream sediments at the reconnaissance stage. However, their use would provide no advantage unless, for some reason, stream sediments were absent or could not be sampled. Conversely, debris flows entering an anomalous drainage from side valleys without mineralization could infill a valley with barren, background material that might truncate or severely dilute stream sediment anomalies that existed prior to the debris flow event. Sediment samples should therefore be taken above and below large debris flows.

Talus cones and alluvial fans are much more local in origin that glacial till or debris flows and could be used to fill in gaps where stream sediments are decoupled from valley walls. However, because talus cone and alluvial fan samples represent a smaller area than sediment samples, a higher sampling density would be necessary to ensure adequate coverage. They are also suitable media for follow-up surveys by taking samples around the base of individual features in anomalous drainage basins.

Although texture varies between surficial deposits, approximately 1 kg of –4mm material is sufficient to provide 50 g of -53μm material (Table 6.11). Samples should be from a representative area of the landform (free from gullying or other localized reworking) and collected several centimeters below ground surface to avoid contamination from wind (or truck) transported material.

In conjunction with ICP-MS analysis small, easily collected water samples can be used to detect anomalous concentrations of trace metals, especially where acidic conditions are prevalent. In addition to being stand-alone data, results from water sampling can corroborate interpretation of stream sediment data, and might, perhaps, avoid the problems associated with dilution of stream sediment anomalies by barren debris flows (though this remains to be tested). Water sampling techniques and procedures are outlined in detail in 3.1.3. pH must be measured at every sediment site, regardless of water samples being collected.

Base-of-slope chemical precipitates are not sufficiently ubiquitous to suggest a standardized sampling procedures. However, as strongly acidic sulfate-rich precipitates are believed to be surface expressions of oxidation of sulfides (and sulfosalts) at depth, collection of small bulk samples (approximately 100g) of precipitates may indicate presence or absence of subsurface mineralization. Other chemical precipitates such as efflorescent coatings or secondary oxides in stream should always be recorded in field notes as they are indicators of metal mobility in the surface environment, and can dramatically increase metal concentrations in stream sediments.

6.4.4 Interpretation of stream sediment surveys

Both Pascua and Lama have displaced gold anomalies, where maximum concentrations can be found several kilometers downstream from mineralization. Interpreting stream sediment data should take this phenomena into account, and follow-up surveys should be designed to sample material several kilometers upstream from the anomalous sample.

The effects of pH can be very pronounced, especially close to mineralization where low pH conditions are prevalent. In acidic streams, mobile pathfinder elements (such as Cu and Zn) may be leached from both stream sediments and surficial media close to deposits. As the pH increases in the stream away from the deposit, the hydromorphic anomalies of pathfinder elements will become more pronounced.

Special attention should be given to the effects of debris flows. Input of material from anomalous debris flows (and glacial till) lengthens the strong sediment anomalies of Pascua-Lama. If these surficial deposits were barren, then it would have the opposite effect on sediment geochemistry. The anomalous dispersion train would be shortened or eliminated as barren material was eroded into the stream system.

6.4.5 Summary recommendations

- For reconnaissance scale exploration stream sediments can be collected at the mouths of 2nd order streams to detect anomalous concentrations of metals (such as Au, Ag, Hg, Pb, Sb, Bi, Te, S, Cu, and Zn). Since supply of sediment to the streams can be complex, bank material must be properly identified, pH must be measured and the presence of chemical precipitates and secondary oxides on the stream bed must be noted.

- 2-3 kg of –2mm material should be collected from high or medium energy environments to obtain a 50 g sub-sample of –75μm or -53μm material for determination of Au by fire assay and multi-element geochemistry by ICP-MS. The *aqua regia* digestion with an ICP-MS finish is of general applicability. However, in neutral-pH environments, a weak leach, such as the cold hydroxylamine leach, may provide better detection of distal hydromorphic anomalies.

- Surface waters can be collected to complement sediments: approximately 15 ml is required and must be filtered to –0.45μm and acidified with ultra-pure acid for preservation. Waters should be analysed by ICP-MS (see 3.1.3 for description).

- The presence of chemical precipitates and secondary oxides on the stream bed must be noted as they can strongly affect metal concentrations.

- To follow-up reconnaissance anomalies, more detailed sampling of stream sediments should be accompanied by sampling around the base of slope of talus cones and alluvial. Approximately 800-900g of –4mm material is needed to obtain a 50 g subsample for Au by fire assay and a multi-element analysis. Interpretation should take into account that mobile elements (e.g. Cu) are likely to be depleted under acidic weathering conditions close to mineralization.

References

Barrick Gold Corporation, 1999. Data from Pascua-Lama deposit from Internet, http://www.barrick.com.

Best, J.L., and Brayshaw, A.C., 1985. Flow separation – a physical process for the concentration of heavy minerals within alluvial channels. Journal Geological Society of London, 142, pp. 747-755.

Boggs, S., 1995. Principles of sedimentology and stratigraphy. Prentice Hall. 774 p.

Carpenter, R.H., and Hayes, W.B., 1980. Annual accretion of Fe-Mn oxides and certain associated trace metals in a stream environment. Chemical Geology, 29, pp. 249-259.

Caughlin, B., 1999. Selective leaches. Geoanalysis with emphasis on selective extractions. 19th International Geochemical Exploration Symposium, Vancouver, B.C.

Caviedes, C.N., and Paskoff, R., 1975. Quaternary glaciations in the Andes of North-Central Chile. Journal of Glaciology, v. 14, pp.155-170.

Chao, T.T., 1984. Use of partial dissolution techniques in geochemical exploration, Journal Geochemical Exploration, 20, pp. 101-135.

Chao, T.T., and Zhou, L., 1983. Extraction techniques for selective dissolution of amorphous iron oxides from soil and sediments. Soil Science Society of America Proceedings, 47, pp. 225-232.

Chao, T.T., 1972. Selective dissolution of manganese oxides from soils and sediments with acidified hydroxylamine hydrochloride, Soil Science Society of America Proceedings, 36, pp. 764-768.

Chao, T.T., and Theobald, P.K., 1976. The significance of iron and manganese oxides in geochemical exploration, Economic. Geology, 71, pp. 1560-1569.

Charchaflie, D., 2001. Personal communication. University of British Columbia.

Chastain, E.A., 2001. Trace metal composition of selected heavy minerals in stream sediments of a high sulfidation epithermal gold deposit of the Chilean/Argentinean Andes. GEOL 501 unpublished report. University of British Columbia.

Chemex, 1999. Fee Schedule.

Christie, T, and Fletcher, W.K., 1999. Contamination from forestry activities: implications for stream sediment exploration programs. Journal Geochemical Exploration, 67, pp. 201-210.

Chouinard, A. and Williams-Jones, A.E., 1999. Mineralogy and petrography of ore and alteration assemblages at Pascua, Chile. Barrick Gold Corporation, internal company report, 5 June, p. 15.

Clifton, H.E., Hunter, R.E., Swanson, F.J., and Phillips, R.L., 1969. Sample size and meaningful gold analysis. United States Geological Survey, Professional Paper 625-C, pp. 17.

Coira, B., Davidson, J., Mpodozis, C., and Ramos, V., 1982. Tectonic and magmatic evolution of the Andes of northern Argentina and Chile. In: Special issue, Magmatic evolution of the Andes, ed., Linares, E., Cordani, U.G., and Munizaga, F., pp. 303-332.

Conic-BF, 1999. Ingenerios Civiles Consultores Ltda Estimacion de caudales minimos Proyecto Lama. Report to Barrick.

Coope J.A. and Webb, J.S., 1963. Copper in stream sediments near disseminated copper mineralization, Cebu, Philippines Republic. Inst. Mining Metall. Trans. 72, pp. 397-406.

Cox, D.P. and Singer, D.A., 1986. Mineral Deposit Model 25e: Descriptive model of epithermal quartz-alunite Au. U.S. Geological Survey Bulletin 1693, 379 pp.

Davidson, J. and Mpodozis, C., 1991. Regional geological setting of epithermal gold deposits, Chile. Economic Geology, v. 86, pp. 1174-1186.

Day, S., 1985. Sampling stream sediments for gold in mineral exploration, Southern British Columbia. Unpublished M.Sc. thesis, University of British Columbia.

Day, S.J, and Fletcher, W.K., 1989. Effects of valley and local channel morphology on the distribution of gold in stream sediments from Harris Creek, British Columbia, Canada, Journal of Geochemical Exploration, 32, pp. 1-16.

Day, S.J. and Fletcher, W.K., 1991. Concentration of magnetite and gold at bar and reach scales in a gravel-bed stream, British Columbia, Canada, Journal of Sedimentary Petrology, 61, No. 6, pp. 871-882.

Deering, M.F., Mohr, E.T., Sypnieuwski, B.F., and Carlson, E.H., 1983. Regional hydrogeochemical patterns in groundwater of northern western Ohio and their relation to Mississippi Valley-type mineral occurrences. Journal of Geochemical Exploration, 19, pp. 225-241.

Deyell, C., 2001. Personal communication. Summary of mineralization at Pascua. University of British Columbia.

Deyell, C., 2000. Personal communication. University of British Columbia.

Drever, J.I., 1997. The Geochemistry of Natural Waters. Prentice Hall, 3rd ed., 436 p.

Evans, A.M., 1993. Ore geology and industrial minerals. Blackwell Science. 389 p.

Fletcher, W.K., 1981. Analytical methods in geochemical prospecting, Handbook of Exploration Geochemistry, Elsevier Science, Amsterdam, 255 p.

Fletcher, W.K., 1997. Stream sediment geochemistry in today's exploration world, In: A.G. Gubins, Proceedings of Exploration '97: Fourth decennial international conference on mineral exploration, p. 249-260.

Fletcher, W.K. and Day, S.J., 1989. Behavior of gold and other heavy minerals in drainage sediments: some implications for exploration geochemical surveys, Trans. Inst. Min. Metall., 98, B130-B136.

Fletcher, W.K., Dousset, P.E. and Bin Ismail, Y., 1987. Elimination of hydraulic effects for cassiterite in a Malaysian stream. Journal of Geochemical Exploration, 28, pp. 385-408.

Fletcher, W.K. and Loh, C.H., 1996. Transport equivalence of cassiterite and its application to stream sediment surveys for heavy minerals, Journal of Geochemical Exploration, 56, pp. 47-57.

Fletcher, W.K., and Muda, 1999. Influence of selective logging and sedimentological process on geochemistry of tropical rainforest streams, Journal of Geochemical Exploration, 67, pp. 211-222.

Geotechnica, 1999. Estudio de Impacto Ambiental Proyecto Minero Pascua. Report for Barrick.

Giblin, A., 1994. Natural waters as sample media in drainage geochemistry. In: M. Hale and J.A. Plant, Drainage geochemistry. Handbook of Exploration Geochemistry Vol 6.

Hall, G.E.M., 1998. Analytical perspective on trace element species of interest in exploration. Journal of Geochemical Exploration, 61, pp. 1-19.

Hall, G.E.M., Vaive, J.E., Beer, R., Hoashi, M. 1996. Selective leaches revisited, with emphasis on the amorphous Fe oxyhydroxide phase extraction. Journal of Geochemical Exploration, 56, pp. 59-78.

Hansuld, 1966. Behavior of Molybdenum in secondary dispersion media. Mining Eng. 18, 12, pp. 73-77.

Hawkes, H. E., 1976. The downstream dilution of stream sediment anomalies, Journal of Geochemical Exploration, 6, pp 345-358.

Hearil, G., Lagos, J., Vivallow, W., 1999. Gold dispersion in Andean desert environments (Atacama, Chile). Journal of Geochemical Exploration, 66, pp. 427-439.

Heberlein, 2000. Personal communication.

Hedenquist, J.W., Izawa, E., Arribas, A., White, N.C., 1996. Epithermal gold deposits Styles, characteristics and exploration. Resource Geology special publication 1. Society of Resource Geology.

Hitzman, M., 1997, GEOL 401 Introduction to mineral deposits, Colorado School of Mines.

Hobday, J. and Fletcher, W.K., 2001. Stream sediment surveys in mountainous terrain, Slesse Creek, British Columbia, Poster presented at Cordilleran Roundup.

Horsnail, R.F., Nichol, I., and Webb, J.S., 1969. Influence of variations in secondary environment on the metal content of drainage sediments. Colorado School of Mines Quart., v. 64, pp. 307-322.

Hou, Z., 1997. Sediment budget of gold and magnetite and their distribution in stream sediments in lower Harris Creek, South-Central British Columbia, Canada, Unpub. Ph.D. thesis. University of British Columbia, 228 p.

Hou, Z., and Fletcher, W.K., 1996. The relations between false gold anomalies, sedimentological processes and landslides in Harris Creek, British Columbia, Canada, Journal of Geochemical Exploration, 57, pp. 21-30.

Informes Gesoestudios, 1994. Report to Barrick.

Ingamells, C.O., 1981. Evaluation of skewed exploration data- the nugget effect. Geochim. Cosmochim. Acta, v. 45, p. 1209-1216.

Jannus, R.R., 1995. Reduced and oxidized high sulfidation deposits of the El Indio District, Chile. Unpublished Ph.D. thesis, Harvard University,

Kay, S.M., Mpodozis, C., and Coira, B., 1997. Neogene magmatism, tectonism, and mineral deposits of the Central Andes. SEG Special Publication 7. Geology and Ore deposits of the Central Andes. Skinner, B.J., editor.

Lalonde, J.P., 1983. Groundwater geochemistry in Abitibi volcanic Belt of Quebec. Journal of Geochemical Exploration, 19, pp. 207-223.

Leaver, M.E., 2000. personal communication. CANMET, Natural Resources Canada.

Leybourne, M.I., Goodfellow, W.D., Boyle, D.R., 1999. Hydrogeochemical, isotpoic and rare earth element evidence for contrasting water-rock interactions at two undisturbed Zn-Pb massive sulfide deposits, Bathurst Mining Camp, N.B., Canada. Journal of Geochemical Exploration, 64, pp. 237-261.

Lliboutry, L., 1997. Glaciers of the dry Andes. http://pubs.usgs.gov/prof/p1386i/chile-arg/dry/index.

Maksaev, J.V., Moscos, D.R., Mpodozis, M.C, Nasi, P.C., 1984. The volcanic and plutonic units of the upper Cenozoic in the High Cordillera of north Chico (29°-31°S); geology, hydrothermal alteration and mineralization. Revista Geologica de Chile; 21, pp 11-51.

Martin, M,W, Clavero, R.J., Mpodozis, M.C., 1995. Tertiary geologic development of the high Andes El Indio belt, Chile. In: Abstract with programs, Geological Society of America, 27, 6, 409 p.

Moranzana, F., 1972. Application of talus sampling to geochemical exploration in arid areas: Los Pelambres hydrothermal alteration area, Chile. IMM Trans. 81:B26-B33.

Morgan, J.J. and Stumm, W., 1964. Colloid-chemical properties of mangese dioxide. Journal of Colloid Science, v. 19, pp. 347-359.

Mpodozis, C., and Cornejo, P., 1988, Hoja Pisco Elqui, 1:250,000: Santiago, Servicio Nac. Geologica Mineria, Carta Geol. Chile, no. 68, 163 p.

Nasi, C., Moscoso, R., and Maksaev, V., 1990. Hoja Guanta, 1:250,000: Servicio Nac. Geologica Mineria, Carta Geol. Chile, no. 67, 140 p.

Nichol, I., Closs, L.G., Lavin, O.P., 1987. Sample representivity with reference to gold exploration. Exploration '87 Proceedings, p. 609-624.

Nichol, I., Hale, M., Fletcher, W.K., 1994. Drainage geochemistry in gold exploration. In: M. Hale and J.A. Plant, Drainage geochemistry. Handbook of Exploration Geochemistry, Vol. 6.

Nordstrom, D.K., Alpers, C.N, Ptacek, C.J., Blowes, D.W., 2000. Negative pH and extremely acidic mine waters from Iron Mountain, California. Environmental Science and Technology, 24 (2), 254-258.

Perel'man, A.I. (1967). Geochemistry of epigenesis. Plenum Press, New York, 266 p.

Phillips, J.S.; Thompson, R.F., 1967. Statistics for Nurses. The Macmillan Company, 550 pp.

Reid, I. and Frostick, L.E. 1985. Role of settling, entrainment and dispersive equivalence and of interstice trapping in place formation. Journal Geological Society of London, 142, pp. 739-746.

Robinson, G.D., 1983. Heavy metal adsorption by ferromanganese coating on stream alluvium: natural controls and implications for exploration. Chemical Geology, 38, pp. 157-174.

Rose, A.W. 1975. The mode of occurrence of trace elements in soils and stream sediments applied to geochemical exploration. Transactions of the 5th International Geochemical Exploration Symposium, pp. 691-705.

Rose, A.W., Hawkes, H.E., and Webb, J.S., 1979. Geochemistry in mineral exploration, second edition, Academic Press, New York, 657 p.

Rittenhouse, G., 1943. The transportation and deposition of heavy minerals. Geological Society of America Bulletin, 54, pp. 1725-170.

Rubey, W.W., 1933. The size distribution of heavy minerals in a water-laid sandstone. Journal Sedimentary Petrology, 3, pp. 3-29.

Sallenger, A.H. 1979. Inverse grading and hydraulic equivalence in grain-flow deposits. Journal Sedimentary Petrology, 49, pp. 553-562.

Saxby, D.W. and Fletcher, W.K., 1986a. Behavior of scheelite in a Cordilleran stream. Presented at GEOEXPO 86, Vancouver, British Columbia.

Saxby, D. and Fletcher, K., 1986b. The geometric mean concentration ratio (GMCR) as an estimator of hydraulic effects in geochemical data for elements dispersed as heavy minerals. Journal of Geochemical Exploration, 26, pp. 223-230.

Sleath, A. and Fletcher, W.K., 1982. In: Prospecting in glaciated terrains, ed., P. Davenport, Geochemical dispersion in a mountain stream, Purcell Mountains, British Columbia. Can. Inst. Min. Metall., 195-203.

Slingerland, R., 1977. The effects of entrainment on the hydraulic equivalence relationships of light and heavy minerals in sands. Journal Sedimentary Petrology, 47, pp. 753-770.

Slingerland, R., 1984. Role of hydraulic sorting in the origin of fluvial placers, Journal of Sedimentary Petrology, V. 54, pp 137-150.

Stanley, C.R. and Smee, B.W., 1989. A test in pattern recognition: defining anomalous patterns in surficial samples which exhibit severe nugget effects – II. Explore, v. 65: 12-14.

Stendal, H. and Theobald, P.K., 1994. Heavy-mineral concentrates in geochemical exploration, In: M. Hale and J.A. Plant, Drainage Geochemistry. Handbook of Exploration Geochemistry, Vol. 6.

Thompson, M. and Howarth, R.J., 1978. A new approach to the estimation of analytical precision. Journal of Geochemical Exploration, v. 9, p. 23-30.

Tianxiang, R., Shaoping, Y., Yinghan, L., 1998. Characteristics of element dispersion and geochemical exploration for concealed ore deposits overlain by loess and red soils in eastern Gansu Province, China. Journal of Geochemical. Exploration, 5, pp. 103-113.

White, N.C and Hedenquist, J,W., 1995. Epithermal gold deposits styles, characteristics and exploration. SEG newsletter No. 23, p 9-13.

APPENDICES

Values greater than the detection limit were changed to the upper limit. Values less than the detection limit were changed to the lower limit.

Table A.1. Gold concentrations in stream sediments at Pascua-Lama. Values at less than or equal to detection limit were changed to the detection limit.

Site No.	Sample No.	UTM-E	UTM-N	Energy	-150 +106μm	-106 +75μm	-75 +53μm	-53μm
1	1	19411623	6752480	high	285	1110	2180	1840
1	2	19411623	6752480	med	40	60	445	370
1	3	19411623	6752480	low	115	385	695	640
2	6	19411012	6753201	high	210	1110	1715	990
2	7	19411012	6753201	med	55	180	340	360
2	8	19411012	6753201	low	40	55	175	435
3	11	19409459	6753605	high	50	165	265	400
3	12	19409459	6753605	med	65	330	150	980
3	13	19409459	6753605	low	45	100	315	325
5	16	19409416	6753736	high	50	105	170	490
5	17	19409416	6753736	med	250	120	115	560
5	18	19409416	6753736	low	45	50	60	305
6	21	19409129	6753684	high	10	15	15	45
6	22	19409129	6753684	med	10	15	10	40
6	23	19409129	6753684	low	10	10	15	70
12	49	19409192	6754140	high	125	760	650	580
12	50	19409192	6754140	med	75	140	485	1060
12	51	19409192	6754140	low	65	170	260	710
13	66	19408242	6754491	high	45	70	135	365
13	67	19408242	6754491	med	60	230	185	390
13	68	19408242	6754491	low	35	65	95	430
14	71	19407493	6754860	high	210	195	520	1065
14	72	19407493	6754860	med	110	575	635	1585
14	73	19407493	6754860	low	40	85	155	560
15	76	19406397	6755270	high	65	120	205	740
15	77	19406397	6755270	med	90	185	675	975
15	78	19406397	6755270	low	45	70	205	410
16	81	19405392	6755433	high	70	90	180	515
16	82	19405392	6755433	med	50	150	300	655
16	83	19405392	6755433	low	60	105	410	1080
17	86	19405422	6755520	high	80	10	260	145
17	87	19405422	6755520	med	5	20	25	45
17	88	19405422	6755520	low	10	10	20	50
18	93	19404355	6755587	high	70	95	170	490
18	94	19404355	6755587	med	55	50	270	435
18	95	19404355	6755587	low	45	55	70	285
19	98	19404449	6755928	high	20	305	150	120
19	99	19404449	6755928	med	15	25	105	185
19	100	19404449	6755928	low	25	30	35	65
20	167	19408527	6753601	med	10	10	5	70
20	168	19408527	6753601	low	10	10	15	70
21	166	19412139	6752587	med	5	50	40	100
21	169	19412139	6752587	low	35	25	100	250
22	170	19407440	6753249	med	5	20	50	60
22	171	19407440	6753249	low	15	10	20	95
23	200	19411198	6752281	med	20	15	5	20
23	201	19411198	6752281	low	5	5	5	10
24	202	19389562	6777042	high	5	5	5	50
24	203	19389562	6777042	med	235	65	150	235
25	321	19388647	6775886	high	5	5	280	100
25	204	19388647	6775886	med	10	220	275	225
26	257	19387864	6772827	high	5	5	5	35

Table A.1. Continued

Site No.	Sample No.	UTM-E	UTM-N	Energy	-150 +106μm	-106 +75μm	-75 +53μm	-53μm
26	258	19387864	6772827	med	5	130	5	20
27	260	19388006	6772617	high	10	265	350	170
27	261	19388006	6772617	med	15	160	305	470
28	262	19388884	6771725	high	135	350	365	470
28	263	19389138	6771339	med	70	90	125	300
29	265	19389954	6768995	high	520	385	290	270
29	266	19389954	6768995	med	990	320	425	295
30	267	19390847	6767116	high	30	545	390	270
30	268	19390847	6767116	med	280	335	300	125
31	269	19391954	6767882	med	5	5	5	290
32	270	19392148	6765356	high	25	25	245	150
32	271	19392148	6765356	med	25	375	340	285
33	272	19393278	6763974	high	435	980	210	315
33	273	19393278	6763974	med	30	20	290	140
34	274	19394506	6763091	high	25	25	415	370
34	275	19394506	6763091	med	15	135	260	370
35	276	19395955	6761937	high	15	20	330	145
35	277	19395955	6761937	med	15	100	100	180
35	278	19395955	6761937	low	20	15	20	105
36	284	19396305	6761773	high	540	325	415	310
36	285	19396305	6761773	med	25	120	130	250
36	286	19396305	6761773	low	10	5	15	115
37	294	19397190	6760198	high	50	1490	1855	820
37	295	19397190	6760198	med	20	15	135	105
37	296	19397190	6760198	low	10	5	15	145
38	299	19398090	6758484	high	25	15	190	355
38	300	19398090	6758484	med	100	240	320	865
38	301	19398090	6758484	low	15	10	20	110
39	289	19396833	6760913	high	125	35	900	250
39	290	19396833	6760913	med	40	715	1060	605
39	291	19396833	6760913	low	10	15	25	85
40	280	19397761	6762537	high	5	5	5	25
40	281	19397761	6762537	med	100	5	170	15
40	282	19397761	6762537	low	5	5	10	30
41	302	19399377	6757564	med	45	45	45	160
41	303	19399377	6757564	low	20	25	45	140

Table A.2. Results of aqua regia digestion of stream sediments.

Site no.	Sample no.	UTM-E	UTM-N	Elev	site pH	Ag (ppm)	Al (%)	As (ppm)	B (ppm)	Ba (ppm)	Be (ppm)	Bi (ppm)
1	1	19411623	6752480	3759	3.2	11.7	0.54	598	10	110	0.25	9.89
2	8	19411012	6753201	3762	3.5	11.7	0.59	390	10	180	0.3	13.4
3	11	19409459	6753605	3756	3.1	23.8	0.55	316	10	120	0.15	21.7
5	18	19409416	6753736	3797	2.8	16.9	0.64	452	10	140	0.2	12.95
6	21	19409129	6753684	3684	7.4	0.8	1.56	424	10	620	3.7	2.97
12	51	19409192	6754140	3705	2.5	21.9	0.6	403	10	110	0.2	20.6
13	66	19408242	6754491	3810	2.5	18.15	0.76	401	10	170	0.25	12.85
14	73	19407493	6754860	3915	1.5	22.3	0.64	434	10	140	0.25	20.7
15	76	19406397	6755270	3798	2.1	20.6	0.64	403	10	160	0.2	17.3
16	83	19405392	6755433	4146	2.1	23	0.68	514	10	170	0.15	21.1
17	86	19405422	6755520	4098	5.8	0.76	1.86	119.5	10	210	1.5	1.98
18	95	19404355	6755587	4272	1.5	14.95	1.03	415	10	160	0.3	14.6
19	98	19404449	6755928	4299	5.3	3	2.13	368	10	280	0.7	5.6
20	168	19408527	6753601	3855	6.6	0.86	1.56	478	10	540	2.5	2.44
21	166	19412139	6752587	3670	5.9	3.8	2.64	1265	10	340	2.55	5.25
22	171	19407440	6753249	3891	8.8	0.9	1	890	10	680	2.05	3.96
23	200	19411198	6752281		7	0.24	2.34	492	10	180	1.75	1.23
24	321	19388647	6775886		7.1	2.08	2.06	72.2	10	370	1.2	3.33
25	203	19389562	6777042		7.1	1.84	2.32	67.4	10	420	1.6	3.74
26	258	19387864	6772827	2628	7	0.24	2.53	14	10	220	1	0.96
27	261	19388006	6772617	2748	6.8	2.84	2.1	80.2	10	320	1.25	3.69
28	263	19389138	6771339	2874	6.7	2.94	3.29	105	10	440	2	3.82
29	266	19389954	6768995	2830	6.7	2.78	2.27	89	10	400	1.3	4.43
30	268	19390847	6767116		6.4	2.42	5.65	111.5	10	310	3.05	3.11
31	269	19391954	6767882	3250	6.8	0.44	2.38	16.4	10	160	1.5	2.21
32	271	19392148	6765356	3390	6.4	3.5	3.32	124	10	390	1.8	4.76
33	272	19393278	6763974	3504	6	2.74	3.72	129	10	330	2.1	3.63
34	275	19394506	6763091	3420	5.3	3.32	2.88	135	10	350	1.35	4.97
35	276	19395955	6761937	35450	4.9	2.44	2.9	102.5	10	370	1.55	4.21
36	286	19396305	6761773	3708	4.2	3.82	4.36	138	10	180	1.6	3.98
37	294	19397190	6760198		4.5	3.94	2.92	161	10	260	1.4	4.68
38	301	19398090	6758484	4047	4.1	6.72	1.72	241	10	270	0.95	7.96
39	289	19396833	6760913	3603	4	4.5	2.55	171	10	420	1.4	4.88
40	282	19397761	6762537	3864	4	0.24	1.92	42.4	10	330	0.95	2.19
41	302	19399377	6757564		5.6	4.26	1.95	354	10	230	1.35	4.75

Table A.2. Continued

Site no.	Ca (%)	Cd (ppm)	Co (ppm)	Cr (ppm)	Cu (ppm)	Fe (%)	Ga (ppm)	Ge (ppm)	Hg (ppm)	K (%)	La (ppm)	Mg (%)
1	0.07	0.22	2.4	13	142	15	5.6	0.1	3.67	0.33	10	0.18
2	0.07	0.18	2.2	10	115.5	7.49	4.5	0.1	6.03	0.37	10	0.23
3	0.09	0.22	3.6	9	131.5	4.81	3.5	0.1	12.45	0.39	10	0.22
5	0.07	0.3	2.8	16	130	7.35	4.7	0.1	6.08	0.48	10	0.27
6	0.58	1.28	9.8	10	48.6	5.3	4.1	0.1	0.24	0.21	30	0.38
12	0.07	0.26	4.4	19	173	6.48	4.2	0.1	16.5	0.44	10	0.24
13	0.14	0.38	3.4	17	148	5.44	4.8	0.1	6.22	0.43	10	0.33
14	0.06	0.22	3.2	10	128.5	6.36	4.4	0.1	13.45	0.58	10	0.23
15	0.08	0.36	3.6	14	121	5.34	4.5	0.1	10.35	0.44	10	0.25
16	0.05	0.3	2	8	107.5	6.11	4.8	0.1	8.94	0.6	10	0.23
17	0.3	0.46	12.4	19	83.5	5.37	6.5	0.1	0.16	0.5	10	0.49
18	0.08	0.4	3.2	8	95.6	5	5.7	0.1	3.47	0.55	10	0.4
19	0.22	0.34	10	20	94.3	5.97	7.7	0.1	0.86	0.64	10	0.76
20	0.3	0.48	11	12	55.7	7.65	4.2	0.1	0.26	0.19	20	0.33
21	3.09	1.16	36.6	12	412	5.6	5.7	0.1	2.45	0.21	10	0.72
22	0.58	1.88	11	12	93.9	7.58	4.6	0.1	0.35	0.23	30	0.31
23	2.07	0.62	41.2	13	88.7	4.67	5.6	0.1	0.1	0.21	10	0.8
24	0.47	2.94	17.4	20	290	4.45	5.5	0.1	0.71	0.21	10	0.61
25	0.57	5.94	23.6	27	416	4.83	5.8	0.1	1.74	0.2	20	0.64
26	1.51	0.26	15.2	37	68.9	3.87	7	0.1	0.16	0.11	20	1.35
27	0.39	3.1	18.2	22	312	4.81	5.8	0.1	1.01	0.21	10	0.57
28	0.5	12.45	34	25	624	5.35	6.3	0.1	2.18	0.25	20	0.61
29	0.43	4.64	21.8	21	336	4.8	6.1	0.1	1.29	0.24	10	0.64
30	0.42	14.7	38.6	19	943	4.08	5.2	0.1	0.44	0.29	20	0.55
31	1.32	0.42	15	73	204	4.1	12.4	0.1	0.2	0.15	20	1.34
32	0.54	6.7	23.8	23	439	4.85	6.6	0.1	0.91	0.34	20	0.76
33	0.44	9.62	31	21	534	4.62	6.6	0.1	1.02	0.34	20	0.72
34	0.34	1.72	17.2	24	292	5.48	6.3	0.1	0.88	0.31	10	0.63
35	0.31	1.36	18.4	28	325	5.88	6.7	0.1	1.09	0.3	10	0.61
36	0.21	0.44	7.6	23	262	8.31	4.8	0.1	1.91	0.21	10	0.39
37	0.35	0.74	10.8	29	168.5	5.56	6.3	0.1	0.78	0.29	20	0.48
38	0.32	0.52	9	26	113	7.89	6.1	0.1	2.46	0.35	10	0.53
39	0.38	1.44	17.6	24	298	6.65	7.2	0.1	0.84	0.35	20	0.66
40	0.34	0.54	20.6	27	103	5.51	6.8	0.1	0.13	0.46	10	0.76
41	0.51	1.74	13.4	17	192.5	5.22	6.5	0.1	0.48	0.57	30	0.67

Table A.2. Continued

Site no.	Mn (ppm)	Mo (ppm)	Na (%)	Ni (ppm)	P (ppm)	Pb (ppm)	S (%)	Sb (ppm)	Sc (ppm)	Sr (ppm)	Te (ppm)
1	190	5.8	0.06	9	430	222	1.98	6.8	1	40	2.35
2	220	4.6	0.07	6	340	260	1.28	8	1	41	2.55
3	200	4.4	0.07	7	280	224	1.91	9.8	1	42	3.15
5	240	6	0.09	10	390	184	1.7	7.2	1	55	3.2
6	2800	7	0.05	12	730	1745	0.36	6.3	6	62	0.35
12	220	5.8	0.08	11	350	214	2.1	9	1	45	3.4
13	300	6	0.09	11	410	184	1.48	6.5	1	54	2.95
14	210	5.4	0.1	7	350	272	1.95	9.4	1	59	3.9
15	245	6	0.09	8	360	206	1.71	8.4	1	51	3.3
16	235	5.2	0.1	7	360	274	1.76	9.5	1	68	4.3
17	680	4	0.08	14	920	46	0.72	0.7	7	80	0.35
18	410	6.4	0.14	6	470	256	1.68	4.8	1	96	3.75
19	780	3	0.15	14	810	214	1.26	1.8	5	96	2.45
20	2050	3.4	0.04	11	870	1000	0.47	5.7	7	58	0.35
21	2330	2.4	0.09	14	790	56	0.57	4.2	6	141	0.65
22	6210	12.2	0.05	11	1060	2140	0.4	6.7	5	72	0.6
23	2260	1	0.13	15	800	22	0.31	1.9	6	151	0.3
24	2410	11.2	0.07	18	680	66	0.29	1.1	4	78	0.65
25	4760	12.6	0.07	25	810	64	0.28	1.1	4	96	0.6
26	1405	4	0.07	26	1120	16	0.06	0.3	7	173	0.05
27	2290	12.6	0.07	19	680	74	0.32	1.2	4	63	0.75
28	7150	20.8	0.08	33	780	90	0.42	1.3	4	79	0.9
29	3260	11.4	0.08	21	700	78	0.38	1.3	4	71	0.85
30	9720	30	0.1	29	770	88	0.51	1.6	4	78	0.8
31	1475	9.2	0.04	31	1690	32	0.17	0.4	6	64	0.15
32	4210	11.6	0.1	27	740	106	0.49	1.4	5	90	0.95
33	6460	16.2	0.09	25	750	110	0.48	1.5	5	84	0.95
34	1860	10.8	0.09	17	750	114	0.55	1.7	5	89	1.15
35	1735	13.6	0.08	20	830	78	0.61	1.2	5	93	1
36	685	14.6	0.05	13	640	102	1.15	2	5	38	0.9
37	955	9.2	0.08	14	940	120	0.7	2.2	4	75	1
38	765	2.4	0.1	13	830	184	0.76	3.1	4	62	1.6
39	1725	7.8	0.08	16	850	140	0.49	2.4	5	95	1.15
40	655	9.8	0.16	20	670	24	1.01	0.3	5	106	1.35
41	2080	1.8	0.17	13	840	302	0.95	3.6	5	87	1.85

Table A.2. Continued

Site no.	Ti (%)	Tl (ppm)	U (ppm)	V (ppm)	W (ppm)	Zn (ppm)
1	0.01	1.74	0.35	98	0.4	64
2	0.01	1.92	0.4	46	0.3	66
3	0.01	2.06	0.35	25	0.5	66
5	0.01	2.2	0.3	46	0.25	78
6	0.01	1.42	1.2	31	0.3	612
12	0.01	2.28	0.35	40	0.35	76
13	0.01	2.1	0.4	36	0.25	98
14	0.01	2.96	0.35	32	0.45	66
15	0.01	2.28	0.35	32	0.45	90
16	0.01	2.88	0.3	33	0.35	74
17	0.04	1.68	3	51	0.1	228
18	0.01	2.6	0.4	24	0.4	118
19	0.03	3.06	1.5	45	0.1	152
20	0.01	1.22	1.3	42	0.2	320
21	0.06	1.38	1.5	84	0.85	338
22	0.01	1.12	1.1	35	0.35	412
23	0.06	0.88	0.95	85	0.4	232
24	0.07	1.14	14.25	50	0.65	676
25	0.08	1.22	17	66	0.7	1260
26	0.2	0.08	24	82	0.85	86
27	0.07	1.36	13.85	57	0.65	738
28	0.07	1.74	26	61	0.75	2340
29	0.07	1.5	12.2	55	0.5	972
30	0.05	1.8	37.7	39	0.8	3330
31	0.18	0.14	229	77	2.65	132
32	0.07	1.9	12.3	50	0.55	1625
33	0.06	2.04	14.1	42	0.45	1790
34	0.06	1.88	8.15	54	0.35	474
35	0.07	1.8	12.35	57	0.3	684
36	0.04	1.24	3	47	0.45	190
37	0.05	1.72	3.95	59	0.55	236
38	0.04	2.04	1.6	73	0.65	188
39	0.07	2.02	3.7	57	0.4	448
40	0.05	2.1	9.4	58	0.15	82
41	0.04	2.68	2.6	44	1.7	416

Table A.3. Results of cold hydroxylamine leach on stream sediments at Pascua-Lama.

Site No.	Ag (ppm)	Al (ppm)	As (ppm)	Au (ppm)	Ba (ppm)	Be (ppm)	Bi (ppm)	Br (ppm)	Ca (ppm)	Cd (ppm)	Ce (ppm)	Co (pp)
1	0.55	390	0.3	0.05	1.6	0.05	0.005	2	430	0.03	0.33	0.25
2	0.44	400	0.3	0.05	2.2	0.05	0.015	2	440	0.02	0.275	0.2
3	1.02	480	3.6	0.2	2.15	0.05	0.02	2	640	0.05	0.23	0.3
5	0.298	473	0.4	0.05	2.15	0.05	0.015	2	460	0.03	0.24	0.25
6	0.038	196	0.7	0.1	108	0.45	0.005	2	2770	0.69	0.95	2.4
12	0.352	493	1.2	0.15	2	0.05	0.04	2	440	0.04	0.25	0.35
13	0.608	678	2.9	0.05	1.15	0.1	0.005	2	960	0.07	0.365	0.55
14	0.442	463	1.9	0.05	2.15	0.05	0.02	2	320	0.03	0.145	0.3
15	0.432	513	2.1	0.05	2.2	0.05	0.015	2	540	0.04	0.19	0.3
16	0.188	554	1	0.05	2.15	0.05	0.045	2	310	0.03	0.14	0.25
17	0.138	603	1.9	0.05	28.3	0.5	0.005	2	1780	0.3	0.995	2.85
18	0.456	868	30.7	0.05	1.7	0.05	0.005	2	550	0.06	0.15	0.4
19	0.63	907	4	0.05	9.25	0.15	0.01	2	1000	0.16	0.295	2.7
20	0.05	829	0.1	0.1	17.15	0.65	0.005	2	1330	0.22	2.11	3.95
21	0.022	12	2.8	0.1	31.2	0.05	0.005	2	14940	0.42	0.4	14.2
22	0.052	27	0.6	0.05	169.8	0.05	0.005	2	3420	1.11	0.41	5.1
23	0.006	19	6.5	0.05	46.2	0.05	0.005	2	8620	0.35	0.355	20.6
24	0.606	503	0.1	0.1	159.6	0.25	0.005	2	1520	2.13	0.85	9.1
25	0.648	370	0.1	0.05	206	0.15	0.005	2	1590	4.59	1.015	14.8
26	0.002	161	0.9	0.05	94.5	0.15	0.005	8	4030	0.17	0.325	1.45
27	0.644	591	0.1	0.05	114.7	0.25	0.005	2	1340	2.14	1.02	9.8
28	0.908	357	0.1	0.15	136.1	0.2	0.005	2	1740	9.77	1.935	22.6
29	0.784	603	0.1	0.05	88.7	0.15	0.005	2	1430	3.38	1.365	13.4
30	0.752	679	0.1	0.15	87.2	0.3	0.005	2	1030	12.9	4.74	31.1
31	NS	NS	NS	NS	NS	NS	NS	NS	NS	NS	NS	NS
32	0.752	429	0.1	0.05	74.2	0.25	0.005	2	2030	5.04	1.65	14.3
33	0.822	569	0.1	0.1	94.3	0.25	0.005	2	1320	8.1	2.84	21.6
34	0.77	691	0.1	0.05	65.9	0.2	0.005	2	1400	1.26	1.545	10.15
35	0.554	1080	0.1	0.15	24	0.3	0.005	2	1080	0.85	1.725	9.8
36	NS	NS	NS	NS	NS	NS	NS	NS	NS	NS	NS	NS
37	0.344	1685	0.1	0.05	23.8	0.15	0.005	2	530	0.3	1.835	2.8
38	0.45	822	0.1	0.05	37.3	0.2	0.005	2	1270	0.27	2.14	1.8
39	0.81	578	0.1	0.05	111.3	0.2	0.005	2	1650	0.78	1.805	8.05
40	0.036	376	0.1	0.15	82.9	0.15	0.005	2	1850	0.26	0.44	11.2
41	0.678	257	4	0.15	28.8	0.25	0.005	2	2380	0.96	0.785	5.2

NS = insufficient sample size for analysis

Table A.3. Continued

Site No.	Cr (ppm)	Cs (ppm)	Cu (ppm)	Dy (ppm)	Er (ppm)	Eu (ppm)	Fe (ppm0	Gd (ppmm	Hg (ppm)	Ho (ppm)	I (ppm)	K (ppm)
1	0.15	0.455	15.05	0.045	0.02	0.01	5380	0.065	0.1	0.005	1.5	15
2	0.05	0.38	14.6	0.035	0.015	0.005	2120	0.055	0.1	0.005	1.1	25
3	0.05	0.22	14.7	0.035	0.015	0.005	695	0.04	0.1	0.005	0.9	20
5	2.5	0.445	16.9	0.035	0.02	0.005	1930	0.045	0.1	0.005	1	15
6	0.05	0.32	1.15	0.225	0.135	0.05	755	0.245	0.1	0.05	1.1	120
12	0.15	0.26	19.1	0.035	0.02	0.005	1855	0.05	0.1	0.005	3.2	20
13	0.25	0.45	36.1	0.065	0.035	0.015	1990	0.07	0.1	0.01	1.3	15
14	0.05	0.26	14.95	0.03	0.015	0.005	1710	0.035	0.1	0.005	1.7	5
15	0.05	0.33	20.3	0.04	0.02	0.005	1510	0.04	0.1	0.005	0.7	15
16	0.05	0.27	16.6	0.02	0.015	0.005	1735	0.03	0.1	0.005	1.2	5
17	0.05	1.47	17.1	0.18	0.115	0.03	315	0.185	0.1	0.04	2.8	250
18	0.15	0.235	29.7	0.04	0.025	0.005	795	0.045	0.1	0.005	0.7	45
19	0.05	0.21	24.4	0.085	0.06	0.02	415	0.115	0.1	0.02	1.7	165
20	0.05	0.905	4.2	0.51	0.24	0.125	870	0.58	0.1	0.09	1.5	120
21	0.2	2.37	19.85	0.015	0.005	0.005	110	0.03	0.1	0.005	62.4	285
22	2.55	0.16	1.4	0.035	0.02	0.005	1830	0.04	0.1	0.005	0.7	115
23	0.05	2.82	6.15	0.02	0.01	0.005	175	0.03	0.1	0.005	25.3	380
24	0.05	0.08	54.3	0.1	0.075	0.01	305	0.1	0.1	0.025	1.4	150
25	0.05	0.09	93.4	0.125	0.075	0.015	320	0.12	0.1	0.025	1.5	125
26	1.3	0.145	0.75	0.02	0.005	0.005	390	0.02	0.1	0.005	4.9	115
27	0.05	0.08	56.8	0.125	0.075	0.02	290	0.125	0.1	0.025	0.9	130
28	0.05	0.08	122.5	0.24	0.155	0.03	375	0.225	0.1	0.055	2.2	155
29	3.7	0.075	78.1	0.165	0.095	0.025	335	0.17	0.1	0.035	1.5	150
30	0.05	0.09	222	0.76	0.45	0.115	305	0.805	0.1	0.16	1.6	120
31	NS	NS	NS	NS	NS	NS	NS	NS	NS	NS	NS	NS
32	0.05	0.075	79.8	0.215	0.135	0.03	345	0.23	0.1	0.045	2.4	140
33	0.05	0.075	117	0.395	0.25	0.065	345	0.42	0.1	0.085	1.4	125
34	0.05	0.07	44.9	0.155	0.08	0.03	360	0.185	0.1	0.035	0.8	145
35	0.05	0.09	31	0.275	0.165	0.045	345	0.305	0.1	0.06	7	80
36	NS	NS	NS	NS	NS	NS	NS	NS	NS	NS	NS	NS
37	2.05	0.095	9	0.145	0.08	0.025	225	0.175	0.1	0.03	0.7	115
38	0.05	0.16	20.8	0.22	0.135	0.03	535	0.25	0.1	0.045	1.5	145
39	0.05	0.1	33.4	0.175	0.1	0.03	290	0.2	0.1	0.04	1.4	135
40	0.05	0.05	15.35	0.13	0.07	0.015	355	0.115	0.1	0.03	2.2	170
41	0.15	0.175	29.3	0.135	0.095	0.015	200	0.14	0.1	0.03	1.7	210

NS = insufficient sample size for analysis

Table A.3. Continued

Site No.	Li (ppm)	Lu (ppm)	Mg (ppm)	Mn (ppm)	Mo (ppm0	Na (ppm)	Nb (ppm)	Nd (ppm)	Ni (ppm)	P (ppm)	Pb (ppm)
1	0.4	0.005	62	28	0.01	40	0.01	0.18	0.3	5	4.1
2	0.4	0.005	63	20.5	0.01	30	0.01	0.21	0.2	5	1
3	0.65	0.005	102	19.3	0.01	10	0.01	0.135	0.25	20	0.6
5	1.25	0.005	69	16.6	0.29	10	0.01	0.18	13.45	5	1
6	0.85	0.015	322	1365	0.01	30	0.01	0.49	0.55	5	150
12	0.9	0.005	93	20.1	0.01	10	0.01	0.165	0.3	5	0.3
13	0.95	0.005	148	39.4	0.01	10	0.01	0.265	0.5	5	0.1
14	0.15	0.005	84	16.4	0.01	10	0.01	0.125	0.25	5	0.1
15	0.8	0.005	80	20.4	0.01	10	0.01	0.13	0.35	5	0.4
16	0.05	0.005	64	13.8	0.01	10	0.01	0.095	0.15	5	0.4
17	0.7	0.015	380	269	0.01	80	0.01	0.59	1	120	1.2
18	1.15	0.005	134	28.4	0.01	10	0.01	0.145	0.55	50	9.5
19	0.65	0.005	126	209	0.01	50	0.01	0.24	0.35	40	0.8
20	1.4	0.025	118	915	0.01	40	0.01	1.43	0.55	5	409
21	3.55	0.005	452	1370	0.12	350	0.01	0.12	1.8	5	0.5
22	1.3	0.005	330	3780	0.33	40	0.01	0.135	15.65	5	27.5
23	3.6	0.005	456	1320	0.03	570	0.01	0.16	3.65	5	0.1
24	1.75	0.005	137	1350	0.01	40	0.01	0.325	2.5	5	0.7
25	2.3	0.005	156	3340	0.03	30	0.01	0.405	5.6	5	0.5
26	1.2	0.005	315	561	0.14	60	0.01	0.12	6.65	50	0.1
27	1.75	0.005	122	1310	0.01	30	0.01	0.395	1.95	5	1
28	3.6	0.02	234	>5000.	0.09	50	0.01	0.68	9.7	5	0.3
29	2.55	0.01	148	2070	0.5	40	0.01	0.53	24.8	5	0.8
30	1.75	0.045	126	>5000.	0.18	20	0.01	2.26	9.1	5	0.3
31	NS	NS	NS	NS	NS	NS	NS	NS	NS	NS	NS
32	1.3	0.015	253	2650	0.05	60	0.01	0.625	4.3	5	0.4
33	0.95	0.03	160	4540	0.08	30	0.01	1.1	5.55	5	0.6
34	0.35	0.01	182	1130	0.01	30	0.01	0.55	1.45	5	0.4
35	0.6	0.02	71	916	0.01	30	0.01	0.955	0.8	5	0.8
36	NS	NS	NS	NS	NS	NS	NS	NS	NS	NS	NS
37	1.25	0.005	17	413	0.25	20	0.01	0.745	12.1	5	1.7
38	1	0.015	80	281	0.01	30	0.01	1.05	0.5	10	3.5
39	0.65	0.01	189	849	0.01	50	0.01	0.685	0.65	5	0.4
40	0.8	0.005	327	246	0.01	30	0.01	0.25	1.7	15	0.1
41	1.05	0.01	379	1045	0.01	40	0.01	0.39	0.95	30	1.7

NS = insufficient sample size for analysis

Table A.3. Continued

Site No.	Pr (ppm)	Rb (ppm)	Sb (ppm)	Se (ppm)	Sm (ppm)	Sn (ppm)	Sr (ppm)	Tb (ppm)	Te (ppm)	Th (ppm)	Ti (ppm)
1	0.045	1.17	0.005	0.5	0.06	0.05	0.8	0.005	0.05	0.02	1
2	0.04	1.33	0.005	0.5	0.055	0.05	0.8	0.005	0.05	0.02	1
3	0.035	1.54	0.035	0.5	0.045	0.05	1.25	0.005	0.05	0.01	1
5	0.04	1.5	0.02	0.5	0.045	0.05	0.8	0.005	0.05	0.01	1
6	0.095	1.71	0.025	0.5	0.33	0.05	10.55	0.04	0.05	0.01	1
12	0.04	1.28	0.035	0.5	0.045	0.05	0.9	0.005	0.05	0.01	1
13	0.055	1.59	0.05	0.5	0.07	0.05	1.15	0.01	0.05	0.01	1
14	0.025	1.64	0.045	0.5	0.04	0.05	0.85	0.005	0.05	0.01	1
15	0.035	1.7	0.04	0.5	0.045	0.05	0.8	0.005	0.05	0.01	1
16	0.025	1.51	0.035	0.5	0.035	0.05	1.15	0.005	0.05	0.01	1
17	0.125	4.9	0.005	0.5	0.17	0.05	4.5	0.03	0.05	0.01	1
18	0.03	2.66	0.015	0.5	0.04	0.05	1.15	0.005	0.05	0.01	1
19	0.05	3.23	0.01	0.5	0.095	0.05	5.9	0.025	0.05	0.1	1
20	0.28	2.47	0.005	0.5	0.475	0.05	5.15	0.085	0.05	0.01	1
21	0.035	4.47	0.41	0.5	0.1	0.05	47	0.005	0.05	0.01	2
22	0.035	1.36	0.025	0.5	0.4	0.05	10.35	0.005	0.05	0.01	1
23	0.04	5.79	0.53	0.5	0.125	0.05	43.8	0.005	0.05	0.01	1
24	0.08	0.94	0.005	0.5	0.305	0.05	11.5	0.015	0.05	0.01	1
25	0.1	1.02	0.005	0.5	0.435	0.05	11.8	0.02	0.05	0.01	1
26	0.035	0.55	0.005	0.5	0.23	0.05	19.9	0.005	0.05	0.01	1
27	0.1	1.02	0.005	0.5	0.255	0.05	7.9	0.02	0.05	0.01	1
28	0.16	1.17	0.015	0.5	0.34	0.05	12.5	0.035	0.05	0.01	1
29	0.125	1	0.02	0.5	0.215	0.05	8.4	0.03	0.05	0.01	1
30	0.48	1.07	0.005	0.5	0.67	0.05	9.2	0.125	0.05	0.01	1
31	NS	NS	NS	NS	NS	NS	NS	NS	NS	NS	NS
32	0.13	1.29	0.01	0.5	0.25	0.05	15.1	0.035	0.05	0.01	1
33	0.25	1.27	0.015	0.5	0.41	0.05	12.85	0.07	0.05	0.01	1
34	0.12	1.18	0.015	0.5	0.185	0.05	7.3	0.025	0.05	0.01	1
35	0.205	1.23	0.005	0.5	0.235	0.05	5.05	0.045	0.05	0.01	1
36	NS	NS	NS	NS	NS	NS	NS	NS	NS	NS	NS
37	0.18	1.02	0.005	0.5	0.21	0.05	6.7	0.025	0.05	0.01	1
38	0.24	1.88	0.005	0.5	0.265	0.05	11.3	0.035	0.05	0.01	1
39	0.15	1.5	0.005	0.5	0.305	0.05	6.75	0.035	0.05	0.01	1
40	0.05	1.31	0.005	0.5	0.17	0.05	7.35	0.02	0.05	0.01	1
41	0.085	2.29	0.045	0.5	0.145	0.05	5.6	0.02	0.05	0.01	1

NS = insufficient sample size for analysis

Table A.3. Continued

Site No.	Tl (ppm)	Tm (ppm)	U (ppm)	V (ppm)	W (ppm)	Yb (ppm)	Zn (ppm)	Zr (ppm)	B (ppm)	Ba (ppm)	Ge (ppm)
1	0.08	0.005	0.03	4.7	0.01	0.02	6.8	0.05	2	0.05	0.1
2	0.08	0.005	0.025	2.35	0.01	0.015	5.8	0.05	2	0.05	0.1
3	0.075	0.005	0.03	1.1	0.01	0.015	7.8	0.05	2	0.05	0.1
5	0.075	0.005	0.025	2.75	0.01	0.015	7.2	0.05	2	0.05	0.1
6	0.18	0.015	0.005	1.15	0.01	0.095	85.2	0.05	2	0.05	0.1
12	0.055	0.005	0.03	1.8	0.01	0.02	9	0.05	2	0.05	0.1
13	0.08	0.005	0.055	3.75	0.09	0.025	17.4	0.05	2	0.05	0.1
14	0.07	0.005	0.025	2.25	0.01	0.015	7	0.05	2	0.05	0.1
15	0.085	0.005	0.03	2.5	0.01	0.015	9.2	0.05	2	0.05	0.1
16	0.08	0.005	0.02	2.65	0.01	0.01	6.6	0.05	2	0.05	0.1
17	0.155	0.015	0.11	1.15	0.01	0.1	21.4	0.05	2	0.05	0.1
18	0.12	0.005	0.07	1.4	0.01	0.015	16.2	0.05	2	0.05	0.1
19	0.145	0.005	0.095	1.1	0.01	0.06	9.4	0.05	2	0.05	0.1
20	0.235	0.03	0.07	0.8	0.01	0.19	25.8	0.05	2	0.05	0.1
21	0.15	0.005	0.065	1.45	0.03	0.005	29.4	0.05	2	0.05	0.1
22	0.08	0.005	0.005	1	0.01	0.015	118	0.05	2	0.1	0.1
23	0.115	0.005	0.01	1.8	0.01	0.005	36	0.05	6	0.05	0.1
24	0.14	0.005	0.14	1.3	0.01	0.05	206	0.05	2	0.05	0.1
25	0.19	0.01	0.165	1.95	0.01	0.06	554	0.05	2	0.1	0.1
26	0.005	0.005	0.11	2.05	0.01	0.005	6.8	0.05	2	0.05	0.1
27	0.185	0.01	0.19	0.9	0.01	0.065	196	0.05	2	0.05	0.1
28	0.25	0.02	0.26	1.7	0.01	0.115	970	0.5	2	0.2	0.1
29	0.18	0.015	0.235	0.9	0.01	0.08	321	0.05	2	0.05	0.1
30	0.26	0.06	0.93	1.6	0.01	0.325	1035	0.05	2	0.3	0.1
31	NS	NS	NS	NS	NS	NS	NS	NS	NS	NS	NS
32	0.19	0.02	0.3	1.1	0.01	0.105	431	0.05	2	0.1	0.1
33	0.245	0.035	0.365	1.1	0.01	0.2	489	0.05	2	0.15	0.1
34	0.18	0.01	0.175	0.7	0.01	0.065	79.4	0.05	2	0.05	0.1
35	0.185	0.02	0.335	0.75	0.01	0.13	80.2	0.05	2	0.05	0.1
36	NS	NS	NS	NS	NS	NS	NS	NS	NS	NS	NS
37	0.135	0.01	0.105	0.35	0.01	0.075	20	0.05	2	0.05	0.1
38	0.2	0.02	0.09	0.5	0.01	0.115	29.6	0.05	2	0.05	0.1
39	0.21	0.015	0.07	0.7	0.01	0.08	51.6	0.05	2	0.05	0.1
40	0.055	0.01	0.33	0.85	0.01	0.055	5	0.05	2	0.05	0.1
41	0.135	0.015	0.035	1.2	0.01	0.08	70.2	0.05	2	0.05	0.1

NS = insufficient sample size for analysis

Table A.3. Continued

Site No.	Hf (ppm)	In (ppm)	La (ppm)	Re (ppm)	Ta (ppm)	Y (ppm)	pH
1	0.01	0.005	0.15	0.001	0.01	0.215	2.3
2	0.01	0.005	0.12	0.001	0.01	0.185	2.2
3	0.01	0.005	0.1	0.001	0.01	0.165	2.2
5	0.01	0.005	0.135	0.001	0.01	0.185	2.2
6	0.01	0.005	0.345	0.001	0.01	1.735	4.4
12	0.01	0.005	0.115	0.001	0.01	0.19	2.2
13	0.01	0.005	0.16	0.001	0.01	0.335	2.3
14	0.01	0.005	0.075	0.001	0.01	0.125	2.2
15	0.01	0.005	0.09	0.001	0.01	0.155	2.2
16	0.01	0.005	0.065	0.001	0.01	0.11	2.2
17	0.01	0.005	0.425	0.001	0.01	1.175	2.8
18	0.01	0.005	0.07	0.001	0.01	0.19	2.3
19	0.01	0.005	0.115	0.001	0.01	0.57	2.6
20	0.01	0.005	0.8	0.001	0.01	2.3	3.1
21	0.01	0.005	0.21	0.001	0.01	0.16	5.7
22	0.01	0.005	0.245	0.001	0.01	0.34	4.3
23	0.01	0.005	0.2	0.001	0.01	0.16	5.3
24	0.01	0.005	0.335	0.001	0.01	0.895	3.2
25	0.01	0.005	0.38	0.001	0.01	1	3.3
26	0.01	0.005	0.25	0.001	0.01	0.135	3.3
27	0.01	0.005	0.405	0.001	0.01	1.035	3.2
28	0.01	0.005	0.52	0.001	0.01	1.895	3.7
29	0.01	0.005	0.565	0.001	0.01	1.31	3.2
30	0.01	0.005	1.39	0.001	0.01	5.47	3.5
31	NS	NS	NS	NS	NS	NS	NS
32	0.01	0.005	0.41	0.001	0.01	1.65	3.4
33	0.01	0.005	0.795	0.001	0.01	2.84	3.4
34	0.01	0.005	0.555	0.001	0.01	1.05	3.3
35	0.01	0.005	0.555	0.001	0.01	1.91	3.3
36	NS	NS	NS	NS	NS	NS	NS
37	0.01	0.005	0.6	0.001	0.01	0.745	3.6
38	0.01	0.005	0.87	0.001	0.01	1.305	2.8
39	0.01	0.005	0.495	0.001	0.01	1.13	3.3
40	0.01	0.005	0.165	0.001	0.01	0.9	3
41	0.01	0.005	0.275	0.001	0.01	0.89	3.2

NS = insufficient sample size for analysis

Table A.4. Results of total digestion on stream sediments at Pascua-Lama.

Site_No	Field #	As (ppm)	Hg (ppb)	Al (%)	Sb (ppm)	Ba (ppm)	Be (ppm)	Bi (ppm)	Cd (ppm)	Ca (%)	Ce (ppm)	Cs (ppm)
1	2	598	2610	5.59	11.8	200	0.9	6.59	0.18	0.29	34	10.45
2	7	391	3290	7.39	5.6	150	0.3	2.68	0.06	0.34	9.18	3.6
3	12	302	9820	8.18	19.4	1350	1.05	12.55	0.24	0.35	37.2	8.1
5	17	423	3690	7.69	15.2	140	1.15	9.43	0.3	0.35	35.6	14.1
6	22	406	210	7.33	17.3	1330	4.25	2.02	1.12	0.71	72.2	37.3
12	50	387	15930	7.63	17.5	180	1.2	10.6	0.3	0.35	37.5	10.4
13	67	384	3810	7.73	15.5	430	1.3	8.45	0.38	0.4	34.7	16
14	72	408	8570	8.15	19.3	630	1.15	13.25	0.28	0.29	37.8	10.7
15	77	396	6580	8.37	18.8	680	1.35	11.7	0.4	0.34	33.6	16.2
16	82	492	5920	8.7	20.7	780	1.1	13.25	0.32	0.24	35.9	14.85
17	87	117	140	8.29	2	510	2.65	1.48	0.48	0.69	80.5	38
18	94	387	2540	10.1	14.6	900	1.55	9.74	0.5	0.31	44.1	23.1
19	99	357	580	9.76	5	600	2.05	3.57	0.38	0.76	59.8	24.2
20	168	437	160	7.33	14.5	2230	3.35	2.17	0.4	0.51	75.3	36.6
21	169	1290	540	7.73	8.1	1270	2.65	1.91	1.02	3.56	55.5	67.1
22	170	842	210	7.8	14	1460	2.8	2.44	1.6	0.65	83.4	31
23	200	493	90	8.37	4.8	490	2.25	1.04	0.58	2.75	49.6	79.4
24	203a	74	290	7.56	3.6	800	2.6	2.3	2.76	1.03	75.3	10
25	204	72	590	7.98	3.1	870	3	2.53	5.52	1.2	91.3	12.05
26	258	17	10	8.02	0.7	540	2.4	0.69	0.26	2.26	74.3	15.65
27	260	79	1130	7.85	3.7	830	2.85	2.48	2.86	1.03	86.3	9.55
28	264	101	1030	8.24	3.7	940	3.15	2.95	10.45	1.11	88.6	10.45
29	266	85	1080	7.91	3.8	840	2.5	2.94	4.24	1.09	77.8	8.7
30	268	106	810	9.41	3.5	630	3.75	1.95	13.55	1.11	75.5	9.65
31	269	17	40	6.14	0.9	380	2.3	1.16	0.4	1.87	83.5	19.2
32	271	117	500	8.73	4.5	810	3.15	2.98	6.36	1.18	89.6	13.8
33	273	116	460	9.06	4.1	730	3.2	2.28	8.52	1.15	82.1	13.25
34	275	124	950	8.67	4.9	950	2.65	3.04	1.62	1.04	77.7	10.35
35	277	85	540	8.39	3.6	840	2.9	2.65	1.3	0.96	76.9	9.65
36	285	124	1030	8.9	4.7	640	2.95	2.5	0.46	0.89	70.1	10.5
37	295	127	610	8.44	5	720	2.45	2.82	0.62	1.51	88.7	10.85
38	300	228	2430	8.02	8.9	1310	2.1	5.22	0.48	1.33	83.9	15.65
39	290	146	810	8.24	5.9	990	2.55	3.6	1.34	1.12	88.3	14.25
40	281	43	40	8.87	1.3	670	2.25	1.57	0.54	0.79	65.7	7.65
41	302	352	330	9.35	8.6	690	2.75	2.99	1.66	1.33	97.6	25.8

Table A.4. Continued

Site_No	Cr (ppm)	Co (ppm)	Cu (ppm)	Ga (ppm)	Ge (ppm)	Fe (%)	La (ppm)	Pb (ppm)	Li (ppm)	Mg (%)	Mn (ppm)	Mo (ppm)
1	23	2.6	151	19.8	1.3	14.1	15.5	366	9.8	0.29	260	6.8
2	22	1	120	9.2	0.7	6.92	4	502	3.6	0.35	275	2
3	21	3.8	130	27.3	1.6	4.25	17.5	532	11	0.32	255	5.4
5	28	3.2	135	26.2	1.6	6.69	16	406	13	0.42	310	7.4
6	23	10.2	52	22	2.4	4.67	32.5	1590	41.4	0.57	2450	8.4
12	31	4.8	170	26.5	1.6	6.03	16	438	12.8	0.38	300	7.4
13	26	3.8	139	27.1	1.6	4.58	15.5	374	15.6	0.45	335	7.6
14	22	3.4	133	27.8	1.6	5.39	17	524	12.2	0.36	265	6
15	25	4.2	132	29.3	1.6	5.16	15	428	16.4	0.43	325	7
16	19	2.2	100	29.9	1.5	5.43	16.5	526	13.8	0.39	275	7.2
17	38	17.4	111	24.4	1.9	6.46	36.5	72	22.8	0.76	775	6.2
18	20	3.8	103	33.7	1.6	4.56	23.5	458	22	0.69	480	7.4
19	44	10.2	105	26.6	1.6	5.87	27	272	21.8	1.06	955	3.6
20	29	11	59	21	2.3	6.91	34.5	930	46.4	0.55	1875	4.2
21	25	37.4	432	18.5	2.6	6.17	24.5	100	81	1.03	2340	4
22	27	11.2	92	24.2	2.1	6.79	37.5	1955	33.6	0.53	5450	14.2
23	26	43.2	112	19	2	5.44	26.5	32	46	1.23	2400	2.8
24	32	17.6	284	20	1.6	3.93	34	108	38.2	0.74	2250	11.8
25	44	25.4	417	21	1.7	4.66	41.5	104	45.4	0.83	4510	13.8
26	71	18.4	76	21.3	1.7	4.44	36	26	51.2	1.71	1525	5
27	39	18.4	320	20.5	1.7	4.51	39.5	122	36.6	0.73	2310	13.2
28	49	32.8	577	19.6	1.6	4.89	39	130	36.2	0.76	6440	21.4
29	36	22.2	332	20.6	1.7	4.42	35.5	128	31.2	0.8	3110	12.6
30	30	39.8	869	17.9	1.3	3.73	33	126	29.6	0.75	8600	31.6
31	86	15.8	196	21.1	1.8	3.85	37	46	75.4	1.37	1520	9.6
32	38	25.6	446	22.1	1.6	4.43	41.5	150	37.8	0.95	4020	13.2
33	35	30.6	563	21.3	1.6	4.24	37.5	144	36.2	0.95	5950	17
34	39	17.8	308	22	1.5	5.29	37	170	30.2	0.86	1960	11.4
35	42	19.2	326	21.9	1.6	5.24	36	118	30.2	0.81	1700	14.4
36	37	8.6	284	19	1.6	7.94	33	164	27.8	0.63	895	15.8
37	45	11.4	170	20.3	1.7	5.43	42	164	27.4	0.81	1280	8.4
38	46	10.8	125	23.8	1.8	7.71	41	280	29.4	0.89	1110	2.8
39	41	18.2	298	23.7	1.8	6.24	42	202	37.6	0.84	1740	8.2
40	43	21.2	105	23.9	1.5	5.09	30	38	19.8	1.03	775	11.4
41	45	15	218	26.2	2.1	5.02	46.5	342	37.6	1	2130	2.2

Table A.4. Continued

Site No	Ni (ppm)	Nb (ppm)	P (ppm)	K (%)	Rb (ppm)	Ag (ppm)	Na (%)	Sr (ppm)	Ta (ppm)	Te (ppm)	Tl (ppm)	Th (ppm)
1	6.6	6.8	660	1.81	83.8	8.55	0.81	195	0.5	2.35	3.08	8.8
2	2.4	3.2	660	2.37	35.8	3.75	1	265	0.15	1.1	1.32	2.4
3	6.4	9.2	640	2.55	94.2	21.4	1.01	289	0.4	3.3	3.52	9
5	9.4	8.8	740	2.43	114.5	14.85	1	272	0.55	3.9	4.3	9.8
6	13	14.6	900	2.1	163	1.8	1.2	166	0.55	0.4	3.02	10
12	10.4	9.8	690	2.43	108.5	19.05	0.99	263	0.45	4.45	4.06	9
13	9.8	8	680	2.38	123.5	13.5	1.02	255	0.4	3.85	4.1	8.8
14	6.2	9	680	2.6	109.5	18.6	0.96	293	0.4	4.35	4.6	9.6
15	9.6	7.8	670	2.52	125	18.85	1.02	274	0.5	4.25	4.36	9.2
16	5	8.6	690	2.73	117	18.45	0.92	302	0.5	4.8	4.88	9.8
17	20.8	14	1190	1.94	180.5	1.3	1.18	268	0.65	0.5	3.38	19
18	6	8.6	790	2.85	181.5	11.5	1.11	362	0.45	4.5	5.88	11.8
19	14.2	11.8	1010	2.65	218	2.45	1.18	258	0.55	2.55	6.62	19.8
20	11	14.8	970	2.03	157.5	1.65	1.29	163	0.8	0.35	2.68	12.2
21	21.6	10.6	1030	1.56	106	3.05	1.25	318	0.45	0.9	1.94	8.8
22	11.2	12.8	1320	2.26	168	1.85	1.08	202	0.6	0.65	3.16	12.8
23	21	11	1070	1.6	105.5	1.4	1.44	350	0.5	0.5	1.46	8.2
24	21.2	12.4	780	2.14	131	2.4	2.14	212	0.6	0.9	2.04	15.2
25	29.6	14.6	940	2.1	134.5	2.85	2.13	246	0.8	0.8	2.06	21.6
26	35	14.4	1370	1.85	109	1.5	1.99	391	0.75	0.05	0.62	17.2
27	22	12.6	800	2.11	131	2.5	2.18	214	0.85	1	2.16	17.2
28	38	12.4	880	1.93	118	2.55	1.93	203	0.65	1.05	2.52	18.6
29	23.8	13	810	2.07	123.5	2.85	2.14	216	0.75	1.1	2.52	20.2
30	29.6	9.4	850	1.61	98.8	2.5	1.66	206	0.55	1	2.5	12.2
31	32.6	18.8	1980	1.36	109	1.75	1.66	172	1.05	0.05	0.56	32
32	29.6	12.4	850	2	132	3	1.85	219	0.6	1.15	2.94	17.2
33	28	11	890	1.97	126	2.5	1.87	228	0.5	1.15	2.84	14.2
34	19.4	11.2	910	2.06	117	3.4	1.93	253	0.6	1.55	2.82	18.2
35	22	11.4	950	1.97	121	2.75	1.94	232	0.7	1.2	2.76	15.8
36	14.6	11.2	740	1.81	109.5	3.75	1.89	170	0.75	1.25	2.08	17.2
37	17	13.6	1070	1.84	108.5	3.45	2.1	262	0.9	1.1	2.16	16.4
38	16.8	13.8	1020	1.99	127.5	6.6	1.76	252	0.95	2.15	3.34	19
39	19.2	12.8	970	2.05	127	4	1.91	235	0.85	1.55	3.1	15.8
40	22.2	9	890	2.27	147	0.6	1.73	256	0.5	1.65	3.78	21.2
41	16.6	12.8	1000	2.45	193	3.3	1.74	268	0.75	2.1	4.84	20.2

Table A.4. Continued

Site_No	Ti (%)	W (ppm)	U (ppm)	V (ppm)	Y (ppm)	Zn (ppm)
1	0.23	2.3	1.2	142	5.8	74
2	0.28	1	0.4	99	1.9	82
3	0.29	4.3	1.4	83	6	78
5	0.3	3.1	1.4	106	6.4	84
6	0.37	2.7	2.4	70	41.2	576
12	0.32	3.7	1.6	100	7.5	88
13	0.28	2.6	1.2	93	5.5	98
14	0.3	3.4	1.4	90	5.8	74
15	0.29	2.8	1.4	96	5	102
16	0.3	3.5	1.2	97	4.9	74
17	0.44	2.2	4.4	122	27.6	360
18	0.36	2.9	1.6	115	6.5	124
19	0.44	2.2	2.4	107	14.8	174
20	0.42	2.2	2.4	84	28.3	344
21	0.53	3.4	2	160	26.9	334
22	0.35	3.1	2.4	87	30.9	392
23	0.6	2	1.6	180	21.8	260
24	0.31	2.3	11.4	79	24.3	624
25	0.38	2.7	14.4	104	31.7	1140
26	0.56	2	21	136	26.9	96
27	0.34	2.5	11.2	91	25.7	688
28	0.34	2.7	19.4	93	34.4	2020
29	0.35	2.7	10.2	90	26	886
30	0.27	4.5	28.8	66	47.2	2840
31	0.46	5.6	264	110	43	126
32	0.35	3	10.4	83	33	1525
33	0.32	2.2	10.8	76	33.9	1800
34	0.37	2.4	6.6	97	20.9	462
35	0.36	2.1	9.8	93	25.2	636
36	0.3	2.2	3	78	18.9	202
37	0.39	2.4	3.4	94	25	236
38	0.43	4.5	2	120	20.4	206
39	0.41	2.7	3.6	94	23.1	446
40	0.34	1.4	8.2	123	18.2	92
41	0.4	7.1	3	97	24.6	422

Table A.5. Results of ICP-MS analysis of stream waters.

Site no.	Sample no.	pH	Ag µg/l	Al mg/l	As µg/l	Ba µg/l	Be µg/l	Bi µg/l	Ca mg/l	Cd µg/l	Co µg/l	Cr µg/l	Cu µg/l	Fe mg/l	Hg µg/l	K mg/l	Mg mg/l	Mn µg/l	Mo µg/l	Na mg/l	Ni µg/l
1	174	3.0	0.05	34.10	7.00	19.10	1.00	0.05	103.00	7.80	32.20	2.50	1830.00	26.30	1.00	3.05	15.70	2980.00	0.10	7.25	23.40
2	175	3.3	0.05	42.10	9.00	19.30	1.00	0.05	133.50	7.70	32.40	2.50	2290.00	33.20	1.00	3.10	19.30	3760.00	0.10	7.30	22.40
3	177	3.0	0.05	81.10	77.00	12.20	2.00	0.05	158.00	15.00	61.90	6.50	4570.00	96.30	1.00	4.05	24.70	6010.00	0.10	7.20	44.20
5	178	2.8	0.05	118.00	117.00	2.80	2.50	0.05	195.00	22.60	89.40	10.00	6760.00	143.50	1.00	4.90	30.80	8550.00	0.10	7.70	65.80
6	180	7.1	0.05	0.29	4.00	31.40	0.50	0.05	103.00	0.10	1.84	0.50	16.20	2.19	1.00	2.20	12.40	1095.00	0.10	5.50	2.00
12	179	2.8	0.05	139.50	118.00	2.90	2.50	0.05	230.00	23.10	90.40	10.00	7890.00	165.50	1.00	5.15	36.20	9880.00	0.10	7.90	65.80
13	182	2.8	0.05	141.00	152.00	2.85	3.00	0.05	217.00	27.30	103.00	12.00	8190.00	176.50	1.00	5.10	33.90	9540.00	0.10	7.60	75.40
14	183	2.8	0.10	140.50	164.00	2.90	3.00	0.05	212.00	28.60	106.50	12.00	8190.00	179.00	1.00	5.15	33.40	9510.00	0.10	7.10	77.20
15	184	2.7	0.05	146.00	167.00	3.05	3.00	0.05	227.00	28.20	106.50	12.00	8630.00	193.50	1.00	5.05	33.90	9870.00	0.10	6.55	78.60
16	187	2.8	0.05	152.50	182.00	2.90	3.00	0.05	221.00	28.60	111.50	13.00	9070.00	202.00	1.00	5.30	35.00	10270.00	0.10	6.80	82.20
17	185	6.6	0.05	0.23	1.00	7.20	0.50	0.05	28.20	0.20	0.38	0.50	21.80	0.43	1.00	1.85	5.73	42.80	0.30	2.60	0.80
18	188	2.5	0.05	330.00	343.00	1.70	5.50	0.05	302.00	71.90	246.00	30.50	24000.00	505.00	1.00	10.80	68.70	22600.00	0.30	6.60	180.50
19	189	6.1	0.05	0.28	1.00	2.90	0.50	0.05	37.70	0.50	2.38	0.50	68.60	0.28	1.00	1.50	5.65	356.00	0.30	3.50	2.20
20	190	7.1	0.05	0.22	6.00	32.50	0.50	0.05	91.70	0.10	1.14	0.50	3.80	1.00	1.00	1.95	11.70	811.00	0.10	5.35	1.20
21	172	6.2	0.05	0.26	8.00	15.55	0.50	0.05	115.50	1.90	11.30	0.50	155.50	4.96	1.00	18.85	17.70	1525.00	1.80	154.50	11.00
22	193	8.2	0.05	0.02	22.00	34.30	0.50	0.05	69.00	0.10	0.18	0.50	0.60	0.21	1.00	1.30	8.80	244.00	0.30	3.95	0.20
23	173	7.8	0.05	0.05	800.00	14.50	0.50	0.05	106.00	0.10	3.64	0.50	1.30	0.26	1.00	25.20	17.70	555.00	3.80	195.00	4.80
24	205	6.6	0.05	0.05	1.00	34.70	0.50	0.05	51.90	1.10	13.00	0.50	1.80	0.14	1.00	1.30	11.35	786.00	5.00	5.45	11.20
25	206	7.0	0.05	0.03	1.00	20.10	0.50	0.05	39.00	0.70	1.06	0.50	2.30	0.10	1.00	1.25	5.81	824.00	4.50	4.75	1.40
26	207	7.8	0.05	0.01	1.00	31.70	0.50	0.05	27.90	0.10	0.06	0.50	0.40	0.08	1.00	0.45	2.69	4.45	11.20	5.10	0.20
27	208	7.4	0.05	0.02	1.00	21.30	0.50	0.05	38.20	1.60	3.30	0.50	1.10	0.09	1.00	1.30	7.96	1200.00	2.60	4.45	4.40
28	210	7.2	0.05	0.02	1.00	22.90	0.50	0.05	39.60	2.10	4.42	0.50	1.50	0.10	1.00	1.35	8.34	1415.00	2.60	4.70	5.40
29	211	7.1	0.05	0.02	1.00	20.20	0.50	0.05	41.00	2.50	4.94	0.50	2.90	0.11	1.00	1.35	8.44	1480.00	2.40	4.50	6.20
30	212	7.1	0.05	0.12	1.00	19.90	0.50	0.05	39.10	2.70	5.04	0.50	12.60	0.32	1.00	1.25	8.39	1440.00	2.60	4.45	6.80
31	213	7.4	0.05	0.00	1.00	15.80	0.50	0.05	26.70	0.10	0.12	0.50	0.10	0.07	1.00	0.50	3.53	1.60	5.50	2.55	0.20
32	215	7.1	0.05	0.02	1.00	17.45	0.50	0.05	43.60	2.90	5.92	0.50	8.40	0.23	1.00	1.45	8.86	1785.00	1.90	4.55	7.00
33	237	5.3	0.05	0.03	1.00	17.75	0.50	0.05	48.40	3.60	7.08	0.50	48.80	0.40	1.00	1.65	9.65	2070.00	1.30	4.75	8.40
34	238	5.2	0.05	0.18	1.00	17.95	0.50	0.05	49.70	3.70	7.66	0.50	95.10	0.45	1.00	1.70	9.85	2200.00	1.00	4.90	8.60
35	239	4.6	0.05	1.59	1.00	21.50	0.50	0.05	54.00	4.20	8.42	0.50	127.50	0.51	1.00	1.80	10.60	2480.00	1.30	5.05	9.60
36	241	4.0	0.05	7.26	1.00	29.90	0.50	0.05	84.70	10.00	18.00	0.50	313.00	1.16	1.00	2.85	14.80	6110.00	0.10	6.55	21.60
37	242	4.8	0.05	10.90	1.00	26.80	1.00	0.05	98.60	12.20	21.70	0.50	395.00	1.62	1.00	3.40	16.70	7430.00	0.10	7.05	26.00
38	243	3.5	0.05	14.20	1.00	18.45	1.50	0.05	107.50	15.90	26.30	0.50	507.00	2.16	1.00	3.80	17.50	8640.00	0.10	6.60	33.60
39	250	3.9	0.05	8.19	1.00	30.80	0.50	0.05	85.80	11.00	18.80	0.50	343.00	1.31	1.00	3.10	15.25	6380.00	0.10	6.70	22.80
40	252	6.0	0.05	0.04	1.00	9.80	0.50	0.05	27.40	0.10	1.36	0.50	0.50	0.08	1.00	0.95	5.66	30.30	2.70	3.55	1.20

Table A.5. Continued

Site no.	P mg/l	Pb µg/l	Sb µg/l	Se µg/l	Sn µg/l	Sr µg/l	Ti µg/l	Tl µg/l	U µg/l	V µg/l	Zn µg/l
1	0.10	6.00	0.05	1.00	0.50	365.00	1.00	0.80	2.15	1.00	1430.00
2	0.10	8.00	0.05	1.00	0.50	360.00	1.00	0.85	2.25	1.00	1785.00
3	0.10	2.00	0.15	1.00	0.50	502.00	1.00	1.30	4.00	22.00	3350.00
5	0.10	2.00	0.05	1.00	0.50	670.00	1.00	1.85	5.55	32.00	4890.00
6	0.10	2.00	0.20	1.00	0.50	180.50	1.00	0.30	0.25	1.00	81.00
12	0.10	2.00	0.05	1.00	0.50	680.00	1.00	1.85	5.70	32.00	5790.00
13	0.10	2.00	0.10	1.00	0.50	751.00	1.00	2.15	7.05	40.00	5700.00
14	0.10	2.00	0.50	1.00	0.50	769.00	1.00	2.15	6.95	41.00	5720.00
15	0.10	2.00	0.10	1.00	0.50	750.00	1.00	2.05	6.90	42.00	6080.00
16	0.10	2.00	0.10	1.00	0.50	785.00	1.00	2.20	7.50	47.00	6270.00
17	0.10	2.00	0.05	1.00	0.50	74.20	19.00	0.05	0.05	1.00	28.00
18	0.10	2.00	0.15	1.00	0.50	1545.00	1.00	3.55	17.00	120.00	15400.00
19	0.10	2.00	0.15	1.00	0.50	77.80	1.00	0.05	0.10	1.00	114.00
20	0.10	2.00	0.30	1.00	0.50	151.50	1.00	0.15	0.25	1.00	45.00
21	0.10	2.00	4.15	2.00	0.50	563.00	1.00	0.50	0.15	1.00	383.00
22	0.10	2.00	0.40	1.00	0.50	114.50	1.00	0.05	0.20	1.00	5.00
23	0.10	2.00	6.85	3.00	0.50	645.00	1.00	0.45	2.00	5.00	7.50
24	0.10	2.00	0.05	1.00	0.50	137.00	1.00	0.05	0.45	1.00	3550.00
25	0.10	2.00	0.05	1.00	0.50	83.00	1.00	0.05	1.25	1.00	2350.00
26	0.10	2.00	0.05	1.00	0.50	102.50	1.00	0.05	7.00	1.00	2040.00
27	0.10	2.00	0.05	1.00	0.50	75.20	1.00	0.05	0.50	1.00	1935.00
28	0.10	2.00	0.05	1.00	0.50	80.10	1.00	0.05	0.45	1.00	845.00
29	0.10	24.00	0.05	1.00	0.50	79.70	1.00	0.05	0.25	1.00	745.00
30	0.10	8.00	0.05	1.00	0.50	82.90	1.00	0.05	0.25	1.00	701.00
31	0.10	2.00	0.05	1.00	0.50	101.50	1.00	0.05	10.10	1.00	536.00
32	0.10	2.00	0.05	1.00	0.50	77.00	1.00	0.05	0.15	1.00	430.00
33	0.10	2.00	0.05	1.00	0.50	78.10	1.00	0.10	0.40	1.00	349.00
34	0.10	2.00	0.05	1.00	0.50	77.40	1.00	0.15	0.95	1.00	311.00
35	0.10	2.00	0.05	2.00	0.50	79.30	1.00	0.15	1.45	1.00	116.00
36	0.10	2.00	0.05	1.00	0.50	110.00	1.00	0.30	2.25	1.00	16.50
37	0.10	2.00	0.05	2.00	0.50	112.00	1.00	0.45	2.50	1.00	39.50
38	0.10	2.00	0.05	3.00	0.50	98.90	1.00	0.55	2.65	1.00	2.50
39	0.10	2.00	0.05	1.00	0.50	110.50	1.00	0.40	2.05	1.00	0.50
40	0.10	2.00	0.05	1.00	0.50	52.80	1.00	0.05	1.50	1.00	1.50

Table A.6. Geochemistry of -53μm fractions of surficial deposits at Pascua-Lama by aqua regia digestion.

Media	Field no.	UTM-E	UTM-N	Elev	pH	Au (ppb) -212+106μm	Au (ppb) -106+53μm	Au (ppb) -53μm	Al (%)	Sb (ppm)	As (ppm)	Ba (ppm)	Be (ppm)	Bi (ppm)
alluvial	102	19404134	6756029	4299	6.9	30	30	185	1.56	2.6	472	310	0.35	5.84
alluvial	103	19404124	6756025	4299	4.7	45	180	125	1.33	1.7	413	240	0.3	5.33
alluvial	104	19404114	6756020	4299	7.1	55	90	195	1.83	2.8	495	280	0.35	6.71
alluvial	109	19405446	6755764		6.8	10	10	30	1.4	1.2	133.5	220	1.6	3.83
alluvial	110	19405467	6755746	4083	4.5	5	5	25	1.54	1.2	128	220	1.05	3.7
alluvial	111	19405601	6755713	3942	6.1	15	190	35	1.86	2.3	191.5	430	1.45	3.87
alluvial	115	19405977	6755642	4107	5.7	15	105	45	1.8	1.6	208	550	1.1	4.76
alluvial	116	19406061	6755636	4155	8	15	25	65	1.42	2.9	298	370	0.6	5.23
alluvial	117	19406193	6755560	4164	7.1	10	10	40	2.13	1.7	234	370	0.55	5.67
alluvial	119	19406239	6755490	4128	5.6	10	5	25	1.41	1.1	122.5	220	1.2	4.02
alluvial	120	19406393	6755488	4065	7.6	5	5	25	1.08	2.6	156	360	1.6	3.76
alluvial	121	19406504	6755494	4011	7	5	10	35	1.47	2.4	157	380	1.45	3.9
alluvial	125	19406864	6755273	3835	6.9	30	10	45	1.77	3.1	202	370	1.4	2.61
alluvial	126	19406914	6755250	3954	4.6	10	30	50	1.6	2.4	171.5	340	1.55	2.18
alluvial	127	19407073	6755191	4035	6.9	5	5	25	1.2	4.1	195	500	1.55	2.13
alluvial	128	19407119	6755122	3942	7	10	10	65	1.1	4.6	238	450	1.4	2.23
alluvial	131	19407300	6755044	3891	6.8	5	5	10	1.94	0.5	23.8	160	1.4	0.66
alluvial	132	19407333	6755030	3996	6.95	5	5	15	1.77	0.4	22.6	160	1.7	0.53
alluvial	133	19407500	6754942	3879	7.25	10	5	15	1.97	0.6	37	180	1.4	0.71
alluvial	136	19407887	6754690	3942	7.5	5	5	15	1.91	0.8	39.8	230	1	0.76
alluvial	144	19404631	6755337	4374	7.1	130	115	840	1.15	13.1	746	330	0.15	9.35
alluvial	145	19404670	6755349	4133	5.2	135	155	840	1.22	9	646	340	0.15	8.47
alluvial	146	19404727	6755355	4182	7.3	150	150	865	0.77	11.7	720	330	0.05	9.09
alluvial	147	19404762	6755284	4272	4.7	95	115	975	1.08	11.6	648	140	0.2	10.6
alluvial	148	19404932	6755257	4059	7.4	130	160	1050	0.53	16.4	738	200	0.05	12.45
debris	14	19409459	6753605	3756	3.5	40	195	255	0.78	4.7	476	190	0.35	6.85
debris	19	19409416	6753736	3797	3.5	25	85	290	0.81	4.8	516	210	0.25	8.41
debris	25	19409129	6753684	3684	4.2	5	10	65	1.72	5.4	572	410	2.15	3.74
debris	52	19409192	6754140	3705	3.5	5	345	200	1.09	4.9	450	220	0.05	5.52

Table A.6. Continued

Media	Field no.	UTM-E	UTM-N	Elev	pH	Au (ppb) -212+106μm	Au (ppb) -106+53μm	Au (ppb) -53μm	Al (%)	Sb (ppm)	As (ppm)	Ba (ppm)	Be (ppm)	Bi (ppm)
debris	69	19408242	6754491	3810	4.1	25	140	300	1.29	3.5	468	200	0.35	5.26
debris	74	19407493	6754860	3915	3.7	25	365	260	1.32	3	419	150	0.35	5.98
debris	75	19407503	6754870	3915	4.1	15	20	280	1.34	3.7	436	230	0.35	5.64
debris	79	19406397	6755270	3798	4.2	25	35	225	1.85	3.4	367	270	0.7	5.68
debris	80	19406407	6755280	3798	3.6	25	65	175	1.87	2.9	358	310	0.6	5.63
debris	84	19405392	6755433	4146	3.7	30	90	330	1.92	4	471	350	0.55	6.36
debris	85	19405402	6755443	4146	3.5	45	45	360	1.9	4.6	492	300	0.45	7.06
debris	89	19405422	6755520	4098	3.8	30	55	220	2.28	2.8	359	390	1	5.24
debris	90	19405430	6755632	4098	4.3	40	110	445	1.88	5.3	502	430	0.55	7.5
debris	91	19405473	6755426	4098	3.8	85	70	320	2.02	4.4	478	410	0.75	6.62
debris	92	19405601	6755500	4098	3.9	30	165	190	2.34	2.6	342	410	0.85	4.77
debris	96	19404355	6755587	4272	4.3	55	120	355	1.56	5.8	562	360	0.25	11.2
debris	97	19404355	6755587	4272	4.5	55	70	440	1.39	12.3	600	220	0.75	12.9
debris	101	19404449	6755928	4299	4.2	45	120	295	1.97	4	602	350	0.35	8.15
debris	156	19409754	6753836		3.3	30	555	330	1.19	4.1	380	230	0.3	5.46
debris	157	19409744	6753399	3882	4.3	10	25	95	1.25	3.6	323	340	0.65	4.29
debris	158	19409890	6753583	3828	4.7	45	50	120	1.11	3.8	303	330	1.35	3.04
debris	159	19408111	6754439	3918	4.1	15	30	185	1.4	3.4	368	230	0.35	5.87
debris	160	19407882	6754331	3909	5.1	25	30	155	2.37	2.7	258	270	0.7	4.76
debris	161	19407594	6754766	3942	4.5	10	15	180	2.35	2.6	256	300	0.5	4.35
debris	162	19407471	6754855	3897	3.7	15	20	180	1.43	3	331	290	0.4	4.81
debris	163	19407048	6754872	3915	4.7	30	35	195	2	3	316	320	0.85	5.31
debris	164	19406912	6755007	3978	4.2	25	45	225	1.73	3.8	395	250	0.3	6.2
debris	165	19406250	6755044	3894	4.5	30	55	270	1.6	3.8	417	190	0.3	7.25
debris	304	19399547	6757587		3.9	20	40	80	1.7	2	190.5	390	0.85	4.33
debris	305	19398916	6757668	3957	4.7	45	145	190	1.91	2.6	219	490	0.6	6.18
debris	306	19398733	6757798	4212	8.3	35	55	250	1.56	3.7	356	480	0.9	6.97
debris	307	19398605	6757771	4042	9	60	295	490	1.32	4.8	380	480	0.6	10.75
debris	308	19398520	6757940	3996	9.5	40	190	285	1.74	3.9	292	590	1	9.17
debris	309	19398452	6757934	3972	9.9	60	75	435	1.63	4	368	490	0.75	7.28
debris	310	19398401	6758071	3912	4.8	30	115	215	1.73	2.8	218	540	0.75	6.02
debris	311	19398224	6758140	4002	4.7	25	75	210	1.56	3.4	316	370	0.75	7.04
debris	312	19398202	6758311	3975	5.1	60	80	355	1.35	4.1	288	490	0.8	8.05

Table A.6. Continued

Field no.	B (ppm)	Cd (ppm)	Ca (%)	Cr (ppm)	Co (ppm)	Cu (ppm)	Ga (ppm)	Ge (ppm)	Fe (%)	La (ppm)	Pb (ppm)	Mg (%)	Mn (ppm)	Hg (ppm)	Mo (ppm)	Ni (ppm)	P (ppm)	K (%)
102	10	0.16	0.08	20	4.8	79.4	6.1	0.1	5.64	10	308	0.54	395	0.31	3.4	12	750	0.69
103	10	0.18	0.11	23	4.4	75.4	5.6	0.1	5.81	10	228	0.57	350	0.41	2	11	780	0.75
104	10	0.24	0.09	20	5	95.8	6.7	0.1	5.69	10	306	0.6	450	0.31	4.4	8	840	0.7
109	10	0.44	0.38	10	7.4	200	4.5	0.1	4.05	20	76	0.39	585	0.21	20.2	8	580	0.46
110	10	0.32	0.27	11	5	157.5	5.2	0.1	4.29	30	68	0.43	430	0.18	21.8	9	640	0.49
111	10	0.54	0.31	15	9.6	88.4	5.9	0.1	5.2	30	104	0.54	1030	0.19	6.4	10	820	0.48
115	10	0.88	0.42	19	12	185.5	5.9	0.1	4.64	20	134	0.63	970	0.38	12.4	14	700	0.43
116	10	0.64	0.37	19	10.2	137	5.2	0.1	4.43	10	186	0.58	775	0.72	8.6	12	690	0.37
117	10	0.4	0.46	19	5.4	178	7.8	0.1	5.8	10	132	0.89	415	0.24	25.4	9	870	0.69
119	10	0.56	0.43	13	7.8	193	5.1	0.1	4.16	20	82	0.52	615	0.16	15.8	9	620	0.45
120	10	1	0.28	10	8	98.9	3.6	0.1	4.42	30	54	0.29	1265	0.18	3.8	9	690	0.43
121	10	0.88	0.45	15	10.4	101.5	4.9	0.1	4.92	30	102	0.52	1690	0.27	4.4	13	840	0.44
125	10	0.74	0.23	12	8.6	138	4.9	0.1	5.33	30	244	0.43	2150	0.16	4	8	890	0.46
126	10	0.92	0.25	10	7	146.5	4.6	0.1	4.82	30	302	0.41	1765	0.12	4	8	930	0.46
127	10	1.96	0.25	8	9.2	108.5	4	0.1	5.33	30	266	0.31	3110	0.27	3	7	920	0.54
128	10	1.54	0.23	10	9	101.5	3.8	0.1	5.21	20	260	0.32	2710	0.89	3.6	6	870	0.49
131	10	0.24	0.32	15	13	309	6.8	0.1	5.43	10	36	0.82	580	0.04	20.4	11	1020	0.39
132	10	0.24	0.32	13	12.2	298	6.3	0.1	5.1	10	18	0.74	540	0.01	19.2	9	990	0.36
133	10	0.22	0.33	13	8.8	281	6.7	0.1	5.06	10	32	0.83	470	0.01	18.8	7	920	0.38
136	10	0.26	0.37	13	8.4	279	6.7	0.1	5.09	10	68	0.76	500	0.04	16.4	8	960	0.42
144	10	0.2	0.08	5	1.6	143.5	5.3	0.1	5.13	10	988	0.23	180	0.21	36.2	2	540	0.55
145	10	0.2	0.07	7	2.6	126.5	5.2	0.1	4.89	10	786	0.33	260	0.28	25.2	5	590	0.5
146	10	0.14	0.04	5	1.4	85.6	3.7	0.1	3.19	10	1000	0.18	140	0.38	45	1	340	0.36
147	10	0.26	0.05	8	2	97.1	4.8	0.1	4.07	10	824	0.28	210	0.35	38.6	4	480	0.44
148	10	0.2	0.04	4	0.8	67.3	3	0.1	2.61	10	1115	0.13	95	0.37	54.7	1	260	0.34
14	10	0.24	0.12	11	3	163.5	5	0.1	7.61	10	326	0.31	365	1.53	6.6	5	480	0.59
19	10	0.18	0.03	6	2.2	113.5	5.3	0.1	8.15	10	238	0.3	260	1.23	6.8	2	520	0.69
25	10	0.38	0.21	10	18	212	4.7	0.1	10.95	20	1515	0.31	3360	0.55	6.8	8	810	0.37
52	10	0.12	0.05	9	3.8	153	6.2	0.1	9.14	10	164	0.33	315	1.92	6.6	4	630	0.67

Table A.6. Continued

Field no.	Sc (ppm)	Se (ppm)	Ag (ppm)	Na (%)	Sr (ppm)	S (%)	Te (ppm)	Tl (ppm)	Ti (%)	W (ppm)	U (ppm)	V (ppm)	Zn (ppm)
102	4	4.5	4.06	0.15	80	1.53	2.4	3.06	0.03	0.15	1.2	47	88
103	4	4	2.04	0.16	67	1.65	2.2	3.34	0.03	0.05	0.95	49	80
104	4	4	5.34	0.15	90	1.57	2.55	3.16	0.02	0.15	1.5	46	100
109	4	6	0.52	0.08	73	0.82	1.1	2.28	0.01	0.15	3.5	34	128
110	5	5.5	0.9	0.08	70	0.86	1.2	1.82	0.01	0.15	3.65	36	134
111	5	4	1.02	0.07	73	0.82	1	3.18	0.02	0.1	1.75	45	192
115	5	4	1.18	0.09	91	0.76	1.05	2.68	0.03	0.15	2.75	50	204
116	4	4.5	1.18	0.08	77	0.66	1.05	3.42	0.03	0.15	1.7	49	160
117	6	7	0.9	0.15	162	1.18	1.3	3.36	0.04	0.15	1.4	63	128
119	4	5.5	0.82	0.08	82	0.79	1.05	1.78	0.02	0.15	3.7	38	144
120	4	5.5	0.58	0.04	38	0.76	0.95	3.96	0.01	0.1	1.15	26	204
121	5	3.5	1.24	0.07	60	0.76	0.95	2.78	0.03	0.15	1.55	40	198
125	5	2.5	1.72	0.06	62	0.78	1.05	1.84	0.01	0.1	1.9	34	388
126	4	2	1.7	0.06	55	0.73	0.9	1.82	0.01	0.1	1.95	31	486
127	4	2.5	1.1	0.05	42	0.9	1.25	2.08	0.01	0.1	1.55	27	472
128	4	2	1.42	0.05	44	0.85	1.25	1.94	0.01	0.15	1.6	29	422
131	5	1.5	0.38	0.08	99	0.61	0.25	0.44	0.03	0.05	0.95	47	104
132	5	0.5	0.32	0.07	93	0.57	0.2	0.32	0.03	0.05	0.85	42	96
133	5	1	0.44	0.07	103	0.57	0.25	0.42	0.03	0.05	0.85	43	96
136	5	1	0.5	0.07	93	0.63	0.35	0.72	0.03	0.05	0.9	43	118
144	2	6.5	7.08	0.15	155	1.5	3.75	2.44	0.01	1.1	0.45	28	48
145	3	5.5	6.44	0.13	120	1.29	2.9	2.48	0.01	0.85	0.55	33	64
146	1	7	4.24	0.08	77	0.89	2.1	1.9	0.02	1.5	0.35	20	38
147	3	9	4.98	0.1	94	1.06	3.6	2.18	0.03	1.25	0.45	25	50
148	1	8	3.36	0.07	63	0.77	2.55	1.76	0.04	1.75	0.25	14	26
14	2	6	5.84	0.09	84	1.59	2.35	2.44	0.01	0.25	0.4	43	94
19	1	7	6.6	0.13	96	1.8	2.45	3	0.01	0.35	0.35	47	60
25	6	2	1.18	0.06	65	0.82	0.5	2.54	0.01	0.2	1.45	51	308
52	3	5	6.24	0.08	85	1.45	1.75	2.62	0.03	0.2	0.7	51	74

Table A.6. Continued

Field no.	B (ppm)	Cd (ppm)	Ca (%)	Cr (ppm)	Co (ppm)	Cu (ppm)	Ga (ppm)	Ge (ppm)	Fe (%)	La (ppm)	Pb (ppm)	Mg (%)	Mn (ppm)	Hg (ppm)	Mo (ppm)	Ni (ppm)	P (ppm)	K (%)
69	10	0.14	0.06	11	4.4	158	7.2	0.1	10.65	10	160	0.44	335	0.95	7.6	6	650	0.8
74	10	0.16	0.05	16	3.8	135	6.8	0.1	7.69	10	172	0.46	345	0.52	9.8	8	660	0.62
75	10	0.14	0.06	10	4.6	181	6.6	0.1	9.21	10	170	0.45	320	1.84	10	6	720	0.79
79	10	0.22	0.11	14	5.8	125	7.7	0.1	7.05	10	196	0.52	445	1.03	6.8	7	720	0.53
80	10	0.2	0.09	14	5.8	110.5	7.6	0.1	6.42	20	172	0.51	485	0.68	6.2	8	800	0.51
84	10	0.24	0.13	13	5.2	143.5	7.9	0.1	6.55	10	236	0.48	400	0.37	8.6	7	810	0.56
85	10	0.22	0.11	12	5.2	148.5	7.9	0.1	6.06	10	314	0.53	455	0.73	10	6	730	0.61
89	10	0.36	0.3	15	6.8	145.5	8.3	0.1	5.6	10	210	0.57	475	0.3	6.2	8	970	0.59
90	10	0.28	0.12	11	5	226	7.6	0.1	5.49	10	410	0.5	430	0.43	13.8	6	770	0.55
91	10	0.3	0.14	12	5.8	129.5	7.9	0.1	5.91	10	330	0.57	520	1.1	10	6	780	0.56
92	10	0.34	0.28	17	6.8	142	8	0.1	5.93	10	206	0.63	490	0.35	6	9	840	0.54
96	10	0.22	0.06	9	4.4	104	6.9	0.1	5	10	342	0.53	395	1.04	6	4	690	0.55
97	10	0.2	0.13	7	6.2	82.6	5.5	0.1	3.78	10	402	0.47	940	0.59	3.8	5	490	0.46
101	10	0.28	0.16	14	4.6	105.5	7.5	0.1	6.05	10	336	0.58	445	0.78	6.6	6	830	0.65
156	10	0.18	0.05	10	5.2	206	6.9	0.1	8.51	10	154	0.38	510	2.03	9.4	5	750	0.59
157	10	0.1	0.27	10	3.2	247	5.6	0.1	5.25	10	758	0.35	375	0.5	5.2	4	600	0.58
158	10	0.56	0.33	9	9	212	4.4	0.1	6.34	30	372	0.33	1500	0.55	3.2	6	900	0.35
159	10	0.14	0.05	12	4.2	119.5	7.5	0.1	6.63	10	154	0.43	325	0.75	6.4	5	660	0.34
160	10	0.22	0.13	18	6.8	143	8.5	0.1	5.51	10	148	0.62	500	0.47	6	10	750	0.38
161	10	0.16	0.11	18	6	123.5	8.1	0.1	5.93	10	138	0.55	465	0.24	6.4	9	730	0.43
162	10	0.14	0.06	14	4.6	102.5	7.1	0.1	6.43	10	162	0.49	370	1	6.8	6	640	0.43
163	10	0.22	0.11	15	6.4	202	7.5	0.1	5.35	10	174	0.61	495	0.84	5.8	9	640	0.4
164	10	0.16	0.07	12	4.6	98.7	7.5	0.1	6.52	10	190	0.53	375	0.83	5.8	6	640	0.38
165	10	0.12	0.06	12	4.4	89.1	7.6	0.1	6.41	10	174	0.45	355	0.96	6	6	670	0.33
304	10	0.62	0.41	6	10.8	90.5	5.8	0.1	3.85	20	154	0.7	1035	0.53	1.6	5	700	0.37
305	10	0.58	0.46	10	9.8	98.8	6	0.1	4.35	20	212	0.77	955	0.75	1.6	7	810	0.44
306	10	1.04	0.39	12	10.2	184	5.5	0.1	4.59	30	336	0.54	1390	1.71	1.6	8	780	0.48
307	10	0.64	0.25	10	6.2	144	4.8	0.1	4.04	20	390	0.37	820	3.28	1.8	6	580	0.44
308	10	0.62	0.4	9	9.2	138.5	6.1	0.1	4.4	10	286	0.63	940	1.69	2.2	6	790	0.42
309	10	1	0.39	11	10	399	5.7	0.1	4.67	30	350	0.53	1320	2.07	1.6	8	810	0.48
310	10	0.6	0.42	10	9	91.7	5.7	0.1	4.07	10	210	0.65	920	1.37	1.4	7	750	0.38
311	10	0.92	0.43	9	10.6	128	5.8	0.1	3.92	20	254	0.55	1280	1.07	1.8	6	760	0.45
312	10	0.7	0.4	9	7.8	113.5	4.8	0.1	3.8	20	280	0.46	960	0.95	1.8	6	640	0.37

Table A.6. Continued

Field no.	Sc (ppm)	Se (ppm)	Ag (ppm)	Na (%)	Sr (ppm)	S (%)	Te (ppm)	Tl (ppm)	Ti (%)	W (ppm)	U (ppm)	V (ppm)	Zn (ppm)
69	4	4.5	6.04	0.09	95	1.71	1.7	3.6	0.03	0.2	0.8	63	78
74	4	4	4.14	0.08	79	1.2	2.05	2.42	0.03	0.15	0.65	54	84
75	4	5	6.04	0.09	106	1.67	1.6	3.14	0.03	0.15	0.85	58	88
79	5	4.5	5.2	0.1	102	1.13	1.8	2.4	0.03	0.15	1.25	54	116
80	5	4	4.92	0.09	82	1.02	1.8	2.62	0.03	0.1	1.3	54	118
84	5	3.5	5.96	0.11	107	1.15	2.2	2.48	0.04	0.2	1.4	58	110
85	5	4	6.7	0.14	127	1.39	2.3	2.58	0.03	0.45	1.2	54	110
89	6	3	4.46	0.13	137	1.12	1.7	2.34	0.04	0.2	1.8	56	158
90	5	4.5	8.22	0.13	123	1.26	2.45	2.54	0.03	0.45	1.1	48	112
91	5	4	6.72	0.12	109	1.19	2.2	2.52	0.03	0.35	1.2	52	122
92	5	3.5	3.48	0.12	141	1.09	1.6	2.14	0.04	0.15	1.5	57	148
96	4	6	10.05	0.13	98	1.28	3	2.8	0.03	0.25	0.8	42	90
97	4	5	8.18	0.1	81	0.98	2.15	1.64	0.03	0.45	0.6	31	78
101	4	5.5	8.46	0.15	128	1.49	3.2	2.94	0.02	0.2	1.1	46	108
156	3	4	4.94	0.07	77	1.31	1.55	2.28	0.03	0.25	0.6	54	90
157	5	3	3.46	0.07	117	1.23	1.1	2.44	0.03	0.1	1.15	43	106
158	5	2	2.32	0.07	62	0.96	0.75	1.5	0.01	0.25	1.25	49	256
159	4	4	5.08	0.06	49	0.67	1.8	1.96	0.04	0.2	1.05	55	82
160	6	3	5.1	0.08	76	0.65	1.4	2.34	0.04	0.15	1.75	59	124
161	6	3	4.32	0.08	83	0.77	1.3	1.8	0.04	0.15	1.65	58	116
162	4	3	3.76	0.07	81	0.85	1.5	2.12	0.04	0.15	0.85	51	94
163	5	3.5	5.32	0.08	67	0.71	1.65	2.12	0.04	0.15	1.45	53	120
164	4	4.5	5.92	0.07	61	0.75	2	2.12	0.04	0.2	1	52	94
165	4	5	6.88	0.06	45	0.62	2.25	2.1	0.04	0.15	1	53	86
304	4	2	3.28	0.13	77	0.65	1.1	1.28	0.05	0.2	1.35	39	178
305	4	2	4.96	0.14	89	0.74	1.25	1.74	0.05	0.25	1.5	48	196
306	4	2.5	5.4	0.13	72	0.94	1.85	2.36	0.03	1.1	1.75	42	310
307	3	3.5	7.88	0.11	61	0.93	2.6	2.54	0.02	0.8	1.45	31	224
308	4	3.5	7.44	0.14	87	0.79	1.9	1.76	0.04	0.35	1.35	47	202
309	4	2.5	6.12	0.14	75	0.96	2.05	2.38	0.03	1.2	1.75	43	324
310	4	2	5.12	0.13	83	0.72	1.3	1.46	0.04	0.25	1.2	47	186
311	4	2.5	5.76	0.14	69	0.81	1.75	1.96	0.04	0.6	1.65	40	224
312	3	2.5	7.72	0.11	67	0.78	1.85	1.62	0.03	0.6	1.25	39	202

Table A.6. Continued

Media	Field no.	UTM-E	UTM-N	Elev	pH	Au (ppb) -212+106μm	Au (ppb) -106+53μm	Au (ppb) -53μm	Al (%)	Sb (ppm)	As (ppm)	Ba (ppm)	Be (ppm)	Bi (ppm)
debris	318	19397592	6759427	3948	7.3	30	135	300	2	2.7	239	350	1.4	6.51
talus	320 (16)	19409459	6753605	3756	5	10	25	25	1.86	2.7	225	420	1.85	3.29
talus	24	19409129	6753684	3684	4.5	10	5	45	2.23	4.4	414	560	1.8	2.98
talus	53	19409192	6754140	3705	3.9	5	25	50	2.41	3.8	242	380	1.8	3.34
talus	105	19405115	6755528	3920	4.7	25	35	95	2.29	2.9	556	370	1.1	5.48
talus	106	19405274	6755617	4132	5.3	20	50	80	3.08	1.7	208	310	0.75	4.31
talus	107	19405264	6755692	3984	4.7	20	65	95	1.98	2.4	354	350	0.7	4.92
talus	108	19405400	6755681	4260	4.5	15	70	95	2.36	2.3	283	400	0.95	5.7
talus	112	19405637	6755706	4020	4.3	15	15	30	2.23	1.5	143	340	2	3.59
talus	113	19405746	6755687	4119	3.9	5	10	45	1.59	1.4	147	310	0.85	3.18
talus	114	19405861	6755707	4017	3.9	5	10	45	1.77	1.8	254	400	1.1	5.04
talus	118	19406182	6755681	4044	5.9	5	15	50	2.19	1.7	204	280	1.05	4.84
talus	122	19406631	6755585	3972	5.1	5	5	20	2.03	2.4	123.5	440	2.05	4.87
talus	123	19406731	6755433	3785	7.1	25	10	60	1.97	2.4	248	350	1.75	4
talus	124	19406802	6755300	3969	7.1	5	10	50	2.2	2.7	173.5	470	1.85	4.19
talus	129	19407190	6755058	3873	3.9	30	55	170	2.06	6.8	485	350	1.35	4.06
talus	130	19407317	6755089	3924	7.2	10	20	75	2.11	4	230	500	1.85	3.77
talus	134	19407470	6754783	4098	3.7	10	25	95	1.66	2.1	195.5	320	0.45	3.56
talus	135	19407781	6754724	3897	4.7	5	45	85	2.2	2.8	197	360	0.7	3.44
talus	137	19408110	6754660	3888	4.4	10	5	30	1.75	3.9	168.5	360	2.3	1.87
talus	138	19408272	6754564	3918	4.7	10	10	70	1.6	2.5	152.5	270	1.05	2.57
talus	139	19404123	6755636	4302	4.9	55	150	495	2.13	8.6	834	350	0.3	12.65
talus	140	19404209	6755466	4230	4.7	95	85	1045	2.17	5.7	732	440	0.05	9.69
talus	141	19404271	6755480	4200	3.5	75	140	725	1.47	4.5	896	240	0.2	10.3
talus	142	19404434	6755381	4266	3.6	60	345	645	1.5	6.9	794	220	0.15	10.25
talus	143	19404517	6755301	4260	4.1	55	60	660	1.57	12.6	848	50	0.1	10.15
talus	149	19405046	6755267	4233	5	40	50	170	1.63	6.9	521	320	0.5	5.36
talus	150	19405066	6755284	4149	5.3	40	110	205	2.02	6.7	498	390	0.3	5.92
talus	151	19405243	6755249	4203	4.8	45	80	235	1.46	4.8	394	360	0.75	6.2
talus	152	19405271	6755302	3912	4.9	55	160	245	1.73	4.9	445	350	0.2	6.34
talus	153	19405414	6755297	4059	4.7	30	45	155	1.63	4.7	451	300	0.7	7.63
talus	154	19405646	6755026		7.1	20	200	190	2.41	3.8	309	240	0.65	5.28
talus	155	19405787	6754970		4.7	25	175	380	1.43	5.1	299	320	0.9	5.09
talus	216	19398005	6758481	3954	7.3	5	15	95	1.13	1.3	89.6	160	0.8	2.72
talus	219	19398679	6758019	3960	6	55	45	100	1.31	2.3	138.5	320	0.75	5.8

Table A.6. Continued

Field no.	B (ppm)	Cd (ppm)	Ca (%)	Cr (ppm)	Co (ppm)	Cu (ppm)	Ga (ppm)	Ge (ppm)	Fe (%)	La (ppm)	Pb (ppm)	Mg (%)	Mn (ppm)	Hg (ppm)	Mo (ppm)	Ni (ppm)	P (ppm)	K (%)
318	10	0.4	0.22	15	9	201	5.8	0.1	4.52	20	194	0.53	890	0.91	3	8	790	0.37
320 (16)	10	0.44	0.24	13	11.6	105.5	5.3	0.1	5.78	10	196	0.35	1595	0.16	4.8	7	710	0.38
24	10	0.36	0.24	10	6.8	90.9	5.5	0.1	6.08	20	634	0.3	1480	0.09	4.4	7	810	0.4
53	10	0.24	0.1	7	13.2	122.5	7.5	0.1	5.55	110	168	0.42	1905	0.17	5.2	6	1100	0.29
105	10	0.6	0.4	15	7.4	235	10.4	0.1	5.51	20	262	0.62	620	0.59	4.6	8	1040	0.66
106	10	0.32	0.38	25	8	189	7.6	0.1	5.14	30	138	0.81	550	0.16	2.4	16	930	0.43
107	10	0.62	0.34	19	8.8	144.5	6.6	0.1	5.14	10	236	0.66	800	0.24	4.4	11	870	0.48
108	10	0.62	0.32	21	10	191	7.3	0.1	5.72	20	196	0.78	1025	0.22	5.8	13	1040	0.53
112	10	1.4	0.63	28	15.2	290	7.5	0.1	5.5	30	238	1.05	1300	0.1	11	19	1060	0.4
113	10	0.82	0.37	18	10.6	139	5.2	0.1	4.36	10	110	0.66	960	0.16	6.4	11	800	0.36
114	10	0.68	0.34	21	13	112.5	6.1	0.1	5.02	10	134	0.7	1020	0.45	7.8	17	750	0.43
118	10	0.72	0.56	24	10.2	127.5	7.4	0.1	4.93	10	98	0.72	765	0.24	9.6	14	780	0.48
122	10	0.96	0.71	16	10.2	92.8	6.6	0.1	5.29	50	156	0.67	2860	0.44	4.2	13	920	0.43
123	10	0.76	0.7	20	9.2	134.5	5.6	0.1	5.02	30	134	0.72	1450	0.23	4.4	13	1210	0.45
124	10	0.76	0.56	19	10.2	224	6.7	0.1	5.14	30	140	0.71	1710	0.31	4.6	14	1110	0.47
129	10	0.42	0.22	15	6.4	100	6.3	0.1	5.14	30	148	0.59	690	0.25	4.6	10	770	0.43
130	10	0.76	0.32	20	9.2	115.5	6.5	0.1	5.33	30	150	0.71	1000	0.2	4.4	13	910	0.43
134	10	0.24	0.12	12	4.8	131.5	5.3	0.1	5.13	10	126	0.5	415	0.35	6.6	7	660	0.42
135	10	0.46	0.23	16	6.4	245	7.7	0.1	8.18	10	122	0.58	560	0.19	7.4	9	900	0.39
137	10	0.5	0.37	9	12	132	5.8	0.1	6.21	30	106	0.67	1200	0.11	7	9	1210	0.64
138	10	0.46	0.33	16	9.4	155	5.5	0.1	4.91	10	98	0.61	730	0.51	8.4	9	810	0.44
139	10	0.22	0.07	10	4	106	7.5	0.1	5.98	10	428	0.53	375	0.24	6.8	5	660	0.59
140	10	0.18	0.05	10	3.4	87.6	8.3	0.1	6.32	10	520	0.51	350	0.11	5.8	4	640	0.5
141	10	0.08	0.05	4	2.2	92.5	9.2	0.1	8.78	10	814	0.32	220	0.19	4.2	1	620	0.63
142	10	0.18	0.05	5	2.4	132	8.7	0.1	8.88	10	830	0.38	250	0.39	5.4	2	820	0.71
143	10	0.26	0.05	5	1.6	187	8.6	0.1	8.58	10	984	0.3	250	0.27	6	3	830	0.87
149	10	1.78	0.24	8	9.8	184.5	6	0.1	6.05	10	822	0.72	1920	0.32	3.6	5	1150	0.49
150	10	1.68	0.34	6	9.6	182	6.9	0.1	6.17	10	748	0.78	1970	0.5	5.4	5	1100	0.51
151	10	0.84	0.41	13	6.6	160	5.3	0.1	4.98	10	468	0.58	900	0.44	7.4	5	1080	0.51
152	10	0.64	0.33	11	6.2	219	5.9	0.1	5.44	10	502	0.59	725	0.26	8.4	7	980	0.58
153	10	0.64	0.22	11	6.4	127.5	6.2	0.1	5.95	10	528	0.55	700	0.36	9	5	970	0.62
154	10	2.16	0.41	17	8.6	164.5	7.3	0.1	5.09	10	478	0.73	1490	0.28	4	10	880	0.65
155	10	2.14	0.31	12	10.4	147	5.2	0.1	5.13	10	450	0.66	1445	0.52	3.6	8	910	0.49
216	10	0.68	0.28	17	7.2	221	4.4	0.1	2.99	20	104	0.48	950	0.17	1.8	10	650	0.17
219	10	0.78	0.34	16	6.2	298	4.9	0.1	3.27	20	200	0.5	945	0.28	3	11	600	0.28

Table A.6. Continued

Field no.	Sc (ppm)	Se (ppm)	Ag (ppm)	Na (%)	Sr (ppm)	S (%)	Te (ppm)	Tl (ppm)	Ti (%)	W (ppm)	U (ppm)	V (ppm)	Zn (ppm)
318	5	1.5	4.64	0.11	54	0.65	1.3	2.1	0.05	0.4	2.3	50	218
320 (16)	5	2	0.84	0.08	132	0.73	0.7	1.4	0.03	0.15	1.2	48	150
24	6	2.5	0.84	0.08	135	0.7	0.7	1.28	0.03	0.2	1.3	37	188
53	6	2.5	1.54	0.05	107	0.52	1.1	1.16	0.02	0.15	1.4	35	174
105	8	3	3.48	0.14	205	1.19	1.8	3.36	0.05	0.15	2.6	53	162
106	7	2	1.44	0.07	154	0.6	0.9	1.9	0.08	0.1	2.75	56	186
107	5	3	2.36	0.12	122	0.99	1.45	2	0.04	0.2	1.85	55	168
108	5	3.5	1.98	0.13	116	1.02	1.6	2.34	0.05	0.2	2	57	200
112	6	3	1.08	0.1	117	0.6	0.85	1.7	0.06	0.15	3.55	64	312
113	4	3	1.32	0.09	80	0.6	0.9	1.4	0.05	0.15	2	52	174
114	5	4	0.98	0.1	84	0.72	1.15	3.02	0.05	0.15	1.85	57	170
118	6	5	1.3	0.09	109	0.77	1.15	3.14	0.03	0.15	2.2	55	166
122	7	2.5	2.48	0.07	74	0.6	0.7	1.96	0.03	0.4	1.8	45	236
123	5	3	1.58	0.08	88	0.67	0.85	2.02	0.04	0.25	1.95	46	246
124	6	2.5	2.08	0.09	89	0.7	0.95	2.04	0.04	0.25	1.95	48	280
129	5	2.5	2	0.08	83	0.75	1.4	2.92	0.03	0.15	1.85	48	164
130	5	2.5	1.58	0.09	85	0.71	1.05	1.86	0.05	0.2	2.05	56	226
134	4	2.5	2.52	0.08	105	0.82	1.1	1.52	0.03	0.05	0.95	43	100
135	5	2.5	1.7	0.08	85	0.69	0.95	1.46	0.04	0.15	1.55	57	166
137	5	4	0.96	0.09	67	1.12	1.1	1.38	0.01	0.05	0.85	40	152
138	4	2.5	1.6	0.07	83	0.73	0.85	1.3	0.03	0.05	1.35	46	134
139	4	6	11.45	0.14	115	1.42	3.2	2.84	0.03	0.45	0.8	46	84
140	4	6	10.55	0.12	106	1.24	3.35	3.3	0.02	0.4	0.75	47	74
141	4	8.5	10.6	0.19	165	1.83	4.2	4.52	0.01	1.1	0.45	39	48
142	3	8.5	10.65	0.19	200	1.96	6.9	3.44	0.01	0.5	0.55	39	60
143	3	10	13.05	0.25	241	2.54	9.25	3.44	0.01	0.55	0.55	32	56
149	4	3.5	4.2	0.13	156	1.12	2.65	2.04	0.01	0.2	0.9	49	376
150	4	3.5	4.84	0.14	156	1.16	2.65	2.34	0.01	0.25	1	45	398
151	3	4	4.9	0.13	127	1.1	2.2	1.98	0.03	0.35	1	41	238
152	4	4	5.14	0.14	150	1.26	2.35	2.36	0.03	0.45	1	44	196
153	3	4.5	3.76	0.16	160	1.46	2.55	2.78	0.03	0.35	1.05	45	164
154	6	4	5.46	0.11	115	0.95	2.3	2.02	0.01	0.15	1.3	45	468
155	3	3	5.08	0.12	115	0.92	1.7	2.04	0.05	0.2	1.4	49	288
216	4	0.5	1.22	0.03	29	0.16	0.45	0.56	0.05	0.2	1.55	45	130
219	4	1.5	2.24	0.05	42	0.36	1.15	1.06	0.04	0.3	1.8	35	226

Table A.6. Continued

Media	Field no.	UTM-E	UTM-N	Elev	pH	Au (ppb) -212+106μm	Au (ppb) -106+53μm	Au (ppb) -53μm	Al (%)	Sb (ppm)	As (ppm)	Ba (ppm)	Be (ppm)	Bi (ppm)
talus	221	19398998	6757266	4278	4.6	10	10	45	2.19	1.7	378	350	1.85	7.12
talus	222	19399142	6757266		4.9	125	40	120	1.48	2.5	368	470	0.6	8.03
talus	223	19399152	6757276		6.8	70	40	145	1.46	3.8	426	80	0.55	11.15
talus	224	19399338	6757241		6.8	55	50	320	0.89	4.4	844	170	0.2	12.5
talus	225	19399595	6757236	4362	7.1	325	1810	1195	0.41	28.5	1230	110	0.05	52.3
talus	226	19400022	6757236	4362	8.4	55	50	285	1.31	6.1	828	60	0.65	12.7
talus	227	19400365	6757359	4404	6.3	115	100	765	0.75	9.3	716	70	0.25	13.75
talus	228	19400595	6757621	4377	5.9	40	50	115	1.94	2.2	378	160	1.4	3.91
talus	229	19399881	6757692	4323	4.7	5	5	10	2.76	0.5	33.8	160	1.15	1.11
talus	230	19399601	6757919	4371	4.6	5	5	10	3.04	0.5	21.2	110	1.9	1.21
talus	231	19399760	6757642	4245	4.7	5	5	20	3.29	0.4	22.6	140	1.2	0.73
talus	232	19398080	6759366	4056	4.5	5	5	5	2.67	0.4	18.6	90	3.8	0.81
talus	233	19398233	6759130	4044	5.3	5	5	5	3.4	0.5	24.4	150	1.75	1.22
talus	234	19398529	6758638	4227	4.7	5	5	5	2.92	0.5	19.8	140	2.45	2.16
talus	235	19398927	6758021	4185	4.7	5	5	20	2.96	0.8	97.2	320	3.05	12.5
talus	236	19399235	6757890	4266	4.8	5	5	15	2.49	0.7	133.5	230	2.35	8.62
till	4	19411623	6752480	3759	7.8	20	5	60	1.45	1.9	115	240	0.65	1.78
till	5	19411633	6752490	3759	8.8	10	10	70	1.26	2.1	127	250	0.8	2.33
till	9	19411012	6753201	3762	9.9	10	10	55	1.46	2.9	195	430	1.1	2.54
till	10	19411022	6753211	3762	5.3	10	10	70	1.26	2.9	161	340	0.8	2.88
till	15	19409505	6753921	3888	7.9	15	30	90	1.39	3.5	212	410	1.05	3.19
till	26	19409129	6753684	3684	8.9	10	10	50	1.11	3.4	217	370	1.25	3.14
till	54	19409192	6754140	3705	6.9	10	15	60	1	3.4	175.5	240	0.8	3.1
till	55	19409202	6754150	3705		825	20	95	1.33	4.8	428	360	0.8	5.34
till	56	19408431	6753680	3900		10	10	65	1.88	2.5	213	230	1.45	2.55
till	57	19408371	6753812	3921	8.25	15	15	55	1.67	2.6	192.5	300	1.4	2.57
till	58	19408405	6753930	3948		25	20	280	1.85	6.4	395	440	0.8	5.62
till	59	19408370	6754117	3915	10.4	15	20	100	1.48	3.2	231	320	0.8	3.67
till	60	19408280	6754212	3924	8.1	380	25	105	1.76	3	253	330	0.8	3.83
till	61	19406316	6754799	3984	7.8	20	20	115	1.68	2.9	246	430	0.85	4.42
till	62	19407010	6754372	4059	7.8	20	15	165	1.72	2.6	220	320	1.25	4.35
till	63	19407270	6754012	3993		55	55	90	1.96	3.2	207	360	1.05	3.29
till	64	19407014	6753667	3945	9.5	25	70	80	0.96	3.5	196.5	350	0.75	4.41

Table A.6. Continued

Field no.	B (ppm)	Cd (ppm)	Ca (%)	Cr (ppm)	Co (ppm)	Cu (ppm)	Ga (ppm)	Ge (ppm)	Fe (%)	La (ppm)	Pb (ppm)	Mg (%)	Mn (ppm)	Hg (ppm)	Mo (ppm)	Ni (ppm)	P (ppm)	K (%)
221	10	5.56	0.27	12	10	107	8.3	0.1	6.19	50	1490	0.53	5010	0.34	8.4	11	1040	0.65
222	10	0.28	0.2	17	6.8	139.5	6.7	0.1	5.03	10	666	0.41	495	0.08	8.2	7	380	0.68
223	10	0.26	0.15	18	5	140.5	8.1	0.1	6.1	10	824	0.31	345	0.1	10.4	7	370	0.87
224	10	0.12	0.01	13	1.2	97.8	11.5	0.1	8.79	10	738	0.12	95	0.07	21	1	330	0.63
225	10	0.08	0.01	8	0.8	49.6	7.3	0.1	3.84	10	1180	0.08	50	1.38	3.4	1	270	0.61
226	10	0.28	0.05	15	1.8	137.5	9.7	0.1	6.77	20	1400	0.17	130	0.09	5.6	4	480	0.99
227	10	0.16	0.01	7	0.2	82.2	5.9	0.1	5.14	20	516	0.04	55	0.72	1.8	1	250	0.9
228	10	1.2	0.4	9	10.6	174	6.8	0.1	5.07	30	194	0.66	1290	0.29	1	7	800	0.58
229	10	0.4	0.81	29	13.4	56.4	7.5	0.1	3.65	20	52	1.25	870	0.02	1	17	980	0.4
230	10	0.62	0.86	35	13	49.2	8.2	0.1	3.83	30	42	1.26	1070	0.03	0.8	21	900	0.37
231	10	0.46	1.01	23	13.2	48	8	0.1	3.76	20	36	1.45	950	0.01	0.6	15	960	0.45
232	10	1.04	0.88	41	14.2	35.4	9.1	0.1	4.24	70	60	1.59	1890	0.05	0.8	31	1000	0.32
233	10	0.4	0.74	32	14.2	47.6	9.4	0.1	4.18	40	50	1.25	1430	0.09	1	24	800	0.29
234	10	0.88	0.75	36	14.6	48.2	8.9	0.1	3.87	40	68	1.27	1525	0.04	1.2	27	830	0.29
235	10	3.44	0.79	38	18.8	60.4	9.5	0.1	6.27	70	154	1.31	4230	0.37	5	32	1070	0.44
236	10	4.08	0.59	35	20.2	220	8.5	0.1	5.77	60	126	1.09	3510	0.2	2.2	33	980	0.4
4	10	0.38	0.43	16	8.6	179	4.3	0.1	4.14	10	104	0.54	615	0.12	3.6	9	960	0.3
5	10	0.44	0.39	13	10	97.7	4.2	0.1	4.03	10	110	0.47	775	0.17	3.4	8	1020	0.28
9	10	0.34	0.2	11	8.6	139	4.6	0.1	3.95	10	164	0.41	1045	0.24	3.4	6	800	0.29
10	10	0.3	0.19	15	8.2	128.5	5.1	0.1	5.03	10	128	0.48	620	0.2	4.8	7	890	0.39
15	10	0.4	0.24	13	5.6	176.5	5.1	0.1	4.61	10	142	0.41	515	0.28	6.6	6	760	0.43
26	10	0.78	0.34	17	9.2	90.8	4.1	0.1	4.23	10	620	0.43	1435	0.21	4.2	10	830	0.29
54	10	0.6	0.2	12	6.2	110.5	4.1	0.1	4.25	10	122	0.37	775	0.21	5.4	6	530	0.3
55	10	0.66	0.19	8	3.6	143.5	4.6	0.1	3.68	10	288	0.47	320	0.18	3.8	5	570	0.33
56	10	0.6	1.27	14	7.6	134	5.7	0.1	4.18	10	194	0.42	1005	0.16	4.4	10	760	0.39
57	10	0.58	0.26	12	7.6	116	5.4	0.1	3.93	20	164	0.44	1050	0.09	4.2	11	660	0.44
58	10	1.34	0.61	11	6	153	6.3	0.1	4.69	10	334	0.47	645	0.15	5.8	7	880	0.44
59	10	0.84	0.21	13	9.6	186.5	5.6	0.1	4.56	10	178	0.44	955	0.29	5.4	9	790	0.38
60	10	0.44	0.22	13	6	165.5	5.8	0.1	4.58	10	172	0.43	490	0.15	4.2	11	720	0.36
61	10	0.74	0.36	19	9.2	186.5	5.5	0.1	4.78	10	218	0.59	1115	0.19	3.8	9	1060	0.44
62	10	0.7	0.38	23	11.2	172	6.1	0.1	5.32	10	194	0.62	1050	0.63	4.8	11	1120	0.5
63	10	0.6	0.41	12	6.6	127.5	6.8	0.1	4.41	20	180	0.5	705	0.03	7	9	780	0.47
64	10	0.46	0.19	9	5.2	62.9	4	0.1	4.55	10	210	0.34	610	0.36	19.6	8	630	0.45

Table A.6. Continued

Field no.	Sc (ppm)	Se (ppm)	Ag (ppm)	Na (%)	Sr (ppm)	S (%)	Te (ppm)	Tl (ppm)	Ti (%)	W (ppm)	U (ppm)	V (ppm)	Zn (ppm)
221	6	1	1.62	0.16	53	1.32	1.8	4.62	0.01	0.15	1.7	34	1090
222	4	2.5	1.36	0.05	46	1.04	1.6	4.62	0.08	0.2	1.3	49	96
223	4	4	1.84	0.08	37	1.49	2.55	6.38	0.06	0.2	1.25	43	82
224	3	8.5	2.6	0.06	18	1.15	4.65	4.96	0.01	0.3	0.65	36	34
225	1	13	12.95	0.06	19	1.15	9.65	2.68	0.02	0.7	0.25	14	20
226	4	5.5	7.08	0.15	33	2	5.4	7.78	0.02	0.35	2.25	31	90
227	1	8.5	5.52	0.11	19	1.81	10.05	5.98	0.01	0.4	0.85	12	54
228	6	2	1.54	0.16	84	1.14	2.35	2.94	0.02	0.45	1.55	35	276
229	5	0.5	0.28	0.06	109	0.11	0.15	0.54	0.15	0.15	1.9	67	132
230	6	0.5	0.16	0.06	91	0.08	0.1	0.52	0.14	0.2	2.05	62	184
231	5	0.5	0.24	0.07	124	0.08	0.15	0.46	0.17	0.15	1.9	64	136
232	8	0.5	0.12	0.04	49	0.01	0.05	0.34	0.12	0.15	1.9	64	204
233	8	0.5	0.24	0.04	66	0.05	0.15	0.38	0.15	0.2	2.3	69	162
234	7	0.5	0.24	0.03	49	0.04	0.05	0.44	0.09	0.25	2.1	66	190
235	10	0.5	0.74	0.11	64	0.62	0.25	3.72	0.04	1.1	3.55	65	762
236	9	0.5	0.46	0.12	69	0.72	0.5	4.96	0.03	0.65	2.8	61	630
4	4	1.5	0.64	0.05	77	0.39	0.55	0.66	0.05	0.15	0.9	54	150
5	4	2	0.86	0.05	64	0.35	0.55	0.62	0.05	0.2	0.95	51	122
9	4	2	1.12	0.05	129	0.47	0.75	1.18	0.04	0.15	1.15	41	148
10	4	2.5	0.9	0.06	135	0.6	0.7	1.14	0.06	0.15	1.1	56	106
15	4	3	1.8	0.07	86	0.67	0.95	1.36	0.03	0.15	1.15	42	156
26	4	2	1.4	0.07	67	0.55	0.75	1.16	0.04	0.2	1.2	49	172
54	3	3	1.14	0.06	61	0.52	0.95	1.12	0.04	0.15	1.1	41	116
55	3	4	1.54	0.07	107	0.59	1.8	1.36	0.01	0.25	0.8	32	152
56	5	2	1.68	0.06	78	1.17	0.7	1.06	0.01	0.15	1.2	38	218
57	4	2	1.36	0.07	71	0.55	0.75	1.1	0.02	0.2	1.3	38	180
58	4	3	2.92	0.07	121	0.83	1.65	1.3	0.02	0.3	1.05	43	334
59	4	3.5	2.14	0.07	85	0.62	1.15	1.34	0.04	0.1	1.35	46	180
60	4	2.5	2.48	0.06	100	0.56	1.1	1.32	0.03	0.1	1.35	45	138
61	4	3	2.66	0.1	103	0.87	1.45	1.48	0.04	0.2	1.2	49	202
62	5	3	3.36	0.1	106	0.88	1.25	1.68	0.05	0.2	1.8	61	184
63	5	2.5	1.94	0.08	100	0.68	0.85	1.34	0.01	0.2	1.25	40	208
64	3	3	1.52	0.09	108	0.96	1	1.56	0.03	0.35	0.95	34	120

Table A.6. Continued

Media	Field no.	UTM-E	UTM-N	Elev	pH	Au (ppb) -212+106μm	Au (ppb) -106+53μm	Au (ppb) -53μm	Al (%)	Sb (ppm)	As (ppm)	Ba (ppm)	Be (ppm)	Bi (ppm)
till	65	19407324	6753675	3987	8.2	35	30	120	1.49	2.5	186	350	0.85	3.71
till	217	19397985	6758572	3998	8	10	20	45	1.1	0.8	55	170	1.55	2.22
till	218	19398181	6758277	4095	7.7	15	10	60	0.81	1.1	74.8	190	0.6	3.43
till	220	19398276	6758019	3860	6.3	15	15	45	0.84	1.4	69.6	190	0.7	3.41
till	297	19396833	6760913	3603	9.5	600	65	80	1.5	0.9	46.4	160	1.15	1.9
till	298	19397761	6762537	3864	6.7	5	5	30	2.84	0.2	9.8	230	1.45	0.58
till	292	19397190	6760120		7.7	25	25	190	1.92	2	131	170	0.5	3.52
till	283	19396305	6761773	3708	4.7	5	5	5	2.18	0.4	9.4	140	1.25	0.62
till	319	19396943	6760972	3963	7.7	5	5	15	2.04	0.4	31	150	1.2	1.02
till	293	19396833	6760913	3603	7.9	10	5	25	2.57	0.3	19.2	130	1.9	1.16

Table A.6. Continued

Field no.	B (ppm)	Cd (ppm)	Ca (%)	Cr (ppm)	Co (ppm)	Cu (ppm)	Ga (ppm)	Ge (ppm)	Fe (%)	La (ppm)	Pb (ppm)	Mg (%)	Mn (ppm)	Hg (ppm)	Mo (ppm)	Ni (ppm)	P (ppm)	K (%)
65	10	0.64	0.39	17	8.2	119	5	0.1	4.15	10	198	0.53	940	0.38	9.8	10	940	0.44
217	10	0.58	0.38	11	6.8	36.8	4.7	0.1	2.73	30	92	0.51	1130	0.12	1.8	8	700	0.18
218	10	0.8	0.26	11	6	163.5	3.7	0.1	2.56	20	150	0.36	1140	0.17	2.4	9	590	0.16
220	10	0.62	0.25	14	5.6	43	3.9	0.1	2.94	10	124	0.36	975	0.11	2	7	610	0.16
297	10	0.48	0.5	24	8.6	101.5	5.3	0.1	3.68	10	56	0.65	715	0.1	1.6	12	940	0.22
298	10	0.38	0.73	35	17.4	60.5	9.9	0.1	4.46	30	22	1.37	1430	0.07	0.8	26	1470	0.16
292	10	0.08	0.04	17	5.4	467	7.3	0.1	13.75	10	98	0.33	360	0.28	5.4	5	830	0.19
283	10	0.24	0.48	31	13.2	57.2	6.5	0.1	3.64	30	22	0.97	860	0.04	1.6	23	810	0.18
319	10	0.64	0.53	35	13	172.5	7.2	0.1	5.16	20	28	0.86	995	0.06	2.8	19	950	0.25
293	10	0.34	0.55	24	11.2	98.2	8.1	0.1	3.31	40	66	1.05	1240	0.04	1.6	20	640	0.22

Table A.6. Continued

Field no.	Sc (ppm)	Se (ppm)	Ag (ppm)	Na (%)	Sr (ppm)	S (%)	Te (ppm)	Tl (ppm)	Ti (%)	W (ppm)	U (ppm)	V (ppm)	Zn (ppm)
65	3	2.5	2.64	0.09	98	0.77	1.05	1.32	0.03	0.25	1.15	43	178
217	5	0.5	0.98	0.03	24	0.12	0.35	0.42	0.02	0.1	0.8	38	152
218	3	0.5	1.12	0.03	21	0.18	0.45	0.64	0.03	0.15	0.95	33	152
220	4	0.5	0.92	0.03	24	0.21	0.5	0.64	0.05	0.15	0.85	40	122
297	4	0.5	0.94	0.04	47	0.15	0.3	0.48	0.08	0.2	1.25	55	130
298	9	0.5	0.22	0.02	51	0.04	0.05	0.18	0.11	0.15	1.05	67	130
292	4	1	2.46	0.02	23	0.39	0.8	2.9	0.09	0.25	1.4	59	98
283	6	0.5	0.1	0.02	64	0.04	0.05	0.18	0.12	0.25	2.1	70	98
319	5	0.5	0.32	0.03	64	0.16	0.15	0.56	0.12	0.25	2.65	81	132
293	6	0.5	0.26	0.02	41	0.05	0.1	0.24	0.07	0.15	2.75	49	144

Table B.1. Texture (%) of stream sediments at Pascua-Lama.

Site no	Energy	-2mm +850μm	-850 +425μm	-425 +212μm	-212 +150μm	-150 +106μm	-106 +75μm	-75 +53μm	-53μm
1	high	33.1%	33.1%	22.9%	4.0%	2.5%	1.4%	0.8%	2.2%
1	med	42.2%	29.6%	18.9%	4.3%	2.0%	1.1%	0.7%	1.2%
1	low	4.7%	54.1%	31.4%	6.2%	1.6%	1.1%	0.5%	0.4%
2	high	25.9%	32.4%	24.2%	6.9%	2.6%	2.3%	1.6%	4.1%
2	med	44.8%	28.1%	17.7%	3.3%	2.1%	1.3%	0.9%	1.7%
2	low	7.3%	8.8%	51.8%	10.9%	8.6%	4.7%	2.6%	5.4%
3	high	30.5%	19.8%	29.3%	8.2%	5.4%	3.7%	2.6%	0.6%
3	med	48.7%	29.4%	13.0%	1.9%	1.0%	0.6%	0.4%	4.9%
3	low	10.5%	55.1%	24.7%	4.1%	2.7%	1.3%	0.5%	1.1%
5	high	28.7%	29.5%	28.1%	5.7%	3.1%	1.8%	1.2%	2.0%
5	med	41.5%	31.8%	17.4%	4.0%	2.1%	1.2%	0.7%	1.4%
5	low	16.8%	15.7%	42.5%	9.8%	6.6%	3.5%	1.7%	3.4%
6	high	41.6%	21.9%	16.9%	7.7%	3.7%	2.7%	1.6%	3.9%
6	med	34.5%	23.7%	16.8%	6.4%	4.3%	3.9%	2.5%	8.0%
6	low	11.0%	26.4%	44.3%	7.7%	3.7%	2.8%	1.3%	2.7%
12	high	55.5%	22.3%	13.6%	3.3%	1.6%	1.1%	0.8%	1.8%
12	med	12.5%	32.6%	38.0%	7.0%	3.9%	2.4%	1.4%	2.2%
12	low	6.4%	52.8%	7.4%	10.9%	10.4%	4.9%	2.8%	4.5%
13	high	46.0%	29.7%	13.1%	2.9%	2.0%	1.4%	1.0%	4.0%
13	med	49.0%	30.4%	14.7%	2.3%	1.4%	0.8%	0.5%	1.0%
13	low	0.6%	5.4%	33.4%	22.8%	16.5%	8.5%	4.0%	8.9%
14	high	20.1%	30.3%	27.2%	6.3%	4.4%	3.2%	2.3%	6.2%
14	med	19.2%	24.2%	30.9%	8.0%	5.2%	3.6%	2.6%	6.1%
14	low	0.3%	0.6%	55.1%	21.7%	10.2%	4.8%	2.6%	4.7%
15	high	31.6%	25.6%	22.0%	6.0%	4.3%	2.9%	2.1%	5.5%
15	med	47.6%	29.8%	16.1%	2.4%	1.5%	0.8%	0.5%	1.2%
15	low	14.9%	27.9%	28.1%	10.2%	6.6%	4.5%	2.5%	5.2%
16	high	45.3%	27.4%	17.5%	3.1%	1.9%	1.2%	0.8%	2.9%
16	med	31.4%	28.7%	25.2%	5.2%	2.6%	1.8%	1.3%	3.7%
16	low	49.5%	7.7%	20.5%	6.8%	5.7%	3.4%	1.9%	4.5%
17	high	39.5%	32.9%	18.2%	3.4%	2.1%	1.2%	0.7%	2.1%
17	med	37.3%	29.8%	19.6%	3.8%	2.4%	1.5%	0.9%	4.8%
17	low	33.0%	31.2%	20.1%	5.0%	3.8%	2.1%	1.1%	3.6%
18	high	56.7%	24.4%	12.8%	1.9%	1.1%	0.7%	0.5%	2.0%
18	med	40.3%	30.4%	17.9%	3.2%	2.1%	1.4%	0.9%	3.8%
18	low	52.2%	23.1%	14.9%	3.5%	2.1%	1.1%	0.7%	2.5%
19	high	40.1%	26.7%	17.0%	3.7%	3.0%	1.9%	1.3%	6.3%
19	med	34.9%	28.3%	19.3%	4.2%	2.8%	1.9%	1.5%	7.0%
19	low	3.5%	20.8%	39.7%	11.7%	8.2%	4.9%	2.9%	8.3%
20	med	33.5%	25.8%	20.2%	6.0%	3.4%	2.6%	2.0%	6.3%
20	low	4.5%	14.0%	35.3%	6.0%	15.9%	8.8%	4.3%	11.2%
21	med	44.3%	34.1%	17.6%	1.8%	1.3%	0.6%	0.3%	0.8%
21	low	20.4%	24.4%	22.4%	10.9%	10.4%	5.4%	2.4%	3.7%
22	med	27.5%	29.5%	30.9%	5.2%	2.6%	1.3%	0.7%	2.2%
22	low	9.4%	18.3%	35.6%	11.8%	9.0%	5.6%	2.9%	7.5%
23	med	34.5%	26.0%	11.9%	24.0%	1.6%	0.7%	0.4%	0.9%
23	low	23.5%	50.5%	14.7%	2.8%	2.4%	2.1%	1.4%	2.7%
24	high	58.4%	22.7%	11.5%	2.2%	1.6%	1.1%	0.8%	1.7%
24	med	58.5%	22.5%	11.5%	2.2%	1.6%	1.0%	0.8%	2.0%
25	high	65.4%	20.1%	9.2%	2.0%	1.3%	0.7%	0.5%	0.8%
25	med	49.4%	28.7%	16.2%	2.0%	1.4%	0.8%	0.5%	1.0%
26	med	55.4%	28.4%	11.9%	1.7%	1.0%	0.5%	0.3%	0.7%

Table B.1. Continued

Site no	Energy	-2mm +850μm	-850 +425μm	-425 +212μm	-212 +150μm	-150 +106μm	-106 +75μm	-75 +53μm	-53μm
27	high	55.4%	21.1%	13.5%	2.7%	1.9%	1.3%	1.1%	3.0%
27	med	64.9%	19.5%	9.9%	1.7%	1.3%	0.8%	0.6%	1.3%
28	high	50.1%	27.7%	14.2%	2.4%	1.6%	0.9%	0.7%	2.4%
28	med	49.5%	28.5%	13.8%	2.7%	1.9%	1.2%	0.8%	1.5%
29	high	49.6%	27.4%	14.1%	2.8%	1.8%	0.7%	1.3%	2.2%
29	med	60.4%	21.2%	11.3%	2.2%	1.4%	1.2%	0.4%	2.0%
30	high	59.1%	19.4%	11.7%	2.7%	1.8%	1.2%	0.8%	3.3%
30	med	49.7%	29.1%	11.7%	2.4%	1.4%	1.0%	0.9%	3.8%
31	med	78.7%	14.8%	4.2%	0.8%	0.5%	0.3%	0.2%	0.3%
32	high	62.7%	19.2%	10.0%	2.4%	1.3%	1.0%	0.6%	2.7%
32	med	42.9%	29.8%	17.9%	2.8%	1.7%	1.2%	0.8%	2.9%
33	high	59.2%	21.8%	11.4%	1.9%	1.4%	1.0%	0.7%	2.5%
33	med	58.0%	22.4%	11.9%	1.8%	1.5%	0.9%	0.8%	2.8%
34	high	29.6%	33.0%	20.7%	4.3%	3.2%	2.3%	1.8%	5.2%
34	med	33.2%	34.5%	19.5%	3.9%	2.4%	1.7%	1.2%	3.6%
35	high	58.9%	21.5%	11.6%	2.1%	1.8%	1.1%	0.8%	2.2%
35	med	58.2%	23.3%	12.6%	1.7%	1.3%	0.9%	0.6%	1.4%
35	low	2.7%	11.8%	33.9%	15.6%	11.9%	8.1%	5.0%	10.8%
36	high	59.3%	21.5%	12.9%	1.8%	1.3%	0.9%	0.6%	1.7%
36	med	43.7%	25.2%	18.8%	3.8%	2.4%	1.8%	1.4%	2.9%
36	low	0.0%	0.7%	10.6%	15.7%	24.4%	20.2%	12.6%	15.9%
37	high	43.4%	30.5%	17.7%	1.5%	2.8%	1.1%	0.8%	2.1%
37	med	48.2%	22.6%	16.8%	4.3%	2.6%	1.9%	1.3%	2.2%
37	low	1.3%	8.3%	30.4%	21.6%	15.6%	9.9%	5.3%	7.6%
38	high	44.7%	30.1%	15.9%	3.4%	1.9%	1.3%	0.8%	1.9%
38	med	30.8%	36.9%	21.1%	3.9%	2.7%	1.7%	1.0%	1.9%
38	low	0.6%	7.9%	46.4%	20.2%	12.7%	6.6%	2.9%	2.9%
39	high	38.7%	33.7%	16.6%	3.4%	2.3%	1.5%	1.0%	2.8%
39	med	38.8%	36.5%	16.2%	2.6%	1.8%	1.1%	0.8%	2.1%
39	low	6.7%	16.4%	36.1%	17.7%	11.3%	5.8%	3.4%	2.6%
40	high	52.8%	26.9%	12.3%	2.0%	1.5%	1.0%	0.8%	2.7%
40	med	55.5%	26.4%	11.5%	1.3%	1.8%	0.8%	0.6%	2.1%
40	low	3.8%	1.8%	1.8%	18.1%	21.8%	17.5%	10.3%	24.9%
41	med	58.4%	23.4%	11.7%	1.8%	1.3%	0.9%	0.6%	1.8%
41	low	17.4%	26.9%	25.8%	9.8%	7.5%	3.8%	2.2%	6.5%

Table B.2. Texture (%) of surficial deposits at Pascua-Lama.

Media	Field no.	-4 +2mm (%)	-2mm +850μm (%)	-850 +425μm (%)	-425 +212μm (%)	-212 +106μm (%)	-75 +53μm (%)	-53μm (%)
alluvial	102	32.45	24.96	15.86	12.59	5.43	3.02	5.68
alluvial	103	33.07	22.47	15.79	11.14	6.35	3.57	7.61
alluvial	104	40.62	26.37	14.06	8.04	4.41	2.38	4.13
alluvial	109	39.57	23.6	11.76	10.7	5.34	1.9	7.13
alluvial	110	32.72	20.29	12.08	12.2	8.19	3.69	10.83
alluvial	111	26.9	18.03	13.02	13.37	9.29	3.97	15.42
alluvial	115	44.87	24.44	15.01	8.22	3.34	1.48	2.63
alluvial	116	31.75	16.71	14.31	16.39	9.83	4.47	6.54
alluvial	117	33.33	14.83	13.18	14.09	8.22	3.77	12.57
alluvial	119	8.18	22.51	13.02	19.38	16.83	7.71	12.37
alluvial	120	54.75	28.59	10.65	3.33	1.14	0.55	0.99
alluvial	121	50.81	21.26	11.45	7.88	4.46	1.92	2.22
alluvial	125	44.74	19.9	9.75	8.37	6.84	3.34	7.05
alluvial	126	33.94	16.53	9.66	9.53	8.32	5.33	16.68
alluvial	127	33.2	20.4	11.51	10.32	7.51	4.55	12.51
alluvial	128	37.29	20.9	12.14	11.63	8.2	5.23	4.61
alluvial	131	32.96	12.2	14.98	13.7	11.48	5.67	9.01
alluvial	132	10.37	6.01	4.1	5.76	13.74	20.48	39.53
alluvial	133	9.61	9.43	7.12	10.37	11.75	12.52	39.2
alluvial	136	16.26	14.94	10.41	11.85	12.24	9.61	24.69
alluvial	144	31.44	26.66	13.31	13.41	5.55	2.47	7.17
alluvial	145	33.84	27.33	15.7	10.79	5.43	2.25	4.67
alluvial	146	22.24	18.93	16.7	18.36	11.27	4.46	8.04
alluvial	147	28.43	25.05	15.7	11.62	7.28	3.51	8.41
alluvial	148	37.98	24.28	12.65	10.54	5.74	2.85	5.96
debris	14	41.97	30.06	17.25	7.18	2.06	0.79	0.69
debris	19	38.51	21.2	18.35	11.56	4.88	2.23	3.27
debris	25	45.29	21.11	19.62	9.2	2.61	1.08	1.1
debris	52	35.89	24.37	18.55	11.18	4.35	2.2	3.45
debris	69	39.64	28.78	17.32	7.09	3.38	1.67	2.12
debris	74	23.87	23.63	27.31	13.3	4.95	2.53	4.41
debris	75	24.93	15.83	19.06	16.07	11.39	5.59	7.13
debris	79	20.19	23.08	21.83	16.01	7.82	3.98	7.09
debris	80	17.8	10.32	17.13	25.61	12.88	5.85	10.41
debris	84	23.99	21.24	16.58	18.2	9.66	4.48	5.84
debris	85	30.74	23.87	15.1	12.41	7.98	4.17	5.72
debris	89	14.83	15.35	20.69	25.54	12.22	4.51	6.86
debris	90	30.86	23.49	14.47	15.5	7.36	3.55	4.77
debris	91	15.47	18.66	20.66	22.22	12.07	4.58	6.36
debris	92	16.5	14.83	20.37	24.39	13.34	4.16	6.39
debris	96	27.62	24.77	18.69	15.16	6.2	2.47	5.09
debris	101	20.42	20.68	18.15	18.69	9.78	4.35	7.94
debris	156	25.69	18.76	24.68	19.54	6.31	2.59	2.43

Table B.2. Continued

Media	Field no.	-4 +2mm (%)	-2mm +850µm (%)	-850 +425µm (%)	-425 +212µm (%)	-212 +106µm (%)	-75 +53µm (%)	-53µm (%)
debris	157	26.4	20.18	14.76	13.88	6.76	6.08	11.95
debris	97	9.72	15.06	26.08	19.5	10.23	5.04	14.36
debris	158	35.22	18.17	19.81	16.35	5.16	2.81	2.47
debris	159	23.33	14.51	9.6	20.78	12.5	7.81	11.48
debris	160	20.98	11.72	14.93	20.91	16.57	6.91	7.99
debris	161	16.67	10.39	13.77	21.68	17.41	8.82	11.25
debris	162	19.96	11.32	11.01	20.64	19.01	9.11	8.94
debris	163	21.69	13.75	18.33	22.66	11.75	5.49	6.34
debris	164	20.33	14.21	18.71	22.55	11.4	4.79	8.01
debris	165	23.12	17.82	19.16	19.09	7.91	5.27	7.64
debris	304	22.16	20.08	16.4	16.46	8.59	4.59	11.71
debris	305	28.88	21.87	24.09	10.78	5.63	3.19	5.56
debris	306	34.91	20.03	17.98	14.86	6.52	2.42	3.28
debris	307	24.88	16.14	19.46	21.12	9.02	3.83	5.54
debris	308	30.62	22.55	22.79	13.18	4.97	2.9	3
debris	309	21.01	15.16	15.25	23.32	13.39	5.6	6.26
debris	310	20.47	15.2	21.89	22.37	8.86	4.5	6.71
debris	311	33.03	18.54	16.14	16.57	6	3.41	6.32
debris	312	17.1	17.77	26.61	17.41	10.21	4.6	6.3
debris	318	26.04	21.1	21.23	19.51	6.53	2.48	3.11
talus	320 (16)	24.99	15.16	8.97	14.1	12.7	8.87	15.22
talus	24	19.58	17.16	11.2	14.9	12.18	7.81	17.17
talus	53	29.87	14.59	8.5	10.52	10.04	2.83	23.66
talus	105	17.87	18.91	24.32	14.36	7.9	3.56	13.07
talus	106	24.79	19.28	15.53	17.14	9.92	4.36	8.98
talus	107	19.39	20.65	21.41	19.64	9.49	3.35	6.07
talus	108	14.09	18.84	20.55	24.59	8.6	3.49	9.85
talus	112	25.35	20.8	13.86	14.32	8.64	5.04	11.99
talus	113	14.01	17.95	18.91	30.2	9.64	3.37	5.93
talus	114	36.55	16.5	13.09	12.62	9.94	2.43	8.88
talus	118	3.58	8.5	16.92	24.87	23.02	9.03	14.09
talus	122	46.61	25.5	10.19	7.79	4.12	2.12	3.66
talus	123	25.33	26.27	13.84	13.75	11.31	5.37	4.12
talus	124	6.87	14.28	20.78	30.26	15.58	5.82	6.42
talus	129	21.58	13.46	8.47	16.5	18.35	6.03	15.61
talus	130	25.79	15.37	14.99	16.47	12.77	7.02	7.6
talus	134	27.81	13.17	10.92	17.04	14.04	4.63	12.4
talus	135	12.87	13.31	12.39	18.42	18.7	9.55	14.76
talus	137	36	14.57	9.44	11.82	8.41	6.09	13.66
talus	138	9.37	10.18	6.88	23.89	24.11	12.58	13
talus	140	20.98	13.39	13.57	18.23	14.04	6.09	13.7
talus	141	35.09	27.45	15.54	8.94	4.58	1.15	7.26
talus	142	58.96	14.93	8.15	8.03	3.94	1.47	4.52

Table B.2. Continued

Media	Field no.	-4 +2mm (%)	-2mm +850µm (%)	-850 +425µm (%)	-425 +212µm (%)	-212 +106µm (%)	-75 +53µm (%)	-53µm (%)
talus	143	2.42	28.99	23.62	17.51	9.31	1.92	16.23
talus	139	37.63	20.68	15.04	13.5	6.31	2.45	4.38
talus	149	29.54	22.39	16.93	10.28	6.3	3.7	10.88
talus	150	25.37	20.79	20.65	16	6.29	3.15	7.75
talus	151	14.51	25.95	26.3	21.61	6.29	2.68	2.67
talus	152	35.74	18.51	15.34	13.54	8.38	3.02	5.46
talus	153	12.59	20.53	25.16	20.06	7.47	2.78	11.41
talus	154	14.82	12.53	10.88	12.43	12.83	8.63	27.87
talus	155	24.5	23.91	14.75	15.56	8.98	4.83	7.46
talus	216	21.97	13.54	13.21	24.17	15.48	6.46	5.17
talus	219	81.05	9.93	1.91	1.36	1.11	1.35	3.29
talus	221	64.24	10.4	4.03	2.88	2.32	2.24	13.89
talus	222	77.35	10.49	1	0.56	0.93	1.13	8.52
talus	223	63.07	15.19	3.18	1.81	1.94	1.72	13.08
talus	224	44.84	19.57	11.81	9.87	7.43	5.02	1.46
talus	225	44.55	17.62	11.27	8.59	5.36	2.67	9.93
talus	226	32.33	19.65	9.99	8.66	5.37	4.05	19.96
talus	227	33.1	33.1	5.25	4.52	3.22	2.74	18.08
talus	228	24.03	23.27	16.39	10.57	6.32	3.56	15.86
talus	229	24.13	19.88	19.06	15.33	8.74	5.17	7.68
talus	230	27.71	20.71	15.17	13.19	8.35	5.6	9.27
talus	231	28.56	27.07	15.26	12.06	5.72	2.7	8.64
talus	232	33.87	21.04	15.38	13.64	5.83	3.78	6.46
talus	233	28.53	22.19	11.62	11.75	6.89	4.42	14.6
talus	234	32.25	26.35	15.41	10.17	5.99	3.46	6.38
talus	235	60.02	20.86	9.52	5.06	1.68	0.84	2.01
talus	236	76.91	18.12	1.58	0.42	0.38	0.49	2.09
till	4	28.76	22.69	13.43	16.85	9.07	5.64	3.57
till	5	45.82	19.43	12.87	9.95	5.5	3.32	3.11
till	9	34.47	19.66	11.73	11.67	7.25	4.47	10.76
till	10	27.27	21.53	12.44	14.71	9.05	5.96	9.05
till	15	15.72	15.65	15.58	20.21	14.72	7.06	11.05
till	26	16.01	14.84	16.83	30.96	12.21	5.58	3.58
till	54	13.41	12.61	15.96	16.55	14.08	8.26	19.13
till	55	17.4	13.35	11.61	11.64	8.65	6.23	31.11
till	56	22.23	18.29	12.3	14.33	11.79	7.73	13.34
till	57	22.83	19.33	10.09	10.35	7.99	5.37	24.05
till	58	12.86	17.5	17.14	18.52	11.31	5.55	17.13
till	59	21.34	16.87	19.09	23.74	1.13	6.02	11.81
till	60	17.42	19.64	19.04	16.21	9.68	5.62	12.37
till	61	8.03	11.39	18.65	32.65	18.99	6.11	4.19
till	62	16.4	14.34	12.3	30.42	21.72	0.58	4.22
till	63	24.57	17.54	7.29	7.93	7.49	4.73	30.45

Table B.2. Continued

Media	Field no.	-4 +2mm (%)	-2mm +850μm (%)	-850 +425μm (%)	-425 +212μm (%)	-212 +106μm (%)	-75 +53μm (%)	-53μm (%)
till	64	14.87	13.52	10.3	14.47	10.42	7.85	28.56
till	65	26.01	8.76	9.42	20.84	19.95	9.35	5.67
till	217	19.3	22.5	14.1	9.8	6.6	5.3	22.3
till	218	46.5	21.8	8.8	6.5	4.7	4.7	7.1
till	220	27.7	18.5	12.5	11.1	8.6	5.7	15.9
till	279	12.8	14	14.9	15	10.7	9	23.6
till	287	25.8	21.2	19.2	12.8	7.5	4.8	8.6
till	288	19.2	34.1	28.3	9.7	3.1	2.1	3.6
till	297	31.2	21.7	24.4	12.7	5	2.7	2.3
till	298	33.1	16.5	11.6	9.8	6.9	6.1	16.1
till	292	19.3	15.8	13.1	17.7	13.5	9.1	11.5
till	283	28.3	16.2	15.8	14.9	9.8	6.6	8.4
till	319	16.9	14.4	12.4	16.2	12.8	13.6	13.8
till	293	26.3	24.4	18.5	11.7	6.4	3.7	9

Table C.1. Results of neutron activation analysis of heavy mineral separates.

Site no	Size fraction	Sb (ppm)	As (ppm)	Ba (ppm)	Br (ppm)	Ce (ppm)	Cr (ppm)	Co (ppm)
1	-75+53µm	30	700	53400	4	200	230	47
1	-106+75µm	25	624	37700	3	170	220	53
37	-75+53µm	17	160	19400	3	300	280	55
37	-106+75µm	10	110	10900	-2	170	160	58

Site no	Size fraction	Au (ppb)	La (ppm)	Hg (ppm)	Mo (ppm)	Sc (ppm)	Se (ppm)	Ag (ppm)
1	-75+53µm	37200	97	-10	21	28.0	-10	17
1	-106+75µm	7800	85	-10	34	24.0	-10	-10
37	-75+53µm	13000	150	-10	11	28.0	-10	-10
37	-106+75µm	3800	92	-10	9	19.0	-10	-10

Site no	Size fraction	Ta (ppm)	Th (ppm)	W (ppm)	U (ppm)	Yb (ppm)	Zn (ppm)
1	-75+53µm	10	54	45	56	20	610
1	-106+75µm	9	34	27	31	14	550
37	-75+53µm	9	52	20	29	12	600
37	-106+75µm	5	29	9	14	7	600

values at or below detection limit indicated by (-)

Table C.2. Results of total digestion of light mineral separates.

Site No.	Size fraction	Au (ppb)	As (ppm)	Hg (ppb)	Al (%)	Sb (ppm)	Ba (ppm)	Be (ppm)	Bi (ppm)	Cd (ppm)	Ca (%)	Ce (ppm)
1	-75+53μm	40	322	160	6.6	7.5	200	1.35	2.5	0.6	0.7	85.9
1	-106+75μm	30	311	70	6.46	7.1	500	1.45	2.52	0.28	0.72	38.2
37	-75+53μm	155	105	70	8.1	4.2	550	2.15	2.2	1.54	1.63	52.3
37	-106+75μm	30	96	50	7.64	3.7	520	1.95	1.98	1.08	1.63	46.9

Site No.	Size fraction	Cs (ppm)	Cr (ppm)	Co (ppm)	Cu (ppm)	Ga (ppm)	Ge (ppm)	Fe (%)	La (ppm)	Pb (ppm)	Li (ppm)	Mg (%)
1	-75+53μm	12.35	11	3.6	128	16.9	1.4	6.63	20.5	302	22.8	0.39
1	-106+75μm	10.65	9	3.2	117	16.2	1.4	6.27	19	289	20.8	0.36
37	-75+53μm	6.75	13	10.4	227	17.3	1.2	3.27	26	130	26.8	0.67
37	-106+75μm	6.1	12	9.2	197	16.9	1.2	3.2	24	120	25	0.64

Site No.	Size fraction	Mn (ppm)	Mo (ppm)	Ni (ppm)	Nb (ppm)	P (ppm)	K (%)	Rb (ppm)	Ag (ppm)	Na (%)	Sr (ppm)	Ta (ppm)
1	-75+53μm	575	3	7.4	7.4	640	2.26	98.8	1.55	1.62	256	0.55
1	-106+75μm	450	3.2	4	6.8	510	2.18	96.2	1.4	1.64	264	0.5
37	-75+53μm	1140	4.8	10.8	7.8	790	2.01	85.6	1.45	2.54	270	0.55
37	-106+75μm	985	4	9.4	7.4	690	1.88	84	1.45	2.43	261	0.55

Site No.	Size fraction	Te (ppm)	Tl (ppm)	Th (ppm)	Ti (ppm)	W (ppm)	U (ppm)	V (ppm)	Y (ppm)	Zn (ppm)
1	-75+53μm	1	2.88	7.4	0.24	1.6	1.4	74	10.9	176
1	-106+75μm	1.1	2.9	7.2	0.2	1.8	1.2	67	9	158
37	-75+53μm	0.7	1.66	7.2	0.23	1.8	2.4	44	18.5	528
37	-106+75μm	0.6	1.56	6.8	0.23	1.6	2.2	43	16.6	432

Table C.3. Results of total digestion of bulk chemical precipitate samples.

Sample no.	UTM-E	UTM-N	Elev	As (ppm)	Hg (ppb)	Al (%)	Sb (ppm)	Ba (ppm)	Be (ppm)	Bi (ppm)	Cd (ppm)	Ca (%)	Ce (ppm)	Cs (ppm)	Cr (ppm)
27	19408938	6753523	3936	198	10	0.84	0.9	120	0.35	0.25	0.02	0.68	4.63	4	4
28	19408938	6753523	3936	141	10	0.37	0.6	60	0.15	0.12	0.02	13.3	3.49	2.45	3
35	19408831	6753546	3777	116	20	0.94	1.3	130	0.05	0.46	0.02	0.06	5.29	2.95	4
36	19408831	6753546	3777	267	20	2.21	3	260	0.6	0.82	0.02	0.95	14.2	7.45	6
37	19408831	6753546	3777	22	10	0.42	0.5	20	0.2	0.18	0.04	17.6	8.53	2.65	1
38	19408647	6753589	3951	75	10	0.97	1	90	0.75	0.34	0.14	15.9	13.2	2.6	1
39	19408647	6753589	3951	552	10	4.84	5	550	1	1.44	0.04	0.81	29.9	13.4	9
40	19408647	6753589	3951	641	10	1.3	2.1	160	0.2	0.56	0.02	0.14	6.85	4.45	6
43	19407937	6753521	3759	21	10	0.28	0.4	30	0.35	0.18	0.06	19.25	5.19	3.55	1
45	19407937	6753521	3759	2	10	0.08	0.6	30	0.15	0.04	0.08	17.4	0.6	0.2	1
46	19407775	6753638	3921	4	10	0.23	0.4	10	0.3	0.12	0.06	19	2.73	5	1
47	19407775	6753638	3921	13	10	0.19	0.3	20	0.05	0.07	0.02	21.2	1.73	0.8	1

Sample no.	Co (ppm)	Cu (ppm)	Ga (ppm)	Ge (ppm)	Fe (%)	La (ppm)	Pb (ppm)	Li (ppm)	Mg (%)	Mn (ppm)	Mo (ppm)	Ni (ppm)	Nb (ppm)	P (ppm)	K (%)
27	3	9	2.5	1	(+)25.0	2	27	4.2	0.22	455	0.6	1	0.8	150	2.48
28	2.2	3	1.1	0.4	12.15	1.5	27	2.6	0.12	185	0.2	4.4	0.4	100	0.96
35	2.6	13	3.1	1.2	(+)25.0	2.5	46	1.4	0.03	140	1	0.2	1	200	1.21
36	3.2	22	6.3	1	(+)25.0	7	75	7.6	0.09	225	2.8	0.8	2.2	260	2.03
37	1.8	1	0.9	0.1	0.71	2.5	18.5	5.4	0.24	195	0.2	6.2	0.2	10	0.23
38	3.2	9	2.4	0.1	0.97	4.5	29	12.4	0.66	730	0.8	6.8	1	70	0.46
39	4.2	34	13.8	1.3	12.8	14	160	6.8	0.16	375	4.8	0.8	5.4	500	2.15
40	1	10	4.1	1.2	(+)25.0	3.5	44.5	2.4	0.08	125	3.2	0.6	1	230	0.58
43	0.8	1	0.6	0.1	0.11	1	20	8.4	0.4	580	0.2	6.2	0.2	10	0.14
45	0.6	7	0.3	0.1	10.95	0.5	18	0.2	0.01	60	0.2	4.6	0.2	10	0.18
46	2.6	3	0.5	0.1	0.13	0.5	13	9	0.55	795	0.2	6	0.2	10	0.15
47	0.6	1	0.4	0.1	0.65	0.5	10.5	0.8	0.01	30	0.2	6.4	0.2	10	0.18

Table C.3. Continued

Sample no.	Rb (ppm)	Ag (ppm)	Na (%)	Sr (ppm)	Ta (ppm)	Te (ppm)	Tl (ppm)	Th (ppm)	Ti (%)	W (ppm)	U (ppm)	V (ppm)	Y (ppm)	Zn (ppm)
27	37.2	0.1	0.47	80.4	0.15	0.05	5	1.2	0.02	3.4	0.2	102	1.4	92
28	16.4	0.05	0.17	258	0.05	0.05	2	0.4	0.01	3.1	0.2	82	4.6	46
35	20.8	0.2	0.19	30.6	0.15	0.15	1.38	1.2	0.03	3.8	0.2	98	1.1	108
36	56.8	0.3	0.35	70.7	0.25	0.25	2.52	2.8	0.06	3	0.4	71	2.4	112
37	11.4	0.15	0.21	615	0.05	0.05	0.74	0.2	0.01	2	0.2	2	16.6	28
38	30.6	0.25	0.46	444	0.1	0.15	1.14	1.2	0.03	2.4	0.2	10	14.5	100
39	100	0.5	0.67	138.5	0.85	0.4	2.68	6.8	0.14	15.3	1	69	4.8	84
40	25.2	0.25	0.22	36.6	0.05	0.15	3.52	1.4	0.03	1.4	0.2	66	1.4	56
43	9.6	0.15	0.26	503	0.05	0.05	0.26	0.2	0.01	0.6	0.2	1	28.2	46
45	1.8	0.25	0.02	60.5	0.05	0.05	0.12	0.2	0.01	0.9	0.2	4	1.1	38
46	9.4	0.15	0.27	420	0.2	0.05	0.2	0.2	0.01	7.2	0.2	1	23.6	94
47	4	0.05	0.08	209	0.05	0.05	0.08	0.2	0.01	1.2	0.2	1	4.7	6

Table C.4. Results of ICP-MS analysis of water samples associated with chemical precipitates.

Sample No.		194	195	192	197	244	245	247	248	249
UTM-E		19408938	19408831	19408647	19407937	19398100	19398168	19398029	19400565	19399640
UTM-E2		408938	408831	408646	407937	398100	398168	398029	400565	399640
UTM-N		6753523	6753546	6753589	6753521	6758429	6758387	6758375	6757637	6757990
Elev		3936	3777	3951	3759	3984	3954	3852	4446	4206
pH		2.9	3	2.8	2.9	3.4	4	5.8	5.1	6.5
Ag	μg/l	0.1	0.1	0.1	0.1	0.05	0.05	0.05	0.05	0.05
Al	mg/l	9.2	8.3	8.9	7.5	3.87	12.1	0.011	0.241	0.007
As	μg/l	1.0	1.0	95.0	1.0	1	2	1	1	3
Ba	μg/l	2.5	6.4	7.3	9.4	10.25	16.4	70.9	3.8	1
Be	μg/l	2.5	2.0	2.5	4.0	0.5	0.5	0.5	0.5	0.5
Bi	μg/l	0.1	0.1	0.1	0.1	0.05	0.05	0.05	0.05	0.05
Ca	mg/l	402.0	350.0	387.0	808.0	71	100	39.9	37.7	16.85
Cd	μg/l	0.5	0.2	0.1	0.6	3	18.1	0.1	0.7	0.1
Co	μg/l	13.7	11.7	10.2	6.3	4.64	26.8	0.06	5.96	0.16
Cr	μg/l	0.5	0.5	1.0	0.5	0.5	0.5	0.5	0.5	0.5
Cu	μg/l	3.5	3.4	3.5	10.1	127.5	381	0.4	26.8	8.4
Fe	mg/l	1.1	4.0	22.2	6.5	0.18	0.38	0.11	0.12	0.05
Hg	μg/l	1.0	1.0	1.0	1.0	1	1	1	1	1
K	mg/l	12.0	11.7	9.6	10.8	2.9	2.7	1	1.2	1.1
Mg	mg/l	30.8	28.3	31.0	46.0	10.15	19.25	9.76	8.42	2.83
Mn	μg/l	3820.0	3780.0	4770.0	12480.0	1415	9960	5.1	888	4.9
Mo	μg/l	0.1	0.1	0.1	0.1	0.1	0.5	1.1	0.1	0.1
Na	mg/l	15.8	14.3	14.4	21.8	5.2	6.4	4.05	4.7	4.25
Ni	μg/l	14.6	12.8	12.0	8.6	7.8	29.8	0.2	4	0.2
P	mg/l	0.1	0.1	0.1	0.1	0.1	0.1	0.1	0.1	0.1
Pb	μg/l	2.0	2.0	2.0	4.0	2	2	2	2	2
Sb	μg/l	0.1	0.1	0.1	0.1	0.05	0.05	0.05	0.05	0.05
Se	μg/l	1.0	1.0	1.0	2.0	1	2	1	1	1
Sn	μg/l	0.5	0.5	0.5	0.5	0.5	0.5	0.5	0.5	0.5
Sr	μg/l	676.0	588.0	600.0	1340.0	53.5	135	154	50.6	12.25
Ti	μg/l	1.0	1.0	1.0	1.0	1	1	1	1	1
Tl	μg/l	4.4	4.0	2.9	1.6	0.45	0.55	0.05	0.05	0.05
U	μg/l	0.4	0.4	0.4	0.3	0.7	2.9	1.3	0.15	0.4
V	μg/l	1.0	1.0	6.0	1.0	1	1	1	1	1
Zn	μg/l	347.0	355.0	422.0	545.0	665	3620	4	100.5	2.5

Table D.3. Results of duplicate analysis of stream sediments after cold hydroxylamine leach.

Ag (ppm)		Al (ppm)		As (ppm)		Au (ppm)		Ba (ppm)		Be (ppm)	
original	duplicate	original	duplicate	original	duplicate	original	duplicate	original	duplicate	original	duplicate
0.352	0.314	493	519	1.2	0.9	0.15	0.1	2	1.85	0.05	0.05
0.036	0.042	376	380	0.1	0.2	0.15	0.1	82.9	70.3	0.15	0.2
0.784	0.752	603	595	0.1	0.1	0.05	0.25	88.7	91.2	0.15	0.15

Bi (ppm)		Br (ppm)		Ca (ppm)		Cd (ppm)		Ce (ppm)		Co (ppm)	
original	duplicate	original	duplicate	original	duplicate	original	duplicate	original	duplicate	original	duplicate
0.04	0.015	2	2	440	410	0.04	0.03	0.25	0.255	0.35	0.4
0.005	0.005	2	2	1850	1840	0.26	0.28	0.44	0.39	11.2	11.1
0.005	0.005	2	2	1430	1400	3.38	3.39	1.365	1.315	13.4	12.7

Cr (ppm)		Cs (ppm)		Cu (ppm)		Dy (ppm)		Er (ppm)		Eu (ppm)	
original	duplicate	original	duplicate	original	duplicate	original	duplicate	original	duplicate	original	duplicate
0.15	0.05	0.26	0.255	19.1	21.1	0.035	0.045	0.02	0.025	0.005	0.005
0.05	0.05	0.05	0.045	15.35	14.8	0.13	0.115	0.07	0.075	0.015	0.02
3.7	0.05	0.075	0.07	78.1	71.5	0.165	0.15	0.095	0.105	0.025	0.025

Fe (ppm)		Gd (ppm)		Hg (ppm)		Ho (ppm)		I (ppm)		K (ppm)	
original	duplicate	original	duplicate	original	duplicate	original	duplicate	original	duplicate	original	duplicate
1855	1895	0.05	0.055	0.1	0.1	0.005	0.005	3.2	0.9	20	5
355	355	0.115	0.12	0.1	0.1	0.03	0.025	2.2	2.4	170	170
335	290	0.17	0.155	0.1	0.1	0.035	0.035	1.5	2.8	150	150

Li (ppm)		Lu (ppm)		Mg (ppm)		Mn (ppm)		Mo (ppm)		Na (ppm)	
original	duplicate	original	duplicate	original	duplicate	original	duplicate	original	duplicate	original	duplicate
0.9	0.25	0.005	0.005	93	99	20.1	23.3	0.01	0.01	10	10
0.8	0.75	0.005	0.01	327	323	246	243	0.01	0.01	30	30
2.55	1.9	0.01	0.01	148	149	2070	1970	0.5	0.03	40	40

Nb (ppm)		Nd (ppm)		Ni (ppm)		P (ppm)		Pb (ppm)		Pr (ppm)	
original	duplicate	original	duplicate	original	duplicate	original	duplicate	original	duplicate	original	duplicate
0.01	0.01	0.165	0.185	0.3	0.35	5	5	0.3	0.1	0.04	0.04
0.01	0.01	0.25	0.215	1.7	1.75	15	15	0.1	0.1	0.05	0.045
0.01	0.01	0.53	0.48	24.8	3.1	5	5	0.8	0.4	0.125	0.11

Table D.3. Continued.

Rb (ppm)		Sb (ppm)		Se (ppm)		Sm (ppm)		Sn (ppm)		Sr (ppm)	
original	duplicate	original	duplicate	original	duplicate	original	duplicate	original	duplicate	original	duplicate
1.28	1.27	0.035	0.03	0.5	0.5	0.045	0.055	0.05	0.05	0.9	0.85
1.31	1.29	0.005	0.005	0.5	0.5	0.17	0.175	0.05	0.05	7.35	7.15
1	1.03	0.02	0.01	0.5	0.5	0.215	0.215	0.05	0.05	8.4	8.6

Tb (ppm)		Te (ppm)		Th (ppm)		TI (ppm)		Tl (ppm)		Tm (ppm)	
original	duplicate	original	duplicate	original	duplicate	original	duplicate	original	duplicate	original	duplicate
0.005	0.005	0.05	0.05	0.01	0.01	1	1	0.055	0.05	0.005	0.005
0.02	0.02	0.05	0.05	0.01	0.01	1	1	0.055	0.05	0.01	0.01
0.03	0.025	0.05	0.05	0.01	0.01	1	1	0.18	0.165	0.015	0.015

U (ppm)		V (ppm)		W (ppm)		Yb (ppm)		Zn (ppm)		Zr (ppm)	
original	duplicate	original	duplicate	original	duplicate	original	duplicate	original	duplicate	original	duplicate
0.03	0.065	1.8	1.85	0.01	0.01	0.02	0.02	9	9.8	0.05	0.05
0.33	0.325	0.85	0.95	0.01	0.01	0.055	0.06	5	4.8	0.05	0.35
0.235	0.175	0.9	1	0.01	0.01	0.08	0.08	321	310	0.05	0.05

B (ppm)		Ga (ppm)		Ge (ppm)		Hf (ppm)		In (ppm)		La (ppm)	
original	duplicate	original	duplicate	original	duplicate	original	duplicate	original	duplicate	original	duplicate
2	2	0.05	0.05	0.1	0.1	0.01	0.01	0.005	0.005	0.115	0.115
2	2	0.05	0.05	0.1	0.1	0.01	0.01	0.005	0.005	0.165	0.14
2	2	0.05	0.05	0.1	0.1	0.01	0.01	0.005	0.005	0.565	0.375

Re (ppm)		Ta (ppm)		Y (ppm)		pH	
original	duplicate	original	duplicate	original	duplicate	original	duplicate
0.001	0.001	0.01	0.01	0.19	0.205	2.2	2.2
0.001	0.001	0.01	0.01	0.9	0.905	3	2.8
0.001	0.001	0.01	0.01	1.31	1.275	3.2	3.1

*c16385D Table D.1. Results of laboratory duplicates for Au determination in stream sediments.

Field no.	Size fraction	Original	Duplicate
170	-150+106μm	5	10
16	-150+106μm	50	40
258	-150+106μm	5	5
273	-150+106μm	30	15
167	-150+106μm	10	10
86	-106+75μm	10	10
49	-106+75μm	760	55
290	-106+75μm	715	285
73	-106+75μm	85	110
278	-106+75μm	15	30
99	-75+53μm	25	380
168	-75+53μm	5	90
66	-75+53μm	135	125
262	-75+53μm	185	80
286	-75+53μm	25	15
21	-53μm	45	50
50	-53μm	1060	1165
281	-53μm	15	50
202	-53μm	50	45
266	-53μm	295	245
267	-53μm	270	285
299	-53μm	355	310
296	-53μm	145	140
93	-53μm	490	485

Table D.4. Results of duplicate analysis of stream sediments after total digestion.

As (ppm)		Hg (ppb)		Al (%)		Sb (ppm)	
original	duplicate	original	duplicate	original	duplicate	original	duplicate
387	402	15930	17430	7.63	7.68	17.5	18.2
43	40	40	60	8.87	8.99	1.3	1.3
85	84	1080	490	7.91	7.83	3.8	3.9

Ba (ppm)		Be (ppm)		Bi (ppm)		Cd (ppm)	
original	duplicate	original	duplicate	original	duplicate	original	duplicate
180	540	1.2	1.15	10.6	11.5	0.3	0.26
670	680	2.25	2.35	1.57	1.54	0.54	0.58
840	870	2.5	2.2	2.94	2.93	4.24	4.08

Ca (%)		Ce (ppm)		Cs (ppm)		Cr (ppm)	
original	duplicate	original	duplicate	original	duplicate	original	duplicate
0.35	0.36	37.5	37.1	10.4	10.85	31	29
0.79	0.78	65.7	63.4	7.65	7.8	43	42
1.09	1.08	77.8	72	8.7	8.55	36	35

Co (ppm)		Cu (ppm)		Ga (ppm)		Ge (ppm)	
original	duplicate	original	duplicate	original	duplicate	original	duplicate
4.8	4.8	170	182	26.5	24.9	1.6	1.6
21.2	21	105	107	23.9	25	1.5	1.5
22.2	21.8	332	334	20.6	20.2	1.7	1.7

Fe (%)		La (ppm)		Pb (ppm)		Li (ppm)	
original	duplicate	original	duplicate	original	duplicate	original	duplicate
6.03	5.96	16	17.5	438	406	12.8	12.2
5.09	5.18	30	28	38	34	19.8	22.4
4.42	4.43	35.5	33	128	134	31.2	28

Mg (%)		Mn (ppm)		Mo (ppm)		Ni (ppm)	
original	duplicate	original	duplicate	original	duplicate	original	duplicate
0.38	0.39	300	310	7.4	7	10.4	10.6
1.03	1.05	775	785	11.4	11.6	22.2	22.2
0.8	0.8	3110	3050	12.6	12.4	23.8	23.6

Nb (ppm)		P (ppm)		K (%)		Rb (ppm)	
original	duplicate	original	duplicate	original	duplicate	original	duplicate
9.8	8	690	640	2.43	2.34	108.5	107.5
9	8.4	890	880	2.27	2.31	147	157
13	12.8	810	800	2.07	2.05	123.5	122

Table D4. Cont'd.

Ag (ppm)		Na (%)		Sr (ppm)		Ta (ppm)	
original	**duplicate**	**original**	**duplicate**	**original**	**duplicate**	**original**	**duplicate**
19.05	19.45	0.99	0.97	263	251	0.45	0.45
0.6	0.6	1.73	1.73	256	254	0.5	0.5
2.85	2.55	2.14	2.11	216	226	0.75	0.75

Te (ppm)		Tl (ppm)		Th (ppm)		Ti (%)	
original	**duplicate**	**original**	**duplicate**	**original**	**duplicate**	**original**	**duplicate**
4.45	4.05	4.06	4.02	9	11.8	0.32	0.28
1.65	1.75	3.78	3.78	21.2	12.4	0.34	0.33
1.1	1.05	2.52	2.52	20.2	14.2	0.35	0.34

W (ppm)		U (ppm)		V (ppm)	
original	**duplicate**	**original**	**duplicate**	**original**	**duplicate**
3.7	3.2	1.6	1.4	100	97
1.4	1.6	8.2	8	123	123
2.7	3.1	10.2	10.6	90	92

Y (ppm)		Zn (ppm)	
original	**duplicate**	**original**	**duplicate**
7.5	5.7	88	88
18.2	18.6	92	92
26	25.5	886	880

Table D.5. Results of duplicate analysis of metal concentrations in surface waters.

Al		As		Ba		Be	
Orig	**Dup**	**Orig**	**Dup**	**Orig**	**Dup**	**Orig**	**Dup**
42.1	34.6	9	10	19.3	20.1	1	1.5
0.287	0.173	4	4	31.4	31.6	0.5	0.5
0.23	0.078	1	1	7.2	6.6	0.5	0.5
0.223	0.218	6	6	32.5	33.1	0.5	0.5
8.3	8.41	1	1	6.4	6.95	2	2
0.018	0.019	1	1	21.3	22.1	0.5	0.5
0.003	0.003	1	1	15.8	15.35	0.5	0.5
1.59	1.375	1	1	21.5	21.1	0.5	0.5
12.1	11.45	2	2	16.4	15.7	0.5	1
8.19	7.96	1	1	30.8	31.4	0.5	0.5

Ca		Cd		Co		Cr	
Orig	**Dup**	**Orig**	**Dup**	**Orig**	**Dup**	**Orig**	**Dup**
133.5	107	7.7	8.1	32.4	34.4	2.5	3
103	100	0.1	0.1	1.84	1.66	0.5	0.5
28.2	29.2	0.2	0.2	0.38	0.22	0.5	0.5
91.7	94.4	0.1	0.1	1.14	1.04	0.5	0.5
350	339	0.2	0.2	11.7	11.6	0.5	0.5
38.2	41.3	1.6	1.8	3.3	3.66	0.5	0.5
26.7	25.8	0.1	0.1	0.12	0.04	0.5	0.5
54	49.7	4.2	3.9	8.42	7.78	0.5	0.5
100	93.9	18.1	17.5	26.8	25.5	0.5	0.5
85.8	80.8	11	10.8	18.8	18.75	0.5	0.5

Cu		Fe		K		Mg	
Orig	**Dup**	**Orig**	**Dup**	**Orig**	**Dup**	**Orig**	**Dup**
2290	1880	33.2	27.6	3.1	3.2	19.3	15.9
16.2	11	2.19	1.97	2.2	2.15	12.4	12.85
21.8	6.5	0.43	0.17	1.85	1.95	5.73	6.25
3.8	2.6	1	0.98	1.95	2	11.7	12
3.4	3	3.98	3.99	11.7	11.45	28.3	29.5
1.1	5.8	0.09	0.11	1.3	1.4	7.96	8.3
0.1	0.1	0.07	0.07	0.5	0.45	3.53	3.46
127.5	117.5	0.51	0.47	1.8	1.7	10.6	10
381	371	0.38	0.37	2.7	2.55	19.25	18.7
343	345	1.31	1.31	3.1	3	15.25	14.9

Mn		Mo		Na		Ni	
Orig	**Dup**	**Orig**	**Dup**	**Orig**	**Dup**	**Orig**	**Dup**
3760	3020	0.1	0.1	7.3	7.6	22.4	24.4
1095	1065	0.1	0.2	5.5	5.75	2	1.8
42.8	28.5	0.3	0.3	2.6	2.8	0.8	0.6
811	808	0.1	0.1	5.35	5.55	1.2	1.2
3780	3830	0.1	0.1	14.25	14.95	12.8	12.2
1200	1290	2.6	2.6	4.45	4.65	4.4	4.4
1.6	0.8	5.5	5.5	2.55	2.45	0.2	0.2
2480	2330	1.3	1.2	5.05	4.8	9.6	9.2
9960	9440	0.5	0.5	6.4	6.2	29.8	29.4
6380	6250	0.1	0.1	6.7	6.45	22.8	23

Table D.5. Cont'd.

Pb		Sb		Se		Sr	
Orig	Dup	Orig	Dup	Orig	Dup	Orig	Dup
8	8	0.05	0.05	1	1	360	386
2	2	0.2	0.25	1	1	180.5	177.5
2	2	0.05	0.05	1	1	74.2	74
2	2	0.3	0.3	1	1	151.5	149.5
2	2	0.05	0.05	1	1	588	589
2	2	0.05	0.05	1	1	75.2	78.8
2	2	0.05	0.05	1	1	101.5	99
2	2	0.05	0.05	2	1	79.3	75.6
2	2	0.05	0.05	2	1	135	131
2	2	0.05	0.05	1	1	110.5	109.5

Ti		Tl		U		Zn	
Orig	Dup	Orig	Dup	Orig	Dup	Orig	Dup
1	1	0.85	0.85	2.25	2.4	1785	1435
1	1	0.3	0.3	0.25	0.25	81	76.5
19	1	0.05	0.05	0.05	0.05	28	19.5
1	1	0.15	0.15	0.25	0.25	45	45.5
1	1	3.95	3.95	0.4	0.4	355	361
1	1	0.05	0.05	0.5	0.5	116	121.5
1	1	0.05	0.05	10.1	9.7	0.5	0.5
1	1	0.15	0.15	1.45	1.4	845	797
1	1	0.55	0.5	2.9	2.65	3620	2890
1	1	0.4	0.4	2.05	2.05	2040	2040

Ag		Bi		Hg		P	
Orig	Dup	Orig	Dup	Orig	Dup	Orig	Dup
0.05	0.05	0.05	0.05	1	1	0.1	0.1
0.05	0.05	0.05	0.05	1	1	0.1	0.1
0.05	0.05	0.05	0.05	1	1	0.1	0.1
0.05	0.05	0.05	0.05	1	1	0.1	0.1
0.05	0.05	0.05	0.05	1	1	0.1	0.1
0.05	0.05	0.05	0.05	1	1	0.1	0.1
0.05	0.05	0.05	0.05	1	1	0.1	0.1
0.05	0.05	0.05	0.05	1	1	0.1	0.1
0.05	0.05	0.05	0.05	1	1	0.1	0.1
0.05	0.05	0.05	0.05	1	1	0.1	0.1

Sn		V	
Orig	Dup	Orig	Dup
0.5	0.5	1	1
0.5	0.5	1	1
0.5	0.5	1	1
0.5	0.5	1	1
0.5	0.5	1	1
0.5	0.5	1	1
0.5	0.5	1	1
0.5	0.5	1	1
0.5	0.5	1	1
0.5	0.5	1	1

Table D.6. Results of duplicate analysis for surficial deposits (Au by FA-AAS, other elements by aqua regia ICP-MS).

Au -212+106μm		Au -106+53μm		Au -53μm		Al (%)		Sb (ppm)		As (ppm)	
original	duplicate	original	duplicate	original	duplicate	original	duplicate	original	duplicate	original	duplicate
10	10	20	20	5	5	2.18	2.24	0.4	0.4	9.4	9
2190	825	5	5	60	85	1.45	1.65	1.9	1.9	115	127.5
20	25	5	5	90	120	1.96	1.75	3.2	3	207	198.5
10	20	10	15	175	180	1.87	1.62	2.9	2.9	358	314
10	15	30	30	185	200	1.56	1.98	2.6	2.6	472	486
5	10	30	20	65	55	1.1	1.38	4.6	4.5	238	229
25	30	45	30	195	215	1.83	2.29	2.8	2.8	495	476
25	25	5	10	270	260	1.6	1.49	3.8	4.2	417	422
10	5	10	35	35	30	1.86	1.8	2.3	2.2	191.5	182.5
25	25	5	5	280	300	1.34	1.19	3.7	3.9	436	478
10	5	5	5	380	545	1.43	1.57	5.1	5.3	299	314
5	10	5	5	45	75	1.59	1.69	1.4	1.5	147	161.5
15	15			490	420	1.32	1.22	4.8	4.9	380	405
				440	415	1.39	1.37	12.3	12.3	600	586

Ba (ppm)		Be (ppm)		Bi (ppm)		B (ppm)		Cd (ppm)		Ca (%)	
original	duplicate	original	duplicate	original	duplicate	original	duplicate	original	duplicate	original	duplicate
140	140	1.25	1.2	0.62	0.57	10	10	0.24	0.24	0.48	0.49
240	260	0.65	1	1.78	1.97	10	10	0.38	0.4	0.43	0.47
360	330	1.05	1.05	3.29	3.01	10	10	0.6	0.6	0.41	0.37
310	280	0.6	0.45	5.63	4.48	10	10	0.2	0.16	0.09	0.08
310	290	0.35	0.8	5.84	6.48	10	10	0.16	0.22	0.08	0.1
450	470	1.4	2.05	2.23	2.47	10	10	1.54	1.64	0.23	0.27
280	290	0.35	0.75	6.71	7.01	10	10	0.24	0.2	0.09	0.14
190	190	0.3	0.75	7.25	7.29	10	10	0.12	0.14	0.06	0.05
430	400	1.45	1.45	3.87	3.93	10	10	0.54	0.56	0.31	0.3
230	220	0.35	0.35	5.64	5.33	10	10	0.14	0.14	0.06	0.06
320	350	0.9	1.05	5.09	5.61	10	10	2.14	2.26	0.31	0.33
310	320	0.85	1.35	3.18	3.49	10	10	0.82	0.9	0.37	0.39
480	450	0.6	1.05	10.75	10.65	10	10	0.64	0.66	0.25	0.24
220	210	0.75	0.35	12.9	13.05	10	10	0.2	0.26	0.13	0.12

Table D.6. Continued

Cr (ppm)		Co (ppm)		Cu (ppm)		Ga (ppm)		Ge (ppm)		Fe (%)	
original	duplicate	original	duplicate	original	duplicate	original	duplicate	original	duplicate	original	duplicate
31	32	13.2	13	57.2	57.6	6.5	6.6	0.1	0.1	3.64	3.71
16	16	8.6	9.2	179	192.5	4.3	5.1	0.1	0.1	4.14	4.54
12	11	6.6	6	127.5	116	6.8	6	0.1	0.1	4.41	4.07
14	13	5.8	5.4	110.5	96.4	7.6	6.2	0.1	0.1	6.42	6.08
20	22	4.8	5.2	79.4	86.6	6.1	6.9	0.1	0.1	5.64	6.37
10	10	9	8.8	101.5	104.5	3.8	4.2	0.1	0.1	5.21	5.67
20	20	5	5	95.8	98.1	6.7	7.7	0.1	0.1	5.69	6.06
12	13	4.4	4.6	89.1	87.6	7.6	7.1	0.1	0.1	6.41	6.54
15	15	9.6	9.2	88.4	84	5.9	5.7	0.1	0.1	5.2	5.01
10	11	4.6	4.4	181	173	6.6	6	0.1	0.1	9.21	8.78
12	11	10.4	11.4	147	163.5	5.2	6.2	0.1	0.1	5.13	5.21
18	19	10.6	11.4	139	151.5	5.2	5.9	0.1	0.1	4.36	4.53
10	10	6.2	6.4	144	148	4.8	5.3	0.1	0.1	4.04	3.79
7	8	6.2	5.8	82.6	81.4	5.5	5.3	0.1	0.1	3.78	3.76

La (ppm)		Pb (ppm)		Mg (%)		Mn (ppm)		Hg (ppm)		Mo (ppm)	
original	duplicate	original	duplicate	original	duplicate	original	duplicate	original	duplicate	original	duplicate
30	30	22	24	0.97	1	860	885	0.04	0.01	1.6	1.4
10	10	104	96	0.54	0.6	615	685	0.12	0.23	3.6	3.8
20	10	180	162	0.5	0.46	705	645	0.03	0.01	7	6.4
20	10	172	166	0.51	0.47	485	415	0.68	0.59	6.2	5.6
10	10	308	306	0.54	0.65	395	460	0.31	0.26	3.4	3.8
20	30	260	254	0.32	0.37	2710	2910	0.89	0.28	3.6	3.4
10	10	306	286	0.6	0.66	450	480	0.31	0.34	4.4	4.2
10	10	174	176	0.45	0.45	355	325	0.96	1.05	6	6.2
30	30	104	98	0.54	0.52	1030	1010	0.19	0.18	6.4	6
10	10	170	166	0.45	0.42	320	305	1.84	1.27	10	10.4
10	10	450	428	0.66	0.67	1445	1585	0.52	0.86	3.6	3.6
10	10	110	120	0.66	0.69	960	1000	0.16	0.18	6.4	7
20	20	390	380	0.37	0.33	820	830	3.28	2.19	1.8	2
10	10	402	394	0.47	0.46	940	940	0.59	0.5	3.8	4

Table D.6. Continued

Ni (ppm)		P (ppm)		K (%)		Sc (ppm)		Se (ppm)		Ag (ppm)	
original	duplicate	original	duplicate	original	duplicate	original	duplicate	original	duplicate	original	duplicate
23	23	810	800	0.18	0.18	6	6	0.5	0.5	0.1	0.1
9	9	960	1060	0.3	0.32	4	4	1.5	1.5	0.64	0.82
9	7	780	720	0.47	0.42	5	4	2.5	2.5	1.94	1.7
8	7	800	680	0.51	0.45	5	4	4	4	4.92	4.12
12	10	750	860	0.69	0.77	4	5	4.5	4.5	4.06	4.4
6	9	870	960	0.49	0.52	4	4	2	2.5	1.42	1.48
8	10	840	860	0.7	0.74	4	5	4	4.5	5.34	5.22
6	5	670	610	0.33	0.31	4	4	5	4.5	6.88	7.1
10	12	820	820	0.48	0.48	5	5	4	3.5	1.02	0.9
6	6	720	700	0.79	0.79	4	3	5	4.5	6.04	6.44
8	7	910	980	0.49	0.53	3	4	3	3	5.08	5.52
11	12	800	840	0.36	0.38	4	4	3	3	1.32	1.54
6	6	580	600	0.44	0.46	3	3	3.5	4	7.88	8.82
5	4	490	500	0.46	0.46	4	4	5	5	8.18	7.9

Na (%)		Sr (ppm)		S (%)		Te (ppm)		Tl (ppm)		Ti (%)	
original	duplicate	original	duplicate	original	duplicate	original	duplicate	original	duplicate	original	duplicate
0.02	0.03	64	65	0.04	0.05	0.05	0.05	0.18	0.18	0.12	0.13
0.05	0.06	77	85	0.39	0.41	0.55	0.55	0.66	0.74	0.05	0.06
0.08	0.07	100	93	0.68	0.64	0.85	0.85	1.34	1.24	0.01	0.01
0.09	0.08	82	76	1.02	0.9	1.8	1.6	2.62	2.18	0.03	0.03
0.15	0.17	80	95	1.53	1.69	2.4	2.55	3.06	3.54	0.03	0.03
0.05	0.06	44	53	0.85	0.87	1.25	1.3	1.94	2.18	0.01	0.01
0.15	0.16	90	101	1.57	1.59	2.55	2.65	3.16	3.56	0.02	0.03
0.06	0.05	45	45	0.62	0.61	2.25	2.3	2.1	1.94	0.04	0.03
0.07	0.07	73	71	0.82	0.79	1	0.95	3.18	3.12	0.02	0.02
0.09	0.09	106	99	1.67	1.71	1.6	1.65	3.14	3.16	0.03	0.03
0.12	0.13	115	119	0.92	0.99	1.7	1.85	2.04	2.26	0.05	0.06
0.09	0.09	80	86	0.6	0.61	0.9	0.95	1.4	1.58	0.05	0.05
0.11	0.11	61	53	0.93	0.91	2.6	2.65	2.54	2.62	0.02	0.02
0.1	0.1	81	79	0.98	0.94	2.15	2.2	1.64	1.56	0.03	0.03

Table D.6. Continued

W (ppm)		U (ppm)		V (ppm)		Zn (ppm)	
original	duplicate	original	duplicate	original	duplicate	original	duplicate
0.25	0.25	2.1	2	70	70	98	98
0.15	0.15	0.9	0.85	54	57	150	170
0.2	0.15	1.25	1.1	40	37	208	188
0.1	0.2	1.3	1.1	54	50	118	102
0.15	0.15	1.2	1.4	47	50	88	100
0.15	0.15	1.6	1.85	29	29	422	458
0.15	0.15	1.5	1.65	46	47	100	112
0.15	0.2	1	1	53	52	86	80
0.1	0.15	1.75	1.75	45	44	192	188
0.15	0.2	0.85	0.8	58	60	88	82
0.2	0.2	1.4	1.55	49	52	288	308
0.15	0.15	2	2.15	52	54	174	182
0.8	0.85	1.45	1.5	31	31	224	218
0.45	0.4	0.6	0.6	31	30	78	74

Table F. Conversion between field and laboratory sample numbers. The -53mm fraction for both sediments and surficial deposits analysed for gold and multi-element geochemistry.

Sample media	Field No.	Lab No.	Size fraction	Energy	Sample media	Field No.	Lab No.	Size fraction	Energy
sediment	200	1	-150+106	med	sediment	271	53	-150+106	med
sediment	169	2	-150+106	med	sediment	272	54	-150+106	high
sediment	86	3	-150+106	high	sediment	273	55	-150+106	med
sediment	87	4	-150+106	med	sediment	274	57	-150+106	high
sediment	98	5	-150+106	high	sediment	275	58	-150+106	med
sediment	99	6	-150+106	med	sediment	276	59	-150+106	high
sediment	21	7	-150+106	high	sediment	277	60	-150+106	med
sediment	22	8	-150+106	med	sediment	284	61	-150+106	high
sediment	168	9	-150+106	med	sediment	285	62	-150+106	med
sediment	170	10	-150+106	med	sediment	289	63	-150+106	high
sediment	1	12	-150+106	high	sediment	290	64	-150+106	med
sediment	2	13	-150+106	med	sediment	294	65	-150+106	high
sediment	6	14	-150+106	high	sediment	295	66	-150+106	med
sediment	7	15	-150+106	med	sediment	299	67	-150+106	high
sediment	11	16	-150+106	high	sediment	300	68	-150+106	med
sediment	12	17	-150+106	med	sediment	302	69	-150+106	med
sediment	16	18	-150+106	high	sediment	3	70	-150+106	low
sediment	17	20	-150+106	med	sediment	8	71	-150+106	low
sediment	49	21	-150+106	high	sediment	13	72	-150+106	low
sediment	50	22	-150+106	med	sediment	171	73	-150+106	low
sediment	66	23	-150+106	high	sediment	18	74	-150+106	low
sediment	67	24	-150+106	med	sediment	23	75	-150+106	low
sediment	71	25	-150+106	high	sediment	167	76	-150+106	low
sediment	72	26	-150+106	med	sediment	51	78	-150+106	low
sediment	76	27	-150+106	high	sediment	73	79	-150+106	low
sediment	77	28	-150+106	med	sediment	68	80	-150+106	low
sediment	81	29	-150+106	high	sediment	83	81	-150+106	low
sediment	82	30	-150+106	med	sediment	78	82	-150+106	low
sediment	93	31	-150+106	high	sediment	88	83	-150+106	low
sediment	94	32	-150+106	med	sediment	95	84	-150+106	low
sediment	257	33	-150+106	high	sediment	166	85	-150+106	low
sediment	258	34	-150+106	med	sediment	100	87	-150+106	low
sediment	269	36	-150+106	med	sediment	201	88	-150+106	low
sediment	280	37	-150+106	high	sediment	286	89	-150+106	low
sediment	281	38	-150+106	med	sediment	282	90	-150+106	low
sediment	202	39	-150+106	high	sediment	296	91	-150+106	low
sediment	203a	40	-150+106	med	sediment	291	92	-150+106	low
sediment	321	41	-150+106	high	sediment	301	93	-150+106	low
sediment	204	42	-150+106	med	sediment	278	94	-150+106	low
sediment	260	43	-150+106	med	sediment	303	95	-150+106	low
sediment	261	44	-150+106	high	sediment	200	96	-106+75	med
sediment	262	45	-150+106	high	sediment	169	97	-106+75	med
sediment	263	46	-150+106	high	sediment	86	98	-106+75	high
sediment	264	47	-150+106	med	sediment	87	100	-106+75	med
sediment	265	48	-150+106	high	sediment	98	101	-106+75	high
sediment	266	49	-150+106	med	sediment	99	102	-106+75	med
sediment	267	50	-150+106	high	sediment	21	103	-106+75	high
sediment	268	51	-150+106	med	sediment	22	104	-106+75	med
sediment	270	52	-150+106	high	sediment	168	105	-106+75	med

Table F. Cont'd

Sample media	Field No.	Lab No.	Size fraction	Energy	Sample media	Field No.	Lab No.	Size fraction	Energy
sediment	170	106	-106+75	med	sediment	290	158	-106+75	med
sediment	1	107	-106+75	high	sediment	294	160	-106+75	high
sediment	2	108	-106+75	med	sediment	295	161	-106+75	med
sediment	6	109	-106+75	high	sediment	299	162	-106+75	high
sediment	7	110	-106+75	med	sediment	300	163	-106+75	med
sediment	11	111	-106+75	high	sediment	302	164	-106+75	med
sediment	12	112	-106+75	med	sediment	3	165	-106+75	low
sediment	16	113	-106+75	high	sediment	8	166	-106+75	low
sediment	17	114	-106+75	med	sediment	13	167	-106+75	low
sediment	49	115	-106+75	high	sediment	171	168	-106+75	low
sediment	50	117	-106+75	med	sediment	18	169	-106+75	low
sediment	66	118	-106+75	high	sediment	23	170	-106+75	low
sediment	67	119	-106+75	med	sediment	167	171	-106+75	low
sediment	71	120	-106+75	high	sediment	51	172	-106+75	low
sediment	72	121	-106+75	med	sediment	73	173	-106+75	low
sediment	76	122	-106+75	high	sediment	68	175	-106+75	low
sediment	77	123	-106+75	med	sediment	83	176	-106+75	low
sediment	81	124	-106+75	high	sediment	78	177	-106+75	low
sediment	82	125	-106+75	med	sediment	88	178	-106+75	low
sediment	93	126	-106+75	high	sediment	95	179	-106+75	low
sediment	94	127	-106+75	med	sediment	166	180	-106+75	low
sediment	257	128	-106+75	high	sediment	100	181	-106+75	low
sediment	258	129	-106+75	med	sediment	201	182	-106+75	low
sediment	269	130	-106+75	med	sediment	286	183	-106+75	low
sediment	280	131	-106+75	high	sediment	282	184	-106+75	low
sediment	281	132	-106+75	med	sediment	296	185	-106+75	low
sediment	202	133	-106+75	high	sediment	291	186	-106+75	low
sediment	203a	134	-106+75	med	sediment	301	187	-106+75	low
sediment	321	135	-106+75	high	sediment	278	189	-106+75	low
sediment	204	136	-106+75	med	sediment	303	190	-106+75	low
sediment	260	137	-106+75	med	sediment	200	191	-75+53	med
sediment	261	138	-106+75	high	sediment	169	193	-75+53	med
sediment	262	139	-106+75	high	sediment	86	194	-75+53	high
sediment	263	140	-106+75	high	sediment	87	195	-75+53	med
sediment	264	142	-106+75	med	sediment	98	196	-75+53	high
sediment	265	143	-106+75	high	sediment	99	197	-75+53	med
sediment	266	144	-106+75	med	sediment	21	198	-75+53	high
sediment	267	145	-106+75	high	sediment	22	199	-75+53	med
sediment	268	146	-106+75	med	sediment	168	200	-75+53	med
sediment	270	147	-106+75	high	sediment	170	202	-75+53	med
sediment	271	148	-106+75	med	sediment	1	203	-75+53	high
sediment	272	149	-106+75	high	sediment	2	204	-75+53	med
sediment	273	150	-106+75	med	sediment	6	205	-75+53	high
sediment	274	151	-106+75	high	sediment	7	206	-75+53	med
sediment	275	152	-106+75	med	sediment	11	207	-75+53	high
sediment	276	153	-106+75	high	sediment	12	208	-75+53	med
sediment	277	154	-106+75	med	sediment	16	209	-75+53	high
sediment	284	155	-106+75	high	sediment	17	210	-75+53	med
sediment	285	156	-106+75	med	sediment	49	211	-75+53	high
sediment	289	157	-106+75	high	sediment	50	212	-75+53	med

Table F. Cont'd

Sample media	Field No.	Lab No.	Size fraction	Energy	Sample media	Field No.	Lab No.	Size fraction	Energy
sediment	66	213	-75+53	high	sediment	23	266	-75+53	low
sediment	67	215	-75+53	med	sediment	167	267	-75+53	low
sediment	71	216	-75+53	high	sediment	51	268	-75+53	low
sediment	72	217	-75+53	med	sediment	73	269	-75+53	low
sediment	76	218	-75+53	high	sediment	68	270	-75+53	low
sediment	77	219	-75+53	med	sediment	83	271	-75+53	low
sediment	81	220	-75+53	high	sediment	78	272	-75+53	low
sediment	82	221	-75+53	med	sediment	88	273	-75+53	low
sediment	93	222	-75+53	high	sediment	95	274	-75+53	low
sediment	94	223	-75+53	med	sediment	166	275	-75+53	low
sediment	257	224	-75+53	high	sediment	100	277	-75+53	low
sediment	258	225	-75+53	med	sediment	201	278	-75+53	low
sediment	269	226	-75+53	med	sediment	286	279	-75+53	low
sediment	280	227	-75+53	high	sediment	282	280	-75+53	low
sediment	281	228	-75+53	med	sediment	296	281	-75+53	low
sediment	202	229	-75+53	high	sediment	291	282	-75+53	low
sediment	203a	230	-75+53	med	sediment	301	283	-75+53	low
sediment	321	231	-75+53	high	sediment	278	284	-75+53	low
sediment	204	232	-75+53	med	sediment	303	285	-75+53	low
sediment	260	234	-75+53	med	sediment	200	286	-53	med
sediment	261	235	-75+53	high	sediment	169	287	-53	med
sediment	262	236	-75+53	high	sediment	86	288	-53	high
sediment	263	237	-75+53	high	sediment	87	289	-53	med
sediment	264	238	-75+53	med	sediment	98	290	-53	high
sediment	265	239	-75+53	high	sediment	99	291	-53	med
sediment	266	240	-75+53	med	sediment	21	292	-53	high
sediment	267	241	-75+53	high	sediment	22	294	-53	med
sediment	268	242	-75+53	med	sediment	168	295	-53	med
sediment	270	243	-75+53	high	sediment	170	296	-53	med
sediment	271	244	-75+53	med	sediment	1	297	-53	high
sediment	272	245	-75+53	high	sediment	2	298	-53	med
sediment	273	246	-75+53	med	sediment	6	299	-53	high
sediment	274	247	-75+53	high	sediment	7	300	-53	med
sediment	275	248	-75+53	med	sediment	11	301	-53	high
sediment	276	249	-75+53	high	sediment	12	302	-53	med
sediment	277	250	-75+53	med	sediment	16	303	-53	high
sediment	284	251	-75+53	high	sediment	17	304	-53	med
sediment	285	252	-75+53	med	sediment	49	305	-53	high
sediment	289	253	-75+53	high	sediment	50	306	-53	med
sediment	290	254	-75+53	med	sediment	66	307	-53	high
sediment	294	255	-75+53	high	sediment	67	308	-53	med
sediment	295	256	-75+53	med	sediment	71	309	-53	high
sediment	299	257	-75+53	high	sediment	72	310	-53	med
sediment	300	258	-75+53	med	sediment	76	311	-53	high
sediment	302	259	-75+53	med	sediment	77	312	-53	med
sediment	3	260	-75+53	low	sediment	81	313	-53	high
sediment	8	261	-75+53	low	sediment	82	314	-53	med
sediment	13	262	-75+53	low	sediment	93	315	-53	high
sediment	171	263	-75+53	low	sediment	94	317	-53	med
sediment	18	264	-75+53	low	sediment	257	318	-53	high

Table F. Cont'd

Sample media	Field No.	Lab No.	Size fraction	Energy	Sample media	Field No.	Lab No.	Size fraction	Energy
sediment	258	319	-53	med	sediment	201	372	-53	low
sediment	269	320	-53	med	sediment	286	373	-53	low
sediment	280	321	-53	high	sediment	282	374	-53	low
sediment	281	322	-53	med	sediment	296	375	-53	low
sediment	202	324	-53	high	sediment	291	376	-53	low
sediment	203a	325	-53	med	sediment	301	378	-53	low
sediment	321	326	-53	high	sediment	278	379	-53	low
sediment	204	327	-53	med	sediment	303	380	-53	low
sediment	260	328	-53	med	Surficial	59	1000	-212+106	
sediment	261	329	-53	high	Surficial	60	1001	-212+106	
sediment	262	330	-53	high	Surficial	279	1002	-212+106	
sediment	263	331	-53	high	Surficial	56	1003	-212+106	
sediment	264	332	-53	med	Surficial	287	1004	-212+106	
sediment	265	333	-53	high	Surficial	319	1005	-212+106	
sediment	266	334	-53	med	Surficial	64	1006	-212+106	
sediment	267	335	-53	high	Surficial	283	1007	-212+106	
sediment	268	337	-53	med	Surficial	4	1009	-212+106	
sediment	270	338	-53	high	Surficial	58	1010	-212+106	
sediment	271	339	-53	med	Surficial	293	1011	-212+106	
sediment	272	340	-53	high	Surficial	10	1012	-212+106	
sediment	273	341	-53	med	Surficial	15	1013	-212+106	
sediment	274	342	-53	high	Surficial	57	1014	-212+106	
sediment	275	343	-53	med	Surficial	63	1015	-212+106	
sediment	276	344	-53	high	Surficial	292	1016	-212+106	
sediment	277	345	-53	med	Surficial	62	1017	-212+106	
sediment	284	346	-53	high	Surficial	55	1018	-212+106	
sediment	285	347	-53	med	Surficial	298	1020	-212+106	
sediment	289	348	-53	high	Surficial	61	1021	-212+106	
sediment	290	349	-53	med	Surficial	5	1022	-212+106	
sediment	294	350	-53	high	Surficial	288	1023	-212+106	
sediment	295	351	-53	med	Surficial	9	1024	-212+106	
sediment	299	352	-53	high	Surficial	26	1025	-212+106	
sediment	300	354	-53	med	Surficial	65	1026	-212+106	
sediment	302	355	-53	med	Surficial	217	1027	-212+106	
sediment	3	356	-53	low	Surficial	218	1028	-212+106	
sediment	8	357	-53	low	Surficial	146	1029	-212+106	
sediment	13	358	-53	low	Surficial	133	1030	-212+106	
sediment	171	359	-53	low	Surficial	136	1032	-212+106	
sediment	18	360	-53	low	Surficial	102	1033	-212+106	
sediment	23	361	-53	low	Surficial	125	1034	-212+106	
sediment	167	362	-53	low	Surficial	127	1035	-212+106	
sediment	51	363	-53	low	Surficial	132	1036	-212+106	
sediment	73	364	-53	low	Surficial	144	1037	-212+106	
sediment	68	365	-53	low	Surficial	116	1038	-212+106	
sediment	83	366	-53	low	Surficial	128	1039	-212+106	
sediment	78	367	-53	low	Surficial	131	1040	-212+106	
sediment	88	368	-53	low	Surficial	117	1042	-212+106	
sediment	95	369	-53	low	Surficial	104	1043	-212+106	
sediment	166	370	-53	low	Surficial	148	1044	-212+106	
sediment	100	371	-53	low	Surficial	109	1045	-212+106	

Table F. Cont'd

Sample media	Field No.	Lab No.	Size fraction
Surficial	111	1046	-212+106
Surficial	115	1047	-212+106
Surficial	103	1048	-212+106
Surficial	120	1049	-212+106
Surficial	119	1050	-212+106
Surficial	126	1051	-212+106
Surficial	110	1053	-212+106
Surficial	121	1054	-212+106
Surficial	236	1055	-212+106
Surficial	107	1056	-212+106
Surficial	155	1057	-212+106
Surficial	234	1058	-212+106
Surficial	138	1059	-212+106
Surficial	149	1060	-212+106
Surficial	152	1061	-212+106
Surficial	222	1062	-212+106
Surficial	153	1064	-212+106
Surficial	229	1065	-212+106
Surficial	151	1066	-212+106
Surficial	216	1067	-212+106
Surficial	135	1068	-212+106
Surficial	140	1069	-212+106
Surficial	221	1070	-212+106
Surficial	139	1071	-212+106
Surficial	235	1072	-212+106
Surficial	232	1073	-212+106
Surficial	106	1075	-212+106
Surficial	123	1076	-212+106
Surficial	122	1077	-212+106
Surficial	150	1078	-212+106
Surficial	233	1079	-212+106
Surficial	231	1080	-212+106
Surficial	124	1081	-212+106
Surficial	142	1082	-212+106
Surficial	141	1083	-212+106
Surficial	134	1084	-212+106
Surficial	113	1085	-212+106
Surficial	114	1087	-212+106
Surficial	53	1088	-212+106
Surficial	130	1089	-212+106
Surficial	129	1090	-212+106
Surficial	112	1091	-212+106
Surficial	230	1092	-212+106
Surficial	137	1093	-212+106
Surficial	24	1094	-212+106
Surficial	108	1095	-212+106
Surficial	105	1097	-212+106
Surficial	156	1098	-212+106
Surficial	318	1100	-212+106
Surficial	85	1101	-212+106

Sample media	Field No.	Lab No.	Size fraction
Surficial	89	1102	-212+106
Surficial	84	1103	-212+106
Surficial	80	1104	-212+106
Surficial	91	1105	-212+106
Surficial	160	1106	-212+106
Surficial	158	1108	-212+106
Surficial	165	1109	-212+106
Surficial	96	1110	-212+106
Surficial	90	1111	-212+106
Surficial	159	1112	-212+106
Surficial	311	1113	-212+106
Surficial	161	1114	-212+106
Surficial	157	1115	-212+106
Surficial	163	1116	-212+106
Surficial	69	1117	-212+106
Surficial	25	1119	-212+106
Surficial	79	1120	-212+106
Surficial	101	1121	-212+106
Surficial	164	1122	-212+106
Surficial	19	1123	-212+106
Surficial	309	1124	-212+106
Surficial	308	1125	-212+106
Surficial	74	1126	-212+106
Surficial	14	1127	-212+106
Surficial	162	1128	-212+106
Surficial	304	1129	-212+106
Surficial	306	1131	-212+106
Surficial	52	1132	-212+106
Surficial	92	1133	-212+106
Surficial	297	1134	-212+106
Surficial	312	1135	-212+106
Surficial	310	1136	-212+106
Surficial	305	1137	-212+106
Surficial	16	1138	-212+106
Surficial	307	1139	-212+106
Surficial	59	1140	-106+53
Surficial	60	1141	-106+53
Surficial	279	1142	-106+53
Surficial	56	1143	-106+53
Surficial	287	1144	-106+53
Surficial	319	1145	-106+53
Surficial	64	1146	-106+53
Surficial	283	1147	-106+53
Surficial	4	1149	-106+53
Surficial	58	1150	-106+53
Surficial	293	1151	-106+53
Surficial	10	1152	-106+53
Surficial	15	1153	-106+53
Surficial	57	1154	-106+53
Surficial	63	1155	-106+53

Table F. Cont'd

Sample media	Field No.	Lab No.	Size fraction
Surficial	292	1156	-106+53
Surficial	62	1157	-106+53
Surficial	55	1158	-106+53
Surficial	298	1160	-106+53
Surficial	61	1161	-106+53
Surficial	5	1162	-106+53
Surficial	288	1163	-106+53
Surficial	9	1164	-106+53
Surficial	26	1165	-106+53
Surficial	65	1166	-106+53
Surficial	217	1167	-106+53
Surficial	218	1168	-106+53
Surficial	146	1169	-106+53
Surficial	133	1170	-106+53
Surficial	136	1172	-106+53
Surficial	102	1173	-106+53
Surficial	125	1174	-106+53
Surficial	127	1175	-106+53
Surficial	132	1176	-106+53
Surficial	144	1177	-106+53
Surficial	116	1178	-106+53
Surficial	128	1179	-106+53
Surficial	131	1180	-106+53
Surficial	117	1182	-106+53
Surficial	104	1183	-106+53
Surficial	148	1184	-106+53
Surficial	109	1185	-106+53
Surficial	111	1186	-106+53
Surficial	115	1187	-106+53
Surficial	103	1188	-106+53
Surficial	120	1189	-106+53
Surficial	119	1190	-106+53
Surficial	126	1191	-106+53
Surficial	110	1193	-106+53
Surficial	121	1194	-106+53
Surficial	236	1195	-106+53
Surficial	107	1196	-106+53
Surficial	155	1197	-106+53
Surficial	234	1198	-106+53
Surficial	138	1199	-106+53
Surficial	149	1200	-106+53
Surficial	152	1201	-106+53
Surficial	222	1202	-106+53
Surficial	153	1204	-106+53
Surficial	229	1205	-106+53
Surficial	151	1206	-106+53
Surficial	216	1207	-106+53
Surficial	135	1208	-106+53
Surficial	140	1209	-106+53
Surficial	221	1210	-106+53

Sample media	Field No.	Lab No.	Size fraction
Surficial	139	1211	-106+53
Surficial	235	1212	-106+53
Surficial	232	1213	-106+53
Surficial	106	1215	-106+53
Surficial	123	1216	-106+53
Surficial	122	1217	-106+53
Surficial	150	1218	-106+53
Surficial	233	1219	-106+53
Surficial	231	1220	-106+53
Surficial	124	1221	-106+53
Surficial	142	1222	-106+53
Surficial	141	1223	-106+53
Surficial	134	1224	-106+53
Surficial	113	1225	-106+53
Surficial	114	1227	-106+53
Surficial	53	1228	-106+53
Surficial	130	1229	-106+53
Surficial	129	1230	-106+53
Surficial	112	1231	-106+53
Surficial	230	1232	-106+53
Surficial	137	1233	-106+53
Surficial	24	1234	-106+53
Surficial	108	1235	-106+53
Surficial	105	1237	-106+53
Surficial	156	1238	-106+53
Surficial	318	1239	-106+53
Surficial	85	1240	-106+53
Surficial	89	1241	-106+53
Surficial	84	1242	-106+53
Surficial	80	1243	-106+53
Surficial	91	1244	-106+53
Surficial	160	1245	-106+53
Surficial	158	1247	-106+53
Surficial	165	1248	-106+53
Surficial	96	1249	-106+53
Surficial	90	1250	-106+53
Surficial	159	1251	-106+53
Surficial	311	1252	-106+53
Surficial	161	1254	-106+53
Surficial	157	1255	-106+53
Surficial	163	1256	-106+53
Surficial	69	1257	-106+53
Surficial	25	1259	-106+53
Surficial	79	1260	-106+53
Surficial	101	1261	-106+53
Surficial	164	1262	-106+53
Surficial	19	1263	-106+53
Surficial	309	1264	-106+53
Surficial	308	1265	-106+53
Surficial	74	1266	-106+53

Table F. Cont'd

Sample media	Field No.	Lab No.	Size fraction
Surficial	14	1267	-106+53
Surficial	162	1268	-106+53
Surficial	304	1269	-106+53
Surficial	306	1271	-106+53
Surficial	52	1272	-106+53
Surficial	92	1273	-106+53
Surficial	297	1274	-106+53
Surficial	312	1275	-106+53
Surficial	310	1276	-106+53
Surficial	305	1277	-106+53
Surficial	16	1278	-106+53
Surficial	307	1279	-106+53
Surficial	59	1280	-53
Surficial	60	1281	-53
Surficial	279	1283	-53
Surficial	56	1284	-53
Surficial	287	1285	-53
Surficial	319	1286	-53
Surficial	64	1287	-53
Surficial	283	1288	-53
Surficial	4	1290	-53
Surficial	58	1291	-53
Surficial	293	1292	-53
Surficial	10	1293	-53
Surficial	15	1294	-53
Surficial	57	1295	-53
Surficial	63	1296	-53
Surficial	292	1297	-53
Surficial	62	1298	-53
Surficial	55	1299	-53
Surficial	298	1301	-53
Surficial	61	1302	-53
Surficial	5	1303	-53
Surficial	288	1304	-53
Surficial	9	1305	-53
Surficial	26	1306	-53
Surficial	65	1307	-53
Surficial	217	1308	-53
Surficial	218	1309	-53
Surficial	146	1310	-53
Surficial	133	1311	-53
Surficial	136	1313	-53
Surficial	102	1314	-53
Surficial	125	1315	-53
Surficial	127	1316	-53
Surficial	132	1317	-53
Surficial	144	1318	-53
Surficial	116	1319	-53
Surficial	128	1320	-53
Surficial	131	1321	-53

Sample media	Field No.	Lab No.	Size fraction
Surficial	117	1323	-53
Surficial	104	1324	-53
Surficial	148	1325	-53
Surficial	109	1326	-53
Surficial	111	1327	-53
Surficial	115	1328	-53
Surficial	103	1329	-53
Surficial	120	1330	-53
Surficial	119	1331	-53
Surficial	126	1332	-53
Surficial	110	1334	-53
Surficial	121	1335	-53
Surficial	236	1336	-53
Surficial	107	1337	-53
Surficial	155	1338	-53
Surficial	234	1339	-53
Surficial	138	1340	-53
Surficial	149	1341	-53
Surficial	152	1342	-53
Surficial	222	1343	-53
Surficial	153	1345	-53
Surficial	229	1346	-53
Surficial	151	1347	-53
Surficial	216	1348	-53
Surficial	135	1349	-53
Surficial	140	1350	-53
Surficial	221	1351	-53
Surficial	139	1352	-53
Surficial	235	1353	-53
Surficial	232	1354	-53
Surficial	106	1356	-53
Surficial	123	1357	-53
Surficial	122	1358	-53
Surficial	150	1359	-53
Surficial	233	1360	-53
Surficial	231	1361	-53
Surficial	124	1362	-53
Surficial	142	1363	-53
Surficial	141	1364	-53
Surficial	134	1365	-53
Surficial	113	1366	-53
Surficial	114	1368	-53
Surficial	53	1369	-53
Surficial	130	1370	-53
Surficial	129	1371	-53
Surficial	112	1372	-53
Surficial	230	1373	-53
Surficial	137	1374	-53
Surficial	24	1375	-53
Surficial	108	1376	-53

Table F. Cont'd

Sample media	Field No.	Lab No.	Size fraction
Surficial	105	1378	-53
Surficial	156	1379	-53
Surficial	318	1380	-53
Surficial	85	1381	-53
Surficial	89	1382	-53
Surficial	84	1383	-53
Surficial	80	1384	-53
Surficial	91	1385	-53
Surficial	160	1386	-53
Surficial	158	1388	-53
Surficial	165	1389	-53
Surficial	96	1390	-53
Surficial	90	1391	-53
Surficial	159	1392	-53
Surficial	311	1393	-53
Surficial	161	1395	-53
Surficial	157	1396	-53
Surficial	163	1397	-53
Surficial	69	1398	-53
Surficial	25	1400	-53
Surficial	79	1401	-53
Surficial	101	1402	-53
Surficial	164	1403	-53
Surficial	19	1404	-53
Surficial	309	1405	-53
Surficial	308	1406	-53
Surficial	74	1407	-53
Surficial	14	1408	-53
Surficial	162	1409	-53
Surficial	304	1410	-53
Surficial	306	1412	-53
Surficial	52	1413	-53
Surficial	92	1414	-53
Surficial	297	1415	-53
Surficial	312	1416	-53
Surficial	310	1417	-53
Surficial	305	1418	-53
Surficial	16	1419	-53
Surficial	307	1420	-53
Surficial	154	1500	-212+106
Surficial	75	1501	-212+106
Surficial	145	1502	-212+106
Surficial	143	1503	-212+106
Surficial	147	1505	-212+106
Surficial	118	1506	-212+106
Surficial	97	1507	-212+106
Surficial	54	1508	-212+106
Surficial	219	1509	-212+106
Surficial	220	1510	-212+106
Surficial	223	1511	-212+106

Sample media	Field No.	Lab No.	Size fraction
Surficial	224	1512	-212+106
Surficial	225a	1513	-212+106
Surficial	225b	1514	-212+106
Surficial	226	1515	-212+106
Surficial	227	1516	-212+106
Surficial	228	1517	-212+106
Surficial	154	1518	-106+53
Surficial	75	1519	-106+53
Surficial	145	1520	-106+53
Surficial	143	1521	-106+53
Surficial	147	1522	-106+53
Surficial	118	1523	-106+53
Surficial	97	1524	-106+53
Surficial	54	1525	-106+53
Surficial	219	1526	-106+53
Surficial	220	1527	-106+53
Surficial	223	1528	-106+53
Surficial	224	1529	-106+53
Surficial	225a	1531	-106+53
Surficial	225b	1532	-106+53
Surficial	226	1533	-106+53
Surficial	227	1534	-106+53
Surficial	228	1535	-106+53
Surficial	154	1536	-53
Surficial	75	1537	-53
Surficial	145	1539	-53
Surficial	143	1540	-53
Surficial	147	1541	-53
Surficial	118	1543	-53
Surficial	97	1544	-53
Surficial	54	1545	-53
Surficial	219	1546	-53
Surficial	220	1547	-53
Surficial	223	1548	-53
Surficial	224	1549	-53
Surficial	225a	1550	-53
Surficial	225b	1551	-53
Surficial	226	1552	-53
Surficial	227	1553	-53
Surficial	228	1554	-53

Appendix E

Geochemical Procedure - G132 Package

Sample Decomposition: Aqua Regia Digestion
Analytical Method: Inductively Coupled Plasma - Atomic Emission Spectroscopy (ICP - AES)
Inductively Coupled Plasma - Mass Spectrometry (ICP-MS)

A prepared sample (0.50 grams) is digested with aqua regia for at least one hour in a hot water bath. After cooling, the resulting solution is diluted to 15ml with demineralized water, mixed and analyzed by inductively coupled plasma-atomic emission spectrometry. Following this analysis, the results are reviewed to ensure that base metal concentrations are less than 1%, with the exception of silver, bismuth, and tungsten which have upper analytical limits of 100, 500 and 1000 ppm, respectively. Samples that meet these criteria are then diluted and analysed by ICP-MS. Samples which exceed the Upper Limits as outlined below will be treated as regular G32 digestions and all detection limits will apply as per that method. The analytical results are corrected for inter-element spectral interferences.

	Element	Symbol	Detection Limit	Upper Limit	Analytical Technique
	ICP-AQ Digestion	n/a	n/a	n/a	
*	Aluminum	Al	0.01%	15 %	AES
*	Antimony	Sb	0.1 ppm	1 %	AES+MS
	Arsenic	As	0.2 ppm	1 %	AES+MS
	Boron	B	10 ppm	10,000 ppm	AES
*	Barium	Ba	10 ppm	1 %	AES
*	Beryllium	Be	0.05 ppm	100 ppm	AES
	Bismuth	Bi	0.01 ppm	1 %	AES+MS
	Cadmium	Cd	0.02 ppm	500 ppm	AES+MS
*	Calcium	Ca	0.01%	15 %	AES
*	Chromium	Cr	1 ppm	1 %	AES
	Cobalt	Co	0.2 ppm	1 %	AES
	Copper	Cu	0.2 ppm	1 %	AES+MS
*	Gallium	Ga	0.1 ppm	1 %	AES+MS
	Germanium	Ge	0.1 ppm	500 ppm	MS
	Iron	Fe	0.01%	15 %	AES
*	Lanthanum	La	10 ppm	1 %	AES
	Lead	Pb	2 ppm	1 %	AES
*	Magnesium	Mg	0.01%	15 %	AES
	Manganese	Mn	5 ppm	1 %	AES
	Mercury	Hg	0.01 ppm	1 %	AES+MS

Geochemical Procedure - G132 Package *(con't)*

	Element	Symbol	Detection Limit	Upper Limit	Analytical Technique
	Molybdenum	Mo	0.2 ppm	1 %	AES+MS
	Nickel	Ni	1 ppm	1 %	AES
	Phosphorus	P	10 ppm	1 %	AES
*	Potassium	K	0.01%	10 %	AES
t	Rhenium	Re	0.005 ppm	50 ppm	MS
*	Scandium	Sc	1 ppm	1 %	AES
	Selenium	Se	0.5 ppm	1,000 ppm	MS
	Silver	Ag	0.02 ppm	100 ppm	AES+MS
*	Sodium	Na	0.01%	10 %	AES
*	Strontium	Sr	1 ppm	1 %	AES
	Sulfur	S	0.01 %	5 %	AES
	Tellurium	Te	0.05 ppm	500 ppm	MS
*	Thallium	Tl	0.02 ppm	1 %	AES+MS
*	Titanium	Ti	0.01%	10 %	AES
*	Tungsten	W	0.05 ppm	1 %	AES+MS
	Uranium	U	0.05 ppm	1 %	AES+MS
	Vanadium	V	1 ppm	1 %	AES
	Zinc	Zn	2 ppm	1 %	AES

*Elements for which the digestion is possibly incomplete.
tReported upon request.

MS - Results are from the ICP-MS Scan
AES - Results are from the ICP-AES Scan
AES+MS - Results are a combination of ICP-AES and ICP-MS scans

Geochemical Procedure - G32m Package

In the G32m package, sample decomposition is achieved with a nitric-aqua regia digestion. One portion of the sample digest is analyzed by ICP-AES for all elements except mercury. In order to obtain a low detection limit for mercury, a second portion of the sample digest is analyzed by flameless atomic absorption spectroscopy.

Sample Decomposition: Nitric Aqua Regia Digestion
Analytical Method: Inductively Coupled Plasma - Atomic Emission Spectroscopy (ICP - AES)

A prepared sample (1.00 gram) is digested with concentrated nitric acid for at least one hour. After cooling, hydrochloric acid is added to produce aqua regia and the mixture is then digested for an additional hour and a half. The resulting solution is diluted to 25ml with demineralized water, mixed and analyzed by inductively coupled plasma-atomic emission spectrometry. The analytical results are corrected for inter-element spectral interferences.

	Element	Symbol	Detection Limit	Upper Limit
	ICP-AQ Digestion	n/a	n/a	n/a
*	Aluminum	Al	0.01%	15 %
	Antimony	Sb	2 ppm	1 %
	Arsenic	As	2 ppm	1 %
*	Barium	Ba	10 ppm	1 %
*	Beryllium	Be	0.5 ppm	0.01 %
	Bismuth	Bi	2 ppm	1 %
	Boron	B	10 ppm	10,000 ppm
	Cadmium	Cd	0.5 ppm	0.05 %
*	Calcium	Ca	0.01%	15 %
*	Chromium	Cr	1 ppm	1 %
	Cobalt	Co	1 ppm	1 %
	Copper	Cu	1 ppm	1 %
*	Gallium	Ga	10 ppm	1 %
	Iron	Fe	0.01%	15 %
*	Lanthanum	La	10 ppm	1 %
	Lead	Pb	2 ppm	1 %
*	Magnesium	Mg	0.01%	15 %

Geochemical Procedure - G32m Package *(con't)*

	Element	Symbol	Detection Limit	Upper Limit
	Manganese	Mn	5 ppm	1 %
	Molybdenum	Mo	1 ppm	1 %
	Nickel	Ni	1 ppm	1 %
	Phosphorus	P	10 ppm	1 %
*	Potassium	K	0.01%	10 %
*	Scandium	Sc	1 ppm	1 %
	Silver	Ag	0.2 ppm	0.01 %
*	Sodium	Na	0.01%	10 %
*	Strontium	Sr	1 ppm	1 %
	Sulfur	S	0.01%	5 %
*	Thallium	Tl	10 ppm	1 %
*	Titanium	Ti	0.01%	10 %
*	Tungsten	W	10 ppm	1 %
	Uranium	U	10 ppm	1 %
	Vanadium	V	1 ppm	1 %
	Zinc	Zn	2 ppm	1 %

*Elements for which the digestion is possibly incomplete.

Sample Decomposition: Nitric Aqua Regia Digestion
Analytical Method: Atomic Absorption Spectroscopy (AAS)

From the same digestion, a portion of the sample is treated with stannous chloride to reduce the mercury. The resulting mercury is volatilized by argon-purging and measured by atomic absorption spectrometry.

Element	Symbol	Detection Limit	Upper Limit
Mercury	Hg	10 ppb	100 ppm

Geochemical Procedure - Selective Leach Packages

Sample Decomposition: Cold and Weak Hydroxylamine Hydrochloride Leach (G985)

Analytical Method: Inductively Coupled Plasma - Mass Spectrometry (ICP-MS)

1. Cold and Weak Hydroxylamine Hydrochloride.
   - A prepared sample (1.0 gram) is mixed with 20 ml of a hydroxylamine hydrochloride solution (0.1 M in 0.01M HNO_3) and rolled for two hours at room temperature. The final solution is then separated from the solids by centrifuging and decanting the supernatant. The solution is then analyzed by ICP-MS and the results are corrected for spectral interferences.

Detection Limit (ppb)

Element	Symbol	Cold Hydroxylamine Leach
Aluminum	Al	1,000
Antimony	Sb	5
Arsenic	As	100
Barium	Ba	50
Beryllium	Be	50
Bismuth	Bi	5
Boron	B	2,000
Bromine	Br	2,000
Cadmium	Cd	10
Calcium	Ca	10,000
Cerium	Ce	5
Cesium	Cs	5
Chromium	Cr	50
Cobalt	Co	50
Copper	Cu	50
Dysprosium	Dy	5
Erbium	Er	5
Europium	Eu	5
Gadolinium	Gd	5
Gallium	Ga	50
Germanium	Ge	100
Gold	Au	50

Hafnium	Hf	10
Holmium	Ho	5
Indium	In	5
Iodine	I	100
Iron	Fe	5,000
Lanthanum	La	5
Lead	Pb	100
Lithium	Li	50
Lutetium	Lu	5
Magnesium	Mg	1,000
Manganese	Mn	100
Mercury	Hg	100
Molybdenum	Mo	10
Neodymium	Nd	5
Nickel	Ni	50
Niobium	Nb	10
Phosphorus	P	5,000
Potassium	K	5,000
Praseodymium	Pr	5
Rhenium	Re	1
Rubidium	Rb	10
Samarium	Sm	5
Selenium	Se	500
Silver	Ag	2
Sodium	Na	10,000
Strontium	Sr	50
Tantalum	Ta	10
Tellurium	Te	50
Terbium	Tb	5
Thallium	Tl	5
Thorium	Th	10
Thulium	Tm	5
Tin	Sn	50
Titanium	Ti	1,000
Tungsten	W	10
Uranium	U	5
Vanadium	V	50
Ytterbium	Yb	5
Yttrium	Y	5
Zinc	Zn	200
Zirconium	Zr	50
Final pH	pH	

Note: After leaching, the final pH of the solution is determined with a pH electrode.

Geochemical Procedure - T27 - Total Metals Package

The majority of metals in the T24 package are determined with a direct ICP-AES measurement following a triple acid digestion. Two elements, lead and silver, are measured by atomic absorption spectroscopy from the same digestion in order to eliminate any possible interelement interferences. The remaining three elements, arsenic, mercury and antimony, are determined individually by optimized geochemical methods.

Sample Decomposition: Triple Acid Digestion
Analytical Method: Inductively Coupled Plasma - Atomic Emission Spectroscopy (ICP - AES)

A prepared sample (0.500 gram) is digested with perchloric, nitric and hydrofluoric acids to dryness. The residue is taken up in a volume of 25 ml of 10% hydrochloric acid and the resulting solution is analyzed by inductively coupled plasma-atomic emission spectrometry. Results are corrected for spectral interelement interferences.

Element	Symbol	Detection Limit	Upper Limit
ICP-HF Digestion	n/a	n/a	n/a
Aluminum	Al	0.01%	25 %
Barium	Ba	10 ppm	1 %
Beryllium	Be	0.5 ppm	1000 ppm
Bismuth	Bi	2 ppm	1 %
Cadmium	Cd	0.5 ppm	500 ppm
Calcium	Ca	0.01%	25 %
Chromium	Cr	1 ppm	1 %
Cobalt	Co	1 ppm	1 %
Copper	Cu	1 ppm	1 %
Iron	Fe	0.01%	25 %
Magnesium	Mg	0.01%	15 %
Manganese	Mn	5 ppm	1 %
Molybdenum	Mo	1 ppm	1 %
Nickel	Ni	1 ppm	1 %
Phosphorus	P	10 ppm	1 %
Potassium	K	0.01%	10 %

<u>Geochemical Procedure</u> - T27 - Total Metals Package *(con't)*

Element	Symbol	Detection Limit	Upper Limit
Sodium	Na	0.01%	10 %
Strontium	Sr	1 ppm	1 %
Titanium	Ti	0.01%	10 %
Tungsten	W	10 ppm	1 %
Vanadium	V	1 ppm	1 %
Zinc	Zn	2 ppm	1 %

Sample Decomposition: Triple Acid Digestion
Analytical Method: Atomic Absorption Spectroscopy (AAS)

From the same digestion, a portion of the sample analyzed by atomic absorption spectrometry.

Element	Symbol	Detection Limit	Upper Limit
Lead	Pb	2 ppm	1 %
Silver	Ag	0.2 ppm	100 ppm

Geochemical Procedure - T27 - Total Metals Package *(con't)*

Sample Decomposition: Nitric Aqua Regia Digestion
Analytical Method: Atomic Absorption Spectroscopy (AAS)

A prepared sample (1.00 gram) is digested with concentrated nitric acid for at least one hour. After cooling, hydrochloric acid is added to produce aqua regia and the mixture is then digested for an additional hour and a half. The resulting solution is diluted to 25ml with demineralized water, mixed and then analyzed by atomic absorption spectrometry with background correction.

Element	Symbol	Detection Limit	Upper Limit
Arsenic	As	1 ppm	1%

Sample Decomposition: Nitric Aqua Regia Digestion
Analytical Method: Atomic Absorption Spectroscopy (AAS)

From the Arsenic digestion, a portion of the sample is treated with stannous chloride to reduce the mercury. The resulting mercury is volatilized by argon-purging and measured by atomic absorption spectrometry.

Element	Symbol	Detection Limit	Upper Limit
Mercury	Hg	10 ppb	100 ppm

Geochemical Procedure - T27 - Total Metals Package *(con't)*

Sample Decomposition: Hydrochloric Acid - Potassium Chlorate Digestion
Analytical Method: Atomic Absorption Spectroscopy (AAS)

A prepared sample (2.00 grams) is digested with concentrated hydrochloric acid and potassium chlorate at low heat. Potassium iodide and ascorbic acid are added to reduce iron. Antimony is then extracted with tri-n-octylphosphine oxide (TOPO) and methyl isobutyl ketone (MIBK). The resulting solution is then analyzed by atomic absorption spectrometry with correction for background absorption.

Chemex Code	Element	Symbol	Detection Limit	Upper Limit
287	Special Digestion with Organic Extraction	n/a	n/a	n/a
22	Antimony	Sb	0.2 ppm	1000 ppm

Appendix E

Environmental Procedure - G392 - ICP-MS Dissolved Metals Package

Analytical Method: Inductively Coupled Plasma - Mass Spectroscopy (ICP - MS)

An aqueous sample is filtered through a 0.45 μm membrane. The filtered sample is then analyzed by inductively coupled - mass spectrometry.

Element	Symbol	Detection Limit	Upper Limit
Total Digestion	n/a	n/a	n/a
Aluminum	Al	0.001mg/l	100,000 mg/l
Antimony	Sb	0.05 ug/l	1000 ug/l
Arsenic	As	1 ug/l	50,000 ug/l
Barium	Ba	0.05 ug/l	50,000 ug/l
Beryllium	Be	0.5 ug/l	1000 ug/l
Bismuth	Bi	0.05 ug/l	1000 ug/l
Cadmium	Cd	0.1 ug/l	50,000 ug/l
Calcium	Ca	0.05 mg/l	100,000 mg/l
Chromium	Cr	0.5 ug/l	50,000 ug/l
Cobalt	Co	0.02 ug/l	50,000 ug/l
Copper	Cu	0.1 ug/l	50,000 ug/l
Iron	Fe	0.01 mg/l	100,000 mg/l
Lead	Pb	2 ug/l	50,000 ug/l
Magnesium	Mg	0.001 mg/l	100,000 mg/l
Manganese	Mn	0.05 ug/l	50,000 ug/l
Mercury	Hg	1 ug/l	1000 ug/l
Molybdenum	Mo	0.1 ug/l	50,000 ug/l
Nickel	Ni	0.2 ug/l	50,000 ug/l
Phosphorus	P	0.1 mg/l	100,000 mg/l
Potassium	K	0.05 mg/l	100,000 mg/l
Selenium	Se	1 ug/l	1000 ug/l
Silver	Ag	0.05 ug/l	1000 ug/l
Sodium	Na	0.05 mg/l	100,000 mg/l
Strontium	Sr	0.05 ug/l	50,000 ug/l
Thallium	Tl	0.05 ug/l	1000 ug/l
Tin	Sn	0.5 ug/l	1000 ug/l
Titanium	Ti	1 ug/l	50,000 ug/l
Uranium	U	0.05 ug/l	1000 ug/l
Vanadium	V	1 ug/l	50,000 ug/l
Zinc	Zn	0.5 ug/l	50,000 ug/l